

Northeastern University Department of Civil and Environmental Engineering

THERMAL BREAK STRATEGIES FOR CLADDING SYSTEMS IN BUILDING STRUCTURES

Report to the Charles Pankow Foundation



CHARLES PANKOW
FOUNDATION

Building Innovation through Research

Kara D. Peterman, Justin Kordas, Julieta Moradei, Kyle Coleman, and Jerome F. Hajjar,
Department of Civil and Environmental Engineering, Northeastern University
James A. D'Aloisio, *Klepper Hahn & Hyatt*
Mark D. Webster, Jason Der Ananian, *Simpson Gumpertz & Heger, Inc.*

May 2017

Executive Summary

This research explores approaches for developing thermal breaks to reduce loss of energy for heating and cooling in steel building structures. Structural steel elements that pass through the building envelope potentially act as thermal bridges due to their ability to conduct heat, transferring interior heat or cooling to the exterior and thus increasing building energy consumption. Condensation and reduced building occupant comfort can also result from thermal bridging. The key goal of this project is to explore and validate several concepts and develop associated design recommendations for mitigating the loss of energy via thermal bridging and other related issues in steel building structures by using a variety of possible solutions. By introducing thermal break strategies to various components throughout the detailing in a structure, we identify practical solutions geared for gaining acceptance and codification as needed for use within the steel construction industry. The scope of this work involves only snug-tight connections.

The scope of this work includes investigation of structural steel shelf angle details to support building cladding, structural steel roof posts to support dunnage on building roofs, and cantilevered structural steel beams to support light canopies. Experimental testing, structural analysis, and thermal analyses were conducted to explore a variety of solutions including different fiber-reinforced polymer (FRP) shims, FRP shapes, and manufactured structural thermal break assemblies (MSTBA). In addition, a methodology is put forward to conduct creep testing on FRP plates loaded in compression through the thickness, and the creep properties of FRP plates used as shims is documented.

Thermal modeling described herein demonstrates the efficacy of the proposed thermal break mitigations strategies. For continuous cladding elements (i.e., shelf angles), the proposed solutions can reduce the thermal conductivity of a system by approximately 50% when compared to an unmitigated broken wall segment. When compared to the conductivity of the unbroken wall element, these solutions result in an improvement of approximately 75%. For discrete cladding details (i.e., roof posts and canopy beams), the improvement is smaller when compared to an unmitigated detail (10-14%, depending on strategy), but more significant when compared to unbroken wall and roof details with no penetrations (60-70%).

Experimental and computational studies on the most successful thermal break strategies provide structural validation of the proposed solutions. The proposed solutions were often seen to impact the failure mode; however, this behavior was not evident until well beyond the design range of the component. In the shelf angles, members with FRP shims were seen to have a decrease in strength compared to members with steel shims. However, shelf angles with FRP shims showed no significant decrease in strength compared to shelf angles without shims due to beneficial changes in the connection geometry. In roof posts and canopy beams, shim mitigation strategies have little to no impact on component behavior. While small differences in strength can be observed (~5%) between mitigated details, this difference is typically due to a difference in shim material properties, and not a system effect.

This report concludes with possible analysis and design recommendations for including thermal breaks in the detailing of shelf angle cladding supports, roof posts, and canopy beams.

Acknowledgements

This material is based upon work supported by the Charles Pankow Foundation, the American Institute of Steel Construction, the American Composites Manufacturers Association (ACMA), the ACMA-Pultrusion Industry Council, the National Science Foundation under Grant No. CMMI-0654176, Simpson Gumpertz & Heger, Inc., and Northeastern University. In-kind support was provided by ArmadilloNV, Bedford Reinforced Plastics, Capone Iron, Creative Pultrusions, Fabreeka, Fastenal, Inframetals, and Strongwell. This support is gratefully acknowledged. Any opinions, findings, and conclusions expressed in this material are those of the authors and do not necessarily reflect the views of the sponsors. For their contributions to this project, the authors would like to thank project team members Mehdi Zarghamee, James Parker, Pedro Sifre, Sean O'Brien, Mariela Corrales, Nathalie Skaf, Elisa Livingston, and Jessica Coolbaugh of Simpson Gumpertz & Heger, Inc., Yujie Yan, Dennis Rogers, Michael MacNeil, and Kurt Braun of Northeastern University, and the members of the Industrial Advisory Panel and the ACMA-Pultrusion Industry Council Technical Advisory Team for this project:

INDUSTRY ADVISORY PANEL

Fiona Aldous	Wiss, Janney, Elstner Associates, Inc.
Glenn Barefoot	Strongwell Corporation
Todd Berthold	Strongwell Corporation
Craig Blanchet	LeMessurier Associates
John P. Busel	American Composites Manufacturing Association
Rodney Gibble	Rodney D. Gibble Consulting Engineers
Robert Haley	ArmadilloNV
Robert Kistler	The Façade Group
Adrian Lane	Owens Corning
Andrea Love	Payette
Alex McGowan	Levelton Consultants, Ltd.
Steve Moore	Fabreeka International, Inc.
Larry Muir	American Institute of Steel Construction
Rick Pauer	CCP Composites
Thomas Schlafly	American Institute of Steel Construction
Tabitha Stine	American Institute of Steel Construction
Dustin Troutman	Creative Pultrusions, Inc.

ACMA-PULTRUSION INDUSTRY COUNCIL TECHNICAL ADVISORY TEAM

Glenn Barefoot	Strongwell Corporation
Todd Berthold	Strongwell Corporation
Stephen Browning	Strongwell Corporation
John P. Busel	American Composites Manufacturing Association
Alfred D'Sousza	Fibergrate Composite Structures, Inc.
Ellen Lackey	University of Mississippi
Bhyrav Mutnuri	Bedford Reinforced Plastics, Inc.
Kevin Spoo	Owens Corning
Jim Tedesco	AOC LLC
Dustin Troutman	Creative Pultrusions, Inc.

Table of Contents

Executive Summary	ii
Acknowledgements.....	iii
Table of Contents.....	iv
1 Introduction	1
1.1 Archetypal building.....	1
1.2 Archetypal cladding details.....	3
1.2.1 Slab-supported shelf angle.....	3
1.2.2 Canopy Beam.....	5
1.2.3 Rooftop Dunnage Post.....	5
1.3 Thermal break mitigation strategies.....	6
1.3.1 Post/beam systems	6
1.3.2 Roof Post Prototype Structures – Mitigation with FRP Shims.....	6
1.3.3 Roof Post Prototype Structures – Replacement with FRP Structural Sections	8
1.3.4 Canopy beam prototype structure – manufactured structural thermal break assembly (MSTBA) solutions	9
1.3.5 Horizontal Beam Prototype Structure – Substitution with FRP Structural Members	9
1.3.6 Slab-supported shelf angle.....	10
1.4 Organization of the Report.....	15
2 Background.....	16
2.1 Overview	16
2.2 Morrison Hershfield (2008)	16
2.1.1 Relieving Angle Models	16
2.1.2 Cantilever Beam Model	19
2.3 The Corus Group (2011)	20
2.1.3 Local Insulation	21
2.1.4 Slotted Steel Sections.....	21
2.1.5 Lower Conductivity Connections	22
2.1.6 Proprietary Solutions	22
2.4 Schoeck Ltd Thermal Bridging Report (2015)	23
2.5 Modern Steel Construction Insert (2012).....	25
2.1.7 Roof Grillage Posts.....	26
2.1.8 Roof Edge Angle.....	27

2.1.9	Shelf Angle Support.....	27
2.1.10	Masonry Lintel.....	28
2.1.11	Cantilever Roof Canopy Beam.....	30
2.6	Kemper Arena Collapse.....	31
3	Thermal Modeling.....	32
3.1	Motivation and Background.....	39
3.2	Scope of Analysis.....	40
3.2	Roof Posts.....	43
3.2.1	Assumptions Made and Differences between Structurally Tested Specimens.....	43
3.2.2	Results.....	44
3.3	Slab-Supported Shelf Angle.....	49
3.3.1	Assumptions Made and Differences between Structurally Tested Specimens.....	49
3.3.2	Results.....	52
3.4	Canopy Beam.....	54
3.4.1	Assumptions Made and Differences between Structurally Tested Specimens.....	54
3.4.2	Results.....	54
3.5	Conclusions.....	56
4	Flatwise Creep Testing of FRP Materials.....	57
4.1	Experimental setup and design.....	57
4.1.1	Test matrix.....	58
4.1	Results.....	59
4.2	Creep stress and time to failure analysis.....	62
4.3	Creep strain analysis.....	64
4.4	Recommendations for Design.....	70
5	Double lap splice bolted steel connections with fiber-reinforced polymer fills.....	74
5.1	Experimental setup and design.....	74
5.1.1	Test matrix.....	74
5.1.2	Test rig.....	75
5.1.3	Load protocol and sensors.....	77
5.2	Results and discussion.....	78
5.3	Design Recommendations.....	85
6	Slab-Supported Shelf Angles.....	87
6.1	Experimental setup and design.....	87
6.1.1	Test matrix.....	87

6.1.2	Test rig and protocol	88
6.1.3	Instrumentation plan	91
6.2	Results and Discussion.....	93
6.2.1	Force-displacement results.....	93
6.2.2	Shelf angle strain results	100
6.2.3	Load cell results	101
6.3	Finite element validation studies.....	103
6.4	Design Recommendations.....	120
6.4.1	Deflections	120
6.4.2	Stresses.....	123
7	Roof Posts and Canopy Beams.....	125
7.1	Experimental setup and design.....	125
7.1.1	Test matrix	125
7.1.2	Test rig and protocol.....	128
7.1.3	Instrumentation plan	131
7.2	Results and Discussion.....	133
7.3	Finite element validation.....	147
7.4	Design Recommendations.....	165
8	Conclusions and Future Work	166
	References.....	168
	Appendix A: Ancillary Test Data	172
A.1	Shelf Angle Base Metal Tensile Tests	172
A.1.1	Shelf angle base metal tensile testing results.....	175
A.2	Roof Post and Canopy Beam Base Plate Base Metal Tensile Tests	179
A.2.1	Test Setup and Methods.....	179
A.2.2	Base plate base metal tensile testing results	180
A.3	Bolt Base Metal Tensile Testing	183
A.3.1	Test Setup and Methods.....	183
A.3.2	Base metal bolt tensile testing results	184
Summary of Results		189
Bolt Testing in Shear and Tension.....		190
A.4	Bolt tensile testing	190
A.5	Bolt shear testing.....	199
A.5.1	Summary of Bolt Tensile and Shear Testing Results	208

A.6 Compression of Fiber Reinforced Polymer Materials.....	209
Appendix B: Proposed Flatwise Compressive Creep Rupture Test Methodology.....	211
Appendix C: Shelf Angle Experimental Test Data.....	217
Appendix D: Roof Post and Canopy Beam Experimental Test Data	239
Appendix E: Thermal Modeling.....	267
Appendix E.1 – Results Sheets for Slab-Supported Shelf Angles	267
Appendix E.2 – Results Sheets for Roof Posts	275
Appendix E.3 – Results Sheets for Canopy Beams	293
Appendix E.4 – Structural Testing Matrix for Roof Posts.....	297
Appendix E.5 – Thermal Modeling Matrix for Roof Posts.....	298
Appendix F: ABAQUS Supplementary Information and Results	299
Appendix F.1: ABAQUS Material Data	299
Appendix F.2: Data Plots	301
Appendix F.3: Deflected Shapes.....	314
Appendix G: Mill Certificates	327

[this page intentionally left blank]

1 Introduction

This research explores approaches for developing thermal breaks to reduce loss of energy for heating and cooling in steel building structures. Structural steel elements that pass through the building envelope potentially act as thermal bridges due to their ability to conduct heat, transferring interior heat or cooling to the exterior and thus increasing building energy consumption. Condensation and reduced building occupant comfort can also result from thermal bridging. The key goal of this project is to explore and validate several concepts and develop associated design recommendations for mitigating the loss of energy and other related issues in steel building structures via thermal bridging by using a variety of possible solutions. By introducing thermal break strategies to various components throughout the detailing in a structure, we identify practical solutions geared for gaining acceptance and codification as needed for use within the steel construction industry.

The scope of this work includes investigation of structural steel shelf angle details to support building cladding, structural steel roof posts to support dunnage on building roofs, and cantilevered structural steel beams to support light canopies. A key goal of this work is to document the structural performance of solutions that are shown to be viable through thermal modeling. Experimental testing, structural analysis, and thermal analyses were conducted to explore a variety of solutions including different fiber-reinforced polymer (FRP) shims within the plies of the steel connections anchoring the shelf angles, roof posts, and canopy beams, as well as fiber-reinforced shapes or manufactured structured thermal break assemblies (MSTBA) that may be used in lieu of the steel members in these structures. In addition, a methodology is put forward to conduct creep testing on FRP plate loaded in compression through the thickness, and the creep properties of FRP plates used as shims is documented. This report concludes with possible analysis and design recommendations for including thermal breaks in the detailing of shelf angle cladding supports, roof posts, and canopy beams.

1.1 Archetypal building

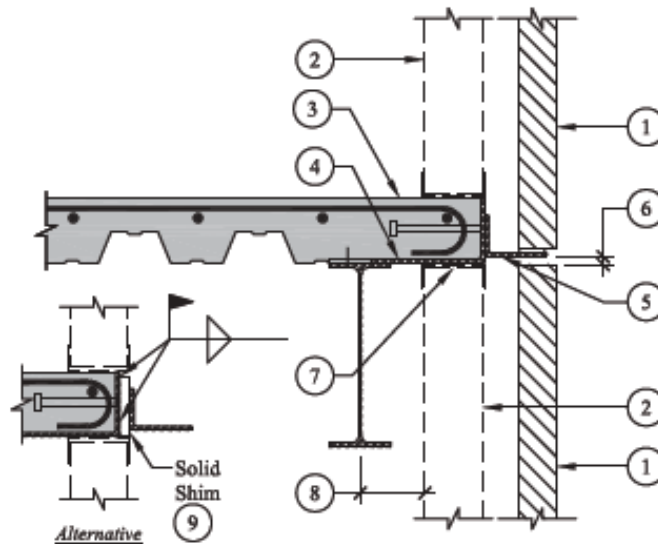
A prototype structure has been selected for this research to help establish realistic parameters for the experimental component of this work and to provide parameters and geometries for parametric thermal modeling investigations. The building system chosen for this research represents a standard steel framed three-story building. To examine thermal performance in different climate zones, the building is hypothetically located in Miami, FL and Fargo, ND, corresponding to the ASHRAE climate zones 1 and 7, respectively. These two climate zones represent the extremes of temperature found in the continental U.S. The lateral force resisting system is assumed to be comprised of special concentrically braced frames (SCBFs). The plan view and elevation views of the archetypal building are shown in Figure 1-1, below.

1.2 Archetypal cladding details

From the range of possible cladding details that span the building envelope, four details were identified by the project industry advisory panel as particularly susceptible to forming thermal bridges. Those are the slab-supported shelf angles to support building cladding, kicker-supported shelf angles to support building cladding, canopy beams to support cantilevered canopies, and rooftop grillage posts to support rooftop dunnage. The subsections below provide typical details for each of these archetypal cladding details.

1.2.1 Slab-supported shelf angle

Shelf angles are commonly used to support exterior brick veneer such that the weight of the bricks is hung off the floor system of the building. Slab-supported shelf angles refer to angles that are connected to the concrete slab floors of a building. As cladding details are installed after the structural system is complete and typically have different tolerances, it is necessary for these details to be adjustable in the field. Currently, standard practice at bolt-supported shelf angles is to cut vertical slotted holes in the shelf angle, such that the shelf angle may be installed on threaded studs or erection bolts. After the shelf angle is positioned on the studs and adjusted vertically, the bolts are tightened to snug-tight, and field welds are added to resist the shelf angle load. A typical slab-supported shelf angle detail, as presented in the AISC Design Guide 22: Façade Attachments in Steel Framed Buildings (Parker, 2008), is shown in Figure 1-3.



(Note: Sheathing and Insulation Not Shown for Clarity, Typ.)

Figure 1-3: Slab-supported shelf angle, from AISC Design Guide 22 (Parker, 2008).

The designed detail for the archetype building in both climate zones is shown in Figure 1-4 and Figure 1-5 below. Sheathing, insulation, and air layers are also illustrated. The 2012 IECC R-value requirements result in mineral wool insulation thicknesses of 1.5 inches in Climate Zone 1 and 3.5 inches in Climate Zone 7.

UNMITIGATED - CLIMATE ZONE 1

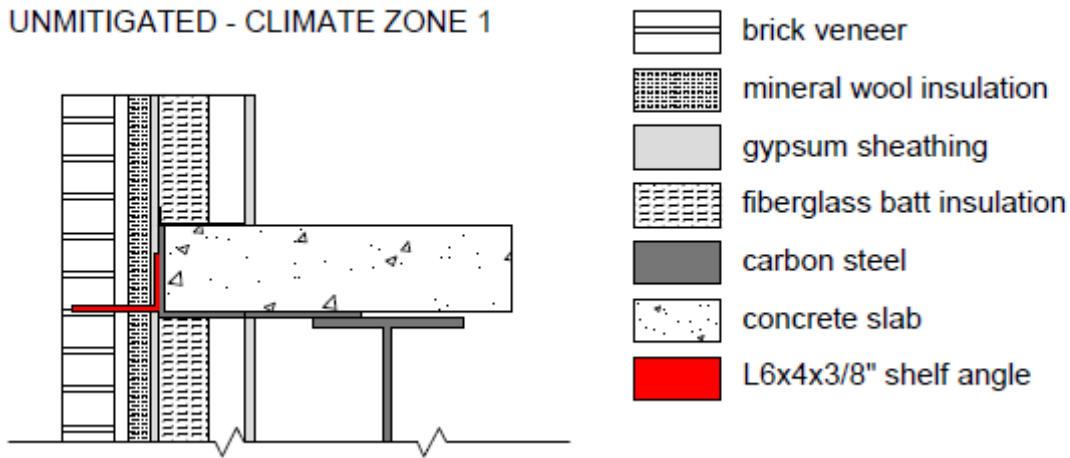


Figure 1-4: Unmitigated slab-supported shelf angle detail, climate zone 1

The brick veneer is detailed as a standard 3 5/8 inches thick. Gypsum drywall sheathing is 5/8 inches thick. Interior cold-formed steel framed partition walls are fastened to the concrete slab. These partition walls contain 3 1/2 inches of fiberglass batt insulation. The concrete slab is poured on a 3 inch deep steel decking and in total, is 6 inch deep (lightweight concrete is assumed). The bent plate pour stop is 3/8 inches thick. Finally, the bent plate is welded to the W21x44 spandrel beam. The climate zone 7 detail is shown in Figure 1-5 with 3.5 inches of mineral wool insulation.

UNMITIGATED - CLIMATE ZONE 7

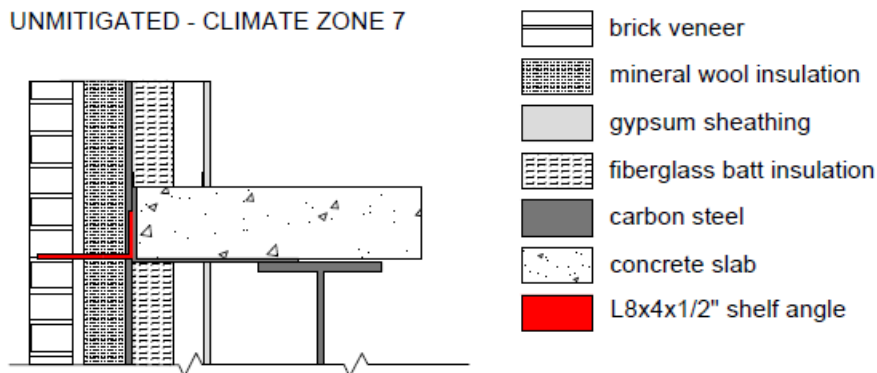


Figure 1-5: Unmitigated slab-supported shelf angle detail, climate zone 7

To accommodate the increased cavity size, a larger shelf angle must be utilized to support the brick veneer, and account for the additional deflections inherent in a longer-legged angle. Both shelf angles are connected to the bent plate pour stop via threaded studs at 36 inch intervals.

1.2.2 Canopy Beam

Elements extending from the edge of a building to form canopies or balconies act as simple cantilevers often connected to the spandrel beams or columns. Figure 1-6 depicts a typical canopy beam detail.

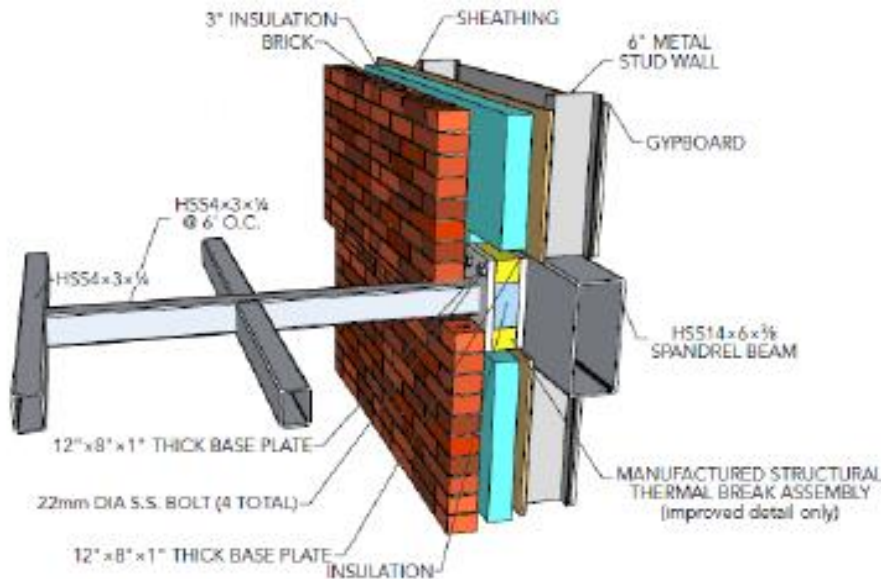


Figure 1-6: Canopy beam typical details (from D'Aloisio 2012)

The canopy beam thermal models include the same wall assemblies and insulation thicknesses as the shelf angle models. This cladding detail is a candidate for shim mitigation, tube shim mitigation, and manufactured thermal break assemblies. These options are discussed later in this report.

1.2.3 Rooftop Dunnage Post

The rooftop dunnage post, shown in Figure 1-7, involves welding a steel pipe onto a base plate, and welding or bolting the ensemble on to a steel beam. The grillage post carries mechanical loads axially and is also subjected to axial, shear, and flexural forces under wind or earthquake loads.

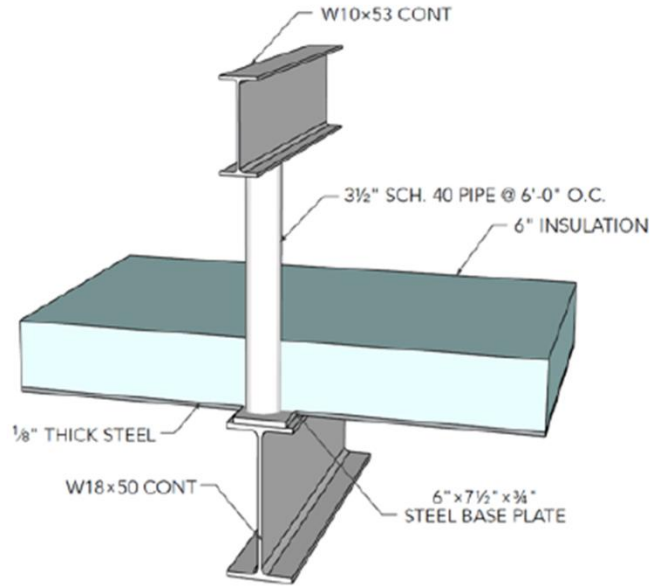


Figure 1-7: Rooftop grillage post examples (from D'Aloisio, 2012).

Insulation in this detail is relatively simple as compared to the wall assemblies: a layer of polyisocyanurate rigid insulation over the deck. The insulation thickness is 3.8 inches for Zone 1 and 6 inches for Zone 7 in conformance with the 2012 IECC. While shims are a logical detail for the roof post (and are explored fully), solutions that span the insulation can also provide thermal break mitigation.

1.3 Thermal break mitigation strategies

The following sections contain the proposed thermal break strategies to be studied in this work for various cases in the building envelope, and how they apply to archetypal details considered in this study. Three strategies are discussed below: adding a thermally improved shim to the system; partial or full replacement of the structural member with a thermally improved member; and manufactured thermal break assemblies.

1.3.1 Post/beam systems

Post/beam systems include (1) roof posts that project through the roof insulation plane to support structures such as mechanical units and photovoltaic panels and (2) beam elements that extend through the wall insulation plane to support structures such as canopies and shading devices. Proposed mitigation details include the addition of thermally improved shims between the post/beam and the interior supports, replacing segments of the post/beams with analogous FRP members, and replacing entire post/beams with an analogous FRP members.

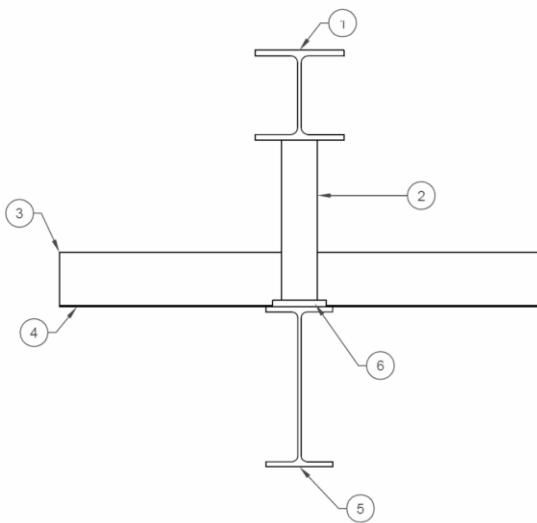
1.3.2 Roof Post Prototype Structures – Mitigation with FRP Shims

FRP plates and bearing pads are natural candidates for thermally improved shims, where the primary load type is compression of the pad; FRP pads can have greater compressive strengths

than carbon steel, though have much lower stiffness. Another alternative is the use of steel foam shims. Steel foam is a relatively new material, made from either forming molten bubbles with steel (hollow sphere foam), or by injecting gas into steel. The thermal conductivity of the material is significantly reduced as a result, while the structural properties are largely maintained.

One challenge in using fiber reinforced polymer shims is their performance under elevated temperatures (fire conditions). Most polymers have no minimum operating temperature, but are limited to the glass transition temperature minus 22 °C. For example, polyurethane has a glass transition temperature of 138 °C so the maximum recommended operating temperature of a polyurethane shim is $138 - 22 = 116$ °C. Once a resin is heated beyond this temperature, strength and stiffness properties are compromised and appropriate reduction factors must be applied for design. Detailed assessment of the structural performance of FRP materials at elevated temperatures is outside the scope of this work.

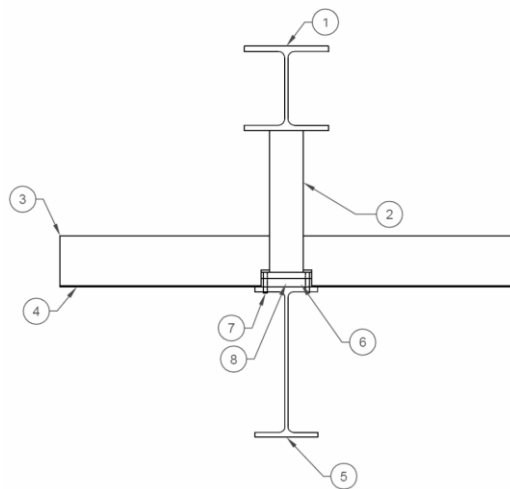
Initial thermal modeling using FRP shims up to 3” thick below the steel post base plate showed improvements in thermal point transmittance of over 30% for both climate zones. Modeling efforts were extended to shims that span the insulation layer. Results of these models are discussed in Chapter 3. Unmitigated and mitigated roof post schematics are shown in Figure 1-8 and Figure 1-9 below. We modeled the steel deck with 1/8” steel plate because software limitations prevented using a thinner cross-section.



ITEM NO.	DESCRIPTION
----------	-------------

1	W Beam – W14x30
2	HSS 3x3x3/16
3	Polyisocyanurate Insulation: 3.8” (Z1), 6” (Z7)
4	1/8” Steel
5	W Beam – W14x34
6	9” x 9” x 1/2” Steel Base Plate

Figure 1-8 - Unmitigated roof post detail



ITEM	DESCRIPTION
1	W Beam – W14x30
2	HSS 3x3x3/16
3	Polyisocyanurate Insulation: 3.8" (Zone 1), 6" (Zone 7)
4	1/8" Steel
5	W Beam – W14x34
6	9" x 9" x 1/2" Steel Base Plate
7	3/4" Dia. Bolt (Typ.)
8	Thermally Improved Shim – 1", 2", 3" FRP or Stainless Steel

Figure 1-9 - Mitigation strategy - thermally improved shim

As insulation layers can be as thick as 6 inches for roof post details, strategies that span the insulation layer must be considered. Stacking shims, with options to adhere with structural adhesive or epoxy, presents one solution to this problem. Figure 1-10 demonstrates these shim strategies.

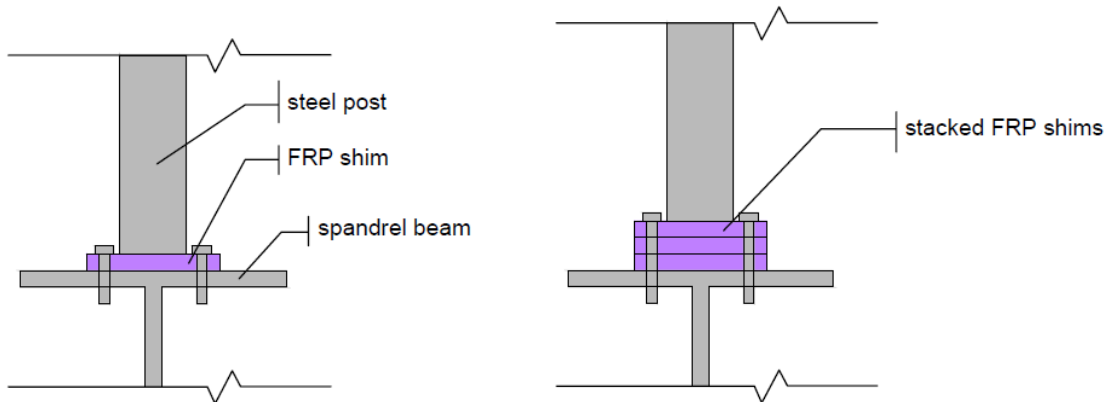
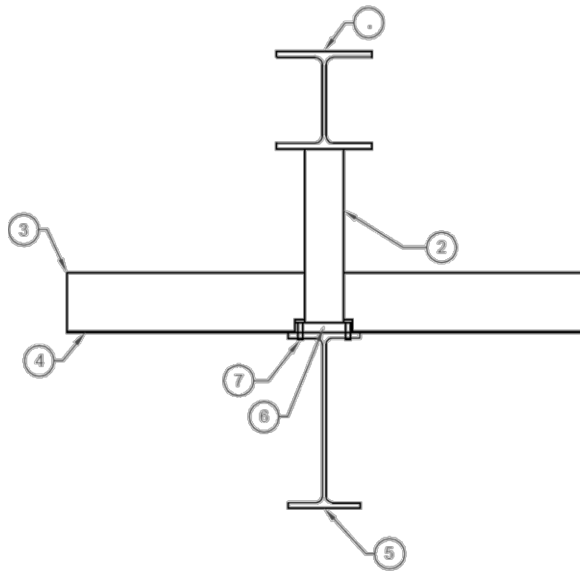


Figure 1-10: Shim mitigation strategies for roof post detail demonstrating single shim and stacked shims configurations.

1.3.3 Roof Post Prototype Structures – Replacement with FRP Structural Sections

In this work, we explore the thermal and structural performance of roof post details mitigated with FRP segments and full FRP replacement, such as shown in Figure 1-11 - Mitigation strategy - thermally improved postFigure 1-11.

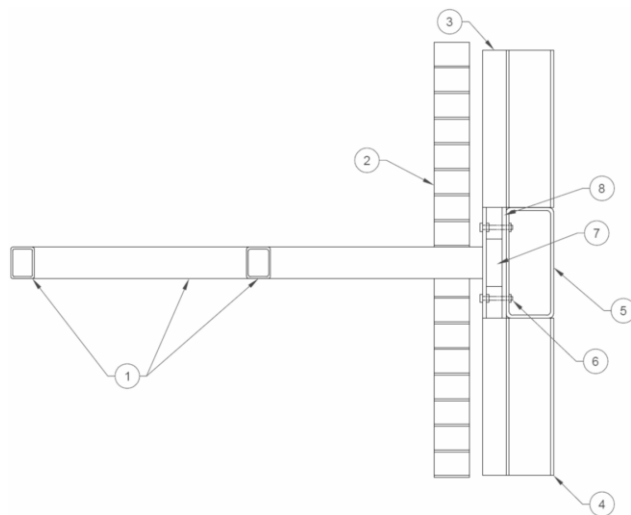


ITEM	DESCRIPTION
1	W Beam – W14x30
2	FRP square tube, 4x4x1/2
3	Polyisocyanurate Insulation – 3.5” (Zone 1), 6” (Zone 7)
4	1/8” Steel
5	W Beam – W14x34
6	6” x 7 1/2” x 3/4” FRP Plate 1/2” Dia. Bolt (Typ.)

Figure 1-11 - Mitigation strategy - thermally improved post

1.3.4 Canopy beam prototype structure – manufactured structural thermal break assembly (MSTBA) solutions

MSTBA solutions are available that can be used in the design of cantilevered members such as those used to support a balcony (an example is shown in Figure 1-12). These solutions often involve forces substantially larger than those considered in this study.

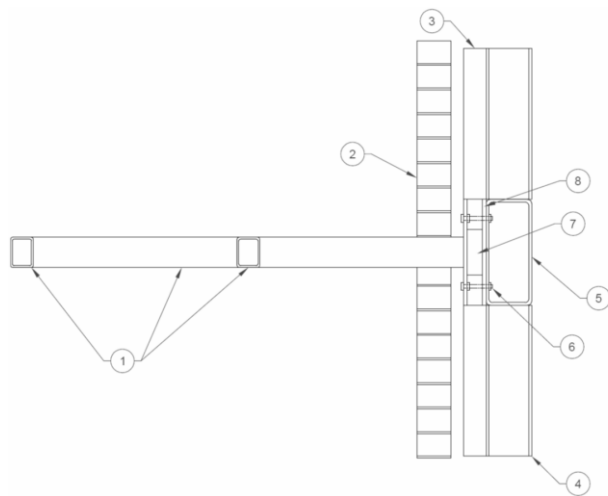


ITEM	DESCRIPTION
1	HSS Cantilevered Beam
2	Brick Veneer
3	Mineral Wool Insulation – 1.5” (Z1), 3.5” (Z7)
4	6” Cold-Formed Steel Studs with 3.5” fiberglass batt insulation
5	HSS 14x6x3/8
6	M22 bolt
7	Thermally Improved Shim – FRP or Stainless Steel
8	180 mm x 80 mm plate

Figure 1-12 - Mitigation Strategy - MSTBA Solution

1.3.5 Horizontal Beam Prototype Structure – Substitution with FRP Structural Members

Options for using FRP structural members as cantilevers are being considered to evaluate their effectiveness as a thermal break strategy.

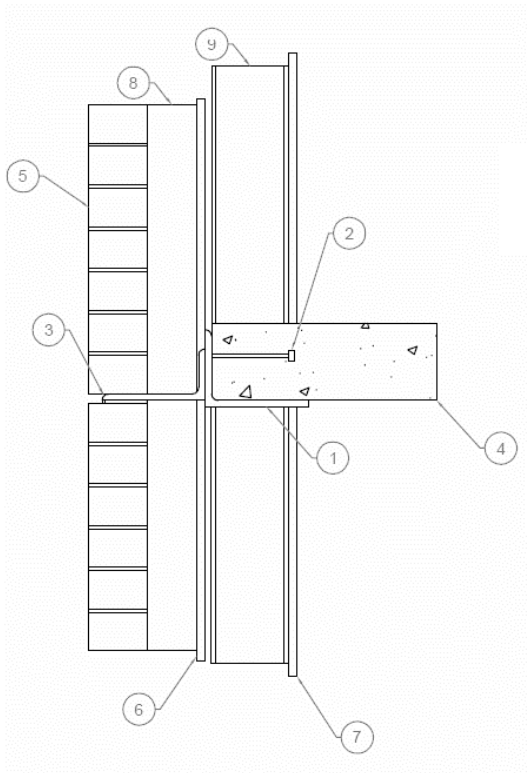


ITEM	DESCRIPTION
1	FRP Cantilevered Beam – 4x4x1/2
2	Brick Veneer
3	Mineral Wool Insulation – 1.5” (Z1), 3.5” (Z7)
4	6” Cold-Formed Steel Studs with 3.5” fiberglass batt insulation
5	HSS 14x6x3/8
6	3/4” Bolt (Typ.)
7	Thermally Improved Shim – FRP or Stainless Steel
8	1/2” Thick Steel Plate (Typ.)

Figure 1-13 - Mitigation Strategy - Substitution with FRP

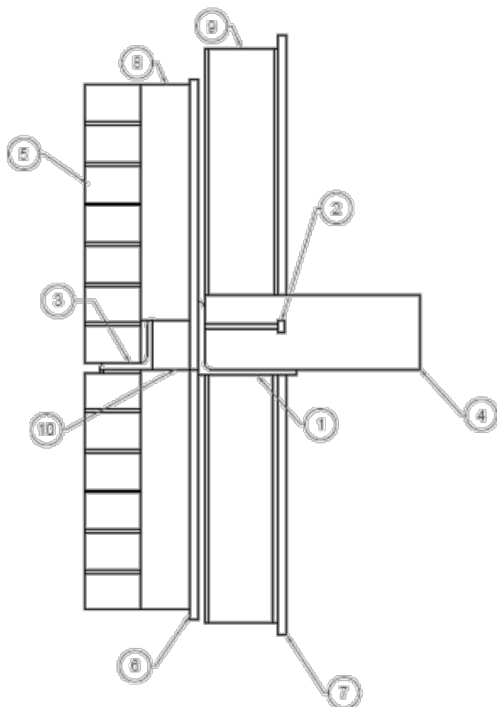
1.3.6 Slab-supported shelf angle

Slab-supported shelf angle thermal bridges may be mitigated by thermally-improved shims, FRP shelf angles, or stainless steel elements. Shim sizes are 3” wide by the length of the shelf angle vertical leg (in the case of the study, 4”), with a through-bolt located at the center of the vertical leg and shim. Stainless steel elements may require welding to carbon steel in some configurations, which requires special welding procedures. Also, any moisture condensing from a dew point condition may create galvanic corrosion between the dissimilar metals. Engineers implementing this type of strategy should consider these issues. The unmitigated and mitigated configurations are shown in Figure 1-14 and Figure 1-15 below.



ITEM	DESCRIPTION
1	3/8" Bent Plate (6x14)
2	5/8" Dia. Stud @ 30" O.C.
3	Shelf Angle - L6x4x5/16, L7x4x3/8
4	6" Concrete Slab
5	Brick Veneer
6	5/8" Sheathing
7	5/8" Gypsum Board
8	Mineral Wool Insulation: 1.5" (Z1), 3.5" (Z7)
9	6" Cold-Formed Steel Studs with 3.5" fiberglass batt insulation

Figure 1-14 - Unmitigated Detail



ITEM	DESCRIPTION
1	3/8" Bent Plate (6x14)
2	5/8" Dia. Stud @ 30" O.C.
3	Shelf Angle - L6x4x5/16, L7x4x3/8
4	6" Concrete Slab
5	Brick Veneer
6	5/8" Sheathing
7	5/8" Gypsum Board
8	Mineral Wool Insulation: 1.5" (Z1), 3.5" (Z7)
9	6" Cold-Formed Steel Studs with 3.5" fiberglass batt insulation
10	Stainless Steel WT4x20 @ 24" O.C.

Figure 1-15 - Mitigation Strategy - Stainless Steel WT Section

Pultruded FRP sections are available in polyester resins and vinylester resins (phenolic resins, also explored in this work, are not typically pultruded into shapes, and are limited to plate). Pultruded sections are not isotropic; the material properties change for loading along the orientation of the fibers or perpendicular to them. Furthermore, “off-the-shelf” pultruded FRP sections are limited in section sizes. When designing FRP shelf angles for the same loading as steel shelf angles, the required sections are thicker than those currently being pultruded. One alternative is to adhere FRP plate stiffeners to the section to increase the thickness using Pliogrip™ adhesive, as illustrated in Figure 1-16.

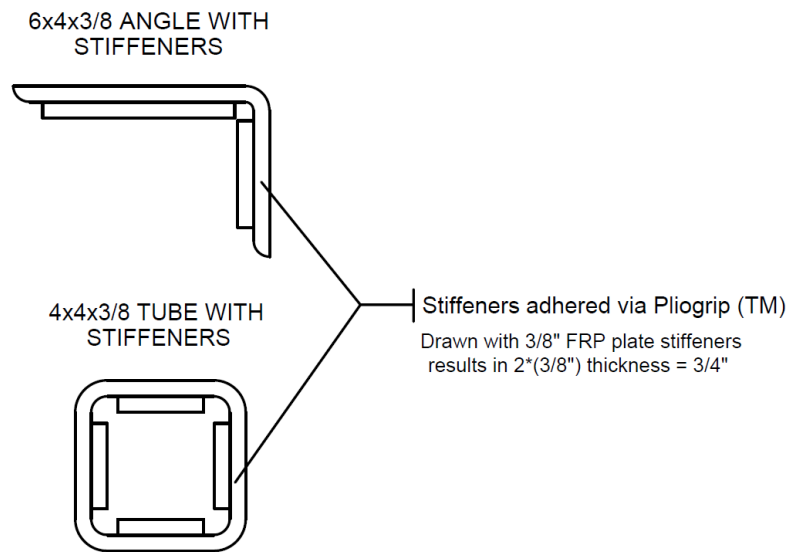
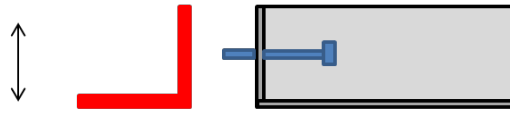


Figure 1-16: Illustration of plate stiffeners of angle and tube sections

Hypothetically, FRP plate stiffeners may also be replaced with steel plates using the same Pliogrip™ adhesive. While this approach is more costly, it provides a compromise between thermal properties and strength. FRP pultruded sections, however, cannot be welded to steel, and must be bolted with structural steel bolts. While steel shelf angles are often installed with bolts in slotted holes, they typically depend on field welds for strength. Despite the promise of custom stiffened FRP structural shapes, this study is limited to available pultruded shapes.

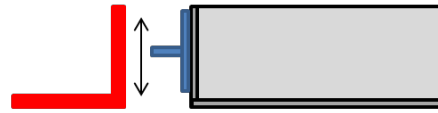
Adjustability in the field must be considered when using FRP members: since the common approach of using slotted holes may not be utilized parallel to the load, adjustability must be attained through a different method. Figure 1-17 shows the proposed solution to this challenge: the adjustment plate. A stainless steel (or carbon steel) plate with a pre-welded threaded stud is welded in the field using procedures specific to stainless-to-carbon steel welding. A shelf angle with standard round holes may then be placed accurately on the adjustment plates.

Original detail:



Angle height is adjustable due to long slotted holes

Proposed detail:



*Additional plate with stud pre-welded can be field-adjusted on slab
Shelf angle has standard holes*

Figure 1-17: Original slotted hole adjustment detail and proposed adjustment plate detail.

The adjustment plate detail also facilitates the use of various thermally improved shims, as discussed in the shelf angle chapter of this report. Alternatively, slab embeds with vertical adjustment can achieve a comparable structural integrity while maintaining field adjustability.

The following details are analyzed computationally for thermal viability and tested experimentally for structural viability. These details include using thermally improved members such as FRP or stainless tube as a bridge between the relieving angle and the slab, a large FRP shim, and an FRP angle. The concept behind FRP and stainless tube shims is illustrated in Figure 1-18.

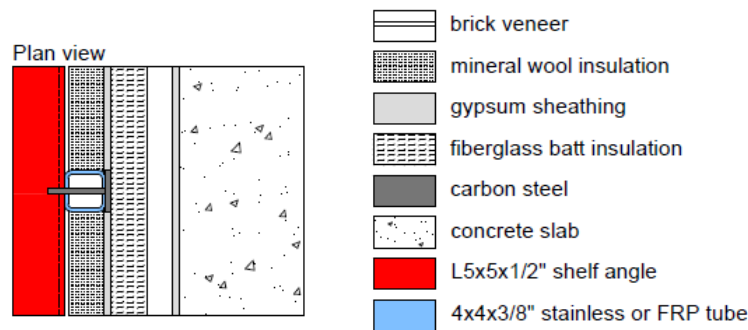
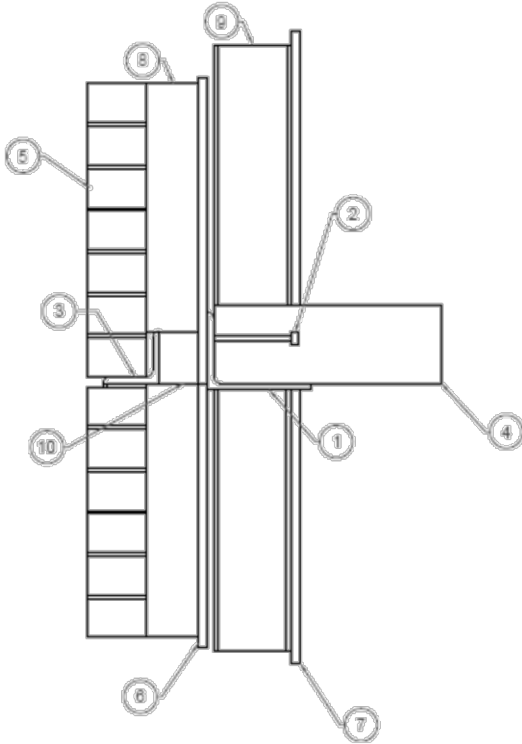
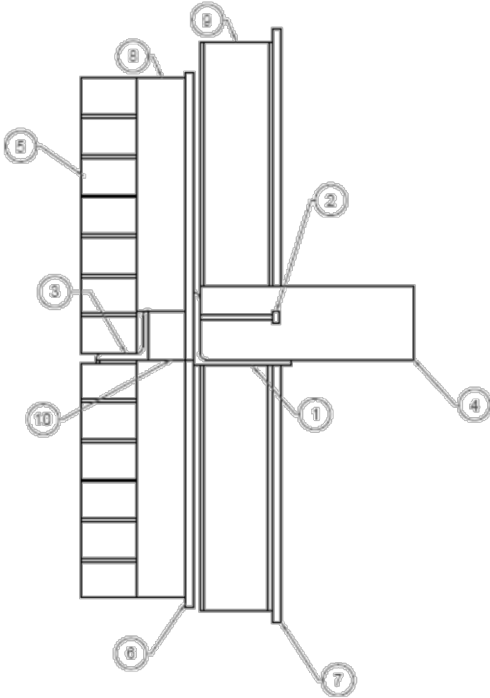


Figure 1-18 - Tube shim mitigation illustration, in elevation and plan views



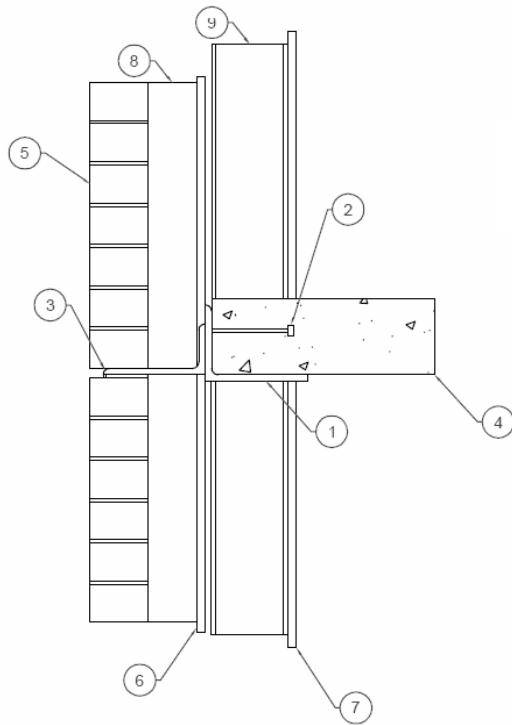
ITEM NO.	DESCRIPTION
1	3/8" Bent Plate (6x14)
2	1/2" Dia. Stud @ 36" O.C.
3	Shelf Angle – L6x4x5/16, L7x4x3/8
4	6" Concrete Slab
5	Brick Veneer
6	5/8" Sheathing
7	5/8" Gypsum Board
8	Mineral wool insulation
9	Cold-Formed Steel Studs with 3.5" fiberglass batt insulation
10	FRP or stainless tube

Figure 1-19 - Mitigation Strategy 1 - Thermally Improved Connecting Element



ITEM NO.	DESCRIPTION
1	L8x6x1/2,
2	1/2" Dia. Stud @ 24" O.C.
3	Shelf Angle – L6x4x5/16, L7x4x3/8
4	6" Concrete Slab
5	Brick Veneer
6	5/8" Sheathing
7	5/8" Gypsum Board
8	Mineral Wool Insulation – 1.5" (Z1), 3.5" (Z7)
9	Cold-Formed Steel Studs with 3.5" fiberglass batt insulation
10	Thermally Improved Shim – 1", 2", 3" FRP or Stainless Steel

Figure 1-20 - Mitigation Strategy - Thermally Improved Shim



ITEM NO.	DESCRIPTION
1	L8x6x1/2
2	1/2" Dia. Stud @ 24" O.C.
3	FRP Relieving Angle – L6x4x1
4	6" Concrete Slab
5	Brick Veneer
6	5/8" Sheathing
7	5/8" Gypsum Board
8	Mineral Wool Insulation – 1.5" (Z1), 3.5" (Z7)
9	Cold-Formed Steel Studs with 3.5" fiberglass batt insulation

Figure 1-21 - Mitigation Strategy 3 - FRP Reliving Angle

Throughout this work, several types of FRP material are used. These include vinylester, polyurethane, and phenolic materials. In addition, two proprietary FRP materials were used, designated in this report as Proprietary 1 and Proprietary 2. Their thermal and mechanical properties are listed for comparison along with the other FRP materials.

1.4 Organization of the Report

Chapter 2 of this report details prior research in thermal break strategies and thermal modeling. New thermal break mitigation strategies are analyzed thermally in Chapter 3 to discern the most successful solutions and form recommendations based upon heat transfer results. Chapter 4 contains a formulation of a new testing protocol for the creep response of FRP materials under prolonged loading in flatwise compression (shims under creep loads) and presents results and design recommendations. The experimental performance of double lap splice connections with varying FRP fills is explored in Chapter 5. Chapter 6 examines the performance of unmitigated and mitigated shelf angles. Chapter 7 examines the performance of unmitigated and mitigated roof posts and canopy beams. Chapter 8 provides conclusions for this research as well as recommendations for future research.

2 Background

2.1 Overview

This section provides a brief summary of recent research on thermal bridging of steel structures. Work done by Strachan et al. (1995) presents an overview of the EUROKOBRA thermal bridge database, which provides guidance on thermal bridging effects for many common 2D thermal bridges. Griffith et al. (1997) examined the significance of bolts in the thermal performance of curtain-wall frames and found that steel bolts can reduce thermal resistance when used at close intervals. Kosny et al. (1998) reported that small changes in detail configuration can bring significant improvements in structure performance. Anzi (1999) detailed the methodology of assessing thermal bridging for slab-on-grade floor foundations and shows the capacity of clear wall resistances to affect local transmittance. Dowson et al. (2011) demonstrated the efficacy of using thermally resistant materials on local thermal breaks in glazed windows to reduce overall thermal transmittance. Morrison Hershfield (2008) produced a report examining multiple thermal bridging solutions in envelope systems. Schoeck (2015) sponsored a study of their own thermal bridging products. Totten and Pazera (2009) demonstrated that thermal bridging is the cause of condensation and related problems in steel structures. The Corus Group (2011) published findings on several thermal break strategies to be considered for use in steel structures. Huang (2012) examined the use of silica aerogel in the building insulation layer and found that a reduction in transmittance of up to 50% could be achieved. D'Aloisio et al. (2012) discussed various thermal bridging solutions in common structural details.

Of the literature mentioned, three reports published within the last five years stand out as the most relevant and comprehensive in scope. These reports are the 2008 Morrison Hershfield report, the 2011 Corus Group report, and D'Aloisio et al. (2012), as summarized below.

2.2 Morrison Hershfield (2008)

In 2008, Morrison Hershfield published a report detailing the results of their study on thermal break strategies in steel- and concrete-framed structures. The report examined 40 common building envelope details for mid- and high-rise structures to facilitate ease of access to design recommendations for designers while maintaining sufficient and accurate results. Three-dimensional thermal modeling for the project was conducted using FEMAP and Nx along with Maya's TMG thermal solver. Results were calibrated against public domain thermal performance data and validated by exercises in ISO standards with well-defined problems.

2.1.1 *Relieving Angle Models*

Details 14 and 15 present brick veneer assemblies at a slab intersection with insulation both between the steel studs and in the cavity behind the brick veneer. The difference between the two assemblies is that Detail 14 utilizes a relieving angle bolted directly to the concrete slab while Detail 15 utilizes steel knife plates to offset the angle with intermittent supports, allowing for the

cavity insulation to continue between the shelf angle and the slab edge with discontinuities only at the knife plates.

The shelf angle and slab edge increase the thermal transmittance in Detail 14 by between 37% and 70% compared to unbroken “clear wall” values, depending on existing cavity insulation transmittance. Detail 15 has a slightly lower effect due to the addition of the knife plates to support the shelf angle and the greater continuity of insulation, with thermal transmittance relative to the clear wall increased by 30% to 41% for the same insulation values as Detail 14. This represents a 5% to 17% decrease in linear thermal transmittance by using the knife plate detail.

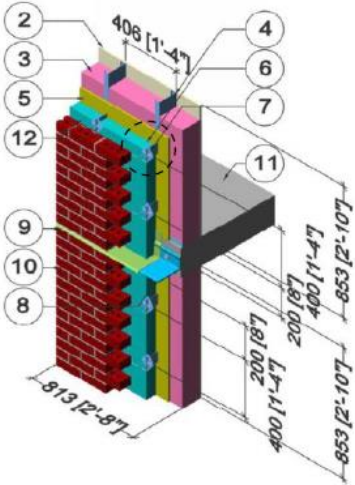


Figure 2-1: Detail 14 Overview (Morrison Hershfield 2008)

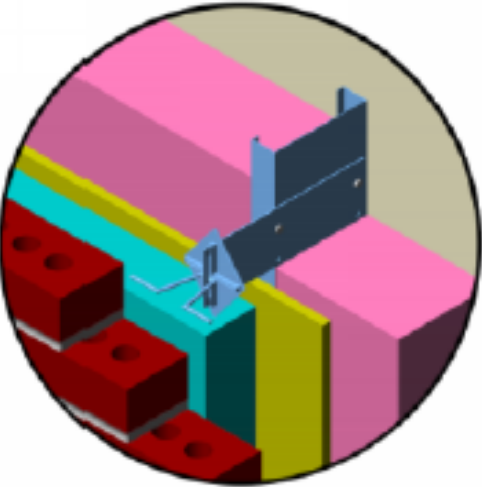


Figure 2-2: Detail 14 Veneer Tie-Back (Morrison Hershfield 2008)

Table 2-1: Component List for Detail 14 (Morrison Hershfield 2008)

ID	Component	Thickness Inches (mm)	Conductivity Btu-in / ft ² -hr-°F (W/m K)	Nominal Resistance hr-ft ² -°F/Btu (m ² K/W)	Density lb/ft ³ (kg/m ³)	Specific Heat Btu/lb-°F (J/kg K)
1	Interior Film (right side) ¹	-	-	R-0.6 (0.11 RSI) to R-0.9 (0.16 RSI)	-	-
2	Gypsum Board	1/2" (13)	1.1 (0.16)	R-0.5 (0.08 RSI)	50 (800)	0.26 (1090)
3	Fiberglass Batt Insulation in Stud Cavity	3 5/8" (92)	0.29 (0.042)	R-12 (2.1 RSI)	0.9 (14)	0.17 (710)
4	3 5/8" x 1 5/8" Steel Studs with Top and Bottom Tracks	18 gauge	430 (62)	-	489 (7830)	0.12 (500)
5	Exterior Sheathing	1/2" (13)	1.1 (0.16)	R-0.5 (0.08 RSI)	50 (800)	0.26 (1090)
6	Exterior Insulation	Varies	-	R5 to R25 (0.88 to 4.4 RSI)	1.8 (28)	0.29 (1220)
7	Brick Ties	14 gauge	347 (50)	-	489 (7830)	0.12 (500)
8	Shelf Angle	3/8" (10)	347 (50)	-	489 (7830)	0.12 (500)
9	Flashing	20 gauge	347 (50)	-	489 (7830)	0.12 (500)
10	Brick Veneer	3 5/8" (92)	5.4 (0.78)	-	120 (1920)	0.19 (720)
11	Concrete Slab	8" (203)	12.5 (1.8)	-	140 (2250)	0.20 (850)
12	Air Gap	1" (25)	-	R-0.9 (0.16 RSI)	0.075 (1.2)	0.24 (1000)
13	Exterior Film (left side) ¹	-	-	R-0.2 (0.03 RSI)	-	-

¹ Value selected from table 1, p. 26.1 of 2009 ASHRAE Handbook – Fundamentals depending on surface orientation

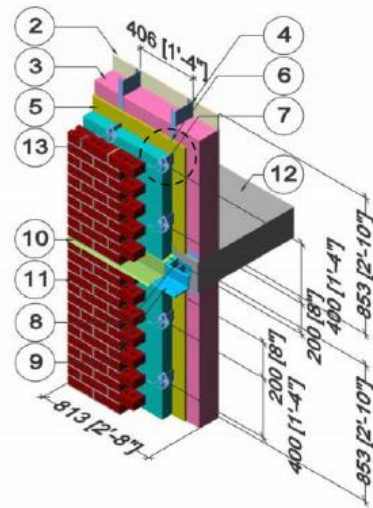


Figure 2-3: Detail 15 Overview (Morrison Hershfield 2008)

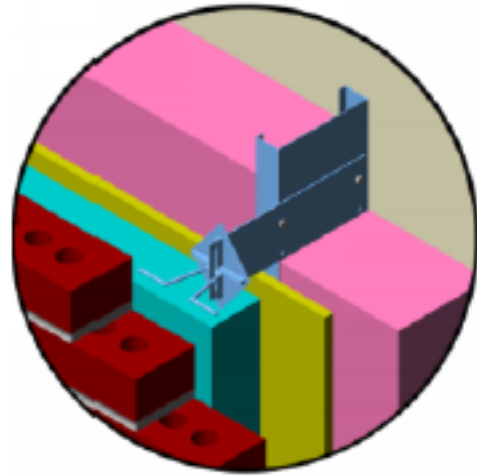


Figure 2-4: Detail 15 Veneer Tie-Back (Morrison Hershfield 2008)

Table 2-2: Component List for Detail 15(Morrison Hershfield 2008)

ID	Component	Thickness Inches (mm)	Conductivity Btu-in / ft ² -hr.°F (W/m K)	Nominal Resistance hr-ft ² -°F/Btu (m ² K/W)	Density lb/ft ³ (kg/m ³)	Specific Heat Btu/lb-°F (J/kg K)
1	Interior Film (right side) ¹	-	-	R-0.6 (0.11 RSI) to R-0.9 (0.16 RSI)	-	-
2	Gypsum Board	1/2" (13)	1.1 (0.16)	R-0.5 (0.08 RSI)	50 (800)	0.26 (1090)
3	Fiberglass Batt Insulation in Stud Cavity	3 5/8" (92)	0.29 (0.042)	R-12 (2.1 RSI)	0.9 (14)	0.17 (710)
4	3 5/8" x 1 5/8" Steel Studs with Top and Bottom Tracks	18 gauge	430 (62)	-	489 (7830)	0.12 (500)
5	Exterior Sheathing	1/2" (13)	1.1 (0.16)	R-0.5 (0.08 RSI)	50 (800)	0.26 (1090)
6	Exterior Insulation	Varies	-	R5 to R25 (0.88 to 4.4 RSI)	1.8 (28)	0.29 (1220)
7	Brick Ties	14 gauge	347 (50)	-	489 (7830)	0.12 (500)
8	Exterior Insulation Behind Shelf Angle	varies	-	R5 to R25 (0.88 to 4.4 RSI)	1.8 (28)	0.29 (1220)
9	Spaced Shelf Angle	3/8" (10)	347 (50)	-	489 (7830)	0.12 (500)
10	Flashing	20 gauge	347 (50)	-	489 (7830)	0.12 (500)
11	Brick Veneer	3 5/8" (92)	5.4 (0.78)	-	120 (1920)	0.19 (720)
12	Concrete Slab	8" (203)	12.5 (1.8)	-	140 (2250)	0.20 (850)
13	Air Gap	1" (25)	-	R-0.9 (0.16 RSI)	0.075 (1.2)	0.24 (1000)
14	Exterior Film (left side) ¹	-	-	R-0.2 (0.03 RSI)	-	-

¹ Value selected from table 1, p. 26.1 of 2009 ASHRAE Handbook – Fundamentals depending on surface orientation

2.1.2 Cantilever Beam Model

Detail 12 is a cold-formed steel stud and horizontal Z-girt assembly with split insulation for the case where a steel beam protrudes through the exterior insulation and is attached to a steel post located within the stud cavity. Given a wall assembly, a single beam penetration increases thermal transmittance by 9% and three beam penetrations increase transmittance by 25%.

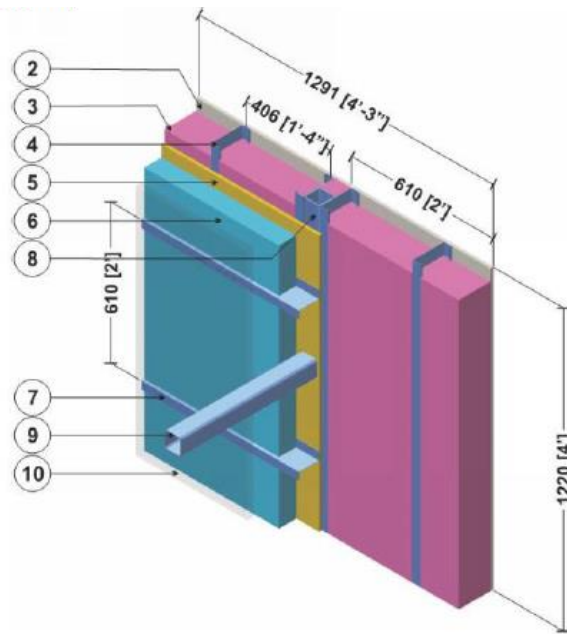


Figure 2-5: Morrison Hershfield Detail 12 Overview (Morrison Hershfield 2008)

Table 2-3: Component List for Detail 12(Morrison Hershfield 2008)

ID	Component	Thickness Inches (mm)	Conductivity Btu-in / ft ² -hr-°F (W/m K)	Nominal Resistance hr-ft ² -°F/Btu (m ² K/W)	Density lb/ft ³ (kg/m ³)	Specific Heat Btu/lb-°F (J/kg K)
1	Interior Film (right side) ¹	-	-	R-0.7 (0.12 RSI)	-	-
2	Gypsum Board	1/2" (13)	1.1 (0.16)	R-0.5 (0.08 RSI)	50 (800)	0.26 (1090)
3	Fiberglass Batt Insulation in Stud Cavity	3 5/8" (92)	0.29 (0.042)	R-12 (2.1 RSI)	0.9 (14)	0.17 (710)
4	3 5/8" x 1 5/8" Steel Studs	18 gauge	430 (62)	-	489 (7830)	0.12 (500)
5	Exterior Sheathing	1/2" (13)	1.1 (0.16)	R-0.5 (0.08 RSI)	50 (800)	0.26 (1090)
6	Exterior Insulation	Varies	-	R5 to R25 (0.88 to 4.4 RSI)	1.8 (28)	0.29 (1220)
7	Horizontal Z-girts w/ 1 1/2" Flange	18 gauge	430 (62)	-	489 (7830)	0.12 (500)
8	Steel Post (HSS 76x76x3.2)	1/8" (3.2)	347 (50)	-	489 (7830)	0.12 (500)
9	Steel Beam (HSS 76x76x3.2)	1/8" (3.2)	347 (50)	-	489 (7830)	0.12 (500)
10	Metal cladding with 1/2" (13mm) vented air space is incorporated into exterior heat transfer coefficient					
11	Exterior Film (left side) ¹	-	-	R-0.2 (0.03 RSI) to R-0.7 (0.12 RSI)	-	-

¹ Value selected from table 1, p. 26.1 of 2009 ASHRAE Handbook – Fundamentals depending on surface orientation

2.3 The Corus Group (2011)

The Corus Group, a United Kingdom based consulting firm, released a document presenting an overview of some results in thermal transmittance due to bridging in steel structures. The report examined different methods of utilizing thermal breaks in framing systems. Details of beams penetrating insulated building envelopes, balcony supports, and brick veneer support systems are included. The Corus Group made use of SAP (Standard Assessment Procedure) 2005 and SBEM

(Simplified Building Energy Model) in calculating energy performance and linear thermal transmittance of assemblies.

2.1.3 Local Insulation

In assemblies where a steel member protrudes through the insulated building envelope, local insulation may be used around the element in order to lengthen the heat flow path, reducing heat transfer. Utilizing this method, internal surface temperatures of the beam were increased from 50.8% to 55.2% that of internal air temperature assuming a freezing temperature externally.

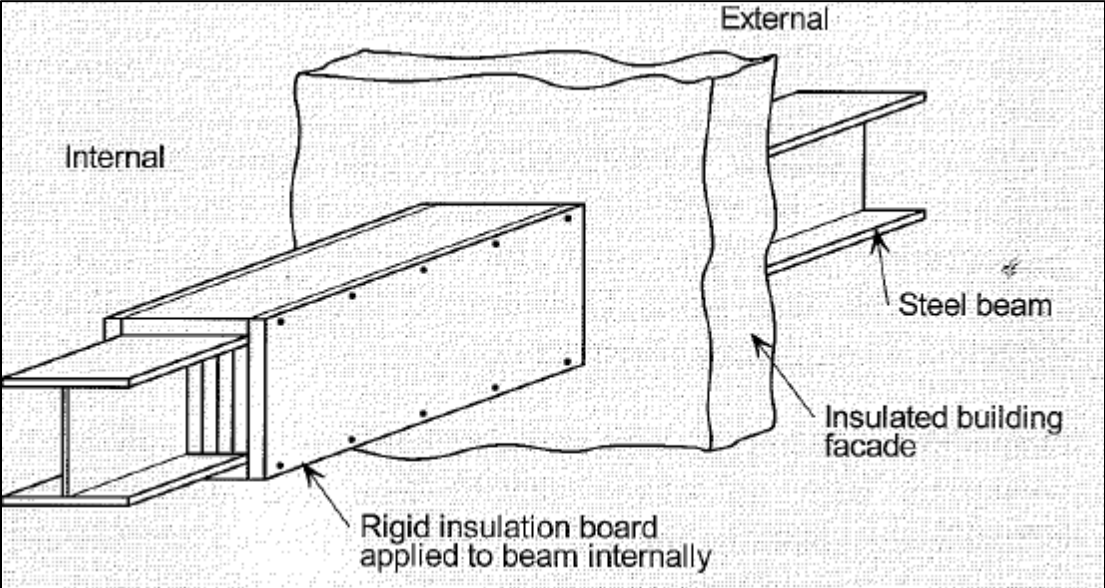


Figure 2-6: Locally Insulated Beam (Corus Group 2011)

2.1.4 Slotted Steel Sections

In assemblies where the heat flow path travels through the web of a slotted channel member, such as in studs, introducing lines of overlapping horizontal lines of slots can increase the thermal resistance of the section by up to a factor of 10. This can result in a loss of some structural integrity, reducing the compressive and flexural strength of the walls by up to 30%.

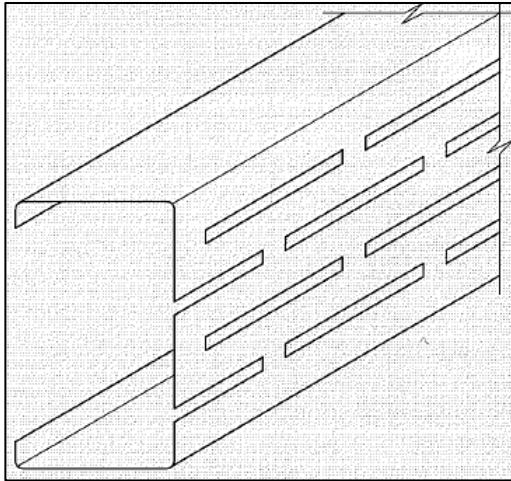


Figure 2-7: Channel Section with Slotted Web
(Corus Group 2011)

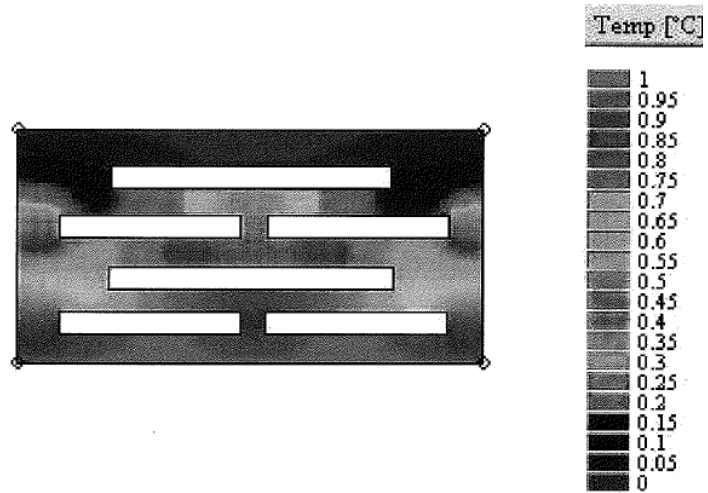


Figure 2-8: Temperature Gradient of a Slotted Channel Section
(Corus Group 2011)

2.1.5 Lower Conductivity Connections

Thermal transmittance in steel framing can be reduced by replacing some steel components with materials that have a lower thermal conductivity. Examples include stainless steel bolts and screws which have a thermal resistance approximately 3 times that of structural carbon steel. However, utilizing stainless steel or other more thermally resistant materials increases the risk of bi-metallic corrosion, though this can be neglected if moisture is not present or if the amount of the more noble metal is significantly lower than that of the less noble metal.

2.1.6 Proprietary Solutions

The Corus Group also examined a proprietary solution to thermal steel bridging, the Schöck Isokorb. In an example model analyzed via a steady state thermal conduction analysis program, the Schöck Isokorb system reduced heat loss due to thermal bridging up to 57% compared to an unmitigated system.

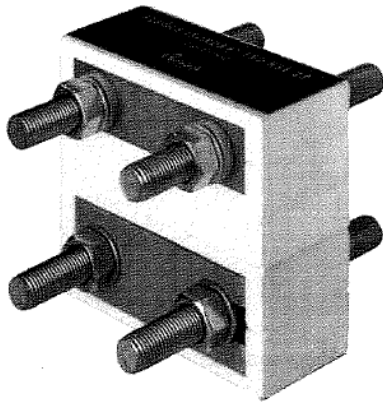


Figure 2-9: Schöck Isokorb Thermal Break (Corus Group 2011)

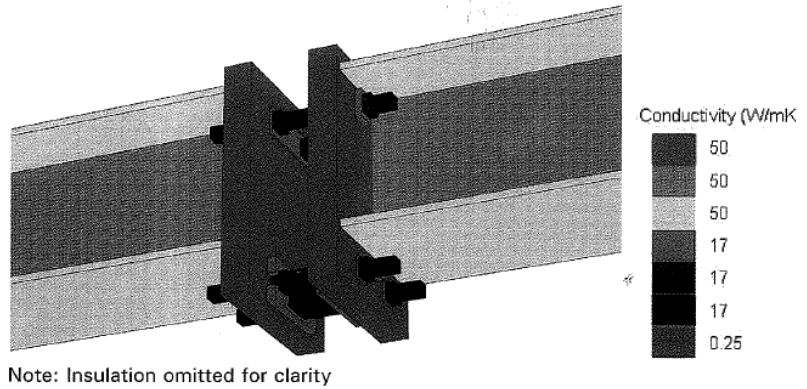


Figure 2-10: Thermal Model (Corus Group 2011)

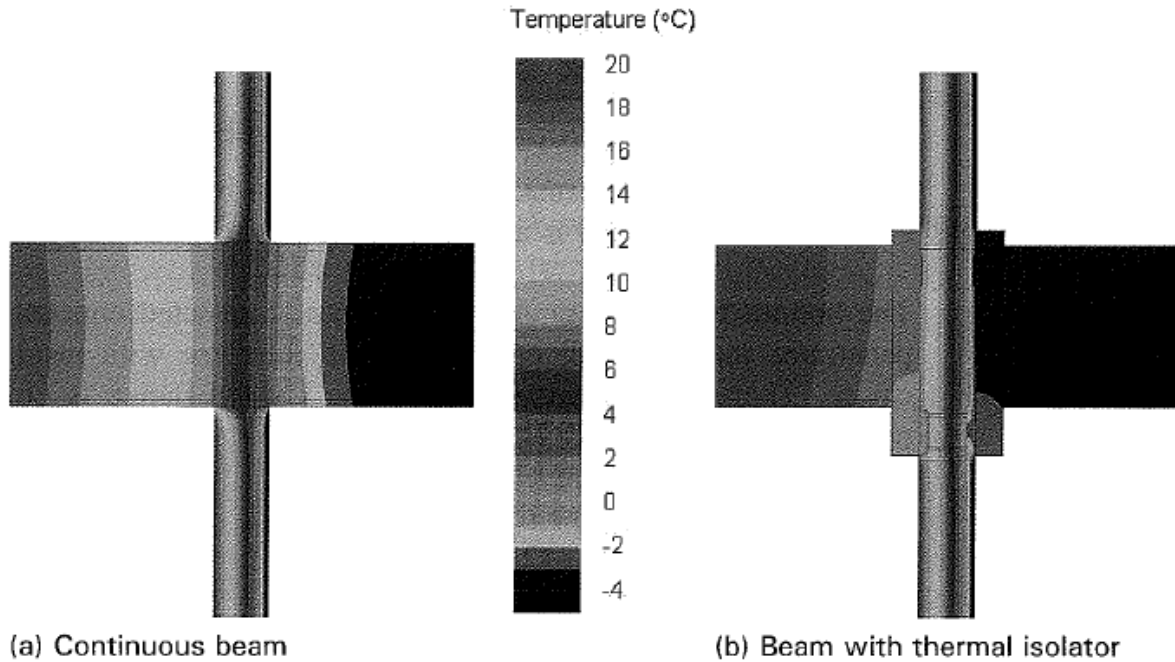


Figure 2-11: Temperature Gradients Resulting from the Model (Corus Group 2011)

2.4 Schoeck Ltd Thermal Bridging Report (2015)

Schoeck Ltd., in a collaborative effort with Oxford Brookes University, published a guide to thermal bridging utilizing their product, the Schoeck Isokorb, in a series of thermal models. This report was published in 2015.

The report begins with a review of thermal bridges, and specifically highlights the difference between linear thermal bridges, in which thermal transmittance occurs constantly along the length

of the thermal bridge, and point thermal bridges, where thermal transmittance is localized, and often lessened. Figure 2-12 and Figure 2-13 demonstrate these differences. While the continuous support does continue to transmit energy in the point thermal bridge example, significant transfer only occurs at the protrusions into the slab.

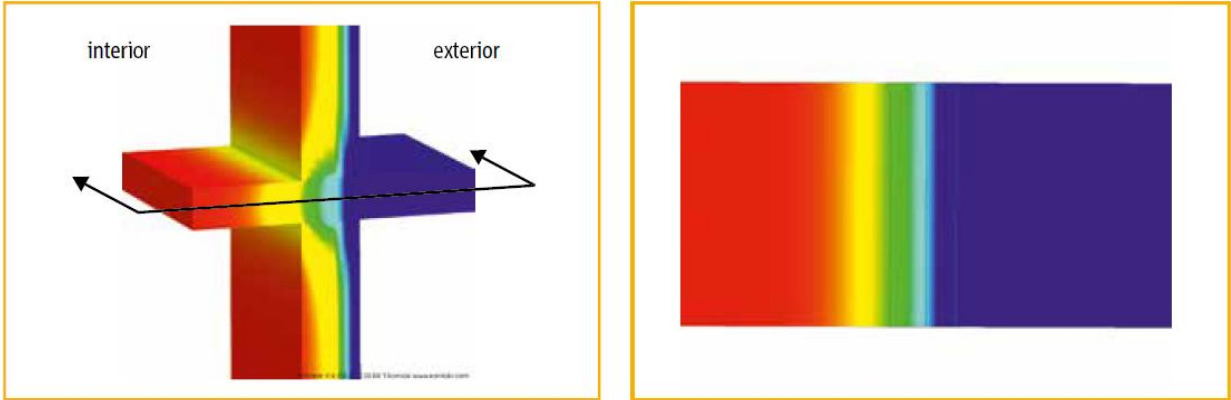


Figure 2-12: Linear thermal bridge in a balcony connection (Schoeck Ltd 2015)

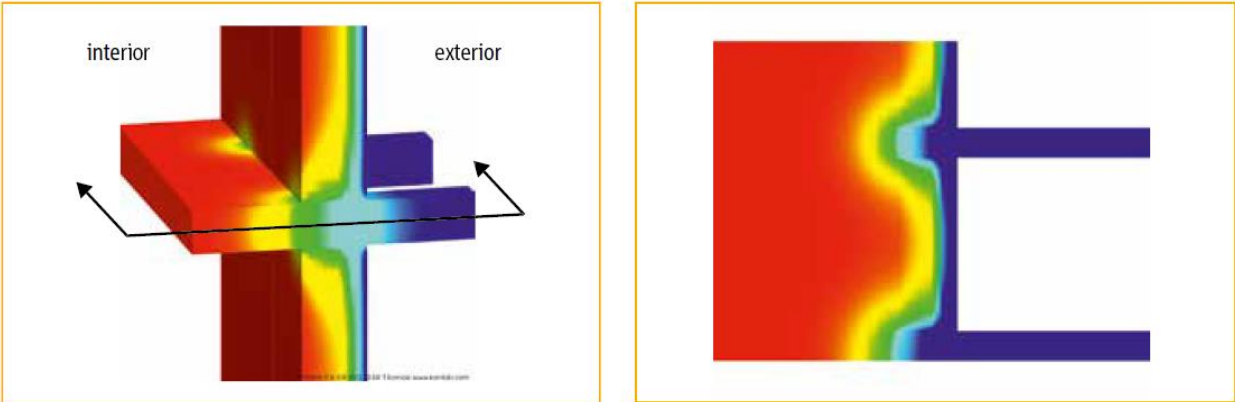


Figure 2-13: Point thermal bridge in a balcony connection (Schoeck Ltd 2015)

While the research report details several types of Schoeck thermal break products used for connections to concrete slabs, the focus of the Northeastern University work is on steel canopies and the Schoeck S22 Isokorb. Figure 2-14 depicts the S22 module installed in a steel canopy.

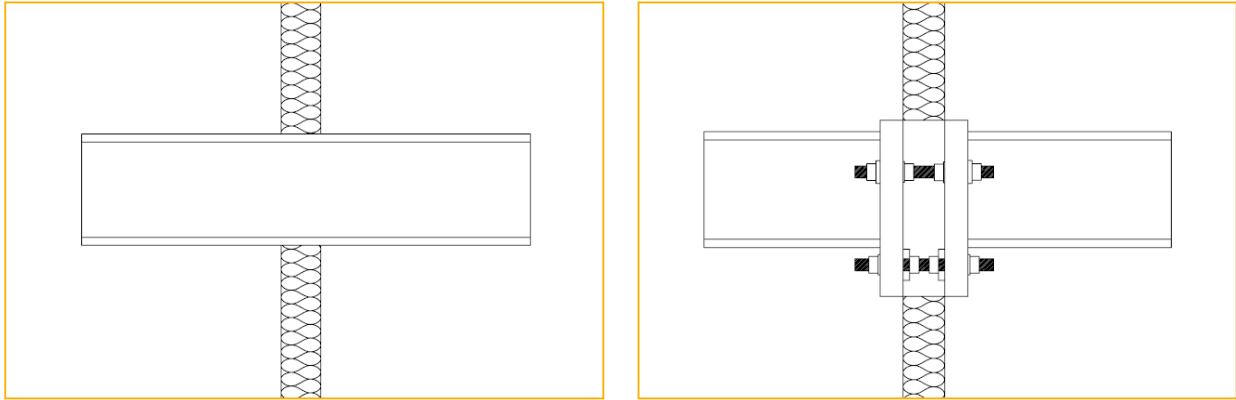


Figure 2-14: Schematic of Schoeck S22 thermal break installed in a steel canopy (Schoeck Ltd. 2015)
 Thermal modeling results for this configuration, compared to an unmitigated detail, are shown in Figure 2-15. The authors report a 66% improvement in point thermal transmission (from 0.77 W/K to 0.26 W/K) with the inclusion of the Isokorb module.

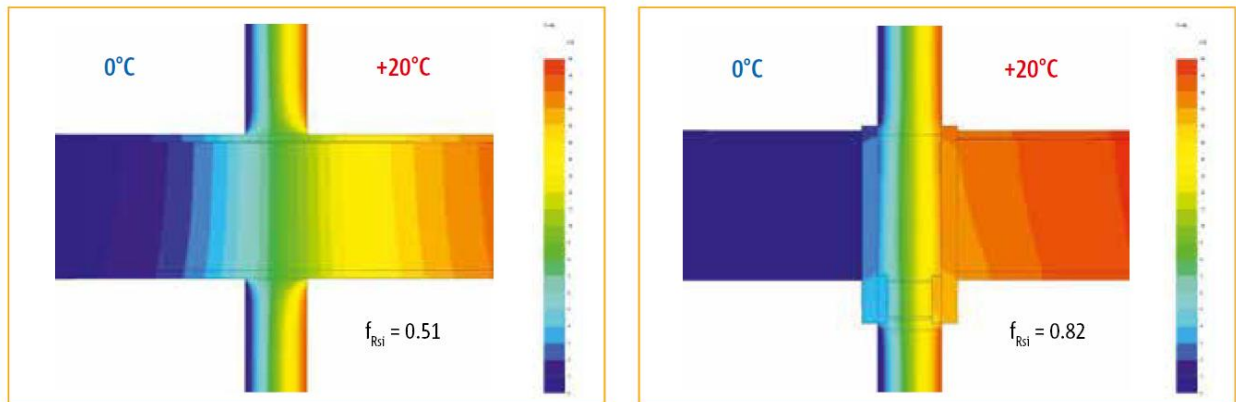


Figure 2-15: Thermal gradient results for continuous beam model (at left) and mitigated model with Schoeck Isokorb product (KST 16 is the European market version of the S22 module) (Schoeck 2015)

Table 2-4: Thermal modeling results for steel canopy detail. (Schoeck 2015)

	Minimum Surface Temperature °C	χ (W/K)	Minimum Temperature factor f_{Rsi}
Continuous Beam	5.7	0.77	0.51
With Isokorb® type KST 16	13.8	0.26	0.82

2.5 Modern Steel Construction Insert (2012)

The Structural Engineering Institute (SEI) Thermal Steel Bridging Task Committee in conjunction with the Sustainability Committee's Thermal Bridging Working Group published a supplement to AISC's *Modern Steel Construction* (MSC) magazine in March 2012. This article examines several

typical thermal bridges in steel-framed structures and presents potential solutions to these assemblies, complete with a limited study on the energy cost benefits and cost effectiveness of the mitigation schemes.

2.1.7 Roof Grillage Posts

The assembly presented in this section is representative of steel posts supporting mechanical rooftop units or other similar equipment such as photovoltaic arrays. The authors examined a 3.5” diameter Schedule 40 steel post assembly spaced at 6’ on center connected to the interior by a wide-flange steel beam and to the exterior assemblage by a continuous wide-flange steel grillage beam. The improved detail places a thermally resistant shim between the post and the interior wide-flange beam. Improvements in thermal transmittance range from 17% to 19% depending on climate, although the incremental costs may outweigh the potential savings, according to their calculations.

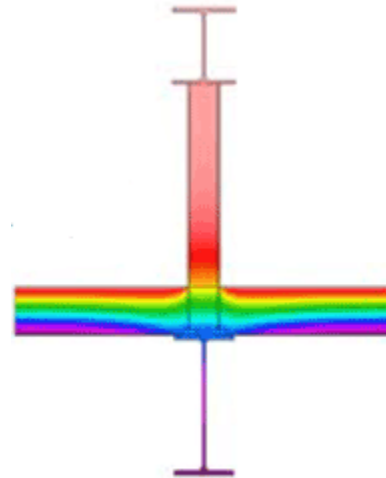
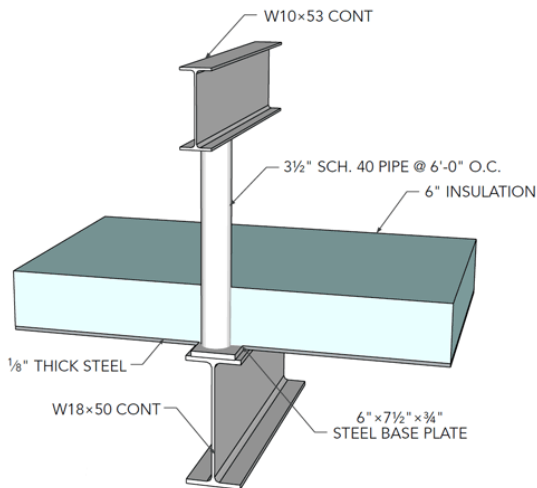


Figure 2-16: Unmitigated roof post (D'Aloisio, et al. 2012) Figure 2-17: Thermal gradient (D'Aloisio, et al. 2012)

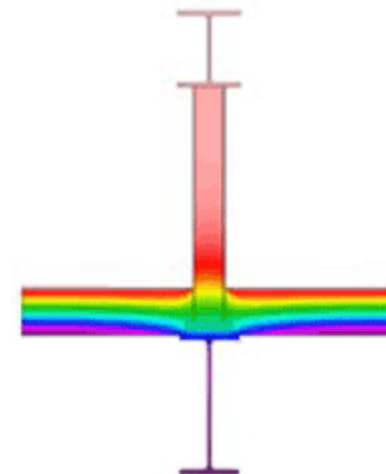
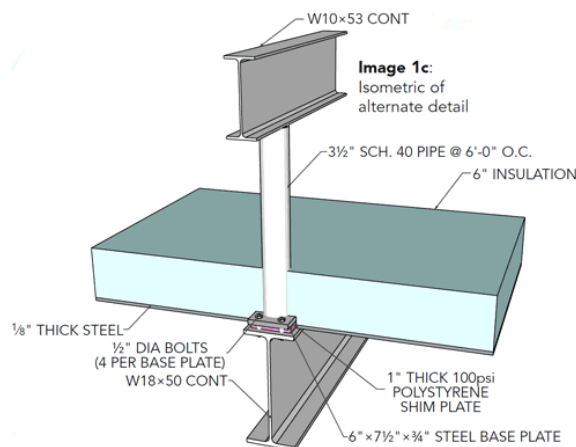


Figure 2-18: Mitigated roof post (D'Aloisio, et al. 2012)

Figure 2-19: Thermal gradient (D'Aloisio, et al. 2012)

2.1.8 Roof Edge Angle

The second section of the MSC supplement examines the intersection of roof and wall planes which contain continuous steel elements that extend between the interior and the exterior. The detail in question utilizes a continuous steel angle along the perimeter of the roof deck connected to another continuous angle that extends out through the roof and wall insulation intersection for the support of roof edge blocking. The alternative detail replaces the second angle with a 6" long angle spaced at 24" on center. The alternate detail improves thermal transmittance by 30% and reduces annual costs by a similar margin.

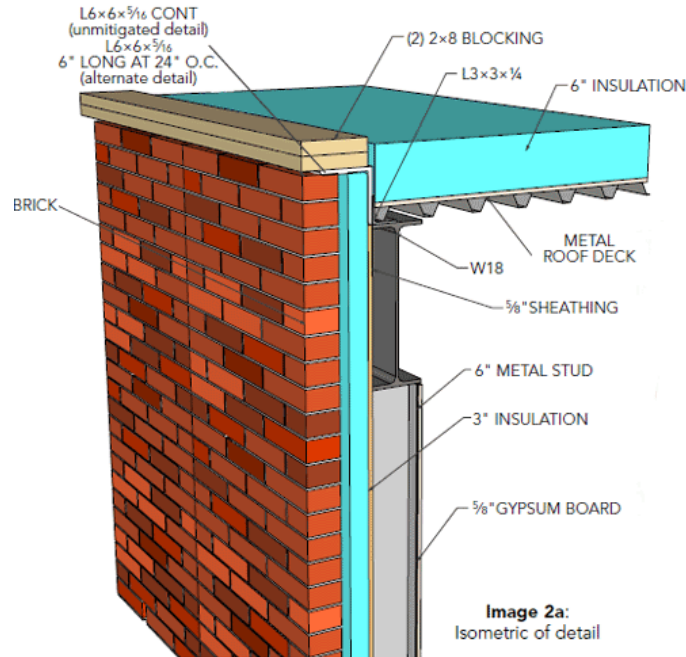


Figure 2-20: Roof Edge Angle, unmitigated (D'Aloisio, et al. 2012)

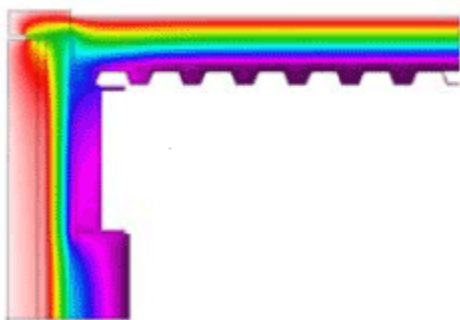


Figure 2-21: Unmitigated gradient (D'Aloisio, et al. 2012)

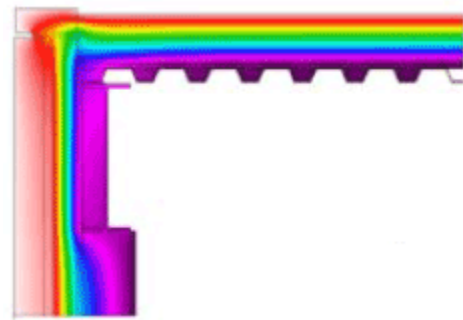


Figure 2-22: Mitigated gradient (D'Aloisio, et al. 2012)

2.1.9 Shelf Angle Support

This detail compares a conventional slab-supported carbon steel relieving angle to a mitigated version using stainless steel knife plates spaced at 24" on center. Stainless steel is approximately three times as thermally resistant as carbon structural steel. The mitigated detail moves the

relieving angle outside of the insulation plane, allowing for more continuous insulation between the relieving angle and slab edge. Thermal transmittance can be reduced up to 77% using this mitigation strategy, making it an ideal candidate for implementation due to its relatively low marginal cost and high savings yield.

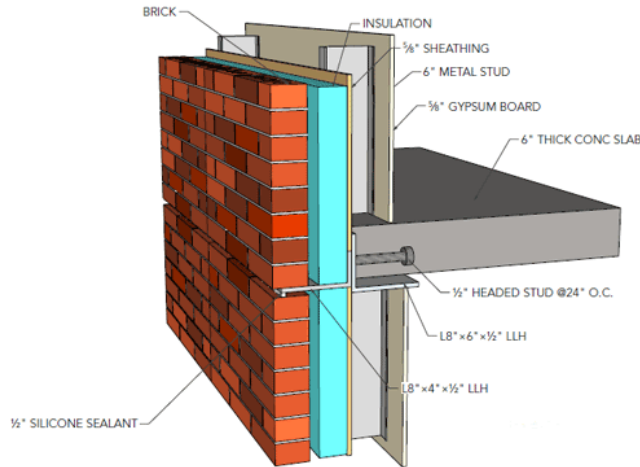


Figure 2-23: Shelf angle, Unmitigated (D'Aloisio, et al. 2012)

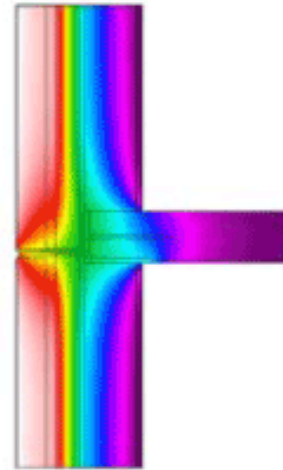


Figure 2-24: Thermal Gradient (D'Aloisio, et al. 2012)

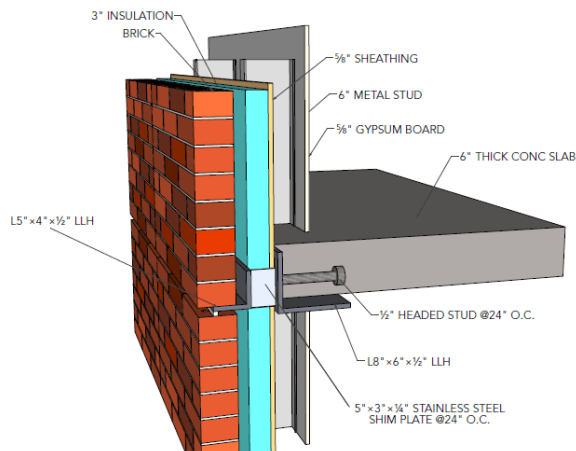


Figure 2-25: Shelf Angle, Mitigated (D'Aloisio, et al. 2012)



Figure 2-26: Thermal Gradient, Mitigated (D'Aloisio, et al. 2012)

2.1.10 Masonry Lintel

This detail is similar to the standard relieving angle support detail except that it is installed over a window opening in the façade. Steel in direct contact with the window frame reduces the effectiveness of any potential improved window design. The authors considered a detail with a 2x piece of wood to act as a thermal separator between interior and exterior steel members. This

modification results in a 26% reduction in thermal transmittance. Unlike the standard relieving angle detail, the potential annual savings do not outweigh the relatively large marginal cost of implementing this solution.

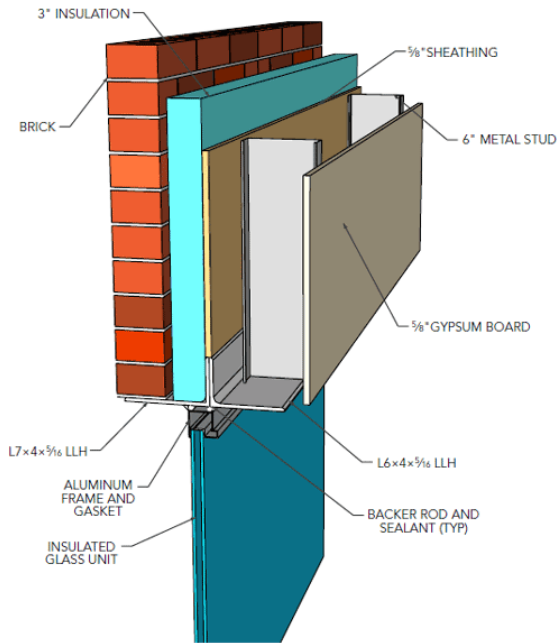


Figure 2-27: Masonry Lintel, Unmitigated (D'Aloisio, et al. 2012)

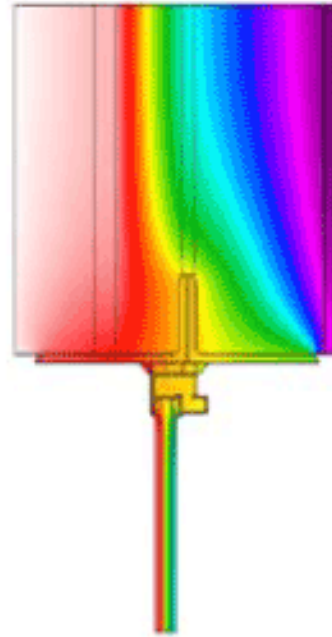


Figure 2-28: Thermal Gradient, Unmitigated (D'Aloisio, et al. 2012)

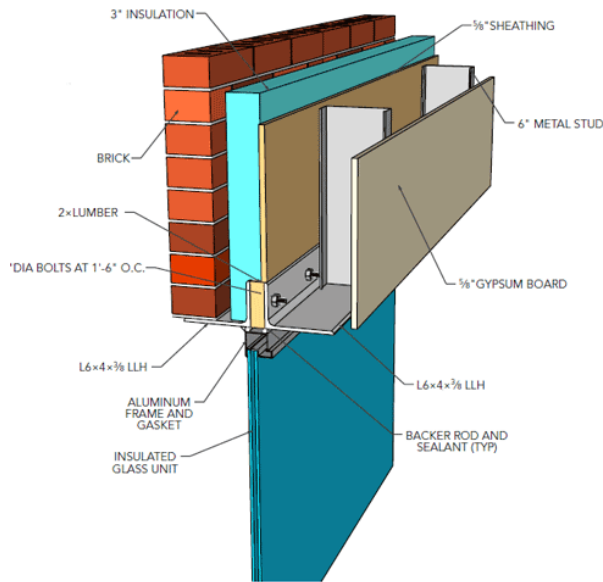


Figure 2-29: Masonry Lintel, Mitigated (D'Aloisio, et al. 2012)

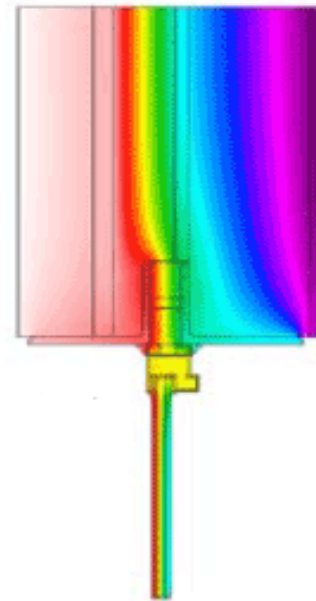


Figure 2-30: Thermal Gradient, Mitigated (D'Aloisio, et al. 2012)

2.1.11 Cantilever Roof Canopy Beam

Cantilever elements that extend out from the faces of buildings, while versatile in their use, create significant thermal bridges where they intersect the insulation plane. The authors examined a prefabricated Manufactured Structural Thermal Break Assembly (MSTBA) for its ability to mitigate thermal bridging created by this type of element. They found that thermal transmittance can be reduced up to 30%, though the annual cost savings are low compared to the relatively high marginal implementation cost, due to the localized nature of this thermal break.

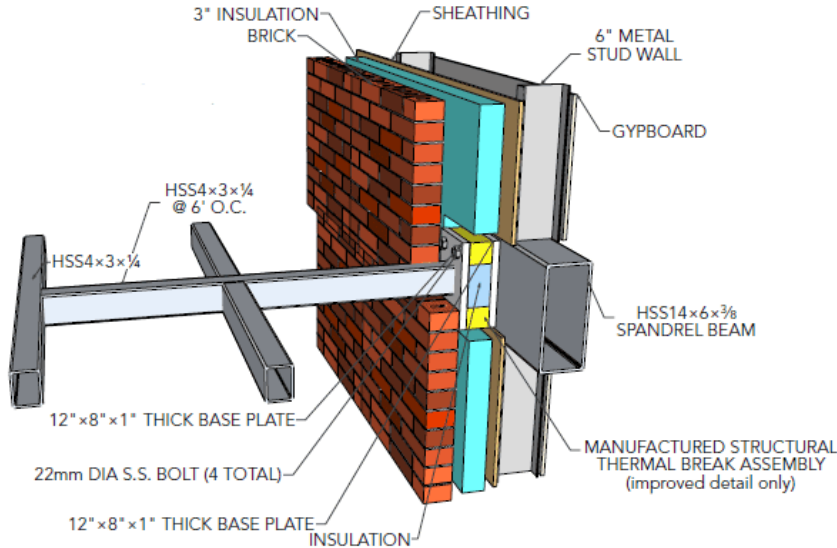


Figure 2-31: Cantilever Roof Canopy Beam, Unmitigated and Mitigated (D'Aloisio, et al. 2012)

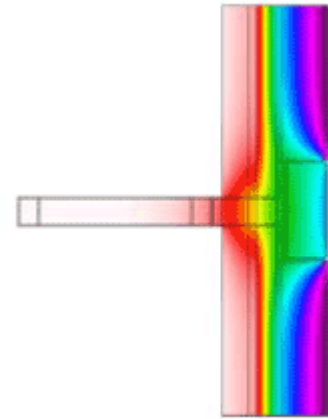


Figure 2-32: Thermal Gradient, Unmitigated (D'Aloisio, et al. 2012)

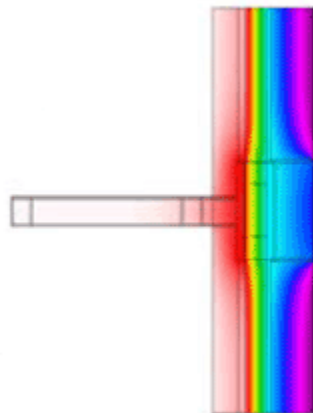


Figure 2-33: Thermal Gradient, Mitigated (D'Aloisio, et al. 2012)

2.6 Kemper Arena Collapse

The 1979 collapse of the Kemper Arena is frequently, but potentially incorrectly, attributed to a fiber reinforced polymer ¼” Micarta plate installed at the base of the connection to the hangers. The authors conducted a review of the available literature on the collapse, notably the official August 1979 report on the Kemper Arena Collapse by consulting engineer James Stratta (Stratta, 1979).

Stratta states that failure of the hanger was due to excessive loading (from a combination of wind, rain, and ponding, oscillations caused by loading, and aeroelastic flutter of the roof membrane), fatigue in the bolts, improper installation of the bolts, and the poor connection between base plate and truss top chord due to deformations in the base plate (induced by welding, measured to be 1/8” on each side of the base plate) and loose construction tolerances. Furthermore, the Stratta predicts that a total of 24,000 oscillations (rocking of the hanger) had occurred during the lifetime of the arena, prior to collapse. As the hanger bolts, A490 bolts, are not specified for unloading and reloading cycles, these oscillations are speculated to have weakened the bolts significantly. According to the report, including factors of safety, the bolts should have carried 600 kips+, and were designed for 210 kips (and, according to the report, rated for 320 kips). Note that according to Table J3.2 in AISC 360-10, the tensile strength of four 1-3/8” dia. A490 bolts is 670 kips. It is not known at what load the pipe hanger bolts failed, but tests at the University of Missouri established that the hanger assembly (including the Micarta plate) had an ultimate capacity of 400 kips. Furthermore, these experiments demonstrated that bending of the base plate did not occur until the hanger assembly was loaded with 200 kips, approaching the design load of the pipe hanger assembly.

The design strength of the hanger assemblies in the Kemper Arena were approximately 210 kips per assembly, while the roof posts examined in the thermal break strategies project have a design compressive strength of 20 kips. Bolts in the hanger were A490, while the cladding details in this work involve A325 or B8 Class 2 bolts. These bolts in the pipe hanger connection failed in tension, and the report on the failure does not attribute this mode to any behavior in the Micarta plate. The assemblies included in this study are also limited to cladding details, and not primary structural systems.

3 Thermal Modeling

Extensive three-dimensional thermal modeling was conducted in this research to evaluate several concepts developed for mitigating loss of energy via thermal bridging in steel structures. Thermal modeling is utilized to compare the thermal transmittance of proposed thermal bridging design solutions.

Three-dimensional thermal modeling of unmitigated and mitigated thermal bridge conditions was performed using the HEAT3 Version 7.0 software by Blocon and the Department of Building Physics at Chalmers Technical University and Lund University in Sweden (Blomberg, T. 2017). The program is validated against the EN ISO 10211 standard. HEAT3 models can be used to calculate the effective U-value (i.e., overall heat transfer coefficient or thermal transmittance) of the mitigated and unmitigated assemblies. The heat equation is solved with explicit forward finite differences using the successive over-relaxation technique in steady-state conduction.

One advantage of HEAT3 is that it accounts for heat transfer in three dimensions and provides extensive graphical capabilities in two and three dimensions for geometry, materials, temperature field, and boundary conditions. Additionally, HEAT3 includes a database of material properties for common building materials that can be edited to include the thermal properties of unique building materials. One of the restrictions is that geometric inputs are modeled in a parallelepiped mesh (i.e., all boundary surfaces are parallel to one of the Cartesian coordinate planes) and thus curved geometries must be approximated as straight line segments.

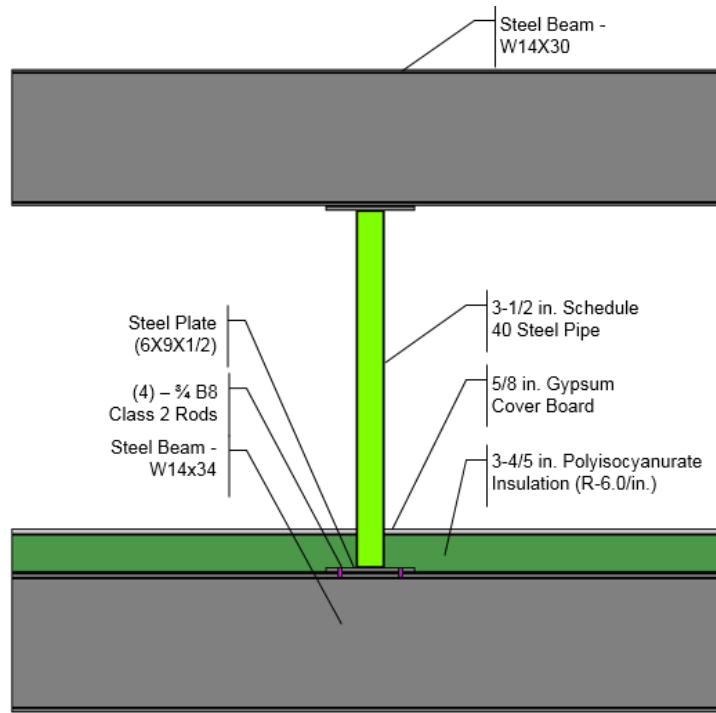
The following archetypal cladding assemblies were modeled in climate zones 1 and 7:

1. Roof posts (e.g., dunnage supports)
2. Slab-supported shelf-angles
3. Canopy beams

In order to differentiate each thermal model, an abbreviated nomenclature is employed. This nomenclature is summarized below and detailed in the following: the first two characters, either RP (roof post) or SA (shelf angle) or CB (canopy beam), correspond to the type of cladding detail; the second letter, either U (unmitigated) or M (mitigated) indicates if a model has a mitigation strategy or not; following this, the fourth number, either 1 (climate zone 1) or 7 (climate zone 7) refers to the thickness of the insulation per code requirements for that climate zone; the fifth number details the structural testing model that the thermal model derives from; specimen repetitions are denoted by a 1 or 2 at the end of the specimen name; and the capital letter at the end of the nomenclature refers to the repetition or variation from the base model.

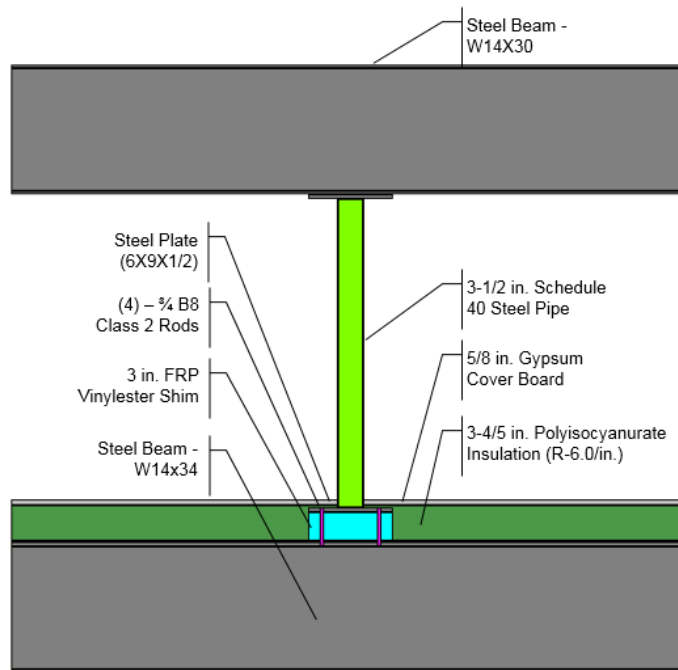
Test Name Nomenclature

RPU7-1-A = roof post (RP), unmitigated (U), climate zone 7 (7),



RPU1-1-B

Figure 3-1: Section view of an unmitigated roof post specimen RPU1-1-B in climate zone 1 (3.8" insulation thickness)



RPM1-2-B

Figure 3-2: Section view of a mitigated roof post specimen RPM1-2-B in climate zone 1 (3.8" insulation thickness) with a 3" thick vinyl ester shim

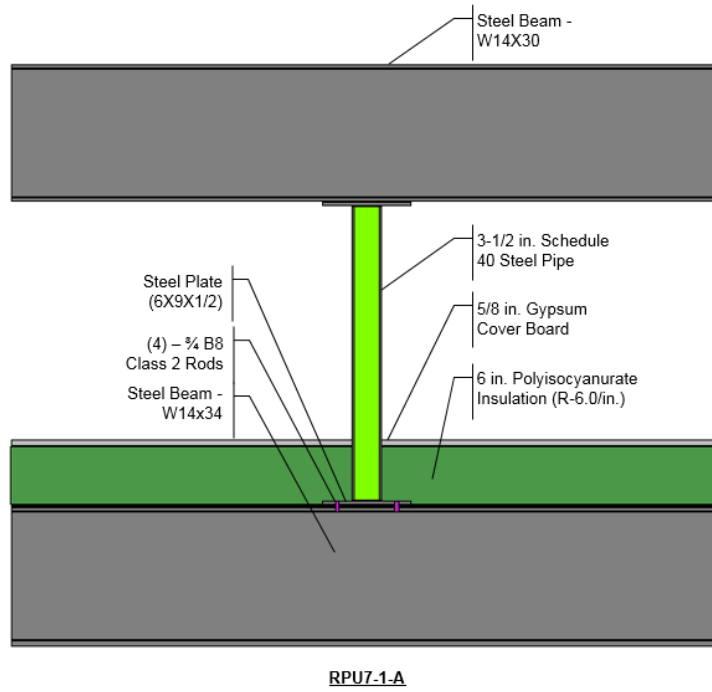


Figure 3-3: Section view of an unmitigated roof post specimen RPU7-1-A in climate zone 7 (6" insulation thickness)

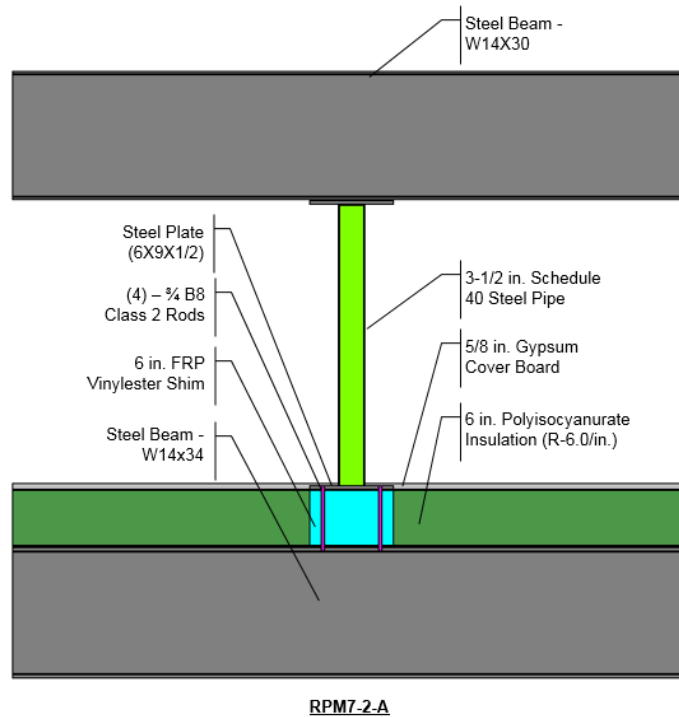


Figure 3-4: Section view of a mitigated roof post specimen RPM7-2-A in climate zone 7 (6" insulation thickness) with a 6" thick vinylester shim

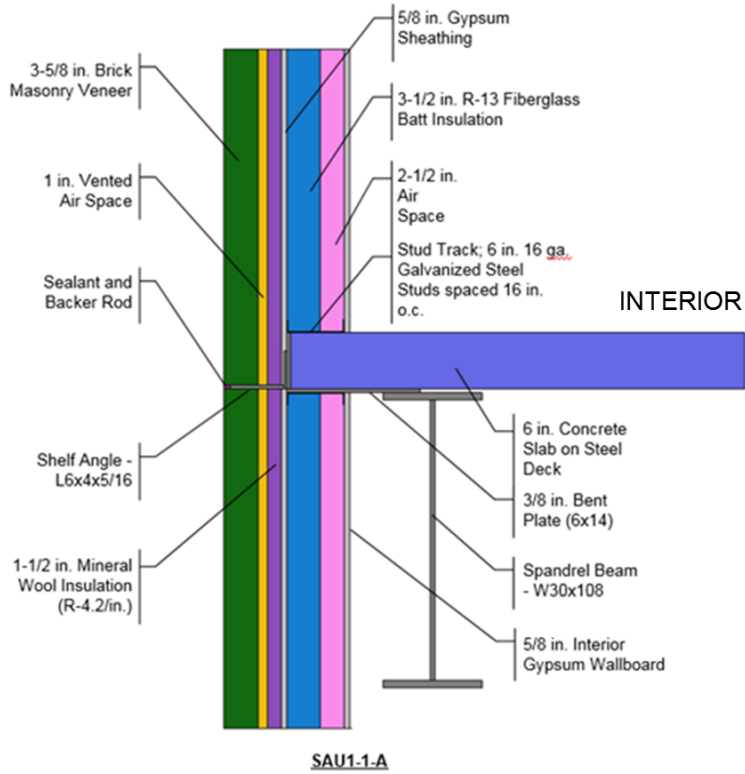


Figure 3-5: Section view of an unmitigated slab-supported shelf angle specimen SAU1-1-A in climate zone 1 (2.5" cavity width)

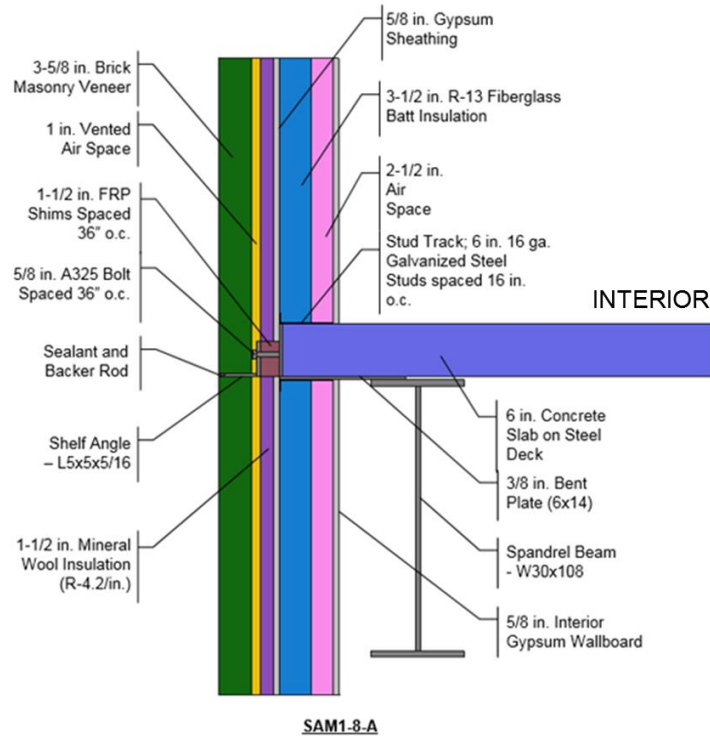


Figure 3-6: Section view of a mitigated slab-supported shelf angle specimen SAM1-8-A in climate zone 1 (2.5" cavity width) with a 1.5" thick vinyl ester shim

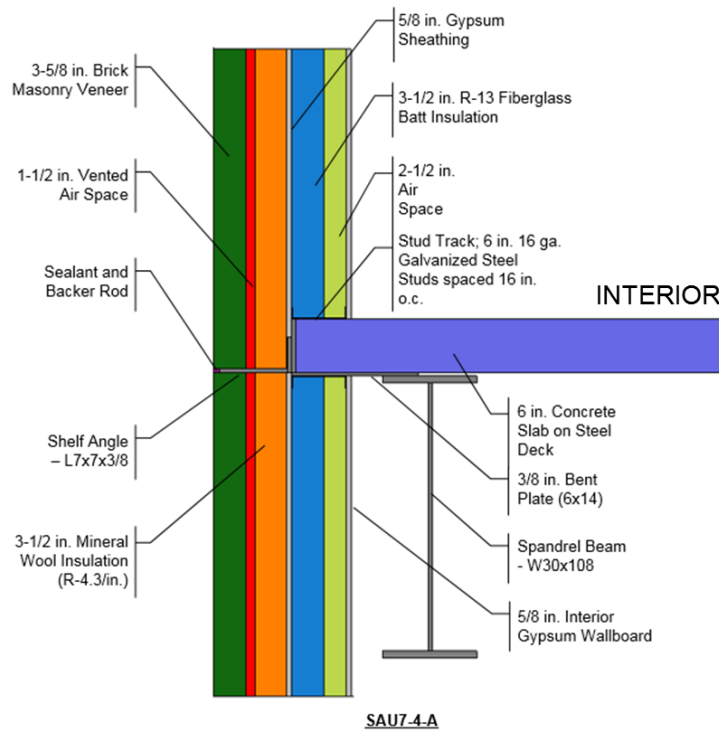


Figure 3-7: Section view of an unmitigated slab-supported shelf angle specimen SAU7-4-A in climate zone 7 (5" cavity width)

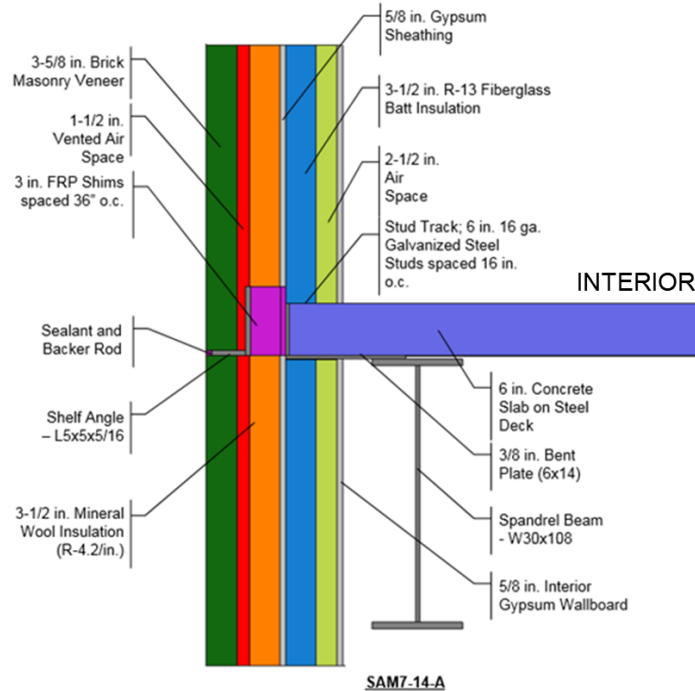


Figure 3-8: Section view of an unmitigated slab-supported shelf angle specimen SAM7-14-A in climate zone 1 (5" cavity width) with a 3" thick vinyl ester shim

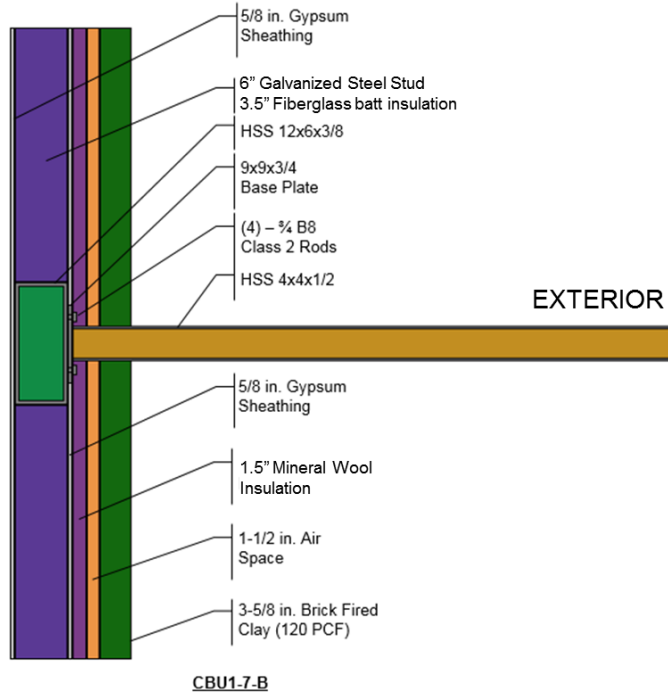


Figure 3-9: Section view of an unmitigated canopy beam specimen CBU1-7-B in climate zone 1 (1.5" insulation thickness).

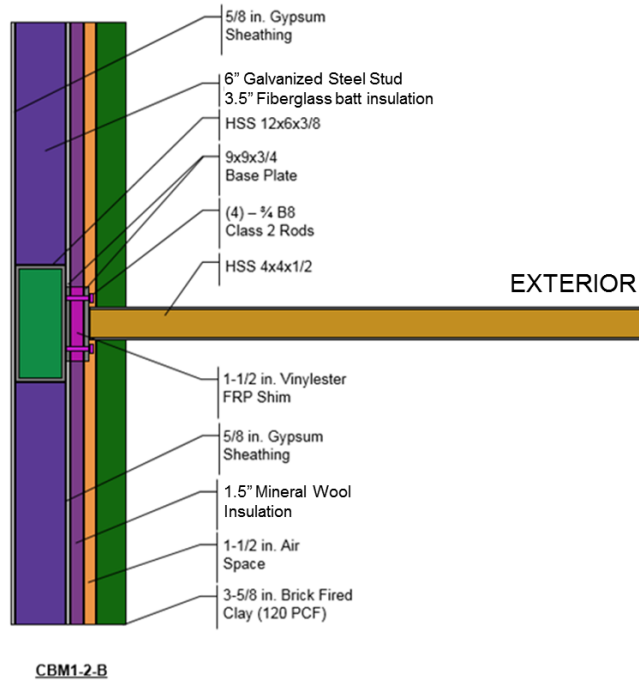
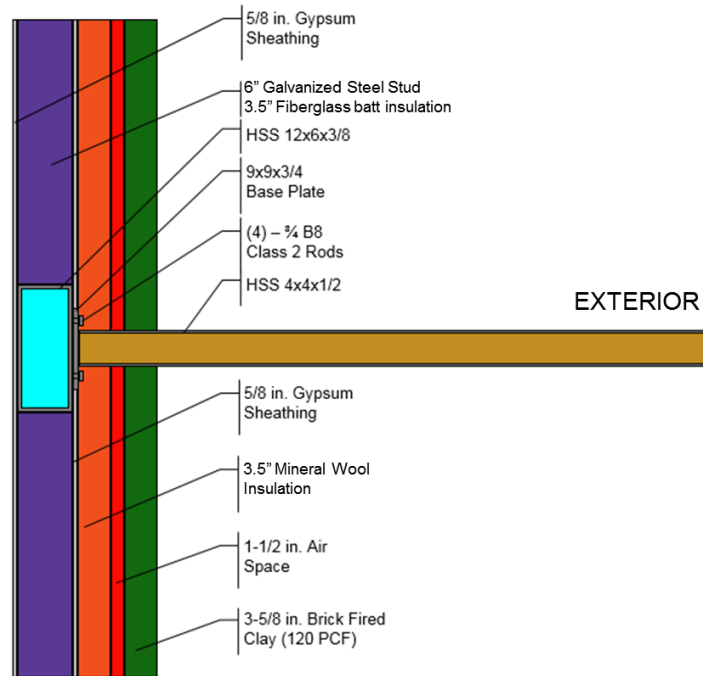
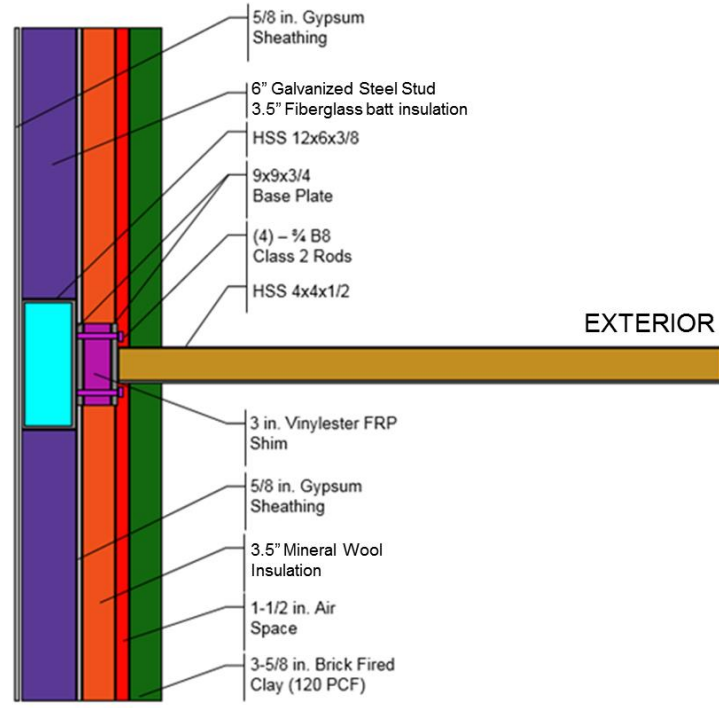


Figure 3-10: Section view of a mitigated canopy beam specimen CBM1-2-B in climate zone 1 (1.5" insulation thickness) with a 1.5" thick vinylester shim.



CBU7-7-A

Figure 3-11: Section view of an unmitigated canopy beam specimen CBU7-7-A in climate zone 7 (3.5” insulation thickness).



CBM7-2-A

Figure 3-12: Section view of a mitigated canopy beam specimen CBM7-2-A in climate zone 7 (3.5” insulation thickness) with a 3” thick vinylester shim.

3.1 Motivation and Background

The modeling results will aid in identifying the most thermally-promising configurations for structural testing and provide a means of exploring alternative design solutions. The objective of this modeling is to analyze the differences in U-value between the different cladding detail mitigation strategies proposed, and to provide guidance on which cladding assemblies to test structurally.

As part of this project, two separate matrices were developed for each type of cladding detail: the structural testing matrix and the thermal modeling matrix (available in Appendix E). The structural testing matrix summarizes all properties and components comprising each cladding detail to be structurally tested. The thermal modeling matrix reflects similar assemblies that were selected to thermally model. For the thermal models, properties and components of the structural testing specimens were altered to analyze the effect on thermal conductivity and explore alternative design solutions. Appendix E illustrates how the thermal modeling matrix was derived from the structural testing matrix.

To minimize the differences between the test assemblies and the thermal models, several assumptions were made to thermally analyze the proposed as-constructed version of the structural tested specimens. Specific assumptions for each type of cladding detail, such as the model size, spacing of bolts, etc., are described the sections that follow. Assumptions pertaining to each type of cladding detail are prescribed below:

- Certain components of the structural test specimens are oversized to control the failure mode. In the thermal models, all components are sized appropriately to resist design/service loads.
- For thermal modeling in HEAT3, surface areas of all materials must be in contact to transmit thermal energy. Thus, all hole diameters are modeled with the same diameter as the fasteners to provide surface contact between the plates and the fasteners. As this eliminates a potentially beneficial air layer and does not account for contact resistance, this is a conservative modeling choice. Because two pieces of material can never be in 100% contact (due to porosity and surface roughness), modeling perfect contact between them represents a worst case scenario.
- All fasteners in the thermal models are stainless steel or carbon steel. The stainless steel fasteners are three times less thermally conductive than the carbon steel fasteners (Baddoo, N. R. 2008). Because the archetypal cladding assemblies are intermittently spaced at the connection points, the thermal conductivity of the bolts themselves contributes to the overall energy transmittance of the system.

3.2 Scope of Analysis

To evaluate the differences in U-value between the proposed cladding assembly detail mitigation strategies, several parameters in the thermal models were varied. The ranges in various parameters are described below:

Unmitigated versus mitigated thermal models: To capture the behavior of the thermal break strategies, unmitigated models (i.e., assemblies with no thermal break strategy) and mitigated models were developed to compare the differences between the thermal efficiency of each mitigation strategy and the unmitigated baseline case. Unbroken wall and roof assemblies without thermal bridges through the continuous insulation layer were also modeled to provide a lower bound for the heat flow in these sub-systems. The following analysis results are presented:

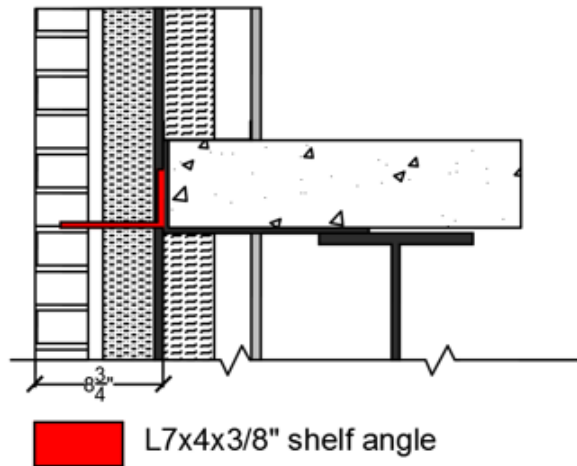
- Average U-value for the modeled assembly.
- Linear Thermal Transmittance (ψ) for the shelf angle thermal bridges.
- Point Thermal Transmittance (χ) for the roof posts and canopy beams.

Linear and point thermal transmittance are calculated using procedures from ASHRAE 1365-RP (ASHRAE 2011). These values may be used by energy modelers to calculate overall wall and roof U-values that account for the type and frequency of thermal bridges present.

Member size: For each assembly, the size of the component passing through the insulation layer was varied. For the roof posts and canopy beams, the member for the thermal modeling specimens varies slightly from the structural testing specimens when the FRP member (i.e., FRP HSS and sleeve) is used as a mitigation strategy. This is due to physical limitations on pultruded shape availability. While it is technically possible for any FRP shape to be customized, the work was limited to readily-available shapes. For this report, parameters of Strongwell Structural Shapes were used (Strongwell 2013).

For the shelf-angle models, detailing recommendations from the AISC Steel Design Guide 22, Façade Attachments to Steel-Framed Buildings (Parker 2008) were followed. FRP shims were the same height as the vertical leg of a shelf-angle and 3” wide. Due to this standard, the shelf angle horizontal leg (i.e., cross-sectional area of steel going through insulation layer in wall) was changed between the unmitigated and mitigated models. This ensures a constant wall cavity thickness across proposed solutions. The unmitigated models have longer angle legs (i.e., L6x4 and L8x4) in comparison to the mitigated models (i.e., L5x5) to meet brick veneer bearing guidelines with the added shim thickness. The L5x5 angle size was chosen since L5x4 angle sizes are not available in the AISC Steel Construction Manual (AISC 2014). Figure 3-13 below demonstrates a constant wall cavity thickness across proposed solutions:

UNMITIGATED - CLIMATE ZONE 7
SAU7-4-A



SHIM MITIGATION - CLIMATE ZONE 7
SAM7-14-A

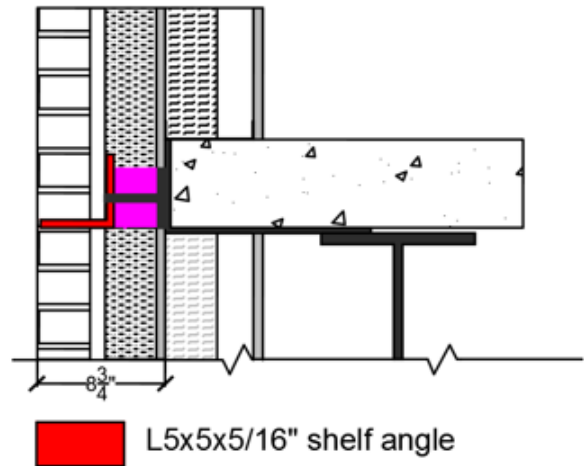


Figure 3-13: Section view of two slab-supported shelf angle specimens with constant wall cavity thicknesses

Connection material and mitigation strategy: In order to thermally test various types of cladding details, different materials were chosen to insert within the cladding assembly or to modify an existing material in order to reduce thermal conductivity. Materials were chosen based on their thermal performance, and Table 3-1 summarizes each material's thermal conductivity. Note that thermal conductivities for the proprietary products (products specifically designed as thermal break pads) are lower than published values for vinylester (Strongwell 2016), phenolic (Strongwell 2016), and polyurethane (Creative Pultrusions 2016) plate (products used for a large range of structural and non-structural applications).

For the roof posts, depending on the climate zone (i.e., climate zone 1 and 7), the code requirement for the roof insulation thickness varies: 3.8 inch thickness for climate zone 1, and 6 inch thickness for climate zone 7. For each climate zone, various shim materials were selected as mitigation strategies (i.e., vinylester, proprietary 1, proprietary 2) and the shim thickness varied to analyze the difference in thermal conductivity. Additionally, alternative mitigation strategies were explored: FRP post, bushings at steel rods, two vinylester shims.

Table 3-1: Summary of thermal modeling materials and thermal properties. Thermal properties for FRP materials are taken directly from publicly available material data sheets provided by the manufacturers. Insulation and air space properties from ASHRAE 90.1

Thermal Properties		
Material	Thermal Conductivity (W/mK)	Thermal Conductivity (BTU-in/hr-ft2-°F)
FRP Shim	0.5769	4.0000
Vinylester Shim	0.5769	4.0000
Phenolic Shim	0.5769	4.0000
Polyurethane Shim	0.5769	4.0000
Proprietary 2 Shim	0.2596	1.8000
Proprietary 1 Shim	0.1889	1.3100
R-35 Polyisocyanurate Roof Insulation	0.0238	0.1653
Air Space	varies	varies
Stainless Steel (B8 Class 2 Rods)	17.0000	117.8689

Climate zone (1 versus 7): The thermal performance of these assemblies is modeled in two climate zones, Zone 1 (primarily cooling climate, i.e., southern Florida) and Zone 7 (primarily heating climate, i.e., Alaska) as defined in the 2012 International Energy Conservation Code (IECC). The purpose of modeling in these two different climate zones is to bound the thermal performance. Each assembly is designed using code insulation values for above-grade metal-framed walls and roofs with continuous insulation above the deck. Table 3-2 summarizes the code-prescribed Residential Use Group R-values for the above-grade exterior wall and roof assemblies included in our study:

Table 3-2: Summary of Code Prescribed R-values for Above-Grade Walls and Roofs (2012 IECC)

	CLIMATE ZONE 1	CLIMATE ZONE 7
ROOFS Insulation entirely above deck	R-20 continuous insulation	R-35 continuous insulation
WALLS, ABOVE-GRADE Metal-framed	R-13 + R-5 continuous insulation	R-13 + R15.6 continuous insulation

The interior and exterior boundary conditions of each HEAT3 model are based on prescribed values in ASHRAE 90.1-2010 and National Fenestration Rating Council (NFRC) 100-2010. Para. A9.4.1 of ASHRAE 90.1-2010 specifies R-Values for air films, but does not specify interior and exterior boundary condition temperatures. The interior and exterior temperatures are based on the NFRC values provided in Para. 4.3.2.D of NFRC 100-2010. The interior and exterior boundary conditions are summarized in Table 3-3 below:

Table 3-3: Summary of Boundary Conditions

Boundary Conditions		
Boundary Conditions	Temperature (°F) (°C)	R-value (m ² ·K/W) (h·ft ² ·°F/Btu)
ASHRAE Exterior	-0.4	0.1700
	-18.0	0.0299
ASHRAE Interior Vertical	69.8	0.6800
	21.0	0.1198
ASHRAE Interior Horizontal, Down	69.8	0.9200
	21.0	0.1620
ASHRAE Interior Horizontal, Up	69.8	0.6100
	21.0	0.1074

3.2 Roof Posts

3.2.1 Assumptions Made and Differences between Structurally Tested Specimens

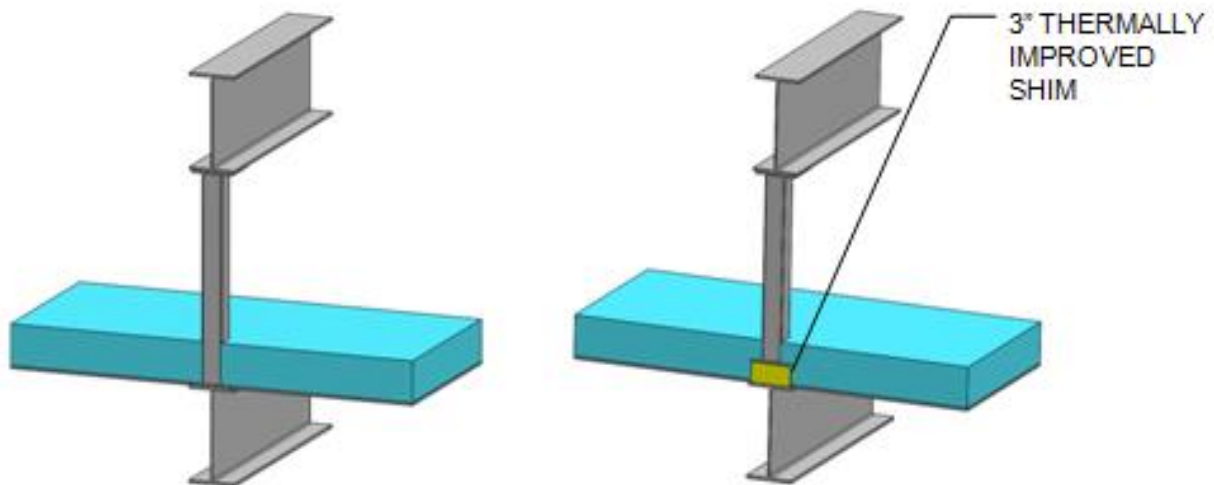


Figure 3-14: Unmitigated (left) and Mitigated (right) Roof Post Typical Detail

The thermal models reflect actual constructible and efficient structurally-designed cladding details as depicted in above in Figure 3-14. The experimental test specimens reflect this, while also considering a desired progression of failure. As a result, thermal models differ in some respects from the structural experimental test specimens, as follows:

- The test specimens are differentiated as ‘designed’ and ‘over-designed.’ The oversized connections meet a testing objective that the primary failure mode of the cladding assembly should not be bolt yielding. For the purpose of thermal modeling, all connections are considered ‘designed’.
- Weld geometry was not modeled in HEAT3, and presence of additional material from weld metal is not taken into consideration (structural test specimens were fabricated with CJP welds).
- All rods are spaced at 6” on center, and in the thermal models are stainless steel with the B8 Class 2 specification (i.e., the stainless steel rods have a lower thermal conductivity than the carbon steel A307 rods used for most structural testing).
- The roof post is steel for every thermal modeling specimen unless otherwise noted, and the beam below the roof insulation is a W14x34, whereas the beam above the roof is a W14x30.
- The structural testing specimens have different sizes of base plates (i.e., 6x9x1/2), cap plates (i.e., 10x10x1), and post lengths. However, thermal models have a uniform post length of 30 inches and their top plates are the same size as their base plates. The structural testing specimens have different post lengths because of the testing configuration restrictions. We modeled more uniform sizes for geometric simplicity. We assumed that these changes would not affect the U-factor of the thermal models.
- Base plates were modeled as rectangles (as is the commonly accepted configuration in the field). For structural test specimens, base plates were tested as square geometries to maintain specimen symmetry.

3.2.2 Results

Several mitigation strategies for roof posts are analyzed, with results summarized in this section. Proof of concept for the FRP shim thermal break mitigation strategy is provided via three-dimensional thermal modeling. Three materials are examined: vinylester, proprietary 1 and proprietary 2. A 72 inch x 120 inch segment of the roof with a central roof post was modeled. A summary of results for roof post cladding details is provided in Appendix E.

A comparison of unmitigated and mitigated thermal models was conducted to identify the difference in U-value (i.e., thermal conductivity) due to the addition of the roof post shim mitigation material. Mitigated thermal models in climate zone 1 are compared to the unmitigated thermal model RPU7-1-B, and similarly models in climate zone 7 are compared to the unmitigated model RPU7-1-A. The mitigated U-values are compared to unmitigated thermal models of the exact same configuration with the shim material removed (see Appendix E for graphics). Figure 3-15 depicts the configuration of the 2 vinylester shims where the green represents air space.

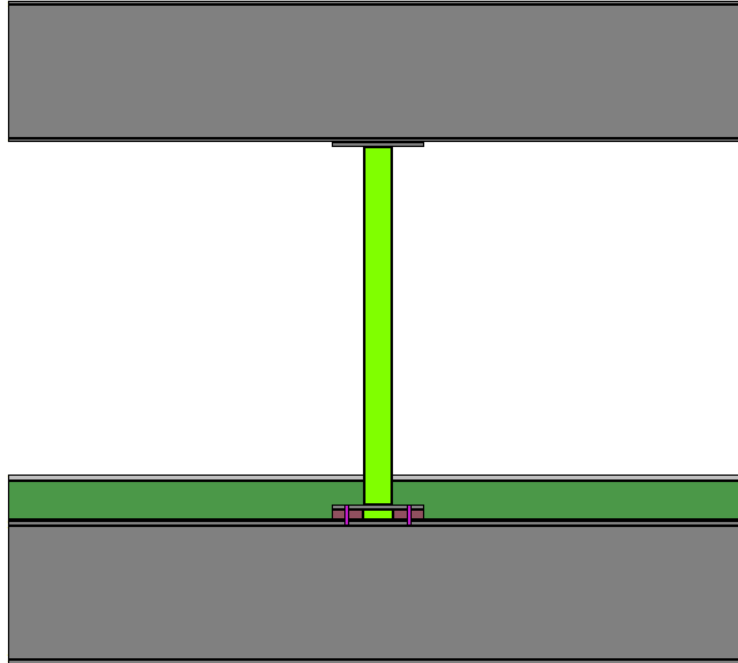


Figure 3-15: Thermal modeling of roof posts in climate zone 1 (3.8” insulation thickness) with two 1” thick vinyl ester shims

Additionally, all thermal models have B8 Class 2 stainless steel rods. However, one thermal model in each climate zone was thermally modeled with A307 rods to compare the difference in thermal conductivity between rod specification types. Table 3-4 below demonstrates the difference in U-values between unmitigated and mitigated strategies. The baselines for comparison are roof posts that pass through the roof insulation layer with no thermal break (“unmitigated model”). The mitigated models include the various thermal break strategies. The models in the gray rows represent the field of the roof with beam but no posts. The table reports the percent reduction in heat flow for each mitigation strategy as well as how the mitigation strategy compares to a roof with no penetrations. This metric is described in more detail below.

Table 3-4: Comparison of Unmitigated and Mitigated Roof Post FRP Shim Mitigation Strategy

UNMITIGATED MODEL		MITIGATED MODEL							COMPARISON
Thermal Model Name	U-Value <i>BTU/h*ft²*F</i>	Thermal Model Name	Mitigation Strategy	Shim Thick <i>in</i>	Insulation Thick <i>in</i>	U-Value <i>BTU/hr ft² °F</i>	χ <i>BTU/hr °F</i>	Δ U-Value <i>BTU/hr ft² °F</i>	% χ Improvement %
climate zone 7									
RPU7-Unbroken	0.0269	RPU7-1-A	none	N/A	6	0.0350	0.49	0.0081	-
RPU7-1-A	0.0350	RPM7-2-A	Vinylester shim	6	6	0.0318	0.29	0.0032	40%
RPU7-1-A	0.0350	RPM7-2-C	Vinylester shim	3	6	0.0325	0.34	0.0025	31%
RPU7-1-A	0.0350	RPM7-11-A	Proprietary 1 shim	6	6	0.0297	0.17	0.0053	65%
RPU7-1-A	0.0350	RPM7-11-B	Proprietary 1 shim	3	6	0.0308	0.24	0.0042	52%
RPU7-1-A	0.0350	RPM7-11-C	Proprietary 1 shim	1	6	0.0325	0.34	0.0025	31%
RPU7-1-A	0.0350	RPM7-12-A	Proprietary 2 shim	6	6	0.0301	0.20	0.0049	60%
RPU7-1-A	0.0350	RPM7-12-B	Proprietary 2 shim	3	6	0.0312	0.26	0.0038	47%
RPU7-1-A	0.0350	RPM7-12-C	Proprietary 2 shim	1	6	0.0328	0.36	0.0022	27%
RPU7-1-A	0.0350	RPM7-1-C	FRP HSS3x3x3/8	N/A	6	0.0273	0.03	0.0077	95%
climate zone 1									
RPU1-Unbroken	0.0416	RPU1-1-B	none	N/A	3.8	0.0517	0.61	0.0101	-
RPU1-1-B	0.0517	RPM1-2-B	Vinylester shim	3	3.8	0.0482	0.40	0.0035	34%
RPU1-1-B	0.0517	RPM1-2-D	Vinylester shim	4	3.8	0.0484	0.41	0.0033	33%
RPU1-1-B	0.0517	RPM1-2-E	Vinylester shim	1	3.8	0.0499	0.50	0.0018	18%
RPU1-1-B	0.0517	RPM1-2-F	2 vinylester shims	1	3.8	0.0492	0.46	0.0025	25%
RPU1-1-B	0.0517	RPM1-2-G	Vinylester shim with bushings at steel rods	1	3.8	0.0491	0.45	0.0025	25%
RPU1-1-B	0.0517	RPM1-2-H	Bushings at steel rods	N/A	3.8	0.0517	0.61	0.0000	0%
RPU1-1-B	0.0517	RPM1-1-D	FRP HSS3x3x3/8	N/A	3.8	0.0422	0.04	0.0095	94%
A307 bolts									
RPU7-7-A	0.0350	RPM7-8-A	Vinylester shim	6	6	0.0342	0.44	0.0009	10%
RPU1-7-B	0.0517	RPM1-8-B	Vinylester shim	3	3.8	0.0501	0.51	0.0016	16%

In climate zone 7, thermal modeling using FRP shims below the steel post base plate shows reductions in thermal point transmittance relative to the unmitigated roof posts ranging from 27% to 65% depending upon thickness and type of shim. While the proprietary products demonstrate superior thermal performance, this is directly related to their R-values, as tabulated earlier in this chapter. FRP posts are the most effective, with a 95% reduction in point transmittance for the zone 7 models. Thermal gradients for the zone 7 modeling efforts are shown in Figure 3-16 below with % reduction in U-value from the unmitigated case.

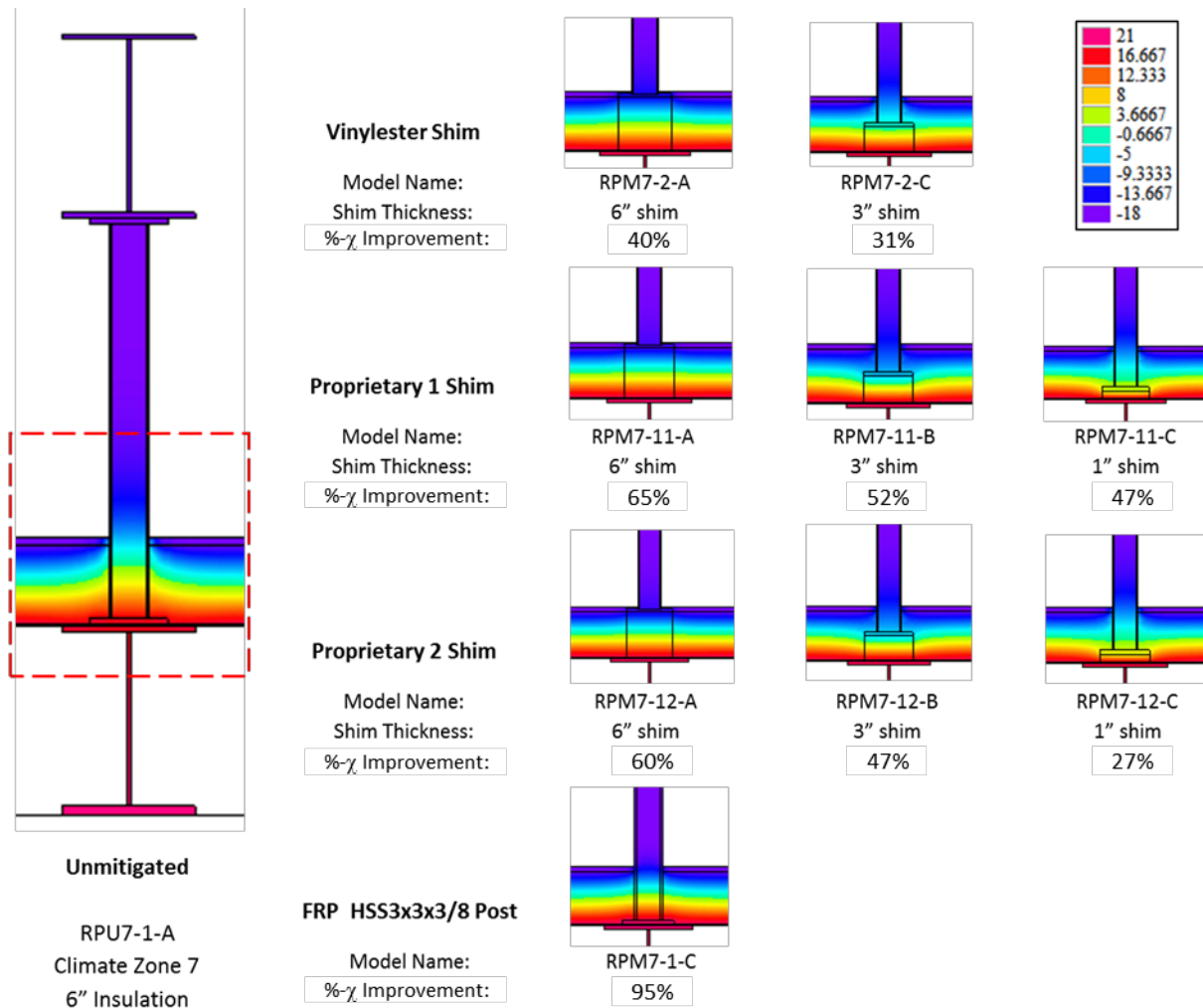


Figure 3-16: Thermal modeling of roof posts in climate zone 7 (6" insulation thickness) 2D results and comparisons

Since roof insulation thicknesses vary, and are based on the R-value of the insulation itself, modeling efforts were extended to account for numerous insulation and shim thicknesses. These results demonstrate that, in particular, thick FRP shims (i.e., 6 inches in thickness) can reduce U-value for the roof post cladding detail.

Figure 3-17 depicts thermal gradient results for the climate zone 1 models. Again, shim thicknesses and materials were varied. As models RPM1-2-D and RPM1-2-B demonstrate, thicker shims do not necessarily result in improved thermal performance if they extend beyond the insulation layer, as in model RPM1-2-D (4" shims with 3.8" insulation). Two 1" thick vinylester shims were analyzed (25% point transmittance reduction) and perform approximately 40% better than the 1" thick single vinylester shim (18% point transmittance reduction). Note that when shim thickness doubles, the change in thermal transmissibility does not increase linearly, due to the impact of the insulation layer. Bushings at the steel rods were modeled with a 1" thick vinylester shim, and yield

a higher energy transmission reduction (25% point transmittance reduction) than the 1” thick vinylester shim without bushings (18% point transmittance reduction).

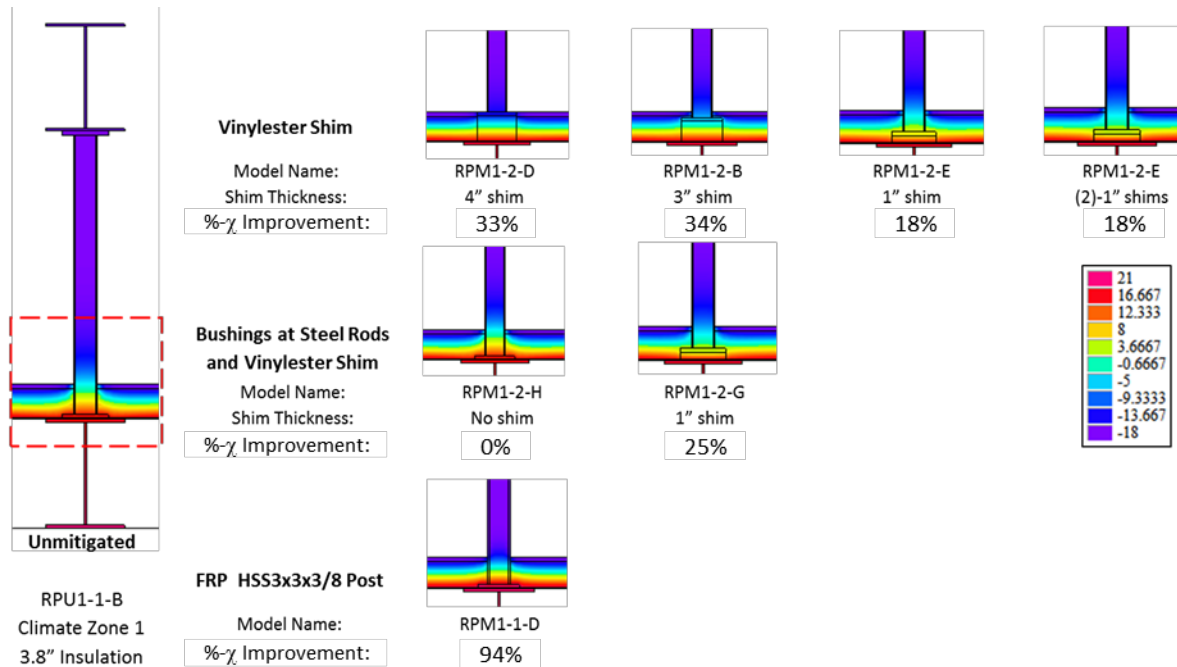


Figure 3-17: Thermal modeling of roof posts in climate zone 1 (3.8” insulation thickness) 2D results and comparisons to unmitigated model performance.

In climate zone 7, thermal modeling using 6” thick FRP shims below the steel post base plate with A307 rods shows an increase in thermal point transmittance of 48% compared to the model using stainless steel rods, while in climate zone 1 using a 3” thick FRP shim the substitution of A307 rods for stainless steel rods results a point transmittance increase of 28%. Figure 3-18 demonstrates the difference in U-values between stainless steel and carbon steel rods for climate zones 1 and 7. While FRP shims alone do improve the thermal performance of a roof post system, it is evident that stainless bolts in conjunction with shims result in a significantly more thermally-efficient system.

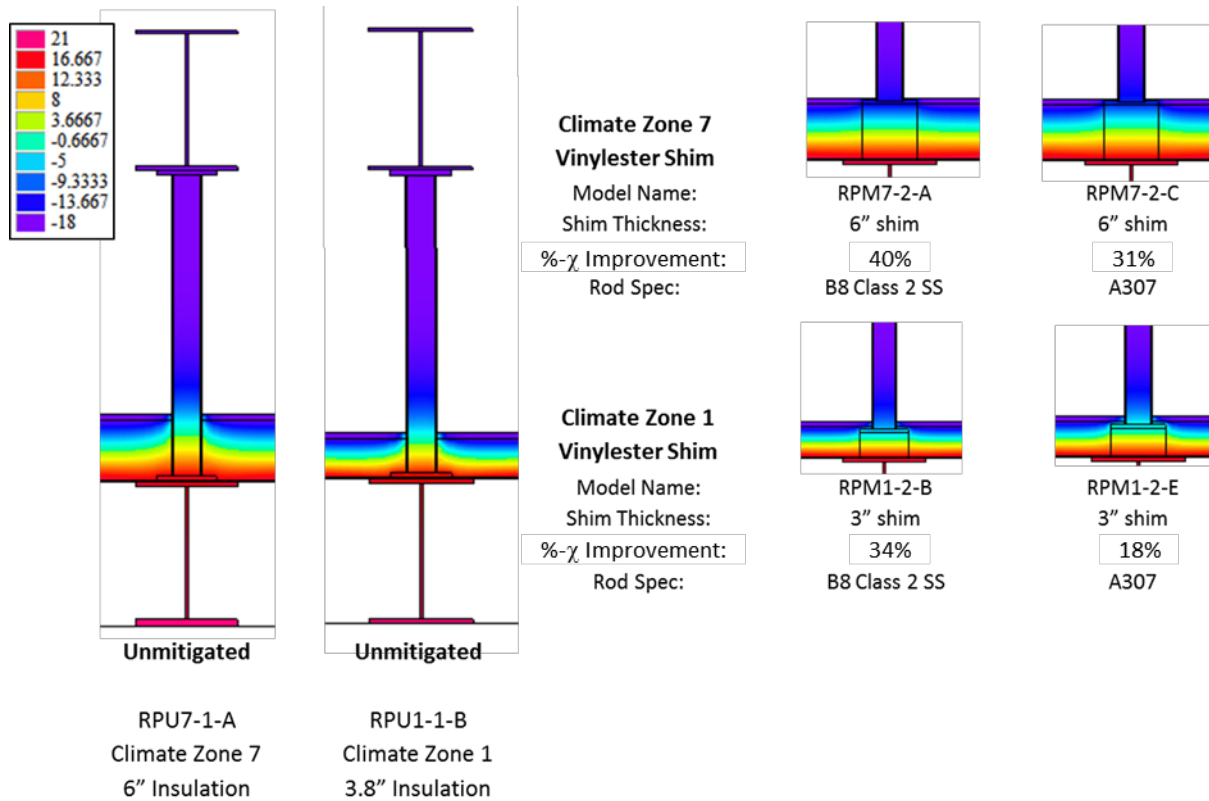


Figure 3-18: Thermal modeling roof posts with alternative rod specs (note that comparisons in χ are to the corresponding unmitigated detail).

3.3 Slab-Supported Shelf Angle

3.3.1 Assumptions Made and Differences between Structurally Tested Specimens

The thermal models reflect actual constructible and efficient structurally-designed cladding details. The experimental test specimens reflect this, while also considering a desired progression of failure.

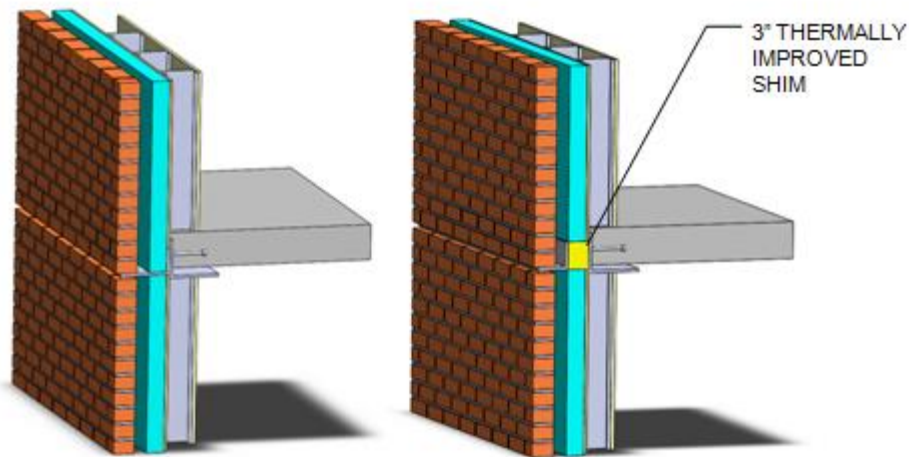


Figure 3-19: Unmitigated (left) and Mitigated (right) Slab-Supported Shelf Angle Typical Detail

As a result, thermal models differ slightly from the structural experimental test specimens, as follows:

- The test specimens are differentiated as ‘designed’ and ‘over-designed.’ The oversized connections meet a testing objective that the primary failure mode of the cladding assembly should not be bolt yielding. For the purpose of thermal modeling, all connections are considered ‘designed.’
- For thermal modeling in HEAT3 (and as discussed for the roof post models), surface areas of all materials must be in contact to transmit thermal energy (i.e., there must not be presence of spaces between surface areas). Due to the restriction of cavities, all hole diameters are modeled as the same diameter as the rods for surface contact between the plates and the rods.
- All rods in the thermal models are classified stainless steel and carbon steel (i.e., A304-SH and A325). The stainless steel rods have a lower thermal conductivity than the carbon steel A304-SH. Because shelf angle bolts are intermittently spaced at the connection points, the thermal conductivity of the bolts themselves contribute to the overall energy transmittance of the system.
- For the shelf-angle models, recommendations from the AISC Steel Design Guide 22, Façade Attachments to Steel-Framed Buildings (Parker 2008), were followed. FRP shims were the same height as the vertical leg of a shelf-angle and 3” wide. To keep the shims bearing completely on the shelf angle horizontal leg (i.e., cross-sectional area of steel going through insulation layer in wall), and to interface with the insulation layer geometries, the shelf angle was changed between the unmitigated and mitigated models. This ensures a constant wall cavity thickness across proposed solutions. The unmitigated models include angles with longer horizontal legs (i.e., L6x4 and L8x4) compared to the mitigated models (i.e., L5x5) so that the shelf angle supports at least 2/3 of the brick veneer thickness without extending past the face of brick in keeping with industry standards (e.g. Parker 2008). The L5x5 angle size was chosen because L5x4 is not a standard angle size in the AISC Steel Construction Manual (AISC 2014).

The original shelf angle designs were 1/2" and 3/8" in thickness. When the angle size was changed per the assumption above, there was a smaller unsupported horizontal shelf angle leg (i.e., 5" versus 7" or 8"). With a smaller angle size and smaller cantilevered leg, we were able to reduce the angle thickness to 5/16". Thinner angles are more thermally-efficient because less steel reduces thermal conductivity. See Figure 3-20 for a 5" versus 7" unsupported horizontal shelf angle leg:

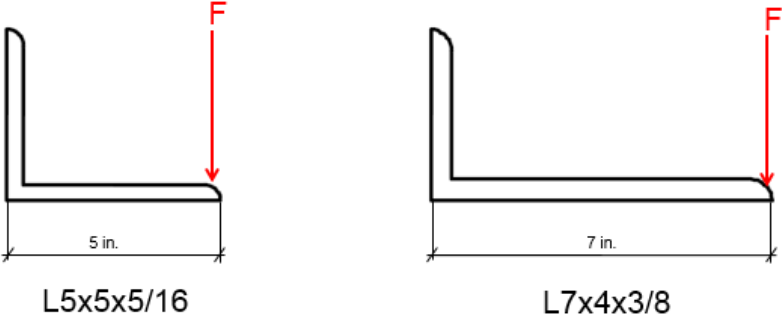


Figure 3-20: Moment arm on two distinct shelf angles

We assumed a full angle length in the model of 80" to incorporate two shims spaced at 36" on center and to account for the wall stud spacing of 16" on center. The full 80" length allows for the model to be cut midway between two shims and two wall studs. The height of the model was 72", and included one floor slab. See Figure 3-21 below for the model spacing as shown on the canopy beam model; since the shelf angle and canopy beams are both installed on exterior walls, basic model geometries were consistent between the two details.

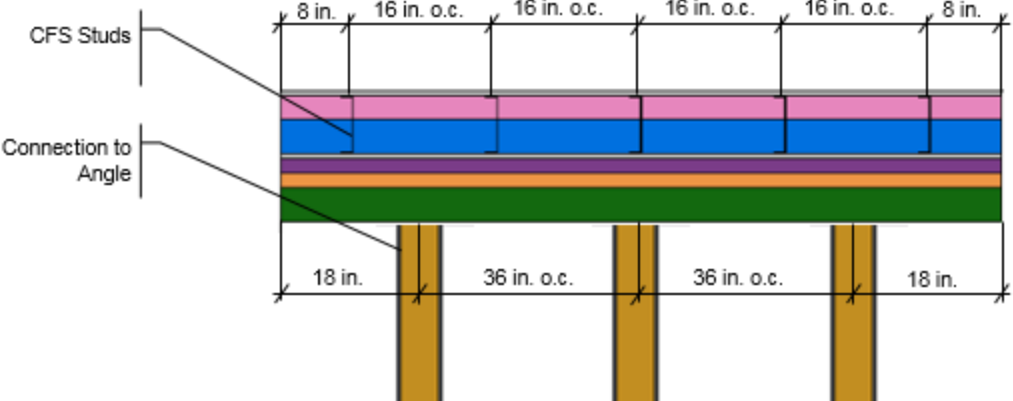


Figure 3-21: Plan view of wall cavity (depicted for canopy beam, but as shelf angle spacing is 36" on center, geometries are applicable for both cladding details)

3.3.2 Results

Several mitigation strategies for slab-supported shelf angles are analyzed, with results summarized herein. Proof of concept for the shim thermal break mitigation strategy is provided via three-dimensional thermal modeling. Three materials are examined (i.e., vinylester, proprietary 1 and proprietary 2) and two separate strategies are modeled (i.e., stainless tube shim and FRP angle).

A comparison of unmitigated and mitigated thermal models was conducted to identify the difference in U-value (i.e., thermal conductivity) due to the addition of the shelf angle shim mitigation material or other assembly. Mitigated thermal models in climate zone 1 are compared to the unmitigated thermal model SAU-1-1-A, and similarly models in climate zone 7 are compared to the unmitigated model SAU7-4-A. The mitigated U-values are compared to unmitigated thermal models of the exact same configuration with the shim material removed (i.e., shelf angles connected directly to the slab plate) (see Chapter 6 for experimental test matrices and graphics). A summary of results for slab-supported cladding details is provided in Table 3-5 below, and in Appendix E. See the discussion for Table 3-4 for further explanation of the result presentation.

Table 3-5: Summary of Results for Slab-Supported Shelf Angle Shim Mitigation Strategy

UNMITIGATED MODEL				MITIGATED MODEL						COMPARISON
Thermal Model Name	U-Value BTU/h ft ² °F	Thermal Model Name	Mitigation Strategy	Shim Thick in	Cavity Width in	Rod Spec	U-Value BTU/h ft ² °F	ψ BTU/hr ft °F	Δ U-Value BTU/h ft ² °F	%- ψ Improvement %
climate zone 7										
Unbroken Wall	0.0373	SAM7-Unbroken	broken by slab edge only	N/A	5	N/A	0.0451	0.047	0.0078	-
SAM7-Unbroken	0.0451	SAU7-4-A	none	N/A	5	A325	0.1123	0.403	0.0672	-
SAU7-4-A	0.1123	SAU7-4-B	stainless bolts	N/A	5	A304-SH	0.1123	0.403	0.0000	0%
SAU7-4-A	0.1123	SAM7-14-A	Vinylester shim	3	5	A325	0.0559	0.065	0.0564	84%
SAU7-4-A	0.1123	SAM7-14-B	Vinylester shim	3	5	A304-SH	0.0526	0.045	0.0597	89%
SAU7-4-A	0.1123	SAM7-17-A	Proprietary 1 shim	3	5	A304-SH	0.0506	0.033	0.0617	92%
SAU7-4-A	0.1123	SAM7-18-A	Proprietary 2 shim	3	5	A304-SH	0.0510	0.035	0.0613	91%
SAU7-4-A	0.1123	SAM7-18-B	Stainless Tube (HSS3x3x3/16)	N/A	5	A304-SH	0.0587	0.081	0.0536	80%
climate zone 1										
Unbroken Wall	0.0562	SAM1-Unbroken	broken by slab edge only	N/A	2.5	N/A	0.0660	0.059	0.0099	-
SAM1-Unbroken	0.0660	SAU1-1-A	none	N/A	2.5	A325	0.1381	0.433	0.0721	-
SAU1-1-A	0.1381	SAU1-1-B	stainless bolts	N/A	2.5	A304-SH	0.1381	0.432	0.0000	0%
SAU1-1-A	0.1381	SAM1-8-A	Vinylester shim	1.5	2.5	A325	0.0823	0.098	0.0558	77%
SAU1-1-A	0.1381	SAM1-8-B	Vinylester shim	1.5	2.5	A304-SH	0.0794	0.080	0.0587	81%
SAU1-1-A	0.1381	SAM1-19-A	FRP L6x4x1/2	N/A	2.5	A304-SH	0.0719	0.035	0.0662	92%

In every thermal model case, the addition of FRP shims to the slab-supported shelf angles improved thermal conductivity by reducing the linear thermal transmittance of the cladding detail by 77% to 92%. There are several factors that cause this increased reduction of thermal transmittance in comparison to the roof post FRP shim addition. For example, shelf angles are only

supported at the location of the shims (i.e., 36" on center) in the mitigated models. Thus, the intermittent spacing of shelf angle supports introduces space for insulation between the steel angle and the concrete slab pour stop, resulting in a reduction in U-value. Comparison to the unbroken system reveal that the mitigation strategies proposed here reach between 58% and 72% of maximum possible mitigation.

The effectiveness of the FRP shims for the shelf angles depend on the material of the shelf angle and the type of steel rod (i.e., stainless steel or carbon steel). Replacing the shelf angle with a FRP angle reduced thermal conductivity by 92% compared to the unbroken shelf angle model, while using stainless steel tube shims reduced thermal conductivity by 80%. Effects of changing the bolt type in addition to adding a shim may be seen between models SAM7-14-A and SAM7-14-B where the A325 bolt type yields a 85% linear thermal transmittance reduction, and the A304-SH bolt type yields a 89% reduction. These results may be visualized via Figure 3-22 and Figure 3-23 below. Note that due to limited variability in FRP angle sizes, FRP angles are only utilized in Climate Zone 1 models, where a smaller angle is acceptable.

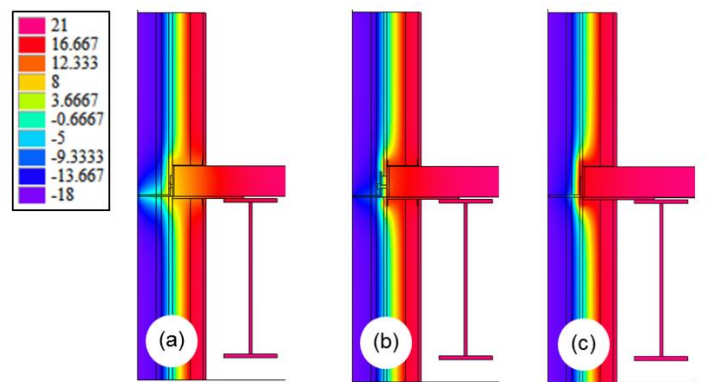


Figure 3-22: Thermal modeling of slab-supported shelf angles in climate zone 1 with a 2.5" cavity width 2D results and comparisons: a) Unmitigated, b) Vinylester shim ($\Delta\psi=81\%$), c) FRP angle ($\Delta\psi=92\%$)

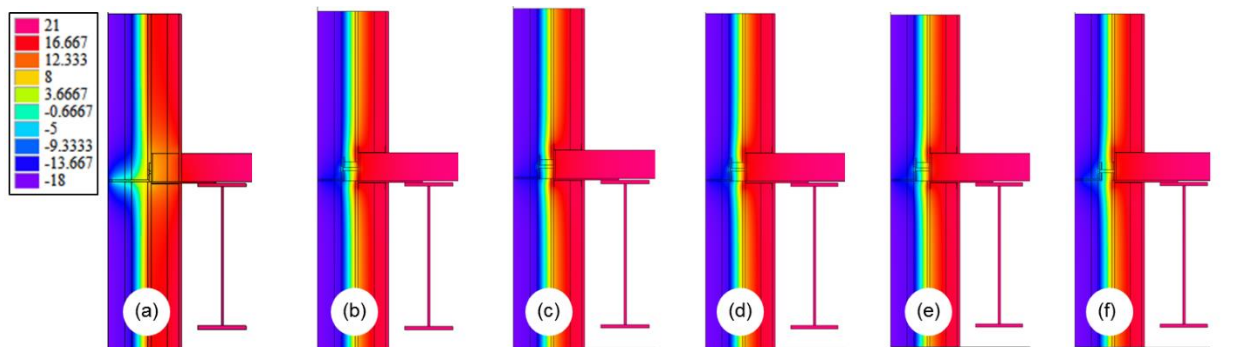


Figure 3-23: Thermal modeling of slab-supported shelf angles in climate zone 7 with a 5" cavity width 2D results and comparisons: a) Unmitigated, b) Vinylester shim with A325 bolts ($\Delta\psi=84\%$), c) Vinylester shim with A304-SH bolts ($\Delta\psi=89\%$), d) Proprietary 1 shim ($\Delta\psi=92\%$), e) Proprietary 2 shim ($\Delta\psi=91\%$), f) Stainless tube shim ($\Delta\psi=80\%$)

3.4 Canopy Beam

3.4.1 Assumptions Made and Differences between Structurally Tested Specimens

The thermal models reflect actual constructible and efficiently-designed cladding details. The experimental test specimens reflect this, while also considering a desired progression of failure. As a result, thermal models differ slightly from the structural experimental test specimens, as follows:

- The test specimens are differentiated as ‘designed’ and ‘over-designed’ to account for the assumption that connections should be oversized to assure that the primary failure mode of the cladding assembly will not be due to yielding at the connections. For the purpose of thermal modeling, all connections are considered ‘designed.’
- All rods in the thermal models are classified stainless steel or carbon steel (i.e., B8 Class 2 and A307, respectively).
- Because a 2.5” cavity is too small to use a 1.5” thermal break when accounting for connection hardware, the unmitigated and mitigated thermal models were modeled with a 3” cavity.
- The same assumptions for the shelf angles are applied for the canopy beam due to their similarity in the segment of the wall and insulation (i.e., wall studs and shim spacing). The main differentiating factor is that the canopy beam models include an HSS support beam instead of an angle at the edge of the slab.
- We are assuming this is a sun-shade overhang (i.e., more lightly loaded balcony) permitting us to detail a 5’ overhang for the canopy beam.
- The width of the model is 80” and the total wall height captured by the model is 72”.

3.4.2 Results

Several mitigation strategies for canopy beams are analyzed, with results summarized in this section. Proof of concept for the shim thermal break mitigation strategy is provided via three-dimensional thermal modeling. Three materials are examined (i.e., vinylester, proprietary 1 and proprietary 2). A summary of results for slab-supported cladding details is provided in Table 3-6 below, and in Appendix E:

Table 3-6: Summary of Results for Canopy Beam Shim Mitigation Strategy

MITIGATED MODEL		UNMITIGATED MODEL								COMPARISON	
Thermal Model Name	U-Value	Thermal Model Name	Mitigation Strategy	Shim Thick	Insulation Thick	Rod Spec	U-Value	χ	ψ	Δ U-Value	% χ Improvement
-	BTU/hr ft ² °F	-	-	in	in	-	BTU/hr ft ² °F	BTU/hr °F	BTU/hr ft °F	BTU/hr ft ² °F	%
climate zone 7											
Unbroken Wall	0.0366	CB-unbroken-zone7	broken by spandrel beam only	-	3	-	0.0415	-	0.029	0.0049	-
CB-unbroken-zone7	0.0415	CBU7-7-A	none	-	3	B8 Class 2	0.0666	0.50	-	0.0251	-
CBU7-7-A	0.0666	CBM7-2-A	Vinylester shim	3	3	B8 Class 2	0.0647	0.46	-	0.0019	8%
CBU7-7-A	0.0666	CBM7-2-C	Vinylester shim	1	3	B8 Class 2	0.0649	0.47	-	0.0017	7%
CBU7-7-A	0.0666	CBM7-11-A	Proprietary 1 shim	3	3	B8 Class 2	0.0590	0.35	-	0.0076	30%
CBU7-7-A	0.0666	CBM7-12-A	Proprietary 2 shim	3	3	B8 Class 2	0.0602	0.37	-	0.0064	25%
climate zone 1											
Unbroken Wall	0.0548	CB-unbroken-zone1	broken by spandrel beam only	-	1.5	-	0.0673	-	0.075	0.0125	-
CB-unbroken-zone1	0.0673	CBU1-7-B	none	-	1.5	B8 Class 2	0.0918	0.49	-	0.0245	-
CBU1-7-B	0.0918	CBM1-2-B	Vinylester shim	1.5	1.5	B8 Class 2	0.0916	0.49	-	0.0002	1%

A comparison of unmitigated and mitigated thermal models was conducted to identify the difference in point thermal transmittance (χ) due to the addition of the canopy beam shim mitigation material. Mitigated thermal models in climate zone 1 are compared to the unmitigated thermal model CBU1-7-B, and similarly models in climate zone 7 are compared to the unmitigated model CBU7-7-B. The mitigated models are compared to unmitigated models of the exact same configuration with the steel angle directly in contact with the slab plate (no shim) (see Appendix E for graphics). Thermal gradients for the canopy beam results are shown in Figure 3-24 below.

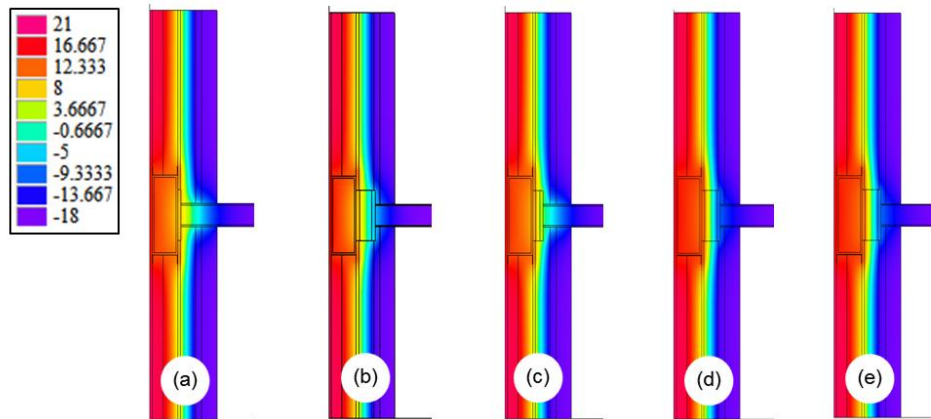


Figure 3-24: Thermal modeling of canopy beams 2D results and comparisons: a) Unmitigated, b) Vinylester shim with 3” thickness ($\Delta\chi=8\%$), c) Vinylester shim with 1” thickness ($\Delta\chi=7\%$), d) Proprietary 1 shim ($\Delta\chi=30\%$), e) Proprietary 2 shim ($\Delta\chi=25\%$)

In every Zone 7 thermal model case, the addition of a FRP shim to the canopy beams improved thermal conductivity by reducing the thermal transmittance of the cladding detail between 7% to 30% for shim thicknesses of 3”. As in the previous sections, insulation properties and shim

materials contribute to the extent of mitigation. However, compared to the unbroken wall model, results are encouraging. Proprietary shims can mitigate point thermal transmittance by 25-30%, while the vinyl ester product mitigates point thermal transmittance by 7-8%.

3.5 Conclusions

The mitigation strategies proposed herein have been parametrically analyzed via the HEAT3 three-dimensional thermal modeling software package. The following parameters were varied across cladding details: shim material, shim thickness, structural member size and material, and connection material. From these results, several conclusions may be formed:

- Using non-conductive shims is a thermally effective means of mitigating thermal bridges. This strategy is especially effective for continuous thermal bridges, where the addition of shims transforms continuous structural elements into discretely-connected elements. This is evident in the shelf angle results, where 3x4" shims installed at the bolt locations significantly reduce the area of steel in direct contact with the concrete slab pour stop. For continuous thermal bridging, the improvement in thermal transmittance via shim mitigation can reach up to 92% of the unbroken shelf angle model.
- Improvement in thermal transmittance is dependent on the thermal properties of the thermally-improved material itself, the insulation layer properties (thickness and R-value) and the thickness of shims with respect to the insulation layer thickness. Shims slightly thicker than the insulation layer, are not as beneficial as shims slightly thinner than the insulation layer. In general, however, thicker shims offer superior thermal performance when they span the insulation layer without protruding from it.
- FRP structural members are very effective at thermal bridge mitigation, in continuous and discrete cladding details.
- Stainless steel bolts offer significant improvement in thermal transmittance, especially in roof posts and canopy beams in which several bolts penetrate the insulation the building envelope.
- Thermally-improved bushings installed at bolt locations offer little to no mitigation
- The results herein justify full-scale structural testing to determine which strategies are optimal for thermal and structural performance.

4 Flatwise Creep Testing of FRP Materials

This chapter summarizes the results of the experimental tests of FRP materials under flatwise compression for prolonged loads (creep). Here, flatwise compression refers to axial compression perpendicular to the fiber mats of the specimens.

4.1 Experimental setup and design

So that the testing equipment could attain the forces required to fail the specimens, 1x1x1” cubes of FRP plate were machined at the Northeastern University STReSS lab. In the absence of a relevant ASTM standard, symmetric specimens were selected, with the goal of limiting the strength of the specimens to that of the test rig load cell. Utilizing existing ASTM standards for tensile creep of fiber reinforced polymers (ASTM C365) and flatwise compressive rupture of polymer matrixes (ASTM D7337), a testing standard for flatwise compressive creep testing of fiber reinforced polymers was developed. This proposed test method is provided in Appendix B of this report.

This series of testing was found to be extremely sensitive to slight variations in specimen geometry. As such, the specimens were milled to flat and parallel on all six sides. Following machining, specimens were measured in each dimension to characterize the geometry of the specimen cube. Using the flat plate attachments for the MTS universal testing machine, the specimens were compressed under force control in which force was applied at 1 kip/second, and maintained until failure of the specimen. Failure of a specimen consisted of crushing of the specimen; typical failure modes are shown in Figure 4-1 below. Note that Proprietary 1 and Proprietary 2 specimens failed similarly to the polyurethane specimens, with a diagonal rupture. Tight interlocks were set so that the machine would automatically shut off once failure had initiated.



Figure 4-1: Typical failure modes for (a) vinylester (b) polyurethane, and (c) phenolic resins.

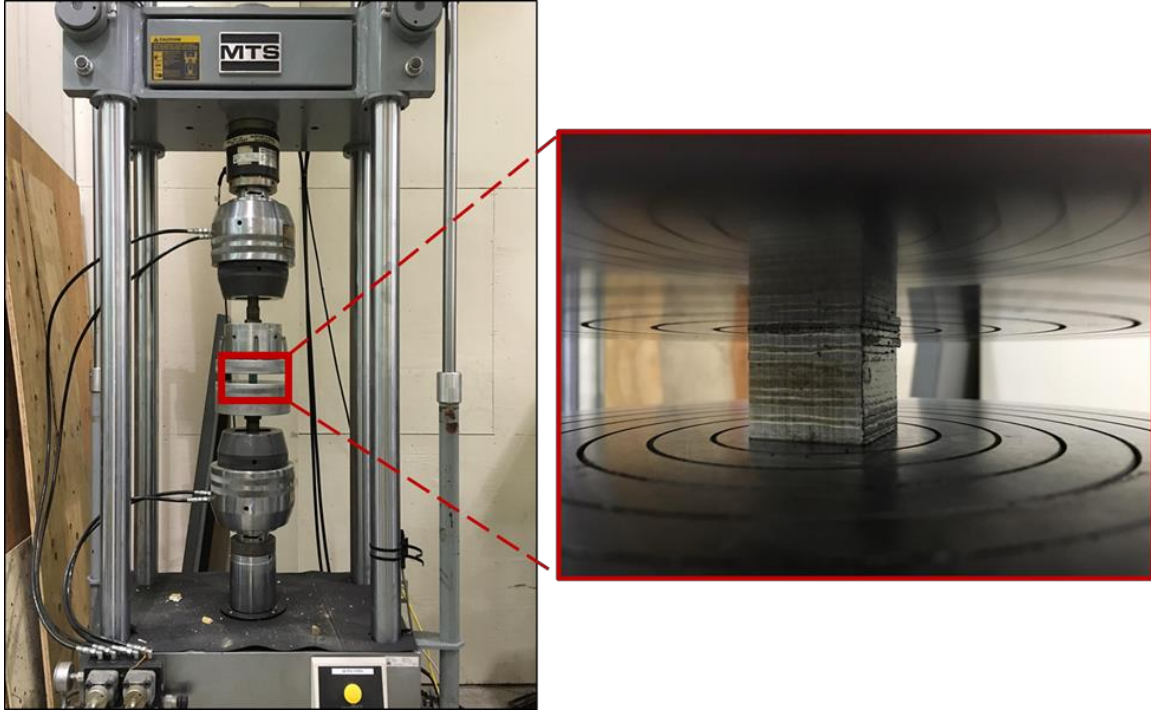
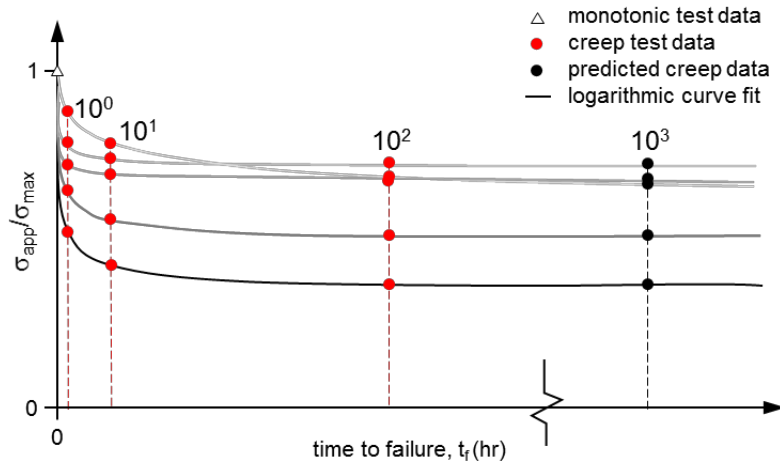


Figure 4-2: Photograph of experimental setup at the Northeastern University STReSS laboratory

4.1.1 Test matrix

The test matrix for creep specimens is based upon the performance of the specimens. Because it is necessary to determine the stress ratios such that failure time is spaced in logarithmic decades, testing is iterative, and the stress ratios used in subsequent tests may be adjusted based on the results of each successful test in which a specimen is tested to failure. Figure 4-3 demonstrates a target test matrix for each material and how the test data is used to predict performance at long term loads.

material	specimen	t_f (hr)
vinylester	1	1
	2	10
	3	100
	4	1000
polyurethane	1	1
	2	10
	3	100
	4	1000
phenolic	1	1
	2	10
	3	100
	4	1000
proprietary 1	1	1
	2	10
	3	100
	4	1000
proprietary 2	1	1
	2	10
	3	100
	4	1000



1. Perform creep tests such that t_f varies by logarithmic decades
2. Fit logarithmic curve to experimental data
3. Predict $(t_f, \sigma_{app}/\sigma_{max})$ for material performance beyond seven days

Figure 4-3: Illustration of utilization of test data to predict long-term performance

The applied stress ratio, $\sigma_{app}/\sigma_{max}$, is based upon the ultimate stress from monotonic flatwise compressive testing, which is summarized in Appendix A. To assess the early regions of the creep curve, testing was focused at higher stress ratios to produce failure times within seven days. While the recommended testing protocol outlined in Appendix B is based upon applied force ratio rather than applied stress ratio, slight differences in the geometry of the specimens (due to limitations in machining accuracy) are better considered via a stress-based approach.

The resulting test matrix, including time to failure and applied stress ratios, is shown in Table 4-1.

4.1 Results

In addition to time to failure and corresponding stress ratio, monotonic strains (ϵ_0), failure strains (ϵ_f), creep strains ($\epsilon_c = \epsilon_f - \epsilon_0$), and slope of the secondary region (m_2) are provided in Table 4-1 below. Monotonic strains are determined from the compressive modulus (determined from monotonic testing, and discussed in Appendix A) and corresponding applied stress using Hooke's Law (Horvath 1998).

Table 4-1: Tabulated results for creep testing across materials

material	test	$\sigma_{app}/\sigma_{max}$ ksi/ksi	specimen properties & loading				t_f , time to failure				ϵ , strains			slope
			F_{app} kip	σ_{app} ksi	σ_{max} ksi	E ksi	<10 ⁰ hr	>10 ⁰ hr	>10 ¹ hr	>10 ² hr	ϵ_0 in/in	ϵ_c in/in	ϵ_f in/in	m_2 in/in/hr
vinylester	3c	0.8	21.28	23.78	29.73	470	0.63	-	-	-	0.051	0.024	0.075	1.53E-02
	1c	0.8	20.98	23.78	29.73	470	-	2.79	-	-	0.051	0.023	0.074	3.10E-03
	2c	0.8	20.93	23.78	29.73	470	-	3.30	-	-	0.051	0.026	0.077	2.82E-03
	5c	0.758	20.78	22.54	29.73	470	-	6.23	-	-	0.048	0.025	0.073	1.27E-03
	6c	0.75	20.10	22.30	29.73	470	-	-	13.4	-	0.047	0.025	0.072	6.55E-04
	4c	0.7	19.11	20.81	29.73	470	-	-	-	132	0.044	0.025	0.069	6.49E-05
	8c*	0.5	14.32	14.87	29.73	470	-	-	43+	-	0.032	-	-	3.65E-05
	7c*	0.4	10.77	11.89	29.73	470	-	-	-	123+	0.025	-	-	1.65E-05
	9c*	0.3	8.26	8.92	29.73	470	-	-	-	165+	0.019	-	-	8.36E-06
											mean	-	-	0.073
										st. dev	-	-	0.003	
polyurethane	1c	0.9	54.68	53.74	59.71	620	0.13	-	-	-	0.087	0.022	0.109	9.00E-02
	2c	0.9	54.45	53.74	59.71	620	0.79	-	-	-	0.087	0.023	0.110	9.37E-03
	3c	0.9	54.01	53.74	59.71	620	-	6.09	-	-	0.087	0.017	0.104	9.70E-04
	4c	0.8	44.03	47.77	59.71	620	-	-	36.9	-	0.077	0.018	0.095	1.46E-04
	5c*	0.78	43.46	46.57	59.71	620	-	-	-	500+	0.075	-	-	5.54E-06
											mean	-	-	0.105
										st. dev	-	-	0.007	
phenolic	8c*	0.875	12.85	14.48	16.55	100	-	-	-	125+	0.145	-	-	2.43E-05
	3c	0.85	12.31	14.07	16.55	100	-	1.92	-	-	0.141	0.109	0.250	1.01E-02
	7c	0.85	12.49	14.07	16.55	100	-	9.63	-	-	0.141	0.119	0.260	1.55E-03
	5c	0.84	12.58	13.90	16.55	100	-	-	73.0	-	0.139	0.114	0.253	1.37E-04
	2c	0.8	12.11	13.24	16.55	100	-	-	-	231	0.132	0.115	0.247	1.30E-04
	1c*	0.8	11.86	12.71	16.55	100	-	-	25+	-	0.127	-	-	2.16E-04
											mean	-	-	0.253
										st. dev	-	-	0.006	
proprietary 1	2c	0.85	27.84	33.56	39.48	450	-	3.08	-	-	0.075	0.016	0.091	6.19E-03
	1c	0.8	28.15	31.58	39.48	450	-	-	16.7	-	0.070	0.024	0.094	1.25E-03
	3c	0.78	27.16	30.79	39.48	450	-	-	-	146	0.068	0.024	0.092	1.05E-04
											mean	-	-	0.092
										st. dev	-	-	0.002	
proprietary 2	1c	0.8	26.76	31.32	39.15	500	0.21	-	-	-	0.063	0.030	0.092	4.31E-02
	2c	0.7	22.49	27.41	39.15	500	-	2.27	-	-	0.055	0.031	0.086	6.71E-03
	6c	0.69	21.63	27.01	39.15	500	-	6.68	-	-	0.054	0.040	0.094	1.60E-03
	5c	0.65	21.13	25.45	39.15	500	-	-	85.4	-	0.051	0.041	0.092	1.09E-04
											mean	-	-	0.091
										st. dev	-	-	0.004	

Creep response curves are typically defined via three distinct regions: the primary, secondary, and tertiary regions. The primary region encompasses the load application, and has a slope equal to the modulus of elasticity of the material. Once the load has plateaued, the strains also begin to plateau and the primary region transitions to the secondary region. In a hypothetical material that does not experience creep strains, the slope of this secondary region would be constant and zero. For materials that do experience creep strain, the slope of the secondary region is constant and non-zero, with the magnitude of the slope approaching zero as the applied stress approaches zero. The tertiary creep region exists only if failure is imminent and represents the end of the constant slope region of the secondary regime. A typical creep response curve is shown in Figure 4-4 below.

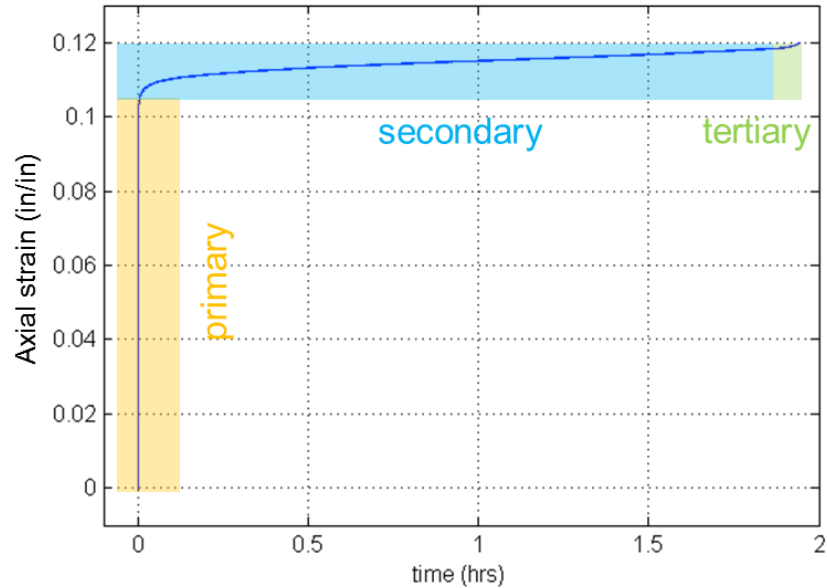


Figure 4-4: standard creep curve with primary, secondary, and tertiary regions illustrated

The failure strain is determined by fitting a straight line to the secondary creep region, and determining the intercept with a vertical line drawn in the tertiary creep region. This concept is illustrated in Figure 4-5 below. For specimens that did not fail (or experience a tertiary creep region), the slope at the time the test was terminated was taken to be the secondary creep region, as these tests ran for weeks before termination, and were thus beyond the primary regime. The slope was determined using the last point prior to termination, and a point at an interval of $0.1 t_f$ prior to the termination point.

Creep strains and failure strains are relatively consistent across material type, with typical variations due to statistical variance in material properties, signifying consistency across testing and stress ratios. The slope in the secondary creep regions also approaches zero as the stress ratio decreases; this phenomena will be discussed in greater detail in subsequent sections.

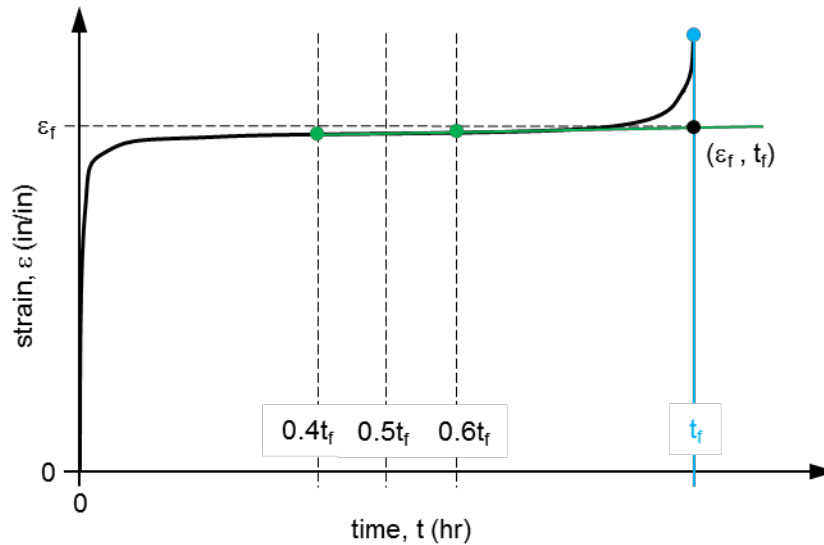


Figure 4-5: Determination of failure strains ϵ_f from strain-time curve

4.2 Creep stress and time to failure analysis

As logarithmically spaced results are desired in creep testing to fully characterize material behavior at long time periods, power equations are commonly used to provide a rigorous means of predicting behavior beyond the realm of realistic test parameters (Horvath 1998, Findley and Khosla 1956, Findley 1960a, Chambers 1984a, Chambers 1984b, Chambers and Mosallam 1994). As such, a power curve to predict the creep response of each material was fit to the creep data for each material tested in this work. These curves may then be used to predict the creep response of materials at times much longer than are typically tested within a creep testing protocol. For the materials tested, stress ratio and time to failure are plotted and fit to an exponential curve. Following this, performance at 500 ($5 \times 10^2 = 20.8$ days), 1,000 ($10^3 = 41.7$ days), 10,000 ($10^4 = 1.14$ years), 100,000 ($10^5 = 11.4$ years), and 1,000,000 ($10^6 = 114.2$ years) hours are predicted (note that these predictions are shown on a logarithmic scale so that data is easily read).

Vinylester data is shown in Figure 4-6, polyurethane in Figure 4-7, phenolic in Figure 4-8, proprietary 1 in Figure 4-9, and proprietary 2 in Figure 4-10. Figure 4-11 aggregates this data to demonstrate how the exponential curve fits perform across all materials included in this survey. The shaded regions in the logarithmically-spaced plots at right represent predicted results, while unshaded points are experimental data. Curve fit equations in terms of x and y correspond to time to failure t_f , and applied stress ratio $\sigma_{app}/\sigma_{max}$, respectively.

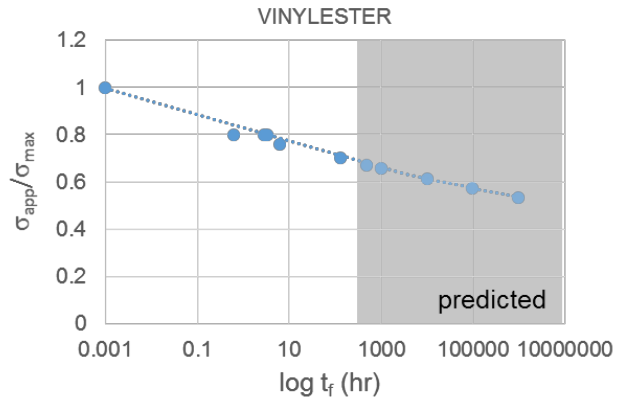
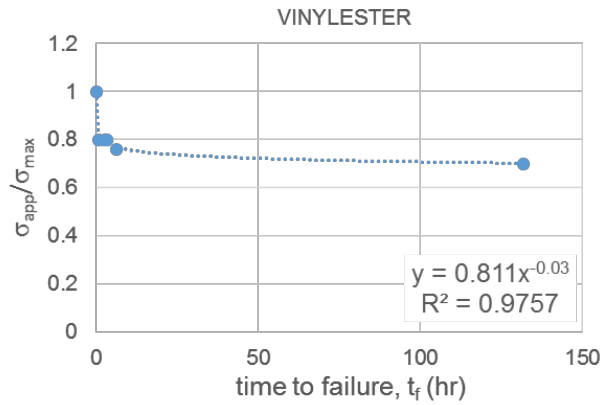


Figure 4-6: Exponential fit to vinylester creep experimental data and predicted failure behavior at long-term loading

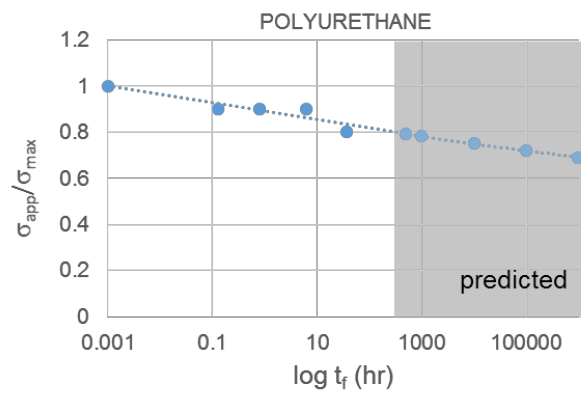
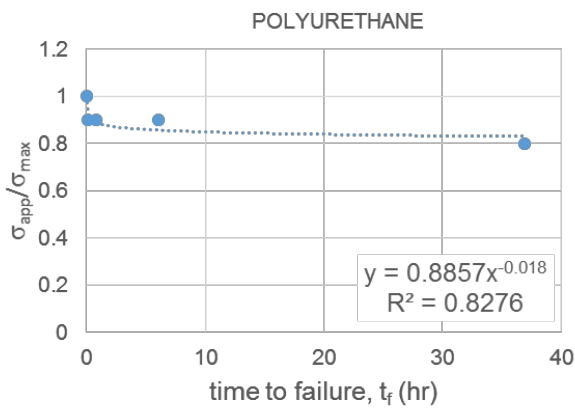


Figure 4-7: Exponential fit to polyurethane creep experimental data and predicted failure behavior at long-term loading

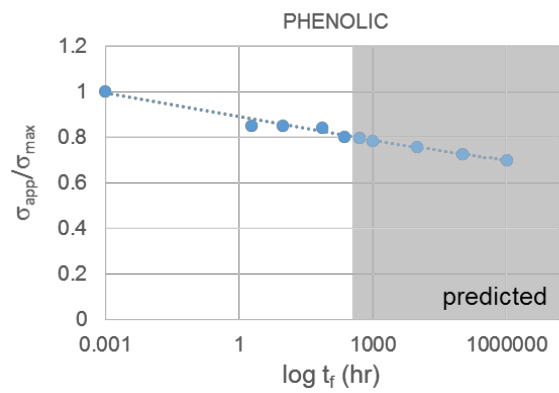
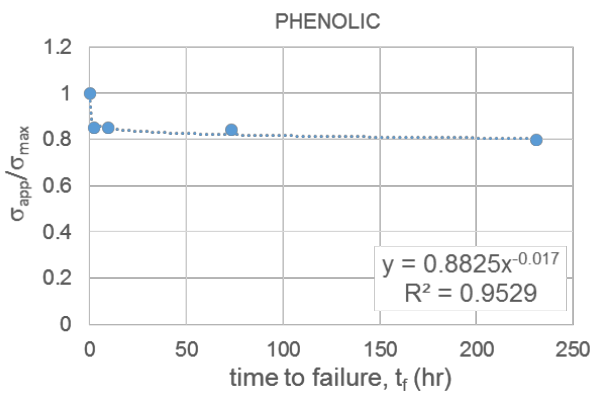


Figure 4-8: Exponential fit to phenolic creep experimental data and predicted failure behavior at long-term loading

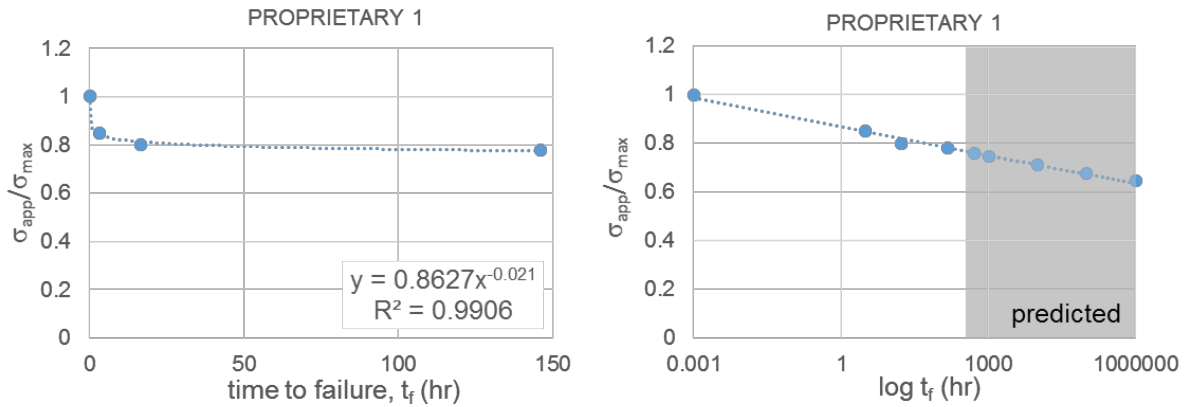


Figure 4-9: Exponential fit to proprietary 1 creep experimental data and predicted failure behavior at long-term loading

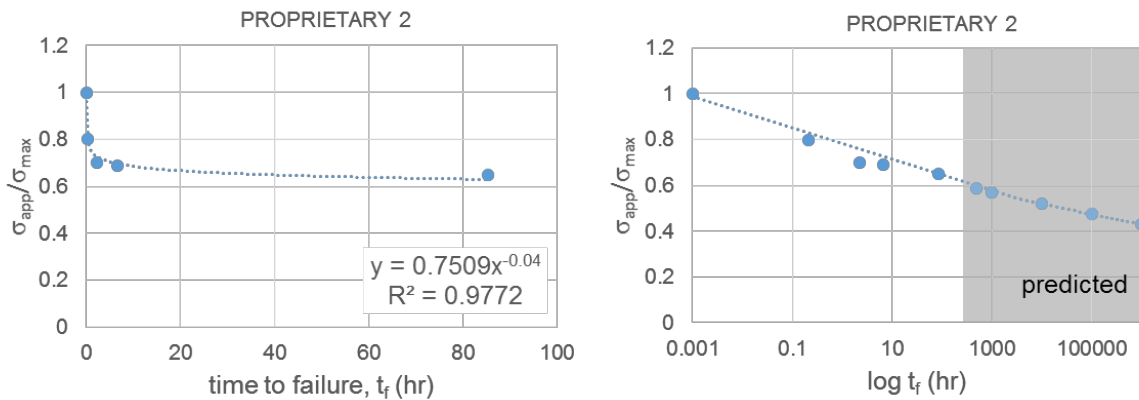


Figure 4-10: Exponential fit to proprietary 2 creep experimental data and predicted failure behavior at long-term loading

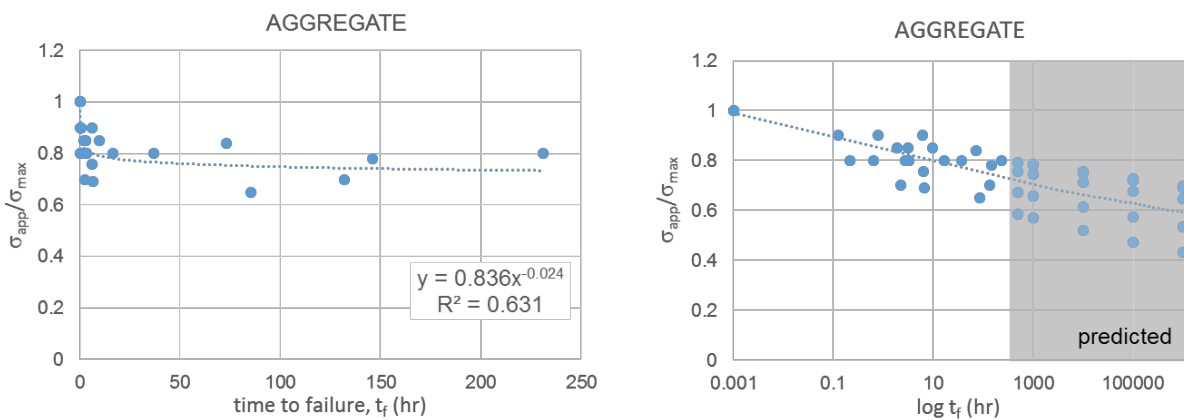


Figure 4-11: Exponential fit to aggregated creep experimental data and predicted failure behavior at long-term loading

4.3 Creep strain analysis

To further quantify creep performance, time series data of axial strain can be used to define and determine behavior. As discussed earlier, in a material that does not experience creep, the slope of

the secondary region will be equal to zero. Thus, the slope of this region provides a means of quantifying the amount a given material creeps under a stress ratio. For the materials tested, time series plots of axial strain are presented, as well as plots of the slope (m_2) of the secondary regions versus the applied stress ratios.

For this approach, tests that did not fail are useful, as many were tested far enough into the response spectrum to be experiencing creep strains, thus permitting calculation of the slope of the secondary creep region. These tests are indicated with dashed lines in the subsequent plots.

Vinylester specimens are presented in Figure 4-12 and Figure 4-13. Polyurethane results are shown in Figure 4-14 and Figure 4-15. Phenolic testing results are given in Figure 4-16 and Figure 4-17. Proprietary 1 results are shown in Figure 4-18 and Figure 4-19, while Proprietary 2 results are shown in Figure 4-20 and Figure 4-21.

Results in general are as anticipated. As stress ratio decreases, m_2 approaches zero. Phenolic resin tests display some inconsistency in the strain results not evident in the stress results, but these inconsistencies (smaller slopes at higher stress ratios) are conservative.

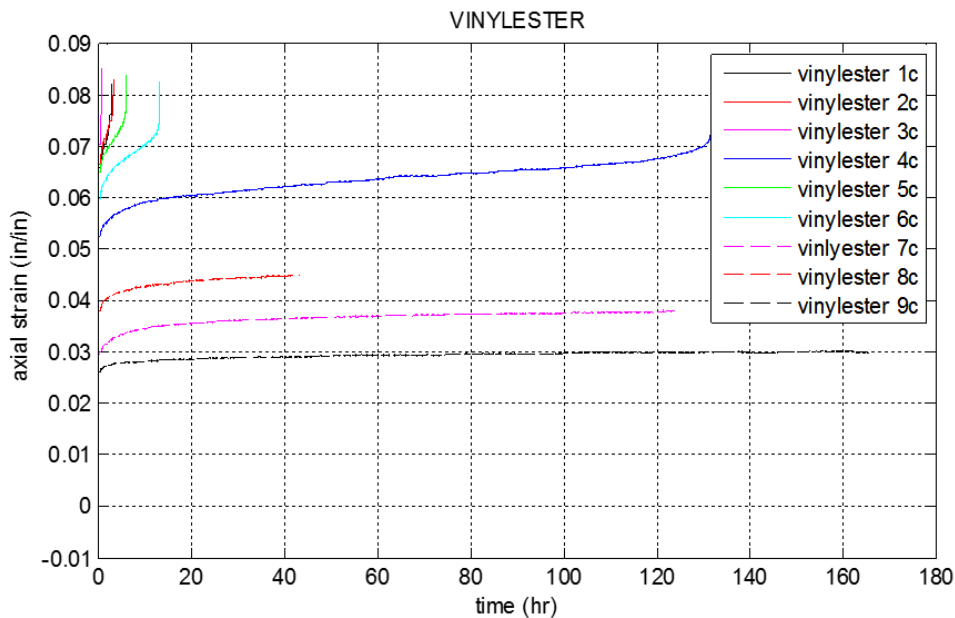


Figure 4-12: Strain versus time for vinylester creep specimens (note: specimens 7c, 8c, and 9c were not tested to failure).

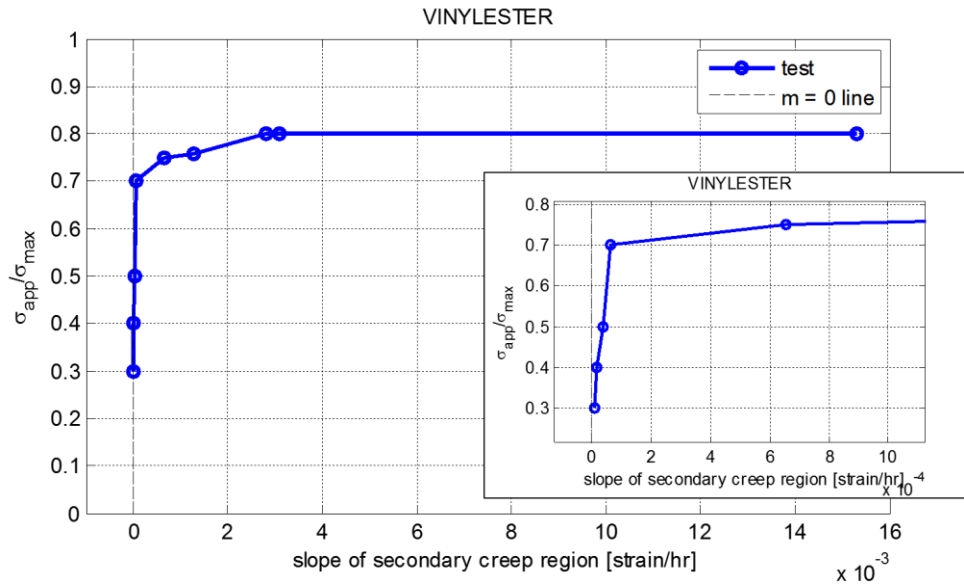


Figure 4-13: Stress ratio versus slope of secondary creep region for vinyl ester specimens. Inset highlights data near zero slope.

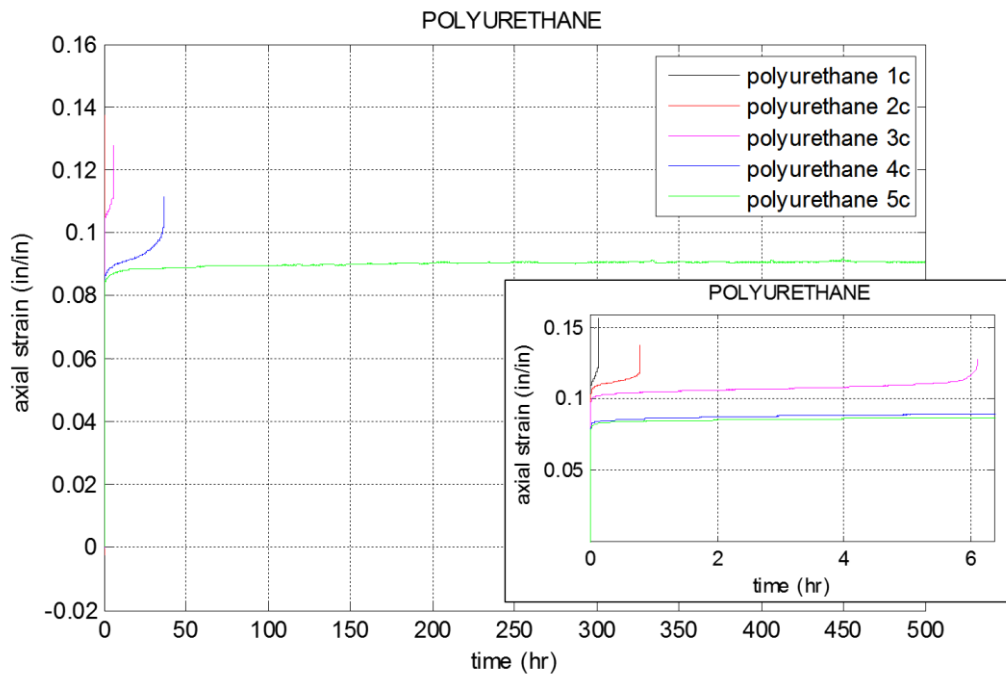


Figure 4-14: Strain versus time for polyurethane creep specimens (note: specimen 5c was not tested to failure). Inset details behavior of specimens with failure time < 6 hr.

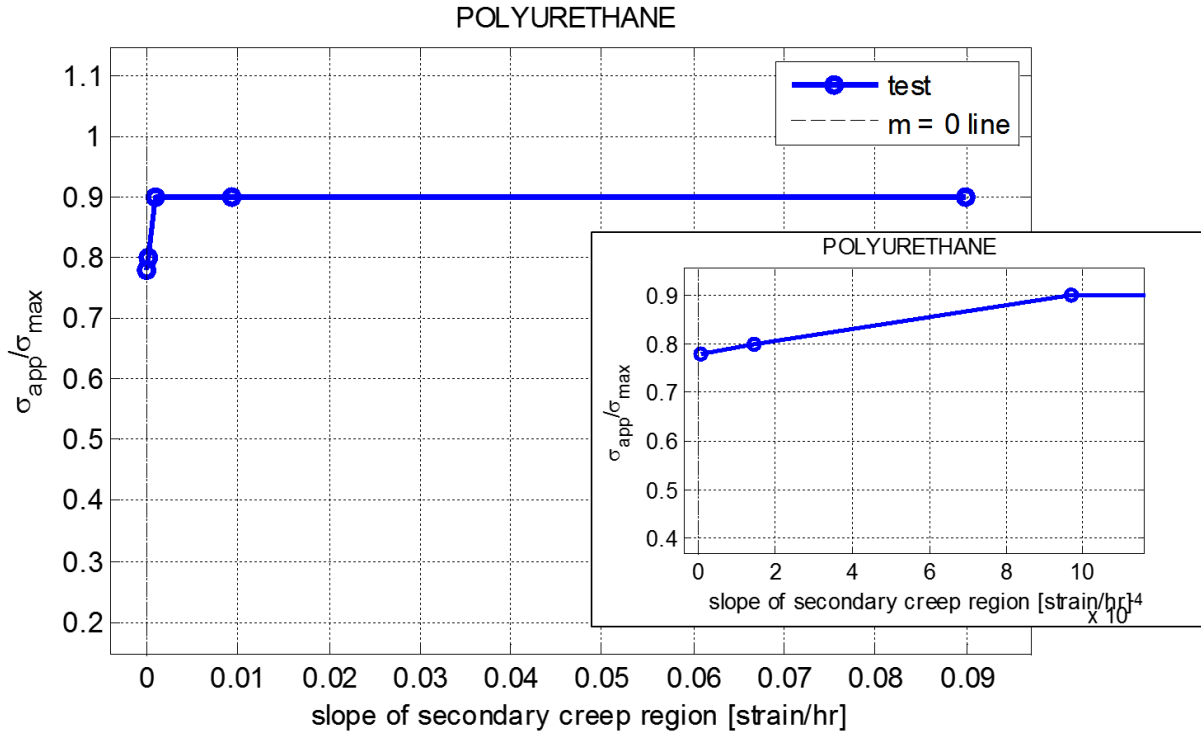


Figure 4-15: Stress ratio versus slope of secondary creep region for polyurethane specimens.

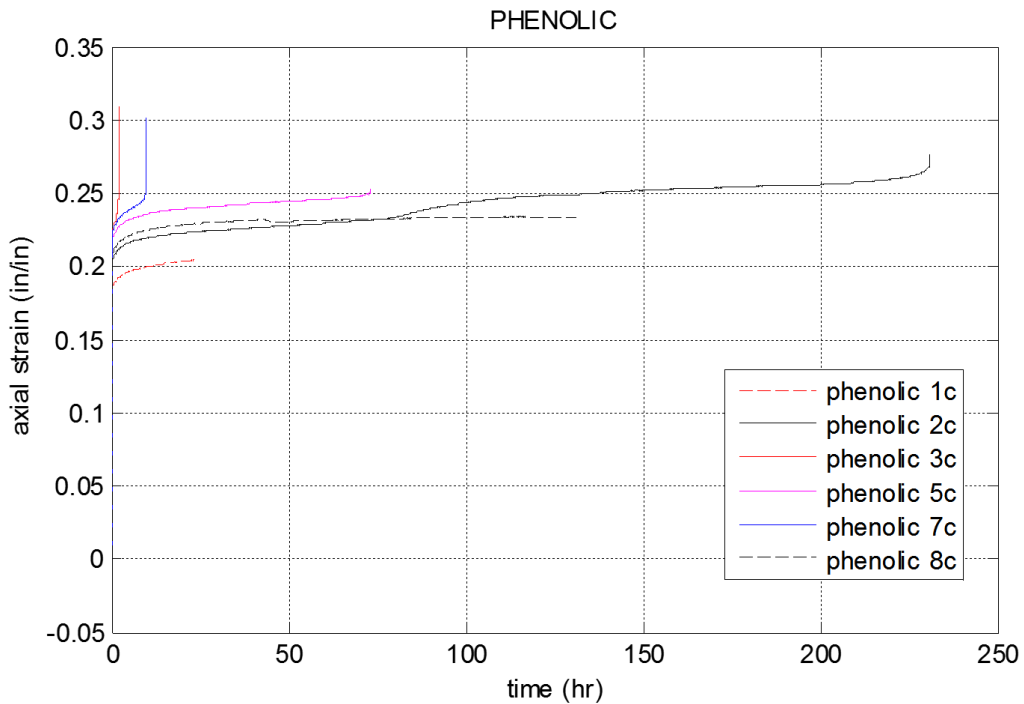


Figure 4-16: Strain versus time for phenolic creep specimens (note: specimens 1c and 8c were not tested to failure).

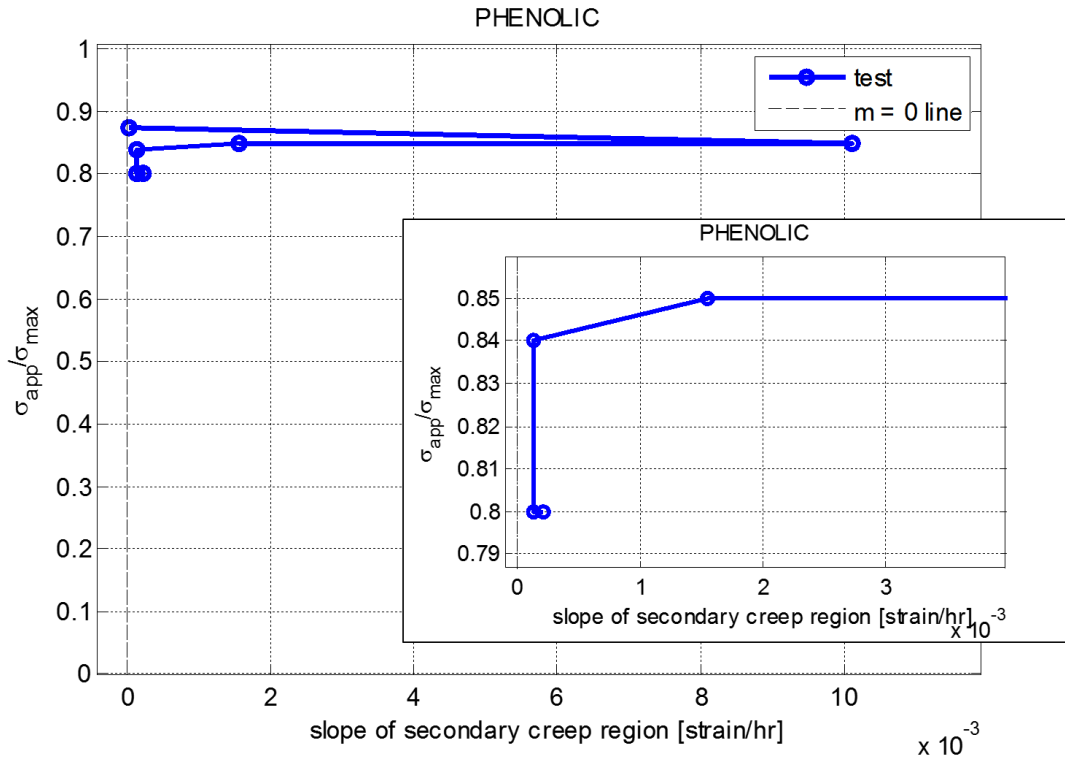


Figure 4-17: Stress ratio versus slope of secondary creep region for phenolic specimens. Inset highlights data near zero slope.

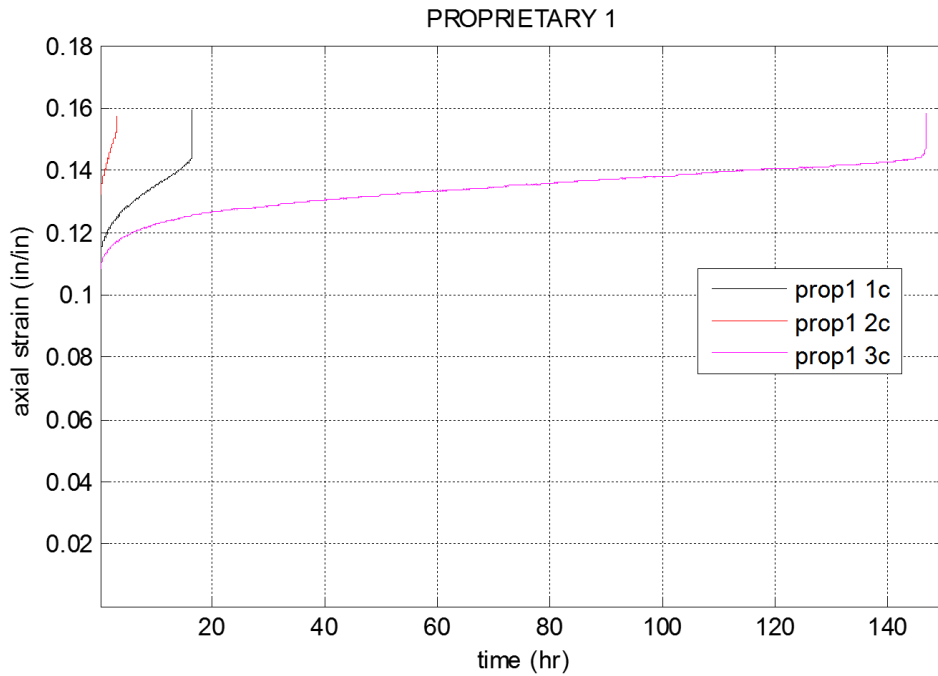


Figure 4-18: Strain versus time for proprietary 1 creep specimens

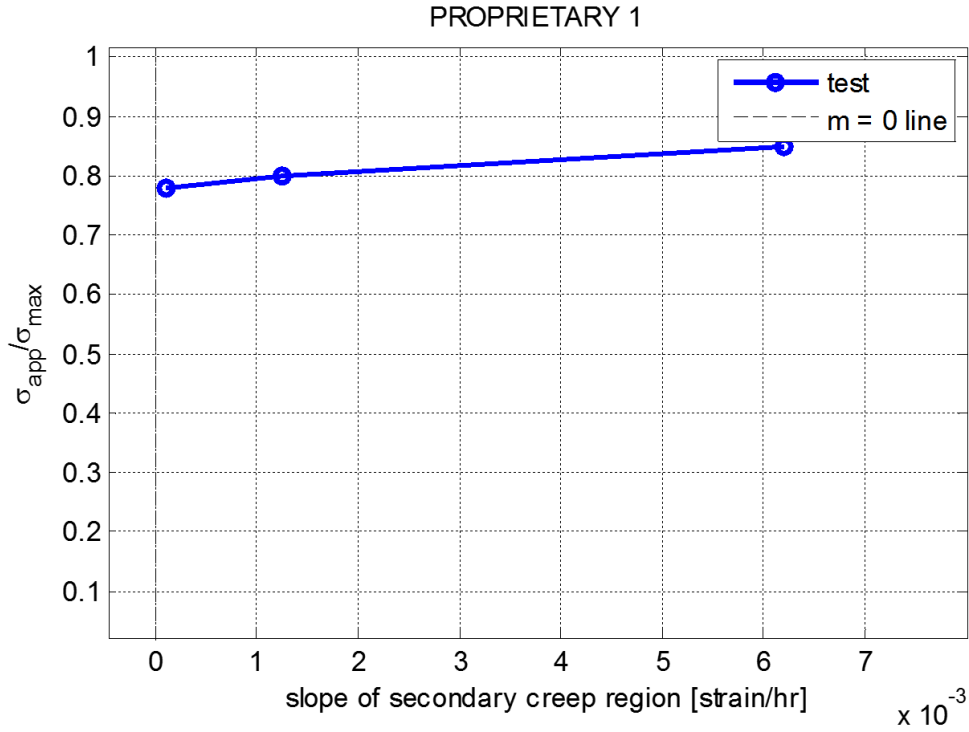


Figure 4-19: Stress ratio versus slope of secondary creep region for proprietary 1 specimens.

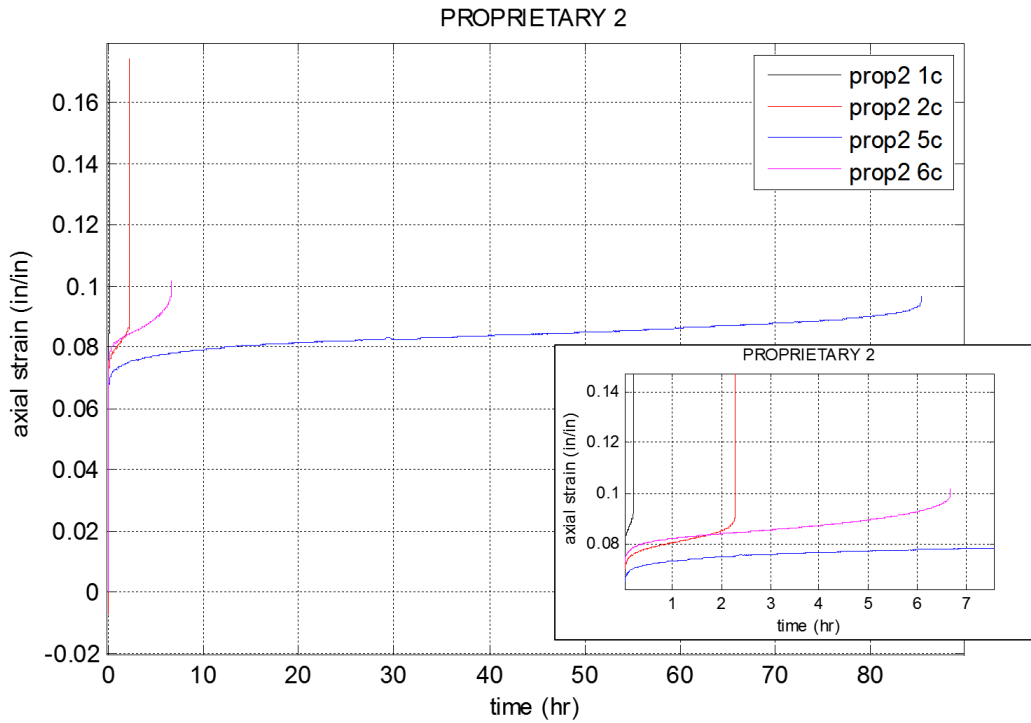


Figure 4-20: Strain versus time for proprietary 2 creep specimens. Inset details behavior of specimens with failure time < 1 hr.

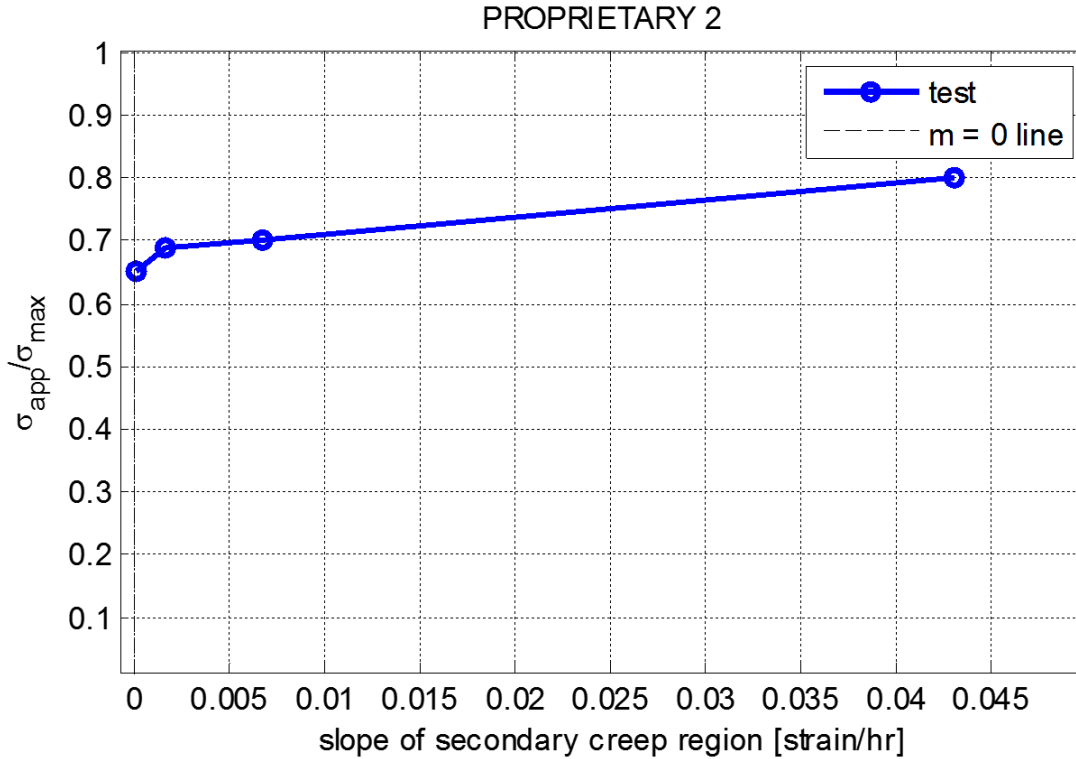


Figure 4-21: Stress ratio versus slope of secondary creep region for proprietary 2 specimens.

4.4 Recommendations for Design

Two methodologies for determining creep behavior have been presented herein. In the first, the applied stress ratio and time to failure were used to predict performance under long-term loads, up to 1,000,000 hours (approximately 114 years). With curve fits to the data, it may be seen that if the materials studied in this work are loaded at a stress ratio below 0.4 (40% of ultimate capacity), there is minimal risk of strain-based failure due to long-term creep within approximately 100 years. Figure 4-22 below identifies this limit on the aggregated data.

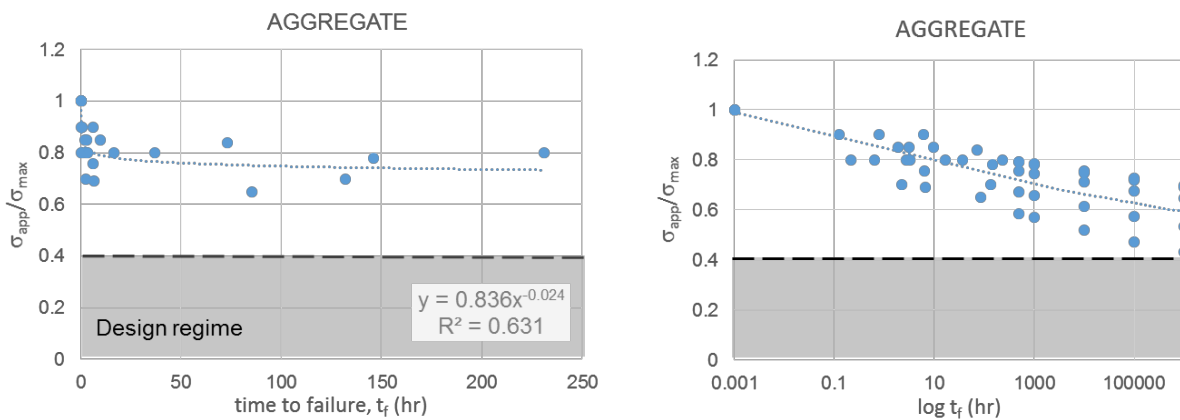


Figure 4-22: Design regime utilizing aggregated stress ratio vs. time to failure curves (reproduced from Figure 4-11)

In the second methodology, time series plots of strain were utilized to determine the slope of the secondary creep region. Hypothetically, materials that do not creep will have zero slope in this regime. Thus, the slopes of this region were determined for aggregated data and are shown in Figure 4-23 below. The proposed stress limit of 0.4 is also shown on the plot, and supports the conclusion that the materials studied in this work have little risk of failure due to creep within approximately 100 years.

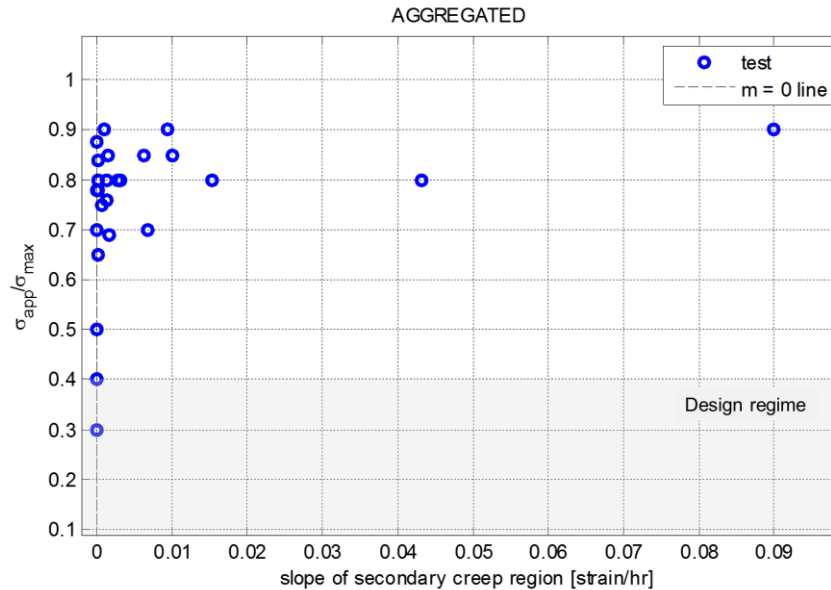


Figure 4-23: Stress ratios and slope of secondary creep region for aggregated data, indicating proposed design regime

While the above discussion identifies how to minimize risk of strain-based failure of the FRP materials in through-thickness compression due to combined elastic strain and creep strain, it is relevant to also try to document how much strain may occur within a design life if the material is loaded at or below a stress ratio of 0.4. The creep test results were thus interpolated to zero stress using the formula shown in Fig. 4-22 for each of the materials to demonstrate the time required to reach various stress ratio levels. As shown in Figure 4-24 and Table 4-2, the five materials studied would require 1.14×10^{96} years for a creep failure at low stress levels – beyond any imaginable service life. At a stress level of 0.3, it is estimated that it would require at least 1,000,000 years to fail in creep. While the data exists to propose unique stress limits on a per-material basis, the 0.4 reduction factor recommendation is conservative, with one material failing at around 100 years and the others failing in a much longer time frame. Capping the stress ratio at a value of 0.3 to 0.35 ensures much longer time frames before failure.

Table 4-2: Stress ratio and time to failure, interpolated to zero stress

time to failure		$\sigma_{app}/\sigma_{max}$				
hours	years	vinylester	polyurethane	phenolic	proprietary 1	proprietary 2
100000	11.41	0.574	0.720	0.726	0.677	0.474
1000000	114.08	0.536	0.691	0.698	0.645	0.432
1E+07	1140.77	0.500	0.663	0.671	0.615	0.394
1E+08	11407.71	0.467	0.636	0.645	0.586	0.359
1E+10	1.14E+06	0.406	0.585	0.597	0.532	0.299
1E+11	1.14E+07	0.379	0.561	0.574	0.507	0.273
1E+12	1.14E+08	0.354	0.539	0.552	0.483	0.249
1E+16	1.14E+12	0.269	0.456	0.472	0.398	0.172
1E+20	1.14E+16	0.204	0.387	0.403	0.328	0.119
1E+30	1.14E+26	0.102	0.255	0.273	0.202	0.047
1E+40	1.14E+36	0.051	0.169	0.184	0.125	0.019
1E+50	1.14E+46	0.026	0.112	0.125	0.077	0.008
1E+100	1.14E+96	0.001	0.014	0.018	0.007	0.000

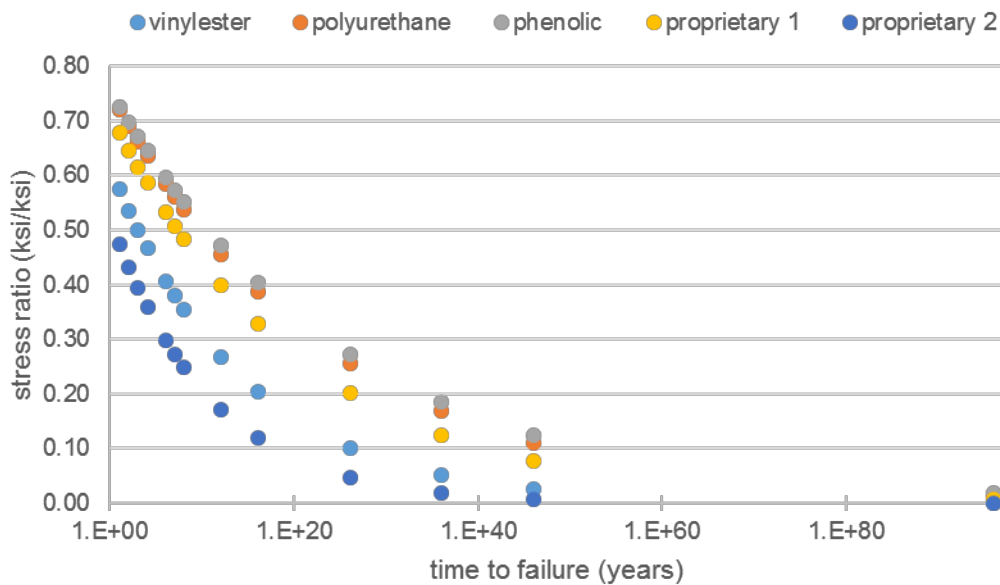


Figure 4-24: Stress ratio and time to failure, interpolated to zero stress

Using the material-specific equations developed in this Chapter, and the following constitutive relationship:

$$\epsilon_0 = \sigma_{max} E \left(\frac{\sigma_{app}}{\sigma_{max}} \right) \quad (1)$$

it is possible to predict the elastic strain for stress ratios unable to be tested to failure. Table 4-3 presents these elastic strain results.

Table 4-3: Prediction of elastic strain ϵ_0 for low stress ratios using material-specific curve fit equations detailed above.

$\sigma_{app}/\sigma_{max}$	vinylester		polyurethane		phenolic		proprietary 1		proprietary 2	
	t_f hours	ϵ_0 in/in	t_f hours	ϵ_0 in/in	t_f hours	ϵ_0 in/in	t_f hours	ϵ_0 in/in	t_f hours	ϵ_0 in/in
0.4	1.71E+10	0.025	1.51E+19	0.039	1.64E+20	0.066	7.86E+15	0.035	6.89E+06	0.031
0.3	2.49E+14	0.019	1.32E+26	0.029	3.67E+27	0.050	6.99E+21	0.026	9.15E+09	0.023
0.2	1.85E+20	0.013	8.00E+35	0.019	8.37E+37	0.033	1.70E+30	0.018	2.31E+14	0.016
0.1	2.00E+30	0.006	4.24E+52	0.010	4.27E+55	0.017	3.67E+44	0.009	7.75E+21	0.008

With these values, plotted at time 0, along with the mean failure strain from Table 4-1, plotted at the time to failure from Table 4-2, the secondary and tertiary creep regions may be approximated by linear interpolation for a given applied stress ratio, as shown schematically in Figure 4-25 below.

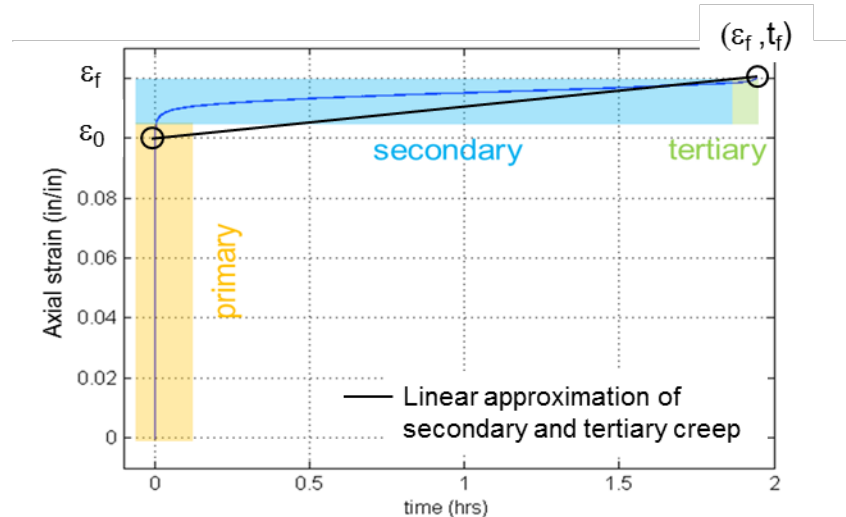


Figure 4-25: Linear approximation of secondary and tertiary creep regions using elastic strain, failure strain, and time to failure.

This linear interpolation can then be used to estimate the total strain, ϵ_{100} , at a common design time span, e.g., 100 years. This in turn provides an estimate for how much the material may creep at a given applied stress ratio. These results are tabulated in Table 4-4, along with proposed creep factors, $(\epsilon_0 + \epsilon_{100}) / \epsilon_0$.

Table 4-4: Strain at 100 years, ϵ_{100} , and creep factor $\epsilon_{100} / \epsilon_0$

$\sigma_{app}/\sigma_{max}$ ksi/ksi	vinylester		polyurethane		phenolic		proprietary 1		proprietary 2	
	ϵ_{100} in/in	$\epsilon_{100}/\epsilon_0$ in/in	ϵ_{100} in/in	$\epsilon_{100}/\epsilon_0$ in/in	ϵ_{100} in/in	$\epsilon_{100}/\epsilon_0$ in/in	ϵ_{100} in/in	$\epsilon_{100}/\epsilon_0$ in/in	ϵ_{100} in/in	$\epsilon_{100}/\epsilon_0$ in/in
0.4	0.025	1	0.039	1	0.066	1	0.035	1	0.039	1.24
0.3	0.019	1	0.029	1	0.050	1	0.026	1	0.023	1
0.2	0.013	1	0.019	1	0.033	1	0.018	1	0.016	1
0.1	0.006	1	0.010	1	0.017	1	0.009	1	0.008	1

Because 100 years is negligible compared to the time at failure for low stress levels (Table 4-3), ϵ_{100} is frequently nominally identical to ϵ_0 . The most notable exception is for Proprietary 2 at the 0.4 stress ratio.

5 Double lap splice bolted steel connections with fiber-reinforced polymer fills

To facilitate the development of design recommendations for thick and thin FRP fills (i.e., shims) in bolted steel connections, localized testing at the connection-level was conducted to characterize the effect of thermal breaks on the shear strength of steel connections. Because these FRP fills behave differently from steel, a complete panel of connection-level testing was conducted to characterize the behavior in bolted steel connections.

The performance of steel fillers in steel bolted connections has been investigated in North America by Lee and Fisher (1968), Frank and Yura (1981), Dusicka and Lewis (2010). Most recently, research by Borello et al. (2009, 2011) and Denavit et al. (2011) led to changes in AISC 360 (2010) related to the use of thick and thin steel fills in steel connections. Steel fills in steel bolted connections in bearing can reduce the strength of these connections by up to 15%; this reduction factor is contingent on the thickness of the steel fills (AISC 2010). The experiments conducted and described herein, while in the context of thermal bridging research, aim to build upon the body of experimental literature dedicated to double lap splice bolted steel connection testing.

5.1 Experimental setup and design

5.1.1 Test matrix

The test matrix is shown in Table 5-1. The bolt sizes included 1/2" and 5/8" diameter A325 carbon steel bolts, as well as 5/8" diameter A304-SH1 strain-hardened stainless steel bolts. Holes were specified as standard holes (bolt diameter + 1/16"), with the exception of tests C10 and C16O, which were specified as oversized. Fill thickness was varied between 1/4" and 1", and beyond 1", the effect of multiple plies was examined up to 3" of total fill thickness. FRP shims greater than 1" were not available from most manufacturers, so thicker tests had multiple plies. For most of the tests, multiple plies were not bonded together, as it was deemed that it may often be common in the field to not bond the plies together. However, most 1" thick material was delivered as two 1/2" plies bonded at the manufacturing site. Fill material was also varied between three different FRP materials, vinylester, phenolic, and polyurethane, and two FRP-based proprietary products. Bolts are specified as snug-tight, as that is deemed to be most commonly used in the field for these applications, and were installed by a single operator for the extent of testing.

Table 5-1: Experimental test matrix detailing bolt type, fill thickness and material, hole size, and rig size.

Test Name	Shim Type	Shim Thickness	Bolt Dia. (in)	Bolt Spec	Hole Size	Rig Thicknesses	
						Top	Bottom
C1	no shim	-	5/8	A325	11/16	4"	4"
C10	no shim	-	5/8	A325	13/16	4"	4"
C2	no shim	-	5/8	A304 SH1	11/16	4"	4"
C3	no shim	-	1/2	A325	9/16	4"	4"
C4	polyurethane	1/4"	5/8	A325	11/16	3.5"	4"
C5	vinylester	1/4"	5/8	A325	11/16	3.5"	4"
C6	phenolic	1/4"	5/8	A325	11/16	3.5"	4"
C7	proprietary 1	1/4"	5/8	A325	11/16	3.5"	4"
C8	proprietary 2	1/4"	5/8	A325	11/16	3.5"	4"
C9	vinylester	2x1/2" multiple plies	5/8	A325	11/16	2"	4"
C10	vinylester	1"	5/8	A325	11/16	2"	4"
C11	vinylester	1"	5/8	A304 SH1	11/16	2"	4"
C12	vinylester	1"	1/2	A325	9/16	2"	4"
C13	vinylester	2x1" multiple plies	5/8	A325	11/16	4"	8"
C14	vinylester	2x1" multiple plies	5/8	A304 SH1	11/16	4"	8"
C15	vinylester	2x1" multiple plies	1/2	A325	9/16	4"	8"
C16	vinylester	3x1" multiple plies	5/8	A325	11/16	2"	8"
C16O	vinylester	3x1" multiple plies	5/8	A325	13/16	2"	8"
C17	vinylester	3x1" multiple plies	5/8	A304 SH1	11/16	2"	8"
C18	vinylester	3x1" multiple plies	1/2	A325	9/16	2"	8"

Tests C9 and C10 directly explore the effect of bonding plies together, with test C9 comprised of two 1/2" unbonded plies and test C10 identical with the exception of using bonded plies.

5.1.2 Test rig

Similar to the work of Frank and Yura (1981), the test rig was constructed of a fixed base, 2" splice plates, and a 2" thick plate from which tension was applied. The rig was fabricated of welded Gr. 50 steel plate. The splice plates were connected to the fixed base via four 3/4" dia. A325 bolts which were installed snug tight along with the specimen bolts.

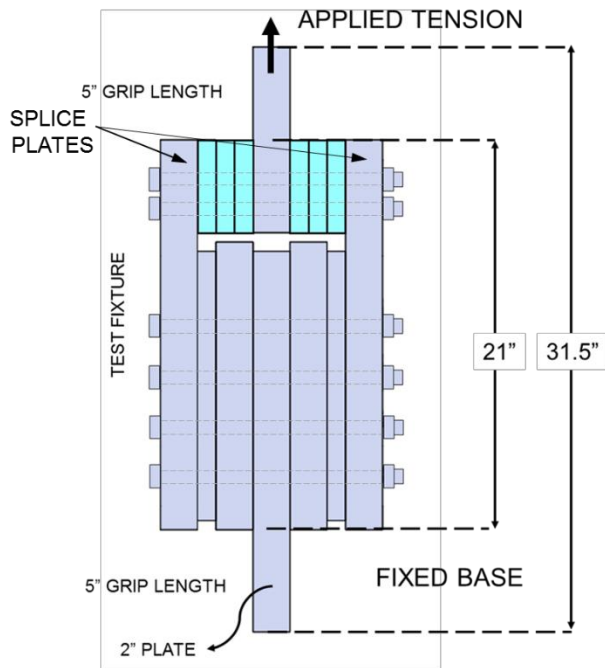


Figure 5-1: Schematic of test rig and photograph of specimen C16 (3" vinylester shims) installed in universal testing machine

Splice plates were 2" thick for all testing, and were flipped between tests such that each splice plate was used for two tests (thus the bearing surface of the splice plate bolt holes was new for every test). The top portion of the rig was variable in thickness to accommodate fill thickness ranging between $\frac{1}{4}$ " and 3". Figure 5-2 illustrates the edge distance, grip length, and specimen hole spacing for the 2" top portion of the rig.

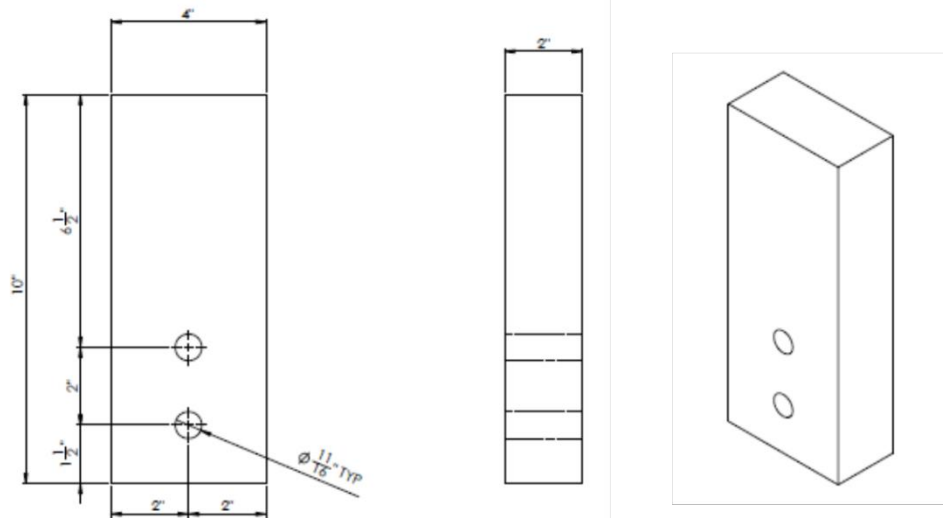


Figure 5-2: Top of rig, detailing specimen hole spacing and edge distance, consistent across testing. Edge distance (1.5") and hole spacing (2" on center) were constant across all specimens. The top rig plate was detailed to be a minimum of 2" thick. As shim configurations were varied throughout testing, the thickness of the top rig plate also varied to maintain structural integrity. To fit within the machine hydraulic grips, however, the gripped portion of the top rig plate could not exceed 2"

thick so a welded built-up configuration was used for a portion of the testing. The various rig configurations are illustrated in Figure 5-3. For tests utilizing the 8" base, bolts were 13" in length, and for tests utilizing the 4" base, bolts were 9" in length.

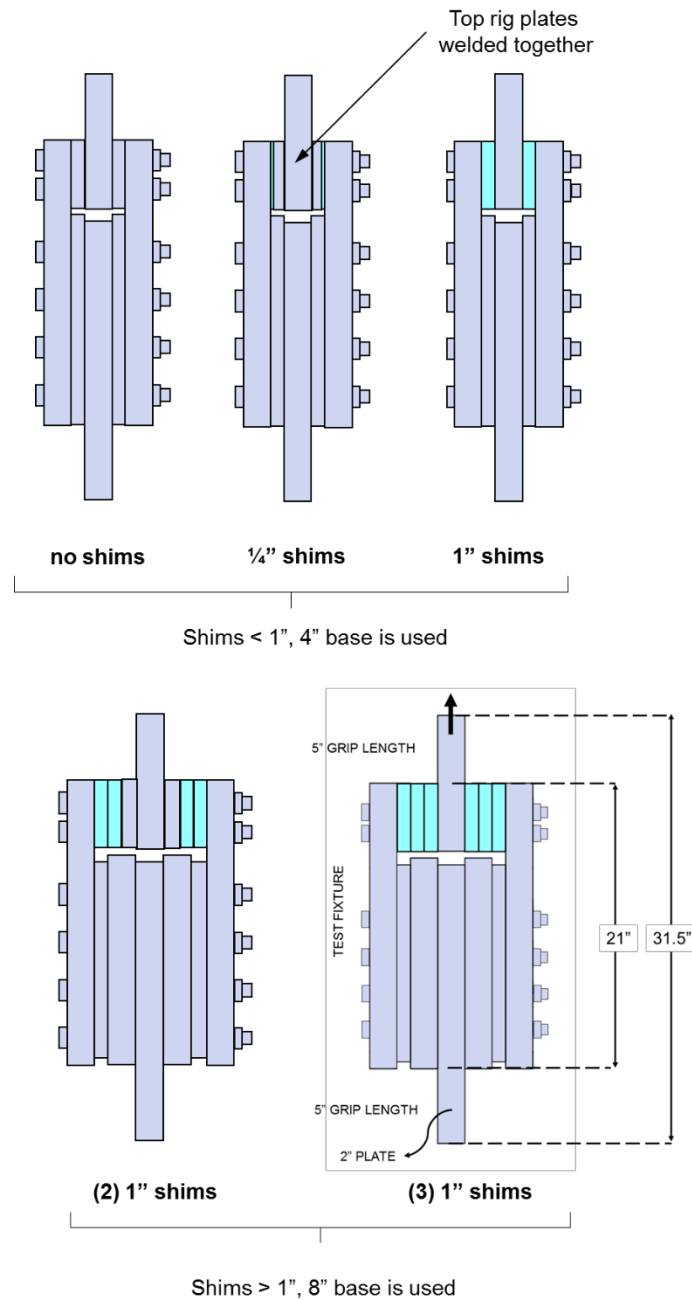


Figure 5-3: Test configuration for fills of varying thickness

5.1.3 Load protocol and sensors

Testing was conducted at the Simpson Gumpertz and Heger laboratory in Waltham, MA, using a Forney 600 kip universal testing machine. The test was controlled by retaining a constant flow of oil to the piston and responded in a manner comparable to a displacement-control test. Specimens

were loaded in monotonic tension at a rate of approximately 0.05 in/min. Actuator force and crosshead displacement (as measured by a linear variable differential transducer) were recorded throughout the tests.

5.2 Results and discussion

Table 5-2 presents the maximum force, crosshead displacement at maximum force ($\delta_{F_{max}}$) and stiffness. The values of P_{nt} are obtained via shear testing of bolts (the results are compiled and discussed in Appendix A). In the table, for bolted connections in shear, $\phi = 0.75$, and the bolt shear strengths were calculated assuming threads were excluded from the shear plane and two shear planes for each of the two bolts in the upper portion of the specimen, using the nominal strength specified in AISC (2010):

$$P_n = F_{nv} A_b \quad \text{Eq 5-1}$$

For the stainless steel bolts, the nominal tensile strength is 125 ksi per Equation 5-1. The nominal stainless steel bolt bearing strength is calculated using the same reduction factor, 0.563, in stress that is taken for the A325 bolts:

$$P_n = 0.563 F_u^{bolt} A_b \quad \text{Eq. 5-2}$$

The value of the bolt bearing strength from tested values (P_{nt}) were obtained using the mean of the tests done for each heat of bolts as reported in Appendix A.

Due to initial slack in the test rig and the presence of rig bolts, stiffness was determined after the engagement of the specimen bolts. This phenomena can be observed in Figure 5-4, at approximately 0.75" of crosshead displacement.

Table 5-2: Displacement at maximum force, maximum force, and stiffness across test specimens, compared to nominal and tested bolt strengths (shim material nomenclature: VE = vinylester, PU = polyurethane, PH = phenolic, P1 = proprietary 1, P2 = proprietary 2). Disaggregated means and standard deviations are given for 5/8" dia. bolts.

Test	Shim	Bolt Spec	NOMINAL STRENGTHS			TESTED STRENGTHS				
			$\delta_{P_{max}}$ in	P_{max} kip	k kip/in	P_n kip	ϕP_n kip	P_{nt} kip	ϕP_{nt} kip	P_{max}/P_{nt} -
<i>5/8" diameter bolts</i>										
C1	-	A325	0.91	116.1	347.6	83.45	62.59	86.06	64.55	1.35
C10	-	A325	0.72	137.4	453.0	83.45	62.59	86.06	64.55	1.60
C2	-	A304 SH1	1.10	129.3	341.9	86.36	64.77	84.50	63.38	1.53
C4	1/4" PU	A325	1.36	119.6	274.9	83.45	62.59	86.06	64.55	1.39
C5	1/4" VE	A325	1.37	117.7	280.1	83.45	62.59	86.06	64.55	1.37
C6	1/4" PH	A325	1.40	117.1	280.1	83.45	62.59	86.06	64.55	1.36
C7	1/4" P1	A325	1.26	112.8	317.1	83.45	62.59	86.06	64.55	1.31
C8	1/4" P2	A325	1.33	118.7	335.5	83.45	62.59	86.06	64.55	1.38
C9	2x1/2" VE	A325	1.66	110.0	78.08	83.45	62.59	86.06	64.55	1.28
C10	1" VE	A325	1.38	111.6	84.86	83.45	62.59	86.06	64.55	1.30
C11	1" VE	A304 SH1	1.91	122.0	72.81	86.36	64.77	84.50	63.38	1.44
C13	2x1" VE	A325	1.56	102.3	77.44	83.45	62.59	84.30	63.23	1.21
C14	2x1" VE	A304 SH1	2.02	103.8	66.47	86.36	64.77	85.79	64.34	1.21
C16	3x1" VE	A325	2.39	100.1	70.63	83.45	62.59	84.30	63.23	1.19
C16O	3x1" VE	A325	1.85	97.3	64.50	83.45	62.59	84.30	63.23	1.15
C17	3x1" VE	A304 SH1	2.56	107.2	70.24	86.36	64.77	85.79	64.34	1.25
<i>1/2" diameter bolts</i>										
C3	-	A325	0.77	74.06	265.2	53.41	40.06	48.26	36.20	1.53
C12	1" VE	A325	1.06	70.64	84.28	53.41	40.06	48.26	36.20	1.46
C15	2x1" VE	A325	1.38	65.10	62.08	53.41	40.06	56.08	42.06	1.16
C18	3x1" VE	A325	1.50	61.53	62.44	53.41	40.06	56.08	42.06	1.10
5/8" dia. Means	< 1" fills		1.18	121.09	328.76	83.81	62.86	85.87	64.40	1.41
	≥ 1" fills		1.91	106.24	76.25	84.03	63.02	85.30	63.98	1.25
	≥ 1" fills A304		2.17	111.00	69.84	86.36	64.77	85.36	64.02	1.30
	≥ 1" fills O		1.85	97.27	64.50	83.45	62.59	84.30	63.23	1.15
5/8" dia. Std Dev	< 1" fills		0.25	8.13	58.29	1.03	0.77	0.55	0.41	0.10
	≥ 1" fills		0.39	6.26	7.78	0.00	0.00	0.96	0.72	0.06
	≥ 1" fills A304		0.35	9.68	3.19	0.00	0.00	0.74	0.56	0.13
	≥ 1" fills O		-	-	-	-	-	-	-	-

Figure 5-4 and Table 5-2 demonstrate a range of behaviors, dependent largely on shim thickness, as well as on bolt material. Stainless steel bolts, while attaining peak strengths comparable to carbon steel bolts, do so at displacements greater than their carbon steel counterparts. Thin shims, designated as shims less than 1" thick, contribute to a slight decrease in stiffness by approximately 20%, and in strength, between 5% and 10%. Tests with 1" shims provided comparable strength of the thin shimmed tests, though not the stiffness, which is reduced by approximately 80%. Beyond 1" shim thicknesses, the reduction in stiffness increases to 82%, although there is no significant difference between 2" shims and 3" shims. The decrease in stiffness is accompanied by a modest decrease in strength, between 15-30%. The same was observed in Borello et al. (2009), who also indicated a strength reduction of 15% when multiple fills (two or more) were included in the

connection, and but only a reduction in stiffness of 20%, likely due to the relative properties of steel shims compared to FRP.

Table 5-3: Disaggregated stiffness and strength results (based on bolt material and hole size) for 5/8” diameter specimens (shim material nomenclature: VE = vinylester, PU = polyurethane, PH = phenolic, P1 = proprietary 1, P2 = proprietary 2)

	Test	Shim	k	k_m/k_{um}	$1 - k_m/k_{um}$	P_{max}	P_m/P_{um}^*	$1 - P_m/P_{um}$	P_{nt}	P_{max}/P_{nt}
	-	-	kip/in	%	%	kip	%	%	kip	-
k_m, P_m mitigated	C1	-	347.6	-	-	116.1	-	-	86.06	1.35
	C10	-	453	-	-	137.4	-	-	86.06	1.60
	C2	-	341.9	-	-	129.3	-	-	84.50	1.53
k_{um}, P_{um} unmitigated	C4	1/4" PU	274.9	79.09%	20.91%	119.6	103.01%	-3.01%	86.06	1.39
	C5	1/4" VE	280.1	80.58%	19.42%	117.7	101.38%	-1.38%	86.06	1.37
	C6	1/4" PH	280.1	80.58%	19.42%	117.1	100.86%	-0.86%	86.06	1.36
	C7	1/4" P1	317.1	91.23%	8.77%	112.8	97.16%	2.84%	86.06	1.31
	C8	1/4" P2	335.5	96.52%	3.48%	118.7	102.24%	-2.24%	86.06	1.38
	C9	2x1/2" VE	78.08	22.46%	77.54%	110	94.75%	5.25%	86.06	1.28
	C10	1" VE	84.86	24.41%	75.59%	111.6	96.12%	3.88%	86.06	1.30
	C11	1" VE	72.81	21.30%	78.70%	122	94.35%	5.65%	84.50	1.44
	C13	2x1" VE	77.44	22.28%	77.72%	102.3	88.11%	11.89%	84.30	1.21
	C14	2x1" VE	66.47	19.44%	80.56%	103.8	80.28%	19.72%	85.79	1.21
	C16	3x1" VE	70.63	20.32%	79.68%	100.1	86.22%	13.78%	84.30	1.19
	C16O	3x1" VE	64.5	14.24%	85.76%	79.3	57.71%	42.29%	84.30	0.94
	C17	3x1" VE	70.24	20.54%	79.46%	107.2	82.91%	17.09%	85.79	1.25
	Means		< 1" fills		87.23%	12.77%	116.58	100.93%	-0.41%	-
		≥ 1" fills		22.37%	77.63%	106.00	91.30%	8.70%	-	1.24
		≥ 1" fills A304		20.43%	79.57%	111.00	85.85%	14.15%	-	1.30
		≥ 1" fills O		14.24%	85.76%	79.30	57.71%	42.29%	-	0.94
Std Dev		< 1" fills		7.97%	7.97%	2.60	2.26%	2.26%	-	0.03
		≥ 1" fills		1.67%	1.67%	5.65	4.87%	4.87%	-	0.05
		≥ 1" fills A304		0.93%	0.93%	9.68	7.48%	7.48%	-	0.13
		≥ 1" fills O		-	-	-	-	-	-	-

* $P_m = P_{max}$ for mitigated (shimmed) specimens, $P_{um} = P_{max}$ for unmitigated (unshimmed) specimens

Disaggregated results from testing are presented in Table 5-3 and Table 5-4, in which shimmed specimens are compared to unshimmed (unmitigated) specimens of identical bolt types. For example, test C11, with stainless steel A304-SH1 bolts, is considered with respect to test C2, also with A304-SH1 bolts. Percent-reductions in strength and stiffness for specimens with shims larger than 1” are approximately 5% larger for stainless bolts than their carbon steel counterparts. Insufficient data exists to calculate representative statistics for oversized hole specimens, but the two existing tests suggest reductions in stiffness are significant, increasing to 40%.

Table 5-4: Disaggregated stiffness and strength results (based on bolt material and hole size) for 1/2" diameter specimens (shim material nomenclature: VE = vinylester, PU = polyurethane, PH = phenolic, P1 = proprietary 1, P2 = proprietary 2)

Test	Shim	k	k_m/k_u	$1 - k_m/k_u$	P_{max}	P_m/P_{um}^*	$1 - P_m/P_{um}$	P_{nt}	P_{max}/P_{nt}
-	-	kip/in	%	%	kip	%	%	kip	-
C3	-	265.2	-	-	74.06	-	-	48.26	1.53
C12	1" VE	84.28	31.78%	68.22%	70.64	95.38%	4.62%	48.26	1.46
C15	2x1" VE	62.08	23.41%	76.59%	65.1	87.90%	12.10%	56.08	1.16
C18	3x1" VE	62.44	23.54%	76.46%	61.53	83.08%	16.92%	46.08	1.34
Means	≥ 1" fills		26.24%	73.76%	65.76	88.79%	11.21%	-	1.32

* $P_m = P_{max}$ for mitigated (shimmed) specimens, $P_{um} = P_{max}$ for unmitigated (unshimmed) specimens

Examining tests C9 and C10, the difference between bonded and unbonded shims of equivalent thicknesses are modest. Bonded shims increased stiffness by 10%, and strength by 1-2%, and ultimately fail along the bond line. Unbonded shims permit increased displacements compared to the bonded case, as the shims first displace to their fullest extent before the shims ovalize from bearing of the bolts.

There is a difference in performance between shims of different materials, although they are within 5-10% of each other. Ultimately, additional testing of the polyurethane, phenolic, and proprietary products is necessary to accurately quantify these variations.

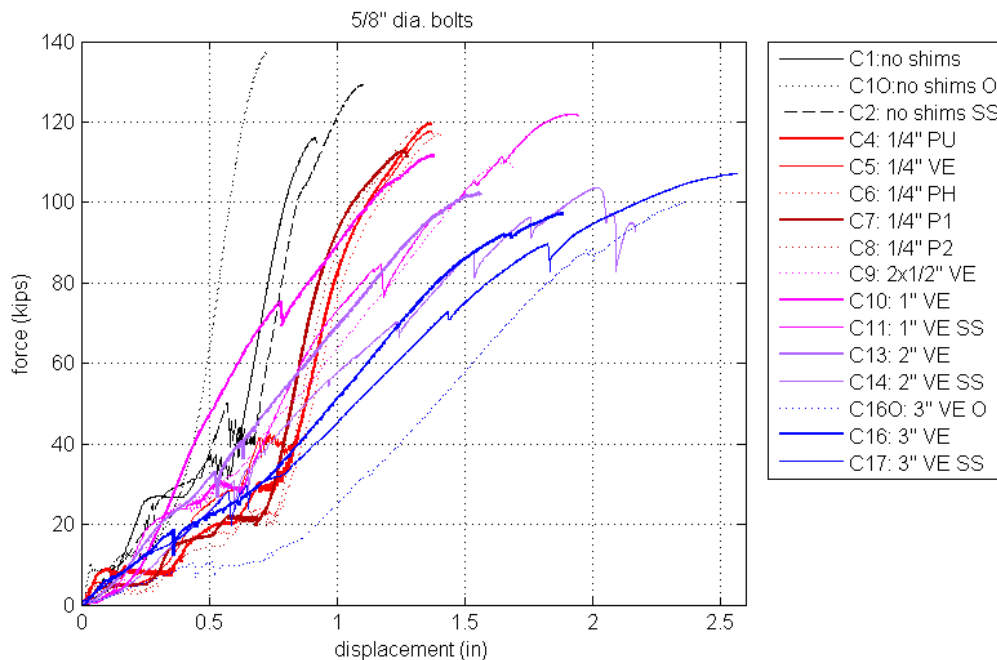


Figure 5-4: Force-displacement behavior of 5/8" diameter bolt specimens (VE = vinylester, PU = polyurethane, PH = phenolic, P1 = proprietary 1, P2 = proprietary 2, SS = stainless steel bolts, O = oversized holes)

Observations from the 5/8" diameter bolt tests are also consistent in the 1/2" diameter bolt tests, as shown in Figure 5-5 below. The trend of decreasing strength and stiffness with increased shim thicknesses is consistent across testing.

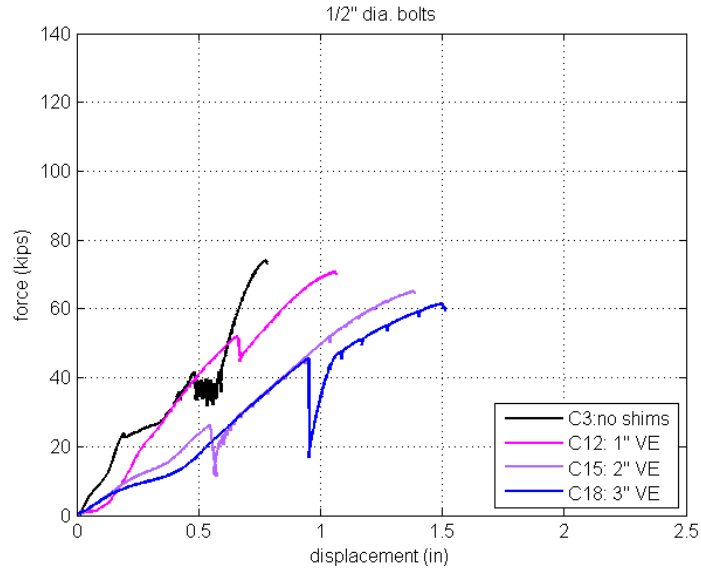


Figure 5-5: Force-displacement behavior of 1/2" diameter bolt specimens (VE = vinylester, PU = polyurethane, PH = phenolic, P1 = proprietary 1, P2 = proprietary 2, SS = stainless steel bolts, O = oversized holes)

Ultimately, two distinct patterns emerge: specimens without shims or with thin shims display a shear response, in which the bolts experience shear with finite tension and bending. In the cases with thick shims, tension and bending on the bolts dominate the response. These patterns are depicted in Figure 5-6 and Figure 5-7 below, evidenced by the unique shapes of the force-displacement response.

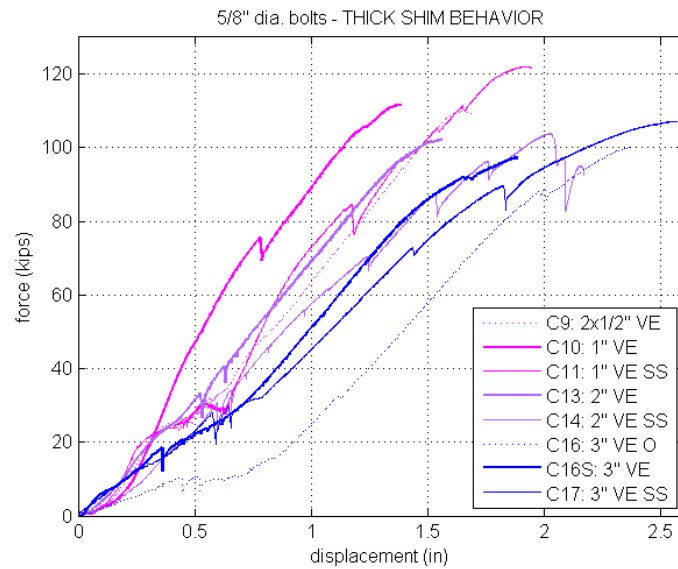


Figure 5-6: Behavior of 5/8" diameter connections tests with thick shims (1" or greater) (VE = vinylester, PU = polyurethane, PH = phenolic, P1 = proprietary 1, P2 = proprietary 2, SS = stainless steel bolts, O = oversized holes)

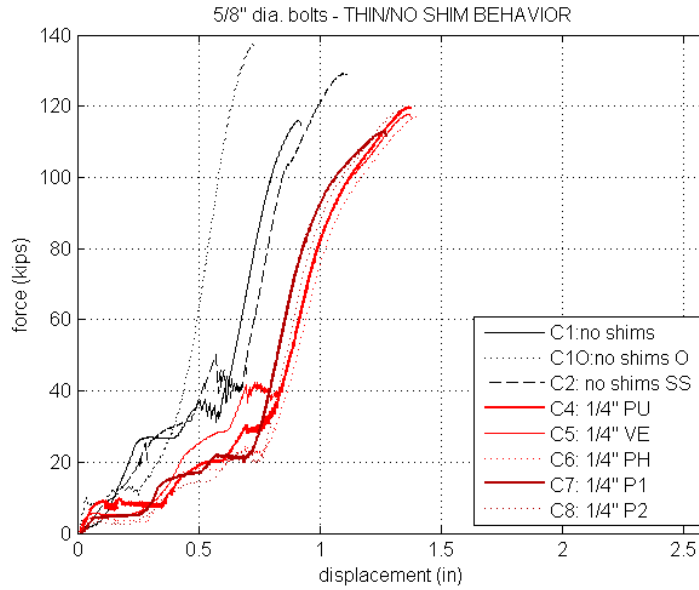


Figure 5-7: Behavior of 5/8” diameter connection tests with thin shims (1/4”) and no shims (VE = vinylester, PU = polyurethane, PH = phenolic, P1 = proprietary 1, P2 = proprietary 2, SS = stainless steel bolts, O = oversized holes)

Figure 5-8 and Figure 5-9 provide demonstrations of the distinct behavior patterns borne out by the data. In the case of thin shims, shear response dominates and the bolt shank deforms little and shears cleanly. In the case of thick shims, the bolt deforms significantly in tension and bending before fracture. Furthermore, the shims ovalize at the holes due to bearing from the bolt and delaminate. While it is ultimately the bolts that dictate failure, the shims influence the overall behavior by permitting additional displacement of the system (thereby decreasing the connection stiffness). The shim failure modes were consistent across testing.



Figure 5-8: Photographs of post-failure specimen bolts from test C1

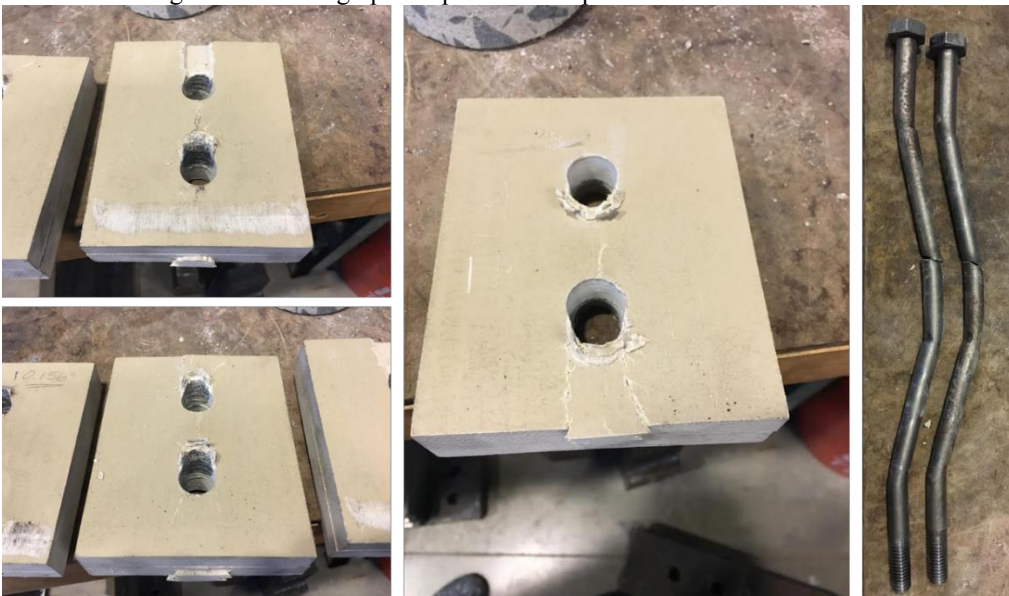


Figure 5-9: Photograph of post-failure specimens from test C16

5.3 Design Recommendations

Figure 5-10 below graphically represents the test-to-predicted ratios vs. shim thickness. As shim thicknesses increase, P_{max}/P_{nt} decreases, though remains above the predicted value using measured properties for all tests performed.

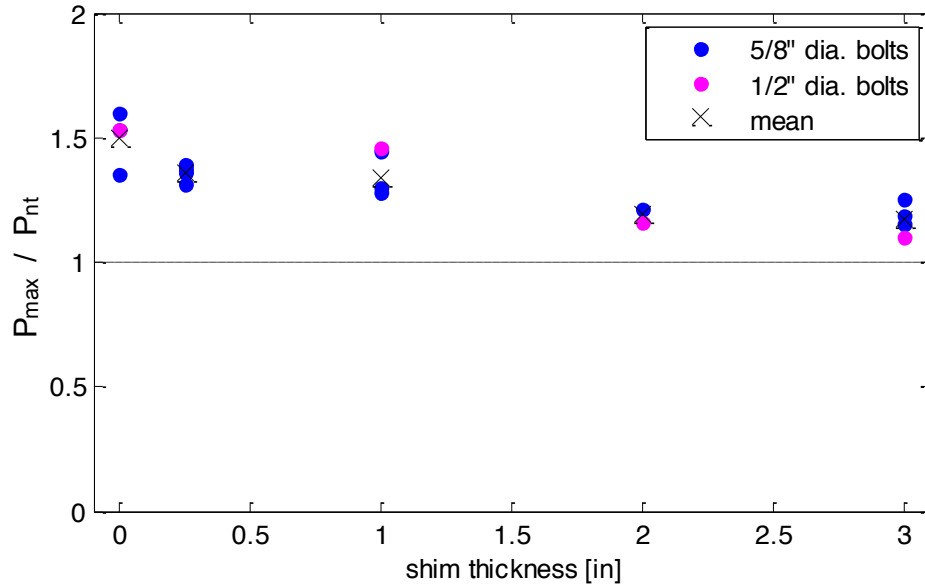


Figure 5-10: Comparison between test-to-predicted ratios per-shim thickness.

Differences between shimmed and un-shimmed specimens are also summarized in Table 5-5 below, which provides an aggregated summary of the results. The mean of test-to-predicted ratio is approximately 1.3, with an average stiffness reduction of 60% and an average strength reduction of 9% when shims are included in the connection. These values increase slightly for thick shims (1" or thicker).

Table 5-5: Summary of aggregated results

Test	k_m/k_u %	$1 - k_m/k_u$ %	P_{max} kip	$P_m/P_{um} * 1 - P_m/P_{um}$ %	P_{max}/P_{nt} -
≥ 1" fills both dia.	24.03%	75.97%	88.75	90.22%	1.28
All	39.51%	58.02%	101.22	90.72%	1.29

As may be seen from Table 5-2, assemblies with shims 2" thick or thicker have approximately a 10%-20% strength reduction from the case with no shims for A325 bolts. The reduction depends on the type of bolt, although all strength values remain above the ancillary bolt tests for bolts taken from the same heat. Shims thinner than 1" show little reduction in strength. A possible reduction formula may thus include a 20% reduction in bolt shear strength for FRP shims of any material that is 1 in. thick or thicker, though it should be noted that all of the data included in this survey are well above $P_{max}/P_{nt} = 1$. However, as bolt overstrength (discussed in Appendix A) is a contributing factor to the reported test-to-predicted ratios, the reduction factor is provided, as this overstrength is not typical.

This reduction factor fits well within the data, as shown in Figure 5-11 below.

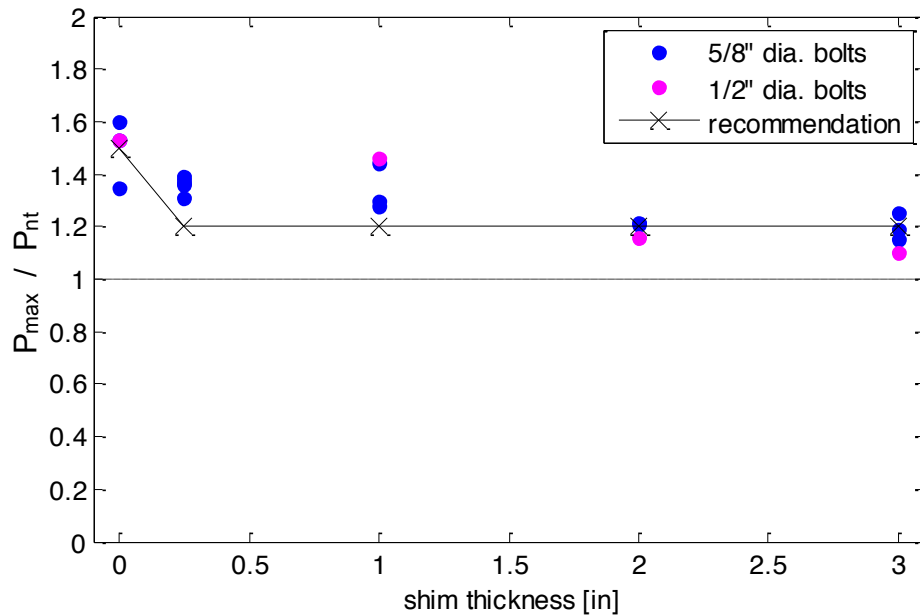


Figure 5-11: Recommended reduction factor of 0.8 for fills 1” or greater superimposed on the test data

For bolts in slip critical connections, Borello et al (2009) reported an approximate 20% reduction in stiffness for specimens with 3.75” steel fills (refer to Fig C.6 in Borello et al (2009)) and a significant increase in connection deformation (approximately 600% of the tests without fills). While the stiffness reductions observed in this series of tests is dramatic, only snug tight connections were examined, and the FRP shims did fail in bearing and delamination, contributing to a loss in stiffness. Ductility was observed to increase by approximately 350%.

6 Slab-Supported Shelf Angles

This chapter summarizes the results of the experimental tests and analyses of shelf-angle tests. Through these experiments, several different types of thermal break strategies were investigated to document their limit states. These solutions, highlighted in Chapter 1, include using a variety of FRP shims in the connection of the shelf angle to its support as well as an FRP section to support the cladding.

6.1 Experimental setup and design

6.1.1 Test matrix

The test matrix for the shelf angle tests is shown in Table 6-1 below. To accommodate for different cavity thicknesses in different Climate Zones (dictated by insulation thickness), two configurations were tested:

- Climate Zone 1: L6x4x5/16 shelf angles, 1.5” shims
- Climate Zone 7: L7x4x3/8 shelf angles, 3” shims

Bolt size and material were also varied in the testing. Efficiently designed specimens utilize 5/8” diameter A325X bolts while over-designed specimens utilize 1” diameter A325X bolts. Strain-hardened stainless steel bolts were also examined, and were up-sized from the efficiently designed case to match strength properties, as the yield strength of the stainless steel bolts was reported as 10 ksi lower than carbon steel bolts. Bolts on the shelf angles were installed at 36” on-center, and the shelf angles were 42” in length. Bolts were installed by a single operator and were specified as snug-tight.

While FRP shims were the focus of the survey, three additional strategies were investigated: pultruded FRP angle in place of a steel angle; carbon steel shims; and carbon steel tube shims (detailed in chapter 3 of this report).

Table 6-1: Experimental test matrix

Test Name	Specimen Type	Mitigation Strategy			Specimen Information			
		Type	Material	Thick (in)	Length	Section	Bolt/Stud Spec	Bolt Dia. (in)*
S1	designed	-	-	-	42	L6x4x5/16	A325	0.625
S2	designed	-	-	-	42	L6x4x5/16	A304-SH	0.75
S3	over-designed	-	-	-	42	L6x4x5/16	A325	1
S4	designed	-	-	-	42	L7x4x3/8	A325	0.625
S5	designed	-	-	-	42	L7x4x3/8	A304-SH	0.75
S6	over-designed	-	-	-	42	L7x4x3/8	A325	1
S7	over-designed	shim	vinylester	1.5	42	L6x4x5/16	A325	1
S8	designed	shim	vinylester	1.5	42	L6x4x5/16	A325	0.625
S9	over-designed	shim	polyurethane	1.5	42	L6x4x5/16	A325	1
S10	over-designed	shim	phenolic	1.5	42	L6x4x5/16	A325	1
S11	over-designed	shim	proprietary 1	1.5	42	L6x4x5/16	A325	1
S12	over-designed	shim	proprietary 2	1.5	42	L6x4x5/16	A325	1
S13	over-designed	shim	vinylester	3	42	L7x4x3/8	A325	1
S14	designed	shim	vinylester	3	42	L7x4x3/8	A325	0.625
S15	over-designed	shim	polyurethane	3	42	L7x4x3/8	A325	1
S16	over-designed	shim	phenolic	3	42	L7x4x3/8	A325	1
S17	over-designed	shim	proprietary 1	3	42	L7x4x3/8	A325	1
S18	over-designed	shim	proprietary 2	3	42	L7x4x3/8	A325	1
S19	over-designed	FRP angle	vinylester	-	42	FRP L6x4x1/2	A325	1
S20	over-designed	tube shim	carbon steel	HSS3x3x3/8	42	L7x4x3/8	A325	1
S21	over-designed	steel shim	carbon steel	3	42	L7x4x3/8	A325	1

*holes are standard holes (bolt diameter + 1/16 inch)

6.1.2 Test rig and protocol

The shelf angle test rig features three main components: the slab plate, to which the specimens are fastened; the load beam which connects to the actuator and directly loads the shelf angle horizontal leg; and a slider support system on which the load beam operates. These components are shown in Figure 6-1 and Figure 6-2 below. The slider system prevents the load beam from rotating out of plane, and maintains alignment with the actuator. Colloquially, the load beam acts as a guillotine.

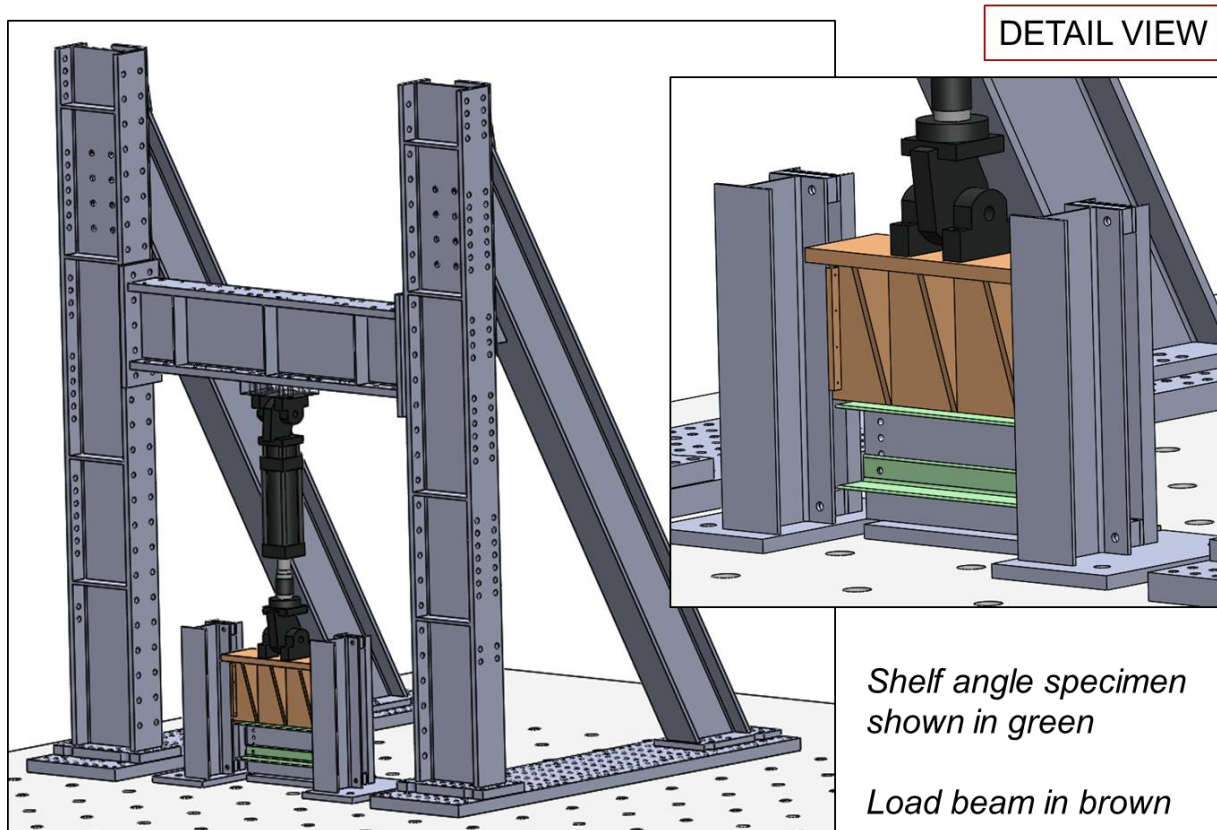


Figure 6-1: Test rig with load beam and specimen configuration shown in inset

While the load beam is of rectangular cross-sections, the load is applied only at the interior corner of the shelf angle. As the shelf angle horizontal leg deflects, the load is concentrated along this line for the remainder of testing. Because the shelf angle is continuously deflecting, the load beam slides along its horizontal leg, though the position of the load beam itself moves only vertically. Specimens were whitewashed prior to testing so that the motion of the load beam can be observed after the test. Photographs of the whitewashed specimens after the test are shown during the discussion of failure modes.

The slab plate is constructed of 2" thick steel, and is supported by two W sections behind the specimen so that the plate remains rigid during testing. This configuration was examined using finite element analysis and was determined rigid.

All tests were displacement-controlled monotonic tests to failure, at a rate of 0.05 in/min. While the design region for these specimens is limited to displacements lower than 0.25", most tests were pushed until 4 or 5" of crosshead displacement to fully-characterize the response.

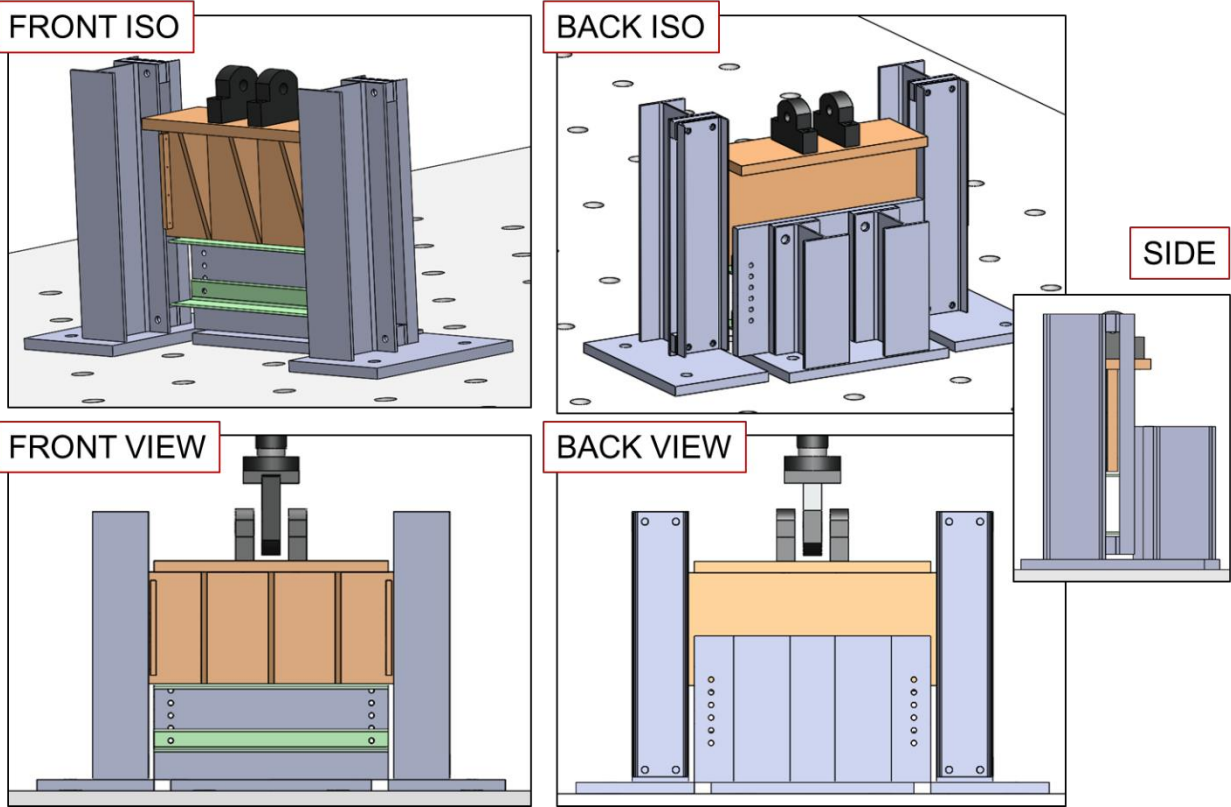


Figure 6-2: Detail views of shelf angle test rig

While the load beam and its location were initially designed to replicate the distance of the concrete slab (where the shelf angle is supported) to the brick veneer, the test rig was fabricated such that when erected this distance was reduced by 0.75". Figure 6-3 demonstrates the as-constructed condition. Note that these values are measured directly from the specimens in the rig.

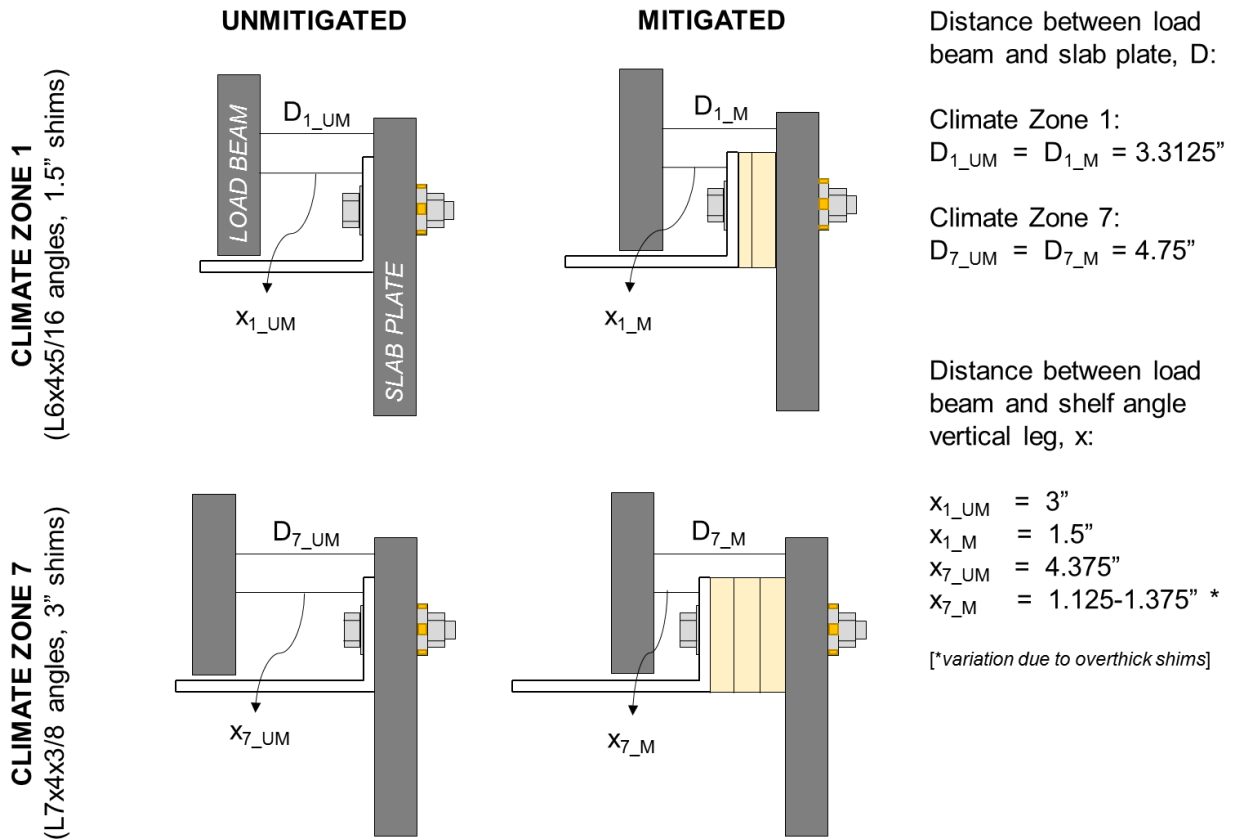


Figure 6-3: Schematic illustrating critical distances between loaded edge, shelf angle, and slab plate (note: drawings not to scale).

6.1.3 Instrumentation plan

To capture the motion of the shelf angle, position transducers were installed on the heel of the shelf angle, measuring in the horizontal and vertical directions. These were mounted on a rigid frame offset from the rig, and attached to the specimen via fishing line and strong magnetic hooks. Strain gauges were installed on the shelf angle horizontal leg heel at three locations: at the center line of the bolts and at the centerline of the angle.

To examine forces in the bolts, custom load cells were constructed and placed on each bolt prior to installation. These load cells act like thick washers (0.25" thick), and were sized to mimic the washers used for the specified bolts. On the circumference of the load cell were four strain gauges, reading compression of the cell. Using the constitutive relationships for the material and the geometry of the load cell, these readings are converted to forces later in this chapter. Load cells were calibrated using a universal testing machine, and compressed while strains were recorded from the gauges. The relation between applied compressive force and measured strain is then used to convert readings to force. Figure 6-4 provides a schematic of the instrumentation plan.

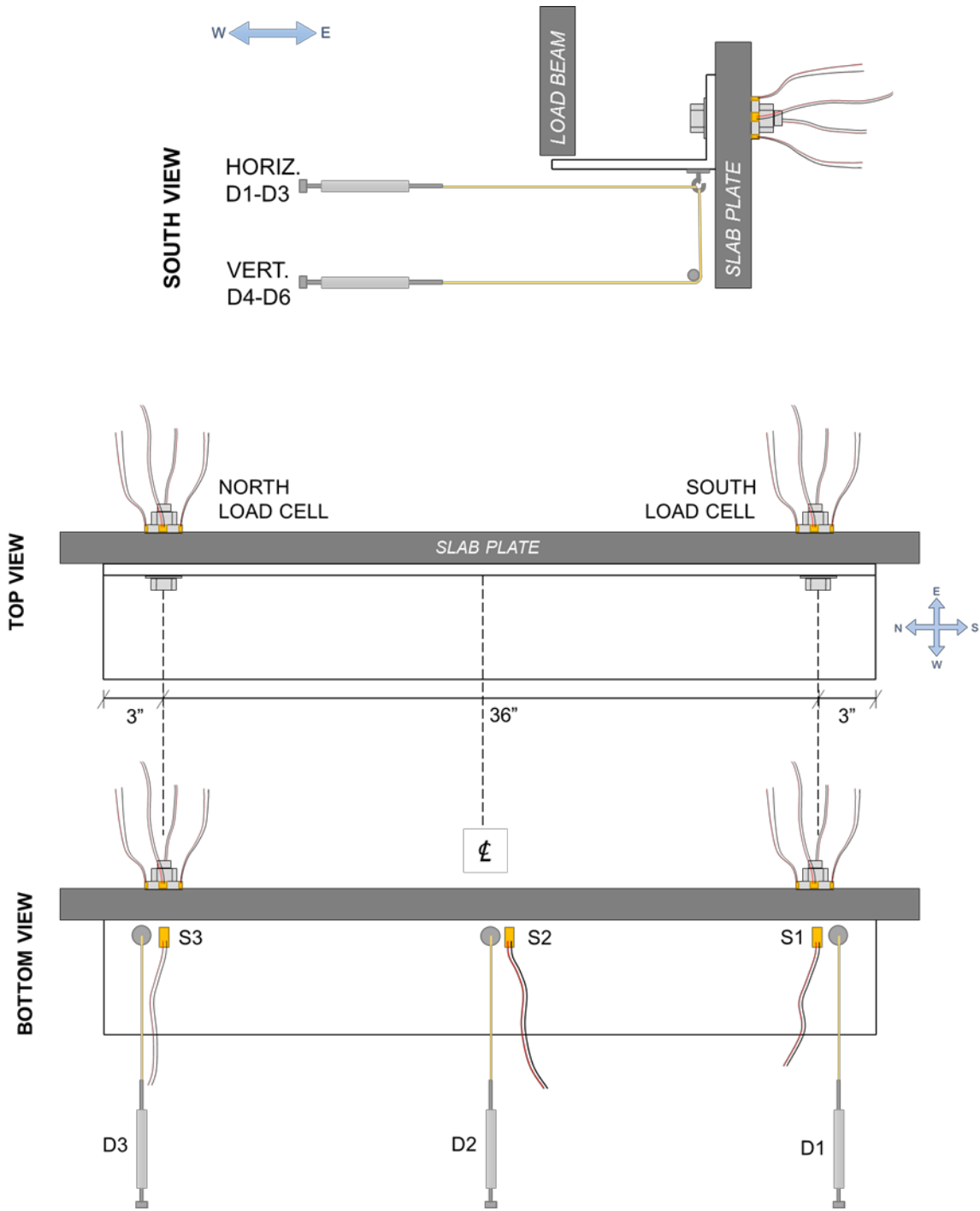


Figure 6-4: Schematic of sensor layout

A photograph of the position transducers and rigid frame is also shown in Figure 6-5 below.



Figure 6-5: Photograph of experimental setup, depicting horizontal position transducers D1-D3 in top row, and vertical position transducers D4-D6 in bottom row, both mounted to rigid frame.

6.2 Results and Discussion

This section presents results from the instrumentation data. For a breakdown of all available raw data for each test, refer to Appendix C.

6.2.1 Force-displacement results

Table 6-2 contains force and initial stiffness results across shelf angle testing. While mitigated specimens do reach larger forces and have increased initial stiffnesses from the unmitigated specimens, this is an artifact of the varying moment-to-shear ratios between specimens, and the decision to keep the wall cavity constant across testing. However, it is important to note that shim mitigation strategies do not negatively impact performance.

Table 6-2: Maximum force and initial stiffness across testing

Mitigation Strategy							
Test Name	Type	Thick <i>in.</i>	Angle	Bolt Spec	Bolt Dia. <i>in.</i>	F_{max} <i>kip</i>	k_i <i>kip/in</i>
<i>climate zone 1 specimens</i>							
S1	-	-	L6x4x5/16	A325	0.625	28.1	35.6
S2	-	-	L6x4x5/16	A304-SH	0.75	21.2	38.1
S3	-	-	L6x4x5/16	A325	1	23.4	45.4
S7	vinylester	1.5	L6x4x5/16	A325	1	40.0	106
S8	vinylester	1.5	L6x4x5/16	A325	0.625	29.6	76.0
S9	polyurethane	1.5	L6x4x5/16	A325	1	29.6	94.4
S10	phenolic	1.5	L6x4x5/16	A325	1	33.5	77.7
S11	proprietary 1	1.5	L6x4x5/16	A325	1	35.9	86.5
S12	proprietary 2	1.5	L6x4x5/16	A325	1	36.6	100
S19	vinylester	-	FRP L6x4x1/2	A325	1	2.76	12.7
<i>climate zone 7 specimens</i>							
S4	-	-	L7x4x3/8	A325	0.625	24.6	31.9
S5	-	-	L7x4x3/8	A304-SH	0.75	26.0	37.7
S6	-	-	L7x4x3/8	A325	1	28.6	26.7
S13	vinylester	3	L7x4x3/8	A325	1	67.2	81.2
S14	vinylester	3	L7x4x3/8	A325	0.625	26.2	64.9
S15	polyurethane	3	L7x4x3/8	A325	1	83.3	84.6
S16	phenolic	3	L7x4x3/8	A325	1	51.2	51.9
S17	proprietary 1	3	L7x4x3/8	A325	1	64.0	75.6
S18	proprietary 2	3	L7x4x3/8	A325	1	65.9	88.2
S20	carbon steel	HSS3x3x3/8	L7x4x3/8	A325	1	55.6	105
S21	carbon steel	3	L7x4x3/8	A325	1	89.8	134

Table 6-3 and Table 6-4, respectively, provide nominal and measured limit state calculations for the shelf angle specimens. Shelf angle bending, shelf angle shear, shim compression, bolt tension, bolt bending, and bolt shear are considered. Equations for these limit states are presented using the design equations outlined in Section 6.4. In this presentation of the results, the maximum force from the experiment is used in place of required strengths to compare to the strengths in each limit state using either nominal or measured material properties. Measured properties include results reported in Appendix A from tensile coupon tests of the shelf angle and bolt materials, and through-thickness compression tests for FRP materials. The design of shelf angle components is typically governed by deflection limits that are breached well below the strengths of these subassemblies; the forces at which the deflections are breached are small, equivalent to the weight of one story of brick cladding, which for the systems considered herein is approximately 1.7 kips (factored) in the prototype structure. In the results tables, test-to-predicted values higher than 1.0 indicate that the maximum experimental load exceeds the limit state, while values lower than 1 indicate that at the maximum load, the limit state was not exceeded. The latter typically corresponds to limit states that were overdesigned for these specimens. As an example, even the smaller bolts in these tests were designed to have conservative values for bolt shear relative to the experimental loads, so as to exercise the limit states on the shelf angle, FRP components, bolt

tension, and bolt bending, rather than being governed by bolt shear. Values presented are for the entire subassembly system (considering two bolts, for example).

As such, because these systems are governed by serviceability limit states, strength limit states aid in describing behavior but are typically engaged at loads well beyond the deflection limits. During the testing, shelf angles were observed to bend and buckle in the vertical leg and rotate about the angle heel. Consistent across testing, the first drops in load relate to shim failure, typically due to delamination along the bond line, if present, of shims made up of multiple layers bonded together. As shown in Figure 6-6 for tests representing Climate Zone 7, drops in force after the peak force are due primarily to compression failure of the shims at the heel of the shelf angle. As the shelf angle has rotated and deformed significantly at this point in the response, the shelf angle bears exclusively on the bottom edge of the shims. Thus, shim compression limit states based on the use of the complete area of the shim do not accurately describe this failure mode, since the bearing area of the shelf angle on the shim changes as the test progresses, and ultimately is reduced to a small portion of the total shim area. Furthermore, compression of the shim base creates interlaminar tension between fiber mat layers on the top half of the shim and results in delamination of the shim.

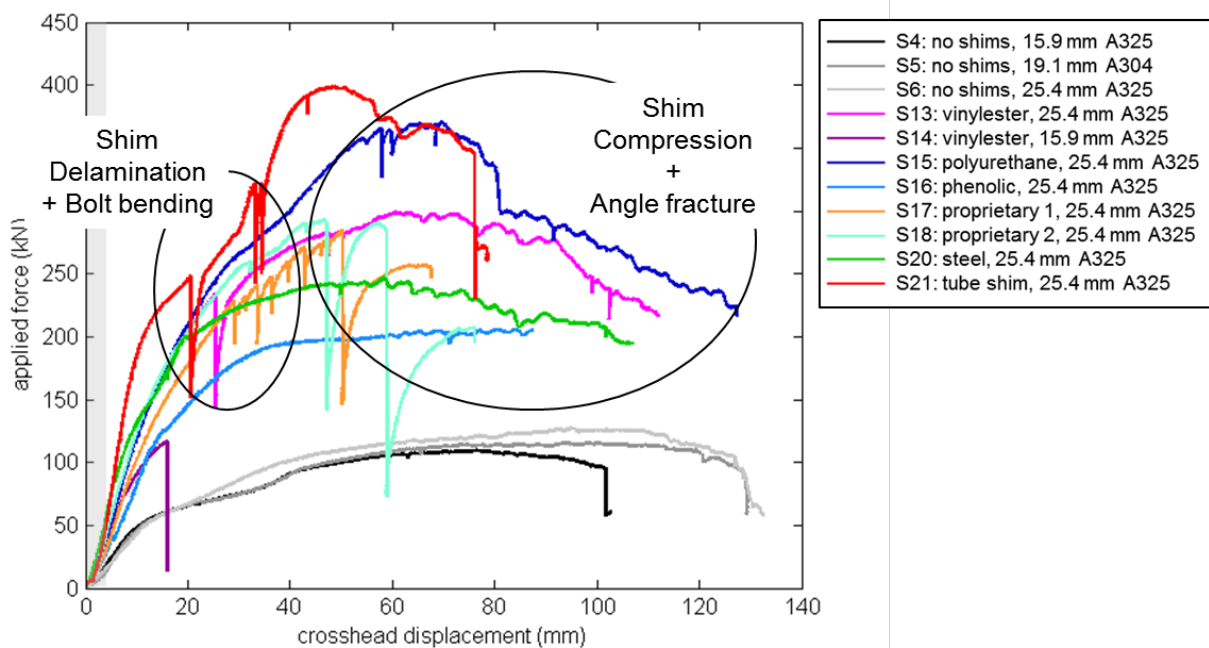


Figure 6-7: Force-displacement results for climate zone 7 specimens, indicating progression of failure for FRP shims.

Bolts were observed to deform significantly during testing, due to bolt bending induced by the eccentric applied force. This bending moment is amplified with the addition of thicker shims. Bolt bending and shelf angle bending were the controlling limit states for the climate zone 1 specimens, which involved a thinner shelf angle than in the climate zone 7 specimens. As the thinner shelf angle is more susceptible to bending and shear, the maximum forces attained were ultimately less

than those of the climate zone 7 specimens, which in turn lessened compression of the shims as well as the bolt limit states for these configurations. The thicker angle increased the strength of the system and the failure modes transitioned to include shim compression and bolt bending.

Ultimately, at extreme deformations all shelf angles experienced fracture near the angle heel on the vertical leg of the angle, indicating the participation of shelf angle bending in the overall response of the specimen. Bolt shear was not a dominant limit state as the bolts were not in pure shear, but rather a combination of shear, tension (exacerbated via the buckling of the vertical shelf angle leg, which pulled on the bolt), and bending (from the rotation of the shelf angle due to the applied loads). The maximum experimental forces were thus dictated primarily by shelf angle slenderness and bolt size.

Table 6-3: Limit states and test-to-predicted ratios across testing using nominal properties (detailed in Section 6.3)

NOMINAL PROPERTIES																
SHELF ANGLE BENDING			SHELF ANGLE SHEAR			SHIM COMP.		BOLT TENSION			BOLT BENDING			BOLT SHEAR		
M_u	M_n	M_u/M_n	f_v	F_v	f_v/F_v	f_{bu}	f_{bu}/F_v	T_{bu}	T_{bn}	T_{bu}/T_{bn}	M_{bu}	M_{bn}	M_{bu}/M_{bn}	V_n	V_b/V_n	
kip-in	kip-in	-	ksi	ksi	-	ksi	-	kip	kip	-	kip-in	kip-in	-	kip	-	
<i>climate zone 1 specimens</i>																
S1	42.16	7.03	6.00	165.30	21.60	7.65	-	-	-	55.22	-	-	4.31	-	41.72	0.67
S2	31.73	7.03	4.51	124.46	21.60	5.76	-	-	-	68.92	-	-	8.28	-	41.53	0.51
S3	35.14	7.03	5.00	137.97	21.60	6.39	-	-	-	141.37	-	-	17.67	-	106.81	0.22
S7	29.99	7.47	4.01	127.19	21.60	5.89	43.32	2.01	43.71	141.37	0.62	59.98	17.67	3.39	106.81	0.37
S8	22.22	7.47	2.97	94.00	21.60	4.35	33.53	1.55	31.32	55.22	1.13	44.44	4.31	10.30	41.72	0.71
S9	22.22	7.47	2.97	94.24	21.60	4.36	32.10	1.49	32.38	141.37	0.46	44.44	17.67	2.51	106.81	0.28
S10	25.10	7.47	3.36	106.44	21.60	4.93	36.25	1.68	36.58	141.37	0.52	50.19	17.67	2.84	106.81	0.31
S11	26.90	7.47	3.60	114.11	21.60	5.28	38.87	1.80	39.21	141.37	0.55	53.81	17.67	3.04	106.81	0.34
S12	27.48	7.47	3.68	116.55	21.60	5.40	39.70	1.84	40.05	141.37	0.57	54.96	17.67	3.11	106.81	0.34
S19	2.07	7.47	0.28	8.78	21.60	0.41	-	-	-	141.37	-	-	17.67	-	106.81	0.03
<i>climate zone 7 specimens</i>																
S4	107.77	14.40	7.49	157.55	21.60	7.29	-	-	-	55.22	-	-	4.31	-	41.72	0.59
S5	113.84	14.40	7.91	166.52	21.60	7.71	-	-	-	68.92	-	-	8.28	-	41.53	0.63
S6	125.09	14.40	8.69	183.19	21.60	8.48	-	-	-	141.37	-	-	17.67	-	106.81	0.27
S13	84.06	10.44	8.05	119.13	21.60	5.52	103.22	4.78	104.14	141.37	1.47	201.74	17.67	11.42	106.81	0.63
S14	32.74	10.44	3.14	46.15	21.60	2.14	42.00	1.94	39.23	55.22	1.42	78.58	4.31	18.21	41.72	0.63
S15	104.10	10.44	9.97	147.54	21.60	6.83	127.83	5.92	128.97	141.37	1.82	249.85	17.67	14.14	106.81	0.78
S16	64.03	10.44	6.13	90.75	21.60	4.20	78.63	3.64	79.32	141.37	1.12	153.67	17.67	8.70	106.81	0.48
S17	80.01	10.44	7.66	113.40	21.60	5.25	98.25	4.55	99.12	141.37	1.40	192.03	17.67	10.87	106.81	0.60
S18	82.36	10.44	7.89	116.73	21.60	5.40	101.14	4.68	102.03	141.37	1.44	197.67	17.67	11.19	106.81	0.62
S20	69.49	10.44	6.66	98.49	21.60	4.56	85.33	3.95	86.09	141.37	1.22	166.78	17.67	9.44	106.81	0.52
S21	112.19	10.44	10.74	159.00	21.60	7.36	137.76	6.38	138.98	141.37	1.97	269.25	17.67	15.24	106.81	0.84

Table 6-4: Limit states and test-to-predicted ratios across testing using measured properties (detailed in Section 6.3)

MEASURED PROPERTIES																
SHELF ANGLE BENDING				SHELF ANGLE SHEAR			SHIM COMP.		BOLT TENSION			BOLT BENDING			BOLT SHEAR	
M_u	M_n	M_u/M_n		f_v	F_v	f_v/F_v	f_{bu}	f_{bu}/F_v	T_{bu}	T_{bn}	T_{bu}/T_{bn}	M_{bu}	M_{bn}	M_{bu}/M_{bn}	V_n	V_u/V_n
<i>kip-in</i>	<i>kip-in</i>	-		<i>ksi</i>	<i>ksi</i>	-	-	-	<i>ksi</i>	<i>ksi</i>	-	<i>kip-in</i>	<i>kip-in</i>	-	<i>kip</i>	-
S1	42.16	9.84	4.28	165.30	30.24	5.47	-	-	-	66.88	-	-	5.23	-	41.34	0.68
S2	31.73	9.84	3.22	124.46	30.24	4.12	-	-	-	81.18	-	-	7.61	-	58.40	0.36
S3	35.14	9.84	3.57	137.97	30.24	4.56	-	-	-	181.32	-	-	22.67	-	110.92	0.21
S7	29.99	10.46	2.87	127.19	30.24	4.21	43.32	2.01	87.71	181.32	0.48	59.98	22.67	2.65	110.92	0.36
S8	22.22	10.46	2.12	94.00	30.24	3.11	33.53	1.55	63.04	66.88	0.94	44.44	5.23	8.50	41.34	0.72
S9	22.22	10.46	2.12	94.24	30.24	3.12	32.10	1.49	64.53	181.32	0.36	44.44	22.67	1.96	110.92	0.27
S10	25.10	10.46	2.40	106.44	30.24	3.52	36.25	1.68	74.84	181.32	0.41	50.19	22.67	2.21	110.92	0.30
S11	26.90	10.46	2.57	114.11	30.24	3.77	38.87	1.80	78.76	181.32	0.43	53.81	22.67	2.37	110.92	0.32
S12	27.48	10.46	2.63	116.55	30.24	3.85	39.70	1.84	80.26	181.32	0.44	54.96	22.67	2.42	110.92	0.33
S19	2.07	10.46	0.20	8.78	30.24	0.29	-	-	-	181.32	-	-	22.67	-	110.92	0.02
S4	107.77	21.67	4.97	157.55	32.52	4.84	-	-	-	33.44	-	-	5.23	-	41.34	0.60
S5	113.84	21.67	5.25	166.52	32.52	5.12	-	-	-	81.18	-	-	7.61	-	58.40	0.45
S6	125.09	21.67	5.77	183.19	32.52	5.63	-	-	-	181.32	-	-	22.67	-	110.92	0.26
S13	84.06	15.72	5.35	119.13	32.52	3.66	103.22	4.78	209.11	181.32	1.15	201.74	22.67	8.90	110.92	0.61
S14	32.74	15.72	2.08	46.15	32.52	1.42	42.00	1.94	79.06	66.88	1.18	78.58	5.23	15.04	41.34	0.63
S15	104.10	15.72	6.62	147.54	32.52	4.54	127.83	5.92	257.21	181.32	1.42	249.85	22.67	11.02	110.92	0.75
S16	64.03	15.72	4.07	90.75	32.52	2.79	78.63	3.64	162.34	181.32	0.90	153.67	22.67	6.78	110.92	0.46
S17	80.01	15.72	5.09	113.40	32.52	3.49	98.25	4.55	199.23	181.32	1.10	192.03	22.67	8.47	110.92	0.58
S18	82.36	15.72	5.24	116.73	32.52	3.59	101.14	4.68	204.60	181.32	1.13	197.67	22.67	8.72	110.92	0.59
S20	69.49	15.72	4.42	98.49	32.52	3.03	85.33	3.95	137.02	181.32	0.76	166.78	22.67	7.36	110.92	0.50
S21	112.19	15.72	7.14	159.00	32.52	4.89	137.76	6.38	221.22	181.32	1.22	269.25	22.67	11.88	110.92	0.81

Figure 6-8 depicts actuator force versus crosshead displacement for Climate Zone 7 specimens (L7x4 angles and 3” shims where applicable). As shelf angles are typically stiffness-controlled details, the region of interest for design purposes (displacements <0.25”) is also shown in the inset. The unmitigated specimens (S4, S5, S6) demonstrate similar performance despite utilizing different bolt sizes, materials, and diameters. While solutions with steel shims or tube shims represent the stiffest and strongest strategies, the FRP shimmed specimens fall within the lower bound defined by the unmitigated strategies and the upper bound defined by the steel shims and tube shims (as shown in Figure 6-8 below). This is due to the assumption that wall cavity thickness must remain constant despite thermal break mitigation, and that shelf angle sizes must also change to accommodate shims. This results in a shorter angle leg, and thus a more favorable moment-to-shear ratio than in the unmitigated details. Drops in load from failure of the shims do not begin to occur until well beyond the elastic region of the response, and beyond 1” of crosshead displacement.

Ultimately, the shelf angles fractured near the angle heel, experienced significant buckling deformations at the midspan, and exhibited local deformations around the bolts. Compression on the base of the shims (where the angle heel comes into contact with the shim) caused both crushing at the base and delamination of the layers at the top.

Specimens with the Proprietary 1, Proprietary 2, and vinylester shims all achieved peak strengths within 5% of each other. The phenolic and polyurethane shims were respectively 30% weaker and 30% stronger than the vinylester shims. These strength variations correspond to the flatwise

compressive strengths of the FRP materials themselves, and suggest that shim behavior does impact specimen behavior at extreme loads.

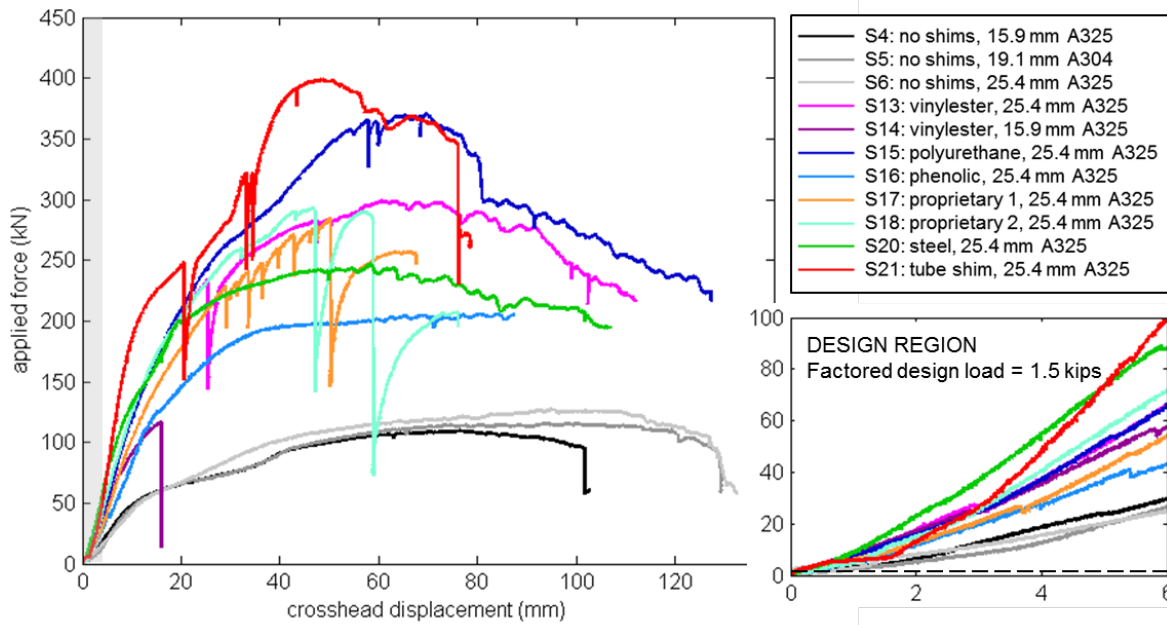


Figure 6-8: Actuator force versus crosshead displacement for Climate Zone 7 (3" shim, L7x4x3/8 angles) specimens, with design region shown in inset.

Similarly, for the Climate Zone 1 specimens, the unmitigated details again provide a lower bound for the force-displacement results. Differences between shim materials are small: while polyurethane shims result in the maximum force, the five various shim materials result in responses within 20% of each other (note that the material properties of the shims themselves vary more than 20%).

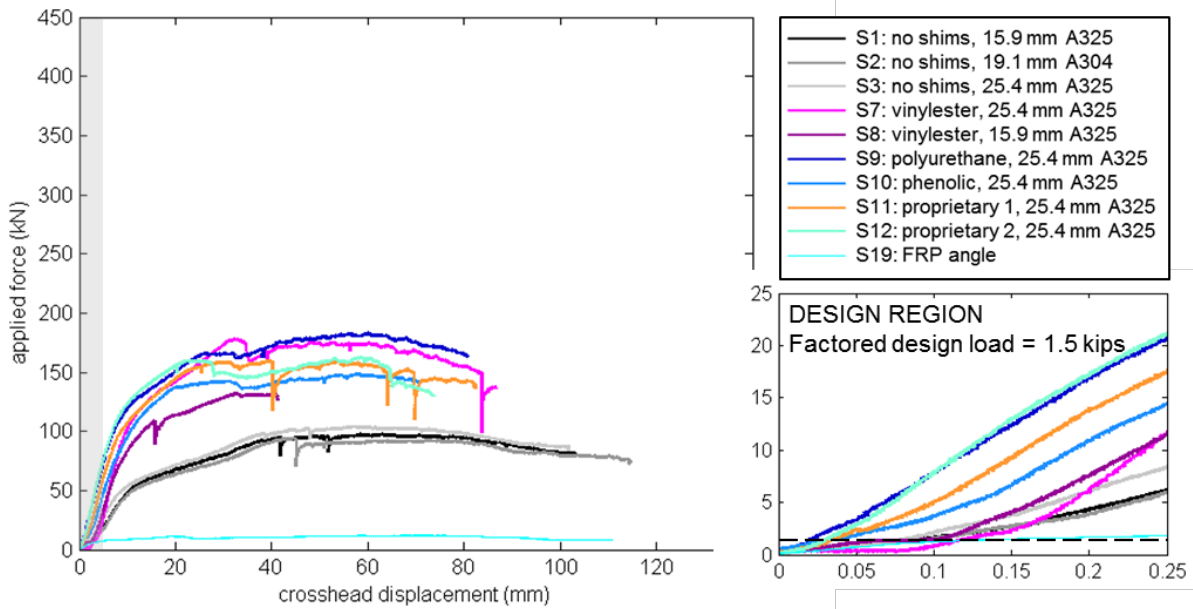


Figure 6-9: Actuator force versus crosshead displacement for Climate Zone 1 (1.5" shim, L6x4x5/16 angles) specimens, with design region shown in inset.

Failure modes resembled those of the Climate Zone 7 specimens, though in most cases shim delamination was less pronounced and due to the thinner shelf angle, since angle deformation dominated the response. Shims failed along the bond line if present, and at varying layers within the cross section if shims were unbonded. Photographs of these modes across all testing are shown in Figure 6-10 below.

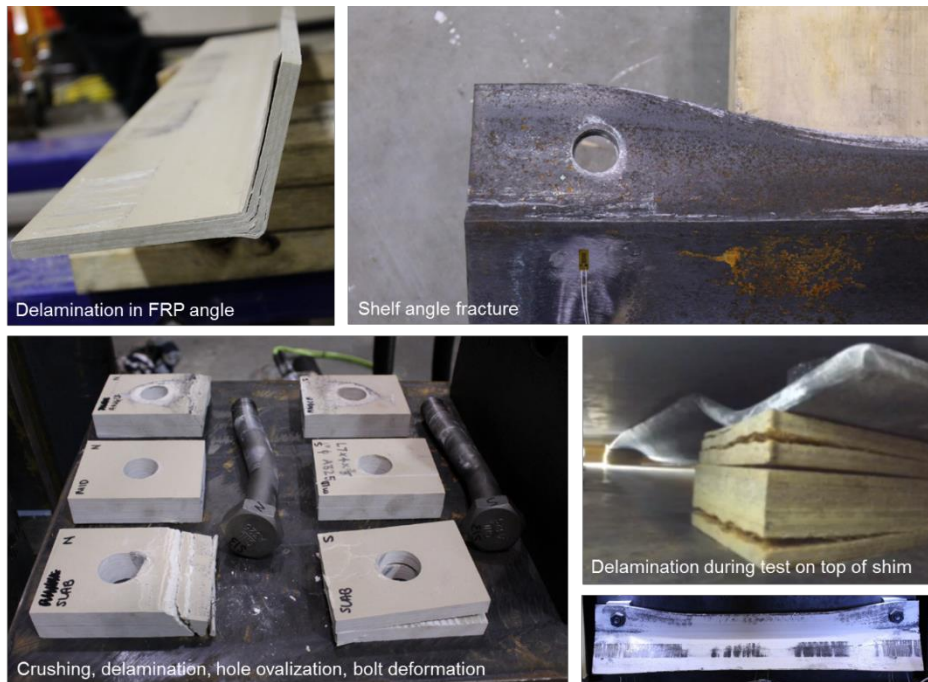


Figure 6-10: Typical failure modes observed during testing

As shown in Figure 6-10, bolts also deformed during testing, though this mode was not critical and likely did not influence performance until the post-peak regime.

The pultruded FRP angle did not perform as well in this series of testing. Prior to testing, it was established that the available pultruded angles were not manufactured thick enough to adequately satisfy design checks. However, as custom pultrusions may be cost-prohibitive, the thickest “off-the-shelf” angle was tested as a part of this program. As Figure 6-9 shows, this angle was significantly less stiff in the design region, and attained a maximum force of approximately 10% of the unmitigated details. The FRP angle delaminated throughout testing and ultimately fractured at the angle heel.

6.2.2 Shelf angle strain results

Data from the strain gauges installed along the heel of the horizontal angle leg, S1, S2, and S3 (shown in Figure 6-4 above) provide a measure of the stresses in the angle, and how the various mitigation strategies impact system performance. This data for Climate Zone 7 specimens is shown in Figure 6-11 below.

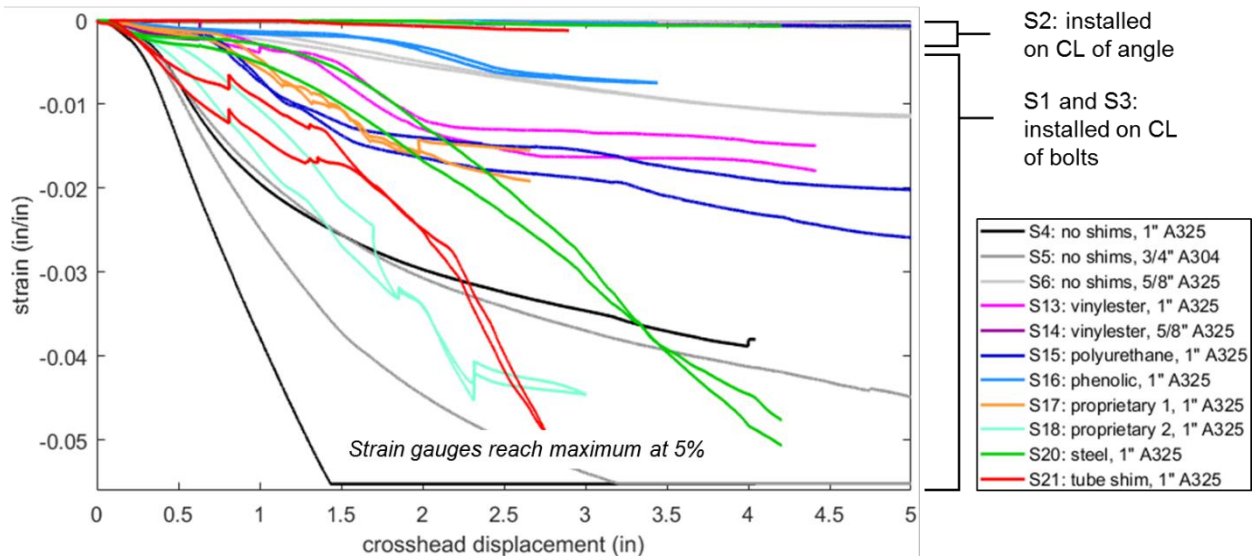


Figure 6-11: Shelf angle strain gauges versus crosshead displacement for Climate Zone 7 (3” shim, L7x4x3/8 angles) specimens

Gauge S2, installed on the center line of the angle consistently demonstrates that the center of the angle is rotating rigidly in the vertical leg, thus resulting in translation of the horizontal leg about the heel (and negligible strain). Gauges S1 and S3 are installed on the centerlines of the bolts and theoretically should be equivalent. Differences in bolt pre-tension likely account for the variation between the two sensors.

Specimen S6, with 5/8” diameter bolts, does not experience significant strain in the angle because forces are concentrated on the bolts, which are the limiting factor for the designed case. As bolts

are increased to 3/4" and 1" diameters (specimens S5 and S6), strains in the angle increase, as the bolts can resist higher forces. In specimens with shims, the response varies. In general, specimens with steel mitigation strategies (S20 and S21) experience larger strains in the shelf angle, while those with FRP mitigation strategies experience less, most likely due to the relative deformability of FRP compared to steel (allowing the shims to compress rather than straining the angle).

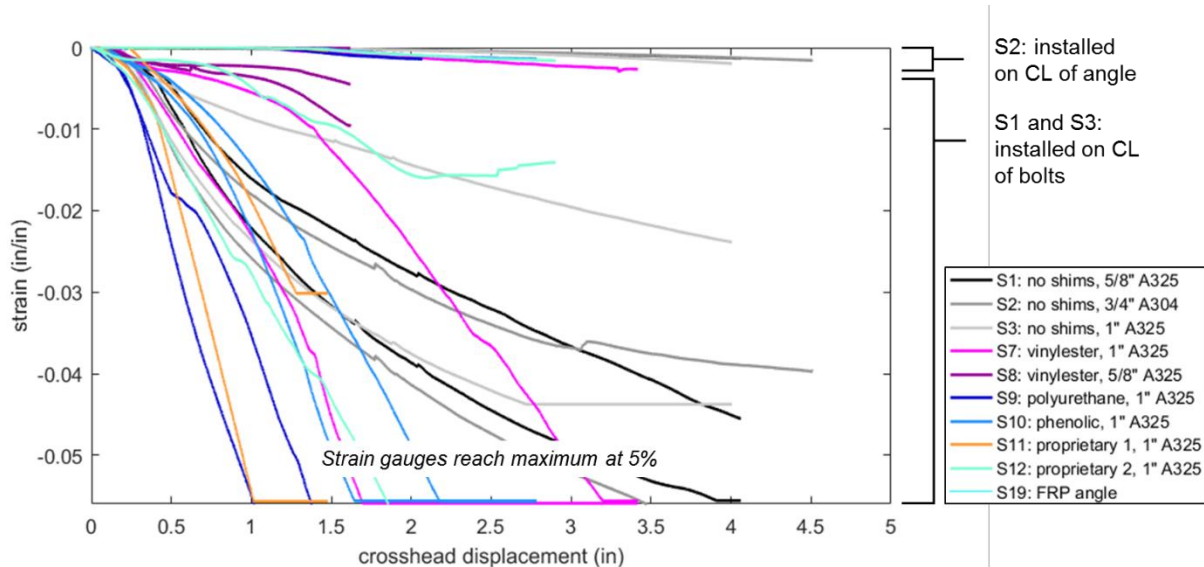


Figure 6-12: Shelf angle strain gauges versus crosshead displacement for Climate Zone 1 (1.5" shim, L6x4x5/16 angles) specimens

The same is not true for the Climate Zone 1 specimens, shown in Figure 6-12. In these tests, the angle size is decreased to L6x4x5/16, and the thinner angle begins to dominate the response, rather than the bolt sizing as in the Climate Zone 7 specimens. This is evident from not only the increased strains, but the slope of the displacement-strain curves, which are significantly greater than those in the Climate Zone 7 results.

As in the Climate Zone 7 specimens, the addition of a mitigation strategy requires pushing the shelf angle further from the support to accommodate the shim while maintaining the wall cavity size. This change alters the moment-to-shear ratios between mitigated and unmitigated details. With thicker angles, bolts and shims dominate response before angle deformation becomes relevant, while for thinner angles, angle deformation occurs before any bolt or shim failure mode.

6.2.3 Load cell results

Using the load cells installed on the bolts, two important quantities can be estimated: the force and variation of the force in the bolts prior to testing, and the variation of the bolt force throughout the test. The strains from the gauges installed at the top and bottom of each load cell are averaged to capture bolt behavior throughout the test.

Figure 6-13 plots the load cell strains (induced by bolts in tension compressing the load cells) as the test progresses for the Climate Zone 7 specimens. For the purpose of this comparative analysis, load cell strains are zeroed at the initiation of the displacement protocol. In specimens with FRP

shims, the shims likely assume some of the pre-tension forces and distribute force away from the bolt. After the initial loading region, forces in the bolt remain relatively constant through the remainder of the test.

Shim failures impact load cell strains, and result in a temporary relaxation of the bolt forces, which equilibrate after force redistribution.

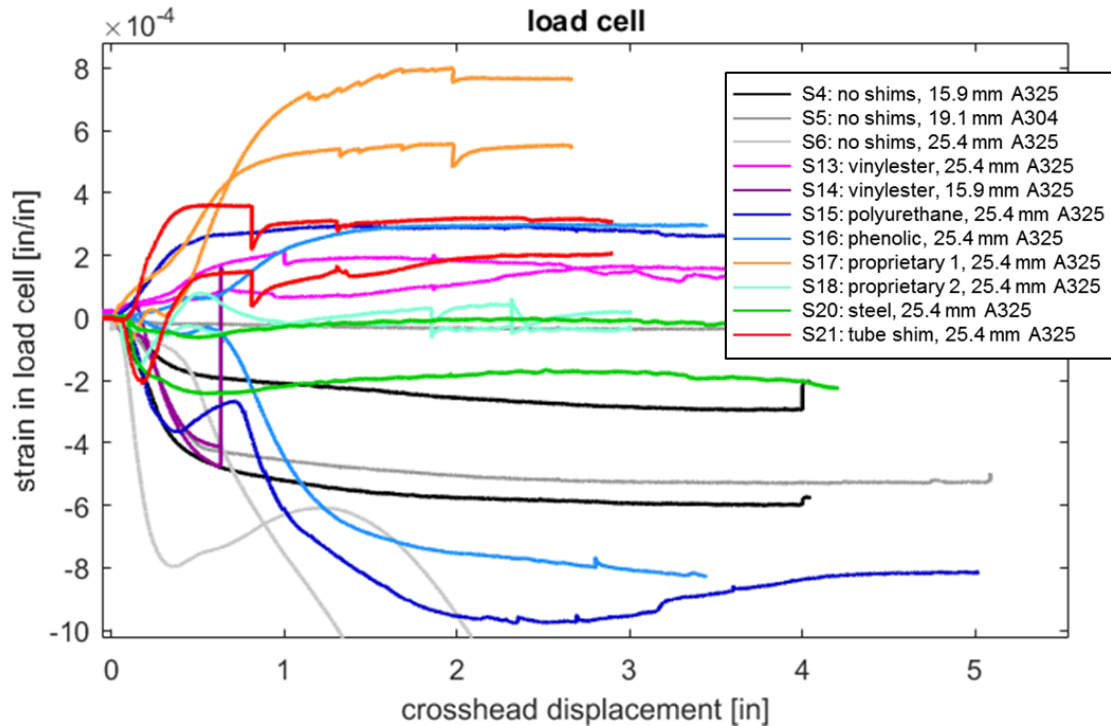


Figure 6-13: Load cell strain readings for Climate Zone 7 (3" shim, L7x4x3/8 angles) specimens

Similar trends are evident in the Climate Zone 1 specimens (Figure 6-14) below. Strain in the load cell (caused by bending and tension from the bolt head) increases in the initial 0.5" of loading, in which the shelf angle vertical leg begins to buckle and pull on the bolts, and typically plateaus for the remainder of the test. While the shelf angle continues to bend and induce bolt bending and tensile modes, the bolt forces remain relatively constant throughout the remainder of the test. This is true whether the specimens have shims or are unmitigated details. Test S8 represents an exception to this rule, as the configuration had 5/8" bolts in consort with 1.5" shims. Increased eccentricity from the shims loads the bolts more severely and bolt forces do not plateau immediately, spiking first before plateauing.

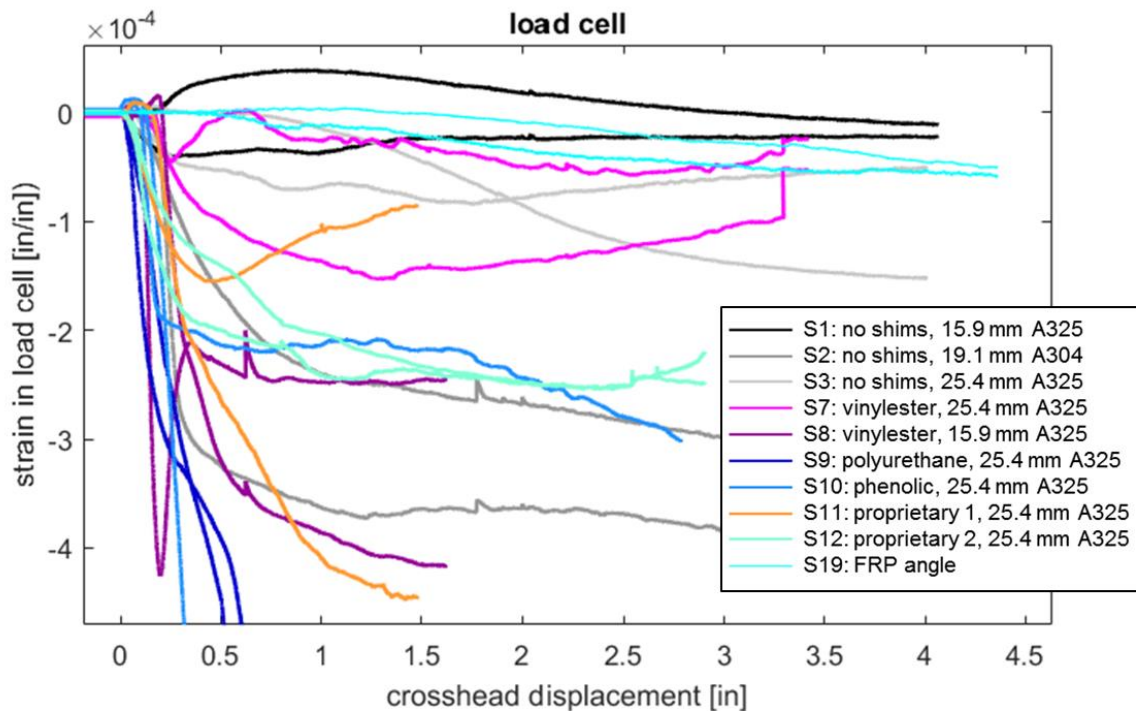


Figure 6-14: Load cell strain readings for Climate Zone 1 (1.5" shim, 6x4x5/16 angles) specimens

6.3 Finite element validation studies

The finite element analyses (FEA) for this research were performed using ABAQUS 6.14-1 (ABAQUS 2014), using the standard analysis solvers.

For each model a mesh with eight node 3D elements with reduced integration were used to improve the convergence rate. Because these elements use a reduced integration, hourglass enhanced section controls were implemented to avoid zero-energy modes due to hourglassing. To accurately portray bending stress, all members in flexure had a minimum of four elements through the cross-section thickness, and the surface mesh was such that the elements through the cross-section had an aspect ratio no larger than 4:1 to reduce the risk of the elements favoring stress along just one of the axes. The largest mesh size dimension used in these models is approximately 0.25 in. Through parametric analysis, it was determined that results are not mesh-dependent.

The components of the models are portrayed in the assembly as a representation of the original component, also known as an instance. Once these instances are in their respective places the surfaces in contact with each other must be defined. This was accomplished by defining master and slave surfaces to interact with each other using surface-to-surface contact. The contact interaction properties used is hard contact in the normal direction of all surfaces and penalty friction, with a coefficient of friction of 0.25, in the tangential direction of all surfaces. Contact in ABAQUS/Standard can cause issues with the start of the analysis because of instantaneous

instabilities between the nodes. The nodes require an extremely small time step to stabilize themselves before the analysis can continue forward. To accomplish this, a dampening factor was instated to absorb some energy from the initiation of the model. This factor is small enough to stabilize the initiation while not affecting the behavior of the model.

The bolts were restrained as if they were within a rigid plate using boundary conditions. This allowed for the bolts to react as expected without the added computational time required for contact. All other surfaces that would typically bear upon a rigid support had the bearing contact represented with compression-only gap elements. These elements were used to restrain the elements from translating along a single direction on the referenced axis.

Various shelf angle models were created to simulate and verify the results of experimental data. The experimental setup being represented is a steel shelf angle manufactured from ASTM A36 structural steel attached to a steel backing plate with either ASTM A325, ASTM A304-SH1, or ASTM A307 bolts. Some assemblies have fiberglass reinforced polymer shims within the connections acting as a thermal break. The thicknesses and combination of thicknesses of the FRP vary to match the experiments. Measured properties include results reported in Appendix A from tensile coupon tests of the shelf angle and bolt materials, and through-thickness compression tests for FRP materials. The loading is assumed to apply continuously increasing pressure evenly across the outstanding leg of the angles.

A comparison between the ABAQUS analyses and the experimental data is presented below. Force and deflection from the models are taken at the same points on the specimen and load frame as they were recorded in the experimental work. Across all testing, models are in excellent agreement with force-displacement results. Shelf angle bending and shear are accurately captured, as are bolt failure modes and shim compression. One behavior the ABAQUS results fail to capture is shim delamination following compression of the bottom edge of the shim. This delamination causes load drops in the first 1-2 inches of displacement (as seen in S8 and S13 force-displacement responses).

Assembly S1 - L6x4x5/16, 5/8 in bolts, no shims

- Angle: L6x4x5/16 – A36 structural steel
- Bolts: 5/8in diameter – A325 structural steel
- Shims: None

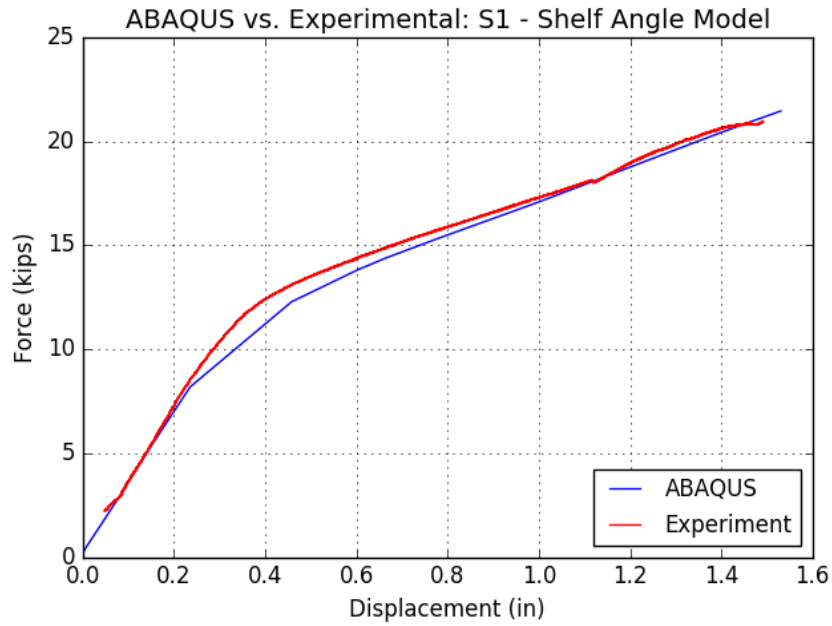


Figure 6-15 Assembly S1 – Force-Displacement, ABAQUS vs. Experimental

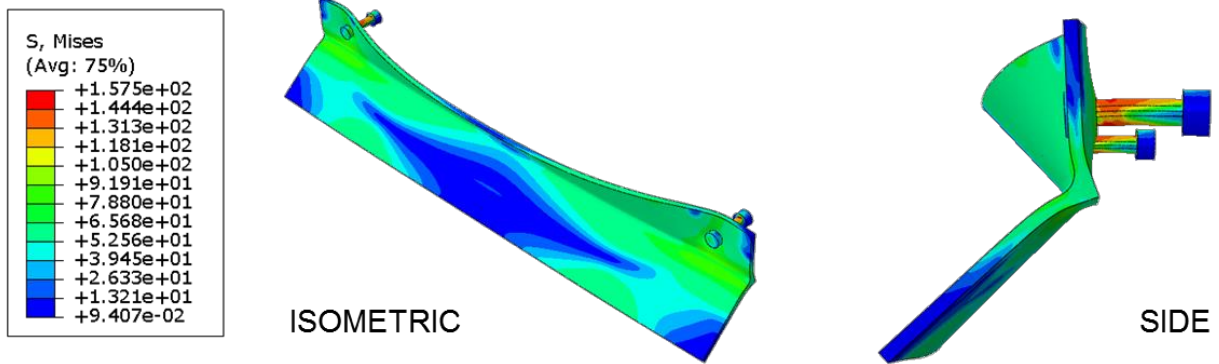


Figure 6-16 Assembly S1 – von Mises stress contour – ISO view

Assembly S7 - L6x4x5/16, 1 in bolts, 1/2 in + 1 in shims

- Angle: L6x4x5/16 – A36 structural steel
- Bolts: 1 in diameter – A325 structural steel
- Shims: 1/2in + 1in Vinylester FRP

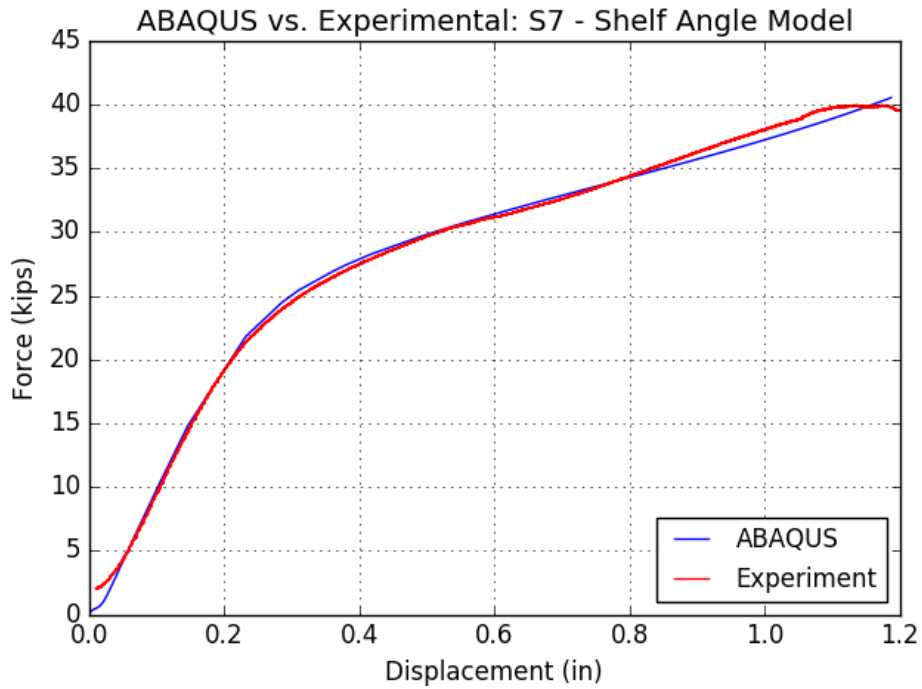


Figure 6-17 Assembly S7 – Force-Displacement, ABAQUS vs. Experimental

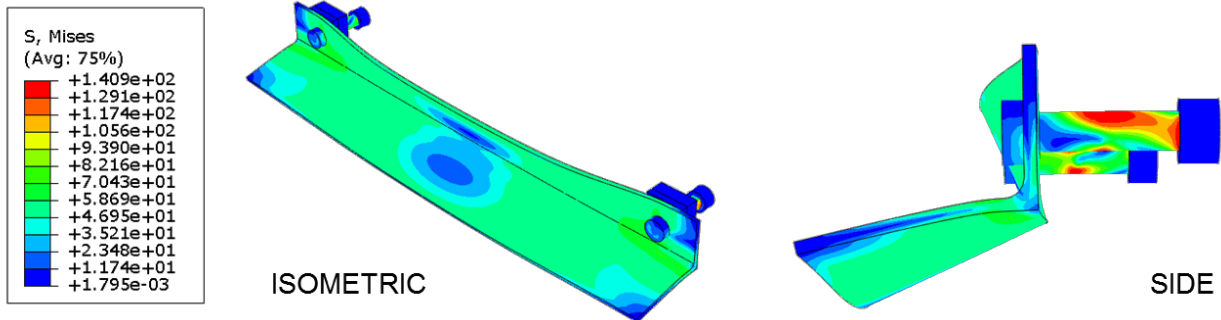


Figure 6-18 Assembly S7 – von Mises stress contour – ISO view

Assembly S8 - L6x4x5/16, 5/8 in bolts, 1/2 in + 1 in shims

- Angle: L6x4x5/16 – A36 structural steel
- Bolts: 5/8in diameter – A325 structural steel
- Shims: 1/2in + 1in Vinylester FRP

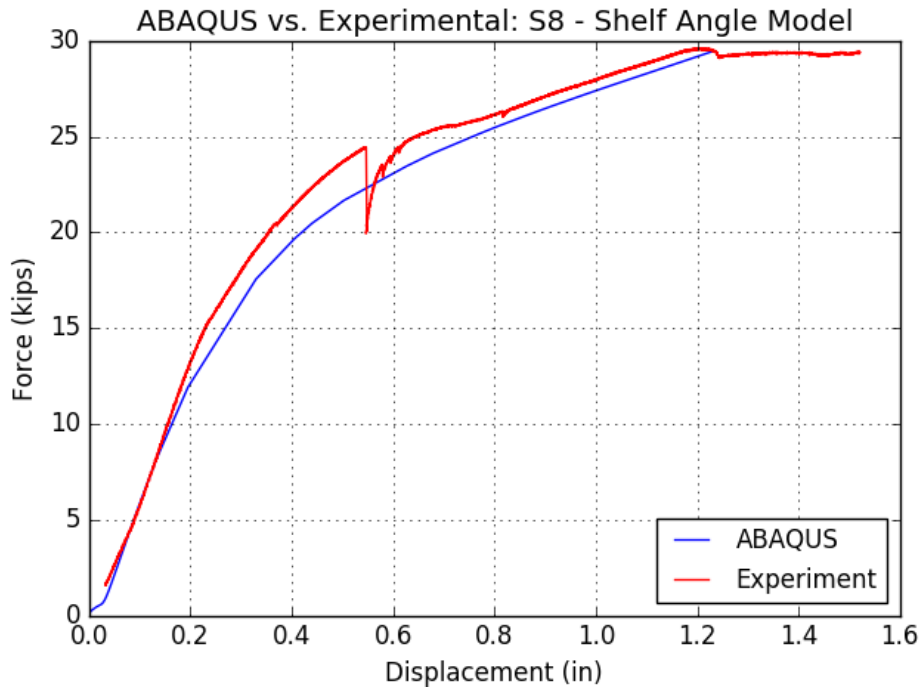


Figure 6-19 Assembly S8 – Force-Displacement, ABAQUS vs. Experimental

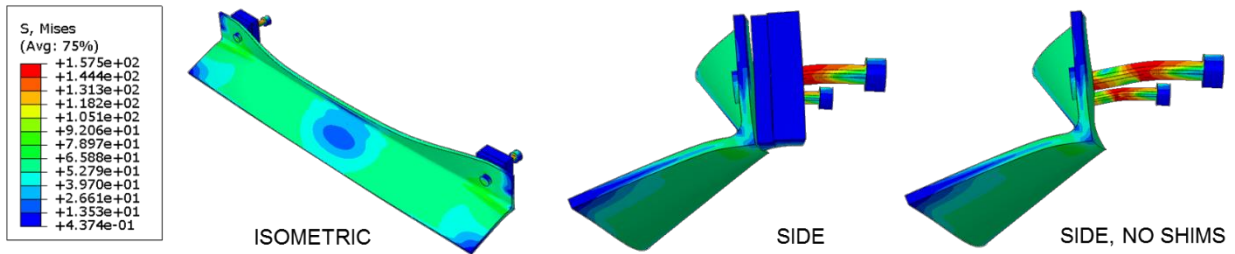


Figure 6-20 Assembly S8 – von Mises stress contour – ISO view

Assembly S9 - L6x4x5/16, 1 in bolts, 1/2 in + 1 in shims

- Angle: L6x4x5/16 – A36 structural steel
- Bolts: 1in diameter – A325 structural steel
- Shims: 1/2in + 1in Polyurethane FRP

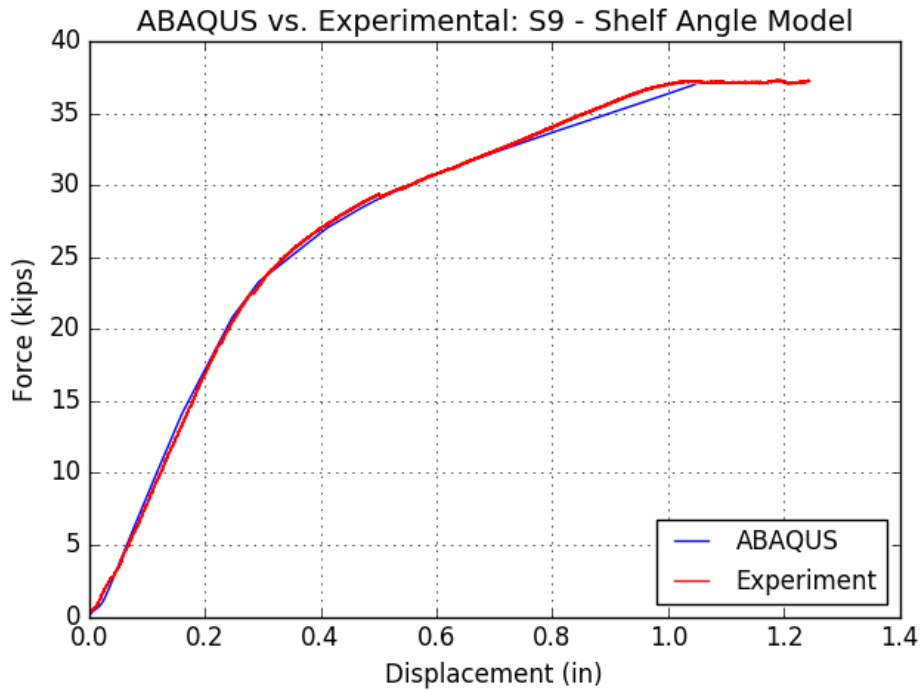


Figure 6-21 Assembly S9 – Force-Displacement, ABAQUS vs. Experimental

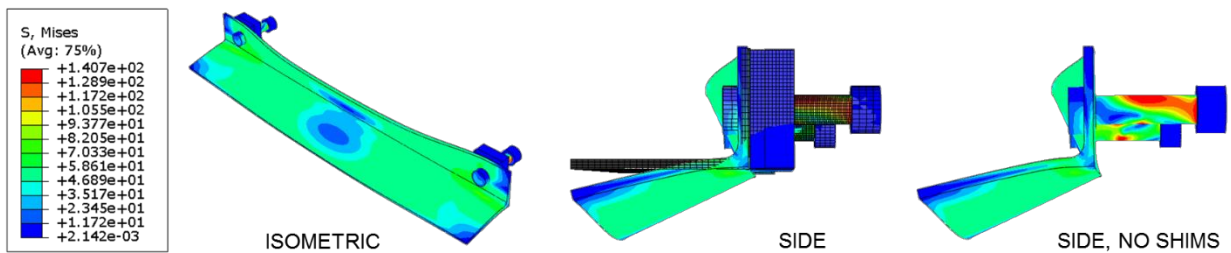


Figure 6-22 Assembly S9 – von Mises stress contour – ISO view

Assembly S10 - L6x4x5/16, 1 in bolts, 1/2 in + 1 in shims

- Angle: L6x4x5/16 – A36 structural steel
- Bolts: 1in diameter – A325 structural steel
- Shims: 1/2in + 1in Phenolic FRP

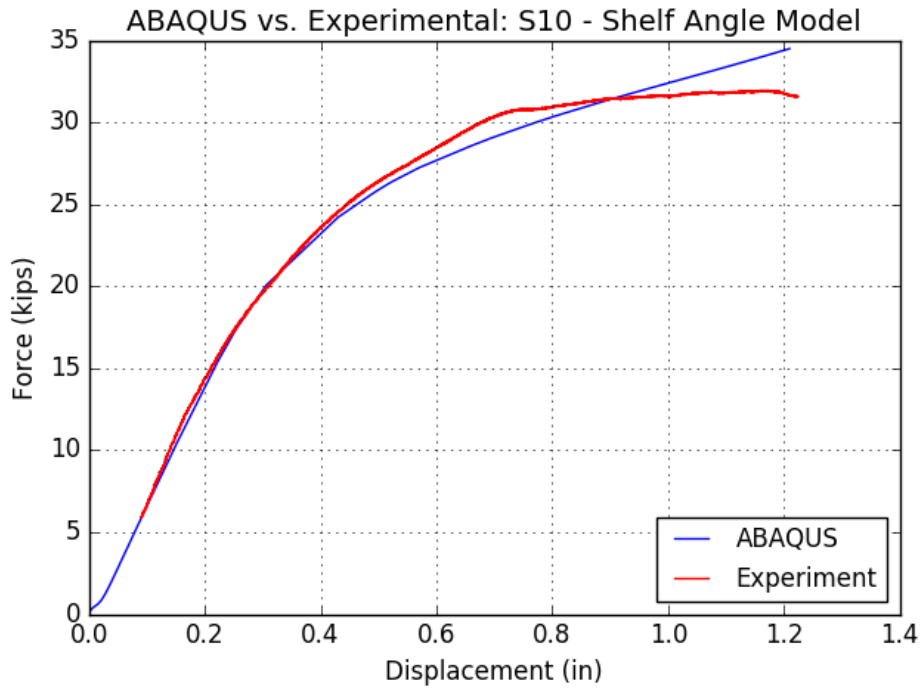


Figure 6-23 Assembly S10 – Force-Displacement, ABAQUS vs. Experimental

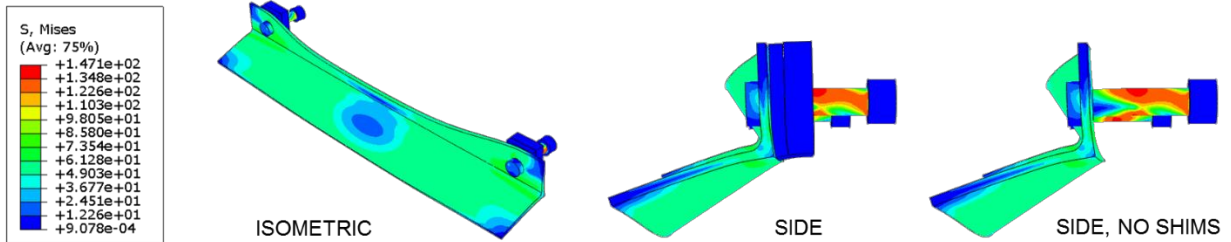


Figure 6-24 Assembly S10 – von Mises stress contour – ISO view

Assembly S11 - L6x4x5/16, 1 in bolts, 1/2 in + 1 in shims

- Angle: L6x4x5/16 – A36 structural steel
- Bolts: 1in diameter – A325 structural steel
- Shims: 1/2in + 1in Proprietary 1 FRP

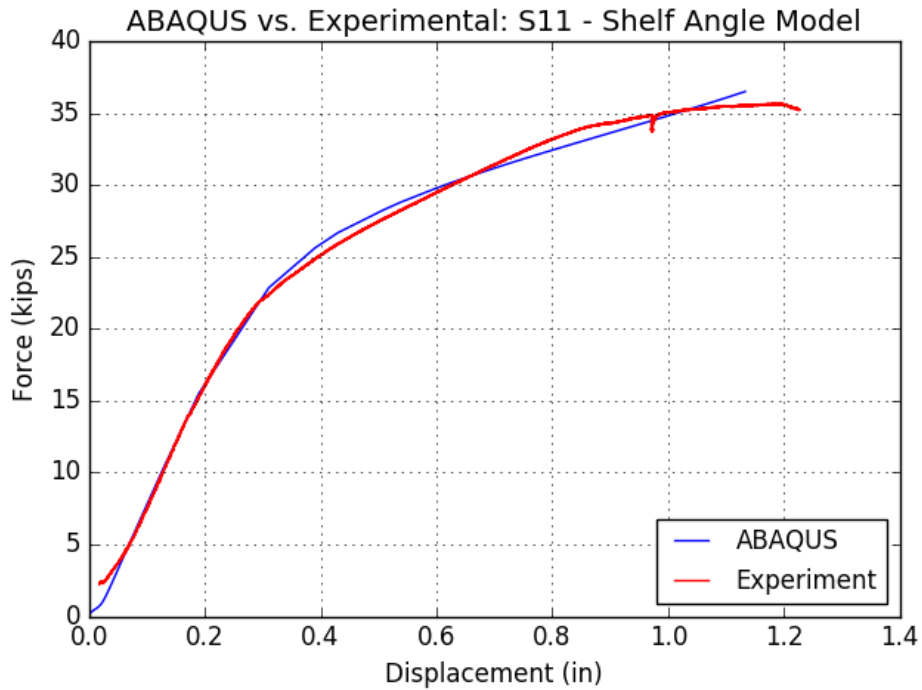


Figure 6-25 Assembly S11 – Force-Displacement, ABAQUS vs. Experimental

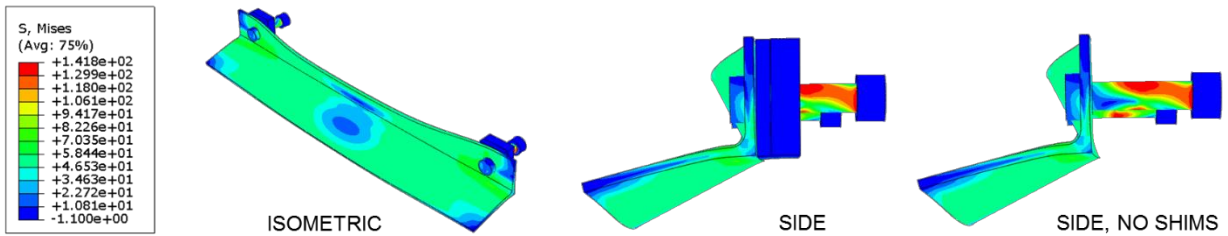


Figure 6-26 Assembly S11 – von Mises stress contour – ISO view

Assembly S12 - L6x4x5/16, 1 in bolts, 1/2 in + 1 in shims

- Angle: L6x4x5/16 – A36 structural steel
- Bolts: 1in diameter – A325 structural steel
- Shims: 1/2in + 1in Proprietary 2 FRP

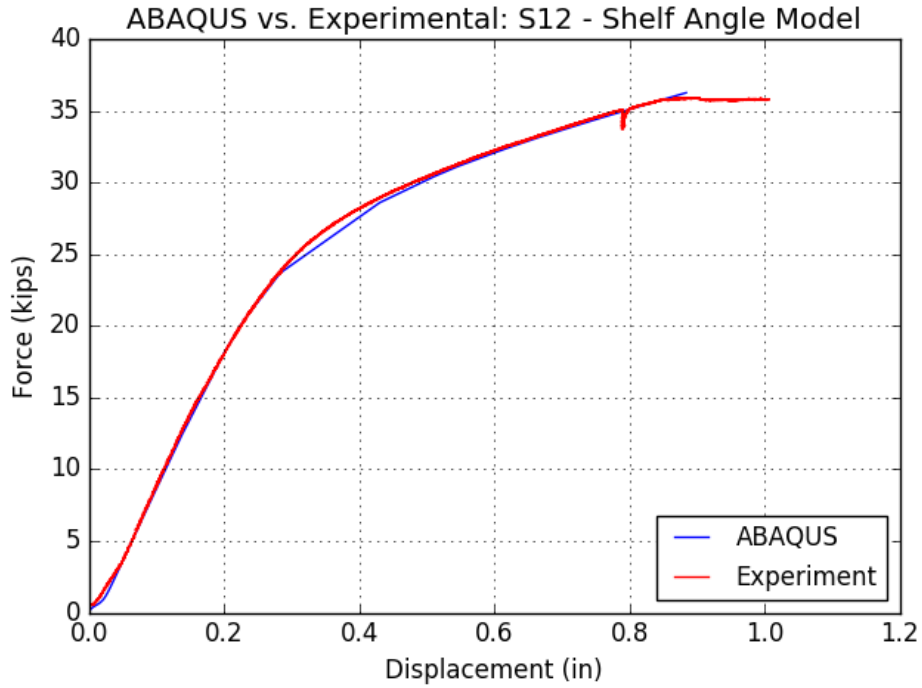


Figure 6-27 Assembly S12 – Force-Displacement, ABAQUS vs. Experimental

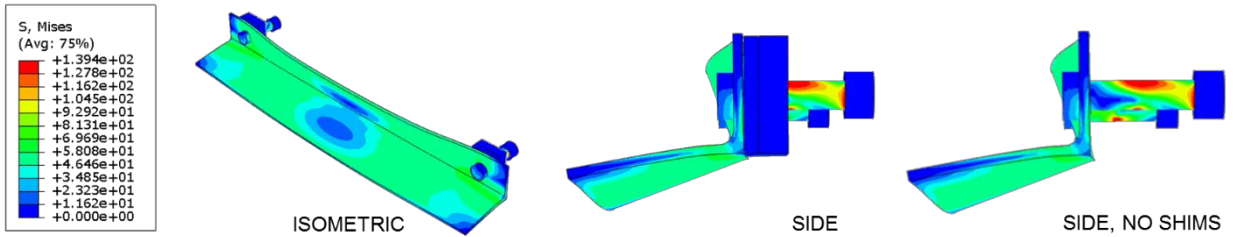


Figure 6-28 Assembly S12 – von Mises stress contour – ISO view

Assembly S13 - L7x4x3/8, 1 in bolts, 3 x 1 in shims

- Angle: L7x4x3/8 – A36 structural steel
- Bolts: 1in diameter – A325 structural steel
- Shims: 3x 1in Vinylester FRP

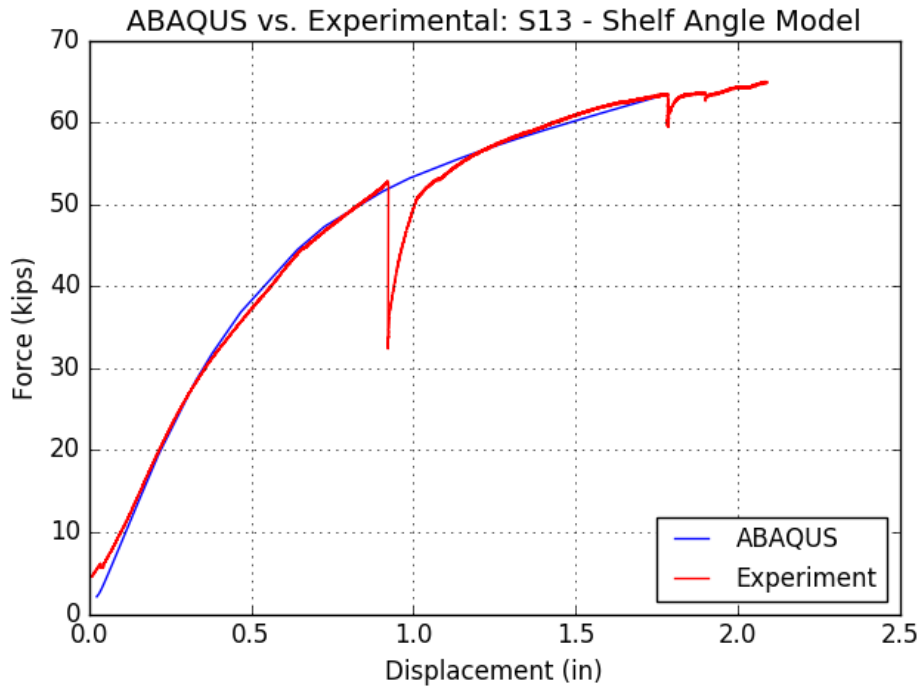


Figure 6-29 Assembly S13 – Force-Displacement, ABAQUS vs. Experimental

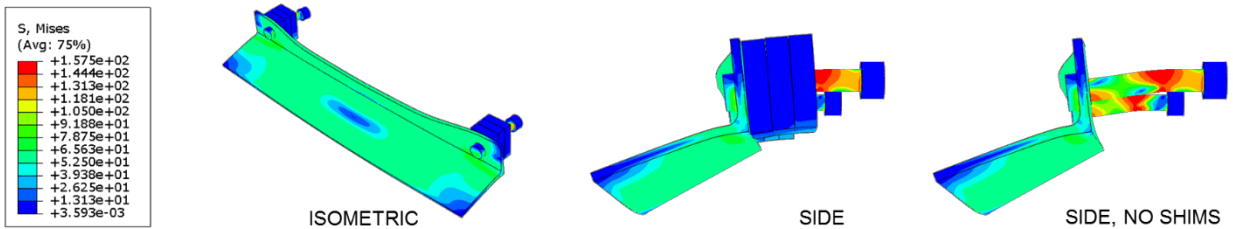


Figure 6-30 Assembly S13 – von Mises stress contour – ISO view

Assembly S14 - L7x4x3/8, 5/8 in bolts, 3 x 1 in shims

- Angle: L7x4x3/8 – A36 structural steel
- Bolts: 5/8in diameter – A325 structural steel
- Shims: 3x 1in Vinylester FRP

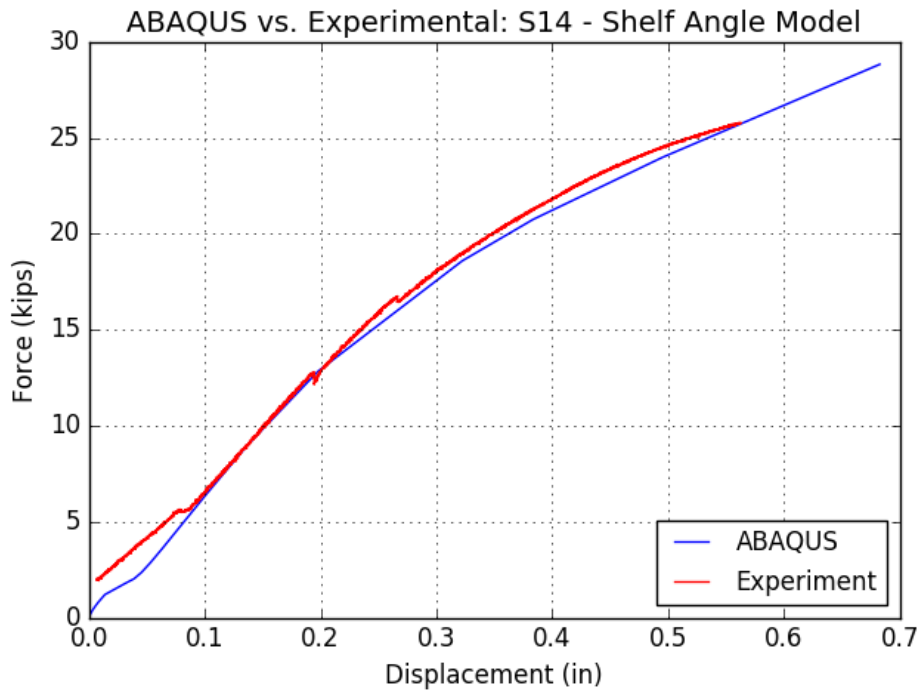


Figure 6-31 Assembly S14 – Force-Displacement, ABAQUS vs. Experimental

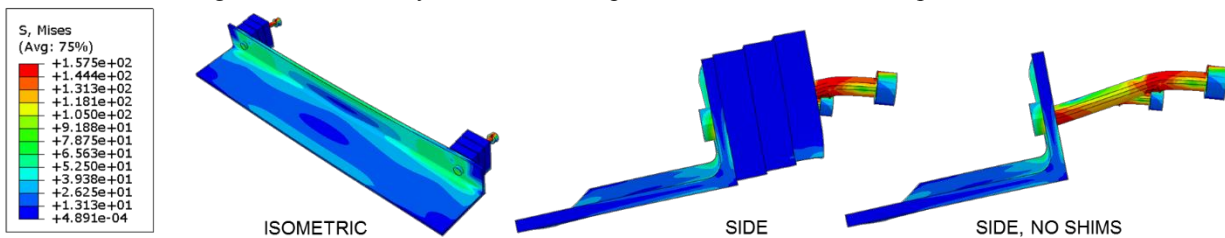


Figure 6-32 Assembly S14 – von Mises stress contour – ISO view

Assembly S15 - L7x4x3/8, 1 in bolts, 3 x 1 in shims

- Angle: L7x4x3/8 – A36 structural steel
- Bolts: 1in diameter – A325 structural steel
- Shims: 3x 1in Polyurethane FRP

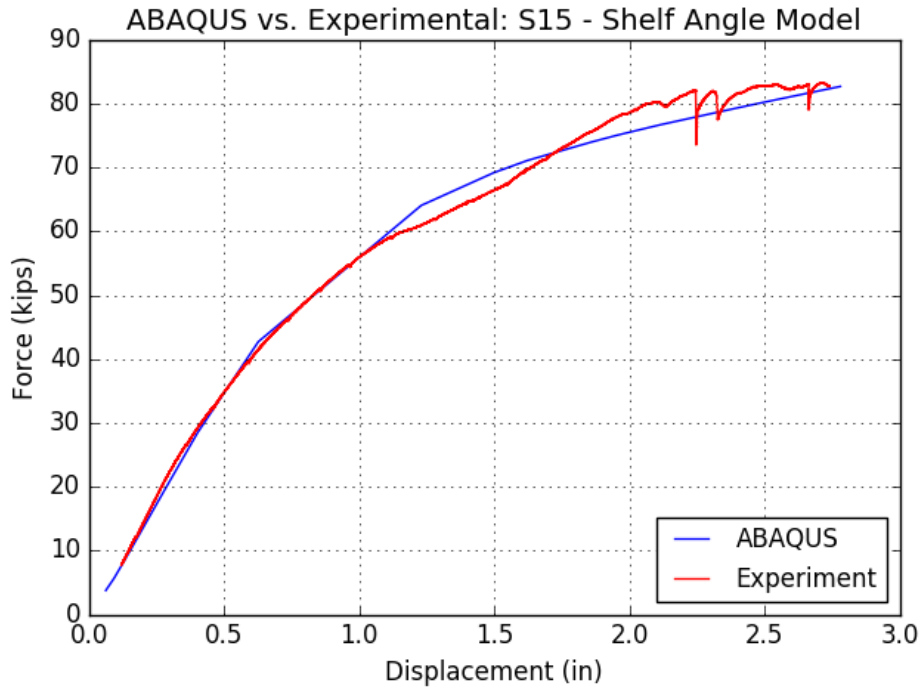


Figure 6-33 Assembly S15 – Force-Displacement, ABAQUS vs. Experimental

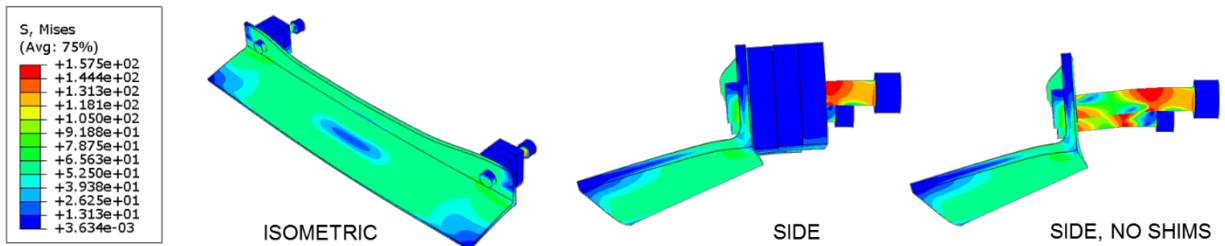


Figure 6-34 Assembly 15 – von Mises stress contour – ISO view

Assembly S16 - L7x4x3/8, 1 in bolts, 3 x 1 in shims

- Angle: L7x4x3/8 – A36 structural steel
- Bolts: 1in diameter – A325 structural steel
- Shims: 3x 1in Phenolic FRP

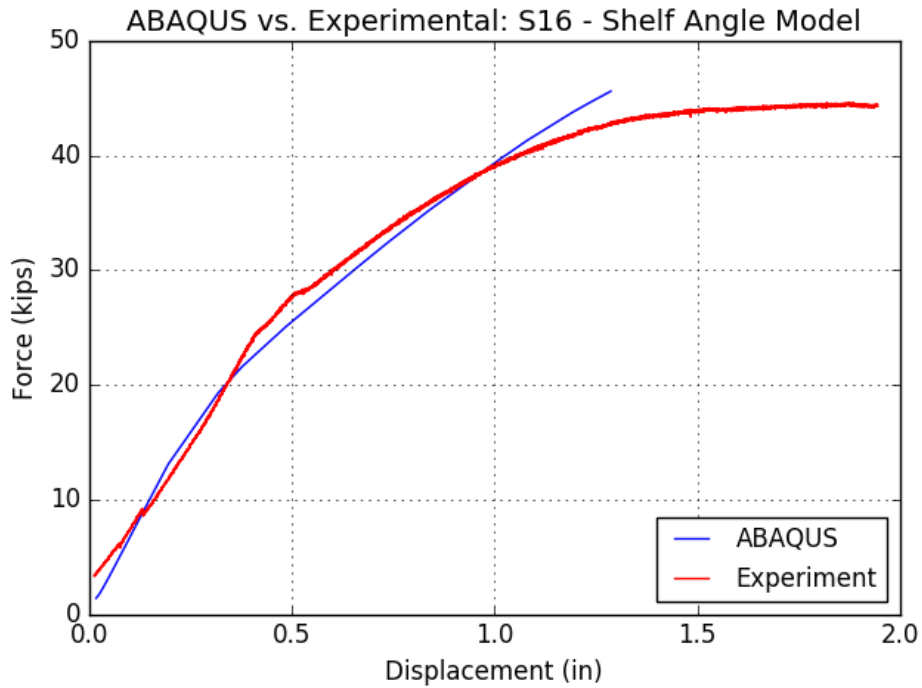


Figure 6-35 Assembly S16 – Force-Displacement, ABAQUS vs. Experimental

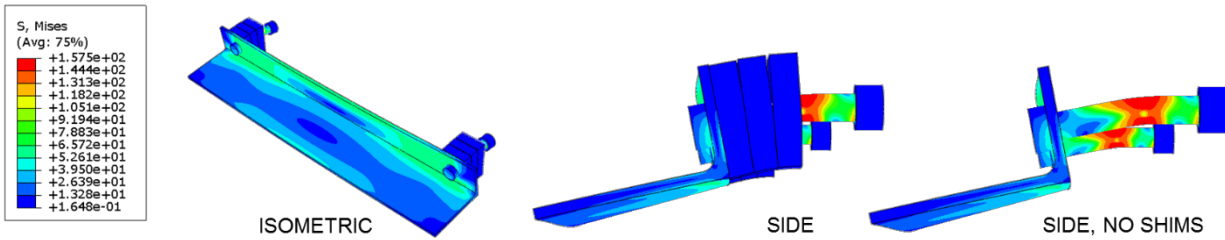


Figure 6-36 Assembly S16 – von Mises stress contour – ISO view

Assembly S17 - L7x4x3/8, 1 in bolts, 3 x 1 in shims

- Angle: L7x4x3/8 – A36 structural steel
- Bolts: 1in diameter – A325 structural steel
- Shims: 3x 1in Proprietary 1 FRP

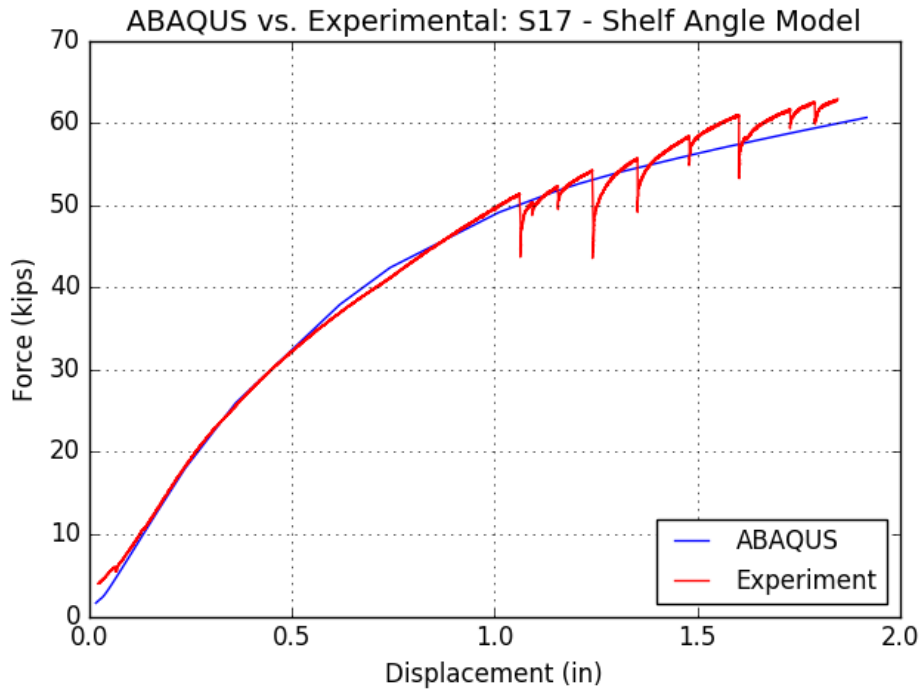


Figure 6-37 Assembly S17 – Force-Displacement, ABAQUS vs. Experimental

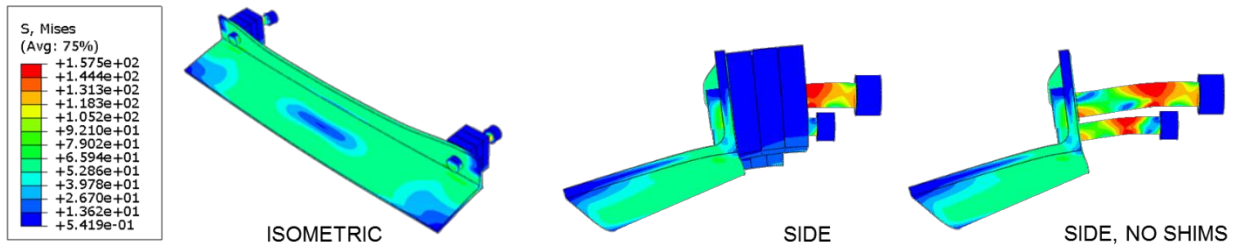


Figure 6-38 Assembly S17 – von Mises stress contour – ISO view

Assembly S18 - L7x4x3/8, 1 in bolts, 3 x 1 in shims

- Angle: L7x4x3/8 – A36 structural steel
- Bolts: 1in diameter – A325 structural steel
- Shims: 3x 1in Proprietary 2 FRP

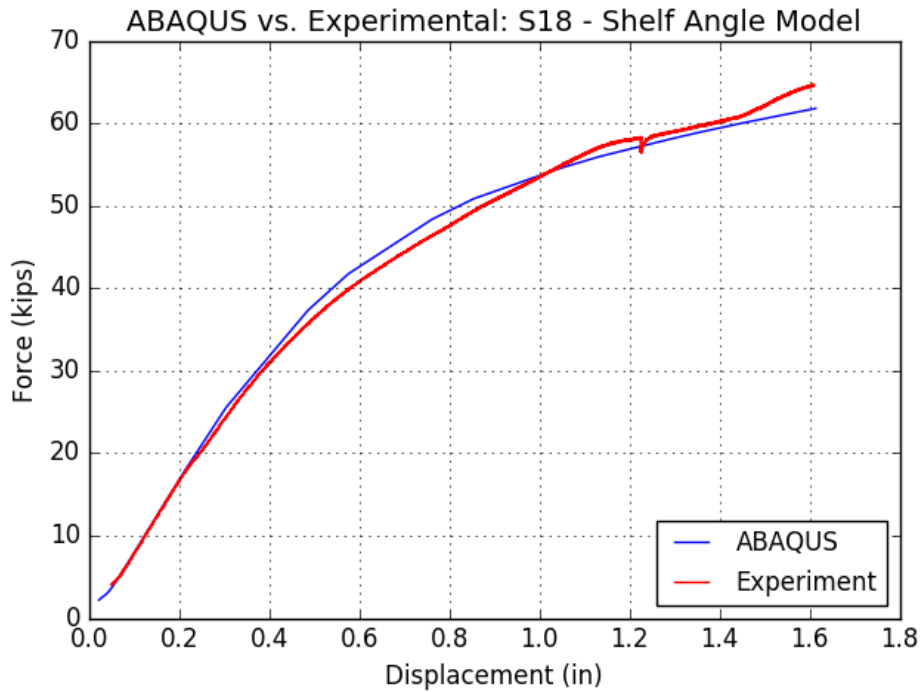


Figure 6-39 Assembly S18 – Force-Displacement, ABAQUS vs. Experimental

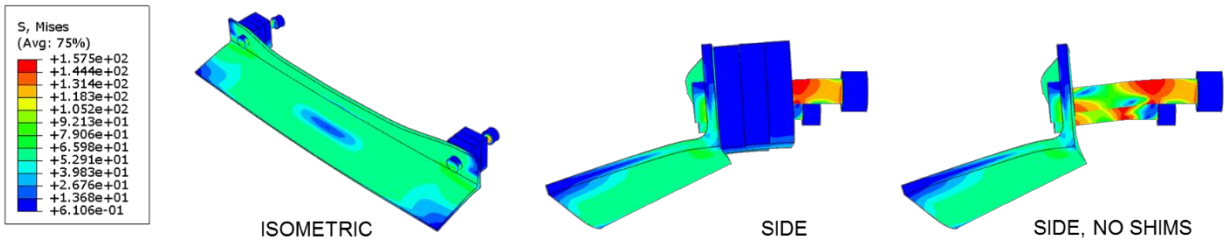


Figure 6-40 Assembly S18 – von Mises stress contour – ISO view

Figure 6-41 the ABAQUS results of assembly S1, S8, and S14. These assemblies are similar to each other as they all have 5/8 in diameter A325X structural steel bolts. The figure demonstrates the performance differences as the FRP shim thickness changes. This shows that an assembly with no shims will deflect more with less load than an assembly with shims included. This is due to the fact the assembly with no shims has continuous bearing against the wall surface. The other two assemblies only have bearing at the shim locations and thus the bending mechanics here include more of the shelf angle as well as the bolts. The minor differences between the two curves with shims is due to the fact that the curve with 3 in. thick shims is a L7x4x3/8, while the curve with 1.5 in. thick shims is a L6x4x5/16.

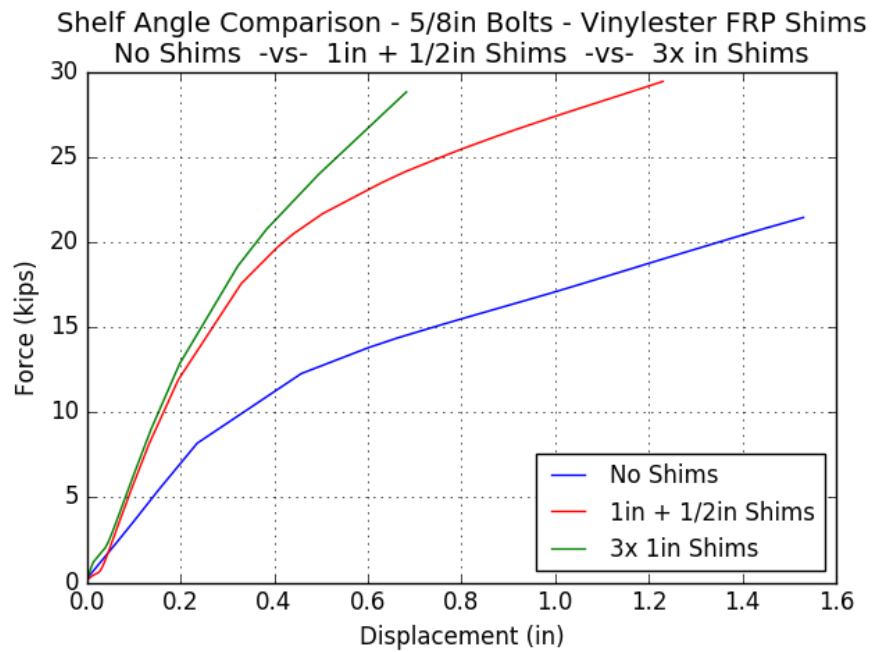


Figure 6-41 Comparison of force-displacement results generated by ABAQUS for shelf angles with 5/8 in bolts

The six curves shown in Figure 6-42 are created from the same geometric model with 1.5 in. thick shims and 1 in. A325X bolts. The only difference is the material properties of the FRP shims within the connection. The figure shows that all the materials are very similar with the exception of phenolic, which has lower strength than the others.

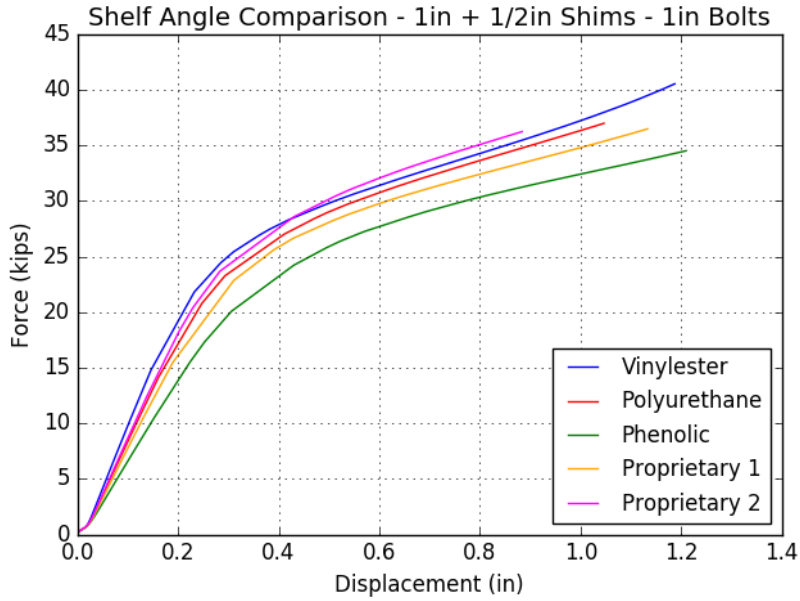


Figure 6-42 Comparison of force-displacement results generated by ABAQUS for shelf angles with 1in + 1/2in shims and 1in bolts

The six curves shown in Figure 6-43 are created from the same geometric model with 3 in. thick shims and 1 in. A325X bolts. The only difference is the material properties of the FRP shims within the connection. The figure shows that all the materials are very similar with the exception of Phenolic which has less strength and stiffness than the others.

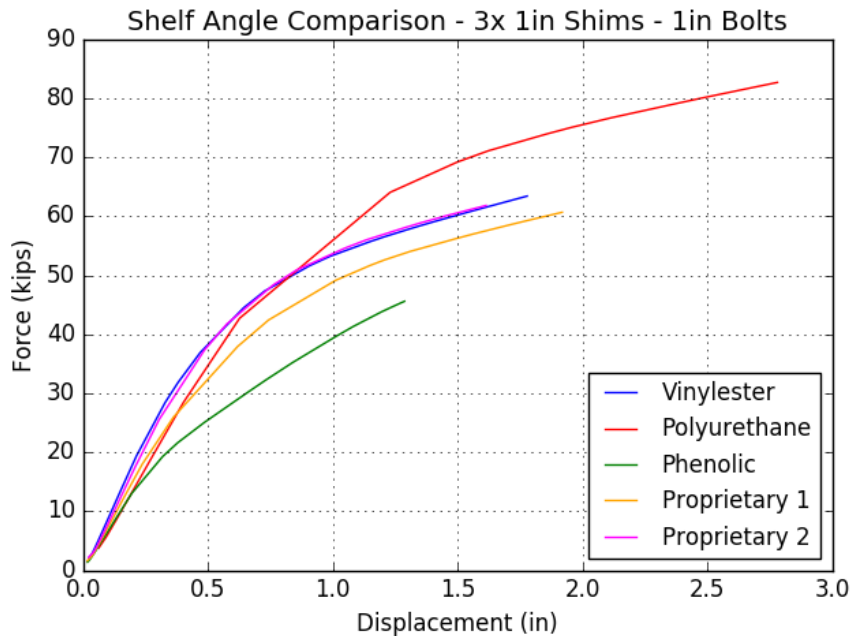


Figure 6-43: Comparison of force-displacement results generated by ABAQUS for shelf angles with 3x 1in shims and 1in bolts

6.4 Design Recommendations

We propose adapting the design procedure developed by Tide and Krogstad (1993) for use with shelf angles incorporating shim-type thermal breaks.

The procedure of Tide and Krogstad (1993) breaks the masonry loads into distributed loads and concentrated loads. The distributed loads account for the weight of the bottom courses of masonry when the mortar is still plastic, allowing the brick veneer to deflect as it loads the supporting shelf angle. The concentrated loads account for the wall stiffness after the mortar in the bottom courses has hardened, allowing the veneer to arch from shelf angle support to support. The methodology accounts for shelf angle displacements and stresses due to bending, shear, and torsion.

To calibrate the methodology to the load tests, we made the following alterations to the procedure:

- Because the test specimens were loaded by a rigid beam, we treated the entire load as concentrated at the support bolts.
- Tide and Krogstad (1993) suggest using the benefit of friction between the masonry and the shelf angle to help resist the imposed loads. We find that neglecting this friction results in closer correlation with the test results.
- Tide and Krogstad (1993) suggest including the width of the shims when calculating the effective length of the angle horizontal leg for bending and torsional effects. We find that neglecting the shim width results in closer correlation with the test results for both FRP and steel shims.
- We simplified the equations for torsional effects due to the concentrated loads.
- To account for the shim effects, we treated the bolts as bending in single curvature and calculated bending effects of the combined shim/bolt system using a linear-elastic composite cross-section bending formulation.

6.4.1 Deflections

Total deflections of the test specimens are the sum of the following five deflection components. We calculate deflection of the angle directly below the corner of the loading beam closest to the angle support. The methodology described below will require modification for continuous constructed shelf angles supporting brick veneer and for calculation of shelf-angle deflection at mid-span between bolts. If the shelf angles are supported by bolts in standard holes, we also recommend adding 1/16 in. to the calculated deflections to account for the hole diameter. The five deflection components considered are:

1. Bending of the horizontal leg of the shelf angle (Δ_d).
2. Torsion on the shelf angle (Δ_t).
3. Bending of the shims (Δ_{sh}).
4. Bolt bending (Δ_b).
5. Bolt shear (Δ_v).

Deflection due to bending of the horizontal leg of the shelf angle:

$$Z = d_a + e + l_o$$

$$I_a = Zt^3/12$$

$$\Delta_d = V_b e^3 / 3EI_a$$

where:

Z = effective width of shelf angle

d_a = depth of vertical leg of shelf angle

e = eccentricity between line of load application and support plane of shelf angle

l_o = distance from bolt to end of shelf angle specimen

I_a = moment of inertia of the horizontal leg of the shelf angle

t = thickness of shelf angle

V_b = vertical load on bolt

E = modulus of elasticity of shelf angle

Deflection due to torsion on shelf angle:

$$\Delta_t = V_b e^2 \left(\frac{Z}{2GJ} \right)$$

where:

G = shear modulus of shelf angle

J = polar moment of inertia of shelf angle

Deflection due to bending of the shims:

$$p = A_b / (b_{sh} d)$$

$$n = E_b / E_{sh}$$

$$k = \sqrt{2pn + (pn)^2} - pn$$

$$\theta_{sh} = \frac{t_{sh}}{2} \left(\frac{V_b (2e + t_{sh})}{A_b d^2 E_{sh} (1-k)(1-k/3)} \right)$$

$$\Delta_{sh} = \frac{V_b t_{sh}^2}{A_b d^2 E_{sh} (1-k)(1-k/3)} \left(\frac{e}{2} + \frac{t_{sh}}{3} \right)$$

where:

A_b = area of bolt

b_{sh} = width of shim

d = distance from bottom of shelf angle to bolt

E_b = modulus of elasticity of bolt

E_{sh} = modulus of elasticity of shim

t_{sh} = thickness of shim

θ_{sh} = rotation of shim at shelf angle interface

Deflection due to bolt bending:

$$\Delta_b = V_b t_{sh}^3 / (3E_b I_b)$$

where:

I_b = moment of inertia of bolt

Deflection due to bolt shear:

$$\Delta_v = V_b t_{sh} / 0.9G_b A_b$$

where:

G_b = shear modulus of bolt

This approach results in good to excellent correlation for the majority of the test results as shown in Table 6-5. Test stiffness is computed using measured actuator loads and displacements in the elastic loading range. The methodology consistently under-predicts stiffness for specimens with phenolic shims, possibly due to variations in material properties of the shims, and the general compressive rupture behavior of phenolic shims (characterized by pulverizing and extensive delamination). The methodology under-predicts the combination of thick shims and small-diameter bolt (test S14). While the 5/8" bolt does increase deflection due to bolt bending, it is possible that the other components of the subassembly mitigate this flexibility.

Table 6-5: Comparison of shelf angle test stiffness and computed stiffness.

Test ID	Shim Material	Shim Thickness (in)	Bolt Diameter (in)	Test Stiffness (lb/in)	Calculated Stiffness (lb/in)	Ratio of Calculated to Measured Stiffness
S7	vinylester	1.5	1	108,000	103,400	0.96
S8	vinylester	1.5	0.625	74,200	82,000	1.11
S9	polyurethane	1.5	1	92,000	107,000	1.16
S10	phenolic	1.5	1	83,600	68,300	0.82
S11	proprietary 1	1.5	1	87,800	102,800	1.17
S12	proprietary 2	1.5	1	105,600	104,300	0.99
S13	vinylester	3	1	84,300	82,700	0.98
S14	vinylester	3	0.625	58,400	32,700	0.56
S15	polyurethane	3	1	83,200	91	1.09
S16	phenolic	3	1	56,700	34,700	0.61
S17	proprietary 1	3	1	73,700	81,300	1.10
S18	proprietary 2	3	1	83,600	84,600	1.01
S21	carbon steel	3	1	149,000	132,800	0.89

6.4.2 Stresses

Stress checks due to concentrated loads at bolts may be completed using a similar methodology (and are performed for the maximum experimental force in Table 6-3 Table 6-4 above). The methodology described below will require modification for continuous shelf angles. See Tide and Krogstad (1993) for additional stress checks due to uniform load on shelf angle. In the equations below, a load factor of 1.4 corresponding to dead load is regularly used in the calculations.

Bending stress in horizontal leg of the shelf angle

$$M_u = 1.4V_b e$$

$$Z_x = Zt^2/4$$

$$\phi M_n = 0.9Z_x F_y$$

Shear stress in shelf angle

$$V_u = 1.4V_b \left(\frac{Z-l_o}{Z} \right)$$

$$f_{vb} = \frac{1.5V_u}{(d_a - (d_b + 1/16))t}$$

$$f_{vt} = V_u e t / J$$

$$f_v = f_{vb} + f_{vt}$$

$$\phi F_v = 0.9(0.6)F_y$$

where:

V_u = factored vertical shear in shelf angle at bolt

f_{vb} = factored beam shear stress in vertical leg of angle

f_{vt} = factored torsional shear stress in angle

f_v = total factored shear stress in angle

d_b = bolt diameter

Z_x = section modulus

Shim factored compressive stress

$$f_{bu} = 1.4 \left[\frac{2V_b(e+t_{sh})}{(1-k/3)k b d^2} \right]$$

Bolt tension and bending stress

$$T_{bu} = \frac{1.4V_b(e_a + t_{sh})}{(1 - k/3)d}$$

$$\phi T_{bn} = 0.75A_b F_{nt}$$

$$M_{bu} = 1.4V_b t_{sh}$$

$$\phi M_{bn} = 0.75Z_b F_{nt}$$

where:

Z_b = section modulus of the bolt

F_{nt} = tensile strength from table J3.2 of AISC 360

F_{nv} = shear strength from table J3.2 of AISC 360

The combined effects of bolt tension and bending may be calculated using Equation H2-1 in the AISC Specification (AISC 2010).

Bolt shear stress

$$V_{bu} = 1.4V_b$$

$$\phi V_{bn} = 0.75A_b F_{nv}$$

7 Roof Posts and Canopy Beams

This chapter summarizes the results of the experimental tests and analyses of roof posts and canopy beams. Two thermal break strategies were investigated to document their limit states and behavior. Chapter 1 details these solutions, including solutions utilizing FRP materials as shims, as well solutions using partial replacement of the structural member under consideration.

7.1 Experimental setup and design

7.1.1 Test matrix

The test matrix for roof posts and canopy beams is presented in Table 7-1 below. Across specimen types, two configurations were considered: oversized specimens in which the bolts, welds, and base plates are increased in size to prevent premature failure and to focus potential failure in the shims and the member, and efficiently-designed specimens in which connections and base plates were designed to factored loads. Shim thickness was varied between 1, 3, and 6 inches. Roof post FRP sleeves were also employed to examine partial member replacement as a potential structural assembly (this detail is discussed in the following paragraphs).

Roof posts were designed to be 2.5 ft in height while canopy beams were designed to be 5.5 ft in length, both representing common construction configurations for their respective cladding details. Base plates were designed as square to maintain symmetry in the experimental testing. Each plate was designed using the recommendations in the AISC Base Plate Design Guide (AISC 2006). It should be noted, however, that to explore a range of potential responses in the base conditions, the base plates for efficiently-designed specimens were thinner than the common industry standard, which is typically $\frac{3}{4}$ ".

Bolts were placed on the base plate at 6" on center, and were both efficiently designed with stainless steel B8 bolts, and oversized with 1" dia. A307 bolts (in accordance with industry practices). Bolts were installed by a single operator and were specified as snug-tight. Holes were specified as standard holes.

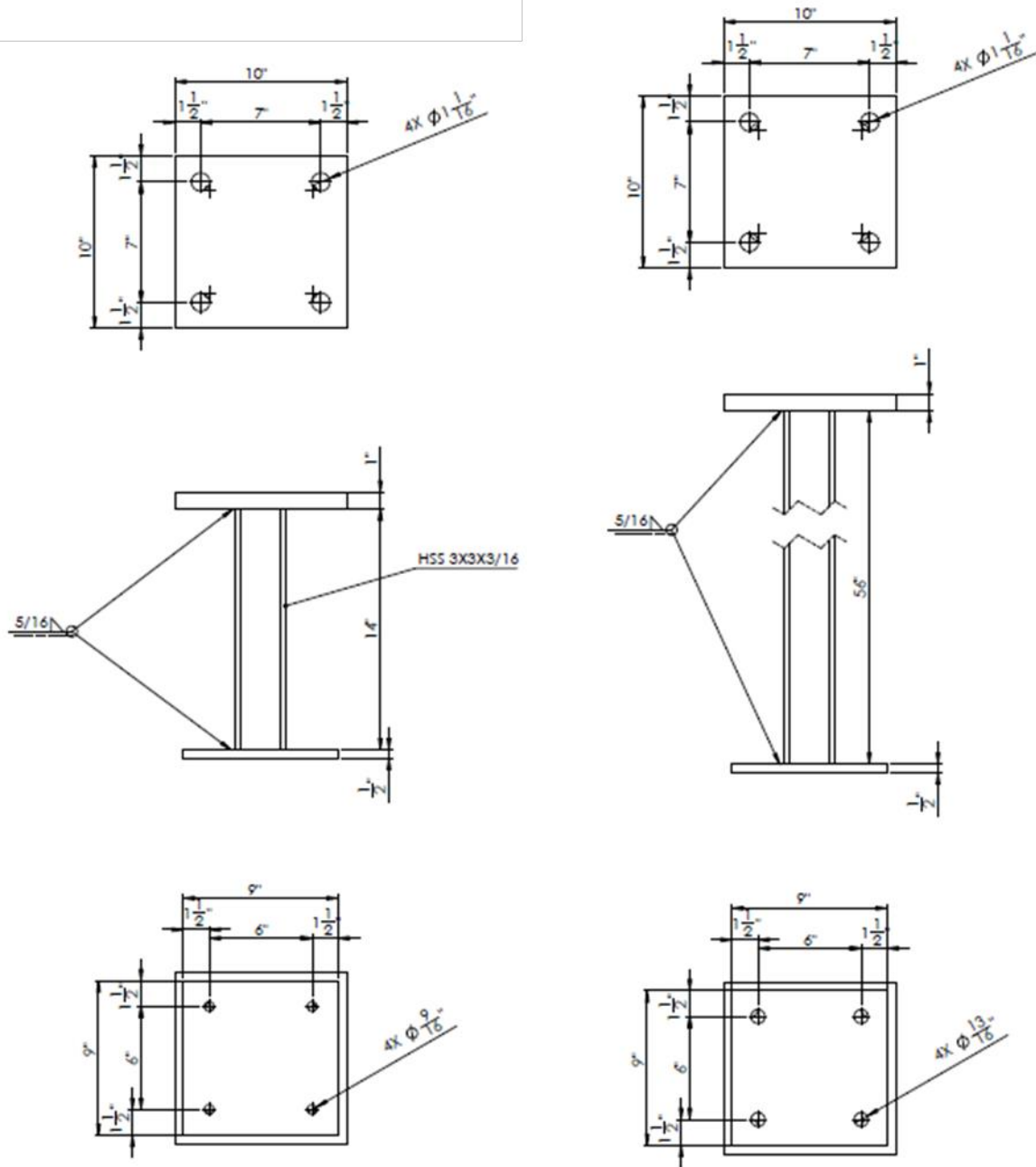


Figure 7-1: Roof post (left) and canopy beam (right) specimen schematics

Roof posts were designed as HSS 3x3x3/16 while canopy beams were designed as HSS 4x4x1/2 (all HSS were specified as ASTM A500, Grade B (46 ksi)). Posts and beams were of constant cross-section throughout the configurations tested. Welds between the post or beam and its base plate typically had the potential to be the critical limit state in these details, and as such, were detailed as complete joint penetration welds to ensure they did not impact response in the design regime.

Table 7-1: Roof post and canopy beam test matrices

	MITIGATION STRATEGY				SPECIMEN INFORMATION					
	Test Name	Specimen Type	Type	Material	Thick (in)	End Plate	Rod Dia. (in)	Rod Spacing (in)	Rod Spec	Loading
ROOF POSTS (AXIAL + LATERAL)	R1	designed	-	-	-	9x9x3/8"	0.5	6" oc	B8 Class 2	Monotonic
	R2	designed	shim	vinylester	3	9x9x1/2"	0.5	6" oc	B8 Class 2	Monotonic
	R3	designed	sleeve	FRP 4x4x1/2	-	9x9x3/8"	0.5	6" oc	B8 Class 2	Monotonic
	R4	designed	-	-	-	9x9x3/8"	0.5	6" oc	B8 Class 2	Cyclic
	R5	designed	shim	vinylester	3	9x9x1/2"	0.5	6" oc	B8 Class 2	Cyclic
	R6	designed	sleeve	FRP 4x4x1/2	-	9x9x3/8"	0.5	6" oc	B8 Class 2	Cyclic
	R7	over-designed	-	-	-	9x9x1/2"	0.75	6" oc	A307	Cyclic
	R8	over-designed	shim	vinylester	3	9x9x1/2"	0.75	6" oc	A307	Cyclic
	R9	over-designed	shim	phenolic	3	9x9x1/2"	0.75	6" oc	A307	Cyclic
	R10	over-designed	shim	polyurethane	3	9x9x1/2"	0.75	6" oc	A307	Cyclic
	R11	over-designed	shim	proprietary 1	3	9x9x1/2"	0.75	6" oc	A307	Cyclic
	R12	over-designed	shim	proprietary 2	3	9x9x1/2"	0.75	6" oc	A307	Cyclic
	R13	over-designed	shim	vinylester	1	9x9x1/2"	0.75	6" oc	A307	Cyclic
	R14	over-designed	shim	vinylester	6	9x9x1/2"	0.75	6" oc	A307	Cyclic
CANOPY BEAMS (LATERAL)										

A schematic of the roof post FRP sleeve detail is shown in Figure 7-2 below, as well as an as-tested photograph of the specimen. Threaded rods that were 0.5” in diameter connect one side of the sleeve to the other, and run through the steel post. The post is broken in the middle to lessen the transfer of heat from interior to exterior. Rod spacings were designed in accordance with AISC 360 (2010) and the LRFD pre-standard for FRP structural members. Availability of pultruded square shapes limited the sleeve to a 4x4x1/2” FRP sleeve, which created slack between the sleeve and post (HSS 3x3x3/16). In an actual structure, this slack could be eliminated via bonding FRP shims to the inside of the sleeve to ensure fit-up.

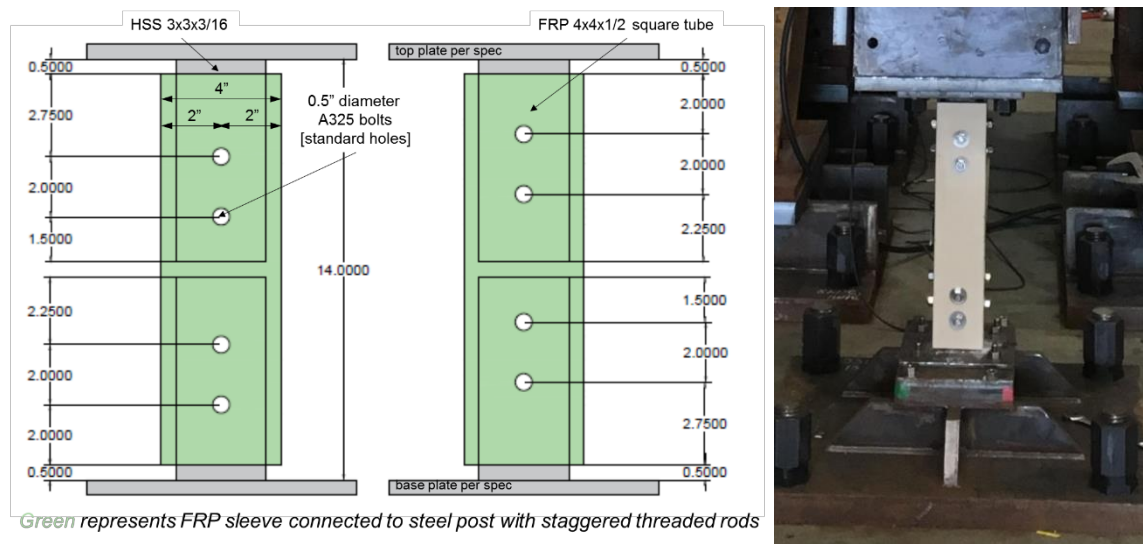


Figure 7-2: Roof post FRP sleeve configuration and photograph of as-tested specimen

7.1.2 Test rig and protocol

The roof post/canopy beam test rig is comprised of two actuators, one lateral and one vertical, a load transfer block, the base (connecting specimen to the strong floor), and the reaction frame. These components are illustrated in Figure 7-3 below.

Roof posts are loaded with a 10 kip axial load to replicate the weight of typical dunnage on the post. After the axial load is applied via the vertical actuator (in load control), the horizontal actuator loads the specimen in displacement control. Canopy beams are intended to be pure cantilevers with zero axial force. To achieve this condition, the vertical actuator counteracts the weight of the load transfer block and half of the horizontal actuator so that the total axial force on the specimen is zero. In both the roof post and canopy beam test setups, the load transfer block is allowed to rotate to simulate a cantilever boundary condition, and is only restrained in the out-of-plane dimension.

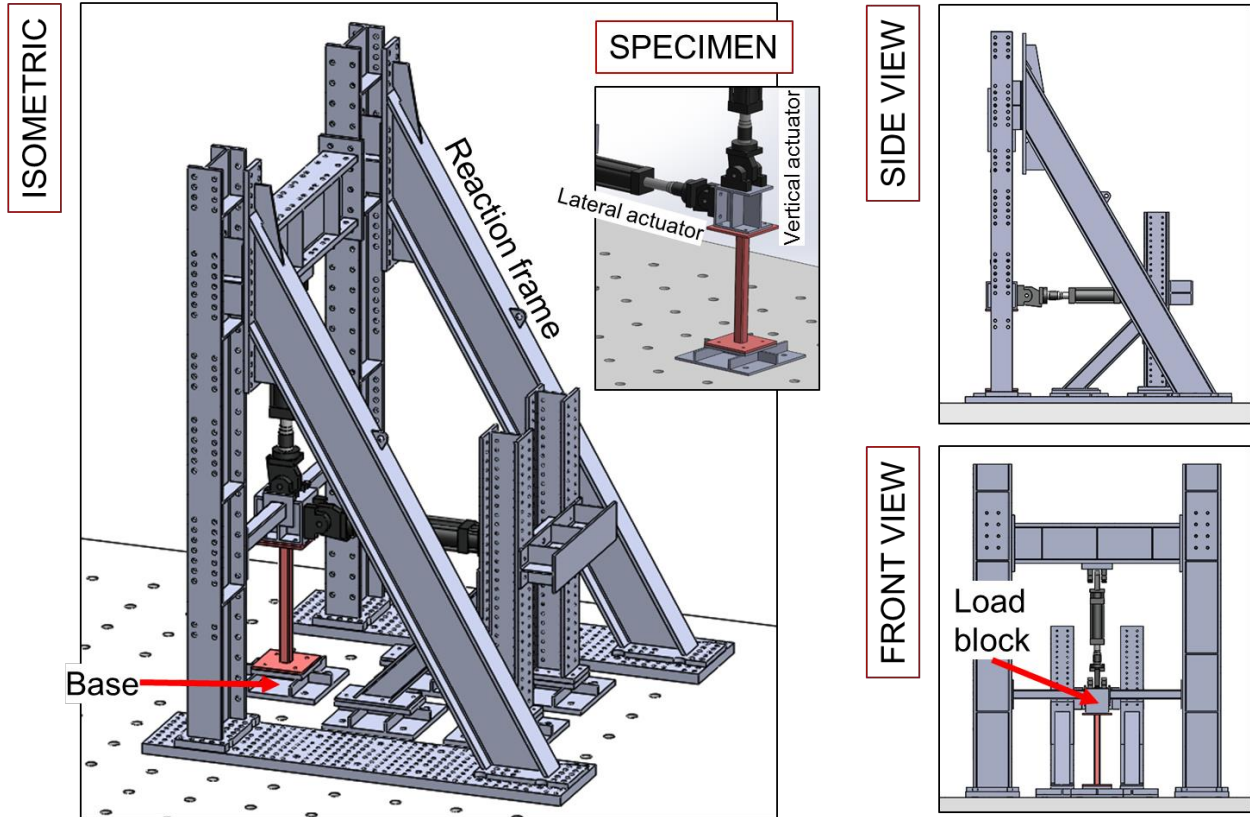


Figure 7-3: Specimen (in red) positioned in the test rig at the Northeastern University STReSS Lab

Load is applied to the top of the specimen (connected to a 1" end plate via a CJP weld) via a load transfer block, which connects the two actuators to the top of the specimen via 1" dia. bolts. The load transfer block is assumed to be rigid and is built up of 1" steel plate (shown in Figure 7-4 below). The horizontal actuator can move vertically up or down as needed, as can the vertical actuator.

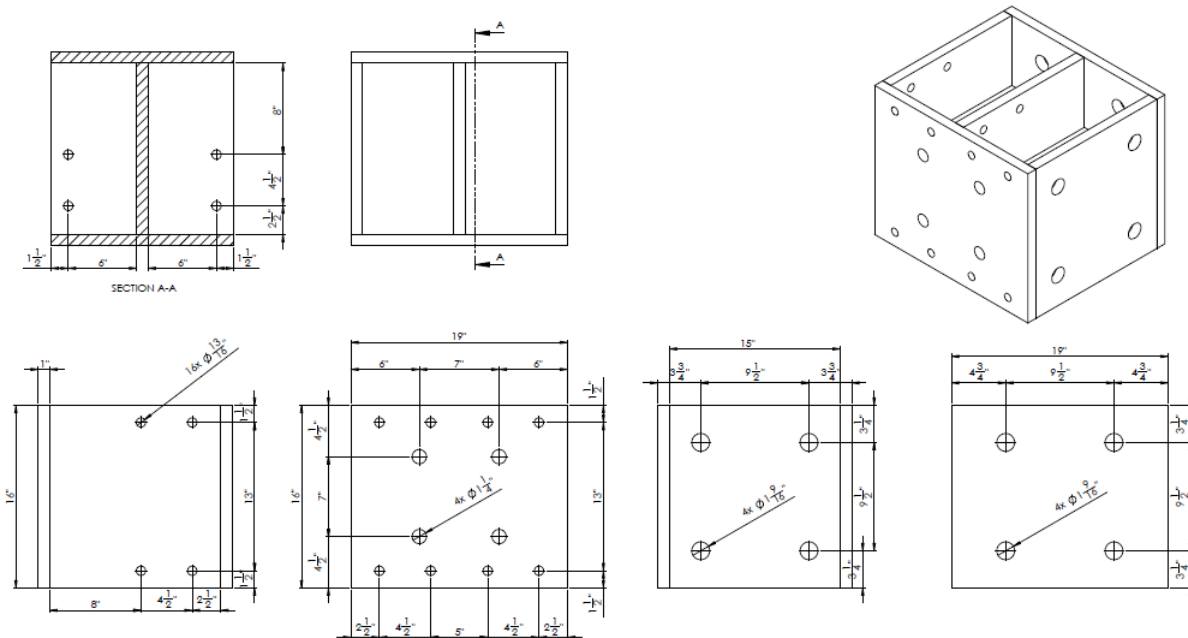


Figure 7-4: Load block detail drawings, interfacing actuator heads with specimen top plates.

Monotonic tests were displacement-controlled for the horizontal actuator, at a rate of 0.18% drift per minute. The vertical actuator was force-controlled throughout testing. Cyclic tests were displacement-controlled for the horizontal actuator, loading at a rate of 2.1% drift per minute, while the vertical actuator remained in load-control. Load rates were taken from the work of Gomez (2010), in which steel posts with base plates were tested cyclically and monotonically. The SAC protocol was used for the cyclic protocol, and was scaled to the exact height of each specimen (which varied due to differing shim thicknesses) such that the load rate and drift targets were consistent across testing. Figure 7-5 presents this protocol for the roof posts, depicting the scaling of the protocol for three different configurations.

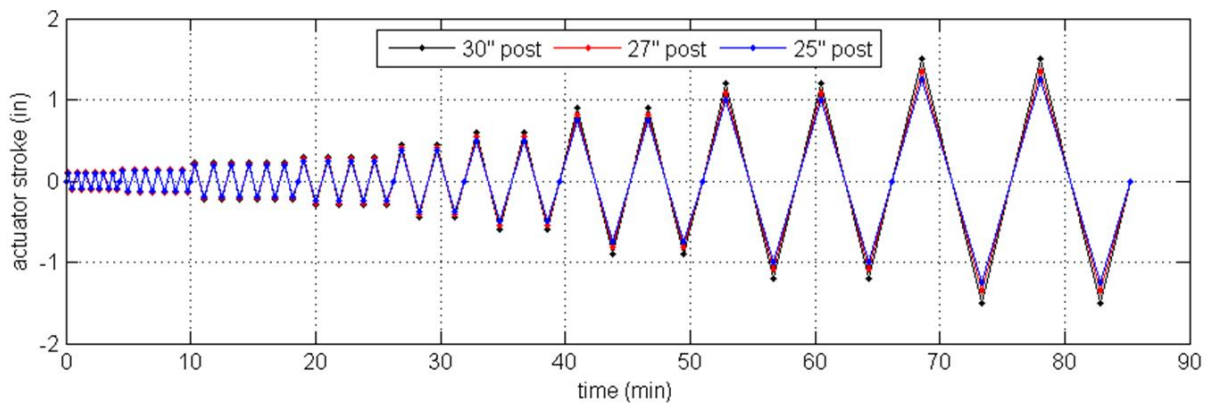


Figure 7-5: SAC protocol scaled for various roof posts height such that load rate (2.1% drift/min) is constant throughout testing

7.1.3 Instrumentation plan

To capture lateral movement of the base plate, LVDTs were installed on the West face of the base plate (cardinal directions and specimen orientation are shown in Figure 7-6 below). They were mounted to strong magnetic frames installed on the base of the rig. Quintuplet LVDTs on the south and east sides of the base plate were oriented vertically to record the buckling of the base plate along its face on these two sides of the member. These quintuplet sensors recorded base plate deformed shapes up until approximately 2% drift, when they typically became misaligned with the base plate due to large deformations, and were removed from the specimen. These quintuples were also mounted via strong magnetic mounting frames affixed to the base of the rig.

Using small LVDTs installed along the vertical dimension of the post/beam, it is possible to calculate the curvature of the post. Two LVDTs were installed along the east and west faces of the HSS specimens. The LVDTs overlap such that their gage lengths were staggered. They were mounted to the HSS itself via aluminum brackets that were glued to the specimen.

Strain gauges were also installed on each specimen. A strain gage was installed on the south and east faces of the base plate, 1" away from the weld to the post. Strain gauges at 2" and 4" up from the base plate were installed on the post/beam on the west and east sides of the specimen. These gauges were intended to provide curvature readings at ranges smaller than what the post/beam LVDTs can reliably record.

Figure 7-6 provides an illustration of the instrumentation plan. Figure 7-7 depicts the sensors as-installed on a test specimen.

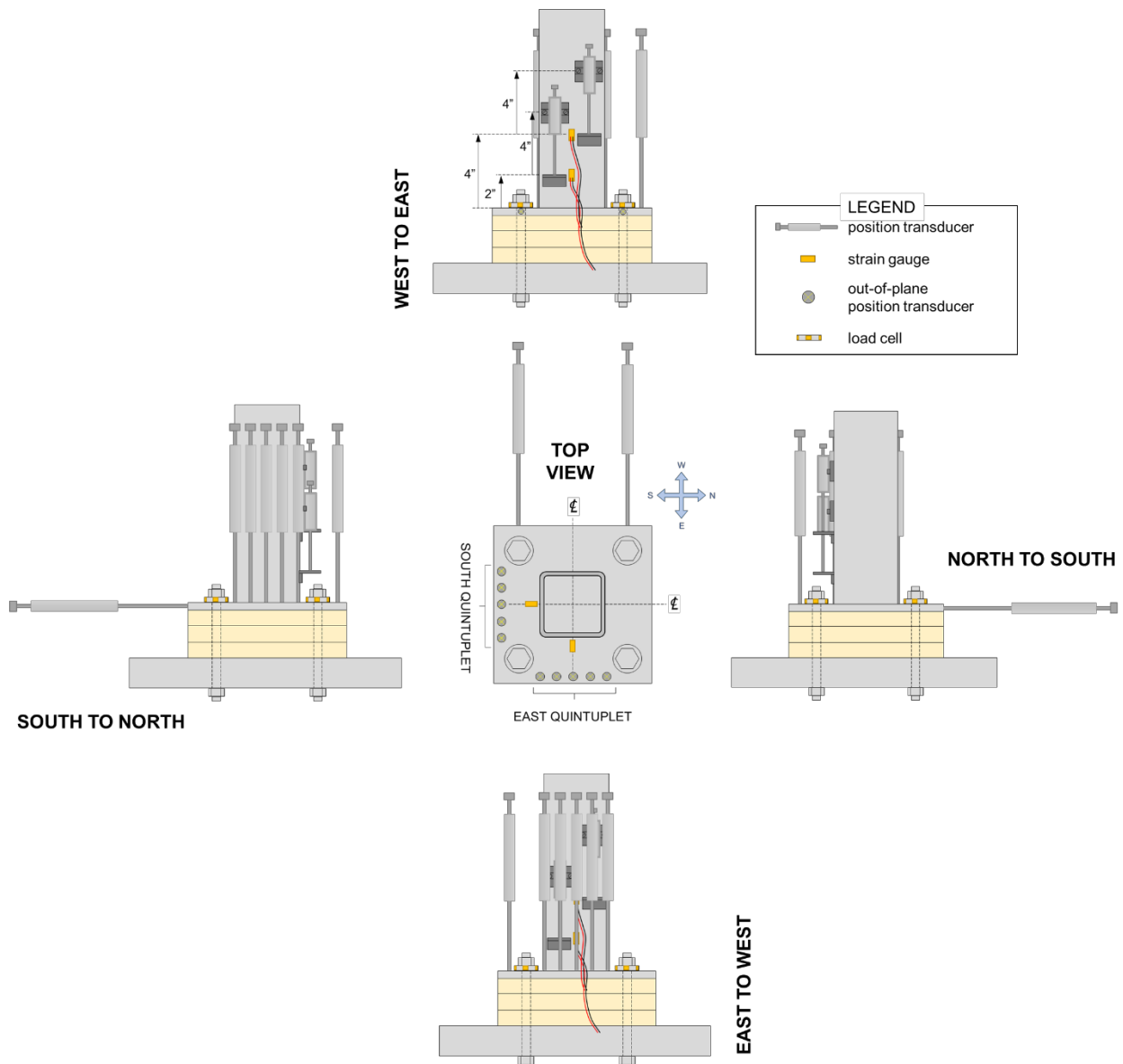


Figure 7-6: Sensor configuration for roof post and canopy beam specimens, with views from each direction

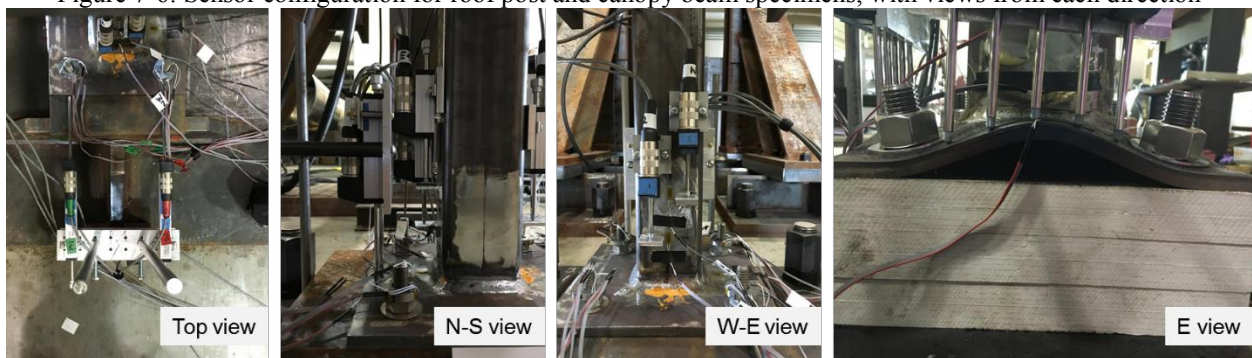


Figure 7-7: Photographs of instrumentation plan from top, North to South, West to East, and East (east view is on a deformed specimen, demonstrating how LVDT sensors are able to read vertical deformations of base plate)

7.2 Results and Discussion

Roof post results are presented in Table 7-2 for nominal test-to-predicted ratios, and Table 7-3 for measured test-to-predicted ratios using measured properties. Measured properties include results reported in Appendix A from tensile coupon tests of the roof posts and canopy beam base plates and bolt materials, and through-thickness compression tests for FRP materials. The roof post and canopy beam base metal was not tested as the tensile coupons were deformed during manufacturing due to residual stresses in the HSS sections; as such, values from mill reports were used for the measured properties. Maximum experimental loads and moments are included, as well as base plate, post bending, shim compression, bolt tension, bolt shear, and bolt bending limit states (equations for these limit states are presented in Chapter 6). To determine the experimental maximum moment, a reduction factor is applied to the height of the specimen (from top of base plate to base of load transfer block) to account for test rig influence on inflection point. These reduction factors are explained in detail in the finite element modeling portion of this chapter. Moment is calculated by multiplying P_{max} by specimen height and the inflection point reduction factor R_f . Results are presented for the system, i.e., four bolts are considered for shear and bending calculations. In the case of bolt tension, two bolts are considered under uplift only (caused by bending of the post). Nominal and measured results calculations are not available for all limit states (shim compression, for example).

Base plate yielding is characterized by yield line diagrams, and relationships for the yield load on the plate are determined from the diagram geometry. Given that all of the base plates tested in the study deformed significantly and buckled, this method is thought to be overly conservative, with test-to-predicted ratios well below 1. The equations developed for these yield forces are shown in Figure 7-8 below.

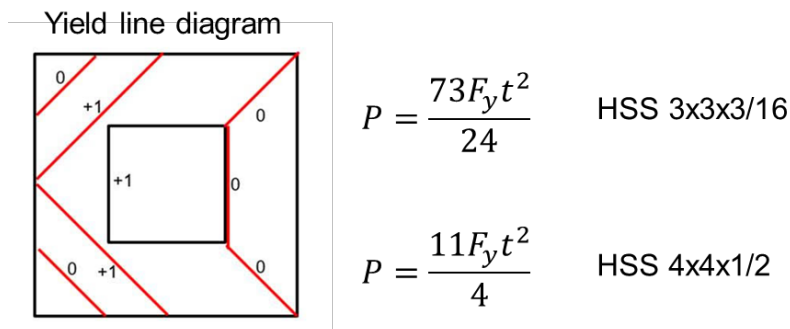


Figure 7-8: Yield line diagram for base plates and post/beams, based on observed deformed shapes

Shim compression for roof posts is determined via a combination of the applied axial force (10 kips) and the compression due to bending moment at the base plate at the maximum force. For canopy beams, which do not have applied axial load, shim compression is based solely on the compressive stresses from bending of the beam.

Based on the tabulated test-to-predicted ratios, bolt bending governs, and is magnified with shims of increasing thickness. However, it should be noted that required strengths for roof posts are approximately 5 kip-ft (60 kip-inches, unfactored, and based upon common design loads recommended by the Industry Advisory Board) during which the specimen responses are still elastic, so all specimens resisted loads well in excess of the factored design loads.

Table 7-2: Roof post results and nominal strength-to-predicted ratios

ROOF POSTS - NOMINAL

Test Name	STRENGTH RESULTS				BASE PLATE YIELDING			POST BENDING	
	P_{max} kip	R_f -	h in	M_u kip-in	P_n kip	P_u kip	P_u/P_n -	M_n kip-in	M_u/M_n -
R1	5.334	0.85	21	95.21	15.40	5.33	0.35	90.84	1.05
R2	8.339	0.85	21	148.85	27.38	8.34	0.30	90.84	1.64
R3	4.39	1	21	92.19	15.40	4.39	0.29	90.84	1.01
R4	5.567	0.85	21	99.37	15.40	5.57	0.36	90.84	1.09
R5	8.69	0.85	15	110.80	27.38	8.69	0.32	90.84	1.22
R6	5.88	1	15	88.20	15.40	5.88	0.38	90.84	0.97
R7	6.88	0.95	21	137.26	27.38	6.88	0.25	90.84	1.51
R8	9.29	0.95	15	132.38	27.38	9.30	0.34	90.84	1.46
R9	6.438	0.95	15	91.74	27.38	6.44	0.24	90.84	1.01
R10	9.44	0.95	15	134.52	27.38	9.44	0.34	90.84	1.48
R11	9.285	0.95	15	132.31	27.38	9.29	0.34	90.84	1.46
R12	9.041	0.95	15	128.83	27.38	9.04	0.33	90.84	1.42
R13	9.31	0.95	15	132.67	27.38	9.31	0.34	90.84	1.46
R14	8.69	0.95	15	123.83	27.38	8.69	0.32	90.84	1.36

Test Name	BOLT TENSION			BOLT SHEAR			BOLT BENDING		
	T_{bn} kip	T_{uplift} kip	T_{uplift}/T_{bn} -	T_n kip	F_{act} kip	F_{act}/T_n -	M_{bn} kip-in	M_{bu} kip-in	M_{bu}/M_{bn} -
R1	30.63	15.87	0.52	36.91	5.33	0.14	1.91	-	-
R2	30.63	24.81	0.81	36.91	8.34	0.23	1.91	25.02	13.07
R3	30.63	15.37	0.50	36.91	4.39	0.12	1.91	-	-
R4	30.63	16.56	0.54	36.91	5.57	0.15	1.91	-	-
R5	30.63	18.47	0.60	36.91	8.69	0.24	1.91	26.07	13.62
R6	30.63	14.70	0.48	36.91	5.88	0.16	1.91	-	-
R7	39.76	22.88	0.58	47.71	6.88	0.14	3.73	-	-
R8	39.76	22.08	0.56	47.71	9.30	0.19	3.73	27.89	7.48
R9	39.76	15.29	0.38	47.71	6.44	0.13	3.73	19.31	5.18
R10	39.76	22.42	0.56	47.71	9.44	0.20	3.73	28.32	7.60
R11	39.76	22.05	0.55	47.71	9.29	0.19	3.73	27.86	7.47
R12	39.76	21.47	0.54	47.71	9.04	0.19	3.73	27.12	7.28
R13	39.76	22.11	0.56	47.71	9.31	0.20	3.73	9.31	2.50
R14	39.76	20.64	0.52	47.71	8.69	0.18	3.73	52.14	13.99

Table 7-3: Roof post results and as-measured test-to-predicted ratios

ROOF POSTS - MEASURED

Test Name	STRENGTH RESULTS				BASE PLATE YIELDING			SHIM COMPRESSION				
	P_{max} kip	R_f -	h in	M_u kip-in	P_n kip	P_u kip	P_u/P_n -	P_n kip	P_{UB} kip	P_{UA} kip	$P_{UB} + P_{NA}$ kip	$(P_{UB} + P_{NA})/P_n$ -
R1	5.334	0.85	21	95.21	17.58	5.33	0.30	-	15.87	10	25.87	-
R2	8.339	0.85	21	148.85	46.92	8.34	0.18	2315	24.81	10	34.81	0.02
R3	4.39	1	21	92.19	17.58	4.39	0.25	-	15.37	10	25.37	-
R4	5.567	0.85	21	99.37	17.58	5.57	0.32	-	16.56	10	26.56	-
R5	8.69	0.85	15	110.80	46.92	8.69	0.19	2315	18.47	10	28.47	0.01
R6	5.88	1	15	88.20	17.58	5.88	0.33	-	14.70	10	24.70	-
R7	6.88	0.95	21	137.26	46.92	6.88	0.15	-	22.88	10	32.88	-
R8	9.29	0.95	15	132.38	46.92	9.30	0.20	2315	22.08	10	32.08	0.01
R9	6.438	0.95	15	91.74	46.92	6.44	0.14	1289	15.29	10	25.29	0.02
R10	9.44	0.95	15	134.52	46.92	9.44	0.20	4649	22.42	10	32.42	0.01
R11	9.285	0.95	15	132.31	46.92	9.29	0.20	3074	22.05	10	32.05	0.01
R12	9.041	0.95	15	128.83	46.92	9.04	0.19	3048	21.47	10	31.47	0.01
R13	9.31	0.95	15	132.67	46.92	9.31	0.20	2315	22.11	10	32.11	0.01
R14	8.69	0.95	15	123.83	46.92	8.69	0.19	2315	20.64	10	30.64	0.01

Test Name	BOLT TENSION			BOLT SHEAR			BOLT BENDING		
	T_{bn} kip	T_{uplift} kip	T_{uplift}/T_{bn} -	T_n kip	F_{act} kip	F_{act}/T_n -	M_{bu} kip-in	M_{bn} kip-in	M_{bu}/M_{bn} -
R1	39.92	15.87	0.40	47.90	5.33	0.11	-	2.49	-
R2	39.92	24.81	0.62	47.90	8.34	0.17	25.02	2.49	10.03
R3	39.92	15.37	0.38	47.90	4.39	0.09	-	2.49	-
R4	39.92	16.56	0.41	47.90	5.57	0.12	-	2.49	-
R5	39.92	18.47	0.46	47.90	8.69	0.18	26.07	2.49	10.45
R6	39.92	14.70	0.37	47.90	5.88	0.12	-	2.49	-
R7	63.83	22.88	0.36	76.60	6.88	0.09	-	5.98	-
R8	63.83	22.08	0.35	76.60	9.30	0.12	27.89	5.98	4.66
R9	63.83	15.29	0.24	76.60	6.44	0.08	19.31	5.98	3.23
R10	63.83	22.42	0.35	76.60	9.44	0.12	28.32	5.98	4.73
R11	63.83	22.05	0.35	76.60	9.29	0.12	27.86	5.98	4.65
R12	63.83	21.47	0.34	76.60	9.04	0.12	27.12	5.98	4.53
R13	63.83	22.11	0.35	76.60	9.31	0.12	9.31	5.98	1.56
R14	63.83	20.64	0.32	76.60	8.69	0.11	52.14	5.98	8.71

Roof posts were observed to bend significantly at the base plate, regardless of plate slenderness. The deformation of the plate allowed the post to rotate about the base plate. As such, stresses were concentrated on the CJP weld, and failure in all specimens ultimately occurred in the heat-affected zone of the weld. In typical roof post details, the base plate is selected based upon economy and rules of thumb, and is significantly over-designed for the detail. Thus, the weld between the post and the base plate may be the limiting factor in a typical design, as it was in the specimen design. However, the weld limit states did not engage in the specimen behavior until beyond 10% drift.

Shims were lightly exercised by the loading, as evidenced by the test-to-predicted ratios. As shims should match the base plate area for maximum thermal performance, shims are large, and forces are evenly distributed across the shim. Shims were not observed to rack back and forth during testing, except in the final stages of lateral loading, when bolt bearing on the shims caused the shims to rub against one another.

Results and nominal test-to-predicted ratios for the canopy beams are presented in Table 7-4 below. Limit states and strength results are determined in the same manner as in the roof post result tables. Results with measured properties are presented in Table 7-5.

Table 7-4: Canopy beam results and nominal strength-to-predicted ratios

CANOPY BEAMS - NOMINAL

Test Name	STRENGTH RESULTS				BASE PLATE YIELDING			POST BENDING	
	P_{max} kip	R_f -	h in	M_u kip-in	P_n kip	P_u kip	P_u/P_n -	M_n kip-in	M_u/M_n -
C1	4.887	0.8	57	222.85	13.92	4.89	0.35	354.60	0.63
C2	5.807	0.8	51	236.93	13.92	5.81	0.42	354.60	0.67
C4	4.539	0.8	57	206.98	13.92	4.54	0.33	354.60	0.58
C5	4.858	0.8	51	198.21	13.92	4.86	0.35	354.60	0.56
C7	6.213	0.95	57	336.43	24.75	6.21	0.25	354.60	0.95
C8	7.04	0.95	51	341.09	24.75	7.04	0.28	354.60	0.96
C9	6.752	0.95	51	327.13	24.75	6.75	0.27	354.60	0.92
C10	7.236	0.95	51	350.58	24.75	7.24	0.29	354.60	0.99
C11	6.962	0.95	51	337.31	24.75	6.96	0.28	354.60	0.95
C12	7.176	0.95	51	347.68	24.75	7.18	0.29	354.60	0.98
C13	7.032	0.95	51	340.70	24.75	7.03	0.28	354.60	0.96
C15	6.804	0.95	51	329.65	24.75	6.80	0.27	354.60	0.93

Test Name	BOLT TENSION			BOLT SHEAR			BOLT BENDING		
	T_{bn} kip	T_{uplift} kip	T_{uplift}/T_{bn} -	T_n kip	F_{act} kip	F_{act}/T_n -	M_{bn} kip-in	M_{bu} kip-in	M_{bu}/M_{bn} -
C1	68.92	37.14	0.54	83.06	4.89	0.06	6.46	-	-
C2	68.92	39.49	0.57	83.06	5.81	0.07	6.46	17.42	2.70
C4	68.92	34.50	0.50	83.06	4.54	0.05	6.46	-	-
C5	68.92	33.03	0.48	83.06	4.86	0.06	6.46	14.57	2.26
C7	70.69	56.07	0.79	84.82	6.21	0.07	8.84	-	-
C8	70.69	56.85	0.80	84.82	7.04	0.08	8.84	21.12	2.39
C9	70.69	54.52	0.77	84.82	6.75	0.08	8.84	20.26	2.29
C10	70.69	58.43	0.83	84.82	7.24	0.09	8.84	21.71	2.46
C11	70.69	56.22	0.80	84.82	6.96	0.08	8.84	20.89	2.36
C12	70.69	57.95	0.82	84.82	7.18	0.08	8.84	21.53	2.44
C13	70.69	56.78	0.80	84.82	7.03	0.08	8.84	7.03	0.80
C15	70.69	54.94	0.78	84.82	6.80	0.08	8.84	40.82	4.62

Canopy beams, despite representing an entirely different structural detail from the roof posts, behave similarly. Bolt bending governs but increased bolt sizes mitigate this limit state more so than in the roof post testing. Canopy beam base plates also deformed significantly during testing, and the yield line methodology is again considered an over-estimate of the strength of these base plates.

Table 7-5: Canopy beam results and as-measured test-to-predicted ratios

CANOPY BEAMS - MEASURED												
Test Name	STRENGTH RESULTS				BASE PLATE YIELDING			SHIM COMPRESSION				
	P_{max} kip	R_f -	h in	M_u kip-in	P_n kip	P_u kip	P_u/P_n -	P_n kip	P_{UB} kip	P_{UA} kip	$P_{UB} + P_{nA}$ kip	$(P_{UB} + P_{nA})/P_n$ -
C1	4.887	0.8	57	222.85	15.89	4.89	0.31	0	37.14	0	37.14	-
C2	5.807	0.8	51	236.93	15.89	5.81	0.37	2315	39.49	0	39.49	0.02
C4	4.539	0.8	57	206.98	15.89	4.54	0.29	0	34.50	0	34.50	-
C5	4.858	0.8	51	198.21	15.89	4.86	0.31	2315	33.03	0	33.03	0.01
C7	6.213	0.95	57	336.43	42.42	6.21	0.15	0	56.07	0	56.07	-
C8	7.04	0.95	51	341.09	42.42	7.04	0.17	2315	56.85	0	56.85	0.02
C9	6.752	0.95	51	327.13	42.42	6.75	0.16	1289	54.52	0	54.52	0.04
C10	7.236	0.95	51	350.58	42.42	7.24	0.17	4649	58.43	0	58.43	0.01
C11	6.962	0.95	51	337.31	42.42	6.96	0.16	3074	56.22	0	56.22	0.02
C12	7.176	0.95	51	347.68	42.42	7.18	0.17	3048	57.95	0	57.95	0.02
C13	7.032	0.95	51	340.70	42.42	7.03	0.17	2315	56.78	0	56.78	0.02
C15	6.804	0.95	51	329.65	42.42	6.80	0.16	2315	54.94	0	54.94	0.02

Test Name	BOLT TENSION			BOLT SHEAR			BOLT BENDING		
	T_{bn} kip	T_{uplift} kip	T_{uplift}/T_{bn} -	T_n kip	F_{act} kip	F_{act}/T_n -	M_{bu} kip-in	M_{bn} kip-in	M_{bu}/M_{bn} -
C1	89.81	37.14	0.41	107.78	4.89	0.05	-	8.42	-
C2	89.81	39.49	0.44	107.78	5.81	0.05	17.42	8.42	2.07
C4	89.81	34.50	0.38	107.78	4.54	0.04	-	8.42	-
C5	89.81	33.03	0.37	107.78	4.86	0.05	14.57	8.42	1.73
C7	113.47	56.07	0.49	136.17	6.21	0.05	-	14.18	-
C8	113.47	56.85	0.50	136.17	7.04	0.05	21.12	14.18	1.49
C9	113.47	54.52	0.48	136.17	6.75	0.05	20.26	14.18	1.43
C10	113.47	58.43	0.51	136.17	7.24	0.05	21.71	14.18	1.53
C11	113.47	56.22	0.50	136.17	6.96	0.05	20.89	14.18	1.47
C12	113.47	57.95	0.51	136.17	7.18	0.05	21.53	14.18	1.52
C13	113.47	56.78	0.50	136.17	7.03	0.05	7.03	14.18	0.50
C15	113.47	54.94	0.48	136.17	6.80	0.05	40.82	14.18	2.88

Figure 7-9 and Figure 7-10 depict force-drift results using the force from the lateral actuator, and backbone curves from the cyclic testing. Notably, shim material does not have a significant impact on peak force. Roof posts are more variable in response than canopy beams, but in both sub-assemblies, nominally identical specimens (save for shim material and thickness) varied by no more than 15%. As shims were not loaded near their maximum capacity, this is anticipated for canopy beams. Roof post testing exercised the shims with an additional 10 kips of axial load, so variability in the force results up to 5% drift may be attributed to compression of the shims (though not failure). Performance is striated based upon shim compressive strength. Polyurethane shims are consistently the strongest shim material, and phenolic the weakest.

Figure 7-11 and Figure 7-12 depict moment-drift results for roof posts and canopy beams, respectively. Moment is reduced via the R_f factors discussed above. Across testing, bolt size and base plate thickness dictate behavior more than bolt material, shim material, and shim thickness. FRP sleeve specimens (roof posts only) attained comparable peak strengths, but were less stiff than unmitigated specimens, or specimens with shims.

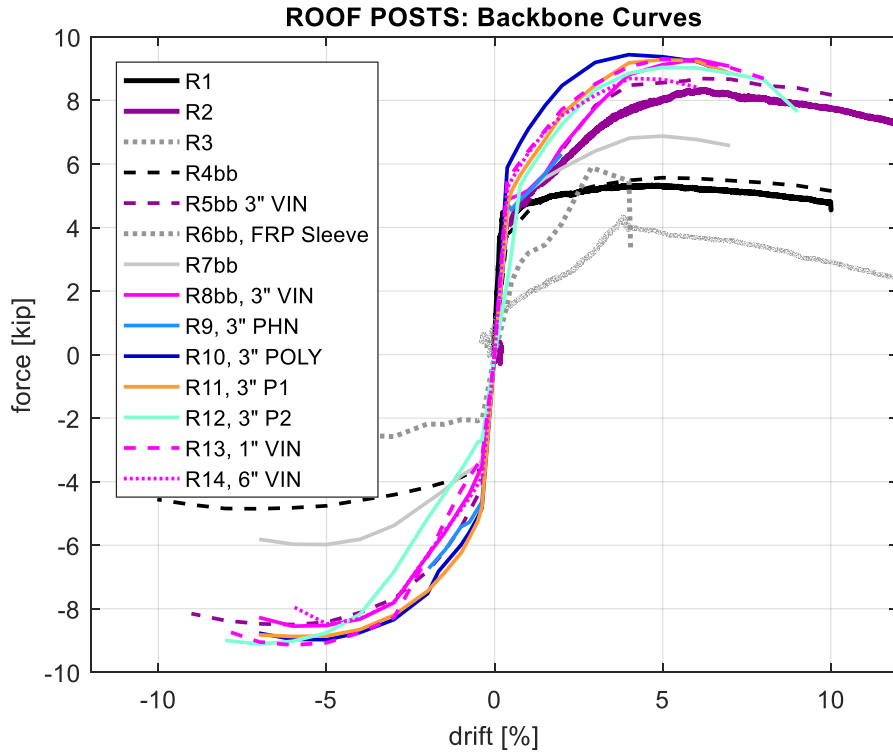


Figure 7-9: Cyclic backbone and monotonic force-drift results for roof post specimens

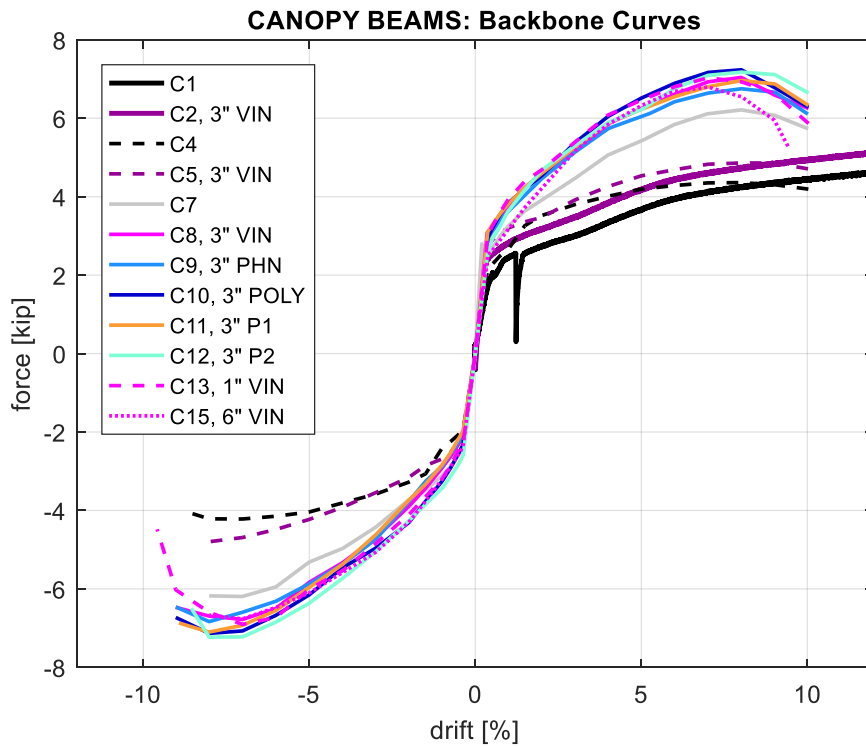


Figure 7-10: Cyclic backbone and monotonic force-drift results for canopy beam specimens

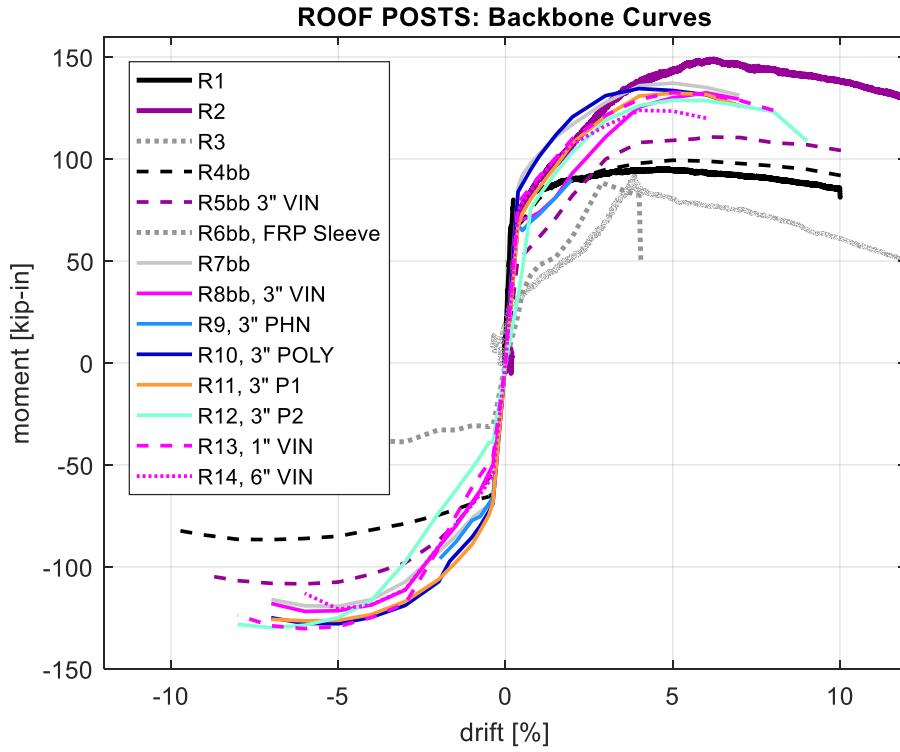


Figure 7-11: Cyclic backbone and monotonic moment-drift results for roof post specimens

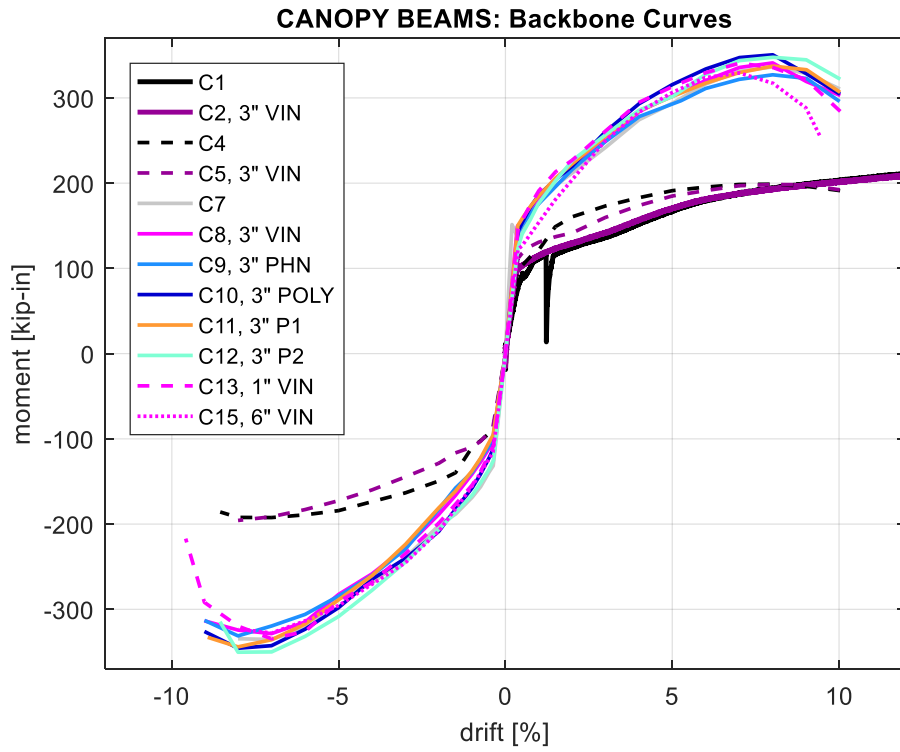


Figure 7-12: Cyclic backbone and monotonic moment-drift results for canopy beam specimens

Representative cyclic plots are shown in Figure 7-13 below for tests C7 and C10, demonstrating the range in behavior between an unmitigated specimen and a specimen with 3” shims. As anticipated, due to the shorter beam height, the shimmed specimen reaches higher moments. Both specimens demonstrate slight pinching, and this behavior is visible in all of the roof posts and canopy beams tested. Pinching in the reverse cycle can be attributed to a stability plate buckling mode as the base plate moves from buckling from loaded edge to loaded edge. Bolt elongation and base plate deformation contribute to damage in the specimen, which reduces its energy dissipating capacity. Force-displacement curves for all tests are shown in Appendix D to this report.

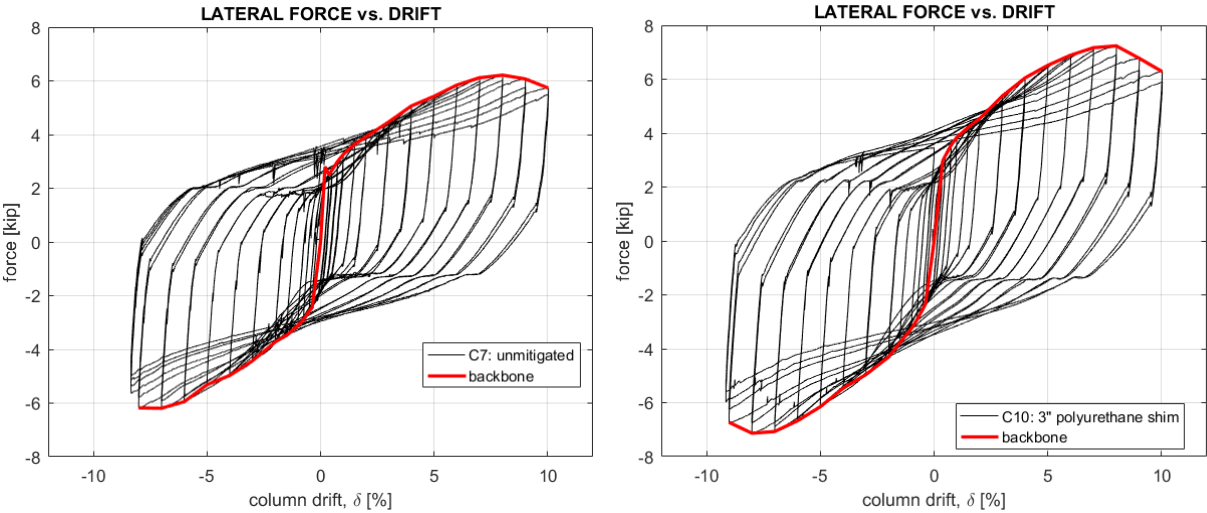


Figure 7-13: Hysteretic curves and backbones for tests C7 (no shim) and C10 (3” polyurethane shim)

Base plate strains (as measured by a strain gauge installed on the east side of the base plate) are shown for unmitigated posts and beams and posts and beams mitigated with vinylester shims (shown in Figure 7-14 and Figure 7-15 respectively). For canopy beams, the elongated specimen size increases strains on the base plate in specimens with thicker plates (C7-15). Shims of increasing thickness contribute to larger strains in the base plate for canopy beams only, in part

due to the longer length of the total specimen with the addition of thick shims. Results for all tests may be found in Appendix D of this report.

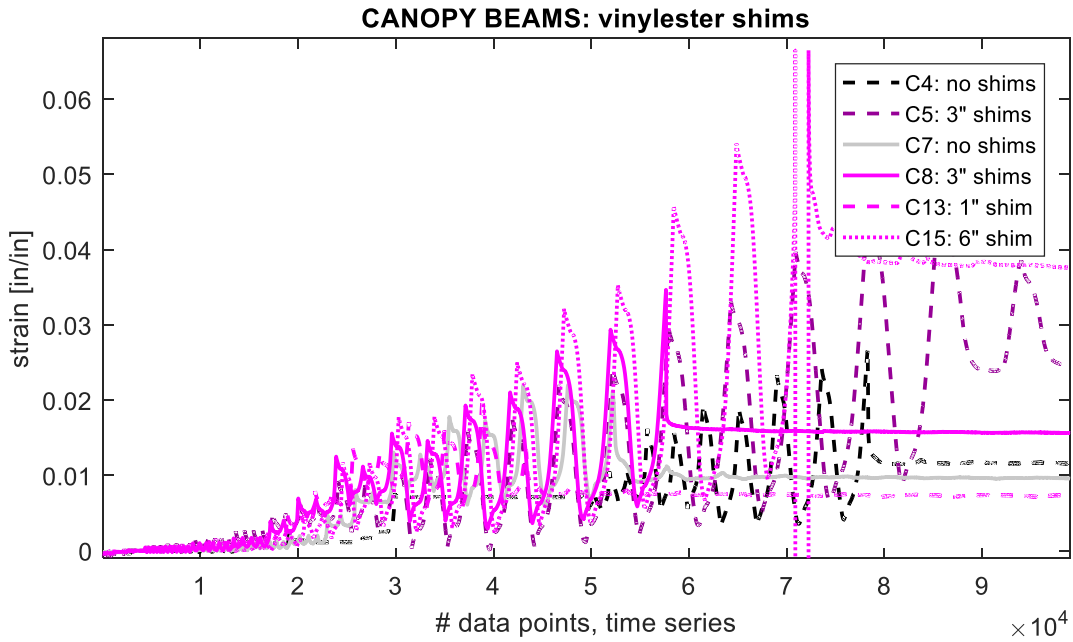


Figure 7-14: East side (loaded side) base plate strains for unmitigated canopy beams and assemblies with vinylester shims of varying thickness

In the roof posts tests, where axial load is applied prior to lateral loading, posts with thinner base plates experience greater base plate strains than those specimens with thicker plates. Shim thickness has no discernible effect on the base plate strains.

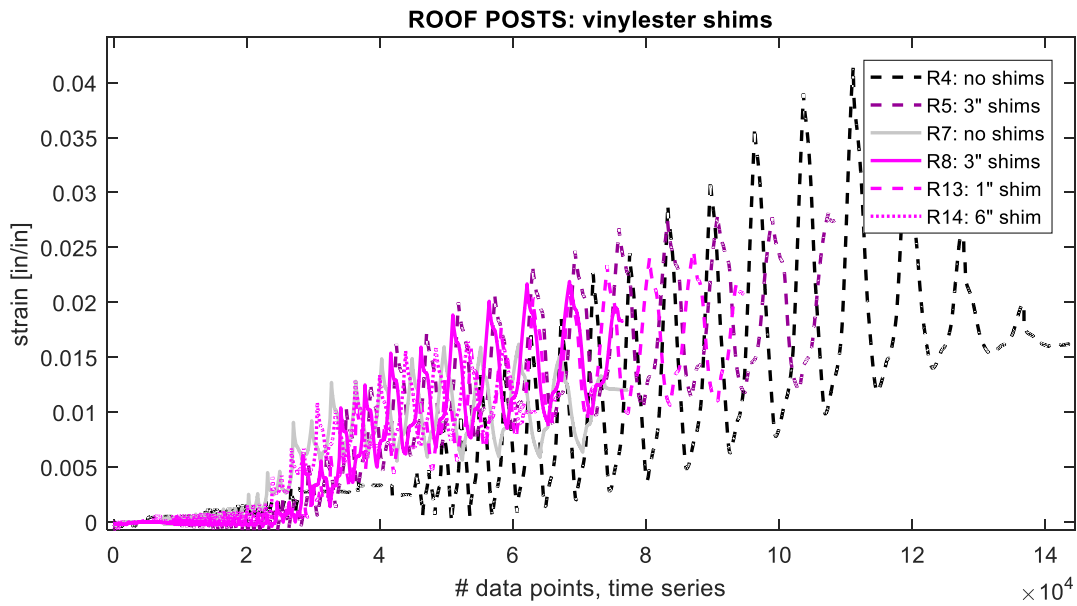


Figure 7-15: East side (loaded side) base plate strains for unmitigated roof posts and assemblies with vinylester shims of varying thickness

Base plate vertical LVDTs (quintuplet sensors) installed on the south and east faces of the base plate capture base plate deformed shapes as the test progresses. While the sensors were removed just beyond 2% drift to prevent damage to the sensors, they capture behavior in the design region for these cladding details. Figure 7-16 presents representative plots of these deformed shapes for tests R7 and R10, which are nominally identical with the exception of the 3” shim in R10. The plotted deformed shape is with respect to the base plate, and does not capture global movement of the base plate (and therefore any shim compression). While R10 does experience larger deformations on the east base plate, the two deformed shapes are within 10% of each other. These plots are provided for every test in Appendix D of this report.

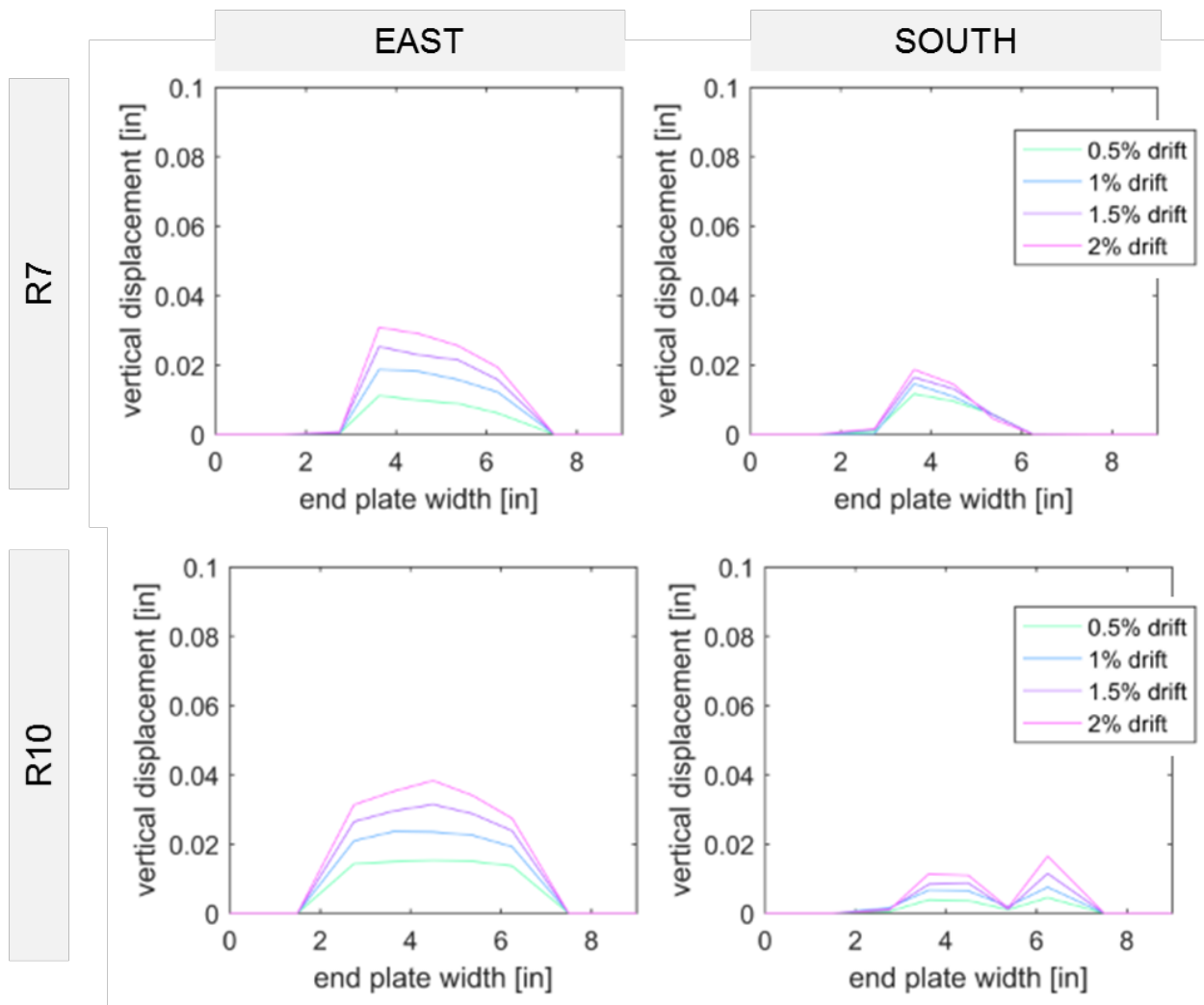


Figure 7-16: Base plate vertical LVDT sensors at design drift levels for R7 and R10 (no shims and 3” shims, respectively) on the south and east faces of the base plate. Specimens are otherwise nominally identical.

Load cell strains on the south load cells are shown for roof posts and canopy beams in Figure 7-17 and Figure 7-18 respectively. Load cell strain gauges (four per gauge) are averaged to produce one measurement per load cell (per rod). Load cells were pre-tensioned while data was recorded, and

then zeroed immediately before application of load. Examining the progression of peaks in load cell strain from cyclic data, it is clear that these peaks plateau, despite the progressing load protocol. Thus, after initial loading cycles, tension in the rods remains approximately constant throughout the test.

ROOF POSTS: load cell strain

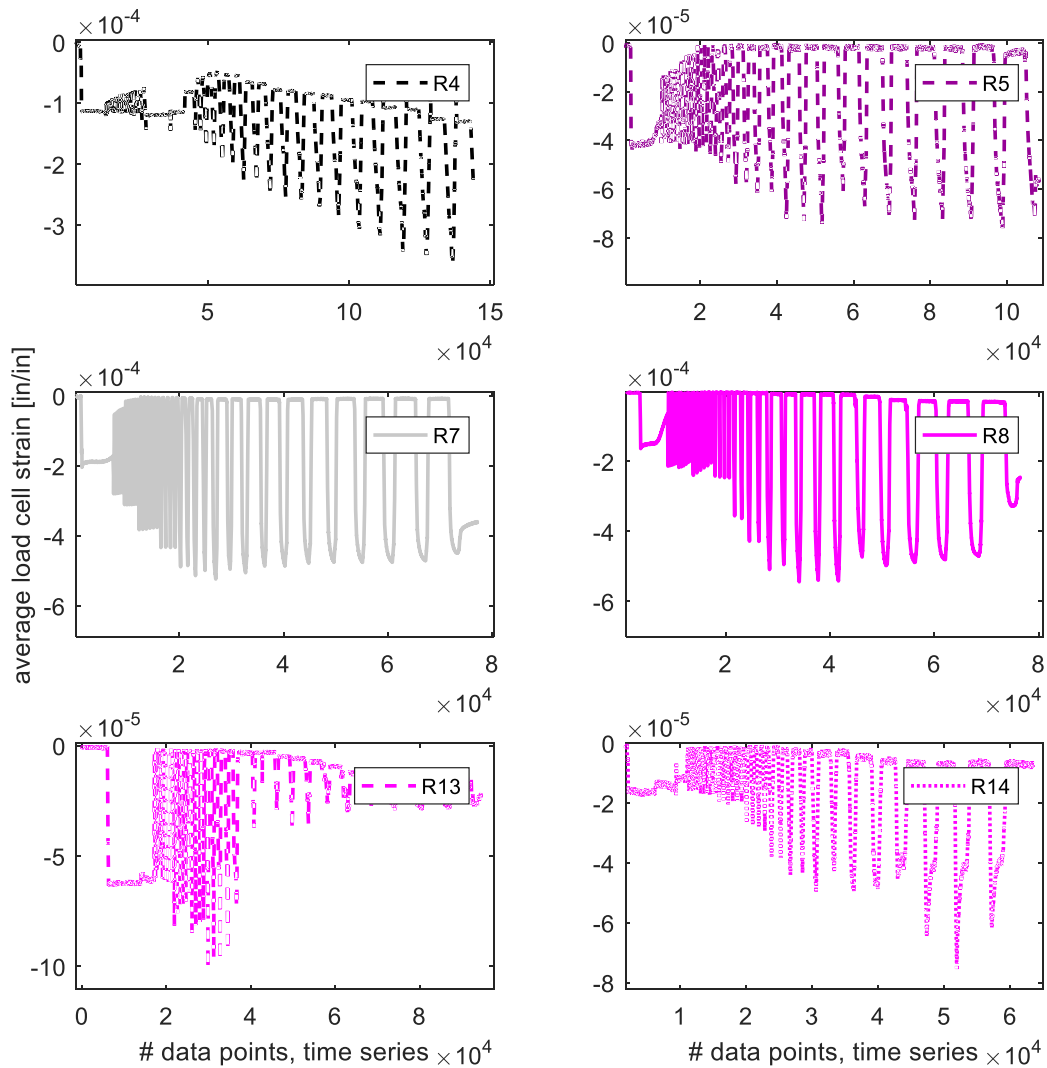


Figure 7-17: Average load cell strain in South load cells for unmitigated roof posts and roof posts with vinylester shims

CANOPY BEAMS: load cell strain

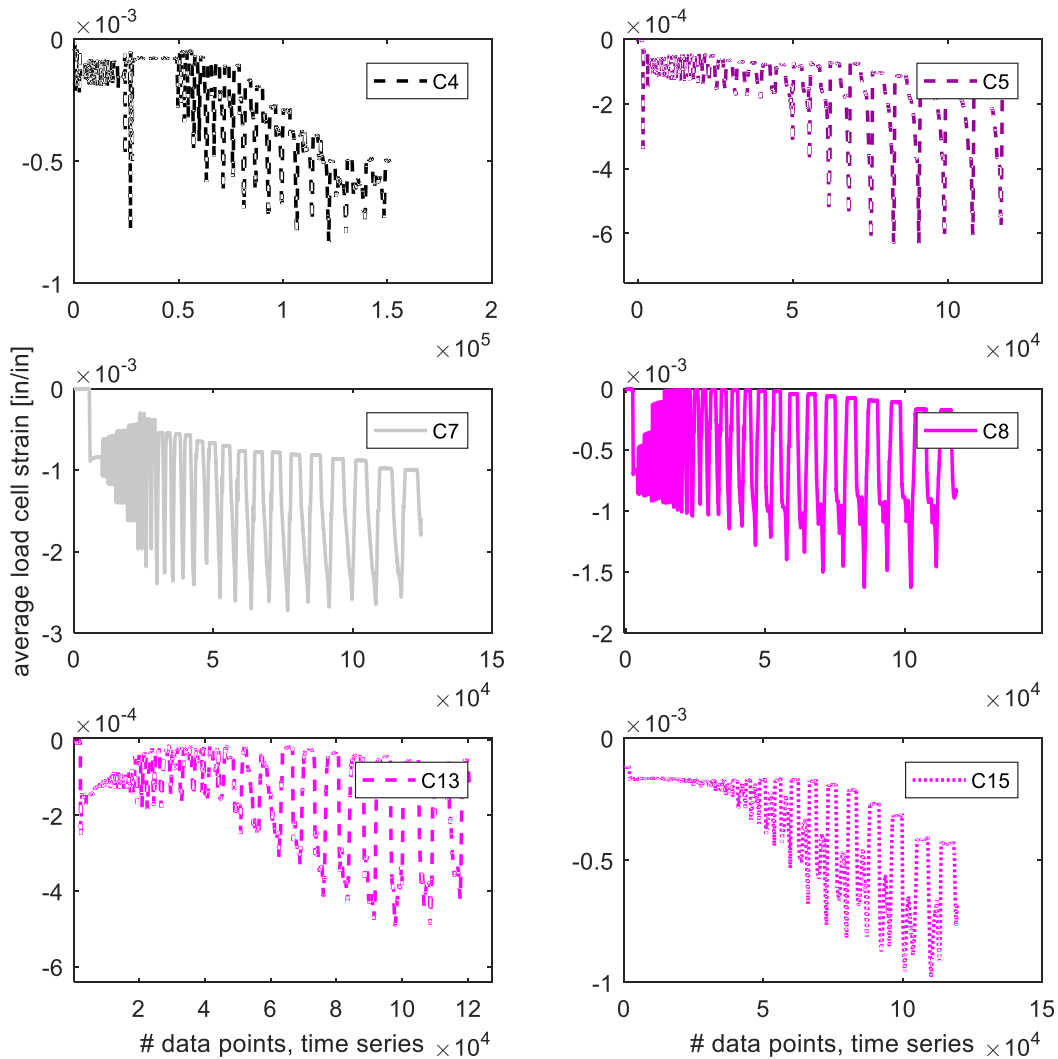


Figure 7-18: Average load cell strain in South load cells for unmitigated canopy beams and canopy beams with vinylester shims

Strains from the load cells may be converted to axial force in the bolts via the load cell calibration curves for each load cell, shown for two of the 1" diameter load cells in the figure below. This calibration was performed in a MTS universal testing machine prior to testing. Load cells were compressed and readings from the load cell strain gauges were recorded at 10 force levels. Applied compression did not exceed or approach the yield stress of the load cells. A linear curve fit is performed on the data, yielding the relationship between stress and applied force as shown in the figure, where the variable y is defined as strain and x is defined as force (see Figure 7-19).

Rearranging terms, anchor force = 20,000 * strain. Using this relationship, it is possible to estimate the force in the load cells and also the compression in the shims at the anchor rod location.

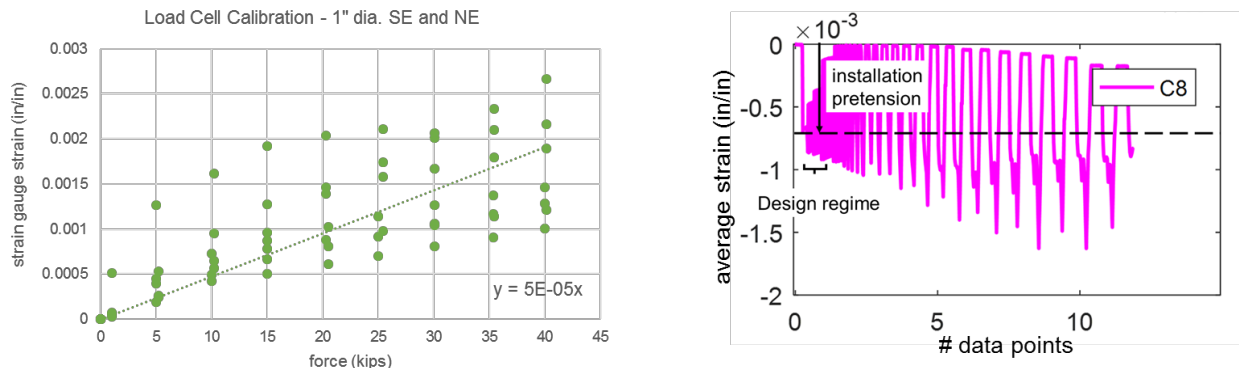


Figure 7-19: At left, load cell calibration curve, with curve fit, at right, detail of Fig. 7-18 demonstrating design regime and installation pretension on bolt.

Figure 7-19 examines test C8. In the design regime (up to 7 kip-ft of moment) average load cell strain consistently remains below 0.001 in/in. Using this overly conservative value and the load cell calibration curves, the force in the anchor rod is estimated to be 20 kips. Assuming that this anchor force is transmitted to the shims via the washers, which, for 1" bolt have an area of 2.25 in², the stress in the shims under the washers is 20 kips/2.25 in² = 8.89 ksi. This simple calculation assumes all stress is concentrated in the washer area and is not distributed to the remainder of the shim. For vinylester shims, as in test C8, 8.89 ksi represents less than 30% of ultimate stress (29.73 ksi, from Appendix A). It is noted that strains from the roof post testing were significantly lower than those recorded in the canopy beam testing and the example presented here represents a conservative scenario.

Photographs of typical failure modes are shown in Figure 7-20 below. The shims remained unaffected by the loading, save for rubbing of the paint finish from the surface of the shim. Holes were not ovalized, and there were no delaminations or failures at the bond line. Fracture of the specimen occurred either in the post/beam above the weld, or in the base plate, below the weld. Fractures universally occurred within the heat-affected zone of the weld (HAZ). Base plate bending was pervasive, and began at the initiation of lateral load. While base plate deformations

were significant across all base plate thicknesses, they were magnified for thinner base plates (pictured).

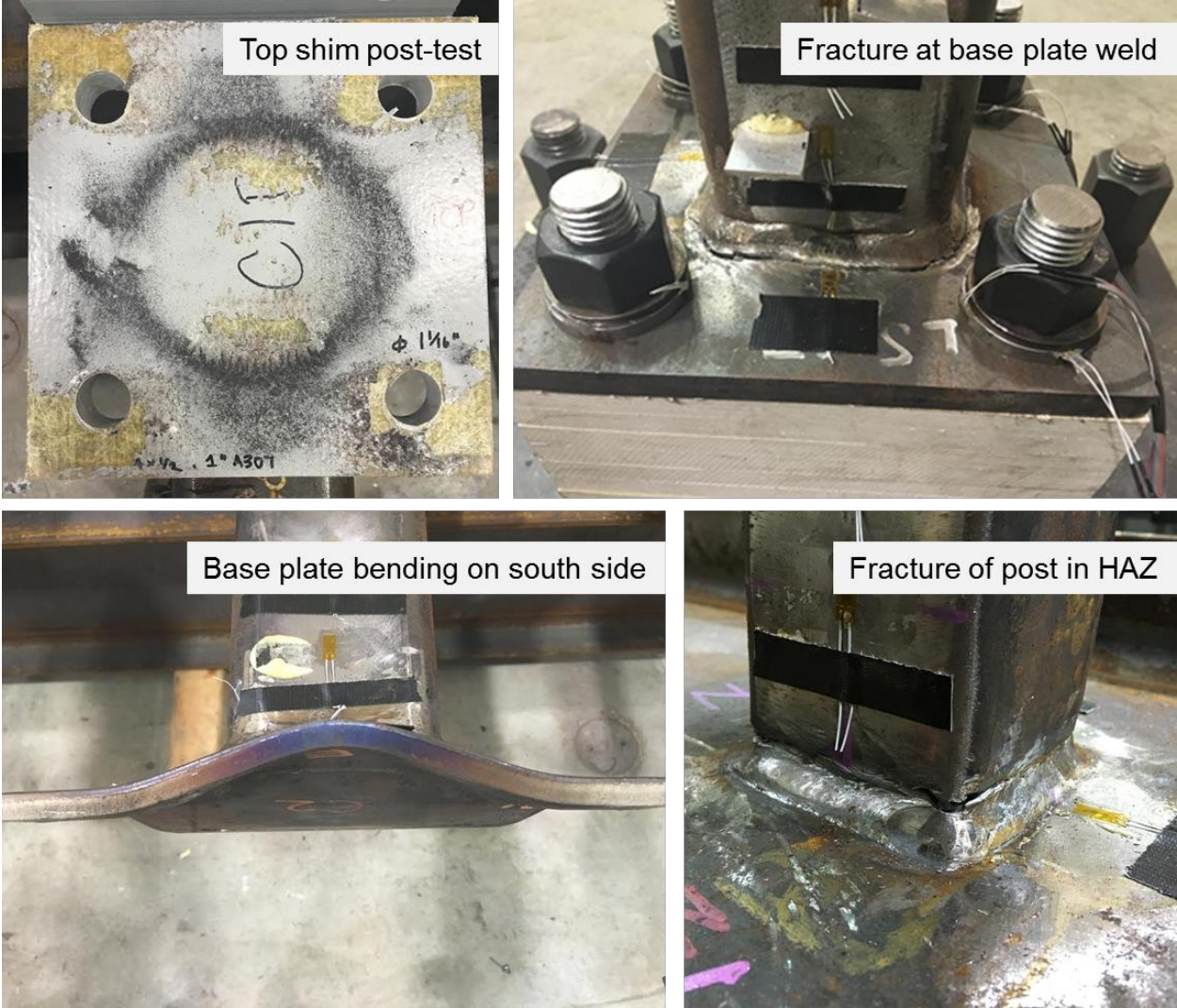


Figure 7-20: Photographs of typical failure modes for roof posts and canopy beams

7.3 Finite element validation

This section summarizes the computational simulations of the roof post and canopy beam specimens. The ABAQUS (2014) models were analyzed using the standard analysis solvers in this work. As the roof post and canopy beam specimens represent relatively light secondary peripheral structures that, compared to base building structures, fail at relatively low loads, the test rig (specifically the actuators and top loading block) was also modeled in ABAQUS to discern any possible influence of the boundary conditions on the experimental results.

Modeling of the specimens: The components of the roof post and canopy beam assemblies are hollow structural sections (HSS), base plates, bolts, and shims. Because of the complexity of the testing setup, representative actuators and a loading block were modeled in these assemblies to capture residual behavior due to internal resistance of the actuator pins and any eccentricities of the loading as the deformations progressed. Each model consisted of 8-node 3D continuum elements (bricks) with reduced integration points and 3D beam elements. The base plate, bolts, and the bottom 12 in. of the HSS are modeled using the brick elements whereas the remainder of the HSS, the loading block, and the actuators are modeled using beam elements. The beam elements are used in portions of the assembly that are expected to remain elastic.

The continuity of the HSS member was kept intact throughout the transition between the brick elements and the beam elements by using kinematic coupling constraints. This restrains the degrees-of-freedom of the top surface of the brick elements to the bottom node of the beam elements. Since the brick elements use reduced integration, hourglass enhanced section controls were implemented to avoid zero-energy modes due to hourglassing (ABAQUS 2014). This section control increases the accuracy by using an advanced strain algorithm that controls hourglassing (ABAQUS 2014). To accurately portray bending stress, all members in flexure had a minimum of four elements through the cross-section thickness, and the surface mesh was such that the mesh through the cross-section had a ratio of 4:1 to reduce the risk of the elements favoring stress along just one of the axes. The largest mesh size used in these models is 0.25 in. Parametric analysis of mesh sizes determined that results were not mesh dependent.

The 3D beam elements that are used in these models are box, pipe, and rectangle. The box and pipe beam elements have hollow cross-sections while the rectangular beam element has a solid cross-section. All of these elements allow for numerical integration along the section to capture any nonlinear material response. The box beam element is used to model the HSS specimen and differed between the canopy beams and roof posts. For the canopy beam this is a 4 in. x 4 in. box section with a wall thickness of 0.465 in. and for the roof post this is a 3 in. x 3 in. box section with a wall thickness of 0.174 in. The pipe beam element is used to represent the actuators from the testing setup and was used to capture any lateral deformations the actuators may have experienced through the loading process. These were modeled with an outside diameter of 5 in and a wall thickness of 0.312 in. The rectangle beam element is used to represent the loading

block from the testing setup and was used to capture the increased rigidity created within the experimental setup. This was modeled with a 6 in. x 6 in. cross section.

All models have contact that needs to be defined between the base plate and the bolts and many have additional contact between shims, shims and bolts, and shims and base plate. This was accomplished by defining master and slave surfaces to interact with each other using surface-to-surface contact. The contact interaction properties used is hard contact in the normal direction of all surfaces and penalty friction, with a coefficient of friction of 0.25, in the tangential direction of all surfaces. Contact in ABAQUS/Standard can cause issues with the start of the analysis because of instantaneous instabilities between the nodes. The nodes require an extremely small time step to stabilize themselves before the analysis can continue forward. To accomplish this, a dampening factor was instated to absorb some energy from the initiation of the model. This factor is small enough to stabilize the initiation while not effecting the behavior of the model, if it was stable [3]. A tie constraint was also used to attach the HSS posts to the base plates.

The bolts were restrained as if they were within a rigid plate using boundary conditions. This allowed for the bolts to react as expected without the added computational time required for contact. All other surfaces that would typically bear upon a rigid support had the bearing contact represented with compression only gap elements. These elements were used to restrain the elements from translating along a single direction on the referenced axis.

Various roof post and canopy beam models were created to simulate and verify the results of experimental data. The experimental setup being represented is a steel hollow structural section (HSS) manufactured from ASTM A500 Gr.50 structural steel attached to a steel backing plate with bolts manufactured from either ASTM A304-SH1 or ASTM A307 structural steel. Some assemblies may have fiberglass reinforced polymer (FRP) shims within the connections acting as a thermal break. With each application, the thicknesses and combination of thicknesses of the FRP vary. Measured properties include results reported in Appendix A from tensile coupon tests of the bolt materials, and through-thickness compression tests for FRP materials. The roof post and canopy beam base metal was not tested as the tensile coupons were deformed during manufacturing due to residual stresses in the HSS sections; as such, values from mill reports were used for the measured properties. In the roof post tests, a vertical actuator is used to apply the axial force to the member, and that load is held constant. A horizontal actuator is used to apply a continuously increasing lateral load at the top of the specimen. The loading application is discussed in more detail below.

Modeling of the test rig: The actuators are attached to the loading block and support nodes using a hinge connection with an internal nonlinear spring. The support nodes have all degrees-of-freedom restrained except the degree of freedom allowing the node to translate in a direction that is parallel to the longitudinal axis of the actuator. The concentrated loads applied to the system were applied at the end of actuators to have them transfer through the actuator and to the specimen

in a way that is similar to the experimental setup. The hinge connectors joined the actuator to the support nodes and to the loading block by providing a revolute constraint between the rotational degrees of freedom. The nonlinear spring within the hinge connector is representative to the internal resistance of the pins on the experimental actuators. They are defined with a rotational stiffness of 200,000 kip-in/rad and a peak moment resistance of 45 kip-in on each hinge connector of the horizontal actuator and 10 kip-in on each hinge connector of the vertical actuator. The hinges were calibrated using an iterative process comparing the force-displacement results of the ABAQUS models to the experimental data and increasing or decreasing peak moment as required. Once a working set of values was decided upon, they were applied to other models and the force-displacement results were compared to their respective experimental results for validation.

The models had a concentrated load applied to the far side of the horizontal actuator that translated through the actuator to the loading block causing lateral deformation and rotation. The load was applied monotonically. In the case of the roof posts, an additional concentrated load of 10 kips was first applied to the top end of the vertical actuator that also translated to the loading block. This load was held constant during application of the horizontal load.

Since the hinges of the actuators are not truly pinned, they cause reverse moment at the top portion of the HSS specimen. The following figures display the model setup and hinge numbers. Figure 7-21 shows the increased stress at the top of the specimen at the start of loading and the relief of stress further along in the loading application on the canopy beams and roof posts. It should also be noted that the inflection point of the specimen rises as the stress at the top of the specimen is relieved.

The following summarizes the modeling results by providing force-displacement comparisons to experimental data, as well as plots of the inflection points of the specimen as the test progresses.

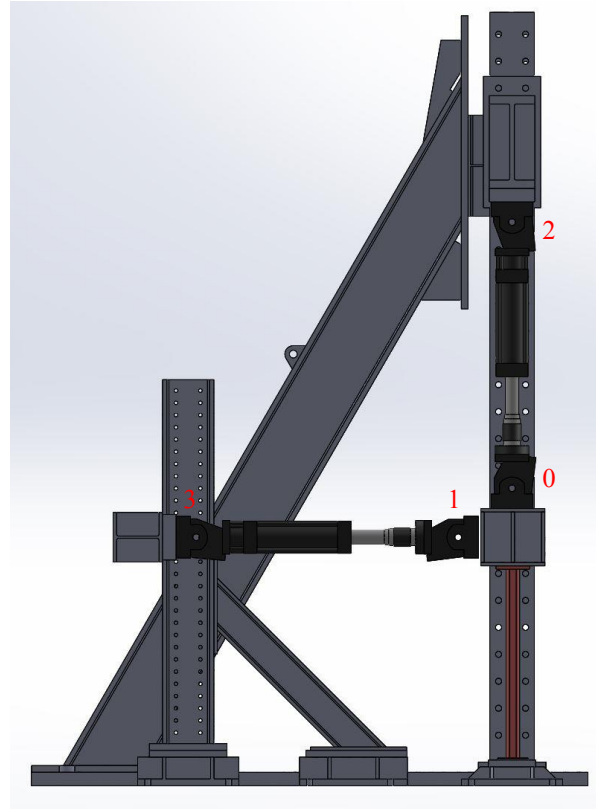
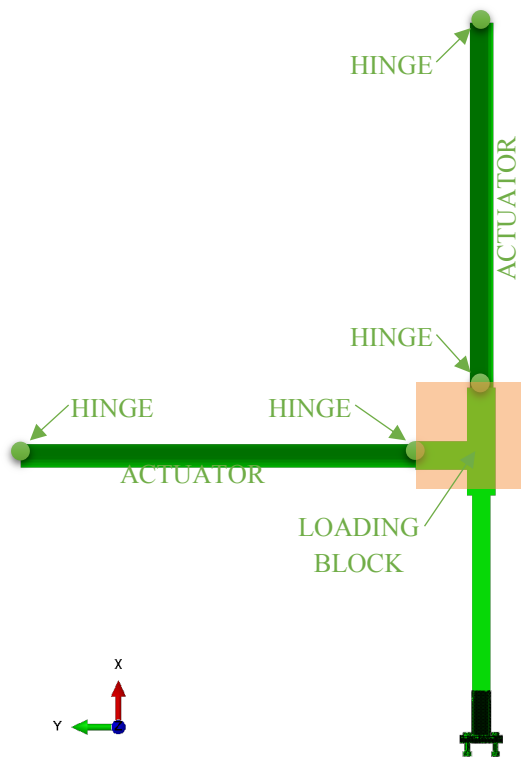


Figure 7-21: (left) System assembly key, (right) Hinge reference numbers

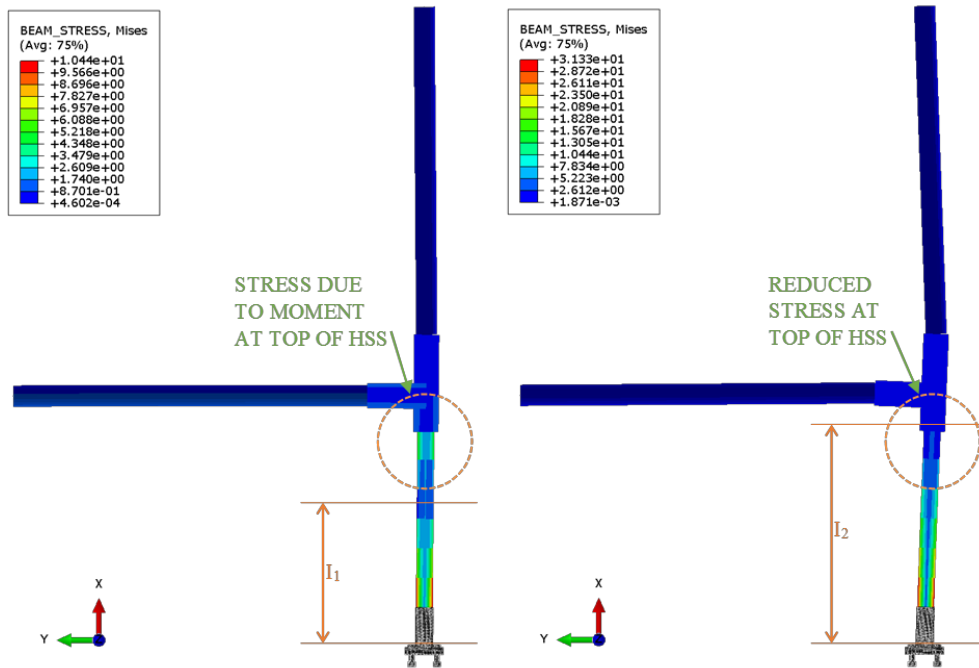


Figure 7-22: (left) Low inflection point, (right) High inflection point

Assembly C1 - HSS4x4x1/2, 3/4in bolts, 3/8in base plate, no shims

- Tube: HSS4x4x1/2 – A500 Gr.50 structural steel
- Bolts: 3/4in diameter – A304-SH1 structural steel
- Base Plate: 3/8in thick – A36 structural steel
- Shims: None

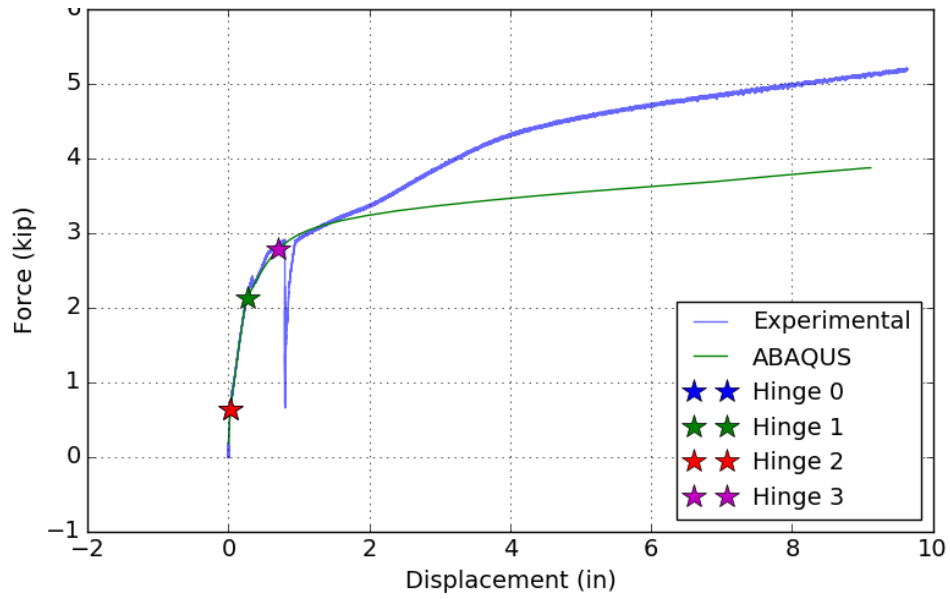


Figure 7-23: Assembly C1 – Force-Displacement, ABAQUS vs. Experimental

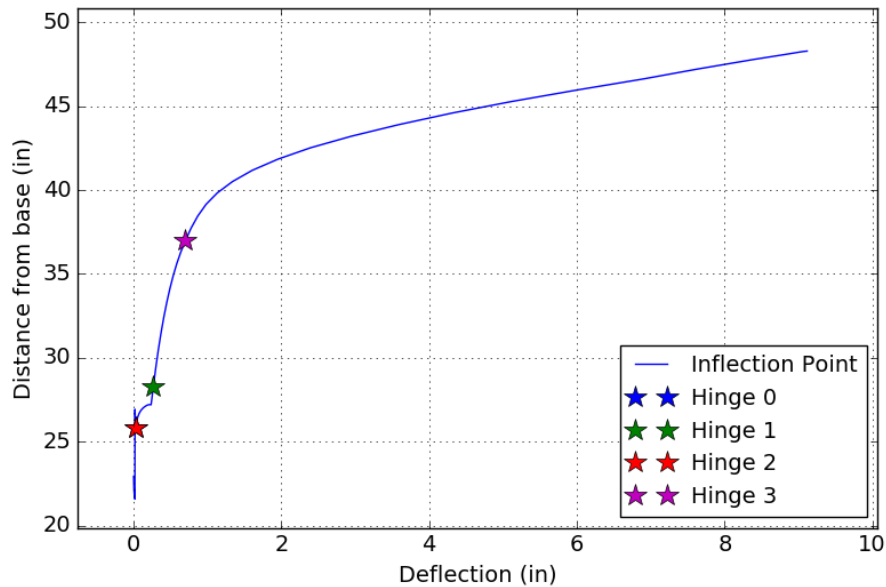


Figure 7-24: Assembly C1 – Inflection Height

Assembly C2 - HSS4x4x1/2, 3/4in bolts, 3/8in base plate, 3in vinylester shims

- Tube: HSS4x4x1/2 – A500 Gr.50 structural steel
- Bolts: 3/4in diameter – A304-SH1 structural steel
- Base Plate: 3/8in thick – A36 structural steel
- Shims: 3in vinylester

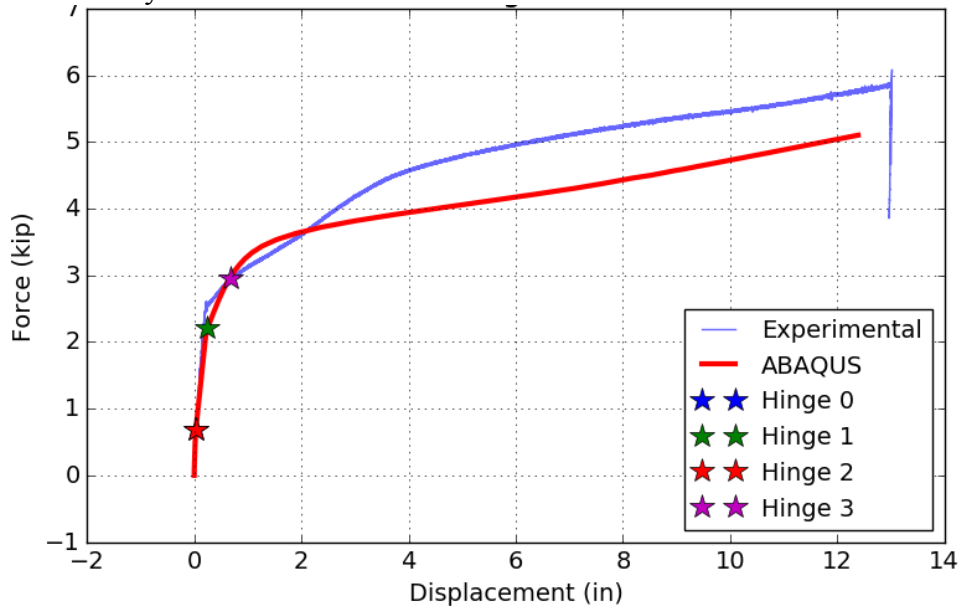


Figure 7-25: Assembly C2 – Force-Displacement, ABAQUS vs. Experimental

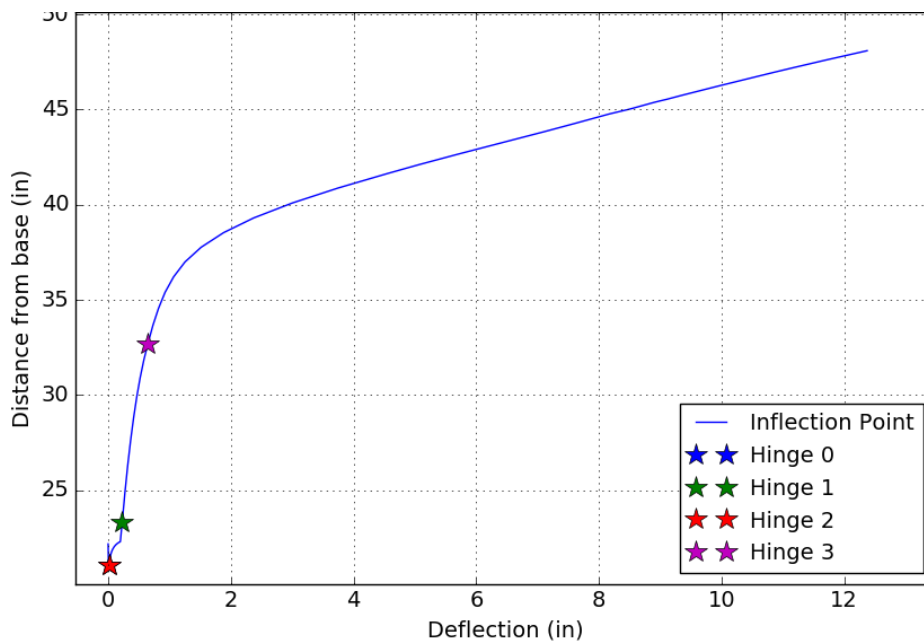


Figure 7-26: Assembly C2 – Inflection Height

Assembly C7 - HSS4x4x1/2, 1in bolts, 1/2in base plate, no shims

- Tube: HSS4x4x1/2 – A500 Gr.50 structural steel
- Bolts: 1in diameter – A307 structural steel
- Base Plate: 1/2in thick – A36 structural steel
- Shims: None

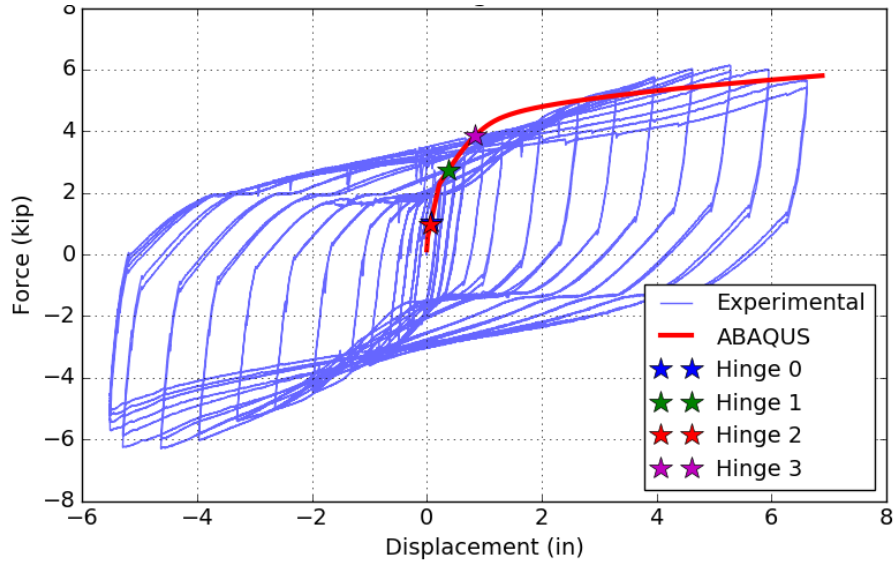


Figure 7-27: Assembly C7 – Force-Displacement, ABAQUS vs. Experimental

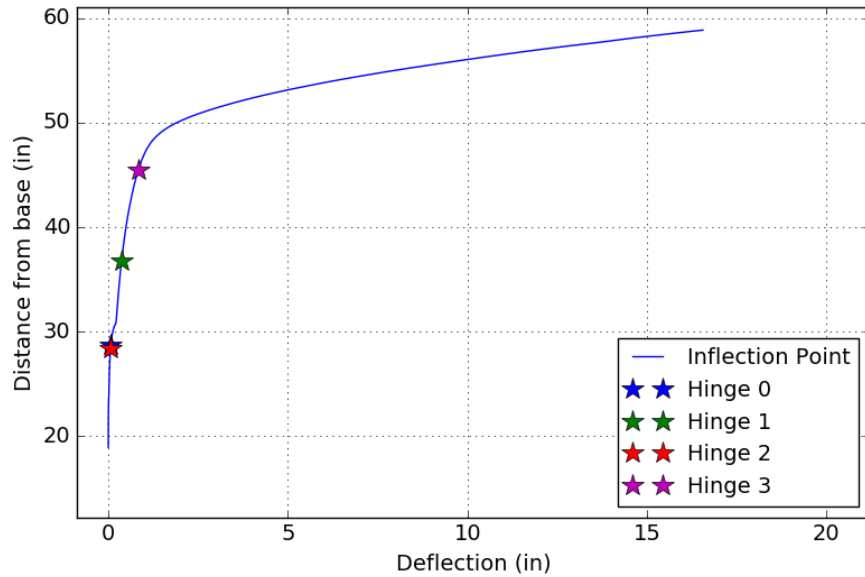


Figure 7-28: Assembly C7 –Inflection Height

Assembly C8 - HSS4x4x1/2, 1in bolts, 1/2in base plate, 3in vinylester shims

- Tube: HSS4x4x1/2 – A500 Gr.50 structural steel
- Bolts: 1in diameter – A307 structural steel
- Base Plate: 1/2in thick – A36 structural steel
- Shims: 3in vinylester

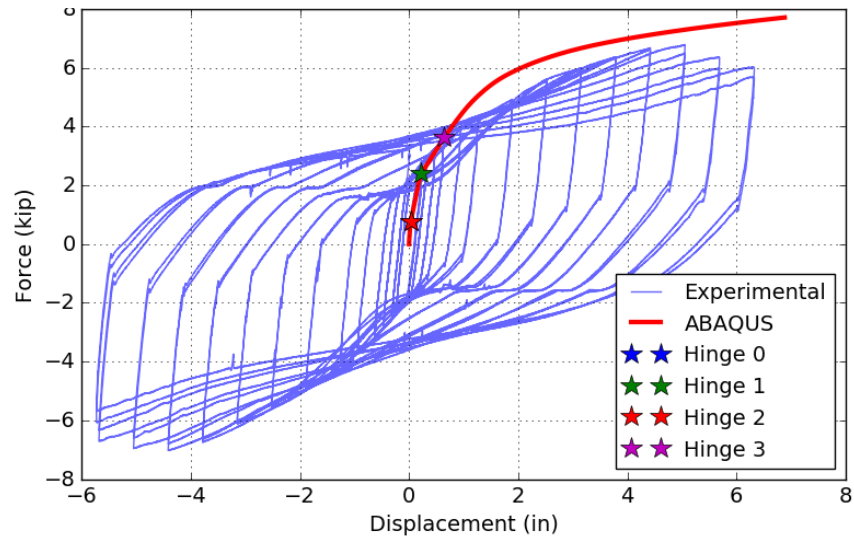


Figure 7-29: Assembly C8 – Force-Displacement, ABAQUS vs. Experimental

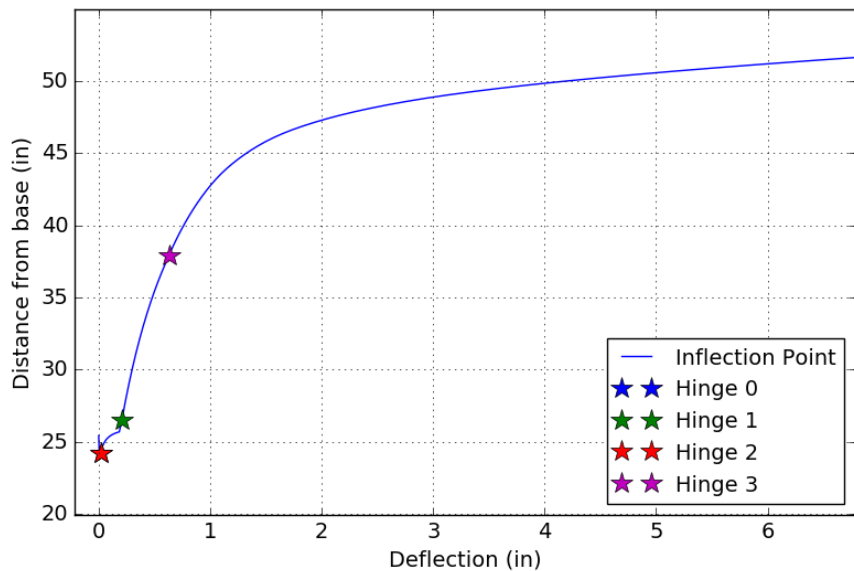


Figure 7-30: Assembly C8 –Inflection Height

Assembly C13 - HSS4x4x1/2, 1in bolts, 1/2in base plate, 1in vinylester shims

- Tube: HSS4x4x1/2 – A500 Gr.50 structural steel
- Bolts: 1in diameter – A307 structural steel
- Base Plate: 1/2in thick – A36 structural steel
- Shims: 1in vinylester

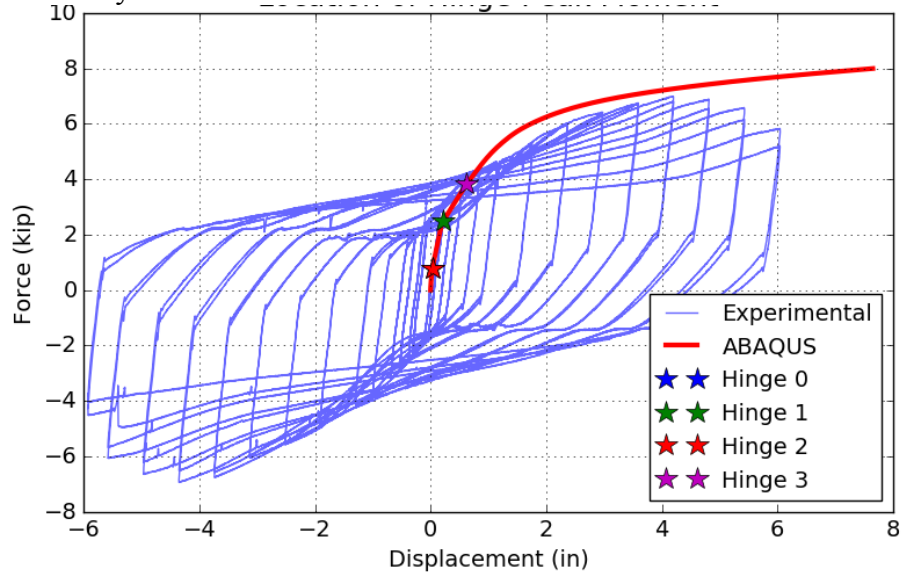


Figure 7-31: Assembly C13 – Force-Displacement, ABAQUS vs. Experimental

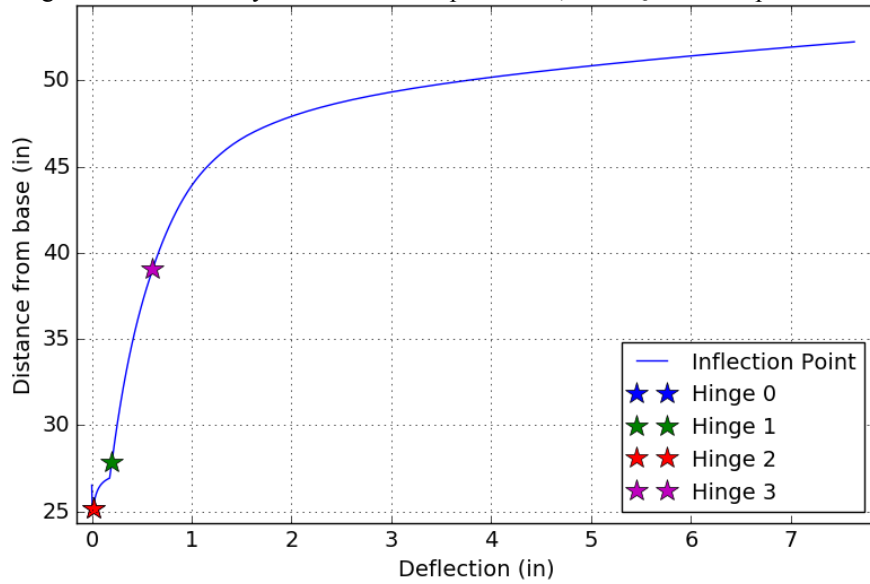


Figure 7-32: Assembly C13 –Inflection Height

Assembly C15 - HSS4x4x1/2, 1in bolts, 1/2in base plate, 6in vinylester shims

- Tube: HSS4x4x1/2 – A500 Gr.50 structural steel
- Bolts: 1in diameter – A307 structural steel
- Base Plate: 1/2in thick – A36 structural steel
- Shims: 6in vinylester

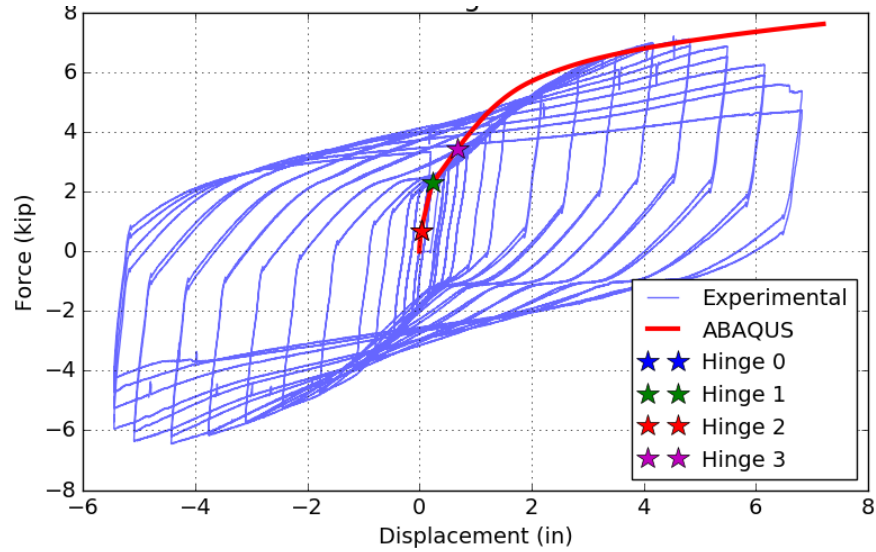


Figure 7-33: Assembly C15 – Force-Displacement, ABAQUS vs. Experimental

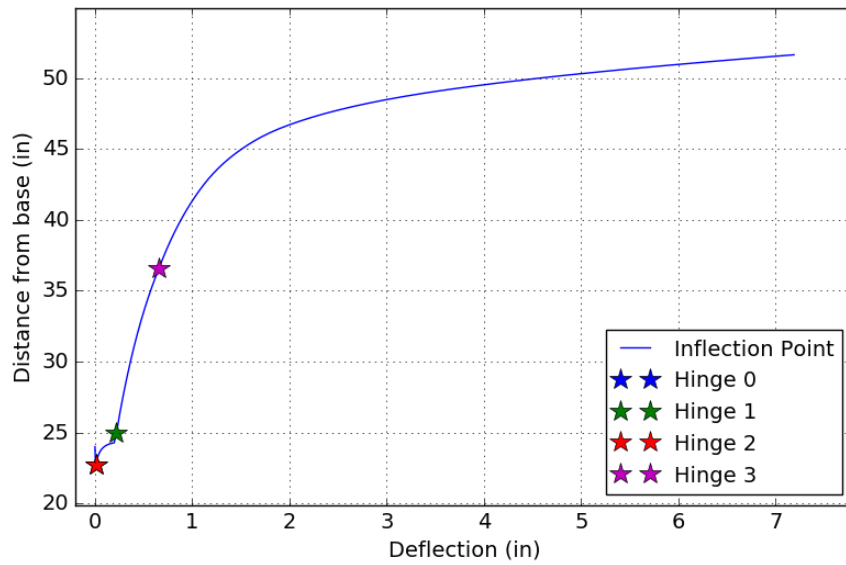


Figure 7-34 Assembly C15 –Inflection Height

Assembly R1 – HSS3x3x3/16, 1/2in bolts, 3/8in base plate, no shims

- Tube: HSS3x3x3/16 – A500 Gr.50 structural steel
- Bolts: 1/2in diameter – A304-SH1 structural steel
- Base Plate: 3/8in thick – A36 structural steel
- Shims: None

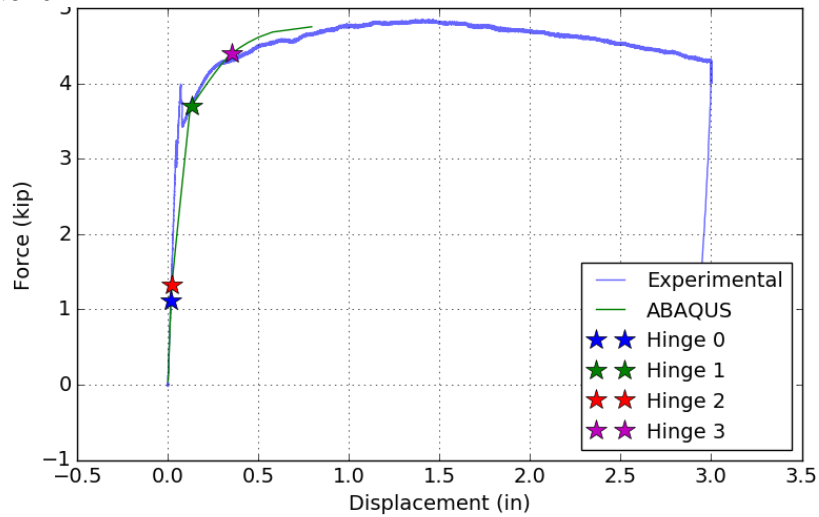


Figure 7-35: Assembly R1 – Force-Displacement, ABAQUS vs. Experimental

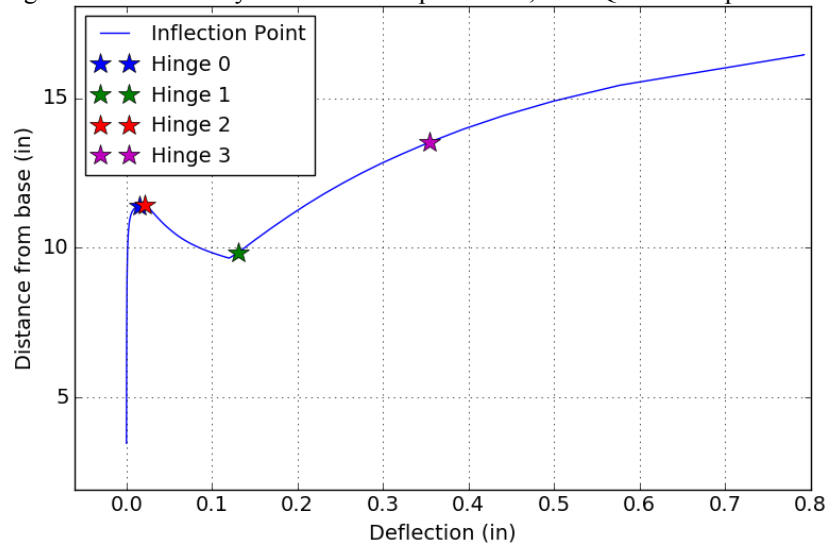


Figure 7-36: Assembly R1 –Inflection Height

Assembly R2 - HSS3x3x3/16, 1/2in bolts, 1/2in base plate, 3in vinylester shims

- Tube: HSS3x3x3/16 – A500 Gr.50 structural steel
- Bolts: 1/2in diameter – A304-SH1 structural steel
- Base Plate: 1/2in thick – A36 structural steel
- Shims: 3in vinylester

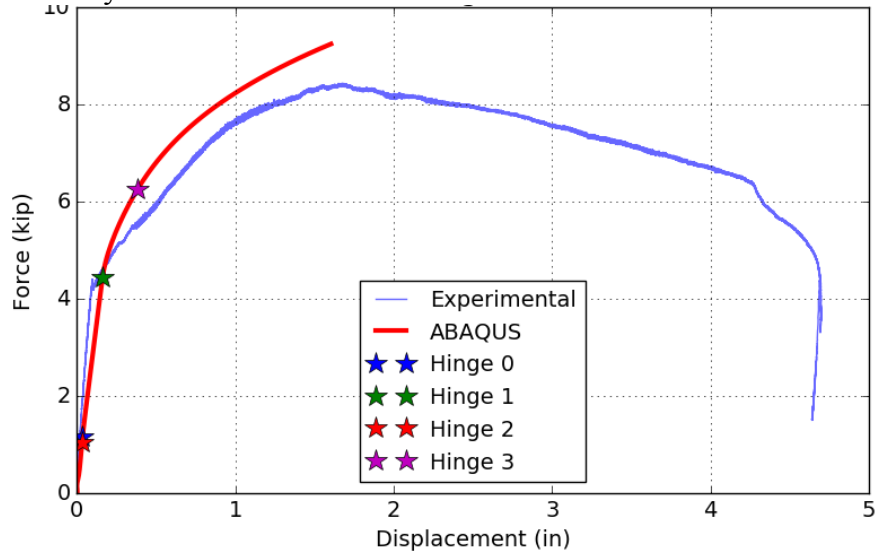


Figure 7-37: Assembly R2 – Force-Displacement, ABAQUS vs. Experimental

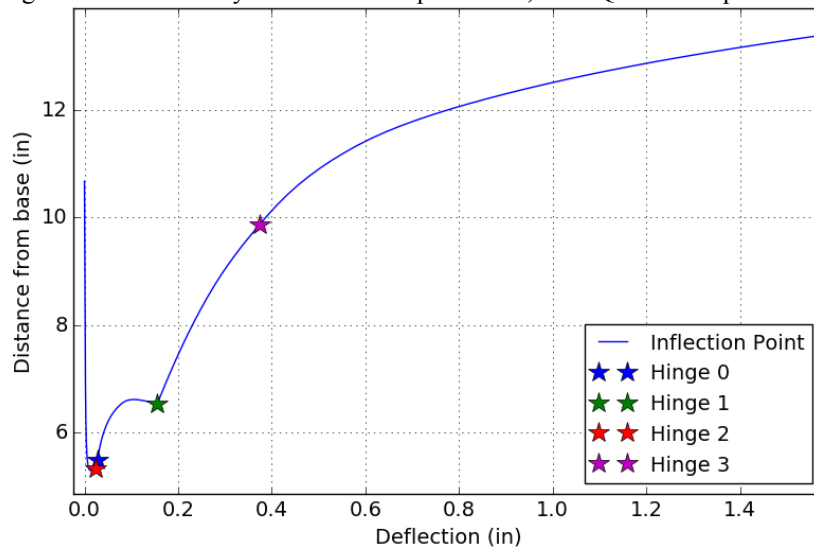


Figure 7-38: Assembly R2 –Inflection Height

Assembly R7 - HSS3x3x3/16, 3/4in bolts, 1/2in base plate, no shims

- Tube: HSS3x3x3/16 – A500 Gr.50 structural steel
- Bolts: 3/4in diameter – A307 structural steel
- Base Plate: 1/2in thick – A36 structural steel
- Shims: None

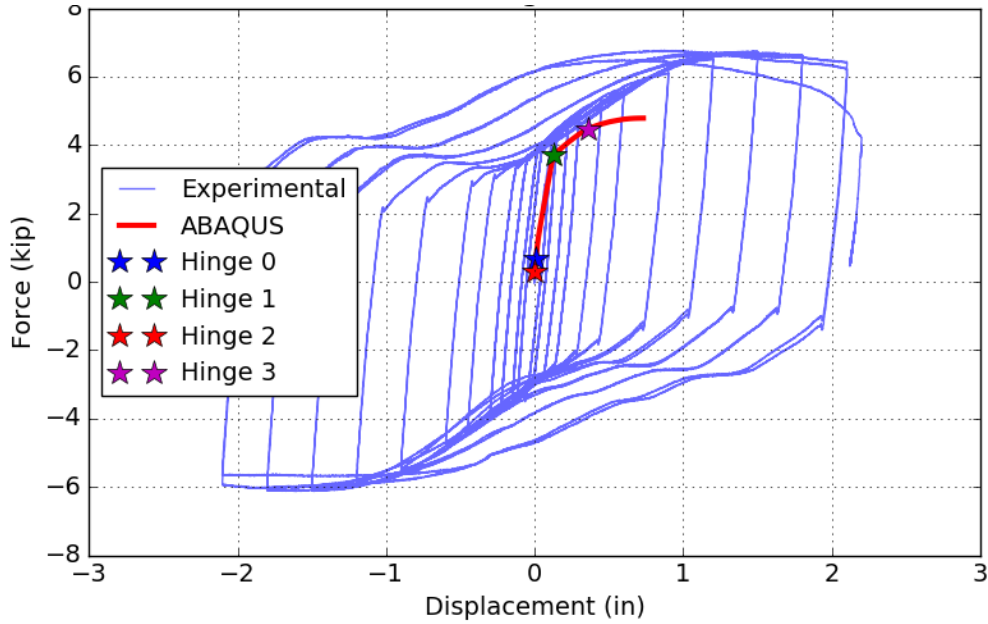


Figure 7-39: Assembly R7 – Force-Displacement, ABAQUS vs. Experimental

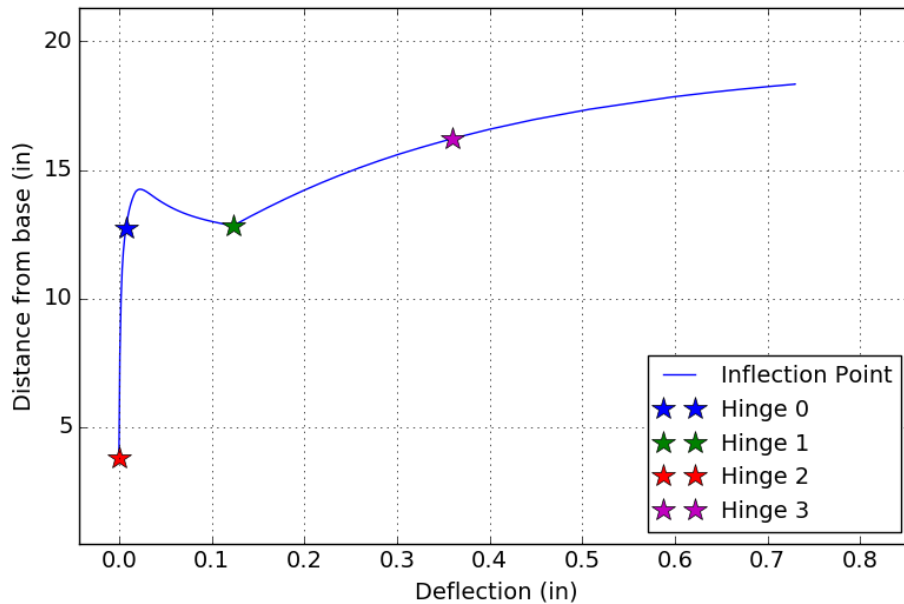


Figure 7-40: Assembly R7 – Inflection Height

Assembly R8 - HSS3x3x3/16, 3/4in bolts, 1/2in base plate, 3in vinylester shims

- Tube: HSS3x3x3/16 – A500 Gr.50 structural steel
- Bolts: 3/4in diameter – A307 structural steel
- Base Plate: 1/2in thick – A36 structural steel
- Shims: 3in vinylester

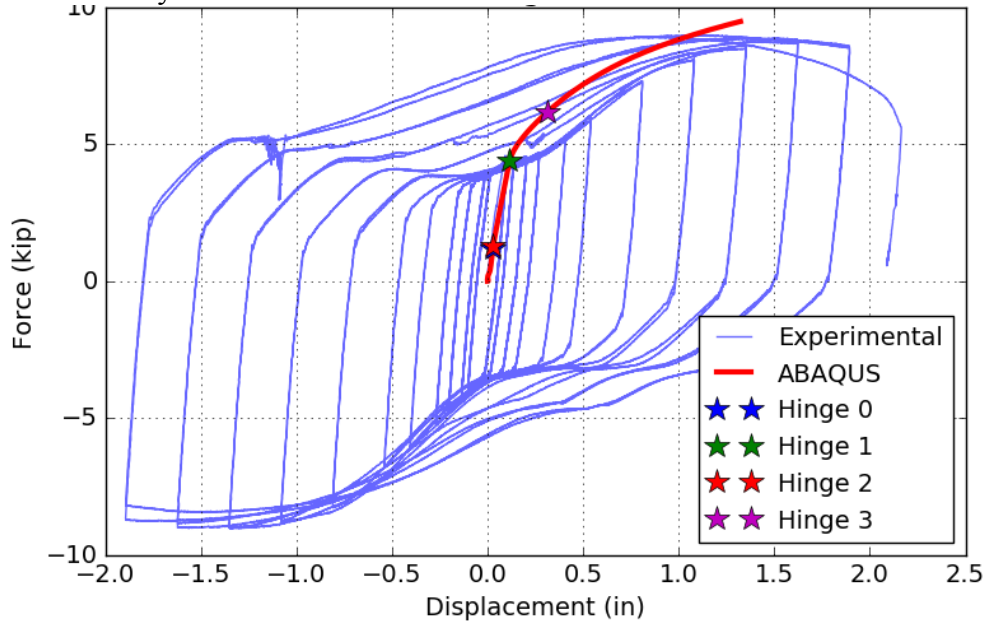


Figure 7-41 Assembly R8 – Force-Displacement, ABAQUS vs. Experimental

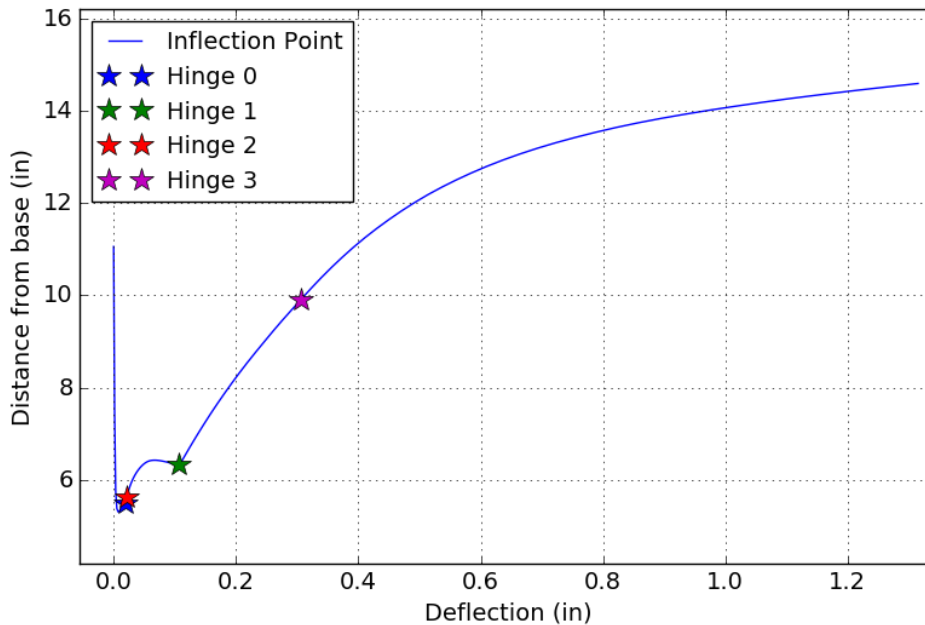


Figure 7-42 Assembly R8 –Inflection Height

Assembly R13 - HSS3x3x3/16, 3/4in bolts, 1/2in base plate, 1in vinylester shims

- Tube: HSS3x3x3/16 – A500 Gr.50 structural steel
- Bolts: 3/4in diameter – A307 structural steel
- Base Plate: 1/2in thick – A36 structural steel
- Shims: 1in vinylester

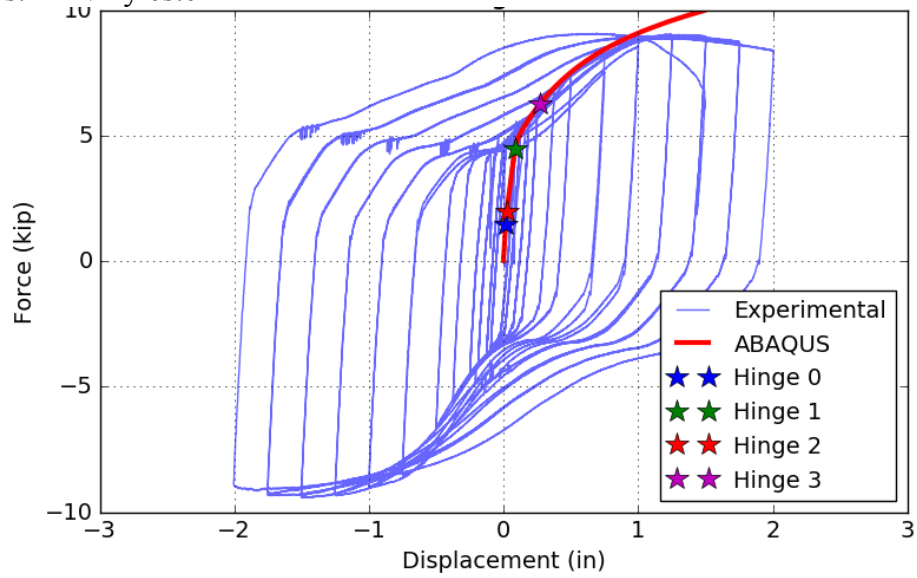


Figure 7-43: Assembly R13 – Force-Displacement, ABAQUS vs. Experimental

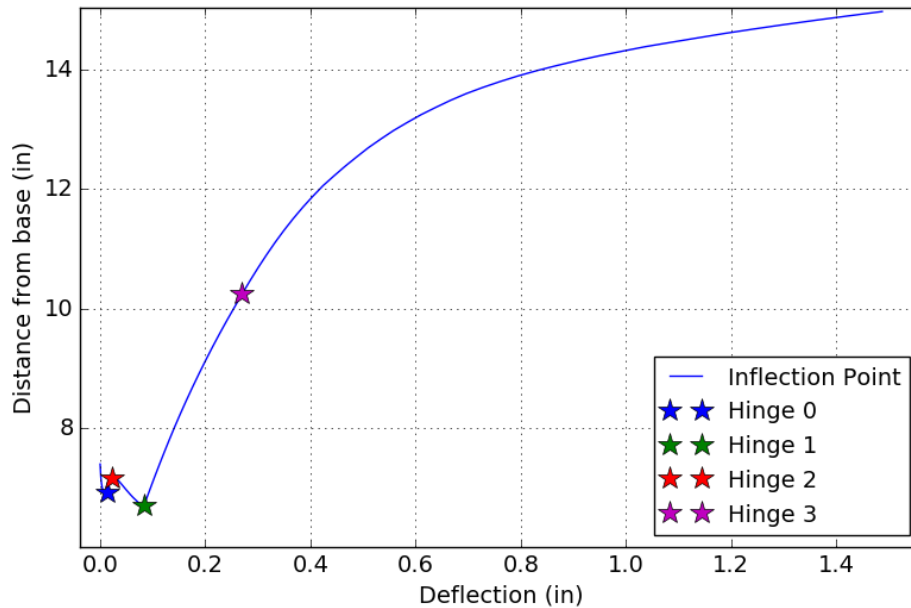


Figure 7-44: Assembly R13 –Inflection Height

Assembly R14 - HSS3x3x3/16, 3/4in bolts, 1/2in base plate, 6in vinylester shims

- Tube: HSS3x3x3/16 – A500 Gr.50 structural steel
- Bolts: 3/4in diameter – A307 structural steel
- Base Plate: 1/2in thick – A36 structural steel
- Shims: 6in vinylester

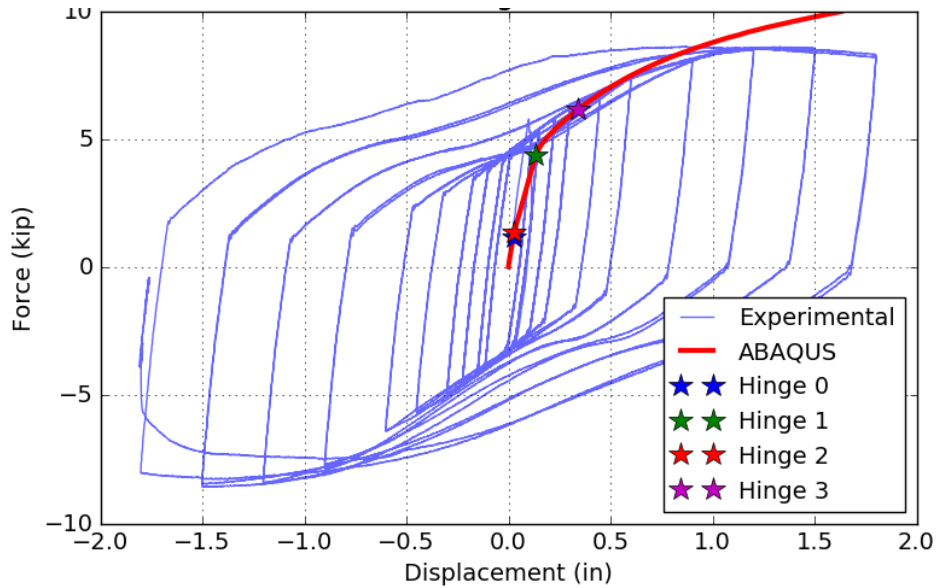


Figure 7-45: Assembly R14 – Force-Displacement, ABAQUS vs. Experimental

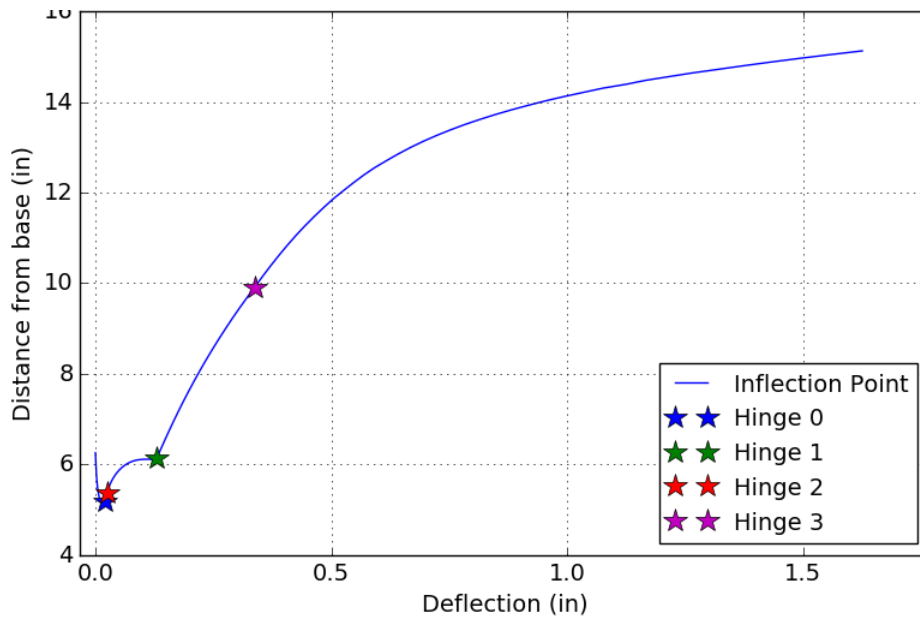


Figure 7-46: Assembly R14 –Inflection Height

Figure 7-47 and Figure 7-48 show the deflected shapes of canopy beams and roof posts, respectively. They show examples of assemblies without shims and with 3 in. and 6 in. thick shim assemblies. The beam stress distribution is similar to each other.

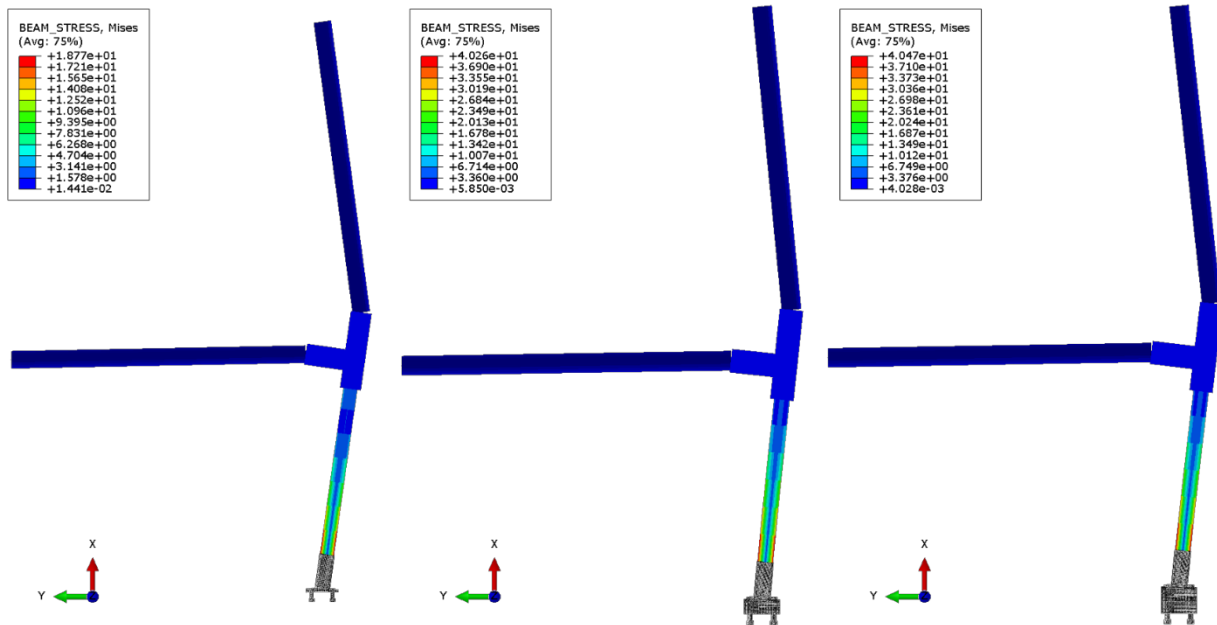


Figure 7-47: Canopy Beam Deflected Shapes: (left) No Shims, (center) 3in Shims, (right) 6in Shims

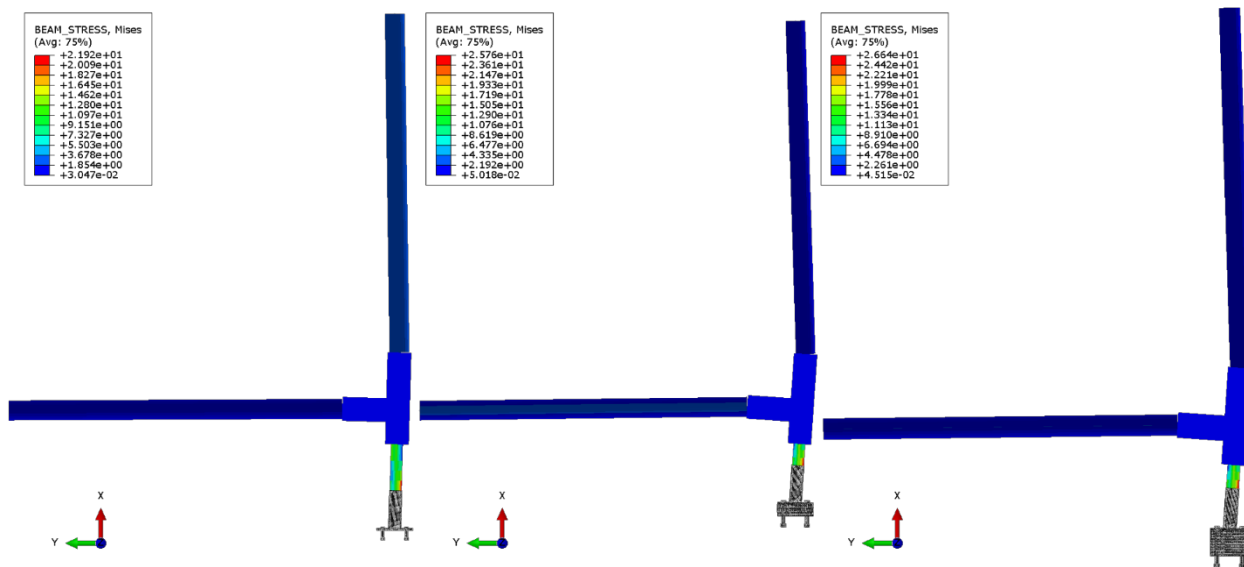


Figure 7-48: Roof Post Deflected Shapes: (left) No Shims, (center) 3in Shims, (right) 6in Shims

Figure 7-49 shows the behavior of the inflection point of all the specimens normalized to the height of the specimen.

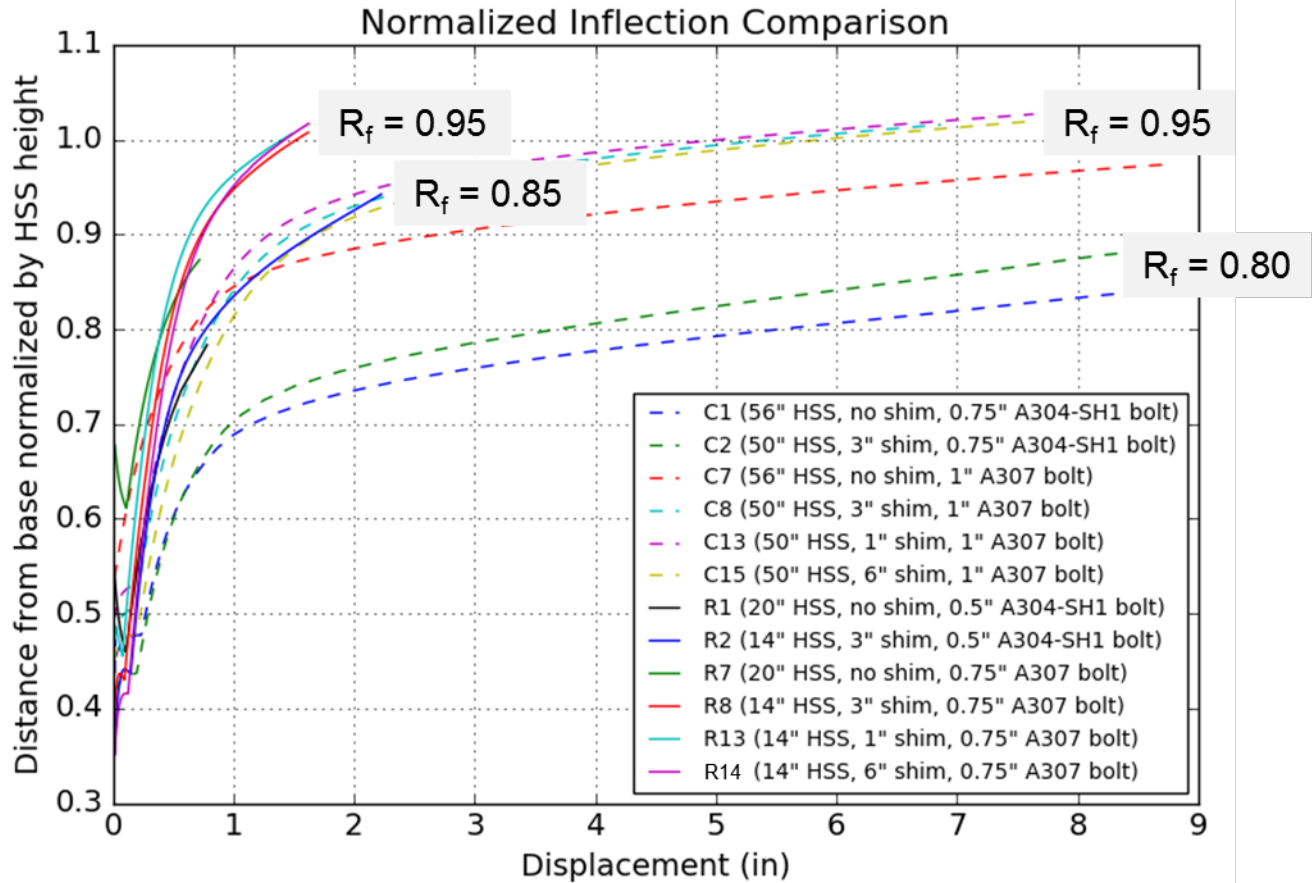


Figure 7-49: Normalized Inflection Comparison

The specimens are organized in four bands of behavior: overdesigned roof posts, efficiently designed roof posts, overdesigned canopy beams, and efficiently design canopy beams. As the normalized inflection point approaches 1, the specimen behaves like a pure cantilever. Strength reduction factors to account for normalized inflection points that do not immediately reach 1 are presented to adjust the experimental data. Table 7-6 presents these reduction factors for all tests, with shaded entries indicating results taken directly from modeled configurations (other reduction factors are interpolated based upon similarities to specimen geometries). In general, bolt size governs the normalized inflection point location, where specimens with overdesigned bolts attain pure cantilever behavior experimentally, and with more immediacy than specimens with smaller base plate anchor bolts.

Table 7-6: Reduction factors, R_f

ROOF POSTS		CANOPY BEAMS	
Test #	R_f	Test #	R_f
R1	0.85	C1	0.80
R2	0.85	C2	0.80
R3	-	C4	0.80
R4	0.85	C5	0.80
R5	0.85	C7	0.95
R6	-	C8	0.95
R7	0.95	C9	0.95
R8	0.95	C10	0.95
R9	0.95	C11	0.95
R10	0.95	C12	0.95
R11	0.95	C13	0.95
R12	0.95	C15	0.95
R13	0.95		
R14	0.95		from model

7.4 Design Recommendations

Canopy beams and roof posts with shims between the base plate and the support structure may be designed using typical industry practices modified to account for the shims. This approach assumes that the shim sizes match the base plate size.

The roof post and base plate may be designed using typical industry practice. The shims and anchor bolts may be designed using an approach similar to the approach described above for shelf angles:

- Determine the compression stress in the shims and the tensile force in the anchor bolts using elastic “plane-sections-remain-plane” analysis. For roof posts with axial load, an iterative solution is required to find the neutral axis. This approach may also be used to estimate the contribution of the shims to bending deflection.
- Neglect the shims when designing for shear below the base plate. Rely on single-curvature bolt bending to resist shear forces. Combine the bolt tensile and bending effects in accordance with AISC combined force equations. This approach may also be used to estimate the contribution of the shims to shear deflection.

8 Conclusions and Future Work

The work detailed herein aims to design, validate, and recommend thermal break strategies for use in steel structures. This was accomplished via computational modeling and experimental testing, including material testing, connection testing, and subassembly testing. Three-dimensional energy transfer thermal modeling explored viable solutions for thermal breaks. Following this, successful thermal solutions were tested as subassemblies. FRP shim mitigation strategies proved both thermally effective and readily constructible. Additional creep and double lap-splice connection testing further documented the behavior. From these efforts, the following is proposed:

- FRP shims are an effective both thermally and structurally at mitigating thermal bridges in steel cladding systems. Solutions for shelf angles, roof posts, and canopy beams involving thick and thin shims consistently performed adequately when compared to unmitigated systems. Strength-based comparisons yielded only minor (5-10%) reductions in shim-mitigated systems, which may be addressed in design.
- Stainless steel shims, while not as thermally beneficial as fiber reinforced polymer shims, can also serve to prevent thermal energy transfer, with no tradeoffs in strength or stiffness compared to using steel shims.
- FRP members demonstrate promise as substitutions for steel structural members, but are not currently pultruded in shapes and thicknesses adequate for structural steel construction. Although the use of custom-pultruded profiles is possible, they were outside the scope of this work because of anticipated cost in practice. The members tested in this work represented readily available sizes and showed strengths and stiffnesses that were below those of comparable steel members. Thicker profiles, e.g., 1 inch in thickness or more, may be adequate to meet strength and serviceability limit states comparable to steel shapes that are currently used.
- Bolted connections with FRP shims must be snug-tight; slip critical connections and pretensioned bolted connections were not explored in this work, and are not presently recommended.
- While thick FRP fills do decrease strength and stiffness in bolted steel connections, the reductions are within those accepted and codified for steel fills. A reduction factor of 0.8 is proposed for fills greater than or equal to 1 inch thick for bolt shear. The results do not justify a reduction factor for FRP shims less than 1 inch thick.
- FRP materials do creep under higher stress ratios. However, FRP materials do not yield and maintain linear stress strain relationships until failure. In addition, their creep behavior was predicted well in through-thickness compression using a testing protocol established in this work. The creep testing data shows that if an applied compressive stress is maintained below 30% to 35% of the monotonic failure stress of the FRP material when loaded in the through-thickness direction, creep is estimated to be negligibly small over a period of 100 years. The combination of compression in the shims due to snug tightening of the bolts combined with applied loading was

typically seen to be below this value at factored design loads in this work. This was verified through experimental data in the canopy beam and roof post tests in this work, for example.

- Stiffness-based design approaches are effective for shelf angle shim design. Design equations presented in this work successfully match experimental stiffness values, all of which are validated via computational modeling. As shelf angles are primarily governed by deflection limits, stiffness alone can characterize the design space for these subassemblies.
- Stainless steel bolts are recommended for building envelope details, and if strain-hardened stainless steel bolts (with strengths approximate to A325 carbon steel bolts) are specified, stainless bolts may be substituted 1:1 for carbon steel bolts.
- Shim mitigation strategies rarely impacted behavior in the design region. Connecting elements (bolts) typically dictated performance in the subassemblies tested. This may be due to several factors, including the choice of lightly loaded cladding details, but for those examined herein, the presence of shims did not alter behavior significantly.
- Innovative details such as an FRP sleeve on roof posts and canopy beams are thermally-sound, and demonstrate promise if specifically designed and constructed for this purpose. Slack in the sleeve contributed to the premature failure of this system, which could be mitigated with a custom pultrusion or a built-up section of FRP shapes and plates.
- Adhering plies to create thicker FRP plates is a common practice in the pultrusion industry. However, failure often occurs along the bond line. While this failure occurs beyond the design region, the impact on response should be recognized.
- Guidelines for design with and use of stainless steel bolts are necessary for their continued adoption, as nomenclature, material properties, and specification recommendations are decentralized and difficult to source.
- Through the range of typical factored loads, the bolts are shown to retain their bolt tension and strength adequately to be used reliably.

Additional creep testing at low stress ratios is warranted to further justify the design regime proposed herein. Details considered in this report were typical of lightly loaded configurations seen in practice. To provide a more comprehensive suite of design recommendations, testing and modeling efforts could be extended to moderately or heavily loaded scenarios. Tests involving custom-pultruded FRP members are also desired, as those tested in this work, representing the largest members available, did not have sufficient strength and stiffness compared to use of steel members with FRP shims in the connections. The performance of FRP materials under elevated temperatures remains an issue that should be addressed in future studies.

References

American Institute of Steel Construction (AISC) (2005). Specification for Structural Steel Buildings, ANSI/AISC 360–05, AISC, Chicago, Illinois.

American Institute of Steel Construction (AISC) (2010). Specification for Structural Steel Buildings, ANSI/AISC 360–10, AISC, Chicago, Illinois.

American Institute of Steel Construction (AISC) (2006). Base Plate and Anchor Rod Design, 2nd ed. AISC, Chicago, Illinois.

American Society for Testing and Materials (ASTM) (2016). Standard Test Methods for Determining the Mechanical Properties of Externally and Internally Treaded Fasteners, Washers, Direct Tension Indicators, and Rivets, ASTM F606/F606M – 16, West Conshohocken, Pennsylvania.

American Society for Testing and Materials (ASTM) (2016). Standard Test Methods for Tension Testing of Metallic Materials, ASTM E8/E8M – 16a, West Conshohocken, Pennsylvania.

Anzi, A. A. (1999). *Evaluation of Thermal Bridging for Slab-on-Grade Floor Foundations*. Department of Civil Engineering, University of Colorado, Boulder, Colorado.

ASHRAE 90.1 (2013). “ANSI/ASHRAE/IES Standard 90.1 – Energy Standard for Buildings Except Low Rise Residential Buildings,” American Society of Heating, Refrigeration, and Air-Conditioning Engineers.

ASHRAE 1365-RP (2011) “Thermal Performance of Building Envelope Details for Mid- and High-Rise Buildings.” American Society of Heating, Refrigeration, and Air-Conditioning Engineers.

Baddoo, N. R. (2008). “Stainless Steel in Construction: A Review of Research, Applications, Challenges and Opportunities,” *Journal of Constructional Steel Research*, Vol. 64, No. 11, pp. 1199-1206.

Blomberg, T. (2001). “HEAT3 Version 4.0 - A PC-program for Heat Conduction in Three Dimensions,” Department of Building Physics, Lund University, Lund, Sweden.

Blomberg, T. (2017). “HEAT3 Version 7.0 - A PC-program for Heat Conduction in Three Dimensions,” Department of Building Physics, Lund University, Lund, Sweden.

Borello D. J., Denavit, M. D., and Hajjar, J. F. (2009). "Behavior of Bolted Steel Slip-Critical Connections with Fillers," Report No. NSEL-017, Newmark Structural Laboratory Report Series, Department of Civil and Environmental Engineering, University of Illinois at Urbana-Champaign, Urbana, Illinois.

Borello D. J., Denavit, M. D., and Hajjar, J. F. (2011). "Bolted Steel Slip-Critical Connections with Fillers: I. Performance," *Journal of Constructional Steel Research*, Vol. 67, No. 3, pp. 379–88.

Clark, P., Frank, K., Krawinkler, H., and Shaw, R., 1997. "Protocol for Fabrication, Inspection, Testing, and Documentation of Beam-Column Connection Tests and Other Experimental Specimens," SAC Steel Project Background Document. October, Report No. SAC/BD-97/02.

Corus Group plc. (2008). *Avoidance of Thermal Bridging in Steel Construction*. The Steel Construction Institute, Ascot, United Kingdom.

D' Aloisio, J., Anderson, J., DeLong, D., Miller-Johnson, R., Oberdorf, K., Ranieri, R., Stine, T., and Weisenberger, G. (2012). "Thermal Bridging Solutions: Minimizing Structural Steel's Impact on Building Envelope Energy Transfer," *Modern Steel Construction*, American Institute of Steel Construction, Chicago, Illinois.

Denavit, M. D., Borello D. J., and Hajjar, J. F. (2011). "Bolted Steel Slip-Critical Connections with Fillers: II. Behavior," *Journal of Constructional Steel Research*, Vol. 67, No. 3, pp. 398–406.

Dowson, M., Harrison, D., Craig, S., and Gill, Z. (2011). "Improving the Thermal Performance of Single Glazed Windows using Translucent Granular Aerogel," *International Journal of Sustainable Engineering*, Vol 4, No. 3, pp. 266-280.

Dusicka, P. and Lewis, G. (2010). High Strength Steel Bolted Connections with Filler Plate," *Journal of Constructional Steel Research*, Vol. 66, pp. 75–84.

EN ISO 10211 (2007). "Thermal Bridges in Building Construction – Heat Flows and Surface Temperatures – Detailed Calculations," International Organization for Standardization, Geneva Switzerland.

Frank K. H. and Yura J. A. (1981). An Experimental Study of Bolted Shear Connections," Report No. FHWA/RD-81/148. Federal Highway Administration, U.S. Department of Transportation, Washington, DC, December.

Griffith, B. Finlayson, E., Yazdani, M., and Arasteh, D. (1997). "The Significance of Bolts in the Thermal Performance of Curtain-Wall Frames for Glazed Facades," *ASHRAE Transactions*, Vol. 104, Part 1.

Hibbitt, Karlsson & Sorensen, Inc. (HKS) (2016). "Abaqus/CAE User's Guide (6.14)," Hibbitt, Karlsson & Sorensen, Inc., Providence, Rhode Island.

Huang, L. (2012). *Feasibility Study of Using Silica Aerogel as Insulation for Buildings*. KTH School of Industrial Engineering and Management, Stockholm, Sweden.

IECC (2012). "International Energy Conservation Code," International Code Council

Kosny, J., Desjarlais, A. O., and Christian, J. E. (1998). *Steel-Framed Buildings; Impacts of Wall Detail Configurations on the Whole Wall Thermal Performance*. Buildings Technology Center, Oak Ridge National Laboratory, Oak Ridge, Tennessee.

Lee, J. H and Fisher, J. W. (1968). "Bolted Joints with Rectangular or Circular Fillers," Report No. 318.6., Fritz Engineering Laboratory, Department of Civil Engineering, Lehigh University, Bethlehem, Pennsylvania, June.

Morrison Hershfield (2011). *Thermal Performance of Building Envelope Details for Mid- and High-Rise Builds*, Morrison Hershfield, New York, New York.

NFRC 100 (2010). "Procedure for Determining Fenestration Product U-factors," National Fenestration Rating Council, National Fenestration Rating Council, Greenbelt, Maryland.

Parker, J. (2008). "Façade Attachments to Steel-Framed Buildings," Design Guide 22, American Institute of Steel Construction, Chicago, Illinois.

Schoeck Ltd (2015) "Schoeck Isokorb: Thermal Bridging Guide," Schoeck, Oxford, United Kingdom, June 2015.

Strachan, P. Nakhi, A., and Sanders, C. (1995). *Thermal Bridge Assessments*. Energy Systems Research Unit, University of Strathclyde. Glasgow, Scotland.

Tide, R. H. R., and Krogstad, V. (1993). "Economical Design of Shelf Angles," *Masonry: Design and Construction, Problems and Repair, ASTM STP 1180*, Melander, J. M. and Lauersdorf, L. R. (eds.), ASTM, Philadelphia.

Totten, P.E. and Pazera, M. (2009). “Thermal Inefficiencies in Building Enclosures – Causes of Moisture Related Performance Problems,” *Forensic Engineering 2009: Pathology of the Built Environment*, American Institute of Steel Construction, Chicago, Illinois, pp. 43-54.

Appendix A: Ancillary Test Data

This appendix presents the ancillary test data reporting material properties of the specimens tested in this research. These measured properties are used to document predicted behavior of the specimens and to calibrate the constitutive relations used in analyses of the specimens.

This appendix contains results and tabulated properties for three different ancillary test programs:

1. Base metal tensile coupon tests of shelf angles, roof post base plates, canopy beam base plates, and specimen bolts.
2. Through-thickness compression testing and tensile coupon testing of FRP materials.
3. Shear and tensile testing of bolts. Testing was performed in the structures laboratory at the University of Cincinnati.

A.1 Shelf Angle Base Metal Tensile Tests

Base metal tensile testing was performed in a 110 kip MTS universal testing machine located in the STReSS Laboratory at Northeastern University. The specimens were clamped with hydraulic grips and data was collected that included the the load on the specimen from the machine load cell, the cross-head displacement, and the displacement from an extensometer installed on the coupon gage length. The test rig and test configuration are shown in Figure A-50.



(a) MTS universal testing machine



(b) Specimen in hydraulic grips

Figure A-50: Universal testing machine used for tensile and compressive testing at the STReSS Lab. There were two shelf angles tested as part of the shelf angle cladding system testing: L6x4x5/16 and L7x4x3/8. All angles of the same size were made from the same heat. Both angles were manufactured from ASTM A36 structural steel. Three coupons were machined from a single angle of each size. Specimens were cut from the midspan of the angle, and were divided amongst the two angle legs.

The specimens were fabricated using a milling machine. The neck was machined to a width of 0.500 in. with a gage length of 2 in. (with an overall specimen length of 8 inches), in accordance with the specimen geometry outlined in ASTM E8 (Figure A-51), and as photographed in Figure A-52 below. The thickness of the coupons was retained as the thickness of the angles.

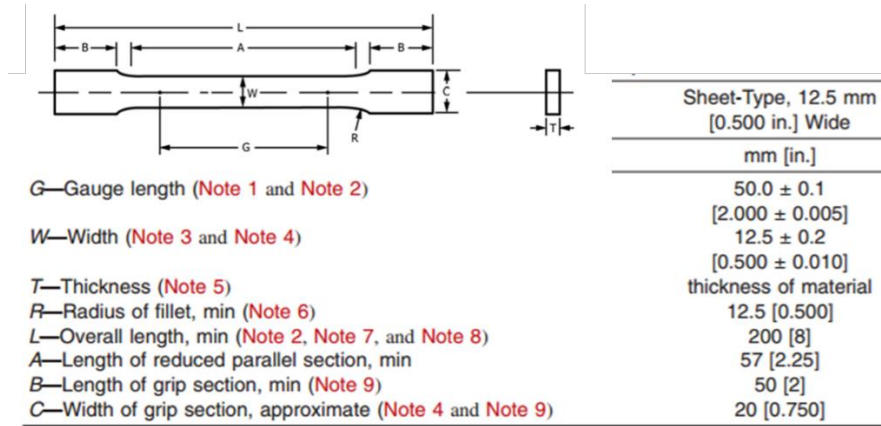


Figure A-51: Test specimen geometry for sheet-type specimens [ASTM E8-16 (2016)].



(a) L6x4x5/16 coupons



(b) L7x4x3/8 coupons

Figure A-52: Photographs of shelf angle coupon specimens

Digital calipers were used to measure the thickness and width within the gauge length at five different locations, as recorded in the tables below.

Table A-7: L6x4x5/16 coupon gage length measurements and cross-sectional area
L6x4x5/16 BASE METAL TENSILE TESTING

measurement #	sample 1		sample 2		sample 3	
	thickness <i>in</i>	width <i>in</i>	thickness <i>in</i>	width <i>in</i>	thickness <i>in</i>	width <i>in</i>
1	0.311	0.474	0.314	0.499	0.316	0.497
2	0.313	0.478	0.315	0.496	0.318	0.492
3	0.314	0.481	0.315	0.493	0.318	0.488
4	0.311	0.48	0.314	0.49	0.318	0.496
5	0.312	0.475	0.314	0.487	0.317	0.484
mean	0.312	0.478	0.314	0.493	0.317	0.491
area [in ²]	0.149		0.155		0.156	

Table A-8: L7x4x3/8 coupon gage length measurements and cross-sectional area
L7x4x3/8 BASE METAL TENSILE TESTING

measurement #	sample 1		sample 2		sample 3	
	thickness <i>in</i>	width <i>in</i>	thickness <i>in</i>	width <i>in</i>	thickness <i>in</i>	width <i>in</i>
1	0.39	0.496	0.39	0.497	0.388	0.496
2	0.388	0.495	0.388	0.492	0.386	0.492
3	0.388	0.492	0.388	0.493	0.386	0.486
4	0.39	0.485	0.389	0.487	0.386	0.484
5	0.389	0.483	0.389	0.485	0.386	0.491
mean	0.389	0.49	0.389	0.491	0.386	0.49
area [in ²]	0.191		0.191		0.189	

A.1.1 Shelf angle base metal tensile testing results

Photographs of failed tensile specimens are shown in the figure below for both shelf angle specimens. With the exception of sample 3 for the L7x4x3/8 angles, failure occurred within the gauge length.



(a) L6x4x5/16 coupons



(b) L7x4x3/8 coupons

Figure A-53: Shelf angle specimens post-test

Force-displacement and stress-strain results are produced in Figure A-54 and Figure A-55 below, for the L6x4x5/16 and L7x4x3/8 angles, respectively.

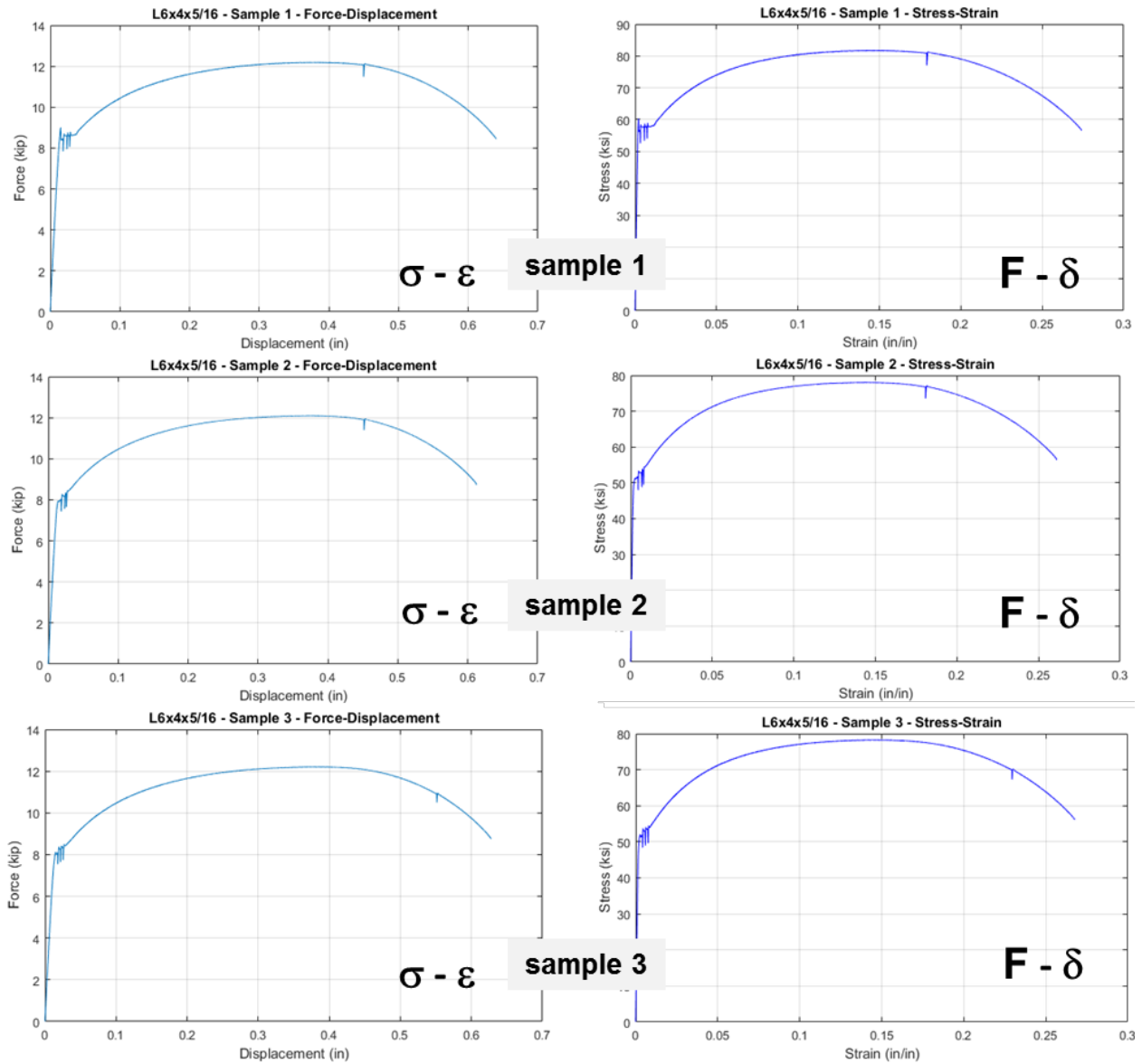


Figure A-54: Force-displacement and stress-strain results for base metal tensile tests of L6x4x5/16 specimen angles

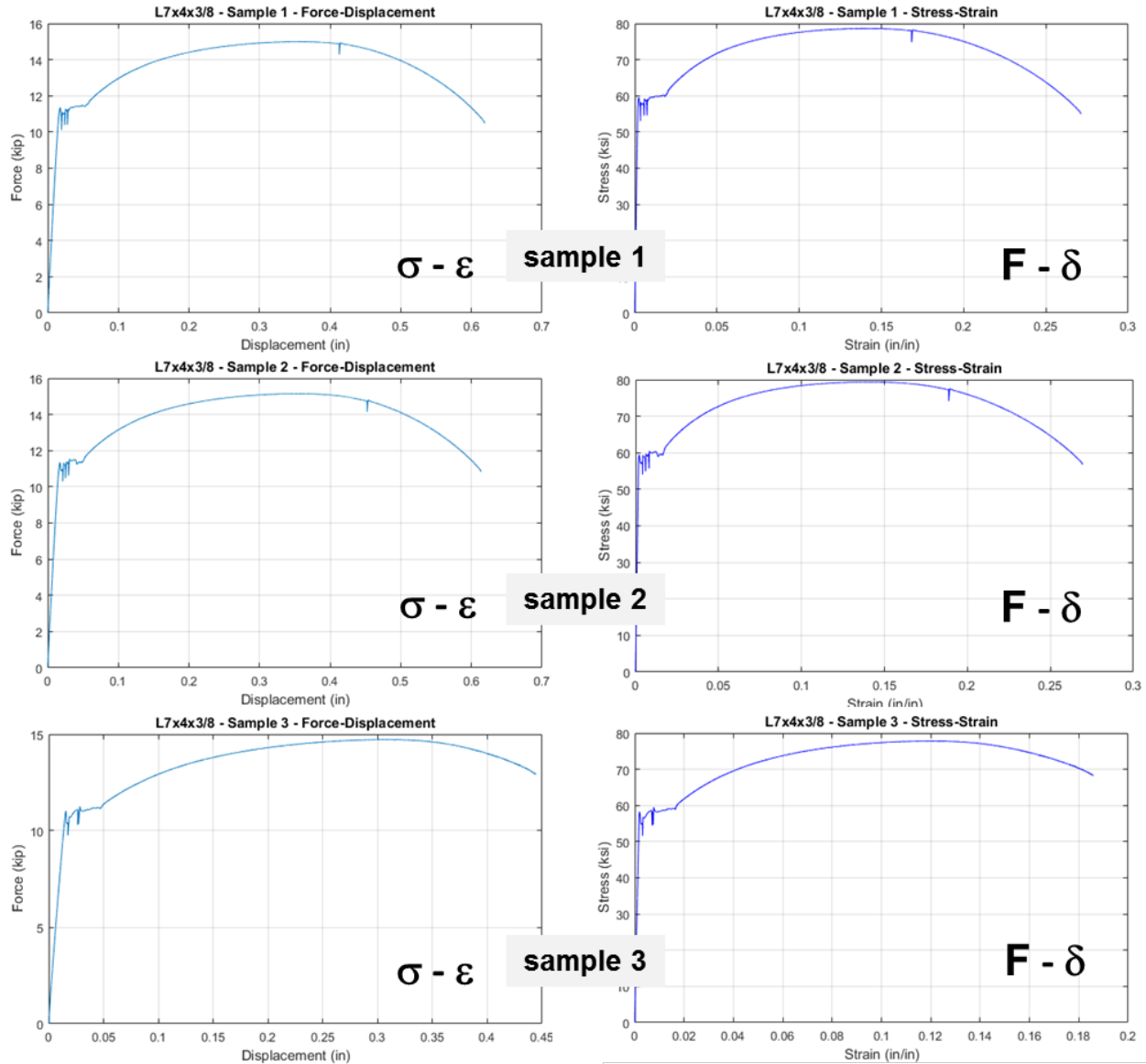


Figure A-55: Force-displacement and stress-strain results for base metal tensile tests of L7x4x3/8 specimen angles. A summary of the material properties as determined from the stress-strain results is shown in Table A-8 below. Modulus of elasticity, static yield stress, dynamic yield stress, and ultimate stress are calculated, as well as the means across samples. Testing demonstrates significantly higher yield stresses than the minimum specified for A36 steel but are not outside typical values for this material. Agreement across samples is within 5%, and within 2% in most cases.

Table A-9: Summary of modulus of elasticity (E), static yield stress (σ_{ys}), dynamic yield stress (σ_{yd}), and ultimate stress (σ_u) across angle base metal tensile testing

L6x4x5/16 BASE METAL TENSILE TESTING					L7x4x3/8 BASE METAL TENSILE TESTING				
	E	σ_{ys}	σ_{yd}	σ_u		E	σ_{ys}	σ_{yd}	σ_u
	<i>ksi</i>	<i>ksi</i>	<i>ksi</i>	<i>ksi</i>		<i>ksi</i>	<i>ksi</i>	<i>ksi</i>	<i>ksi</i>
sample 1	33451	53.30	58.10	81.90	sample 1	31915	54.10	59.84	78.70
sample 2	30320	48.80	51.04	78.10	sample 2	32105	54.90	59.90	79.50
sample 3	30339	49.00	51.44	78.40	sample 3	32928	53.60	59.20	77.90
mean	31370	50.37	53.53	79.47	mean	32316	54.20	59.65	78.70

A.2 Roof Post and Canopy Beam Base Plate Base Metal Tensile Tests

There were two base plates tested, a 3/8 in. thick base plate and a 1/2 in. thick base plate, from the roof post and canopy beam specimens. Base plates were ordered and fabricated with the roof post and canopy beam specimens. Specimens were chosen from one base plate, away from edges to avoid residual stresses formed in manufacturing. All specimens of one plate thickness were sampled from the same base plate. Both of these baseplates were manufactured from ASTM A36 structural steel and were machined into dogbone specimens in accordance with ASTM E8, as in the shelf angle coupons. Figure A-56 depicts these coupons.



Figure A-56: Photographs of base plate coupon specimens

A.2.1 Test Setup and Methods

The specimens were fabricated and measured using the same procedure as described for the shelf angle base metal testing. Measured geometries and cross-sectional areas for the two base plate thicknesses are shown in the tables below.

Table A-10: 3/8" base plate coupon gage length measurements and cross-sectional area
3/8" BASE PLATE BASE METAL TENSILE TESTING

measurement #	sample 1		sample 2		sample 3	
	thickness <i>in</i>	width <i>in</i>	thickness <i>in</i>	width <i>in</i>	thickness <i>in</i>	width <i>in</i>
1	0.366	0.5	0.366	0.496	0.367	0.496
2	0.367	0.51	0.365	0.493	0.366	0.493
3	0.373	0.503	0.366	0.494	0.366	0.5
4	0.369	0.499	0.366	0.497	0.368	0.493
5	0.37	0.495	0.366	0.498	0.367	0.497
mean	0.369	0.501	0.366	0.496	0.367	0.496
area [<i>in</i> ²]	0.185		0.181		0.182	

Table A-11: 3/8" base plate coupon gage length measurements and cross-sectional area
 1/2" BASE PLATE BASE METAL TENSILE TESTING

measurement #	sample 1		sample 2		sample 3	
	thickness <i>in</i>	width <i>in</i>	thickness <i>in</i>	width <i>in</i>	thickness <i>in</i>	width <i>in</i>
1	0.499	0.497	0.5	0.497	0.499	0.502
2	0.499	0.492	0.5	0.492	0.498	0.498
3	0.499	0.487	0.5	0.484	0.499	0.497
4	0.5	0.491	0.5	0.49	0.5	0.495
5	0.499	0.496	0.499	0.496	0.499	0.5
mean	0.499	0.493	0.5	0.492	0.499	0.498
area [in ²]	0.246		0.246		0.249	

A.2.2 Base plate base metal tensile testing results

Figure A-57 depicts the base plate base metal specimens post-test. All of the specimens failed within the gauge length.



(a) 3/8" base plate coupons



(b) 1/2" base plate coupons

Figure A-57: Base plate specimens post-test

Figure A-58 and Figure A-59 depict the force-displacement and stress-strain curves for the three samples cut from the 3/8" base plates and 1/2" base plates, respectively. Note that sample 3 for the 1/2" base plate specimen is significantly higher in strength than the other two samples, increasing the average values for yield stress, as shown in Table A-15.

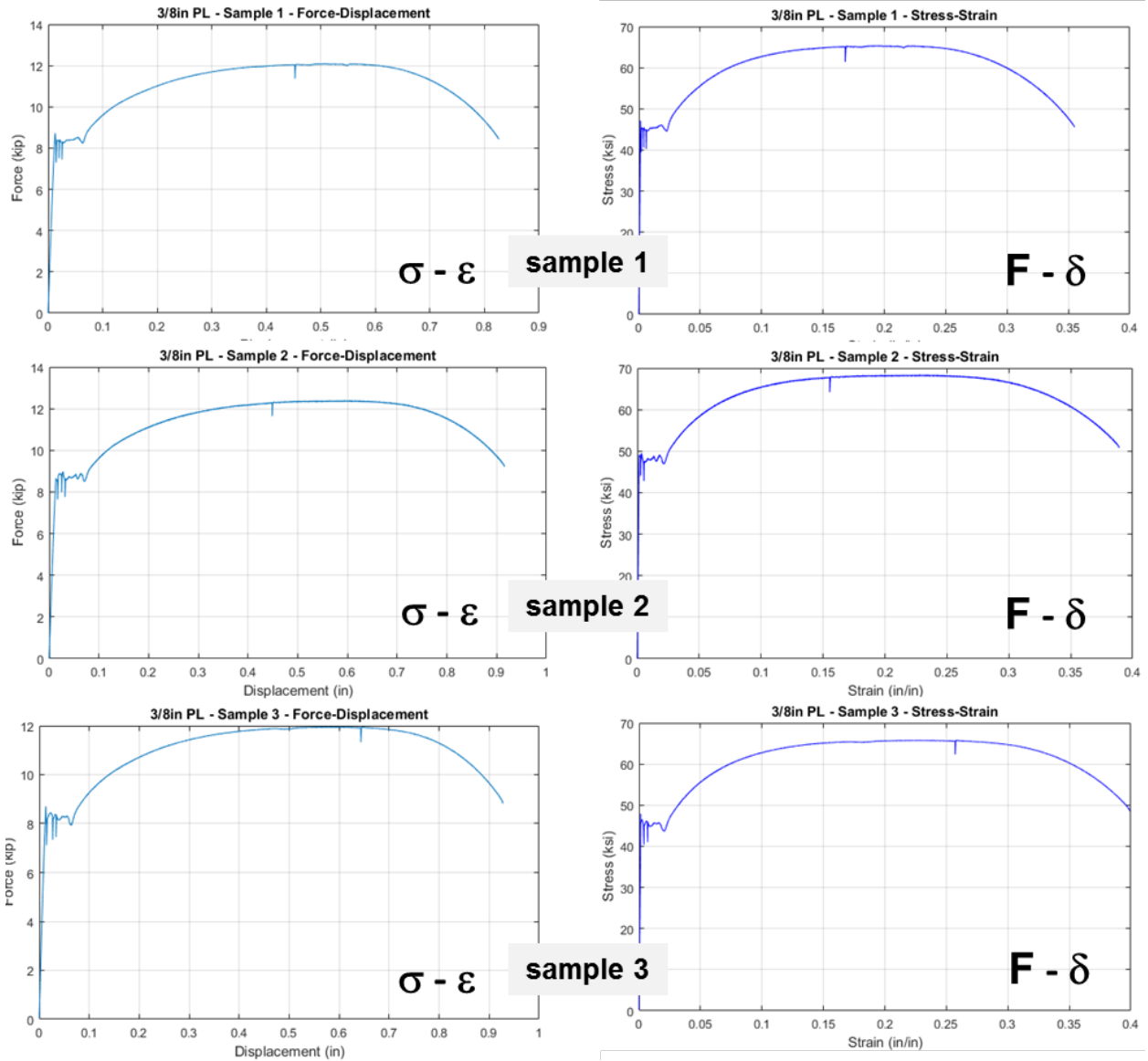


Figure A-58: Force-displacement and stress-strain results for base metal tensile tests of 3/8" base plate specimens

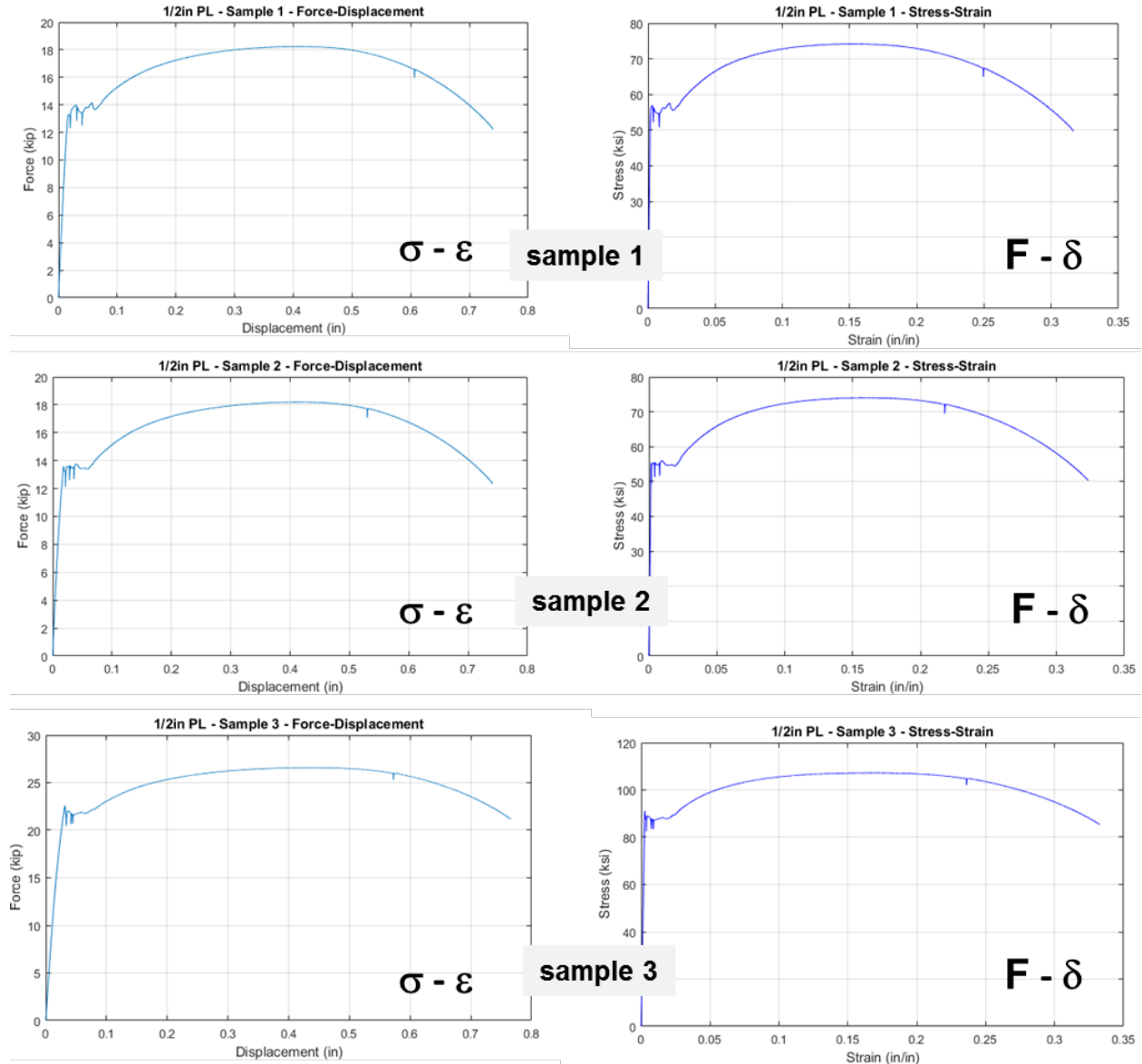


Figure A-59: Force-displacement and stress-strain results for base metal tensile tests of 1/2" base plate specimens
 Table A-33: Summary of modulus of elasticity (E), static yield stress (σ_{ys}), dynamic yield stress (σ_{yd}), and ultimate stress (σ_u) across base plate base metal tensile testing

3/8" BASE PLATE BASE METAL TENSILE TESTING

	E	σ_{ys}	σ_{yd}	σ_u
	<i>ksi</i>	<i>ksi</i>	<i>ksi</i>	<i>ksi</i>
sample 1	33801	40.10	45.60	65.10
sample 2	31661	43.00	48.30	67.50
sample 3	31717	40.23	45.60	65.20
mean	32393	41.11	46.50	65.93

1/2" BASE PLATE BASE METAL TENSILE TESTING

	E	σ_{ys}	σ_{yd}	σ_u
	<i>ksi</i>	<i>ksi</i>	<i>ksi</i>	<i>ksi</i>
sample 1	32669	51.10	55.65	74.30
sample 2	34564	50.80	54.40	74.10
sample 3	35095	83.20	87.70	106.70
mean	34109	61.70	65.92	85.03

A.3 Bolt Base Metal Tensile Testing

There were three bolt materials tested, A307 rod, A325 bolt, and A304 SH-1 bolt, at varying lengths representing the range of possible specimen bolts. For performing tensile coupon tests, all of the bolts and rods were machined to a smaller diameter in accordance to ASTM F606. There were four samples of the A325 bolts, two samples of the A304 SH-1 bolts, and one sample of the A307 rod, corresponding to different lots of bolts based on the different lengths used in the specimens. Bolts were also tested in shear and tension, results of which are presented later in this Appendix.

A.3.1. Test Setup and Methods

The specimens were fabricated using a lathe. The neck of the bolts were machined to a diameter of approximately ½ in. with a gage length of 2 in. Digital calipers were used to measure the thickness and width within the gage length at five different locations.

Table A-34: Specimen measurements and cross-sectional areas for base metal bolt testing

A325 BOLTS					A304-SH1 BOLTS			A307 RODS	
Diameter					Diameter			Diameter	
measurement #	sample 1	sample 2	sample 3	sample 4	measurement #	sample 1	sample 2	measurement #	sample 1
-	in	in	in	in	-	in	in	-	in
1	0.467	0.470	0.473	0.477	1	0.468	0.475	1	0.600
2	0.472	0.469	0.471	0.477	2	0.466	0.475	2	0.601
3	0.471	0.470	0.478	0.475	3	0.467	0.475	3	0.603
4	0.475	0.469	0.477	0.477	4	0.470	0.476	4	0.602
5	0.472	0.470	0.474	0.476	5	0.472	0.477	5	0.602
mean	0.471	0.470	0.475	0.476	mean	0.469	0.476	mean	0.602
area [in ²]	0.174	0.173	0.177	0.178	area [in ²]	0.173	0.178	area [in ²]	0.285

Photographs of the specimens prior to testing are shown in Figure A-60. Threaded regions were kept intact to minimize reduction of the cross-section in the gripped region.



Figure A-60: Photograph of A325 (#3 and #4) and A304-SH1 (#1 and #2) specimens prior to testing

A.3.2 Base metal bolt tensile testing results

Photographs of the tested specimens are shown in Figure A-61 below. Failure consistently occurred within the gauge lengths across testing.



(a) A325 coupons



(b) A304-SH1 coupons

Figure A-61: Photographs of A325 and A304-SH1 specimens after testing

Figure A-62 and Figure A-63 depict the force-displacement results and stress-strain results, respectively, for the A325 bolt base metal testing. Behavior is consistent across the samples tested, with failure occurring at 17% strain.

Force-displacement and stress-strain results for the A304-SH1 base metal tensile testing (strain hardened stainless steel bolts) are presented in Figure A-64.

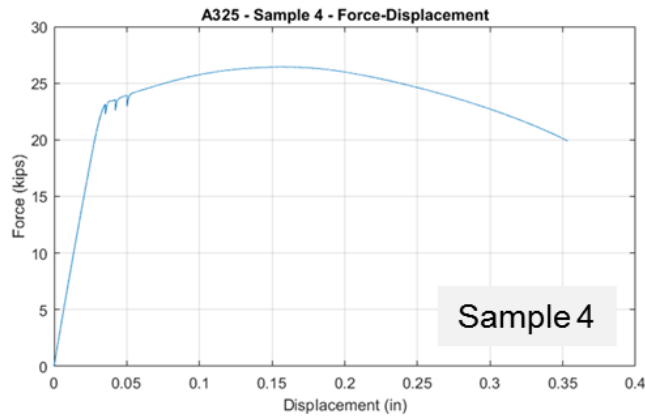
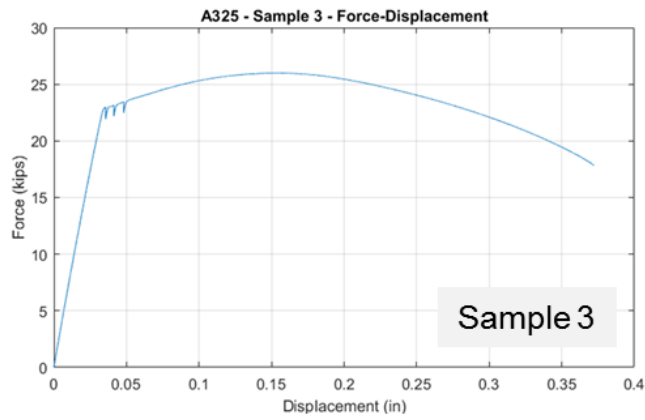
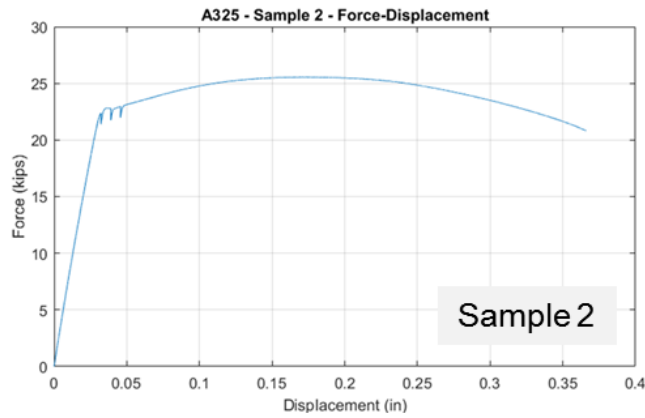
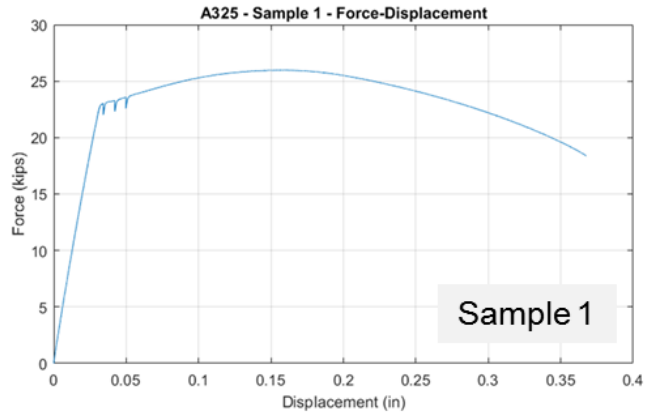


Figure A-62: Force-displacement results for A325 bolt base metal testing

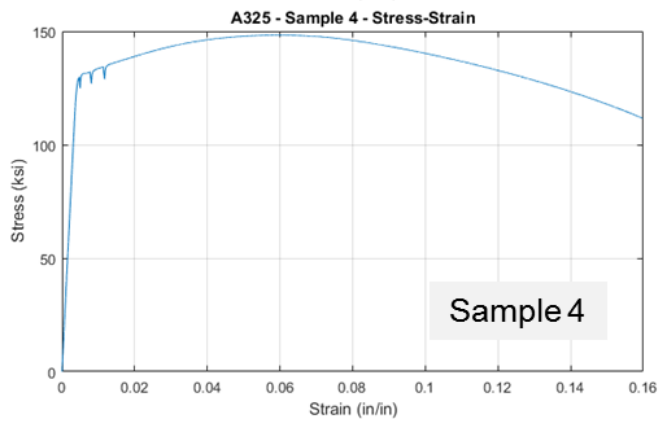
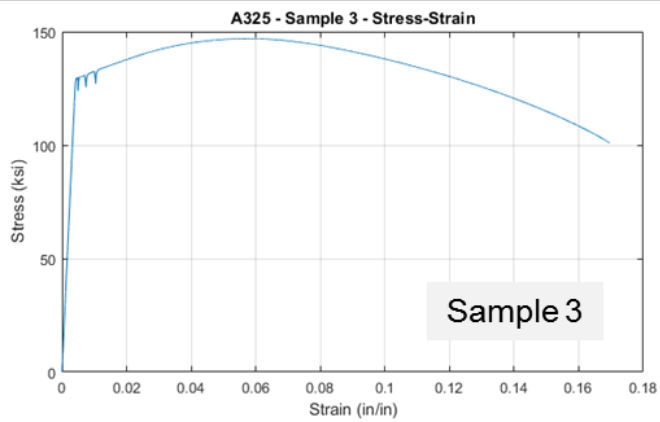
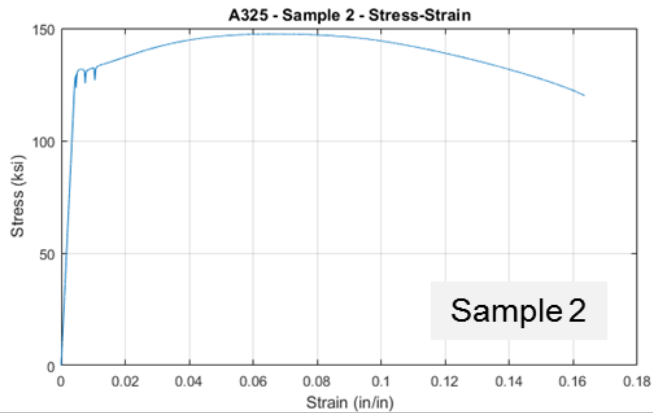
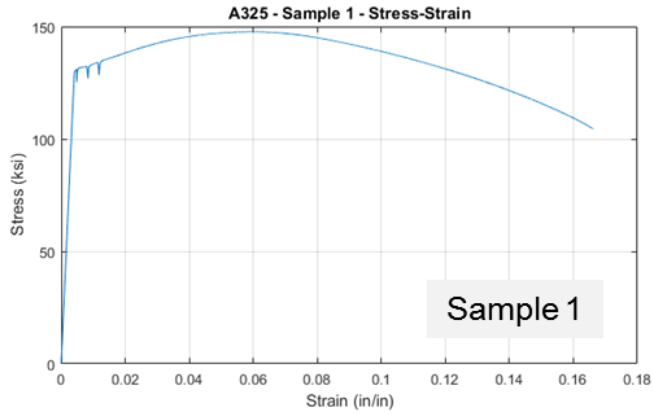


Figure A-63: Stress-strain results for A325 bolt base metal testing

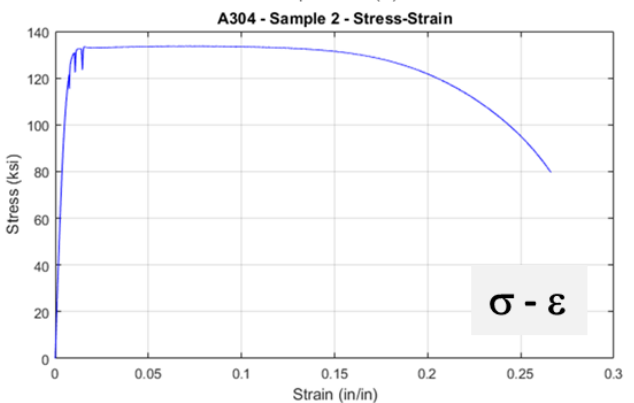
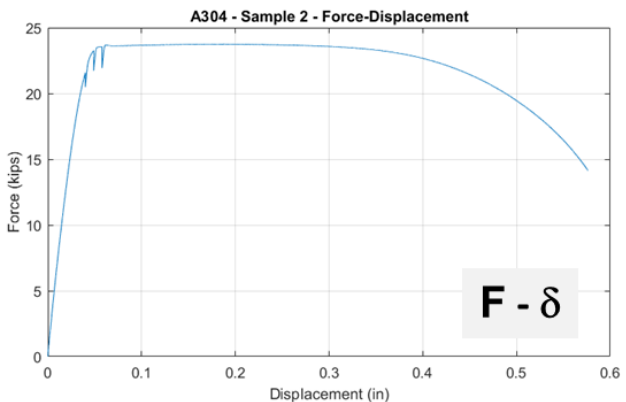
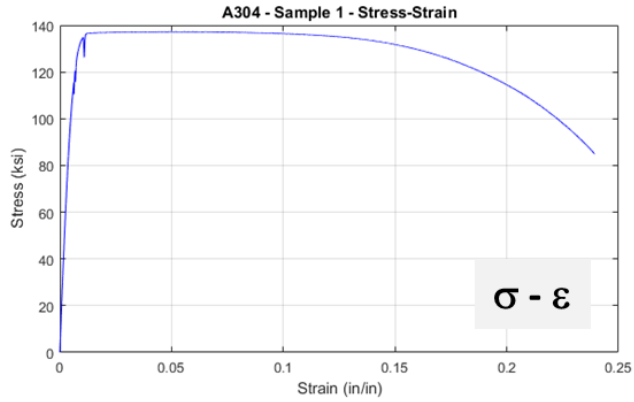
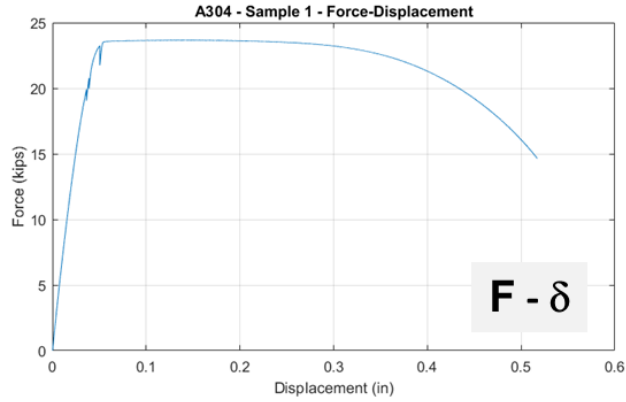


Figure A-64: Force-displacement and stress-strain relationships for A304-SH1 base metal bolt testing
 Force-displacement and stress-strain results for the A307 base metal tensile testing (strain hardened stainless steel bolts) are presented in Figure A-65. Note that there was only one available

sample for base metal testing, but the behavior of the bolt is fully characterized in the subsequent section.

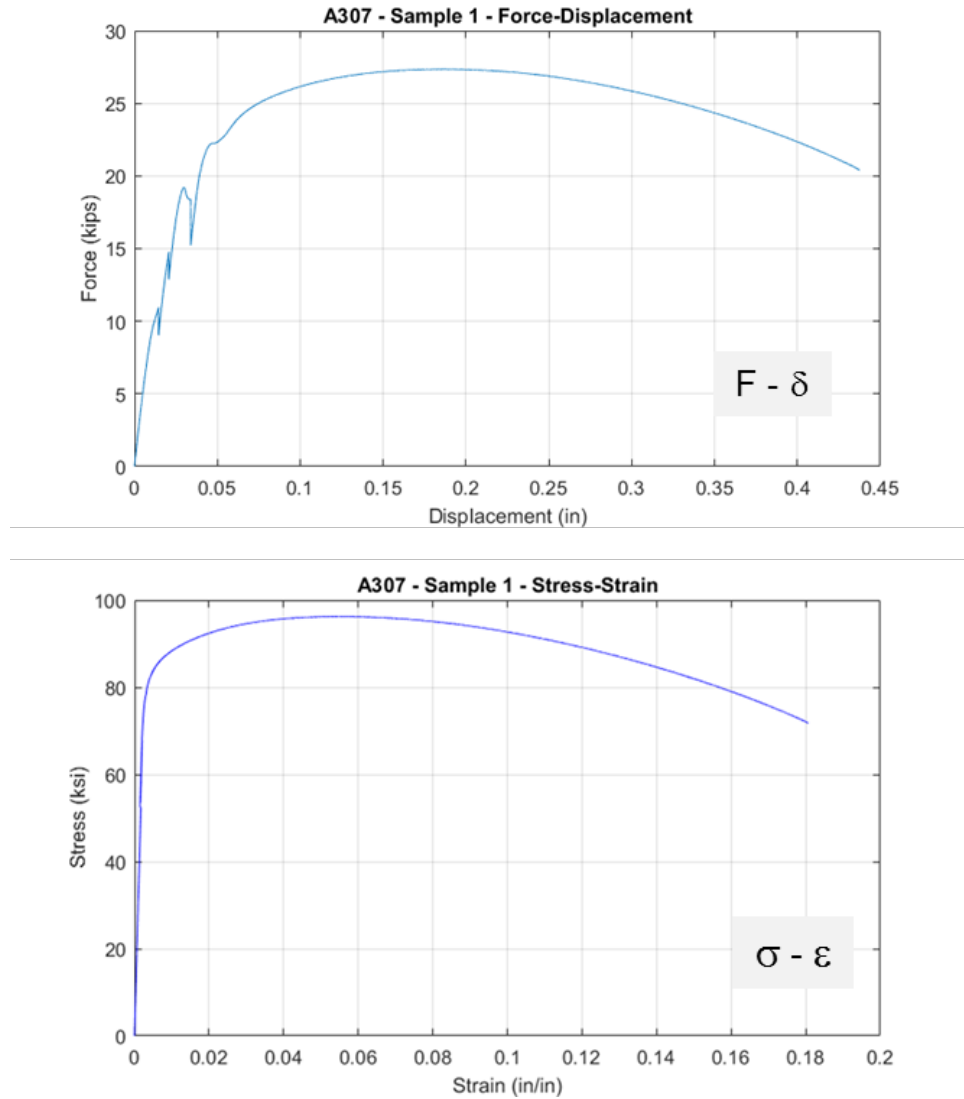


Figure A-65: Force-displacement and stress-strain relationships for A307 base metal bolt testing
Results across all base metal bolt testing are shown in Table A-35 below. Modulus of elasticity, static yield stress, dynamic yield stress, and ultimate stress are reported.

Table A-35: Summary of modulus of elasticity (E), static yield stress (σ_{ys}), dynamic yield stress (σ_{yd}), and ultimate stress (σ_u) across bolt base metal tensile testing

A325 BASE METAL TENSILE TESTING					A304-SH1 BASE METAL TENSILE TESTING				
	E	σ_{ys}	σ_{yd}	σ_u		E	σ_{ys}	σ_{yd}	σ_u
	<i>ksi</i>	<i>ksi</i>	<i>ksi</i>	<i>ksi</i>		<i>ksi</i>	<i>ksi</i>	<i>ksi</i>	<i>ksi</i>
sample 1	31800	126.93	131.70	147.77	sample 1	22893	126.30	132.60	137.30
sample 2	29907	125.40	131.70	147.68	sample 2	22666	120.50	128.60	133.76
sample 3	31164	125.60	130.20	146.96	mean	22780	123.40	130.60	135.53
sample 4	32467	126.93	131.40	148.36					
mean	31179	125.98	131.10	147.67					

A307 BASE METAL TENSILE TESTING				
	E	σ_{ys}	σ_{yd}	σ_u
	<i>ksi</i>	<i>ksi</i>	<i>ksi</i>	<i>ksi</i>
sample 1	30439	-	70.30	96.32

Summary of Results

Table A-15 presents a concise summary of material properties across base metal tests described in this section.

Table A-15: Summary of specimen material properties across testing (modulus of elasticity (E), static yield stress (σ_{ys}), dynamic yield stress (σ_{yd}), ultimate stress (σ_u))

	E	σ_{ys}	σ_{yd}	σ_u
	<i>ksi</i>	<i>ksi</i>	<i>ksi</i>	<i>ksi</i>
L6x4x5/16 angle	31370	50.37	53.53	79.47
L7x4x3/8 angle	32316	54.20	59.65	78.70
3/8" base plate	32393	41.11	46.50	65.93
1/2" base plate	34109	61.70	65.92	85.03
A325 bolt	31179	125.98	131.10	147.67
A304 SH-1 bolt	22780	123.40	130.60	135.53
A307 rod	30439	-	70.30	96.32

Bolt Testing in Shear and Tension

Testing of specimen bolts in shear and in tension was performed at the University of Cincinnati. Testing was in accordance with the standards outlined in ASTM F606-16. Five nominally identical specimens for each bolt or rod type (material and diameter) and length were tested in tension, and five were tested in shear.

A.4 Bolt tensile testing

The tensile test setup designated in ASTM F606 and replicated at the University of Cincinnati is shown in Figure A-66 below.

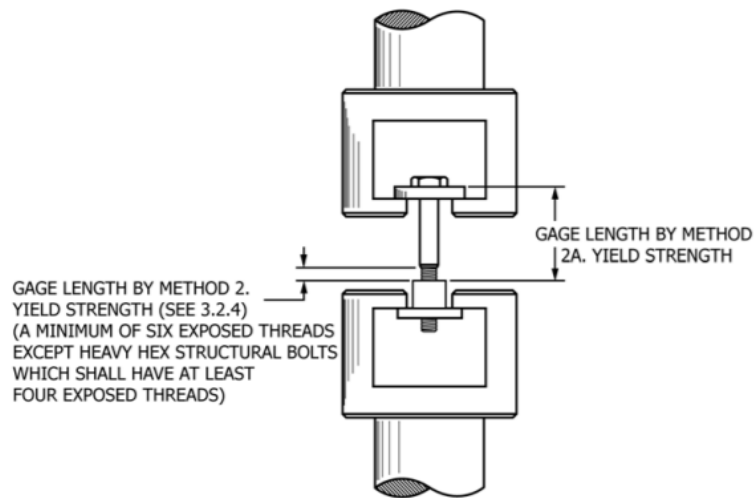


Figure A-66: Typical setup for bolt tensile testing (ASTM F606, 2016)

Force-displacement results for $\frac{1}{2}$ " diameter bolts and rods are shown in Figure A-67 below. While the stainless steel rods (B8 Class 2) achieve similar strengths to the carbon steel bolts, the force-displacement relationship is markedly different, featuring a long plateau after the proportional limit is reached.

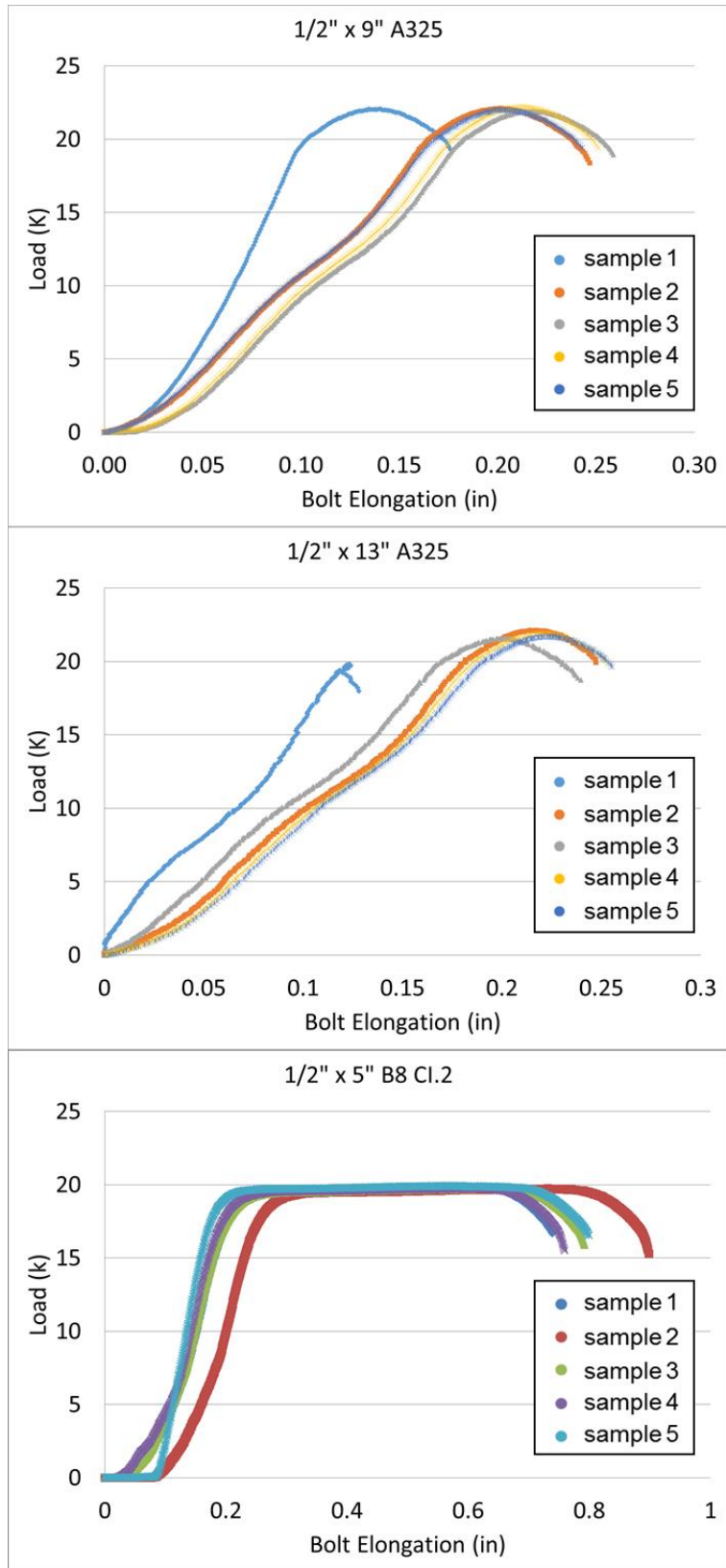


Figure A-67: Force-displacement results for 1/2" diameter bolt and rod tensile testing

The maximum force achieved for each sample is given in Table A-37 below, as well as the means per specimen type. Variation is small among samples. For all result tables within this section, L is the total bolt length, L_S is the shank length, and L_T is the threaded length. P_n is the nominal tensile strength of the bolt while P_u is the ultimate tested tensile strength. Pitch (measured in threads-per-inch, TPI) and diameter are also given.

Table A-37: Maximum force for 1/2" dia. bolts and rods tested in tension

Dia. <i>in</i>	Pitch <i>TPI</i>	L <i>in</i>	L_S <i>in</i>	L_T <i>in</i>	Grade -	P_n <i>kips</i>	Bolt # -	P_u <i>kips</i>
1/2	13	9	8	1	A325	20.58	1	21.96
							2	22.00
							3	21.83
							4	22.10
							5	21.99
							mean	21.98
1/2	13	13	12	1	A325	20.58	1	19.72
							2	22.03
							3	21.50
							4	21.84
							5	21.63
							mean	21.34
1/2	13	5	0	5	B8 Cl.2	20.58	1	19.75
							2	19.61
							3	19.65
							4	19.66
							5	19.82
							mean	19.70

Force-displacement results for 5/8" diameter bolt tensile testing are shown in Figure A-68 below. Change in behavior for the 3.5" long A325 bolts is likely related to the shortness of the specimen compared to the other bolts tested.

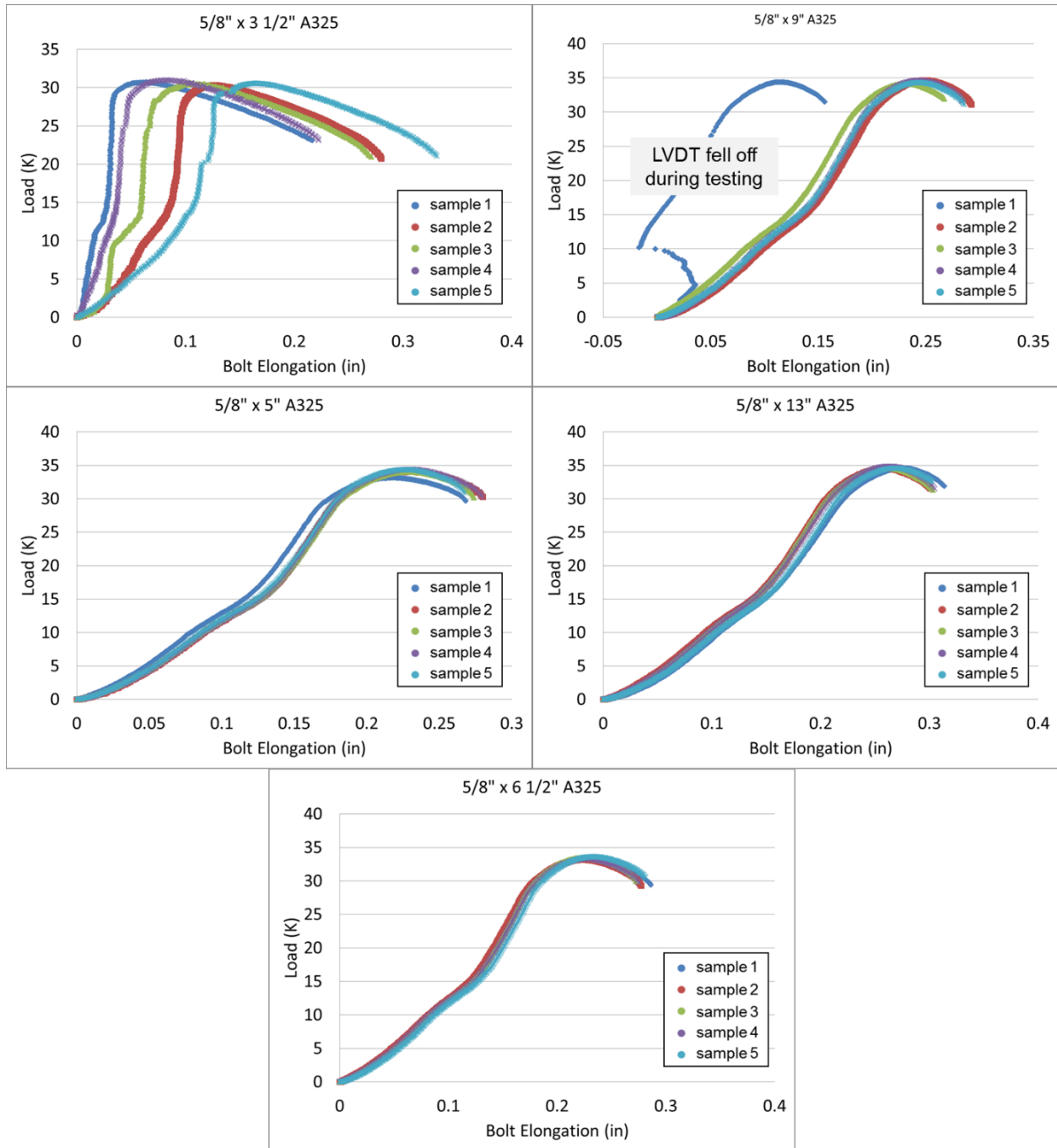


Figure A-68: Force-displacement results for 5/8" diameter bolt tensile testing

Results for each tested sample are given in Table A-38 below. While the shortest bolt tested, samples of 3.5" long A325 bolts, did not reach the same ultimate strength as longer bolt, the ultimate strength is consistent amongst the other bolts.

Table A-38: Maximum force for 5/8" dia. bolts and rods tested in tension

Dia. <i>in</i>	Pitch <i>TPI</i>	L <i>in</i>	L_s <i>in</i>	L_T <i>in</i>	Grade -	P_n <i>kips</i>	Bolt # -	P_u <i>kips</i>
5/8	11	3 1/2	2 1/4	1 1/4	A325	32.77	1	30.62
							2	30.33
							3	30.61
							4	31.09
							5	30.94
							mean	30.72
5/8	11	5	3 3/4	1 1/4	A325	32.77	1	33.57
							2	34.09
							3	33.99
							4	34.34
							5	34.33
							mean	34.06
5/8	11	6 1/2	5 1/4	1 1/4	A325	32.77	1	33.57
							2	33.60
							3	33.77
							4	33.70
							5	33.58
							mean	33.64
5/8	11	9	7 3/4	1 1/4	A325	32.77	1	34.42
							2	34.71
							3	34.08
							4	34.52
							5	34.29
							mean	34.40
5/8	11	13	11 3/4	1 1/4	A325	32.77	1	33.49
							2	34.47
							3	34.62
							4	34.77
							5	34.48
							mean	34.37

Force-displacement results for 3/4" diameter bolts and rods are shown in Figure A-69 below and capacities are tabulated in Table A-39 below.

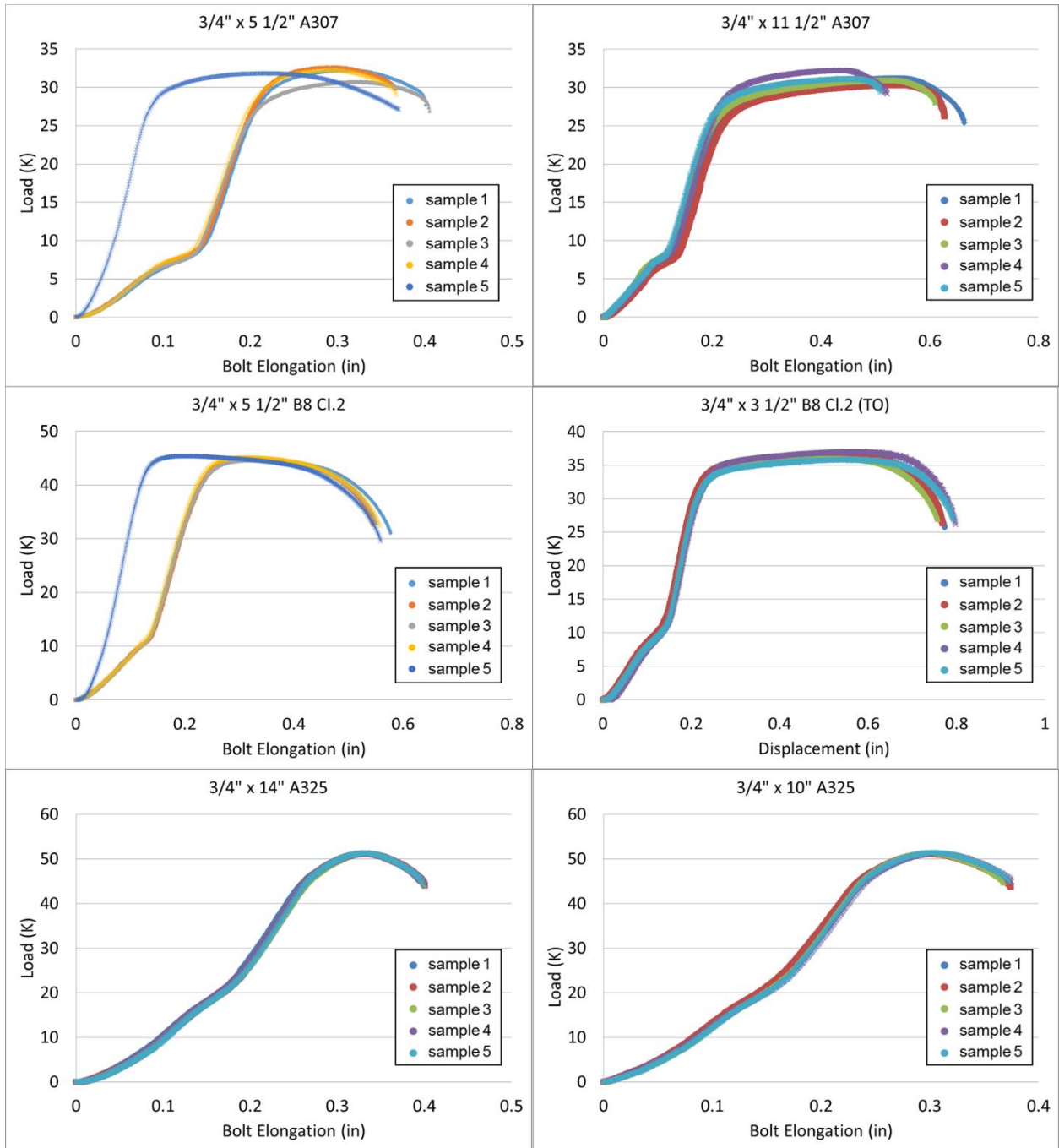


Figure A-69: Force-displacement results for 3/4" diameter bolt and rod tensile testing

Table A-39: Maximum force for 3/4" dia. bolts and rods tested in tension

Dia. <i>in</i>	Pitch <i>TPI</i>	L <i>in</i>	L_s <i>in</i>	L_r <i>in</i>	Grade <i>-</i>	P_n <i>kips</i>	Bolt # <i>-</i>	P_u <i>kips</i>
							1	32.08
							2	32.46
3/4	10	5 1/2	0	5 1/2	A307	33.45	3	30.59
							4	32.08
							5	31.71
							mean	31.78
							1	31.09
							2	30.27
3/4	10	11 1/2	0	11 1/2	A307	33.45	3	30.84
							4	32.11
							5	31.04
							mean	31.07
							1	50.95
							2	51.01
3/4	10	10	8 5/8	1 3/8	A325	48.50	3	51.16
							4	51.20
							5	51.22
							mean	51.11
							1	51.05
							2	51.10
3/4	10	14	12 5/8	1 3/8	A325	48.50	3	51.08
							4	50.96
							5	51.13
							mean	51.06
							1	44.74
							2	44.90
3/4	10	5 1/2	0	5 1/2	B8 Cl.2	48.50	3	44.58
							4	45.15
							5	45.41
							mean	44.96
							1	36.25
							2	36.38
3/4	10	3 1/2	2 1/8	1 3/8	A307	33.45	3	35.86
							4	36.92
							5	35.72
							mean	36.23

Results for 1" diameter bolts and rods are shown in Figure A-70 and capacities tabulated in Table A-40.

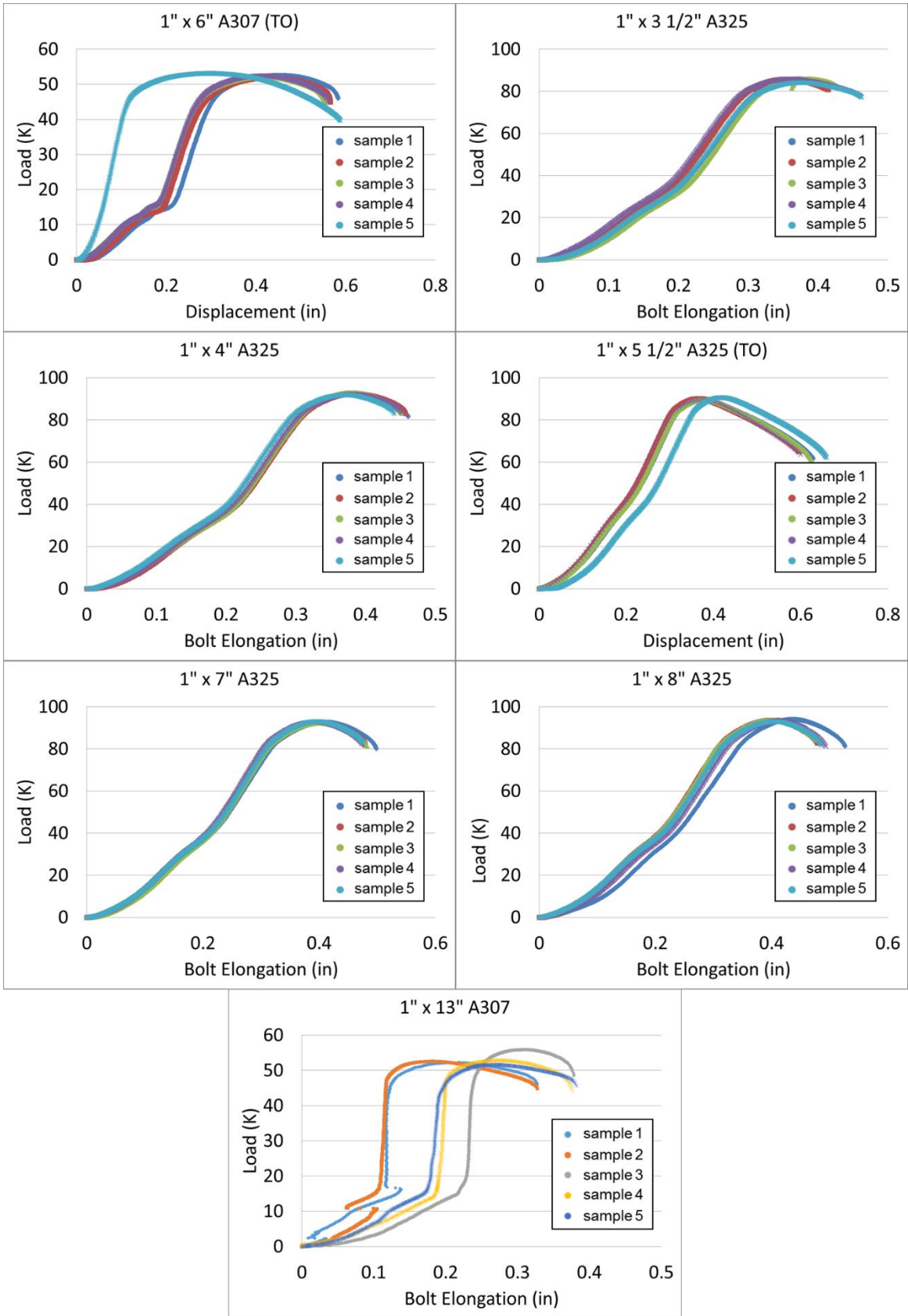


Figure A-70: Force-displacement results for 1" diameter bolt and rod tensile testing

Table A-40: Maximum force for 1" dia. bolts and rods tested in tension

Dia. <i>in</i>	Pitch <i>TPI</i>	L <i>in</i>	L_S <i>in</i>	L_T <i>in</i>	Grade <i>-</i>	P_n <i>kips</i>	Bolt # <i>-</i>	P_u <i>kips</i>
1	8	6	0	6	A307	60.57	1	52.51
							2	51.84
							3	51.95
							4	52.35
							5	53.05
							mean	52.34
1	8	3 1/2	1 3/4	1 3/4	A325	87.83	1	85.68
							2	85.64
							3	85.7
							4	85.7
							5	83.99
							mean	85.34
1	8	4	2 1/4	1 3/4	A325	87.83	1	92.63
							2	92.39
							3	92.76
							4	92.16
							5	91.76
							mean	92.34
1	8	5 1/2	3 3/4	1 3/4	A325	87.83	1	89.15
							2	89.91
							3	89.42
							4	89.75
							5	90.43
							mean	89.73
1	8	7	5 1/4	1 3/4	A325	87.83	1	92.56
							2	92.49
							3	92.08
							4	92.73
							5	92.83
							mean	92.54
1	8	8	6 1/4	1 3/4	A325	87.83	1	93.84
							2	93.40
							3	93.39
							4	93.19
							5	92.83
							mean	93.33
1	8	13	0	13	A307	60.57	1	52.03
							2	52.40
							3	55.80
							4	52.69
							5	51.42
							mean	52.87

A.5 Bolt shear testing

The tensile test setup designated in ASTM F606 and replicated at the University of Cincinnati is shown in Figure A-71 below. The setup is identical for bolts and threaded rods, where threads are included in the shear plane.

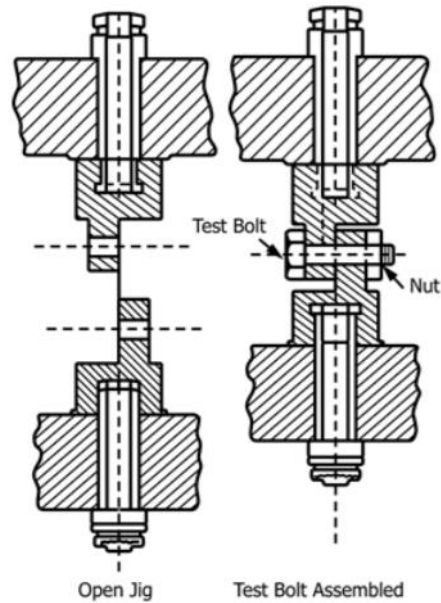


Figure A-71: Typical setup for bolt shear testing (ASTM F606, 2016)

Force-displacement results for 1/2" diameter bolts and rods are shown in Figure A-72 below. With the exception of significant over-strength in one of the 13" A325 samples, results are consistent across testing.

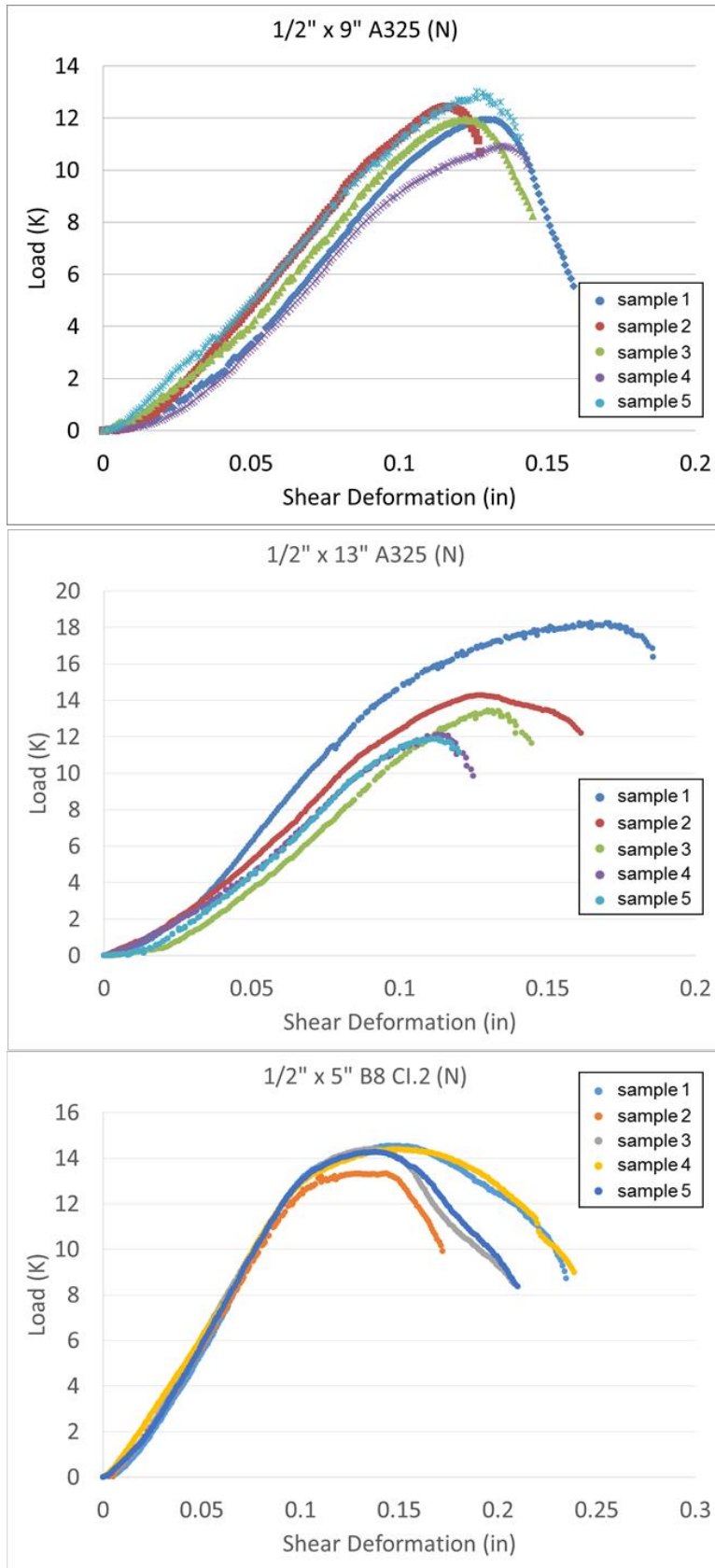


Figure A-72: Force-displacement results for 1/2" diameter bolt and rod shear testing

Bolt shear strengths are given across all 1/2" diameter samples in Table A-41 below.

Table A-41: Maximum force for 1/2" dia. bolts and rods tested in shear

Dia. <i>in</i>	Pitch <i>TPI</i>	L <i>in</i>	L_s <i>in</i>	L_T <i>in</i>	Grade -	P_n <i>kips</i>	Bolt # -	P_u <i>kips</i>
							1	11.95
							2	12.45
1/2	13	9	8	1	A325	12.77	3	11.96
							4	10.94
							5	13.02
							mean	12.06
							1	18.28
							2	14.30
1/2	13	13	12	1	A325	12.77	3	13.47
							4	12.14
							5	11.91
							mean	14.02
							1	14.55
							2	13.43
1/2	13	5	0	5	B8 Cl.2	12.77	3	14.42
							4	14.60
							5	14.32
							mean	14.26

Figure A-73 depicts force-displacement results for 5/8" diameter bolts. Behavior is consistent throughout the range of bolt lengths, and variability is low. Table A-42 provides strengths per sample and the means across specimen types.

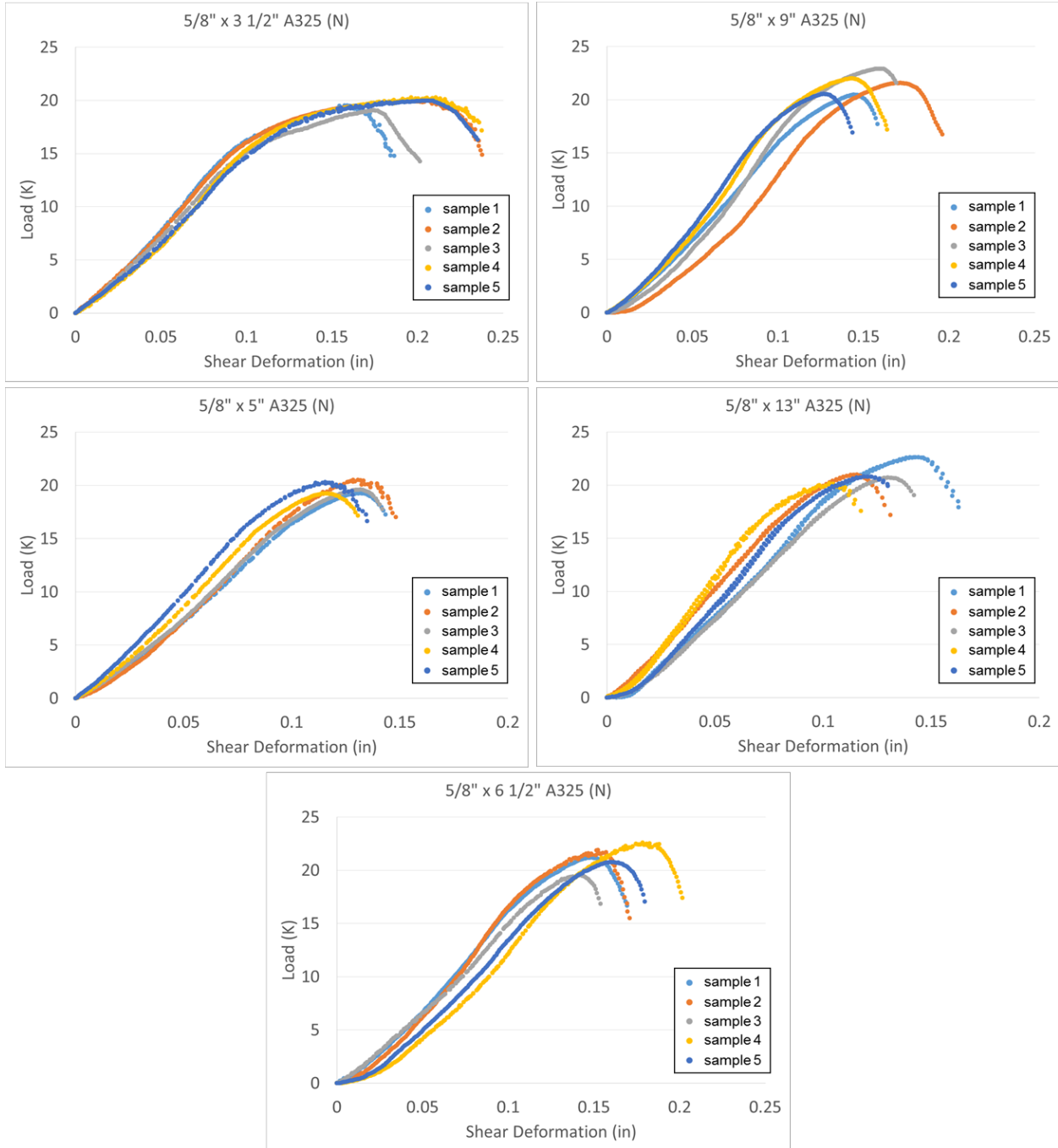


Figure A-73: Force-displacement results for 5/8" diameter bolt and rod shear testing

Table A-42: Maximum force for 5/8" dia. bolts and rods tested in shear

Dia. <i>in</i>	Pitch <i>TPI</i>	L <i>in</i>	L_s <i>in</i>	L_T <i>in</i>	Grade -	P_n <i>kips</i>	Bolt # -	P_u <i>kips</i>
5/8	11	3 1/2	2 1/4	1 1/4	A325	20.34	1	19.54
							2	20.01
							3	19.08
							4	20.30
							5	19.98
							mean	19.78
5/8	11	5	3 3/4	1 1/4	A325	20.34	1	19.28
							2	20.52
							3	19.61
							4	19.26
							5	20.32
							mean	19.80
5/8	11	6 1/2	5 1/4	1 1/4	A325	20.34	1	21.21
							2	21.90
							3	19.55
							4	22.59
							5	20.77
							mean	21.20
5/8	11	9	7 3/4	1 1/4	A325	20.34	1	20.49
							2	21.60
							3	22.92
							4	22.01
							5	20.55
							mean	21.51
5/8	11	13	11 3/4	1 1/4	A325	20.34	1	22.65
							2	21.00
							3	20.72
							4	20.19
							5	20.82
							mean	21.08

Force-displacement results for 3/4" diameter bolts and threaded rods are shown in Figure A-74 below.

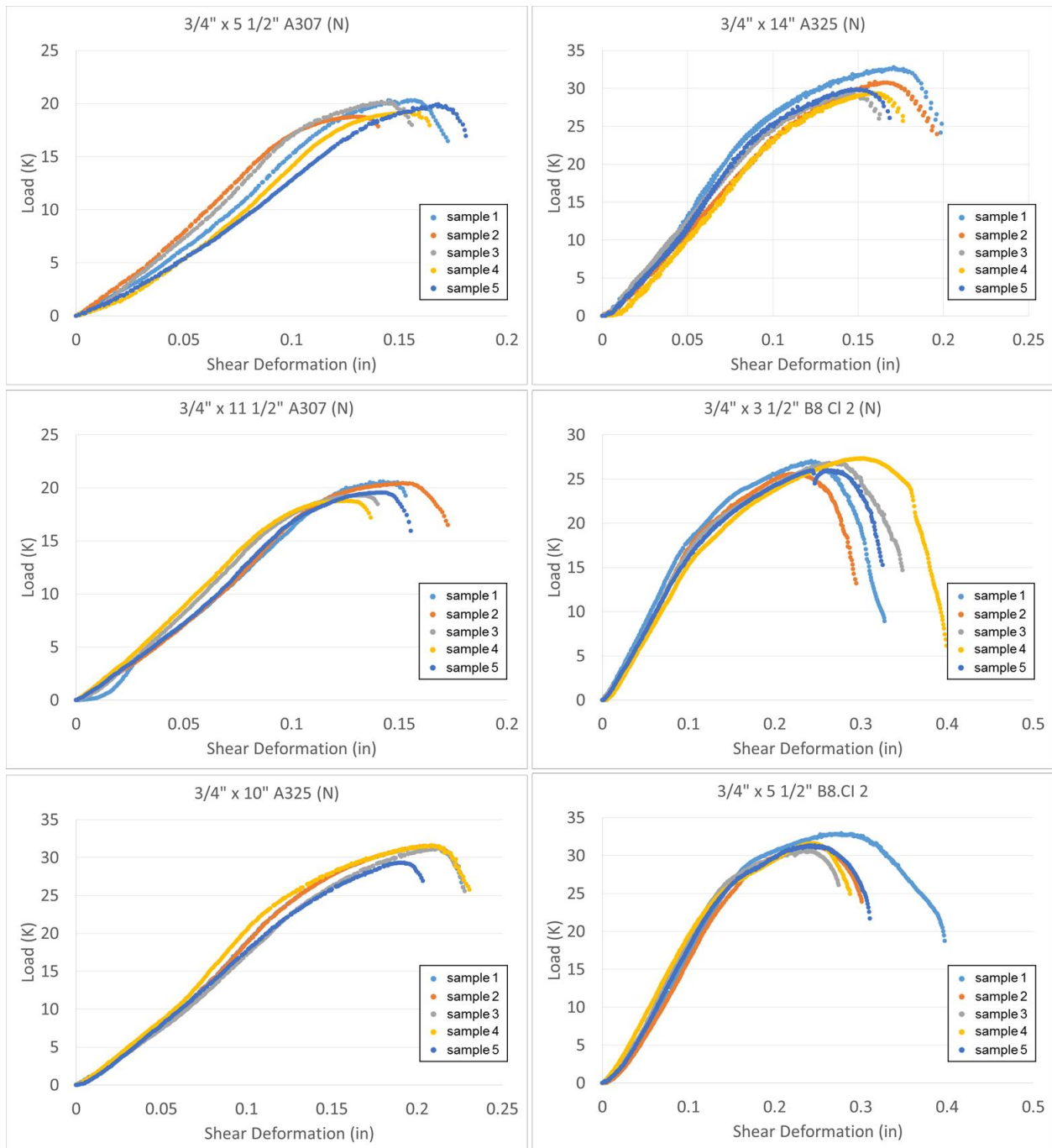


Figure A-74: Force-displacement results for 3/4" diameter bolt and rod shear testing
 Table A-43 summarizes the shear testing results for 3/4" diameter bolts.

Table A-43: Maximum force for 3/4" dia. bolts and rods tested in shear

Dia. <i>in</i>	Pitch <i>TPI</i>	L <i>in</i>	L_S <i>in</i>	L_T <i>in</i>	Grade -	P_n <i>kips</i>	Bolt # -	P_u <i>kips</i>
3/4	10	5 1/2	0	5 1/2	A307	20.90	1	21.10
							2	19.54
							3	20.27
							4	19.62
							5	20.13
							mean	20.13
3/4	10	11 1/2	0	11 1/2	A307	20.90	1	20.49
							2	21.20
							3	20.02
							4	19.53
							5	20.36
							mean	20.32
3/4	10	10	8 5/8	1 3/8	A325	30.10	1	31.47
							2	31.54
							3	31.29
							4	31.65
							5	29.34
							mean	31.06
3/4	10	14	12 5/8	1 3/8	A325	30.10	1	32.79
							2	30.86
							3	29.39
							4	29.39
							5	29.91
							mean	30.47
3/4	10	3 1/2	0	3 1/2	B8 Cl. 2	30.10	1	26.90
							2	25.71
							3	27.80
							4	27.55
							5	26.17
							mean	26.83
3/4	10	5 1/2	0	5 1/2	B8 Cl.2	30.10	1	32.70
							2	31.15
							3	30.64
							4	31.86
							5	31.40
							mean	31.55

The shear behavior of 1" diameter bolts and rods is shown in Figure A-75 while maximum values are recorded in Table A-44.

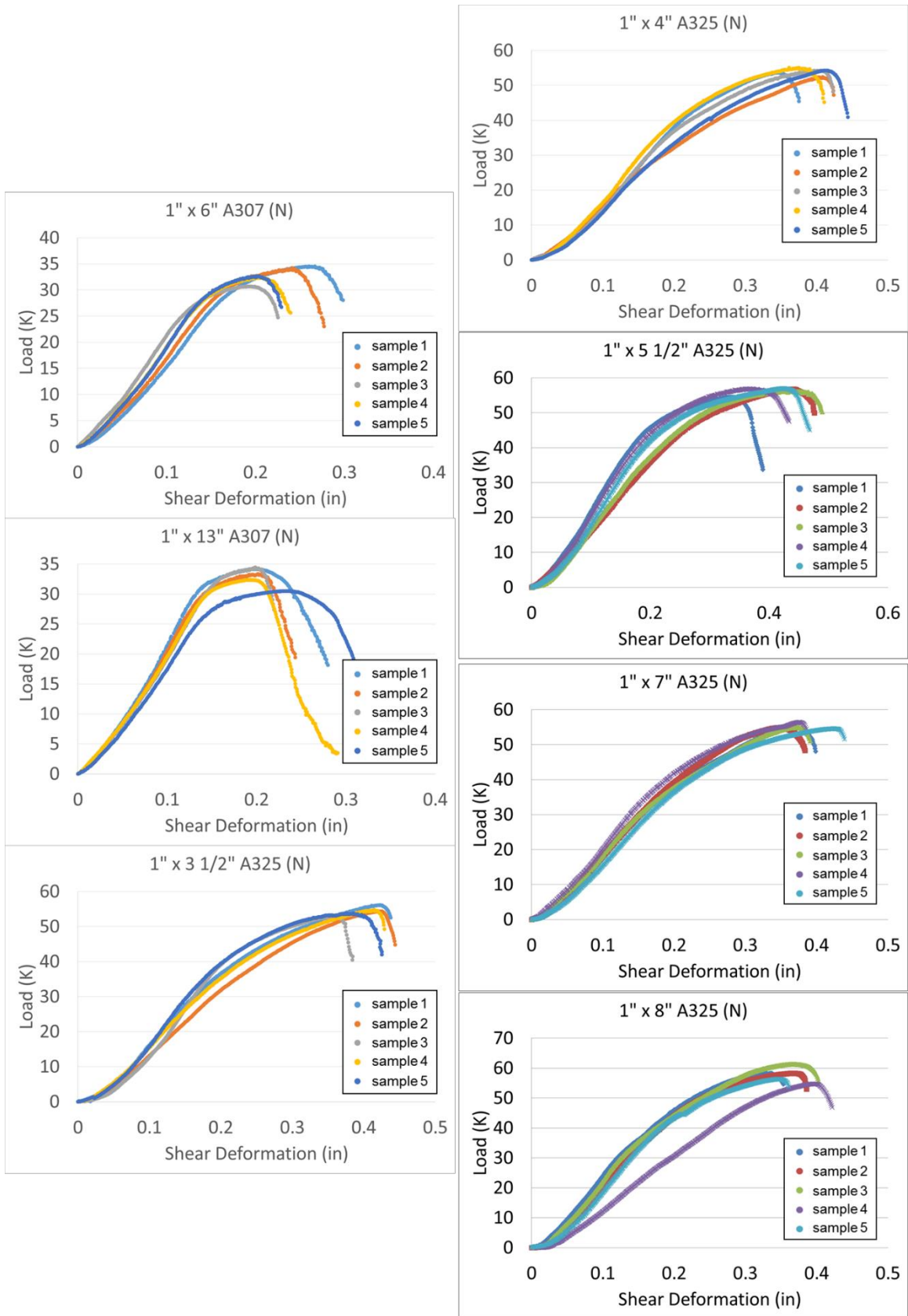


Figure A-75: Force-displacement results for 1" diameter bolt and rod shear testing

Table A-44: Maximum force for 1" dia. bolts and rods tested in shear

Dia. <i>in</i>	Pitch <i>TPI</i>	L <i>in</i>	L_s <i>in</i>	L_T <i>in</i>	Grade <i>-</i>	P_n <i>kips</i>	Bolt # <i>-</i>	P_u <i>kips</i>
1	8	6	0	6	A307	37.86	1	34.50
							2	33.95
							3	32.41
							4	32.29
							5	36.63
							mean	33.96
1	8	13	0	13	A307	37.86	1	34.36
							2	33.47
							3	34.58
							4	32.78
							5	30.64
							mean	33.17
1	8	3 1/2	1 3/4	1 3/4	A325	54.52	1	56.13
							2	54.38
							3	52.79
							4	54.78
							5	53.97
							mean	54.41
1	8	4	2 1/4	1 3/4	A325	54.52	1	53.81
							2	52.40
							3	54.29
							4	55.03
							5	54.27
							mean	53.96
1	8	5 1/2	3 3/4	1 3/4	A325	54.52	1	54.49
							2	56.74
							3	56.16
							4	56.77
							5	56.86
							mean	56.20
1	8	7	5 1/4	1 3/4	A325	54.52	1	54.69
							2	54.95
							3	54.90
							4	56.33
							5	54.46
							mean	55.07
1	8	8	6 1/4	1 3/4	A325	54.52	1	58.04
							2	58.17
							3	61.17
							4	54.60
							5	56.25
							mean	57.65

A.5.1 Summary of Bolt Tensile and Shear Testing Results

Table A-45 presents a summary of results across all tensile and shear bolt testing performed at the University of Cincinnati. The table presents averages across bolt lengths as well as test-to-predicted ratios. Note that because stainless steel bolts are not currently included in AISC 360, nominal values for A325 bolts are used for comparison as the mechanical properties match well with the strain hardened stainless steel bolts and rods.

Table A-45: Summary of tensile and shear testing of specimen bolts

TENSION					SHEAR				
Dia.	Grade	P_n	P_u	P_u/P_n	Dia.	Grade	P_n	P_u	P_u/P_n
<i>in</i>	-	<i>kips</i>	<i>kips</i>	-	<i>in</i>	-	<i>kips</i>	<i>kips</i>	-
1/2	A325	20.58	21.66	1.05	1/2	A325	12.77	13.04	1.02
1/2	B8 Cl. 2	20.58	19.70	0.96	1/2	B8 Cl. 2	12.77	14.26	1.12
5/8	A325	32.77	33.44	1.02	5/8	A325	20.34	20.67	1.02
3/4	A307	33.45	33.03	0.99	3/4	A307	20.90	20.23	0.97
3/4	A325	48.50	51.09	1.05	3/4	A325	30.10	30.76	1.02
3/4	B8 Cl. 2	48.50	40.59	0.84	3/4	B8 Cl. 2	30.10	29.19	0.97
1	A307	60.57	52.60	0.87	1	A307	37.86	33.56	0.89
1	A325	87.83	90.66	1.03	1	A325	54.52	55.46	1.02

A.6 Compression of Fiber Reinforced Polymer Materials

Compression testing of FRP materials utilized in sub-system testing was performed to characterize the performance under shim-type loading, termed flatwise compression. Currently, no ASTM standard exists for the strength testing of these materials perpendicular to the plane of the fibers. Standards do exist for testing parallel to the plane of the fibers, but those were deemed inapplicable.

As failure of the FRP specimens was desired, specimens were designed so that, even with potential over-strength, the MTS universal testing machine was able to supply enough force to the specimen. The limiting factor was not the load cell itself, but the hydraulic grips, which have a compressive capacity of 83.5 kips before the grips begin to slip. With this limit in mind, specimens were cut to 1"x1"x1" cubes (specimens were cut from 1" thick pultruded plate). In early stages of testing, it was discovered that results were sensitive to slight variations in specimen geometry, most notably lack of parallel surfaces in the plane of the fibers. To reduce variability, specimens were machined to flat and parallel with a milling machine.

Photographs of the test setup and of typical failure modes are shown in Figure A-76 below. For all of the specimens testing with the exception of phenolic specimens, failure was in the form of diagonal fracture through the specimen. Phenolic resins displayed a crushing failure as shown in the figure.



Figure A-76: Photographs of typical failure modes and test setup in MTS universal testing rig

Stress-strain results from compressive testing are shown in Figure A-77. Failure was brittle and occurred with little softening of the curve. Results are consistent across material samples.

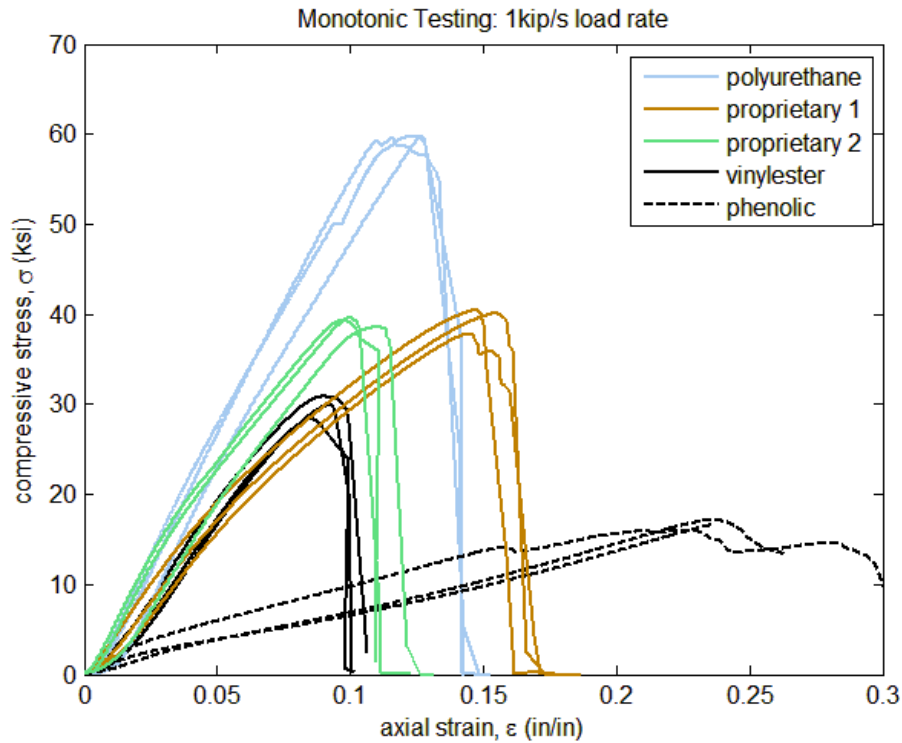


Figure A-77: Stress-strain results for flatwise compression testing of FRP materials

Table A-46 below presents material properties averaged across specimens tested. Modulus of elasticity and ultimate stress are given.

Table A-46: Summary of material properties across specimens

material	E	σ_u
-	<i>ksi</i>	<i>ksi</i>
polyurethane	620	59.71
proprietary 1	450	39.48
proprietary 2	500	39.15
vinylester	470	29.73
phenolic	100	16.55

Appendix B: Proposed Flatwise Compressive Creep Rupture Test Methodology

In this research, creep testing was conducted for fiber reinforced polymers materials subjected to through-thickness compression, referred to as flatwise compressive creep testing. In the absence of a relevant ASTM standard, a testing standard for flatwise compressive creep testing of fiber reinforced polymers is put forward in this appendix and used in this work. Existing ASTM standards for tensile creep of fiber reinforced polymers (ASTM C365) and flatwise compressive rupture of polymer matrixes (ASTM D7337) are used as a basis for this proposed test method.

[PROPOSED] Standard Test Method for Flatwise Compressive Creep Rupture of Fiber Reinforced Polymer Matrix Composite Materials (*adapted after ASTM C365 and D7337*)

1. Scope

1.1 This test method outlines requirements for flatwise compressive creep rupture testing of fiber reinforced polymer matrix (FRP) composite materials used as compressive fills in steel bolted connections.

1.2 Data obtained from this test method are used in design of FRP fills under sustained loading. The procedure for calculating one-million hour creep-rupture capacity is provided in Annex A1.

1.3 The values stated in either SI units or inch-pound units are to be regarded separately as standard. Within the text, the inch-pound units are shown in brackets. The values stated in each system are not exact equivalents; therefore, each system must be used independently of the other. Combining values from the two systems may result in nonconformance with the standard.

1.4 *This standard does not purport to address all of the safety concerns, if any, associated with its use. It is the responsibility of the user of this standard to establish appropriate safety and health practices and determine the applicability of regulatory limitations prior to use.*

2. Referenced Documents

2.1 *ASTM Standards.*¹

C365/C365M Standard Test Method for Flatwise Compressive Properties of Sandwich Cores

D883 Terminology Relating to Plastics

D3878 Terminology for Composite Materials

D5229/D5229M Test Method for Moisture Absorption Properties and Equilibrium Conditioning of Polymer Matrix Composite Materials

D7205/D7205M Test Method for Tensile Properties of Fiber Reinforced Polymer Matrix Composite Bars

D7337/D7337M Test Method for Tensile Creep Rupture of Fiber Reinforced Polymer Matrix Composite Bars

E4 Practices for Force Verification of Testing Machines

E6 Terminology Related to Methods of Mechanical Testing

E177 Practice for Use of the Terms Precision and Bias in ASTM Test Methods

E456 Terminology Relating to Quality and Statistics

E1012 Practice for Verification of Testing Frame and Specimen Alignment Under Tensile and Compressive Axial Force Application

¹ For referenced ASTM standards, visit the ASTM website, www.astm.org, or contact ASTM Customer Service at service@astm.org. For *Annual Book of ASTM Standards* volume information, refer to the standard's Document Summary page on the ASTM website.

3. Terminology

3.1 Terminology in D3878 defines terms relating to high-modulus fibers and their composites. Terminology in D883 defines terms relating to plastics. Terminology in E6 defines terms related to mechanical testing. Terminology in E456 defines terms relating to statistics and the selection of sample sizes. In the event of conflict between terms, Terminology in D3878 shall have precedence of the other terminology standards.

3.2 Definitions of Terms Specific to This Standard:

3.2.1 *creep, n*—time dependent deformation (or strain) under sustained force (or stress).

3.2.2 *creep rupture, n*—material failure caused by sustained force (or stress) over time.

3.2.3 *creep rupture capacity, n*—the force at which failure occurs after a specified period of time from initiation of a sustained force. The predicted force causing failure at 1 million hours is referred to as the million-hour creep rupture capacity. This capacity is determined by the method described in the Annex.

3.2.4 *creep rupture strength, n*—the stress causing failure after a specified period of time from initiation of a sustained force.

3.2.5 *creep rupture time, n*—the lapsed time between the start of a sustained force and failure of the test specimen.

3.2.6 *force ratio, n*—the ratio of a constant sustained force applied to a specimen to its compressive capacity as determined according to Test Method D7205/D7205M.

3.2.7 *nominal cross-sectional area, n*—a measure of cross-sectional area of a bar, determined over at least one representative length, used to calculate stress.

3.3 *Symbols:*

a_1, b_1 = empirical constants

A = nominal or standard cross-sectional area of a bar, see Test Method D7205/D7205M

F_r = stress carried by specimen at rupture

P_r = force carried by specimen at rupture

t = time, hours

Y_c = creep rupture trend line

4. Summary of Test Method

4.1 This test method consists of measuring the time to rupture of a fill subjected to a constant compressive force. Multiple force levels are specified by the method so that a relationship between force and time-to-failure can be derived.

5. Significance and Use

5.1 Flatwise compressive strength and modulus are fundamental mechanical properties of sandwich cores that are used in designing sandwich panels. Deformation data can be obtained, and from a complete force versus deformation curve, it is possible to compute the compressive stress at any applied force (such as compressive stress at proportional limit force or compressive strength at the maximum force) and to compute the effective modulus of the fill.

5.2 This test method provides a standard method of obtaining the flatwise compressive creep rupture strength and modulus for connection fill structural design properties, material specifications, research and development applications, and quality assurance.

5.3 In order to prevent local crushing of some fills, it is often desirable to stabilize the facing plane surfaces with a suitable material, such as a thin layer of resin or thin facings. Flatwise compressive strength data may be generated using either stabilized specimens (reported as stabilized compression strength) or non-stabilized specimens (reported as bare

compression strength). It is customary aerospace industry practice to determine compression modulus only when using stabilized specimens.

5.4 Factors that influence the flatwise compressive strength and shall therefore be reported include the following: fill material, methods of material fabrication, fill geometry (fiber orientation), specimen geometry, specimen preparation, specimen conditioning environment of testing, specimen alignment, loading procedure, and speed of testing.

8. Sampling and Test Specimens

8.1 Specimens shall be representative of the lot or batch being tested. For grid-type FRP specimens, linear test specimens may be prepared by cutting away extraneous material in such a way as not to affect the performance of the part to be used. In the test section of the specimen, no postproduction machining, abrading, or other such processing is permitted.

8.2 During the sampling and preparation of test specimens, all deformation, heating, outdoor exposure to ultraviolet light, and other conditions possibly causing changes to the material properties of the specimen shall be avoided, unless these conditions are specified as part of the test procedure.

8.3 The length of the specimen shall be in accordance with Test Method D7205/D7205M.

8.4 The cross-sectional area of the specimen shall be determined in accordance with either of the two methods described in Test Method D7205/D7205M: nominal area or standard area.

8.5 A 100 mm [4 in.] long specimen shall be used to determine the average moisture content of the as-received or as-conditioned bar before the start of creep rupture testing. The average moisture content shall be determined according to Procedure D, section 3.2.2, of Test Method D5229/D5229M.

8.6 A 100 mm [4 in.] long traveler specimen of the same cross-section geometry and appropriate size shall be used to determine the average moisture content of each bar after creep rupture testing. The ends of creep rupture specimens and traveler specimens shall be sealed with a water resistant sealant such as a high grade, room temperature curing epoxy to avoid end effects. The average moisture content shall be determined according to Procedure D, section 3.2.2, of Test Method D5229/D5229M.

9. Test Matrix

9.1 The quasi-static compressive strength of the specimens as determined by Test Method C365/C365M is used as a basis for selecting the applied compressive forces for creep rupture tests. At each given force ratio—for example, 80 %, 70 %, 60 % of the compressive strength—the applied force must be maintained constant until failure occurs while the time elapsed to rupture of each test specimen is recorded.

NOTE 1—The selection of force ratios is dependent on the fiber architecture and fiber volume fraction for the bar. Material systems with a high resistance to creep rupture (for example, carbon FRP composite) will necessitate the selection of closely-spaced force ratios at stress levels approaching 100 % of the quasi-static compressive strength. Material systems with less resistance to creep rupture (for example, glass FRP composite) will necessitate the selection of widely-spaced force ratios.

9.2 A minimum of four force ratios are required (see Fig. A1.1 for example). A minimum of 5 valid test results are required for each force ratio. For the entire group of tests reported, the range between the longest and shortest recorded rupture times shall be at least three decades. Data from specimens that break before the applied compressive force is fully applied to the specimen shall be disregarded.

NOTE 2—It is suggested that additional specimens be tested at each force ratio, especially for those force ratios that require long times to rupture.

9.2.1 The highest force ratio shall be selected such that at least four specimens in this group ruptures at a time of greater than 1 h.

NOTE 3—The highest force is specified with the aim of minimizing the effects of the initial loading ramp on the creep rupture time.

9.2.2 The lowest force ratio shall be selected such that at least one specimen in this group ruptures at a time of greater than 8000 h.

NOTE 4—The lowest force is specified with the aim of limiting the extent of extrapolation required to determine the one million hour creep rupture capacity.

9.2.3 The remaining force ratios shall be roughly equally spaced in relation to the highest and lowest force ratios determined in 9.2.1 and 9.2.2, respectively.

10. Conditioning

10.1 The recommended pre-test condition is effective moisture equilibrium at a specific relative humidity as established by Test Method D5229/D5229M; however, if the test requestor does not explicitly specify a pre-test conditioning environment, no conditioning is required and the specimens may be tested as prepared.

10.2 The pre-test specimen conditioning process, to include specified environmental exposure levels and resulting moisture content, shall be reported with the test data.

NOTE 5—The term moisture, as used in Test Method D5229/D5229M, includes not only the vapor of a liquid and its condensate, but the liquid itself in large quantities, as for immersion.

10.3 If no explicit conditioning process is performed the specimen conditioning process shall be reported as “unconditioned”.

11. Procedure

11.1 The mounting of the specimen in the test fixture shall be in accordance with Test Method D7205/D7205M.

11.2 Test specimens shall not be subjected to any dynamic effects, vibration, or torsion during testing.

11.3 The full load shall be applied to the specimen in a time between 20 s and 5 min. Time to creep rupture shall be measured from the moment when the specimen has attained the prescribed force.

NOTE 6—The load should be applied in a manner that precludes impact forces on the specimen. For frames using weights to load the specimen, it is suggested that the weights be supported temporarily on a hydraulic jack or pneumatic bladder, and then the load transferred linearly to the specimen by slowly releasing the pressure on the jack or bladder.

12. Validation

12.1 Failure times should not be recorded for any specimen that fails at some obvious flaw, unless such a flaw constitutes a variable being studied.

12.2 Re-examine the means of force introduction into the material if a significant fraction of failures in a sample population occur within or just outside any anchor or grip. Factors considered should include the anchor-to-test frame alignment, anchor material, anchor-to-specimen alignment, anchor filler and bonding agent, grip type, grip pressure, and grip alignment.

13. Report

13.1 Report the following information, or references pointing to other documentation containing this information, to the maximum extent applicable (reporting of items beyond the control of a given testing laboratory, such as might occur with material details or bar fabrication parameters, shall be the responsibility of the requestor):

13.1.1 The revision level or date of issue of this test method.

13.1.2 The date(s) and location(s) of the test.

13.1.3 The name(s) of the test operator(s).

13.1.4 Any variations to this test method, anomalies noticed during testing or equipment problems occurring during testing.

13.1.5 Identification of the material tested including (if available): material specification, material type, material designation, manufacturer, manufacturer's lot or batch number, source (if not from manufacturer), date of certification, expiration of certification, filament diameter, tow or yarn filament count and twist, sizing, form or weave, and matrix type.

13.1.6 If available, description of the fabrication steps used to prepare the bar including fabrication start date, fabrication end date, process specification, cure cycle, consolidation method, and a description of the equipment used.

13.1.7 Description of fiber architecture and surface characteristics of the bar. Indicate the representative length of the bar, if appropriate.

- 13.1.8 If requested, report density, volume percent reinforcement, and void content test methods, specimen sampling method and geometries, test parameters, and test results.
- 13.1.9 Minimum, maximum and average value of the nominal area of the bar and the average bar diameter.
- 13.1.10 Results of any nondestructive evaluation tests.
- 13.1.11 Method of preparing the test specimen, including specimen labeling scheme and method, specimen geometry, sampling method, and bar cutting method. Identification of anchor material, geometry, bonding agent such as expansive cementitious material, and bonding agent preparation and curing information.
- 13.1.12 Calibration dates and methods for all measurement and test equipment.
- 13.1.13 Type of test machine, grips, jaws; grip pressure, grip length and texture of grip faces, and data acquisition sampling rate and equipment type if applicable.
- 13.1.14 Results of system alignment evaluations, if any such evaluations were done.
- 13.1.15 Dimensions of each test specimen.
- 13.1.16 Conditioning parameters and results, use of travelers and traveler geometry, and the procedure used, if other than that specified in the test method.
- 13.1.17 Moisture content of specimen sample at start of creep rupture testing.
- 13.1.18 Environment of the test machine environmental chamber (if used).
- 13.1.19 Number of specimens tested at each force ratio.
- 13.1.20 Time duration of initial loading of each specimen.
- 13.1.21 Average compressive capacity and quasi-static compressive strength of similar specimens from same batch of material as used for the creep rupture specimens.
- 13.1.22 Type of area used for stress calculation: nominal area or standard area.
- 13.1.23 Force ratio, rupture strength and rupture time for each specimen. Include elapsed time of testing for specimens that did not fail. Force ratio versus time curve as defined in [Annex A1](#).
- 13.1.24 Empirical constants a_1 and b_1 from [Eq A1.1](#) of [Annex A1](#), along with regression coefficient R_2 .
- 13.1.25 The million-hour creep-rupture force ratio, rupture capacity, and rupture strength, as defined in [Annex A1](#).
- 13.1.26 Average moisture content of the unloaded traveler specimens, at the end of each test.
- 13.1.27 Failure mode and location of failure for each specimen.

14. Precision and Bias

14.1 *Precision*—The data required for the development of a precision statement is not available for this test method. Precision, defined as the degree of mutual agreement between individual measurements, cannot yet be estimated because of an insufficient amount of data.

14.2 *Bias*—Bias cannot be determined for this test method as no acceptable reference standard exists.

15. Keywords

15.1 bars; composite bars; composite materials; creep rupture; reinforcing bars; compressive properties; compressive strength

ANNEX

(Mandatory Information)

A1. METHOD FOR CALCULATING MILLION-HOUR CREEP RUPTURE CAPACITY

A1.1 Scope

A1.1.1 This Annex describes the method for calculating the million-hour creep rupture capacity of FRP bars given the reported test results.

A1.2 Significance and Use

A1.2.1 The million-hour creep rupture capacity can be used for material screening purposes and in structural design codes to limit the sustained-level stresses in FRP bars.

A1.3 Calculation

A1.3.1 The force ratio versus creep rupture time curve shall be plotted on a semi-logarithmic graph where the force ratio is represented on an arithmetic scale along the vertical axis and creep rupture time in hours is represented on a logarithmic scale along the horizontal axis (see [Fig. A1.1](#)). Tests resulting in no failure (run-outs) shall be included in this plot but should not be included in the calculation of the creep rupture trend line. Run outs should clearly be identified as such on the graph.

A1.3.2 A creep rupture trend line shall be plotted from linear regression of the data by means of the least-square method according to [Eq A1.1](#):

$$Y_c = a_1 - b_1 \log t \quad (\text{A1.1})$$

where:

Y_c = force ratio, expressed as a percentage of quasistatic compressive strength,

a_1, b_1 = empirical constants, and

t = time, h.

A1.3.3 The force ratio at 1 million hours, as determined from the linear extrapolation of the trendline, shall be taken as the million-hour creep-rupture force ratio. The force and stress corresponding to the million-hour creep rupture force ratio are the million-hour creep rupture capacity and the million-hour creep rupture strength, respectively. The million-hour creep rupture strength is calculated according to Eq A1.2, with a precision to three significant digits:

$$F_r = \frac{P_r}{A} \quad (\text{A1.2})$$

where:

F_r = million-hour creep rupture strength of FRP bar, MPa [psi],

P_r = million-hour creep rupture capacity, N [lbf], and

A = cross-sectional area of specimen, mm² [in.²] as determined according to Section 11 of Test Method [D7205/D7205M](#).

Appendix C: Shelf Angle Experimental Test Data

This appendix contains the results from the shelf angle experiments, highlighting the key data for these tests. The results are zeroed at the same time to initiate data collection at a time after the two bolts on each shelf angle specimen had been tightened to a snug tight condition. A template for the layout of the data plots for each tests is shown below:

Actuator Force
vs.
Crosshead Displacement

Shelf Angle Strain Gauges
vs.
Crosshead Displacement

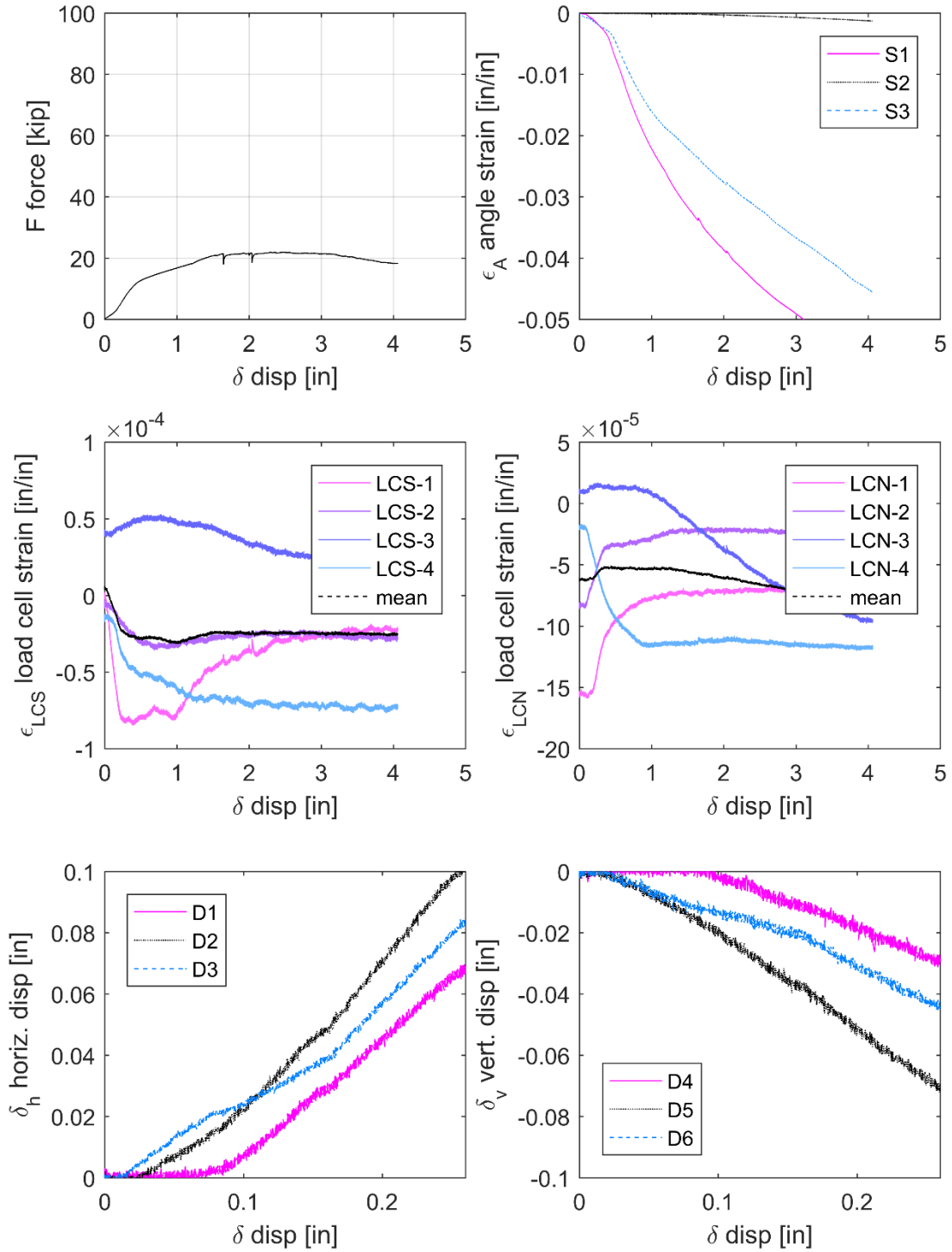
SOUTH
Load Cell Strain Gauges
[and mean]
vs.
Crosshead Displacement

NORTH
Load Cell Strain Gauges
[and mean]
vs.
Crosshead Displacement

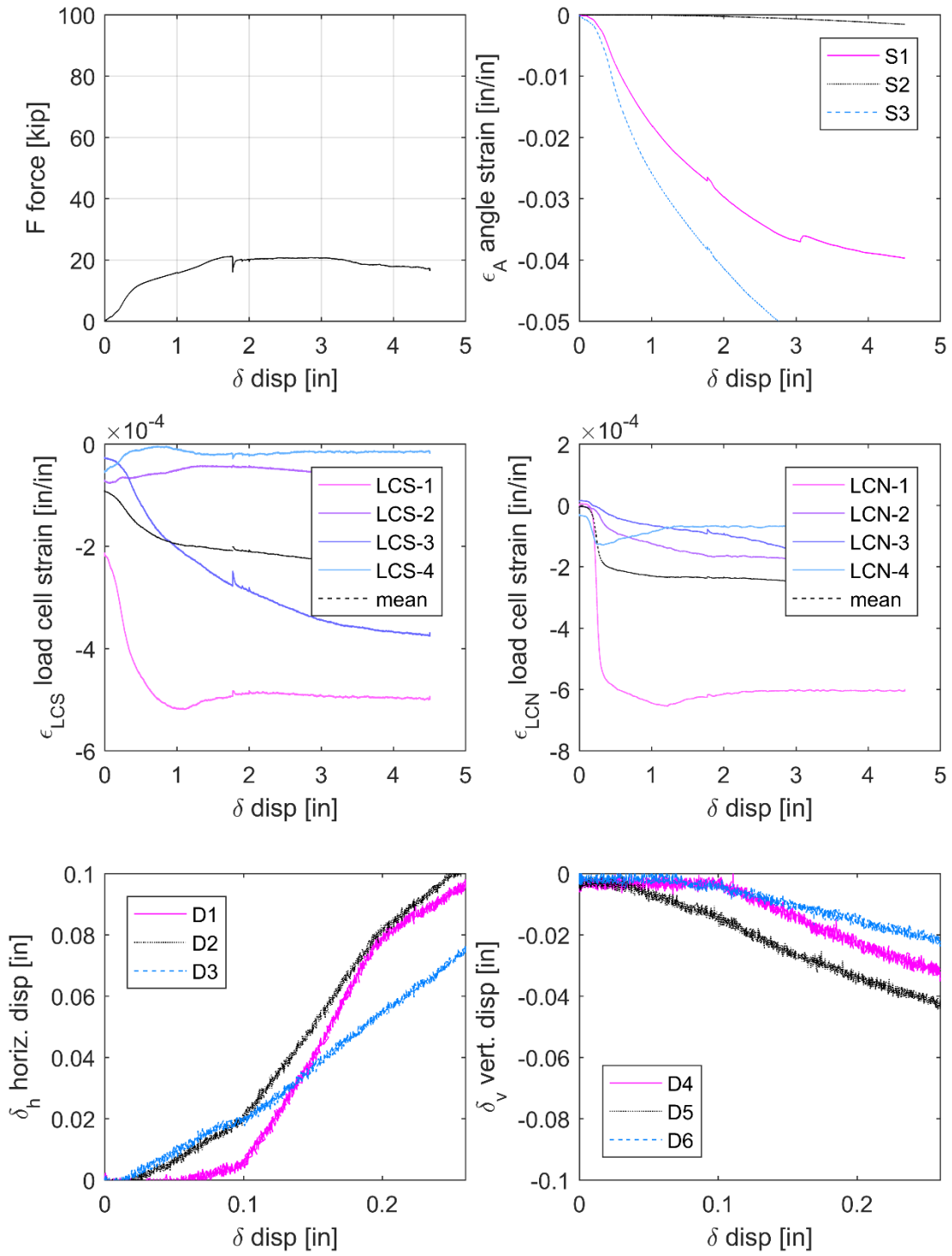
HORIZONTAL
Position Transducers
vs.
Crosshead Displacement
in design region (<0.25")

VERTICAL
Position Transducers
vs.
Crosshead Displacement
in design region (<0.25")

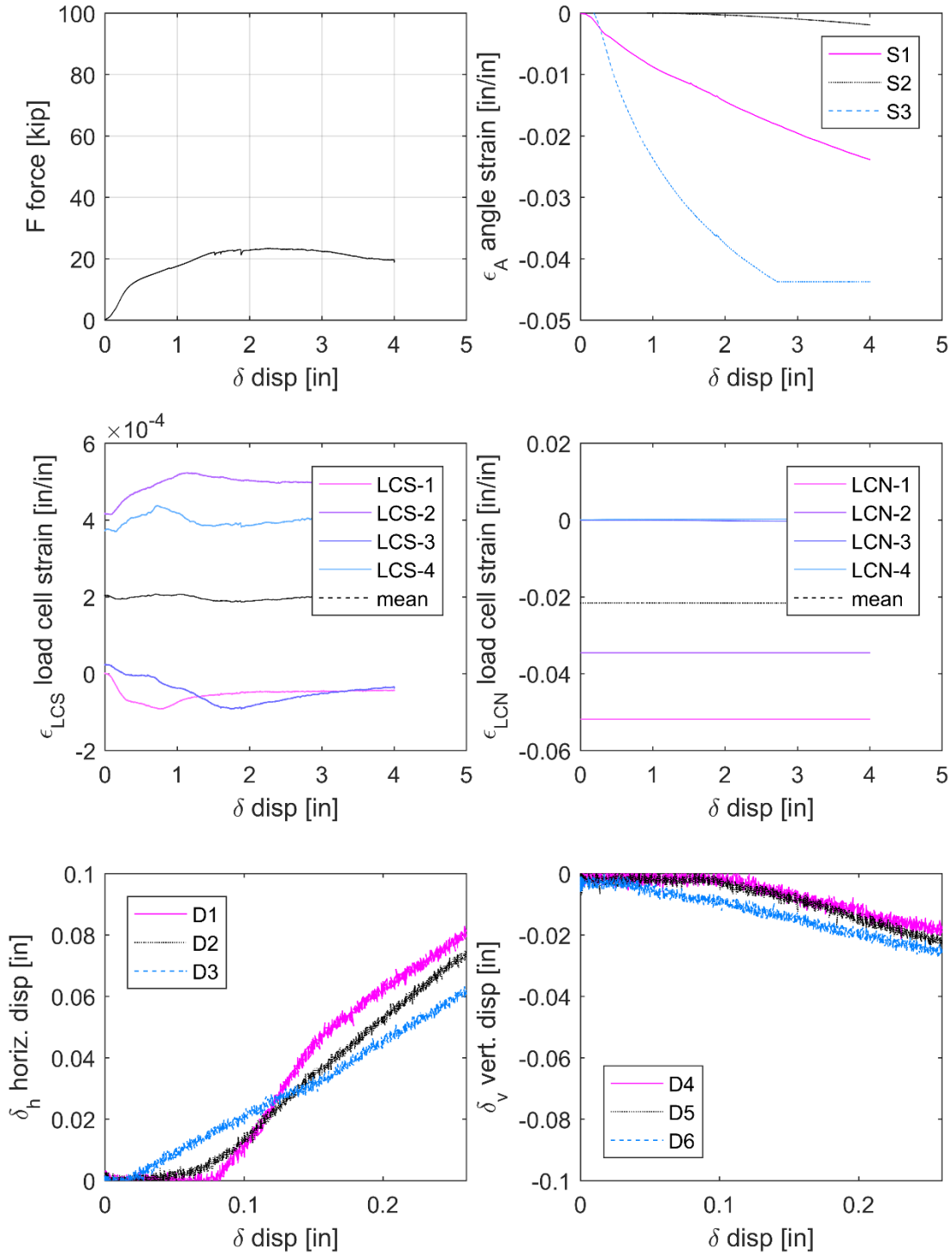
Shelf Angle: S1



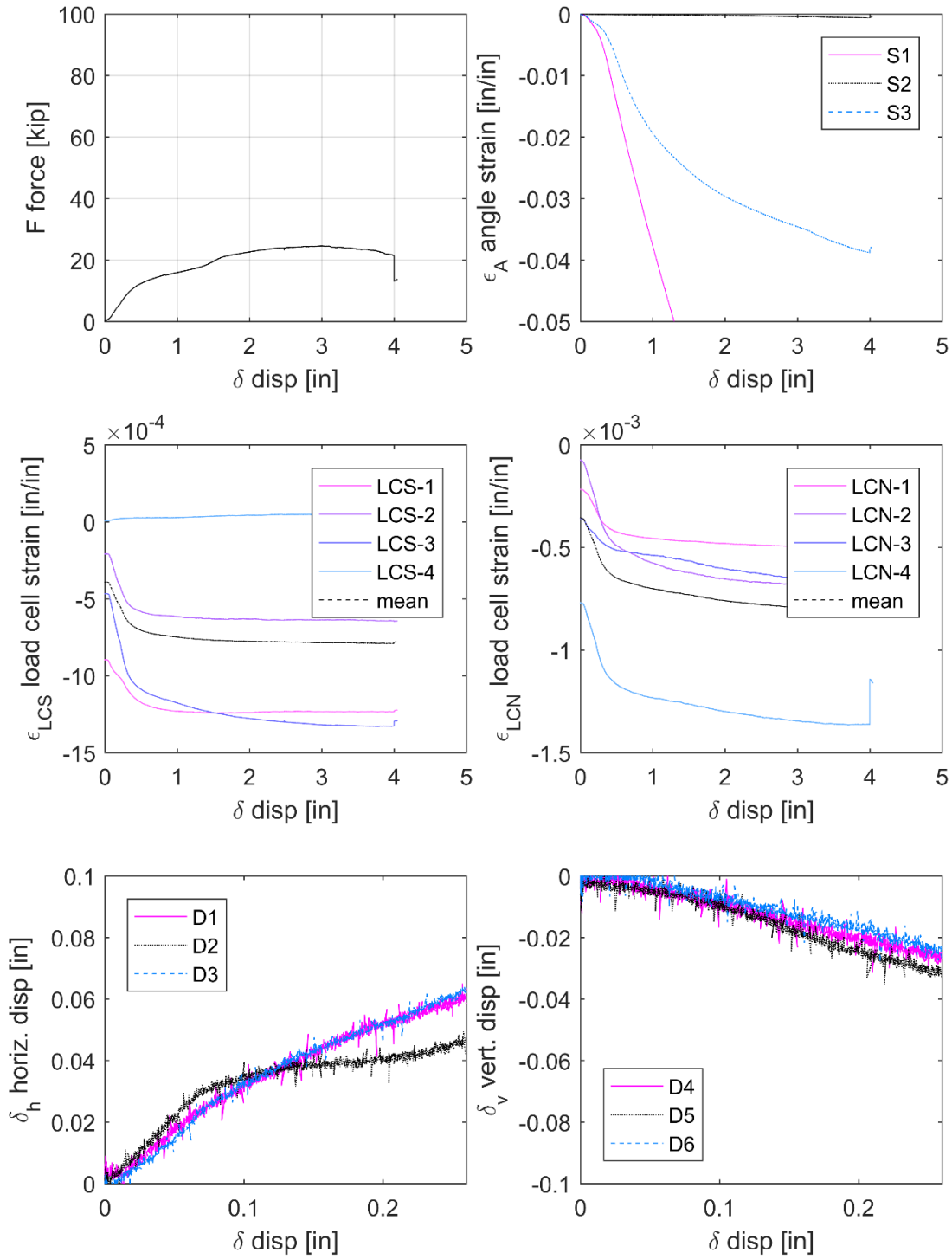
Shelf Angle: S2



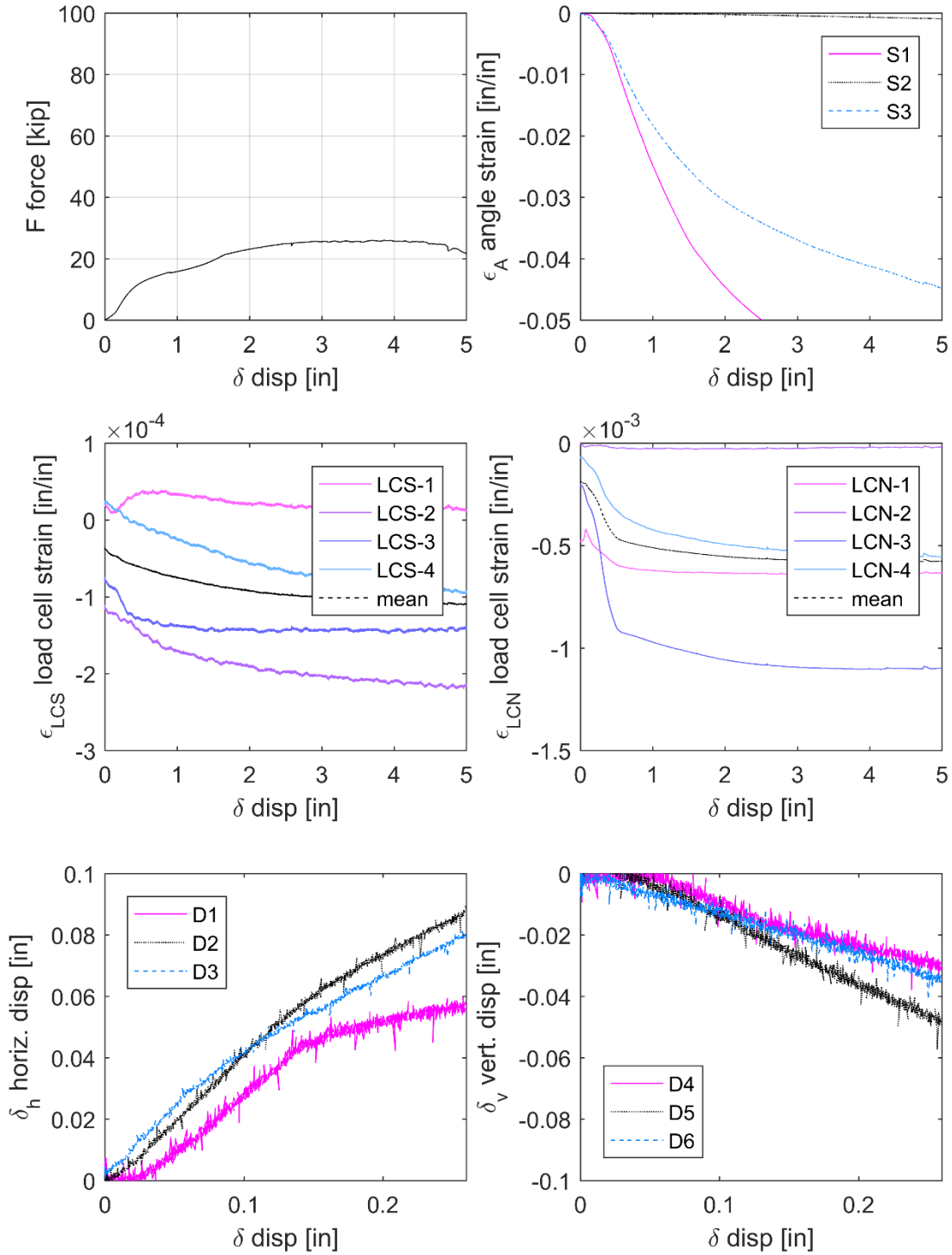
Shelf Angle: S3



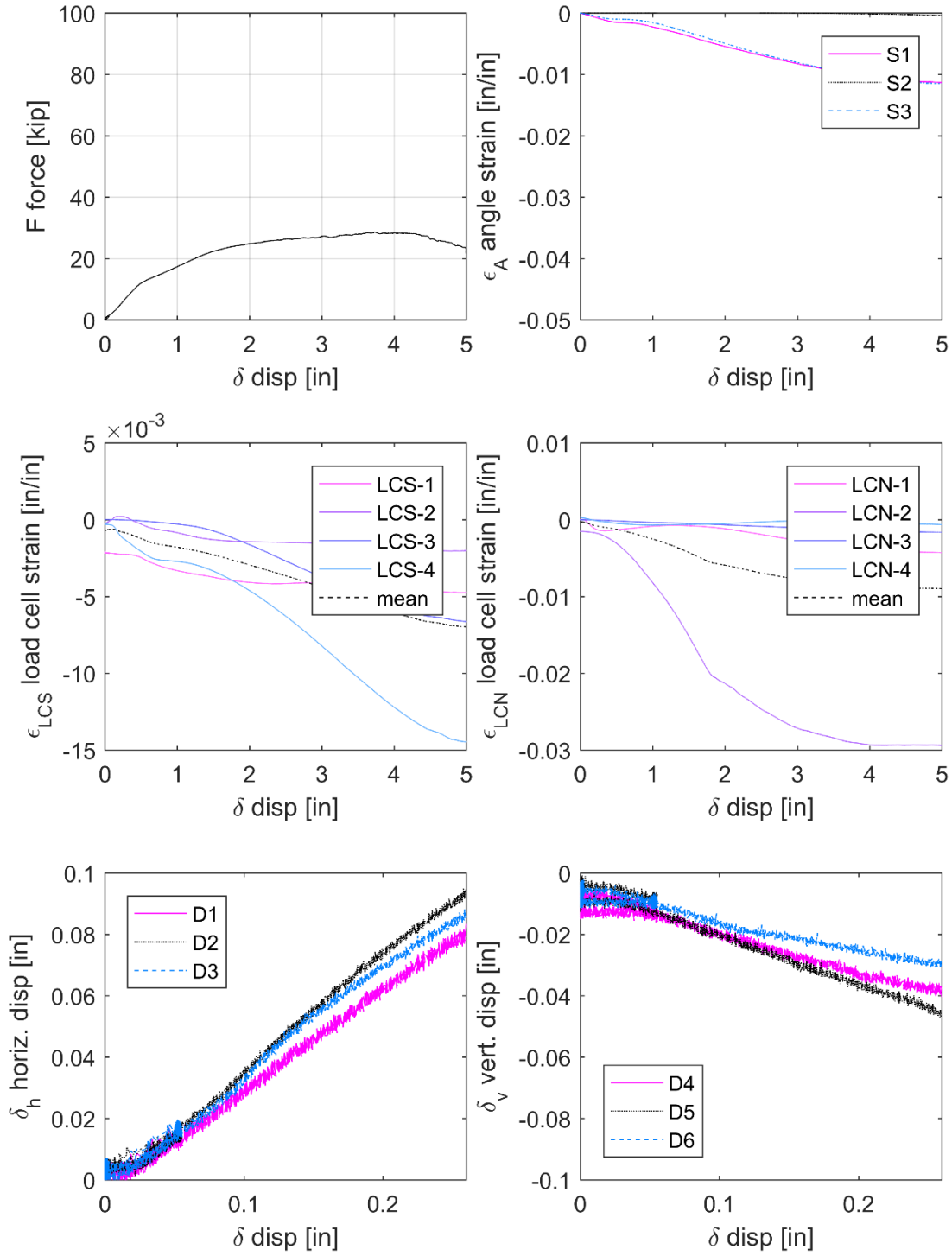
Shelf Angle: S4



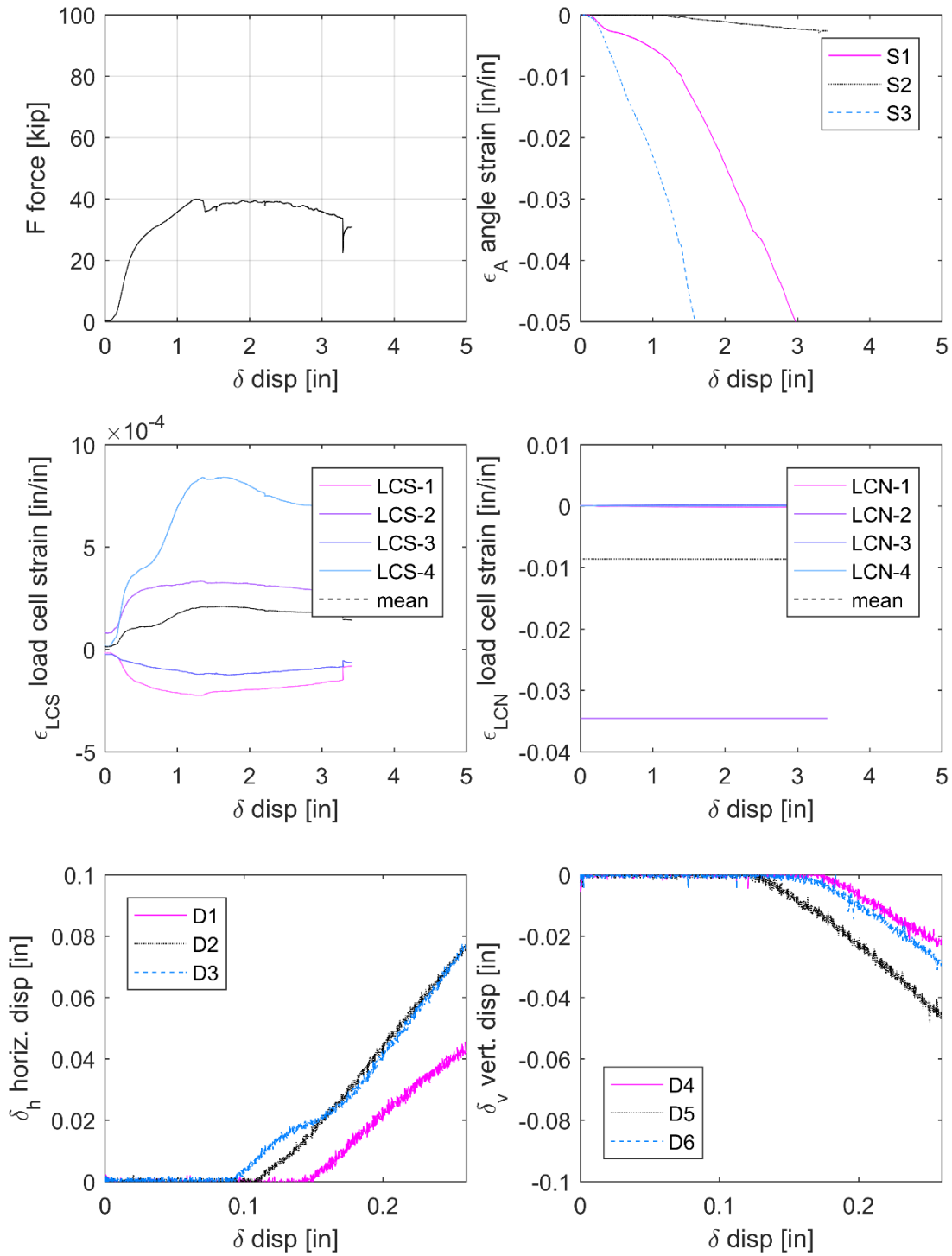
Shelf Angle: S5



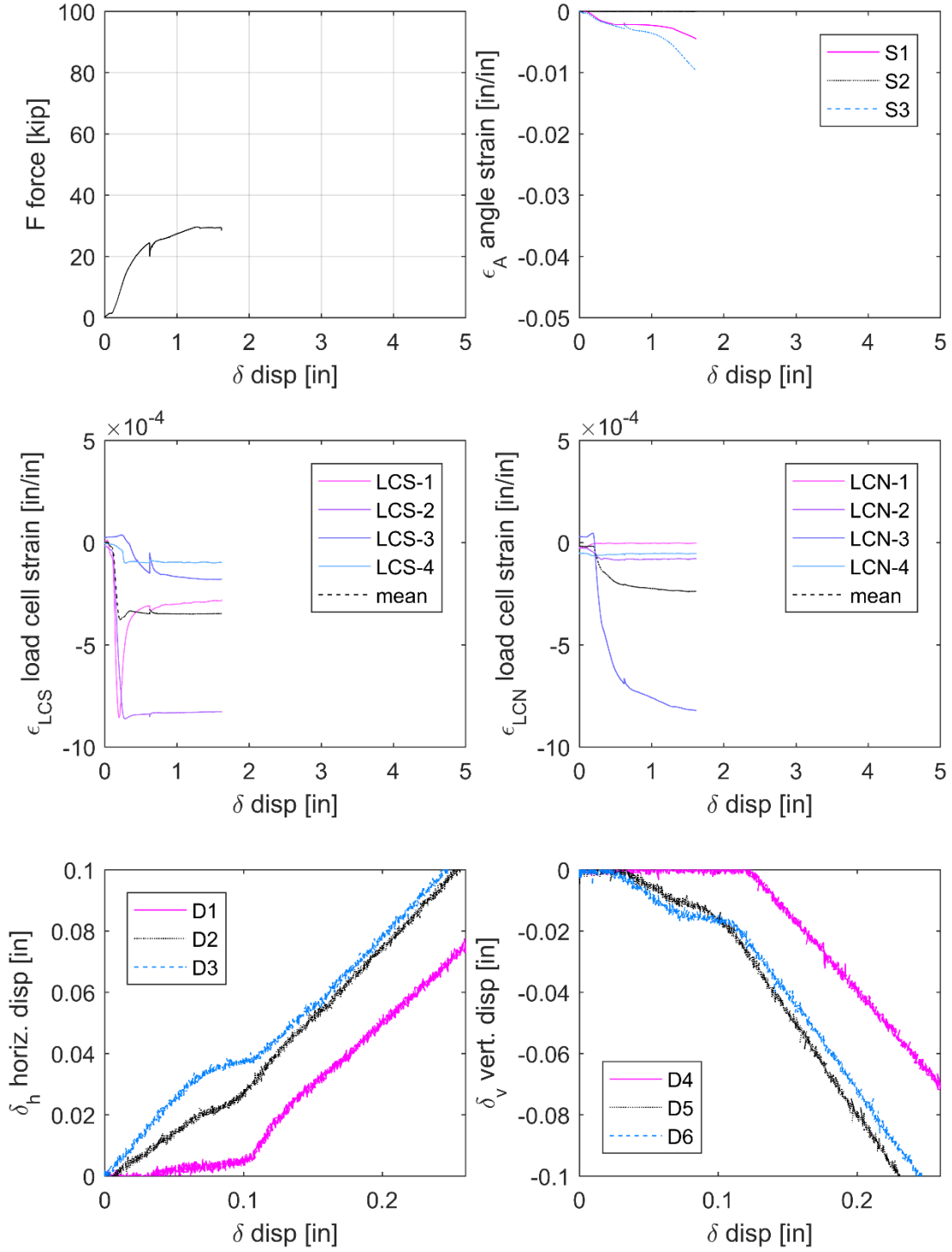
Shelf Angle: S6



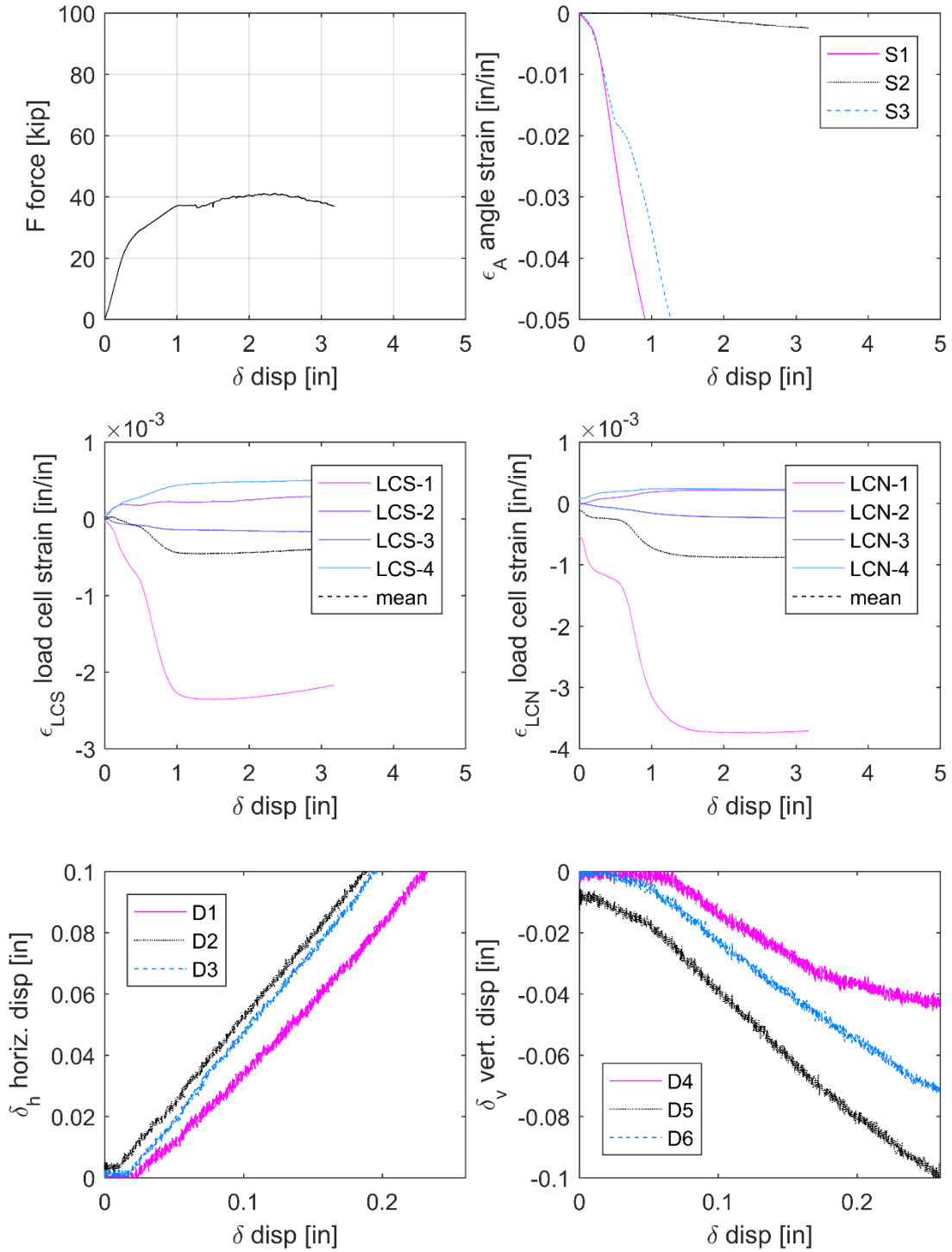
Shelf Angle: S7



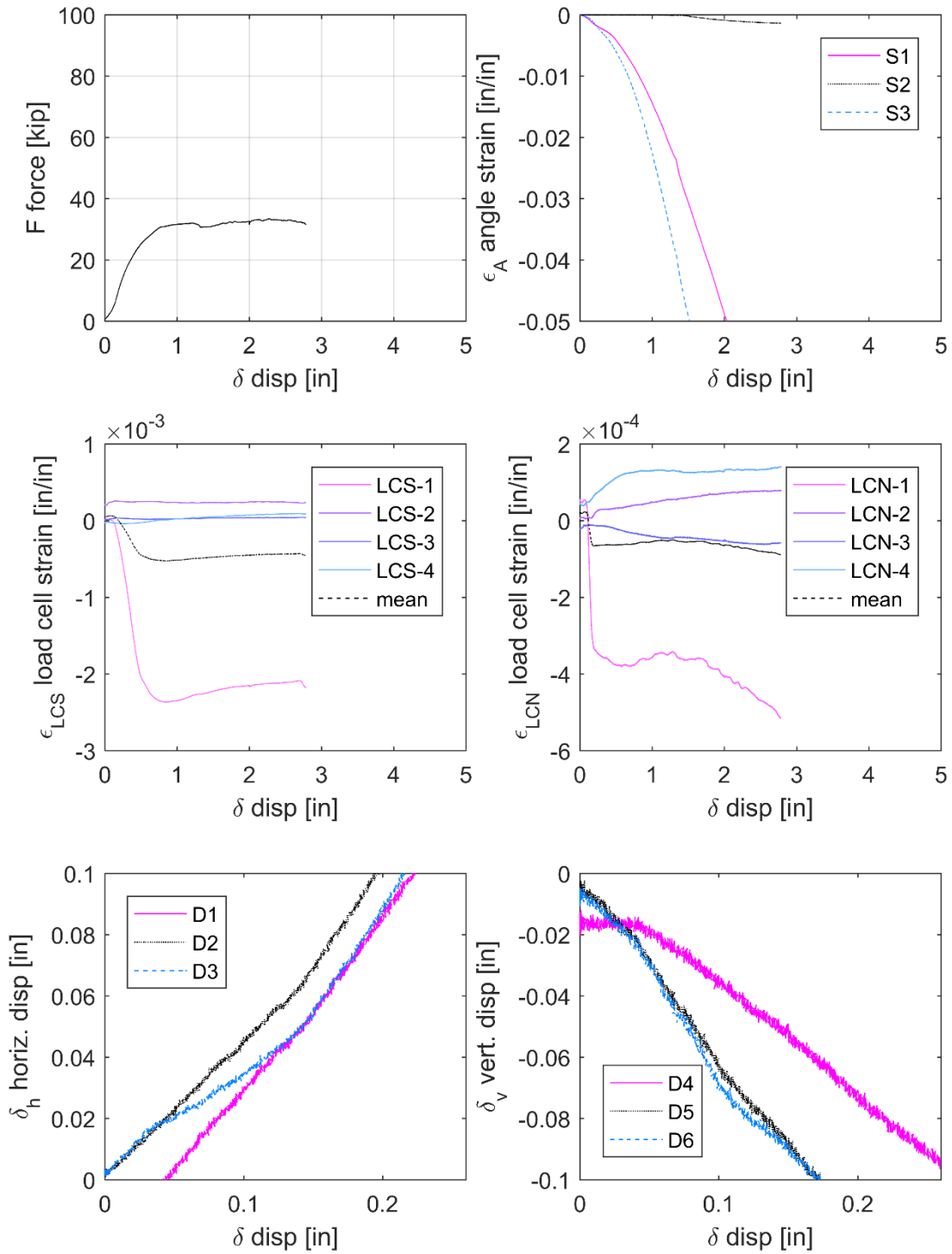
Shelf Angle: S8



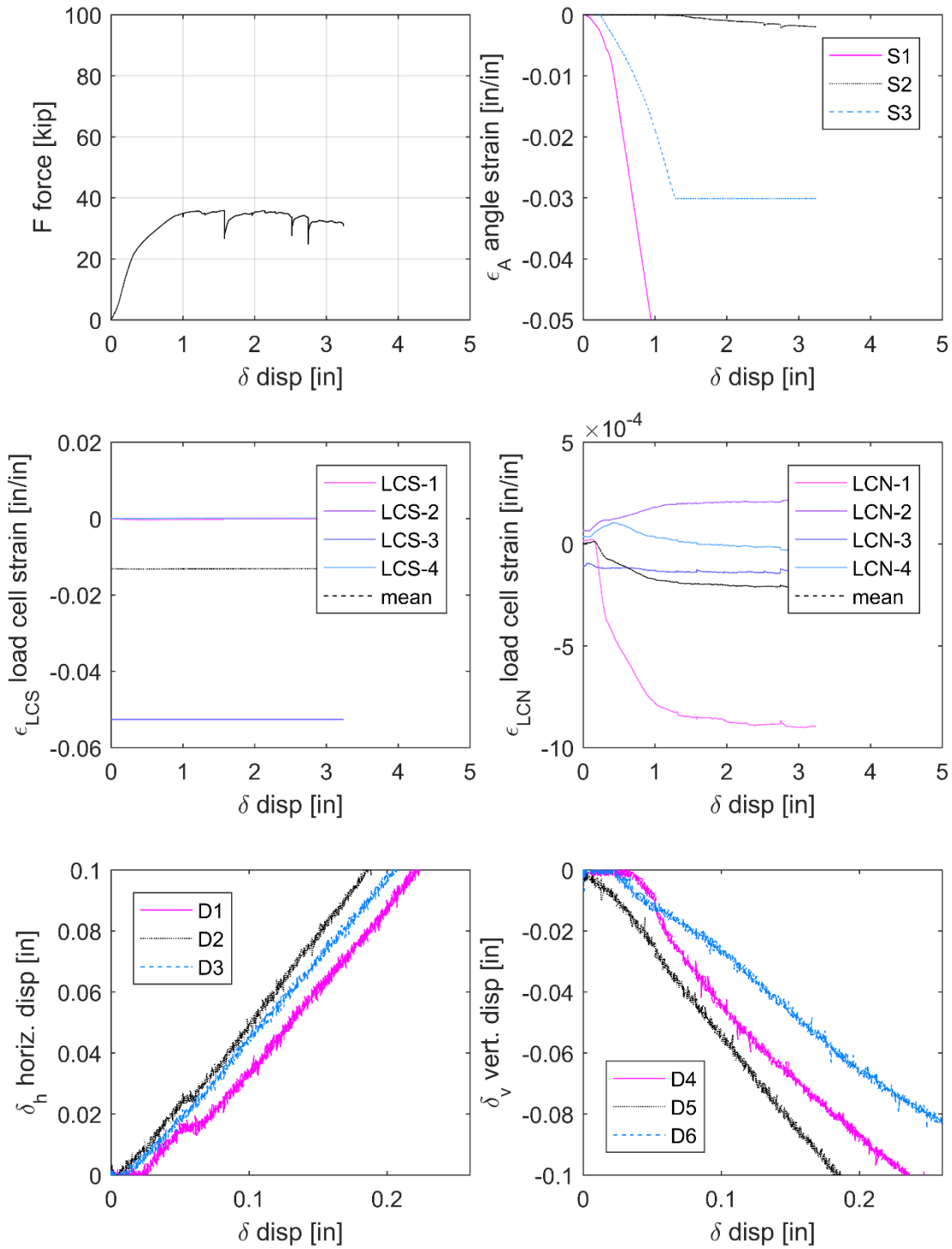
Shelf Angle: S9



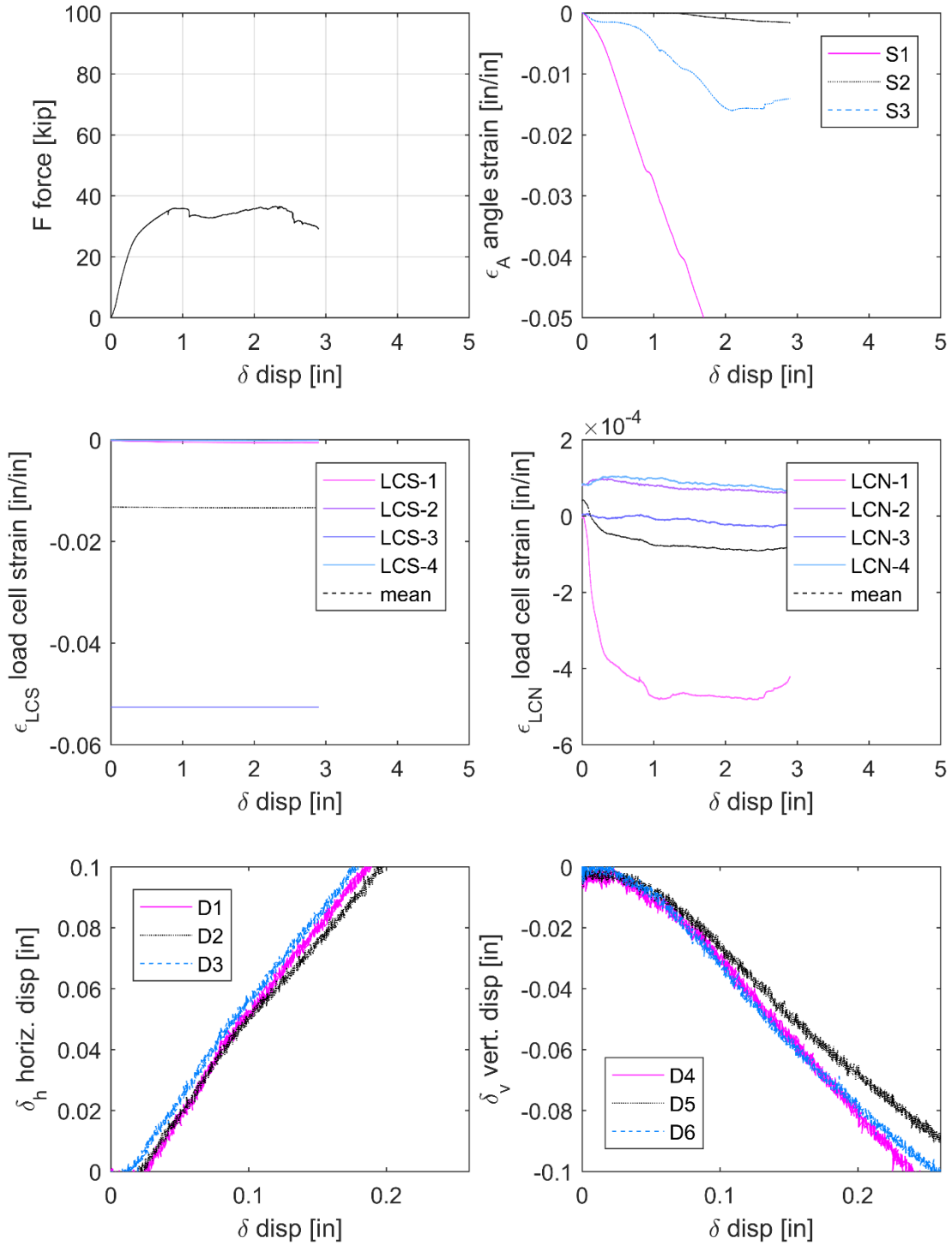
Shelf Angle: S10



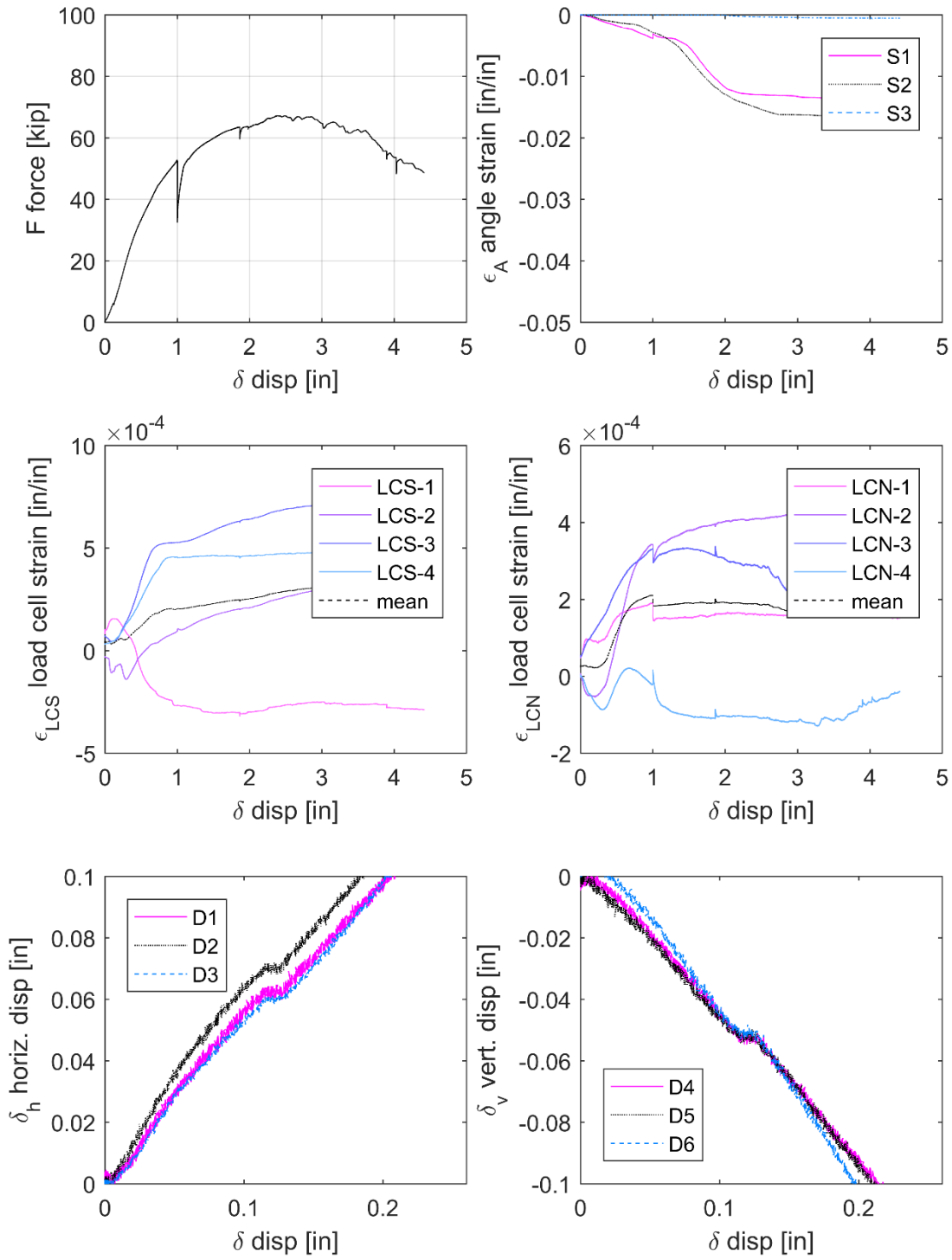
Shelf Angle: S11



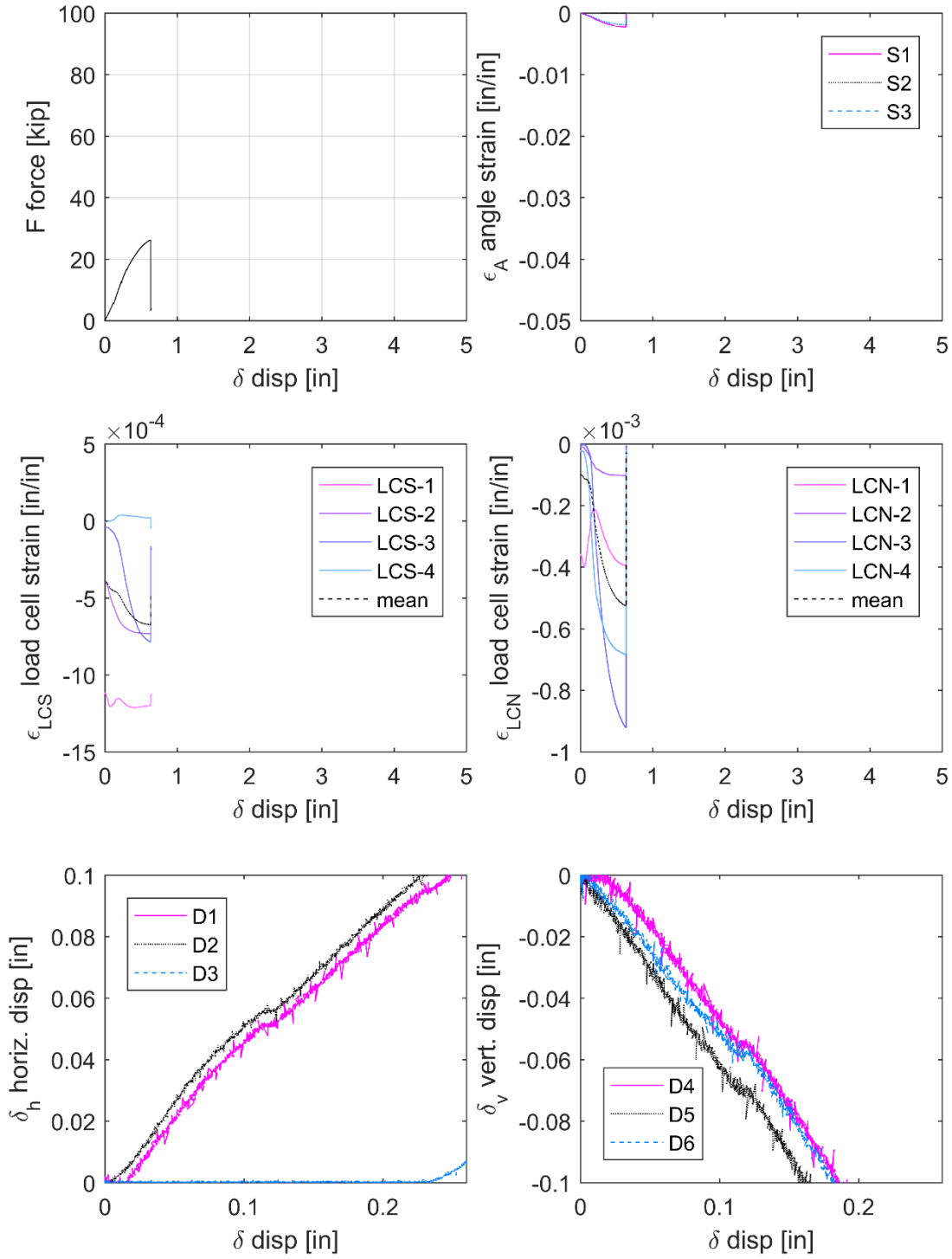
Shelf Angle: S12



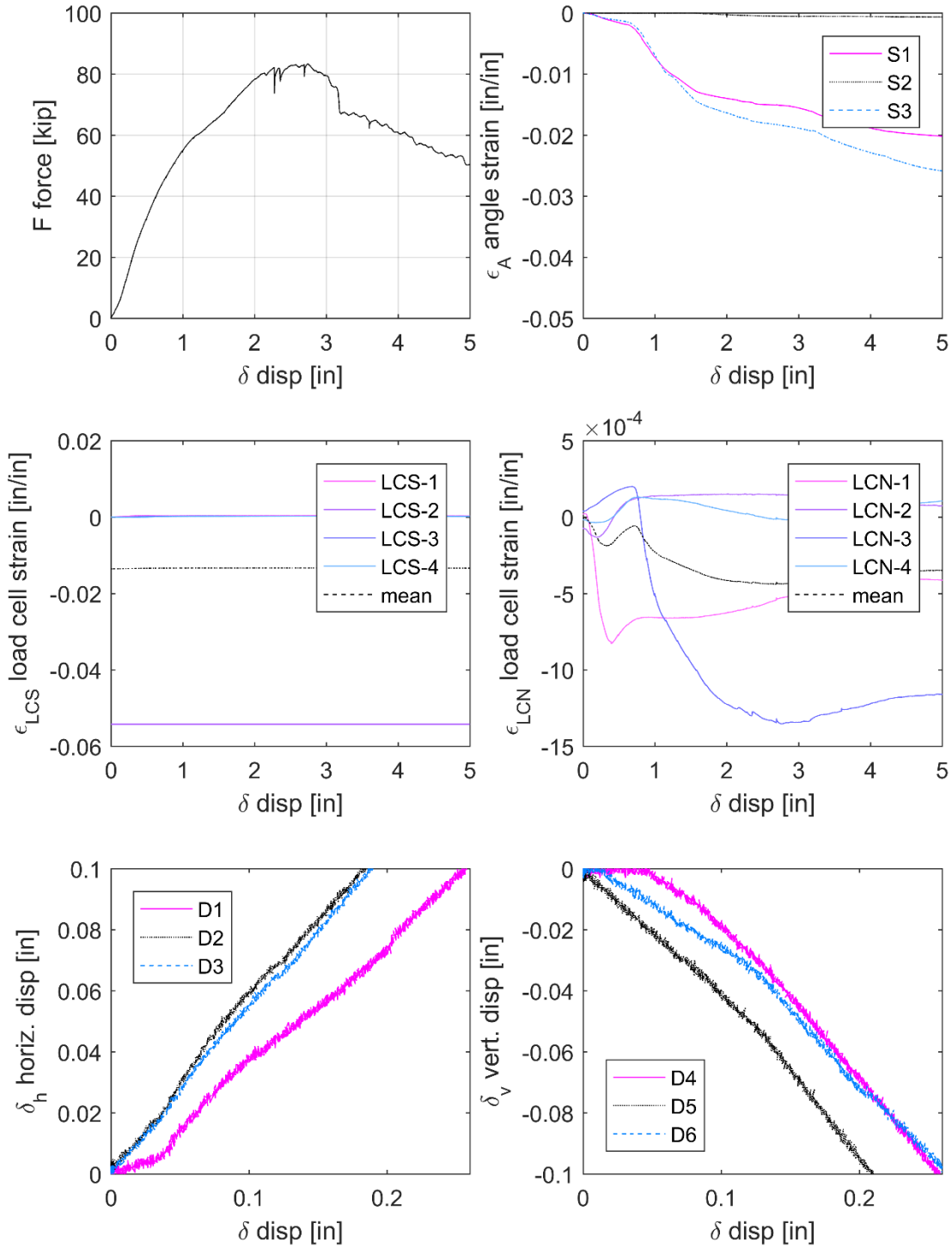
Shelf Angle: S13



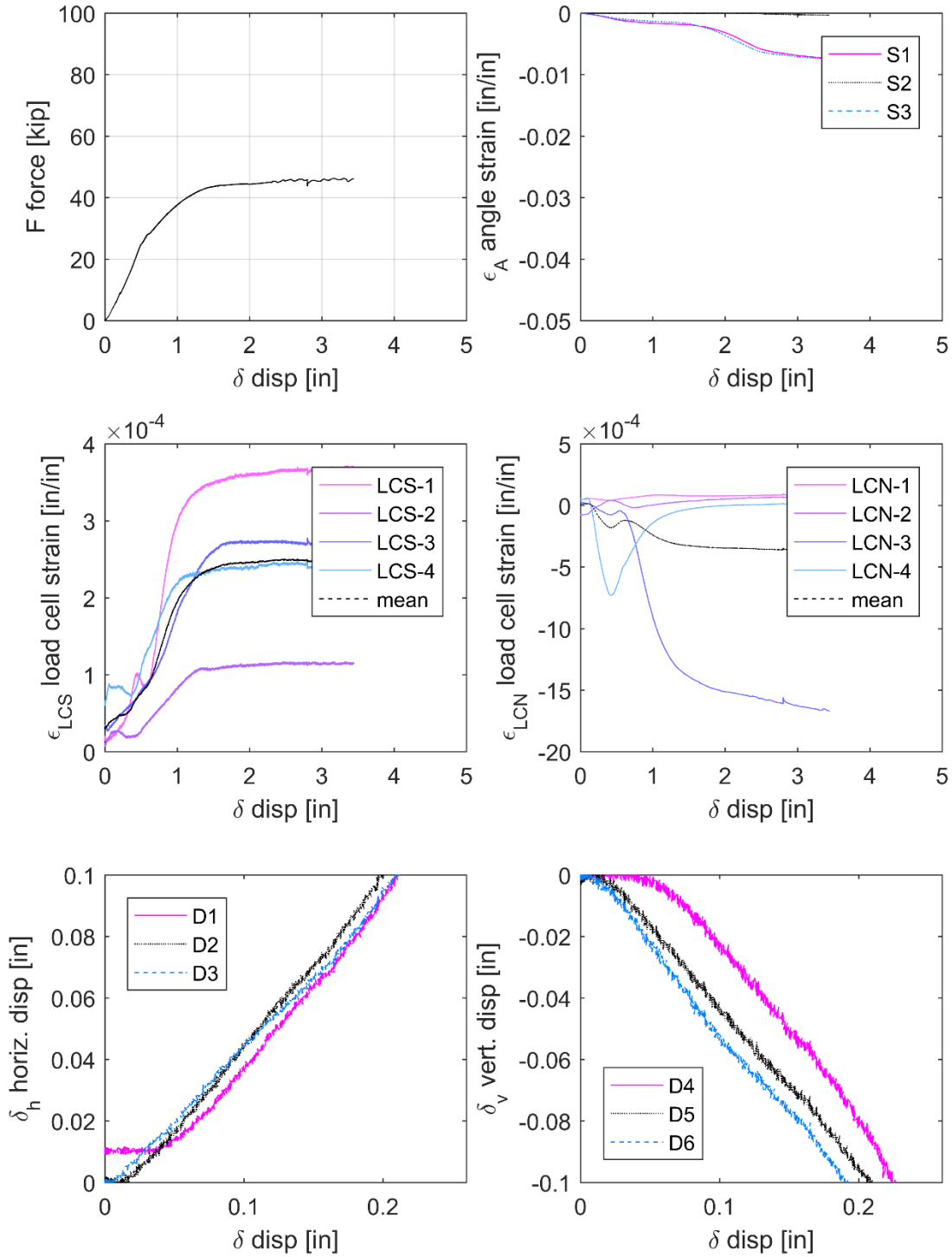
Shelf Angle: S14



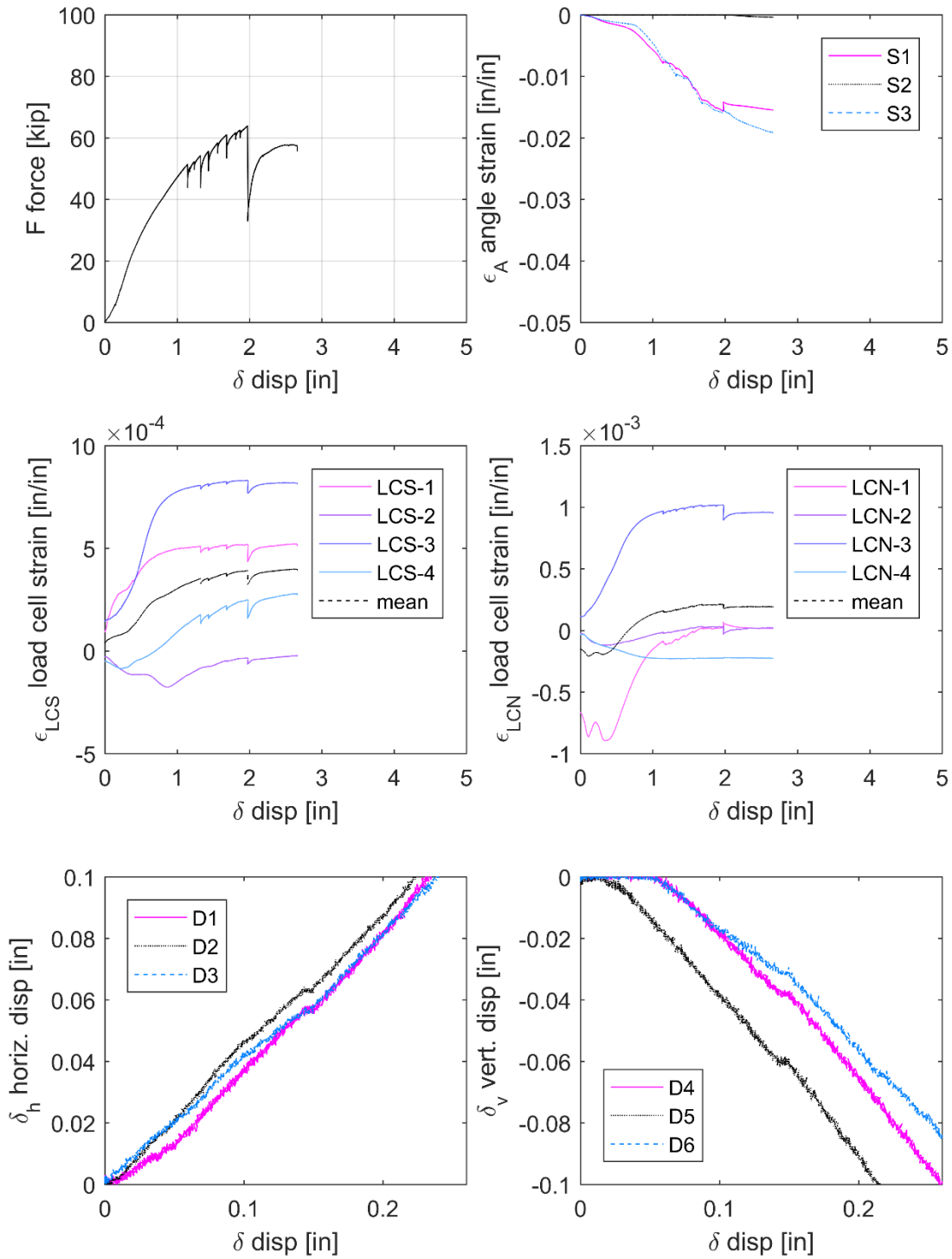
Shelf Angle: S15



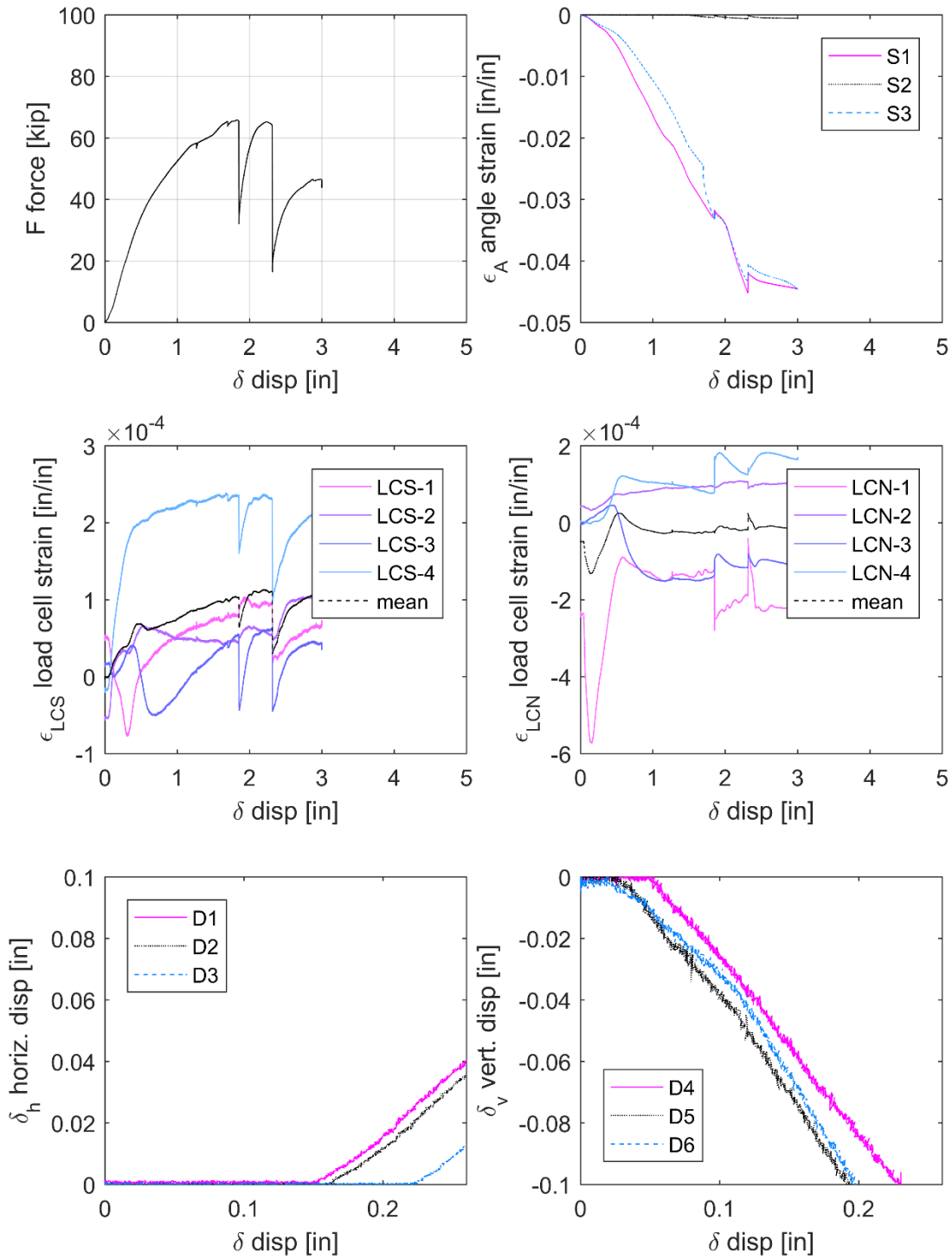
Shelf Angle: S16



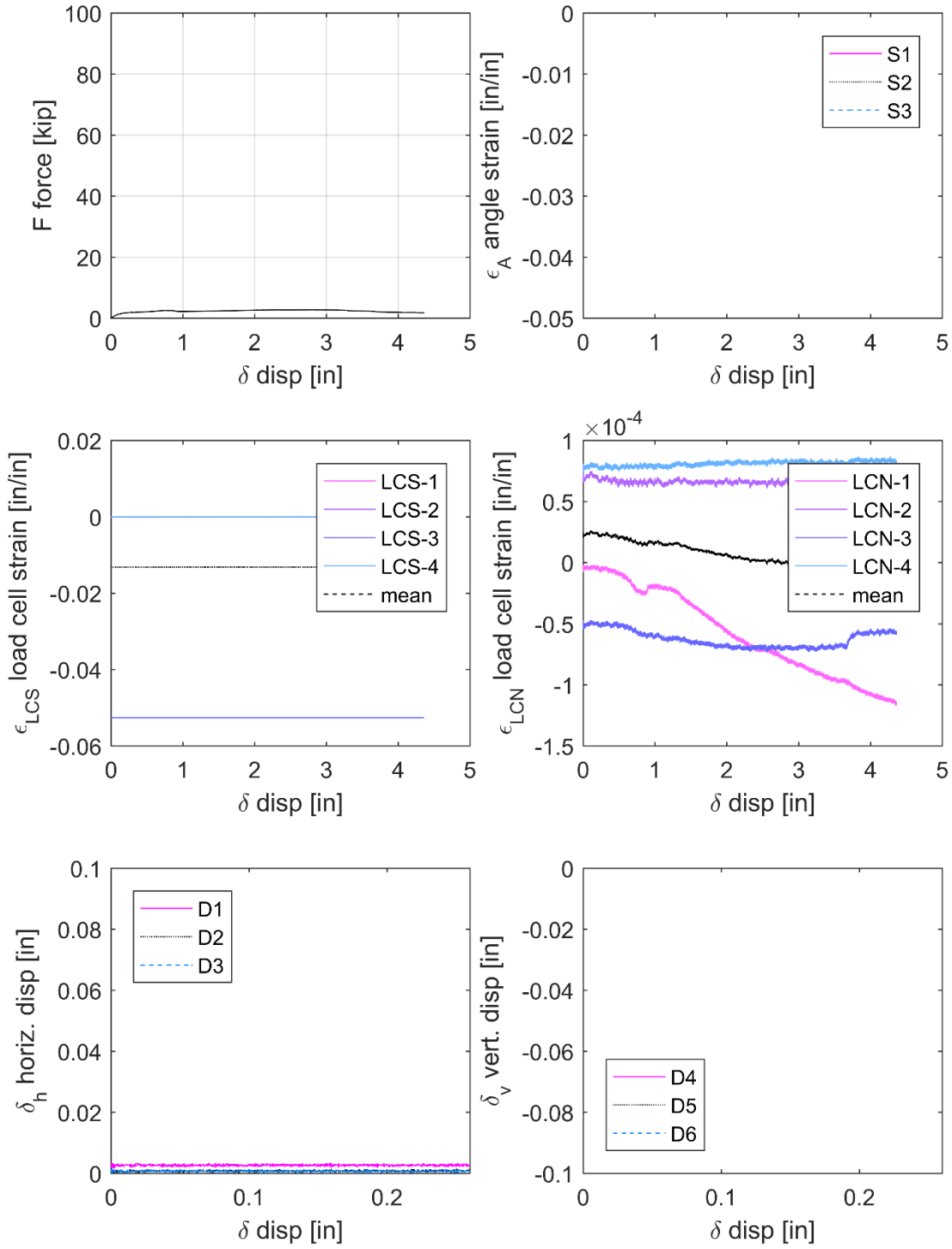
Shelf Angle: S17



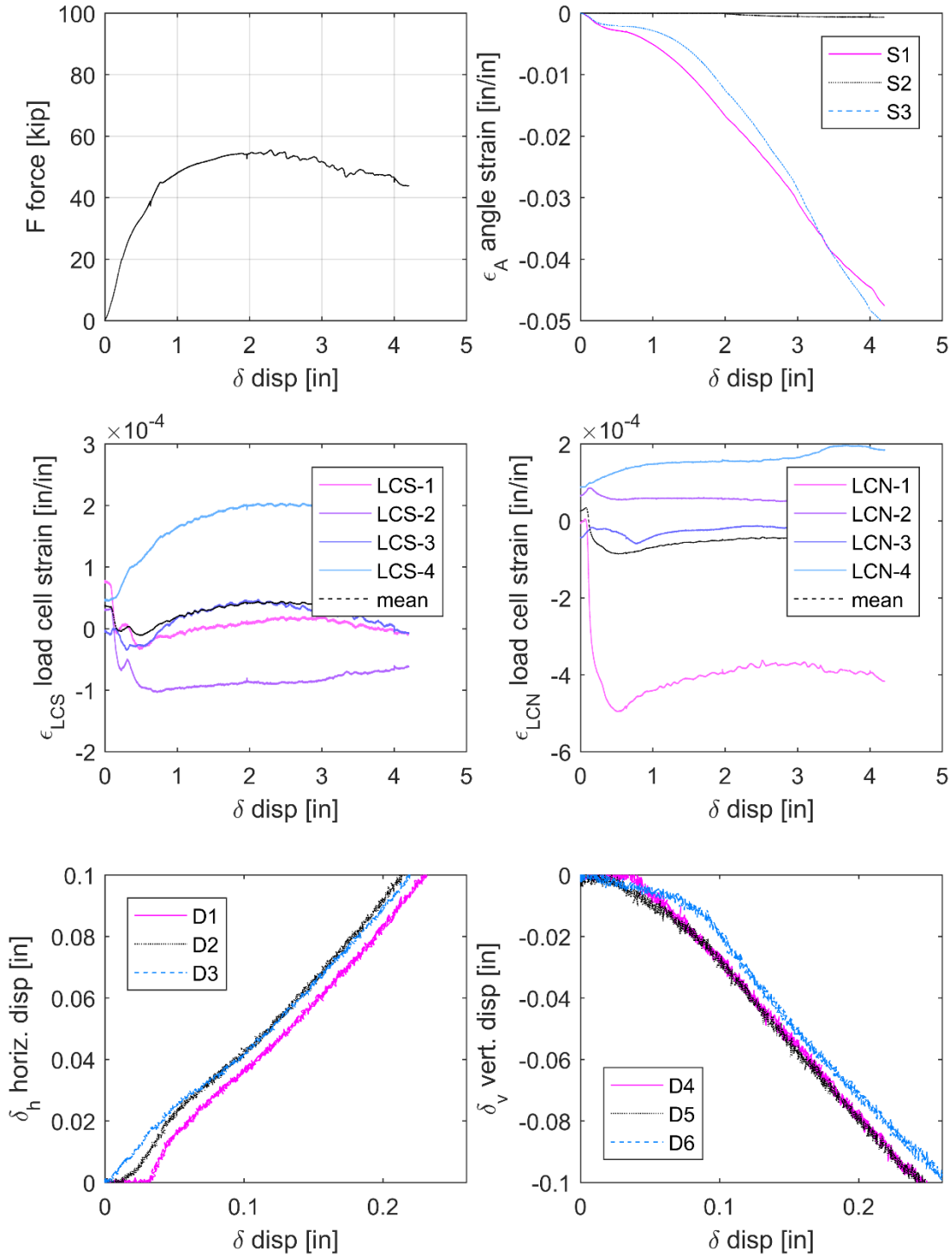
Shelf Angle: S18



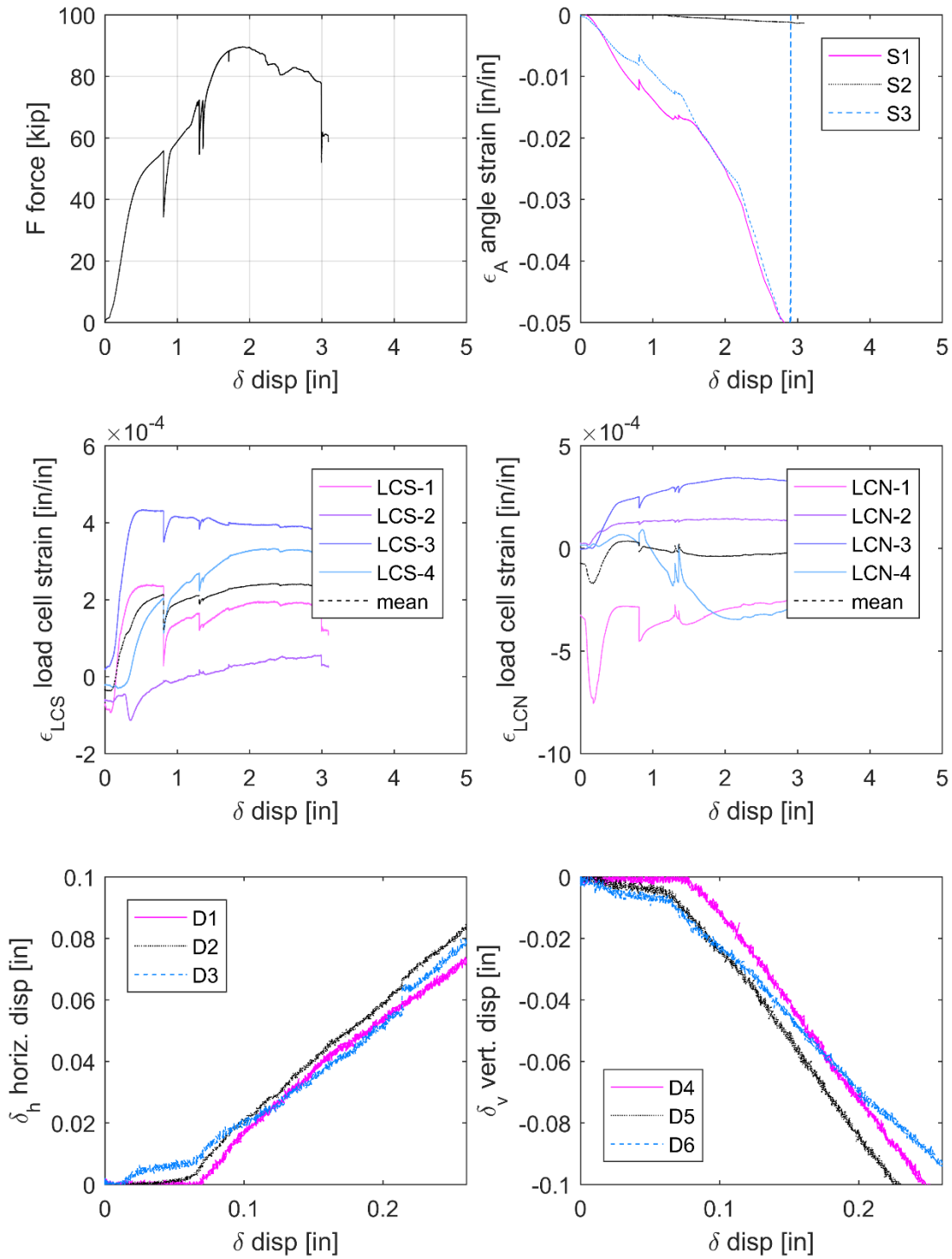
Shelf Angle: S19



Shelf Angle: S20



Shelf Angle: S21



Appendix D: Roof Post and Canopy Beam Experimental Test Data

This appendix contains the results from the roof post and canopy beam experiments, highlighting the key data for these tests. The results are zeroed at the same time to initiate data collection at a time after the four bolts on each specimen had been tightened to a snug tight condition. A template for the layout of the data plots for each tests is shown below. Legends are given in the results for roof post R1, and are identical for the remaining result pages.

Actuator Force
vs.
Drift
(and backbone, if cyclic)

Post/beam curvature
vs.
Drift

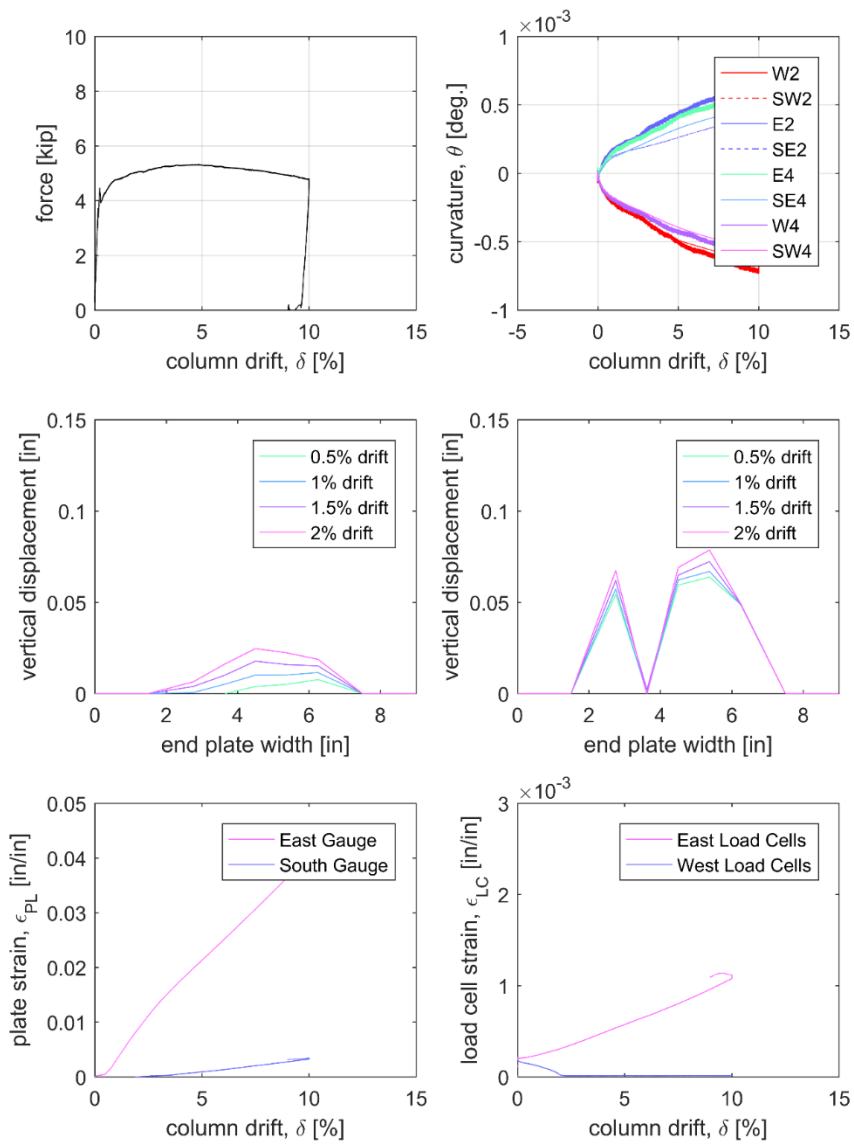
EAST
Base Plate
Vertical deformations

SOUTH
Base Plate
Vertical deformations

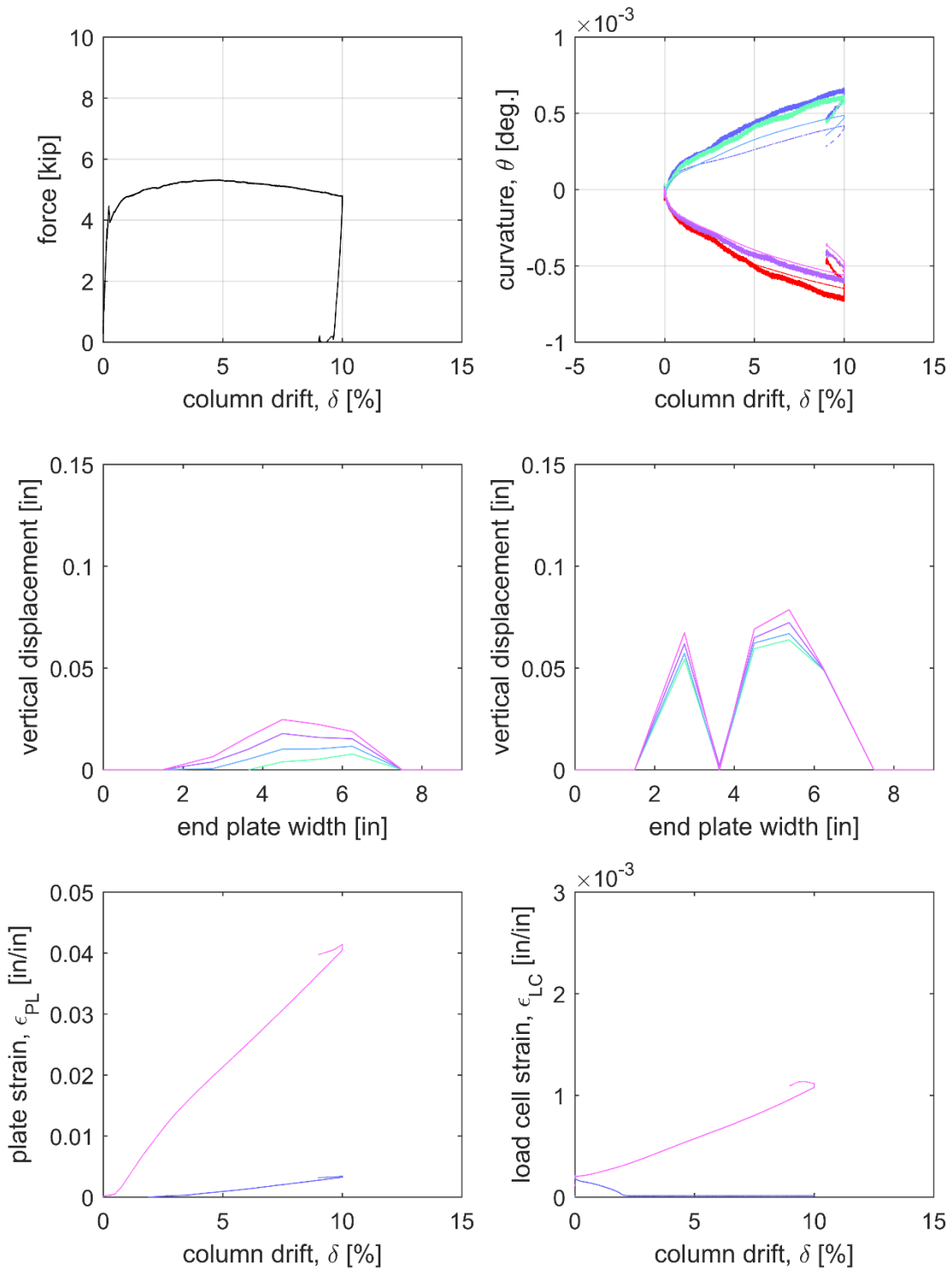
SOUTH and EAST
Base plate strain gauges

EAST and WEST
*Load cell strain gauges
(average of 4 gauges per
Load cell,
average per side)*

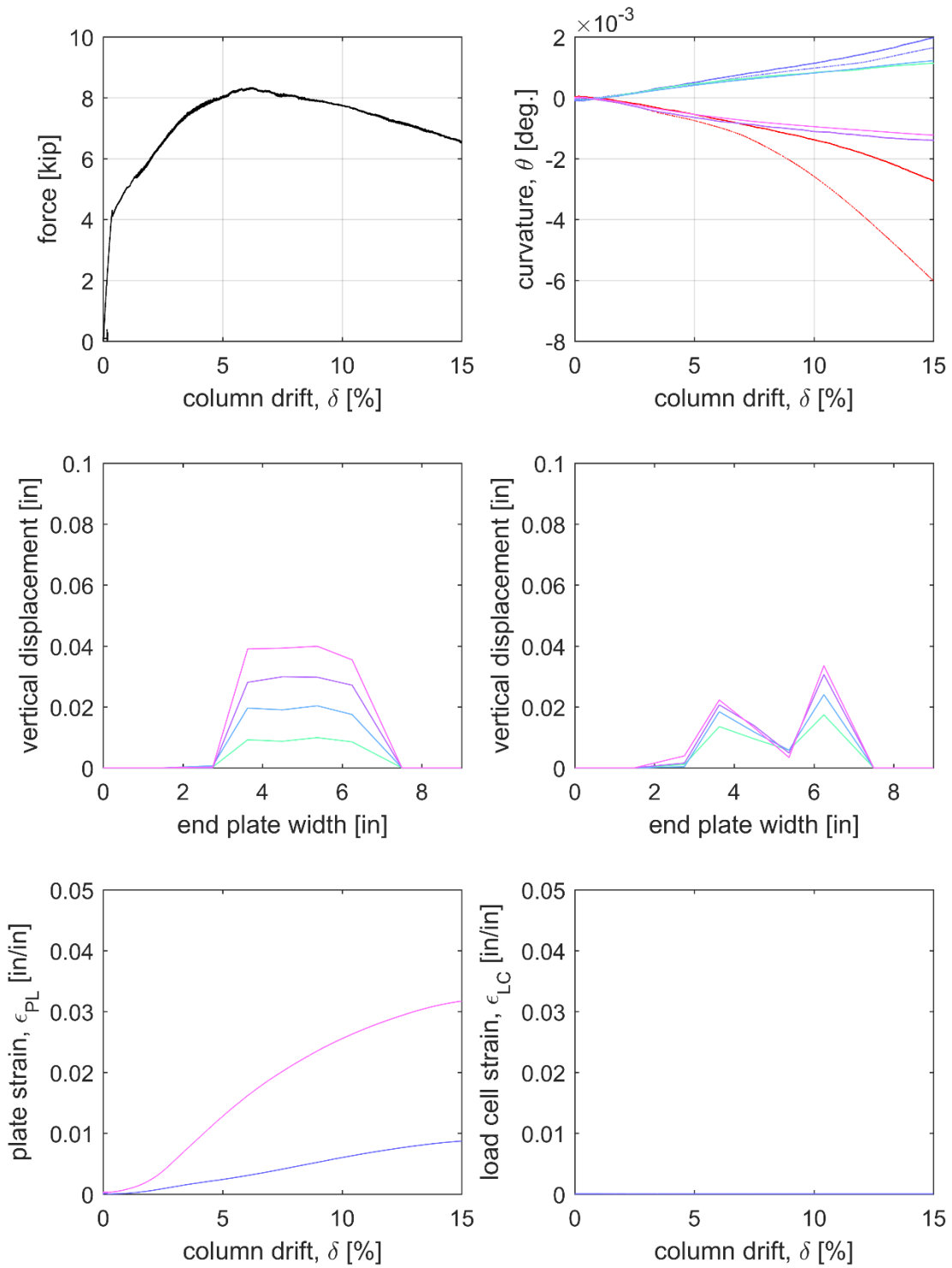
Roof Post: R1



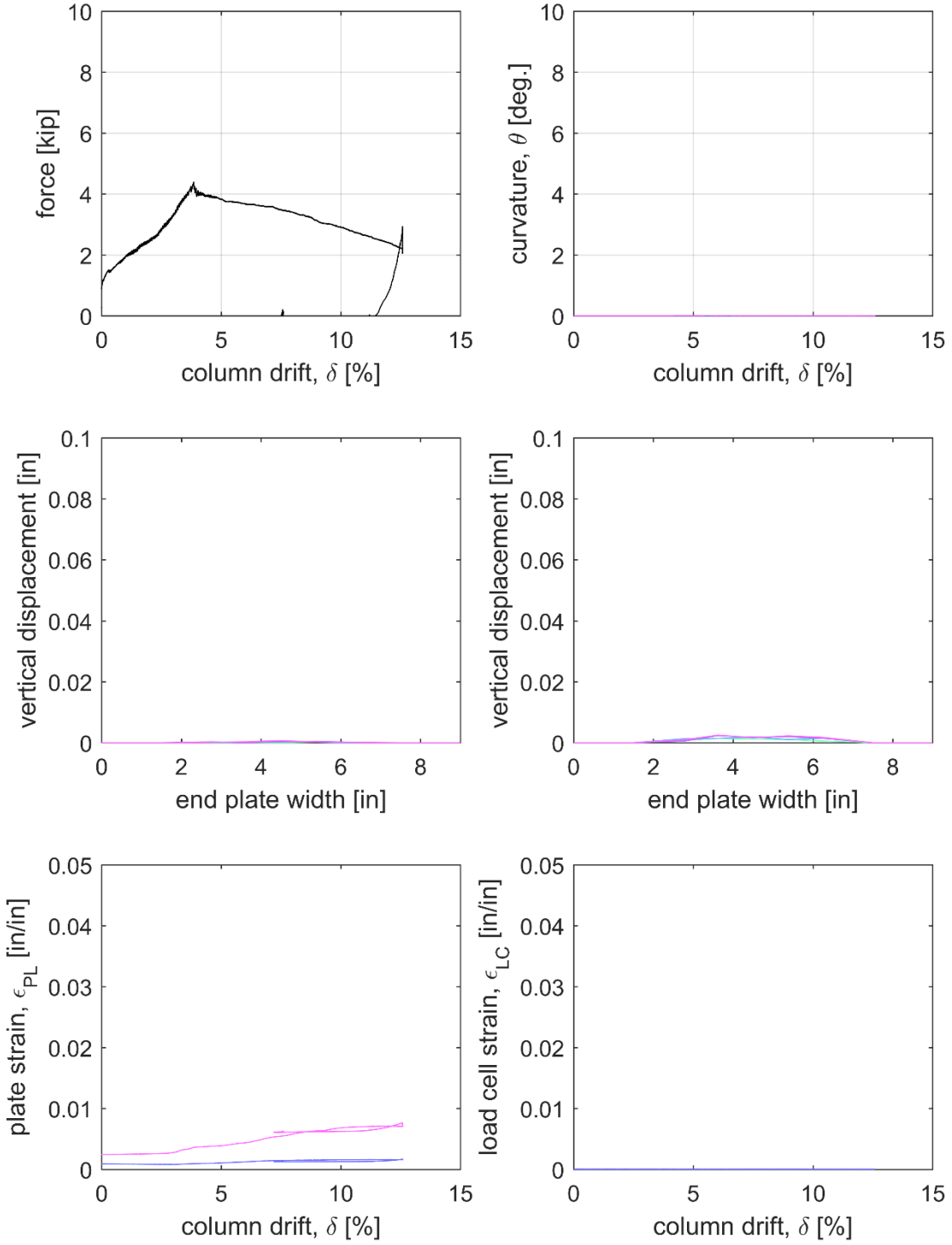
Roof Post: R1



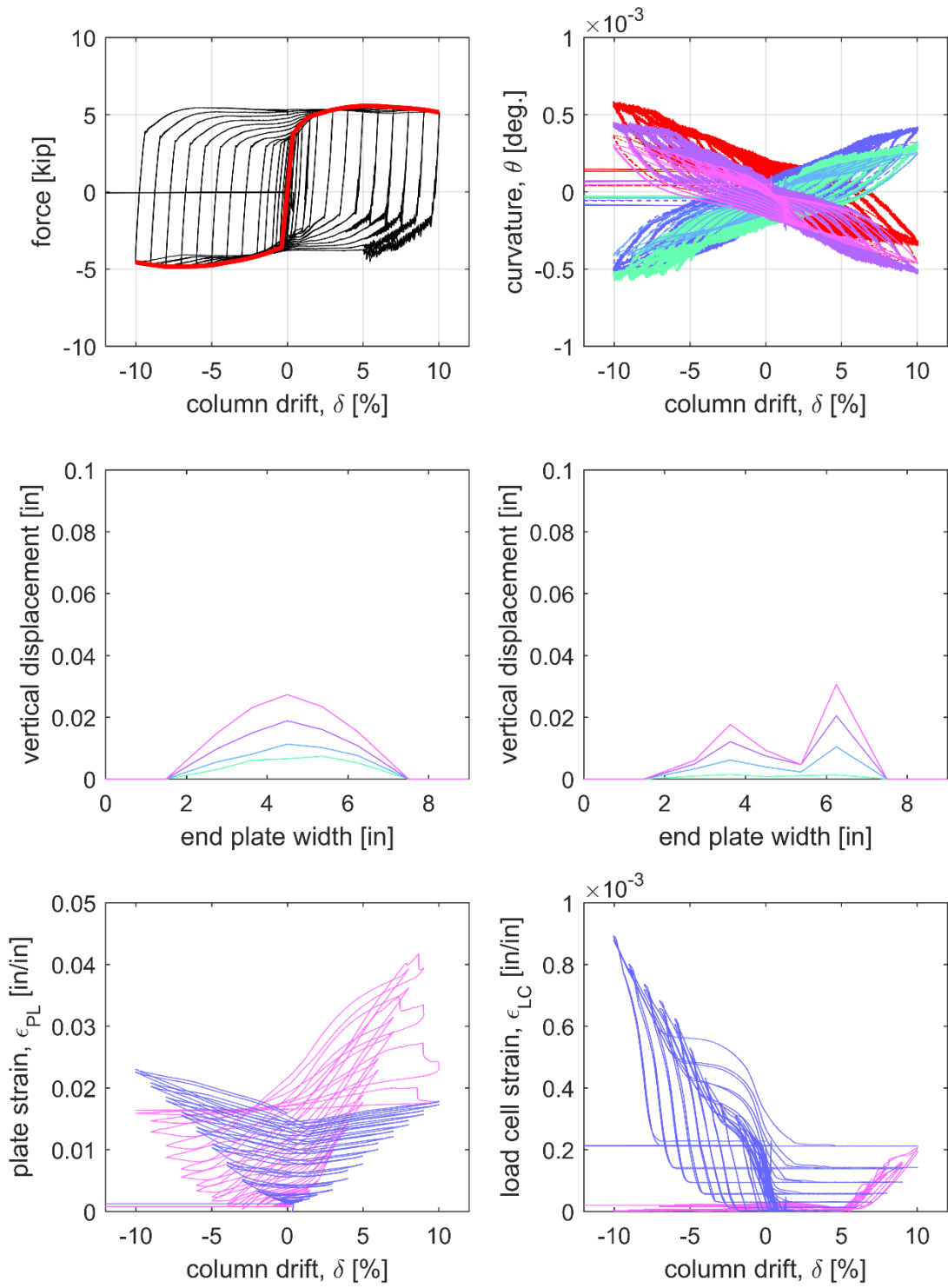
Roof Post: R2



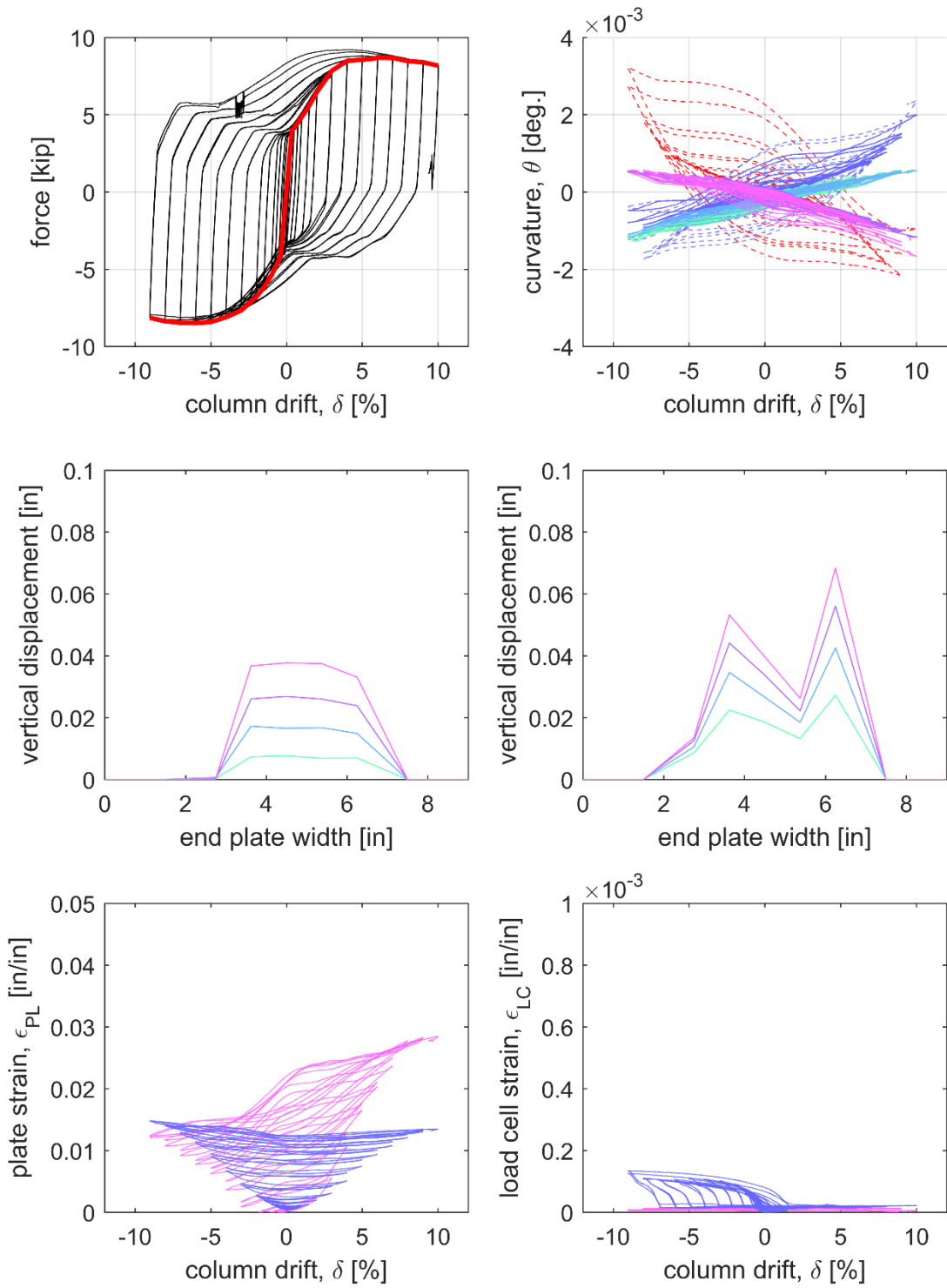
Roof Post: R3



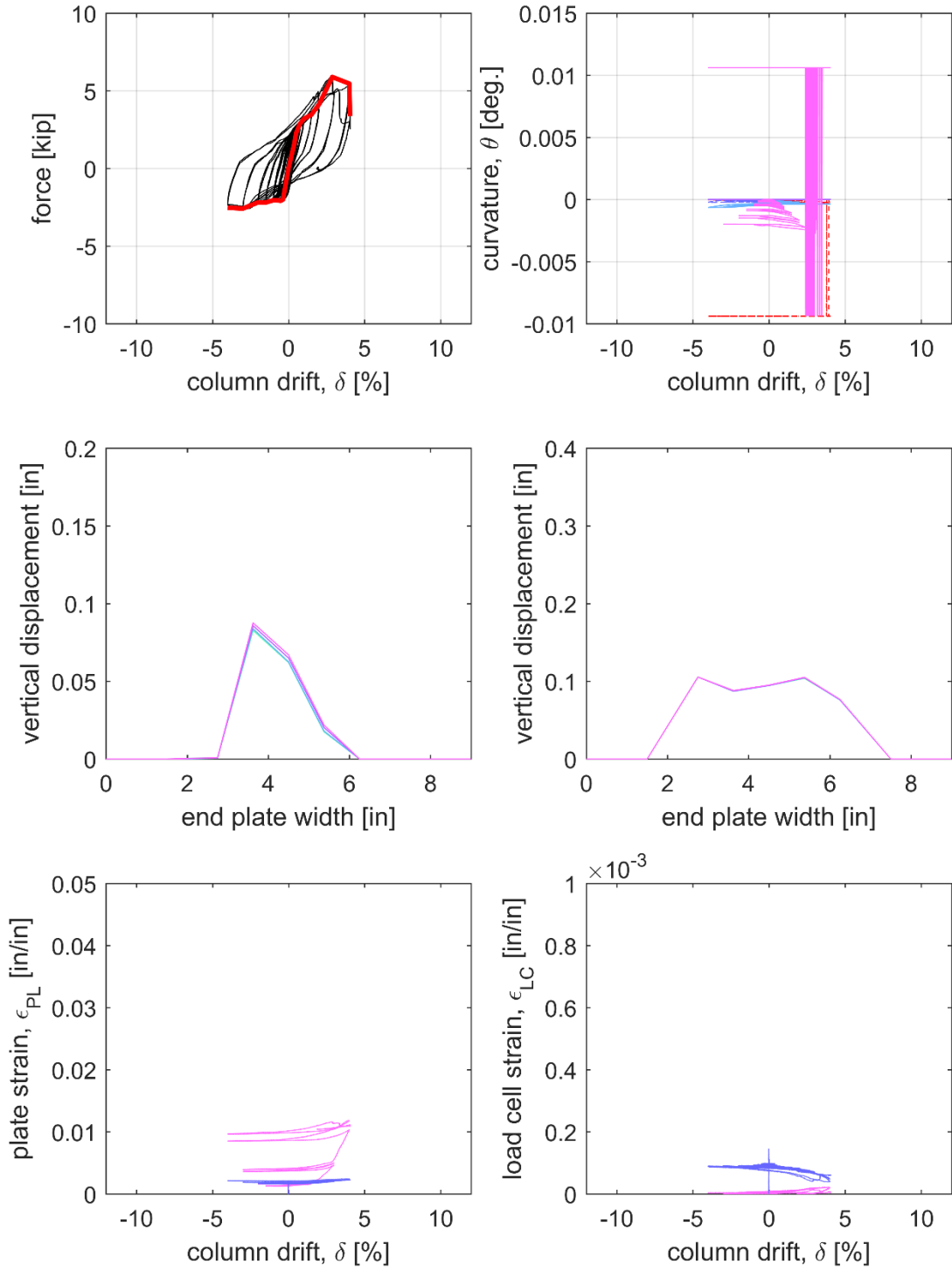
Roof Post: R4



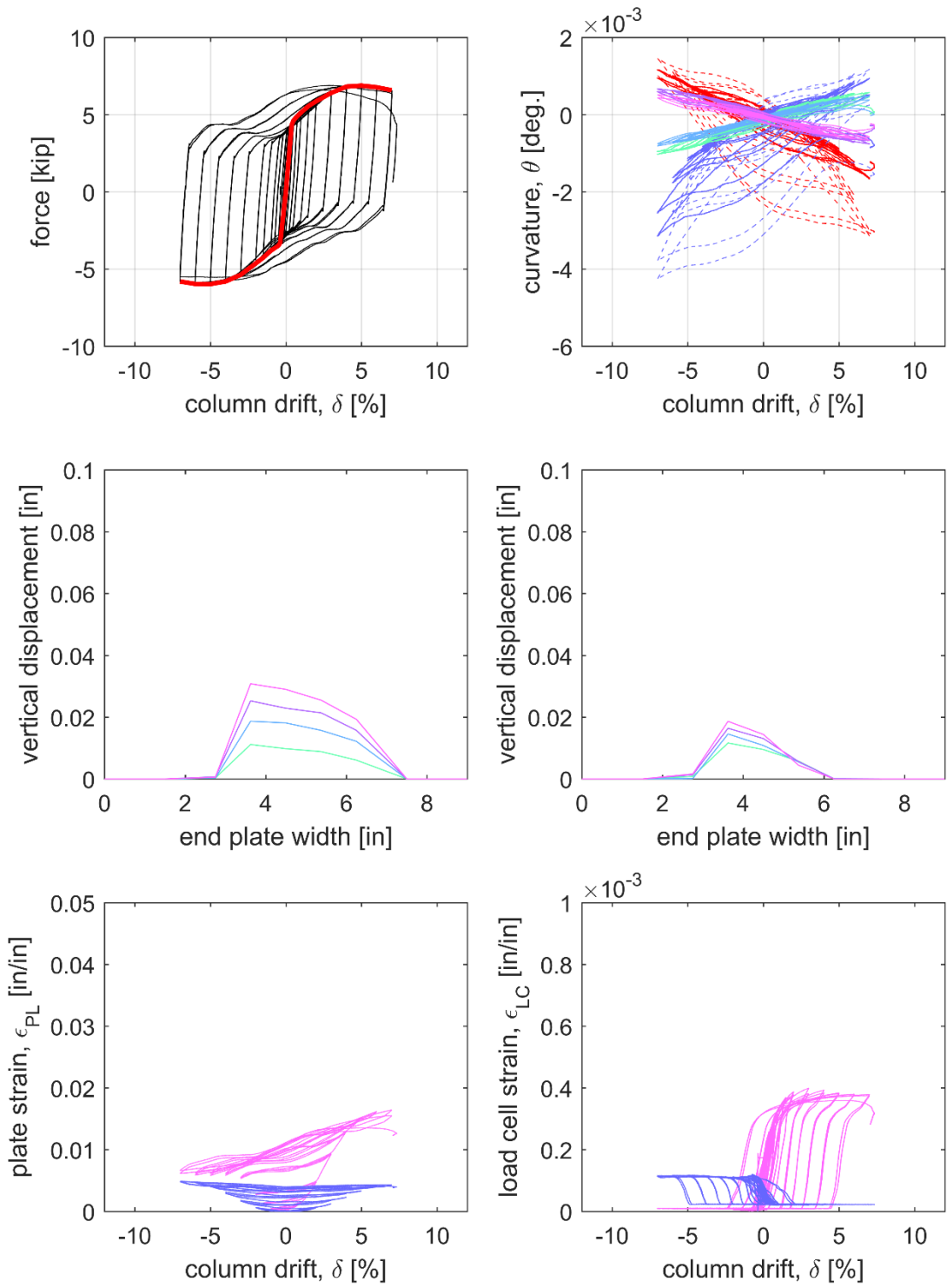
Roof Post: R5



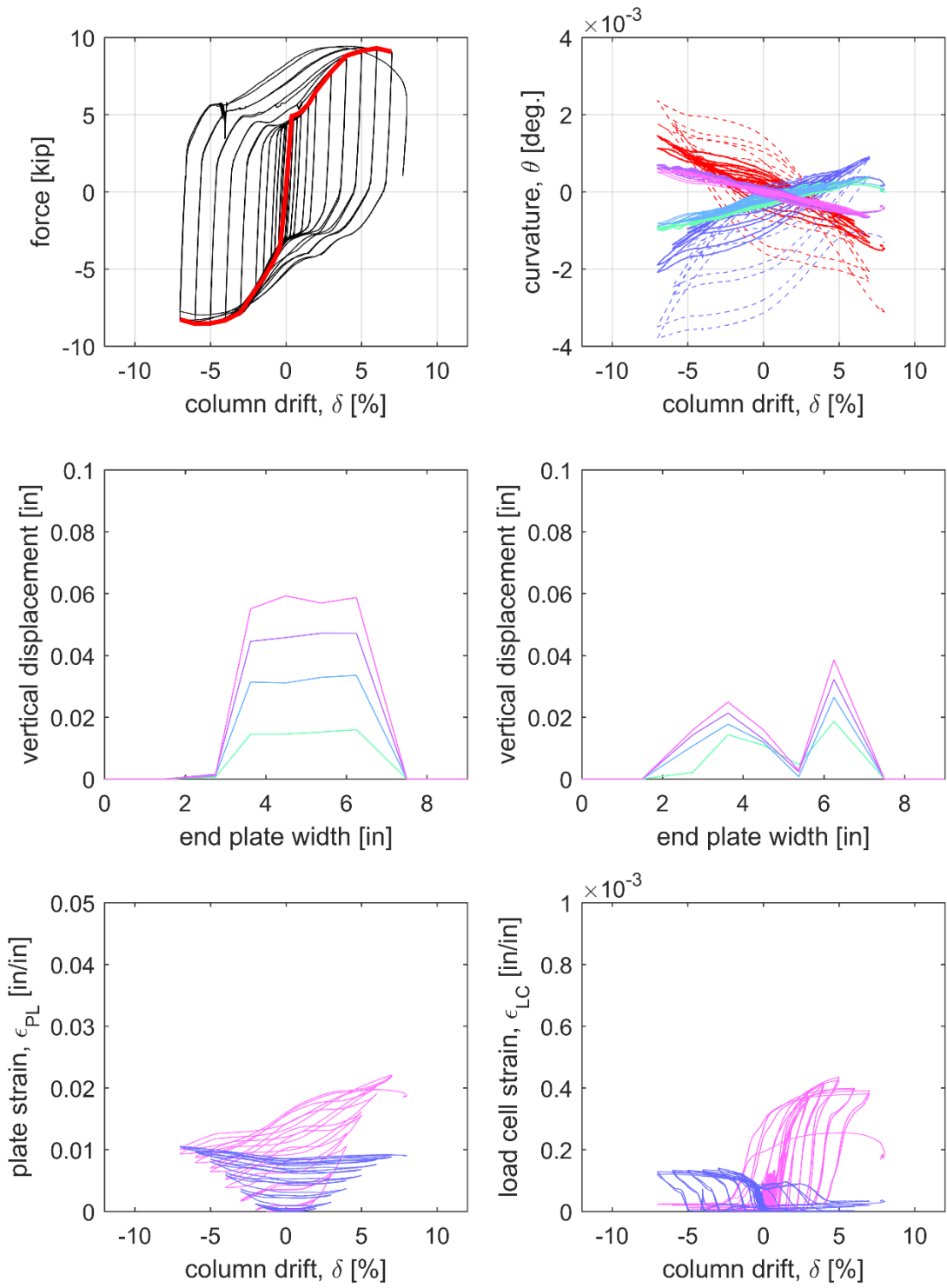
Roof Post: R6



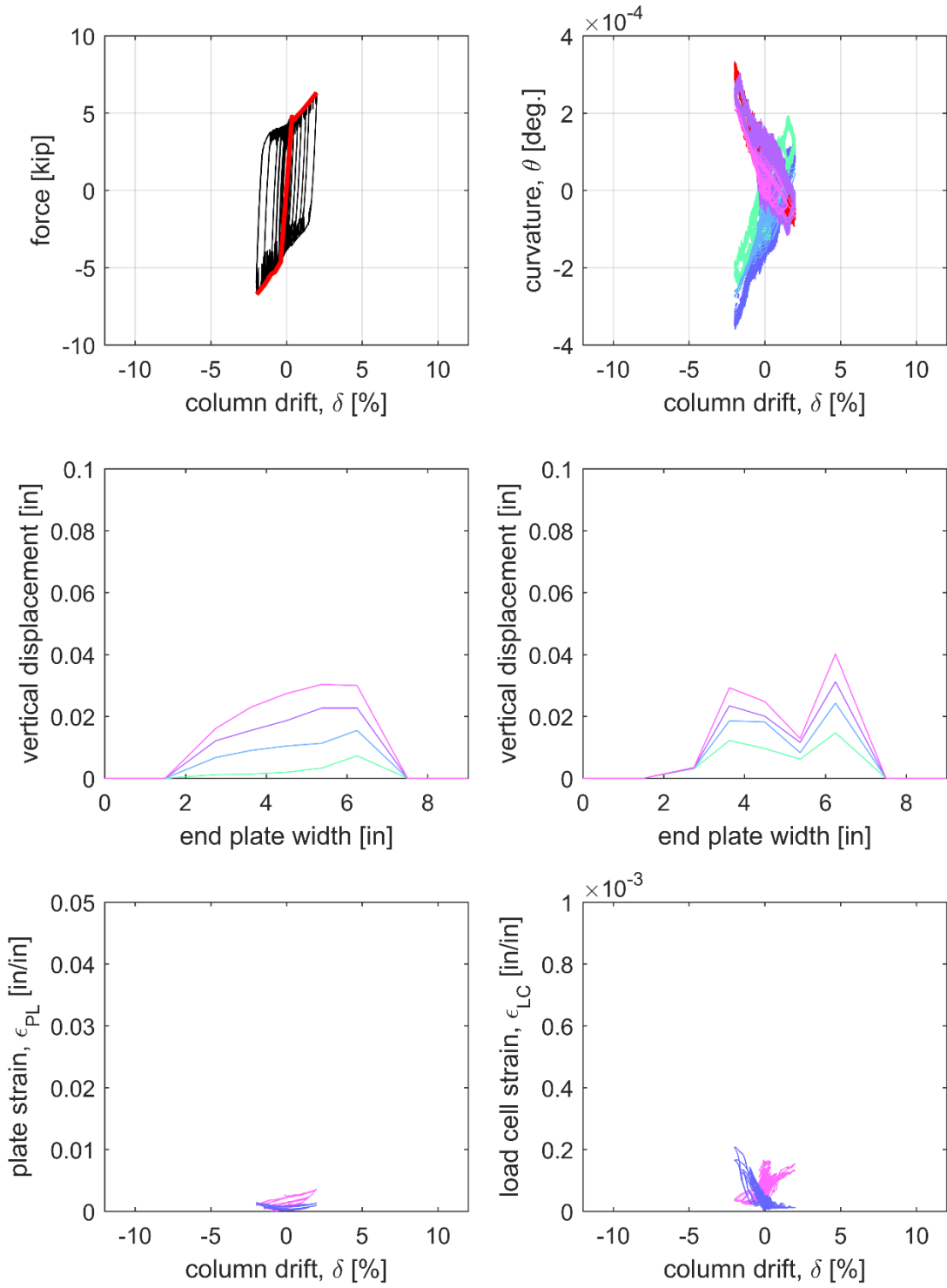
Roof Post: R7



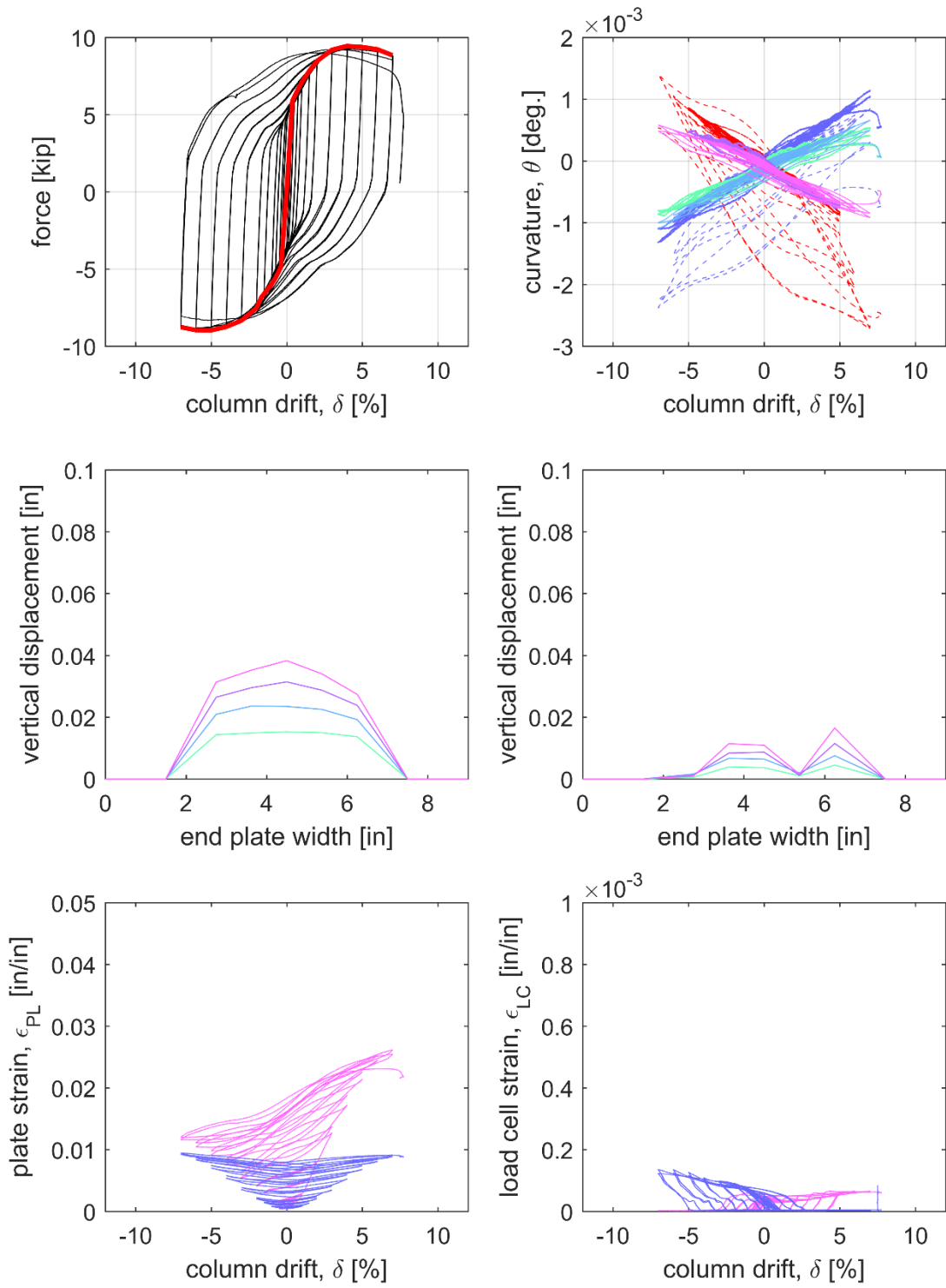
Roof Post: R8



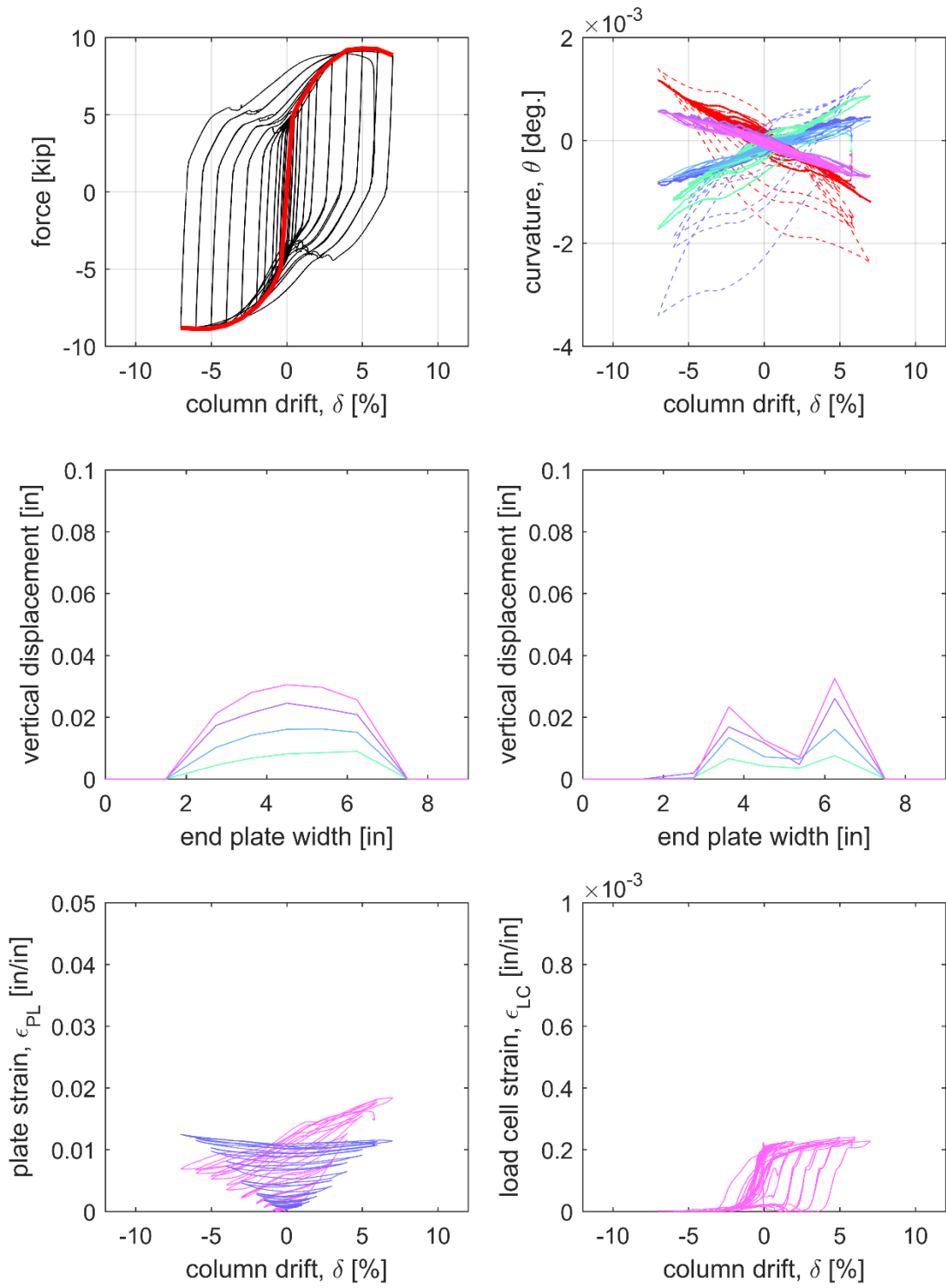
Roof Post: R9



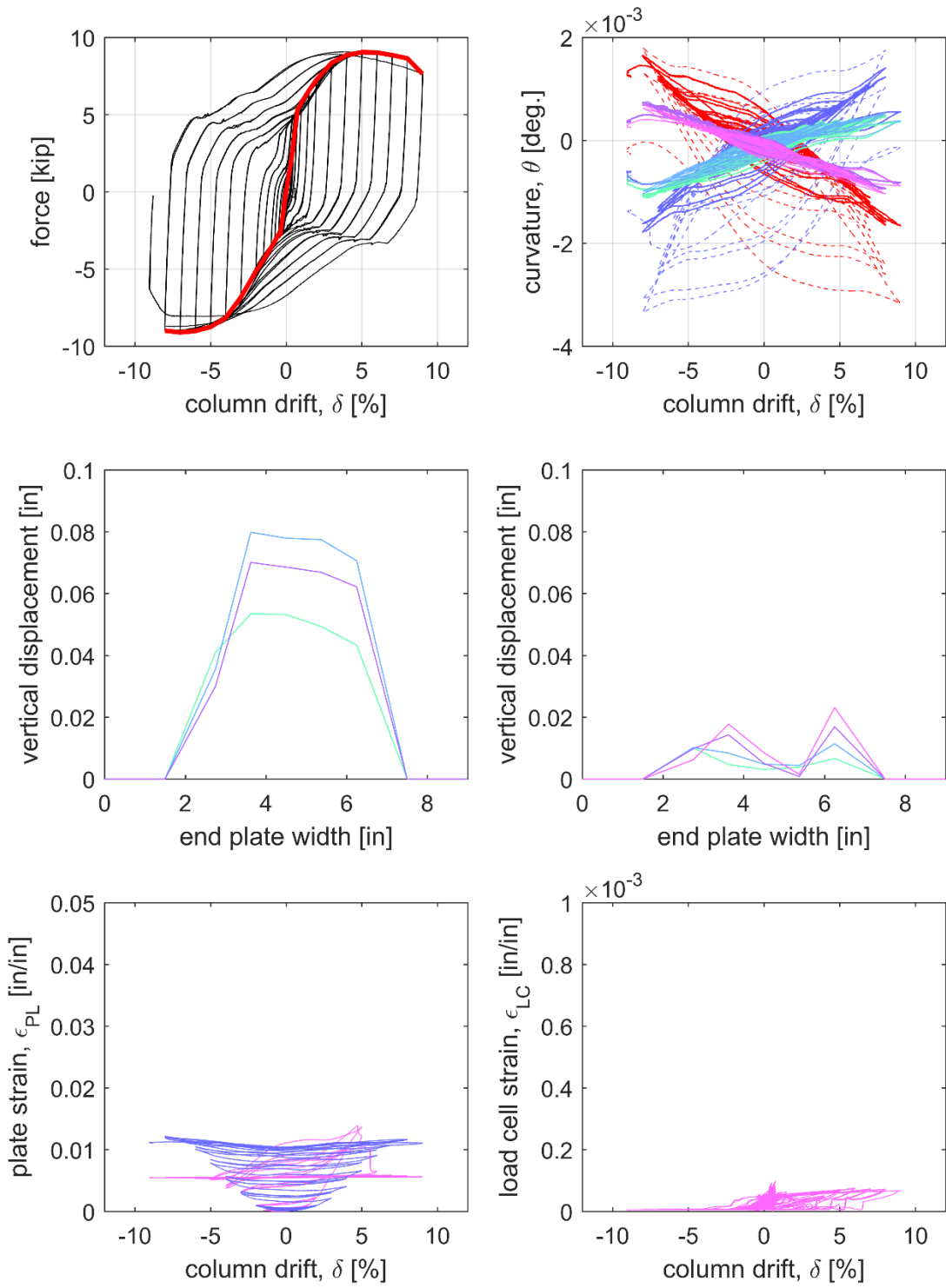
Roof Post: R10



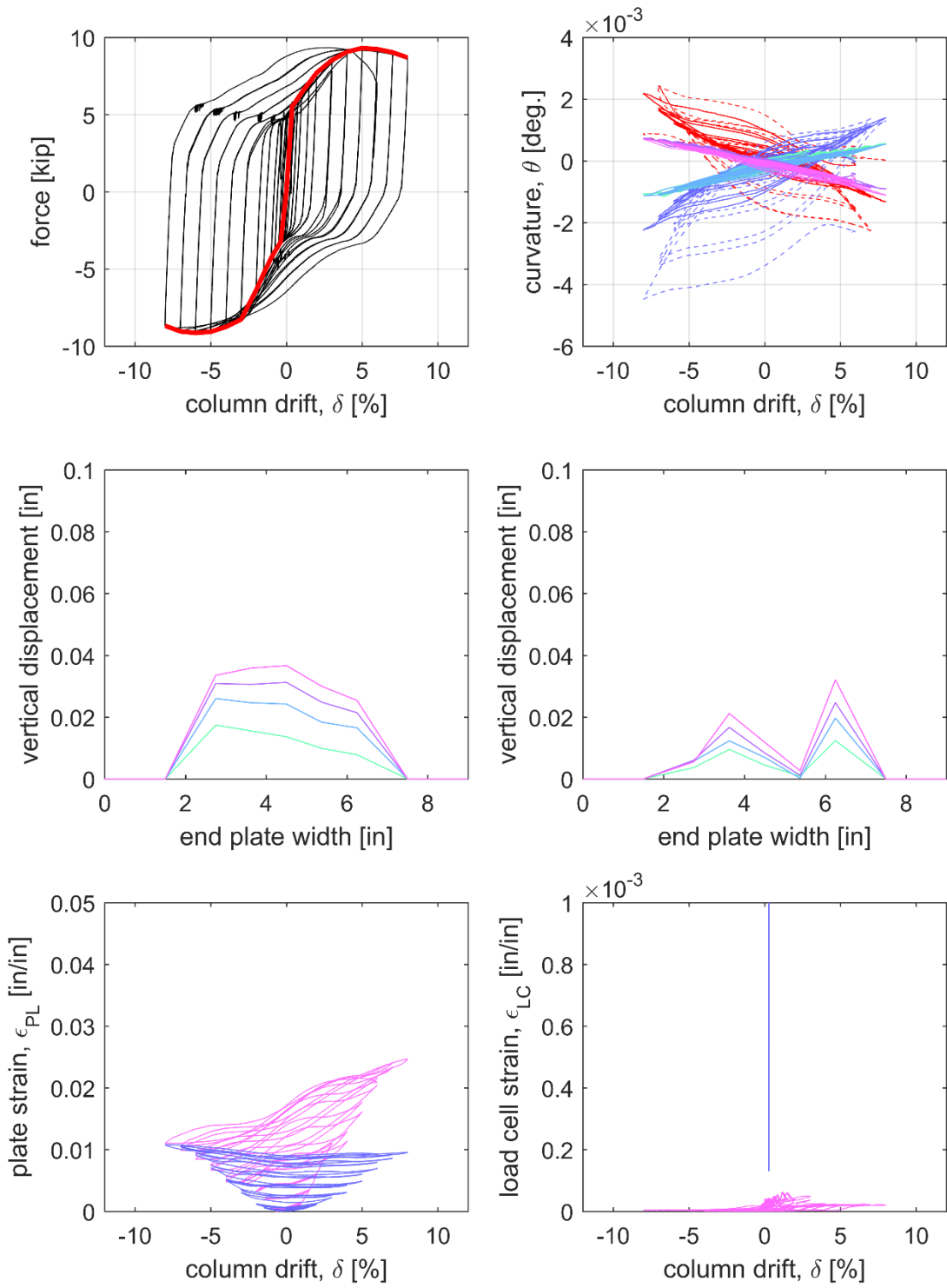
Roof Post: R11



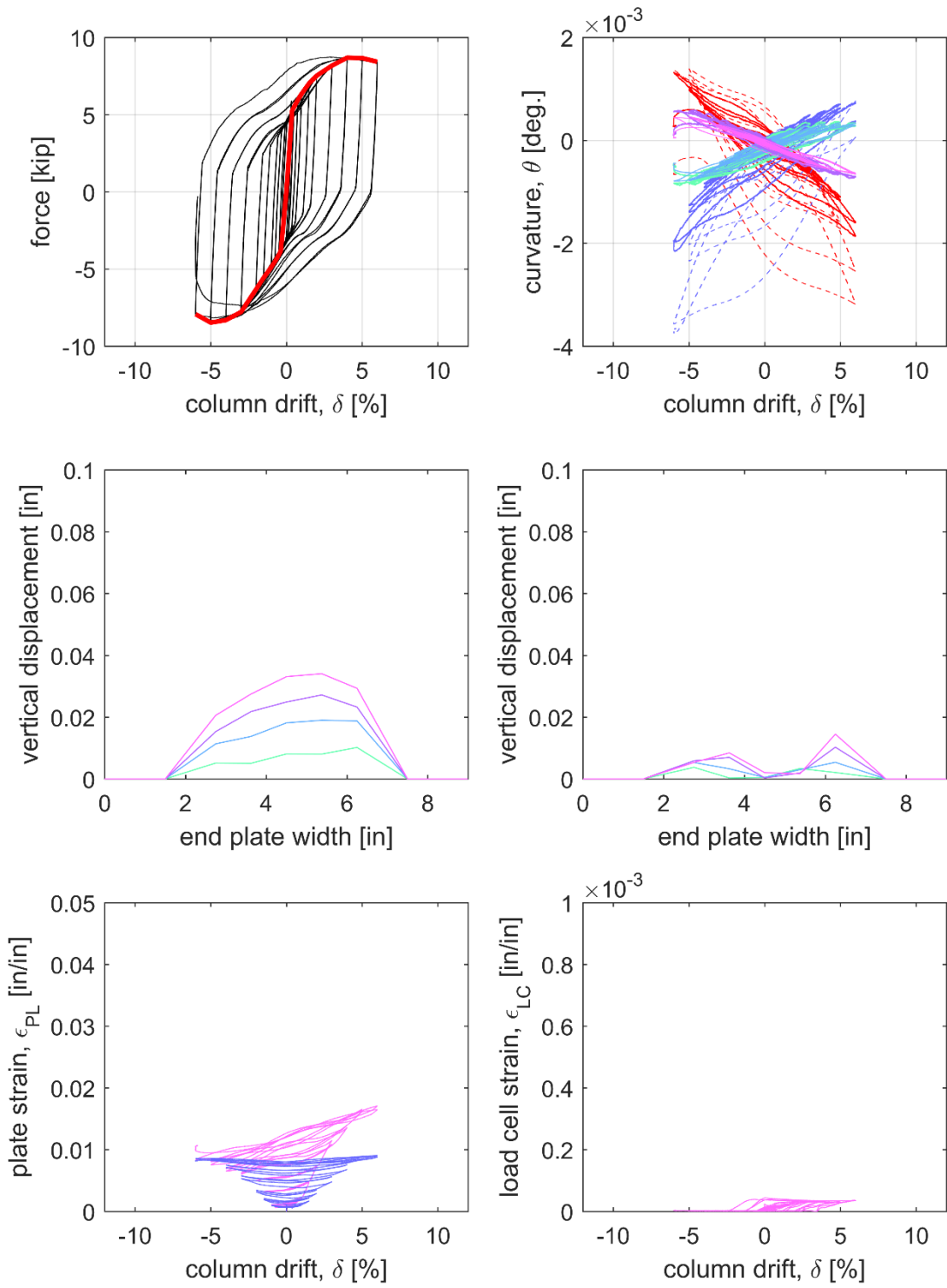
Roof Post: R12



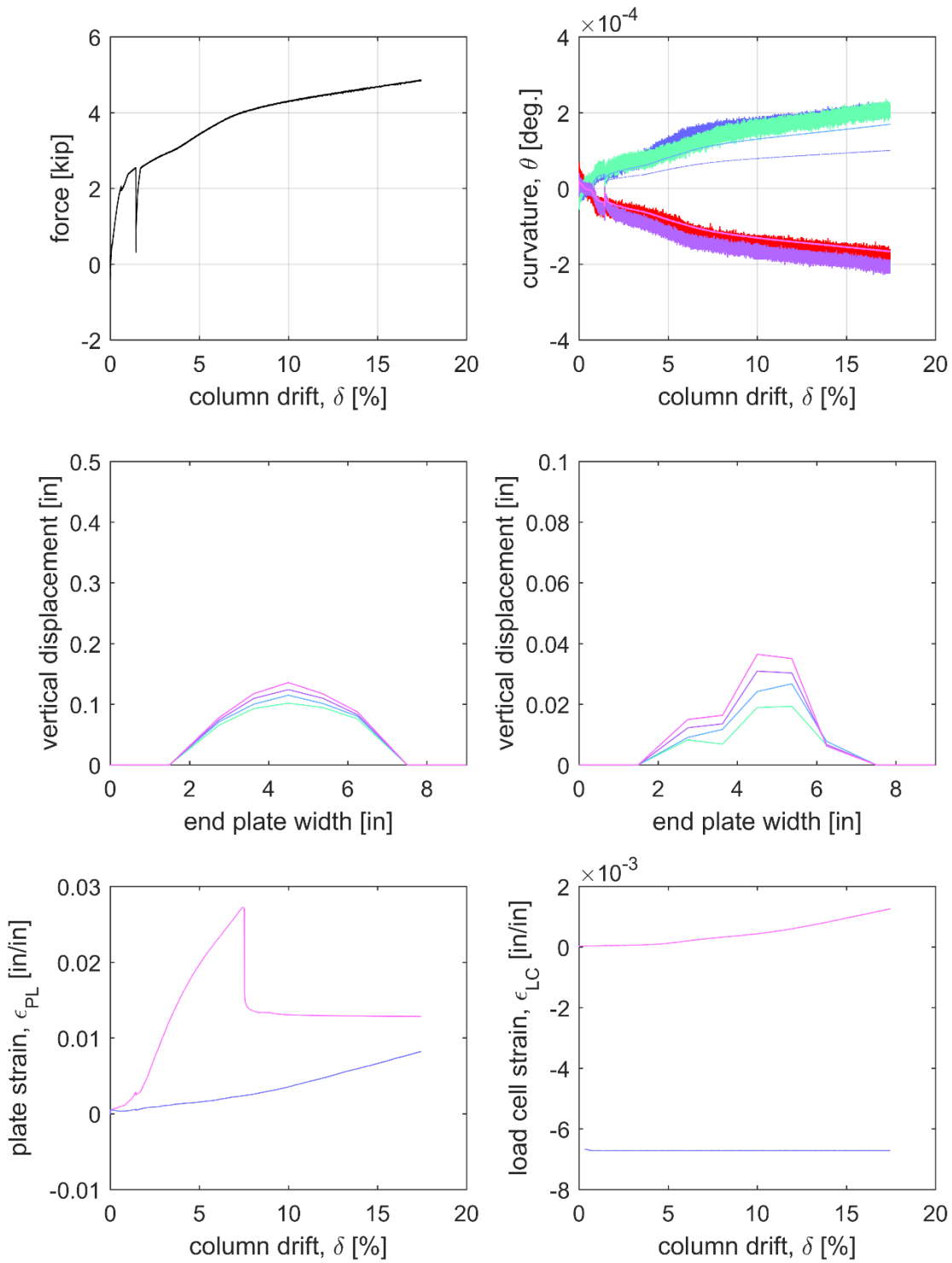
Roof Post: R13



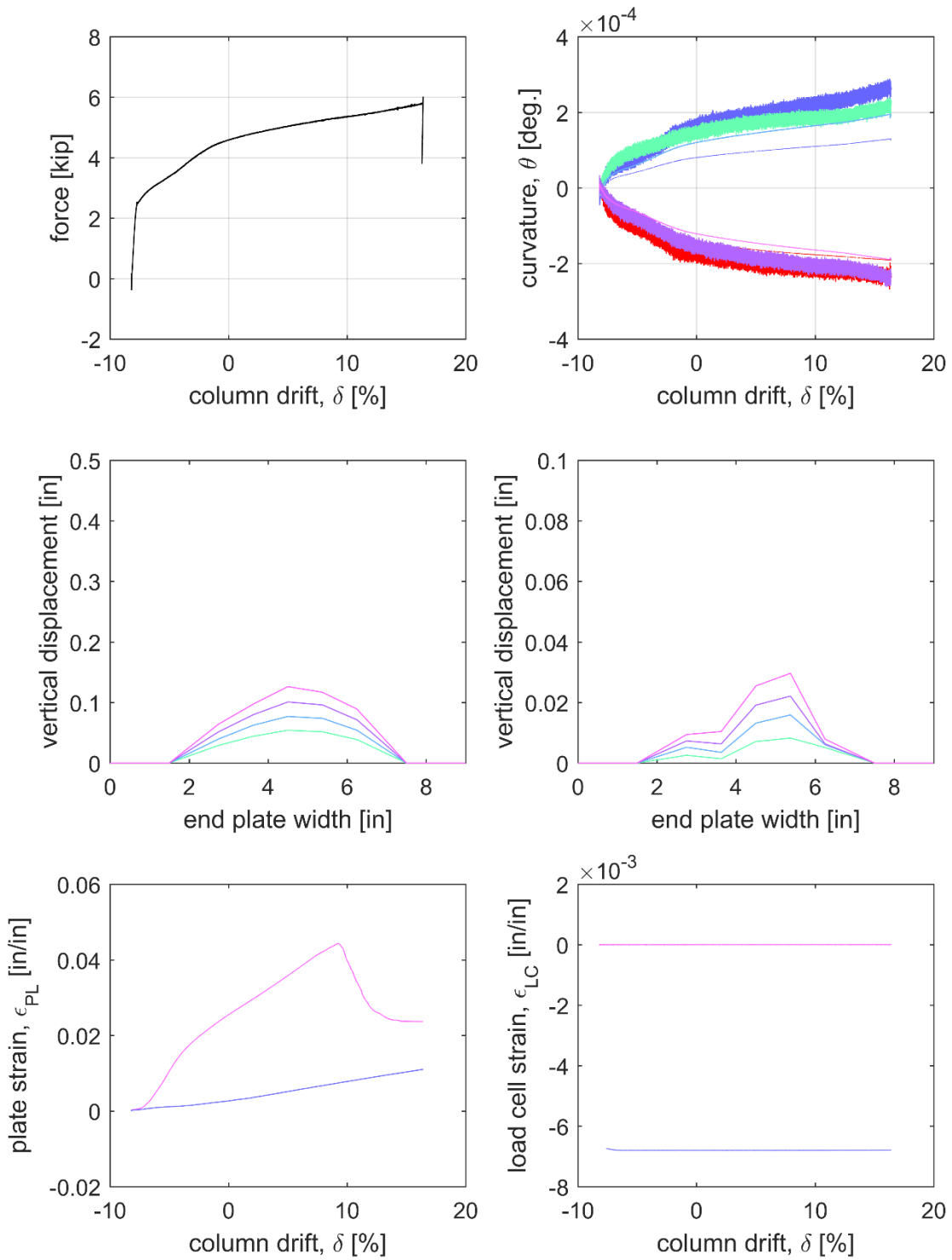
Roof Post: R14



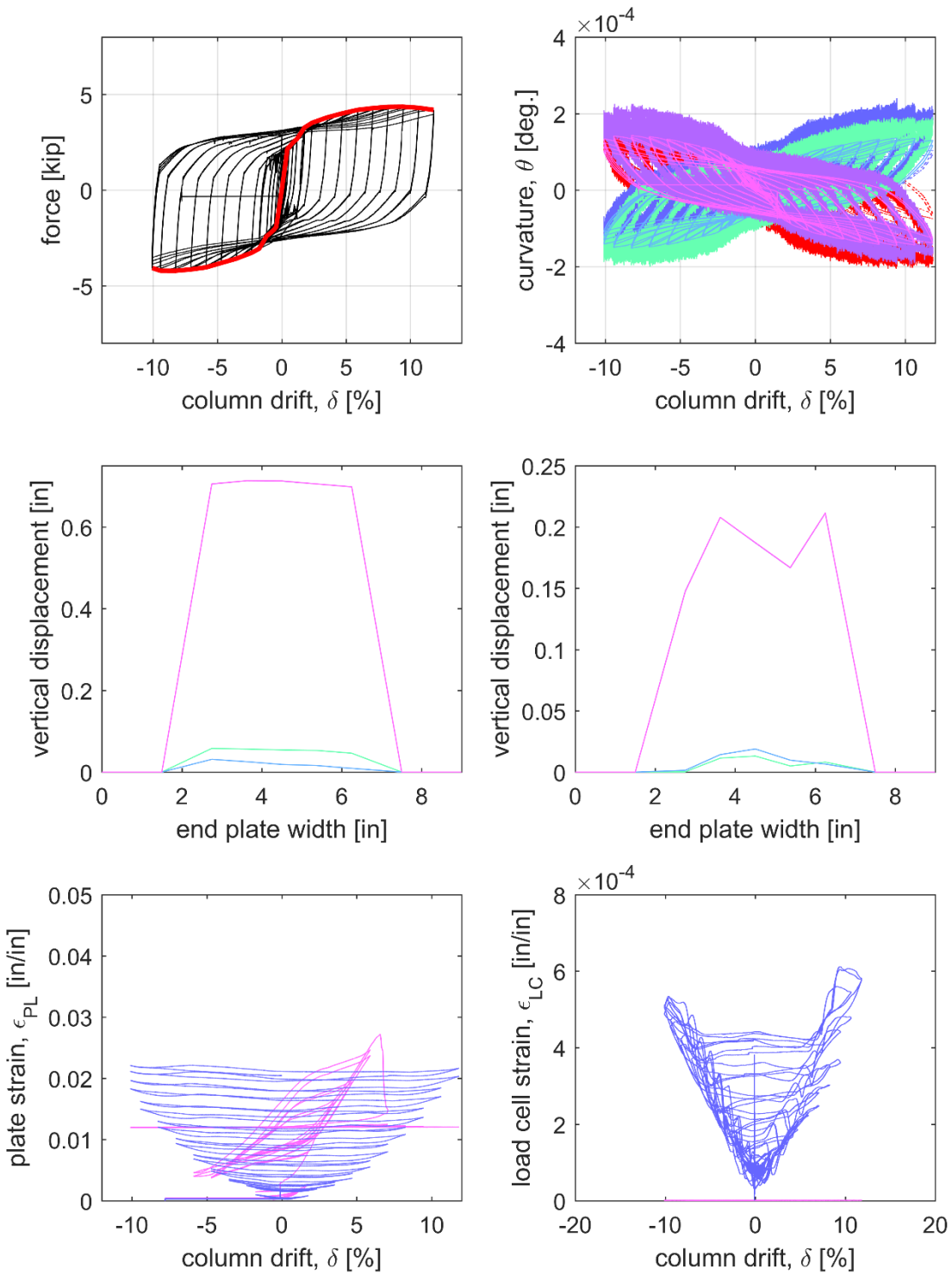
Canopy Beam: C1



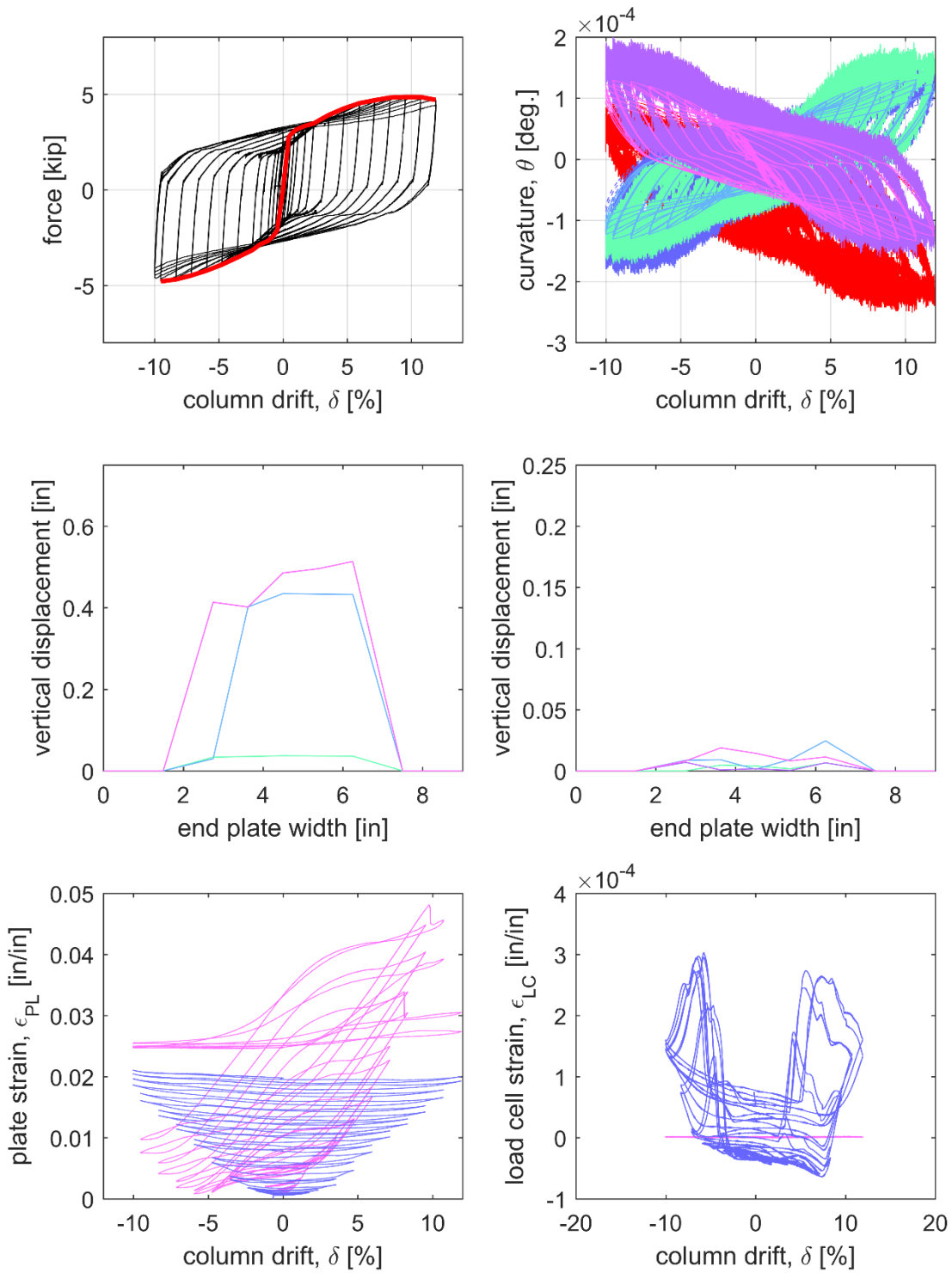
Canopy Beam: C2



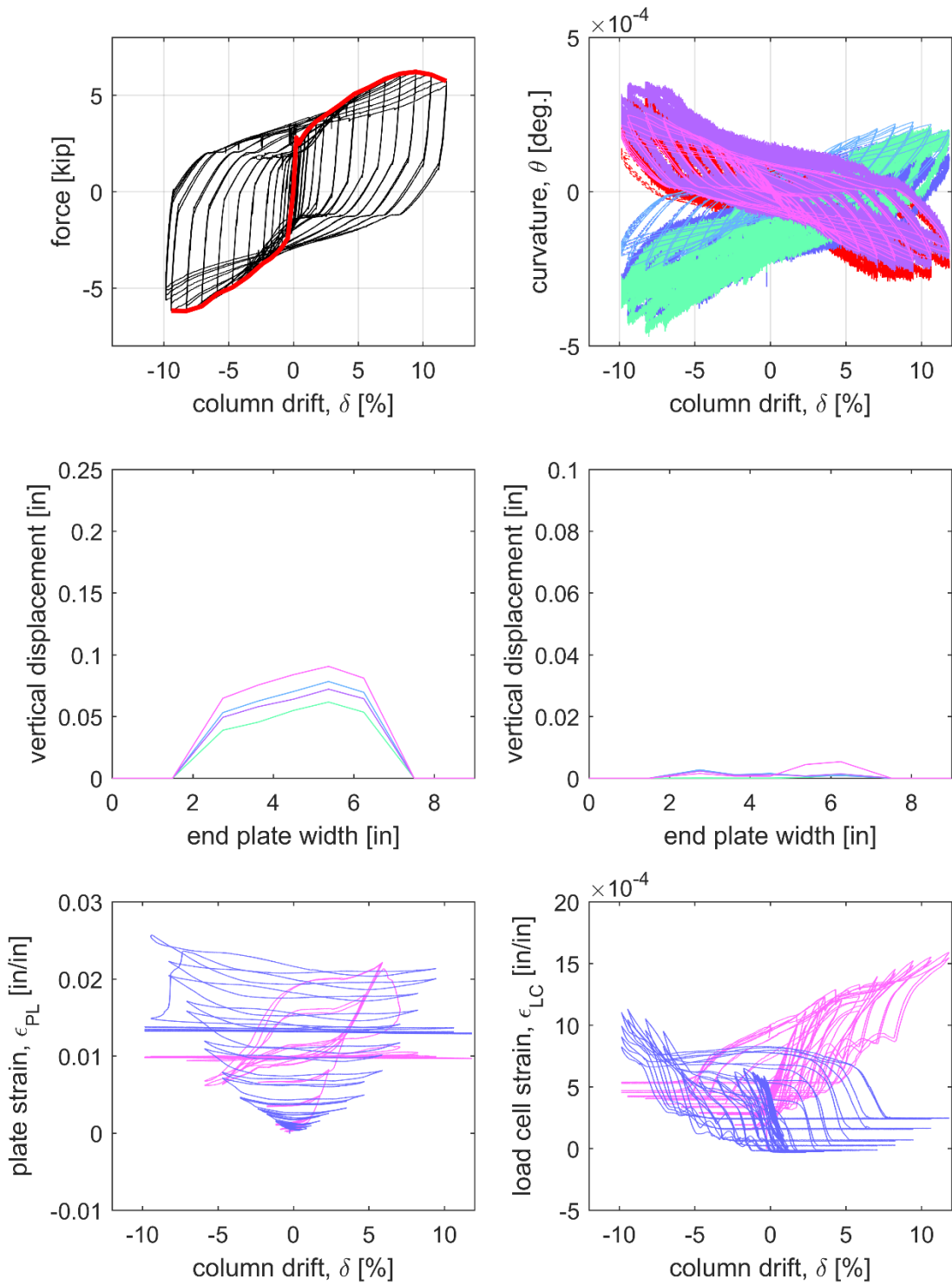
Canopy Beam: C4



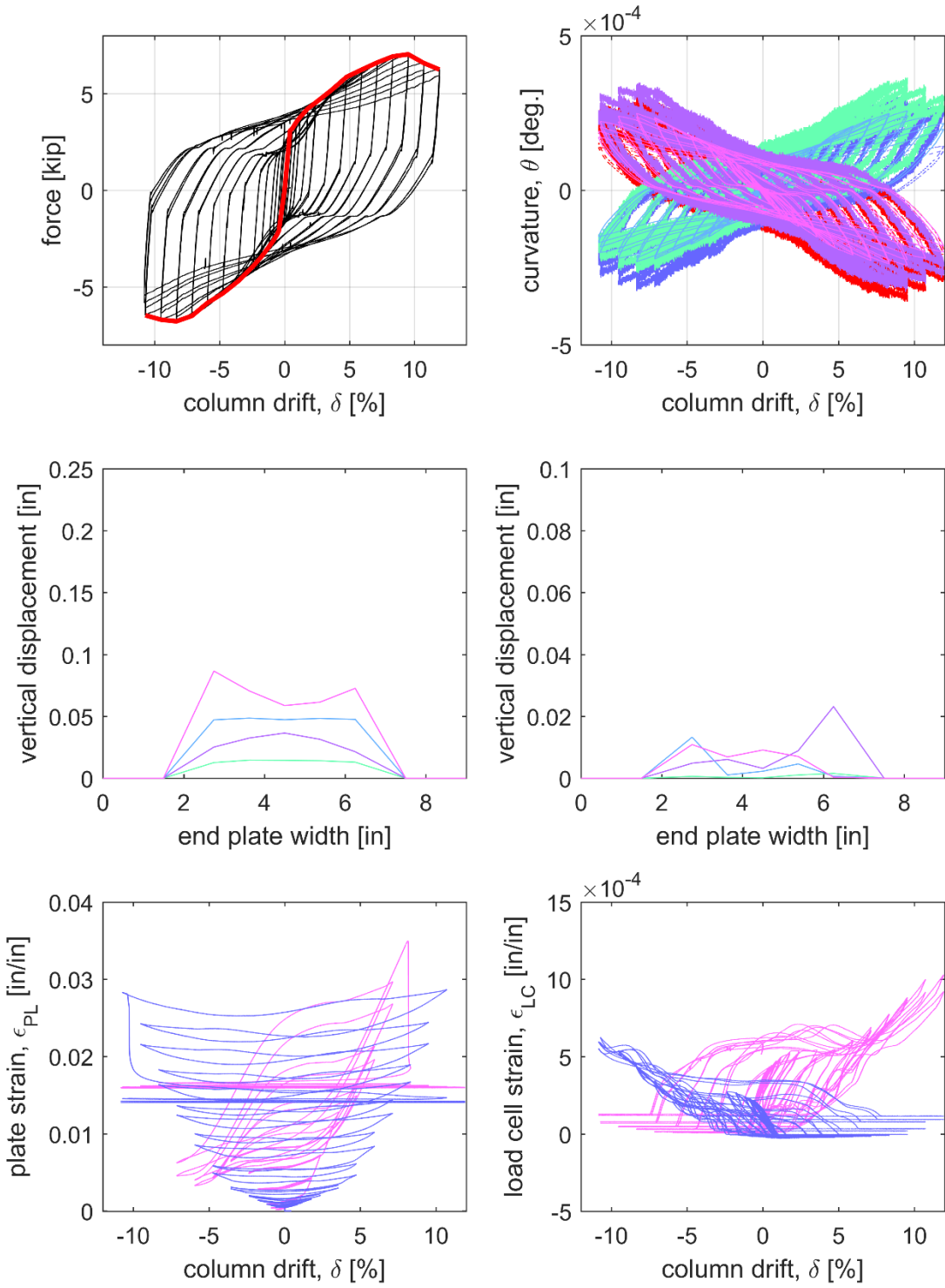
Canopy Beam: C5



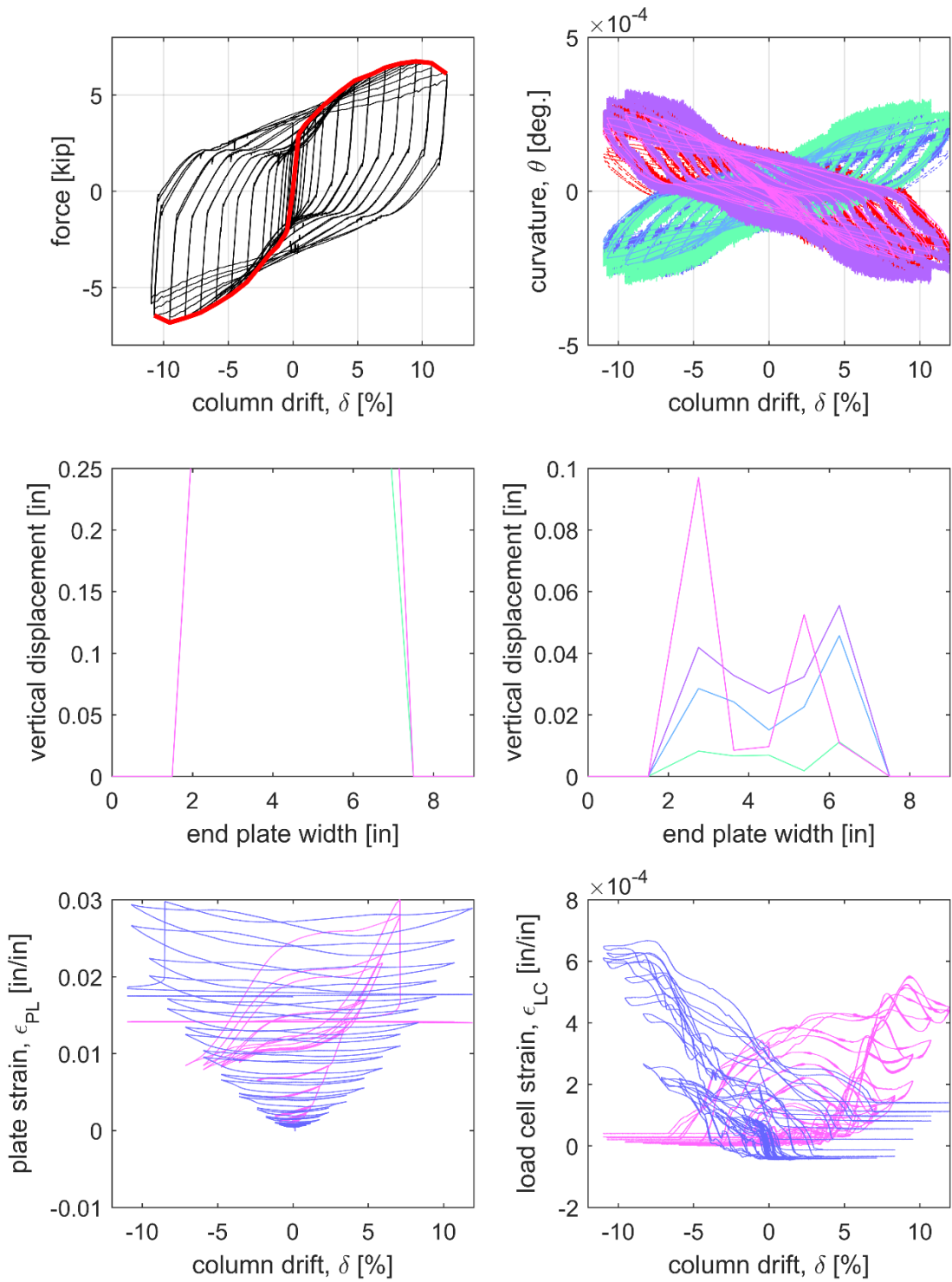
Canopy Beam: C7



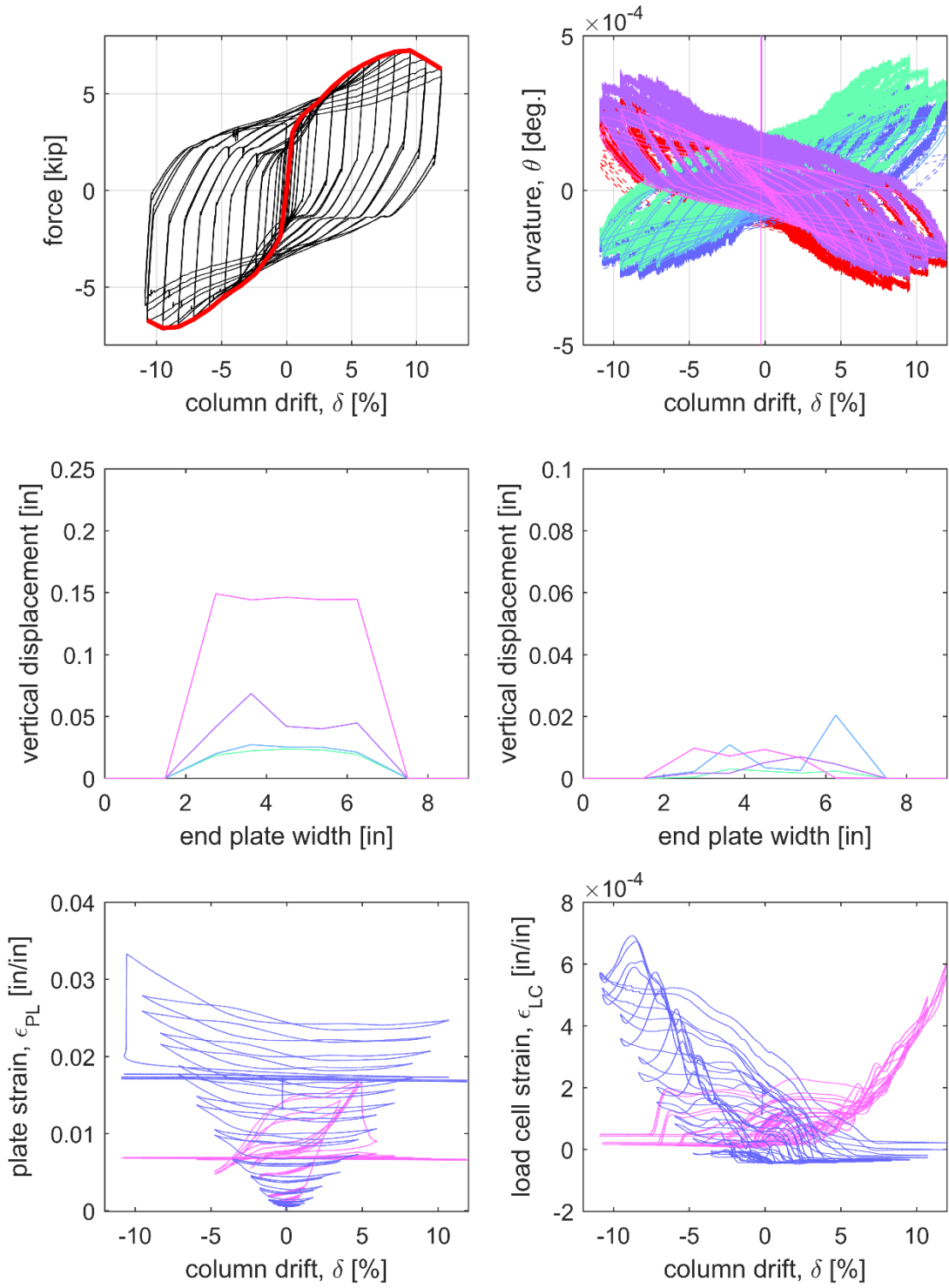
Canopy Beam: C8



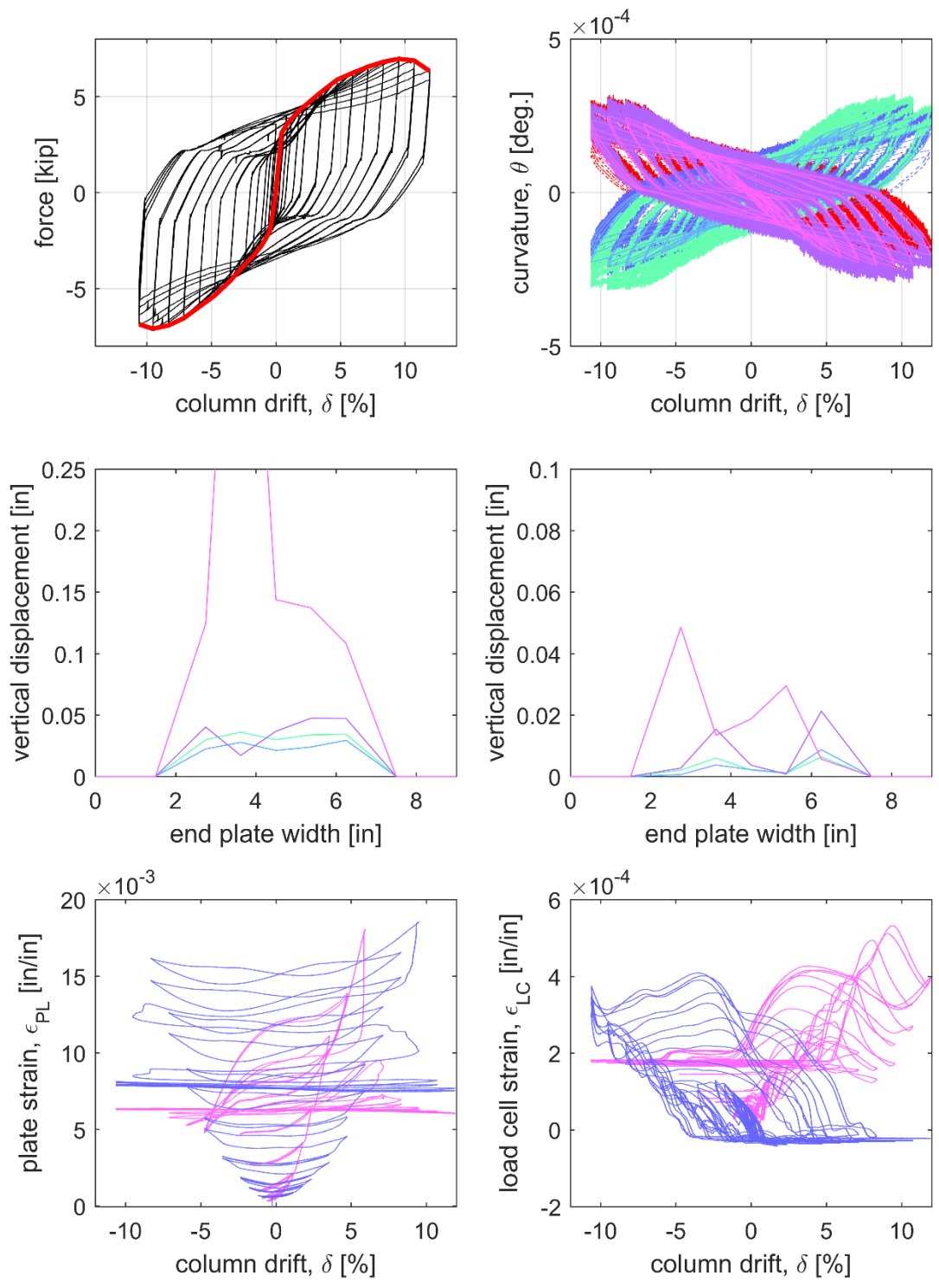
Canopy Beam: C9



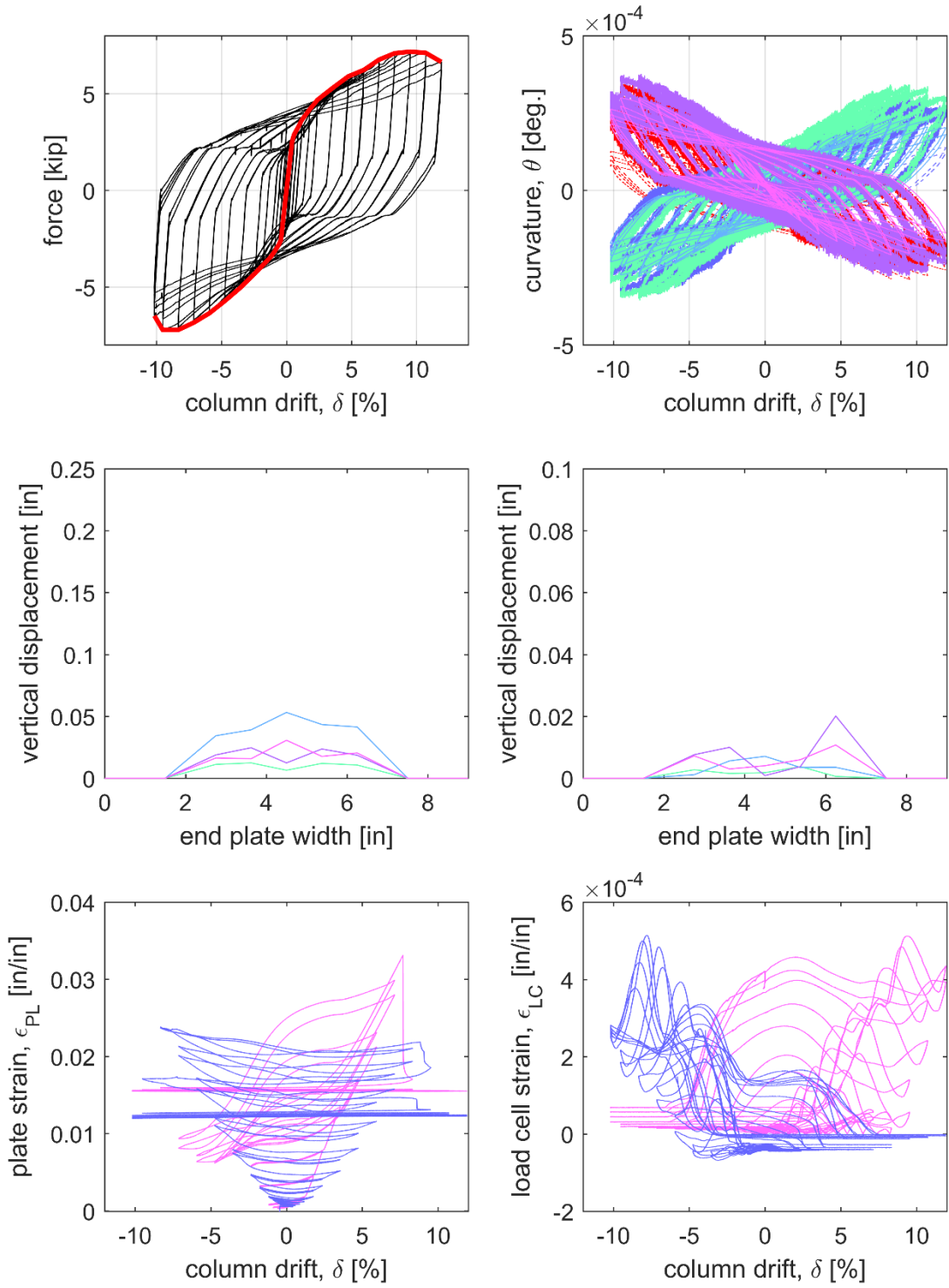
Canopy Beam: C10



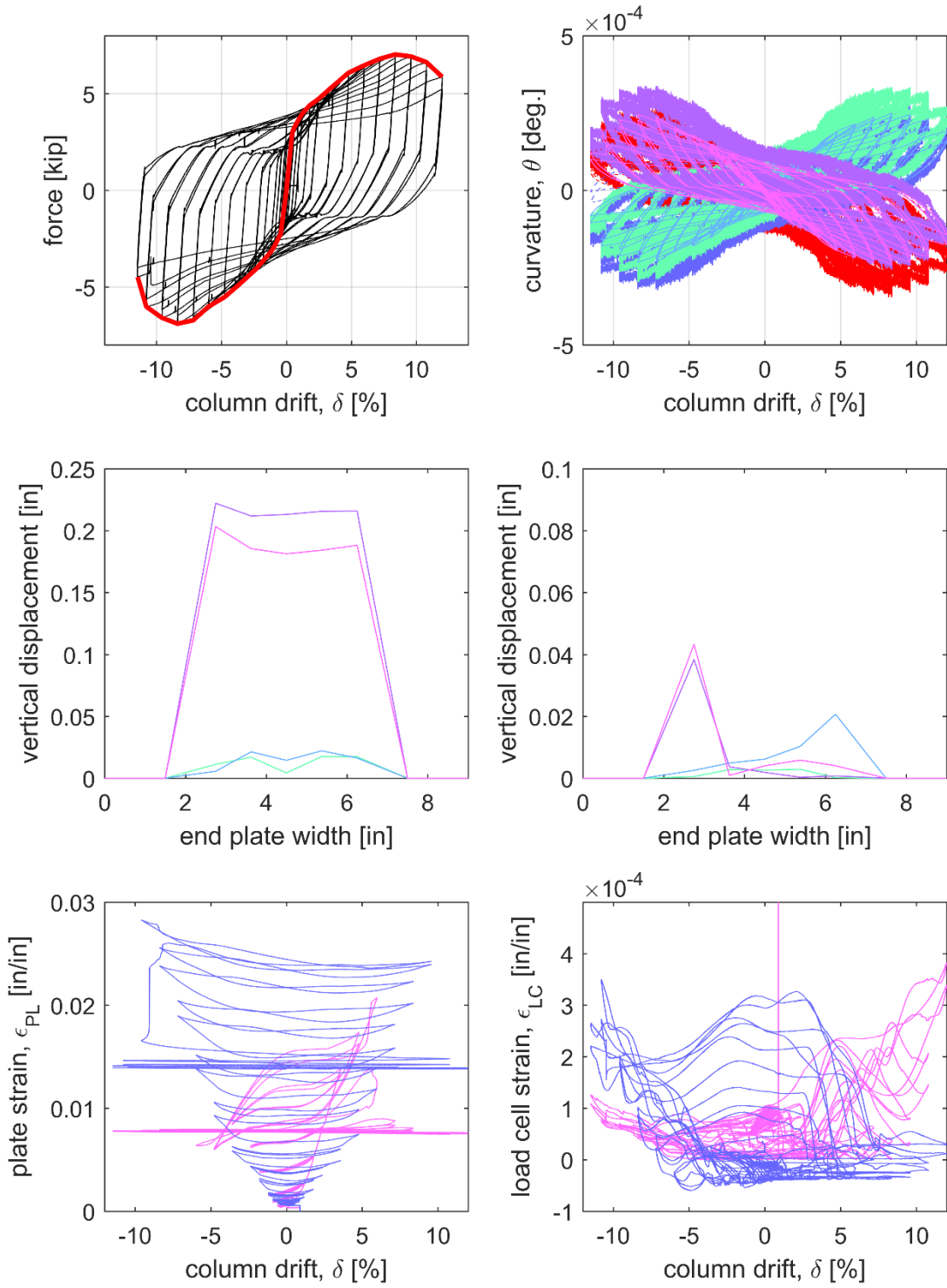
Canopy Beam: C11



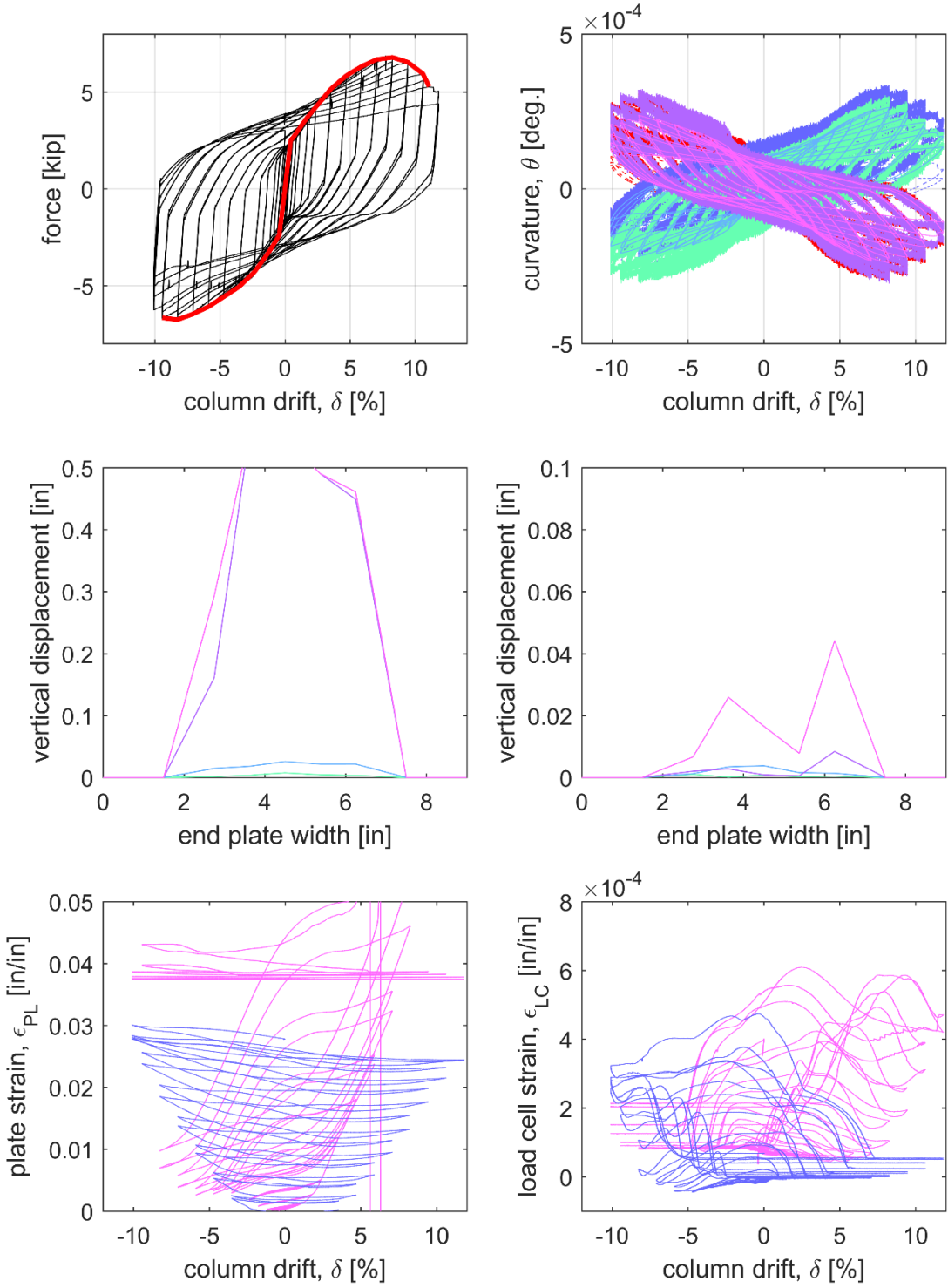
Canopy Beam: C12



Canopy Beam: C13



Canopy Beam: C15



Appendix E: Thermal Modeling

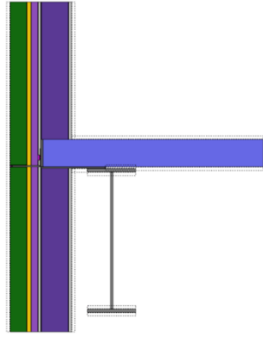
This appendix contains the results from thermal modeling of the thermal break strategies studied in this research.

Appendix E.1 – Results Sheets for Slab-Supported Shelf Angles

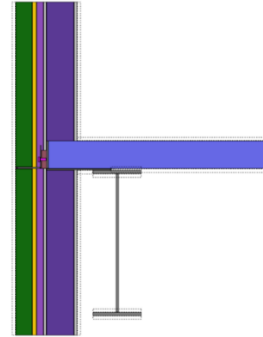
SHELF ANGLE: CLIMATE ZONE 1, 1.5" VINYLESTER SHIM

Detail: Shelf angle
Shelf angle: L5x5x5/16
Angle length: 80"
Mitigation strategy: 1.5" vinylester shim
Fastener: 5/8" dia. A325, 36" o.c.

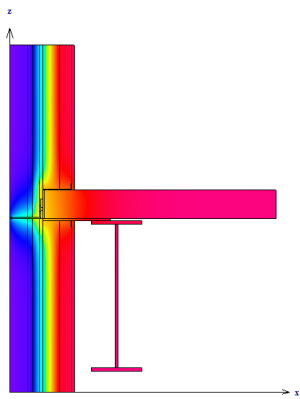
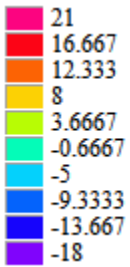
Climate Zone: 1
Exterior Temperature: -0.4 F
Interior Temperature: 69.8 F
Unmitigated filename: SAU1-1-A
Mitigated filename: SAM1-8-A



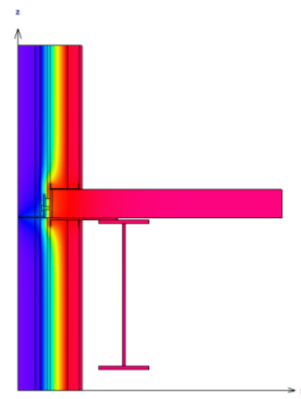
Unmitigated 2D Assembly Section



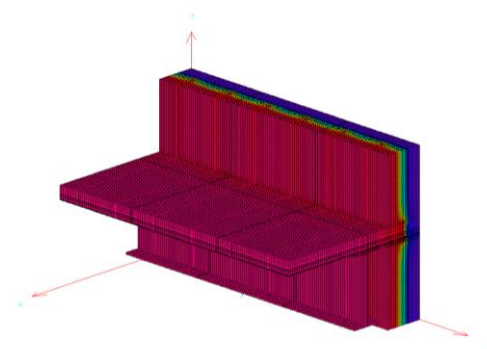
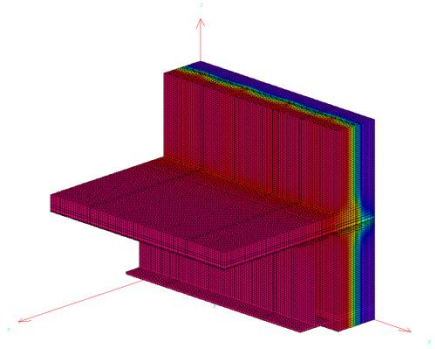
Mitigated 2D Assembly Section



Unmitigated 2D Results Model



Mitigated 2D Results Model

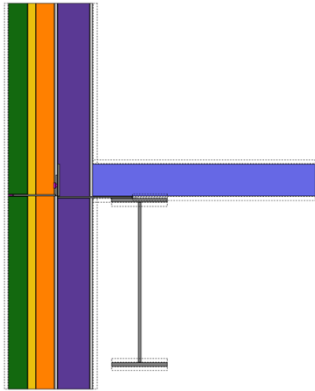


<i>Unmitigated 3D Results Model</i>		<i>Mitigated 3D Results Model</i>	
U-Value Unmitigated (BTU/h ft ² °F)	U-Value Mitigated (BTU/h ft ² °F)	ψ (BTU/hr ft °F)	% Reduction in ψ
0.138	0.082	0.098	77%

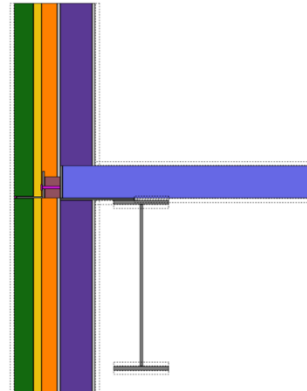
SHELF ANGLE: CLIMATE ZONE 7, 3" VINYLESTER SHIM

Detail: Shelf angle
Shelf angle: L5x5x5/16
Angle length: 80"
Mitigation strategy: 3" vinyl ester shim
Fastener: 5/8" dia. A325, 36" o.c.

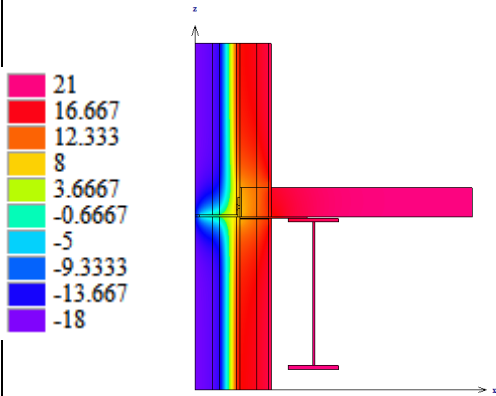
Climate Zone: 7
Exterior Temperature: -0.4 F
Interior Temperature: 69.8 F
Unmitigated filename: SAU7-4-A
Mitigated filename: SAM7-14-A



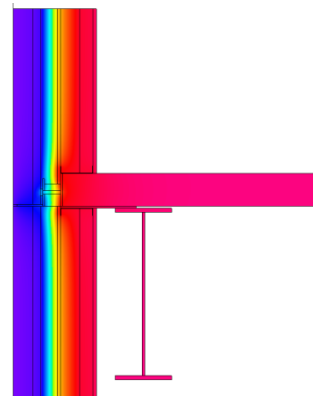
Unmitigated 2D Assembly Section



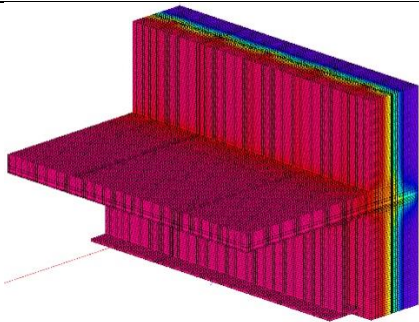
Mitigated 2D Assembly Section



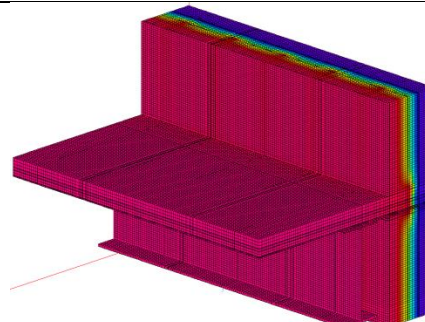
Unmitigated 2D Results Model



Mitigated 2D Results Model



Unmitigated 3D Results Model



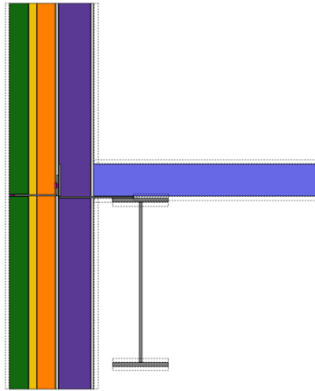
Mitigated 3D Results Model

U-Value Unmitigated (BTU/h ft ² °F)	U-Value Mitigated (BTU/h ft ² °F)	ψ (BTU/hr ft °F)	% Reduction in ψ
0.112	0.056	0.065	84%

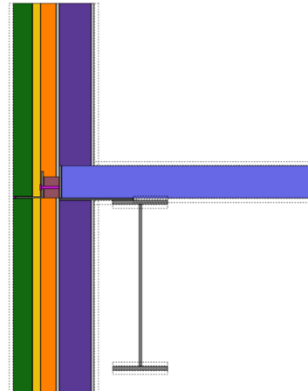
SHELF ANGLE: CLIMATE ZONE 7, 3" VINYLESTER SHIM

Detail: Shelf angle
Shelf angle: L5x5x5/16
Angle length: 80"
Mitigation strategy: 3" vinyl ester shim
Fastener: 5/8" dia. A304-SH, 36" o.c.

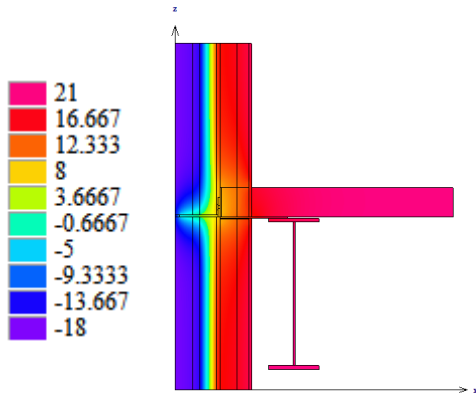
Climate Zone: 7
Exterior Temperature: -0.4 F
Interior Temperature: 69.8 F
Unmitigated filename: SAU7-4-A
Mitigated filename: SAM7-14-B



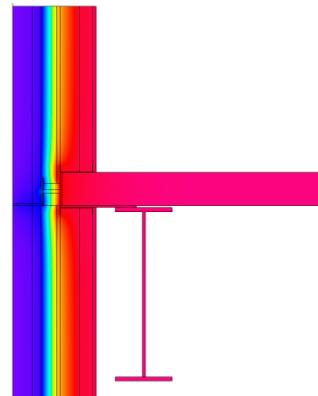
Unmitigated 2D Assembly Section



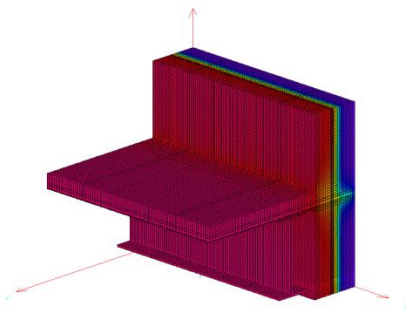
Mitigated 2D Assembly Section



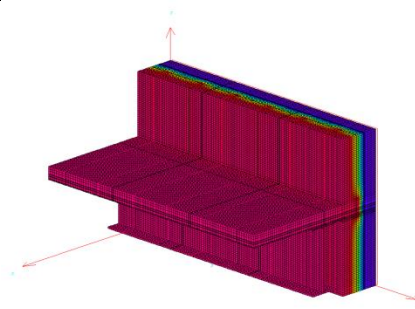
Unmitigated 2D Results Model



Mitigated 2D Results Model



Unmitigated 3D Results Model



Mitigated 3D Results Model

U-Value Unmitigated (BTU/h ft ² °F)	U-Value Mitigated (BTU/h ft ² °F)	ψ (BTU/hr ft °F)	% Reduction in ψ
0.112	0.053	0.045	89%

SHELF ANGLE: CLIMATE ZONE 7, 3" PROPRIETARY 1 SHIM

Detail: Shelf angle

Shelf angle: L5x5x5/16

Angle length: 80"

Fastener: 5/8" dia. A304-SH, 36" o.c.

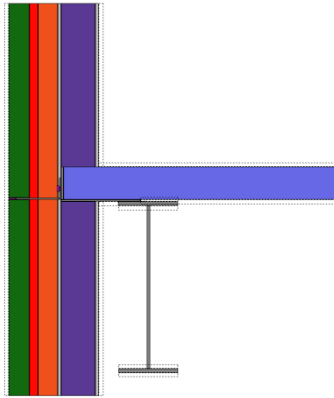
Climate Zone: 1

Exterior Temperature: -0.4 F

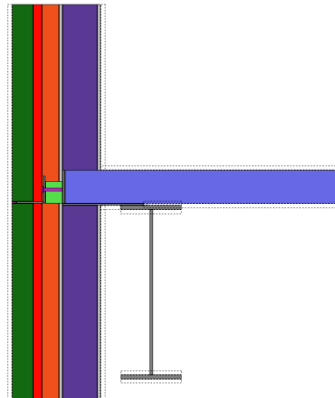
Interior Temperature: 69.8 F

Unmitigated filename: SAU7-4-A

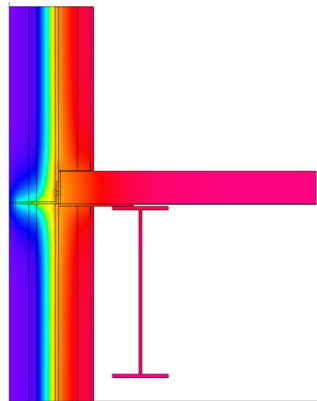
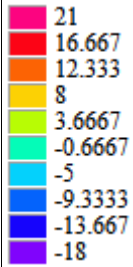
Mitigated filename: SAM7-17-A



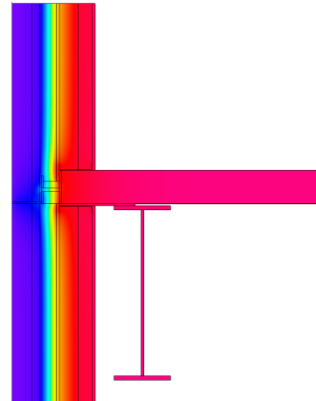
Unmitigated 2D Assembly Section



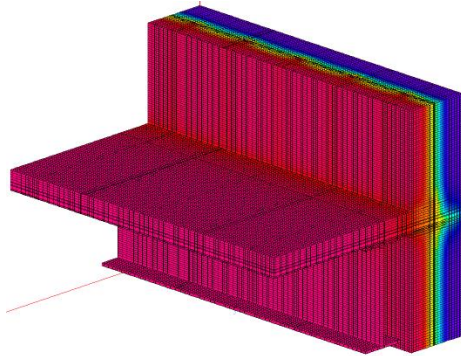
Mitigated 2D Assembly Section



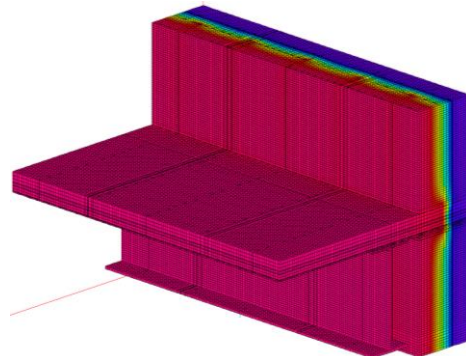
Unmitigated 2D Results Model



Mitigated 2D Results Model



Unmitigated 3D Results Model



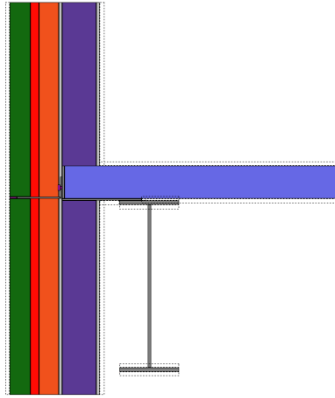
Mitigated 3D Results Model

U-Value Unmitigated (BTU/h ft ² °F)	U-Value Mitigated (BTU/h ft ² °F)	ψ (BTU/hr ft °F)	% Reduction in ψ
0.112	0.051	0.033	92%

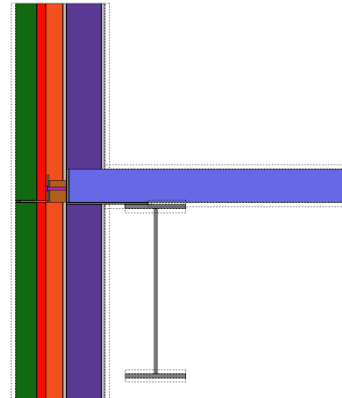
SHELF ANGLE: CLIMATE ZONE 1, 3" PROPRIETARY 2 SHIM

Detail: Shelf angle
Shelf angle: L5x5x5/16
Angle length: 80"
Fastener: 5/8" dia. A304-SH, 36" o.c.

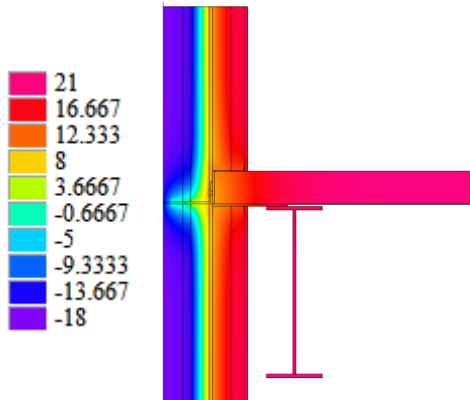
Climate Zone: 7
Exterior Temperature: -0.4 F
Interior Temperature: 69.8 F
Unmitigated filename: SAU7-4-A
Mitigated filename: SAM7-18-A



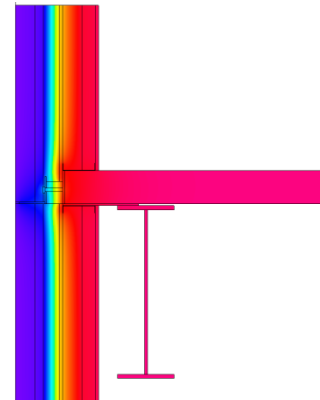
Unmitigated 2D Assembly Section



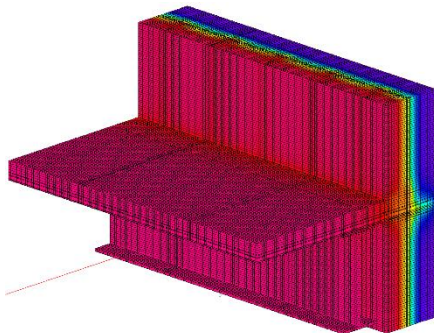
Mitigated 2D Assembly Section



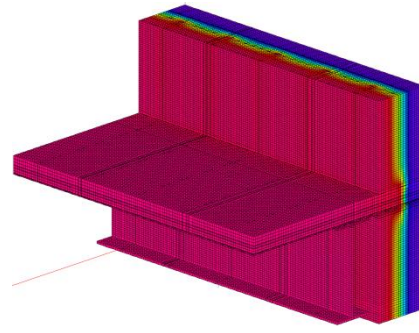
Unmitigated 2D Results Model



Mitigated 2D Results Model



Unmitigated 3D Results Model



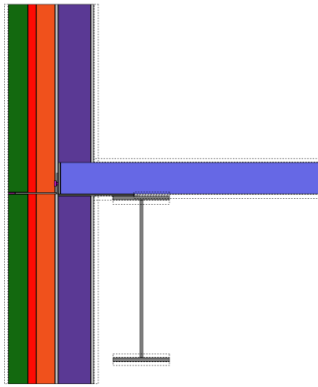
Mitigated 3D Results Model

U-Value Unmitigated (BTU/h ft ² °F)	U-Value Mitigated (BTU/h ft ² °F)	ψ (BTU/hr ft °F)	% Reduction in ψ
0.112	0.051	0.035	91%

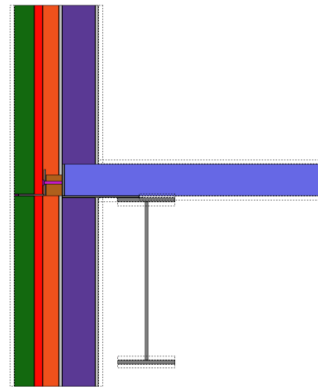
SHELF ANGLE: CLIMATE ZONE 1, STAINLESS HSS3x3x3/16

Detail: Shelf angle
Shelf angle: L4x4x5/16
Angle length: 80"
Fastener: 5/8" dia. A304-SH, 36" o.c.

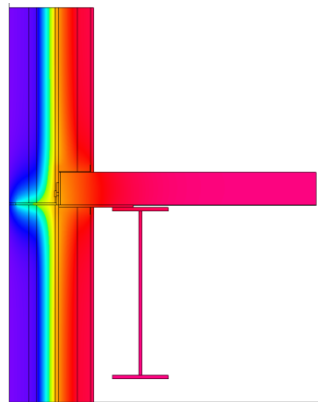
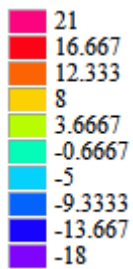
Climate Zone: 7
Exterior Temperature: -0.4 F
Interior Temperature: 69.8 F
Unmitigated filename: SAU7-4-A
Mitigated filename: SAM7-18-B



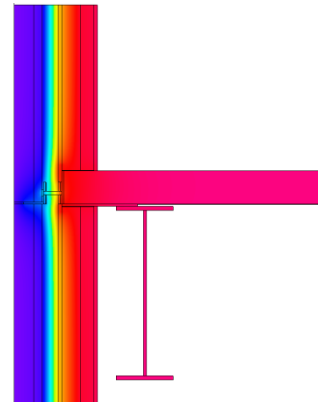
Unmitigated 2D Assembly Section



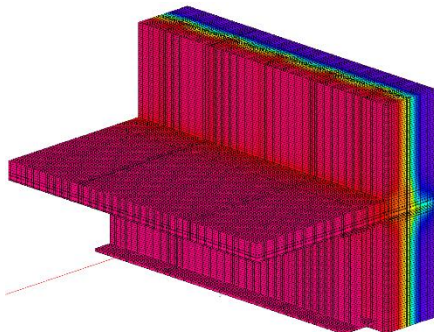
Mitigated 2D Assembly Section



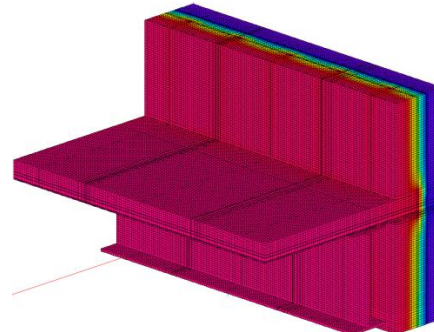
Unmitigated 2D Results Model



Mitigated 2D Results Model



Unmitigated 3D Results Model



Mitigated 3D Results Model

U-Value Unmitigated (BTU/h ft ² °F)	U-Value Mitigated (BTU/h ft ² °F)	ψ (BTU/hr ft °F)	% Reduction in ψ
0.112	0.059	0.081	80%

SHELF ANGLE: CLIMATE ZONE 1, FRP ANGLE

Detail: Shelf angle

Shelf angle: L6x4x1/2

Angle length: 96"

Mitigation strategy: vinyl ester angle

Fastener: 5/8" dia. A325, 36" o.c.

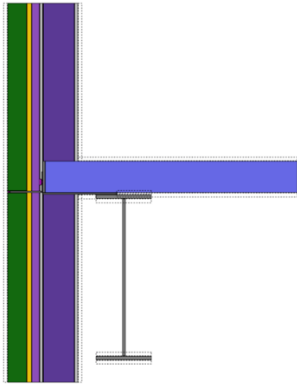
Climate Zone: 1

Exterior Temperature: -0.4 F

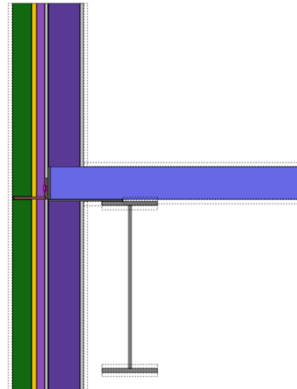
Interior Temperature: 69.8 F

Unmitigated filename: SAU1-1-A

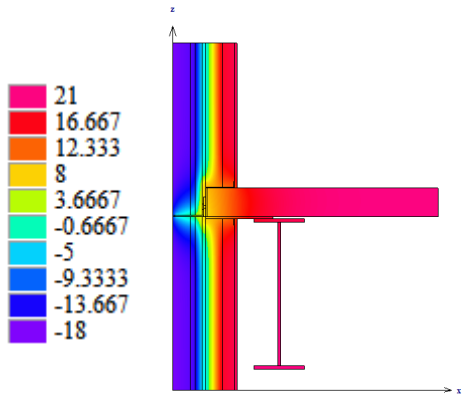
Mitigated filename: SAM1-19-A



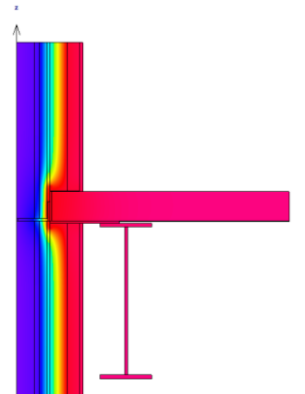
Unmitigated 2D Assembly Section



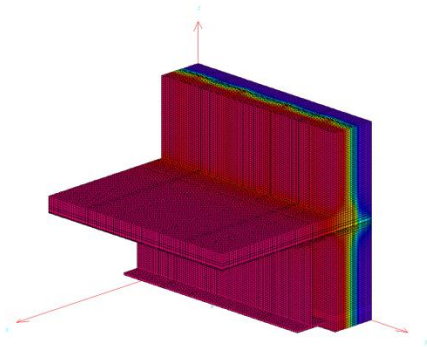
Mitigated 2D Assembly Section



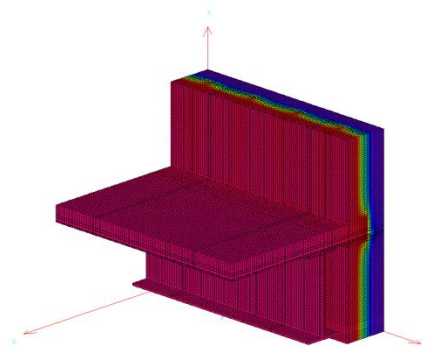
Unmitigated 2D Results Model



Mitigated 2D Results Model



Unmitigated 3D Results Model



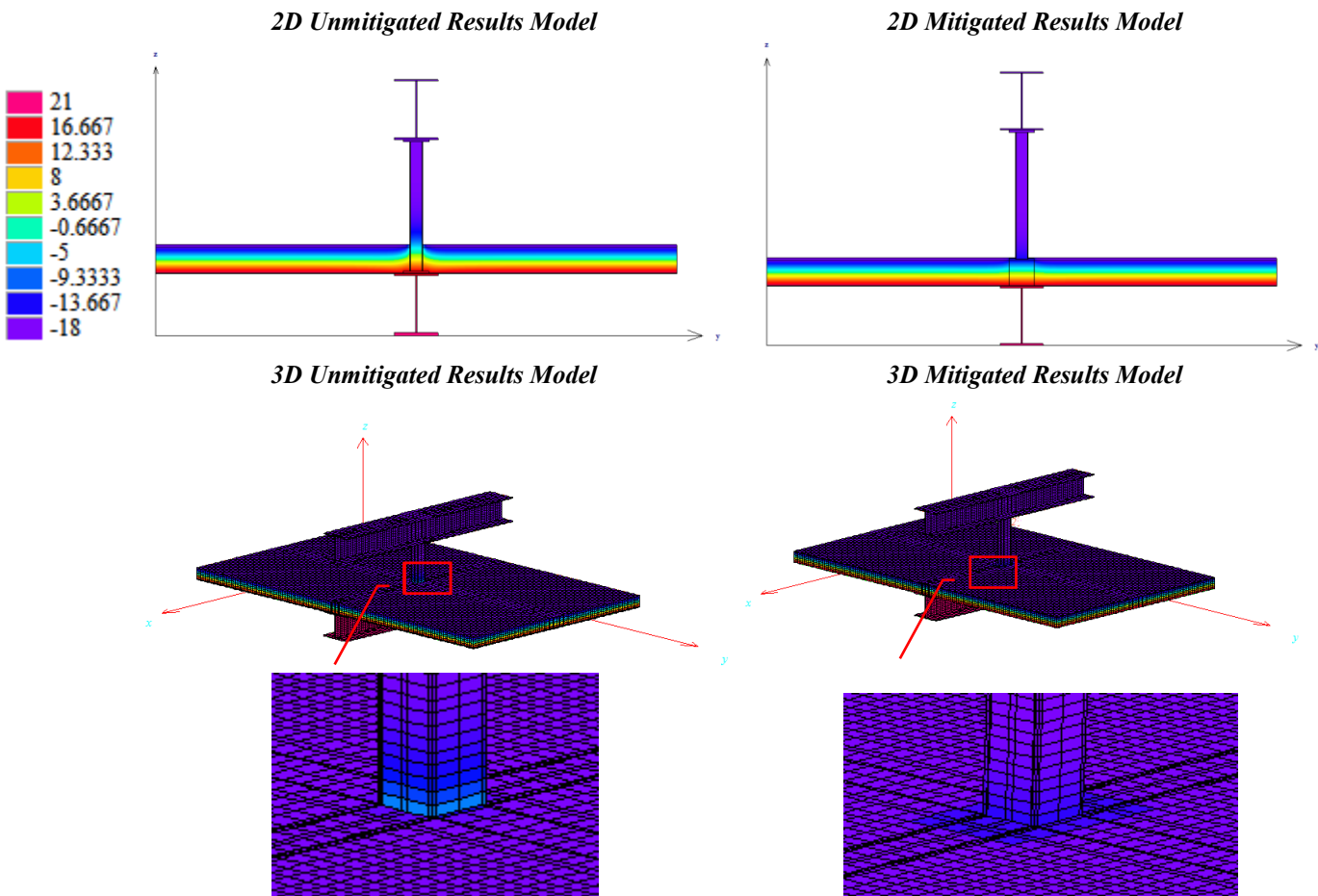
Mitigated 3D Results Model

U-Value Unmitigated (BTU/h ft ² °F)	U-Value Mitigated (BTU/h ft ² °F)	ψ (BTU/hr ft °F)	% Reduction in ψ
0.138	0.072	0.035	92%

Appendix E.2 – Results Sheets for Roof Posts

ROOF POST: CLIMATE ZONE 7, 6" VINYLESTER FRP SHIM

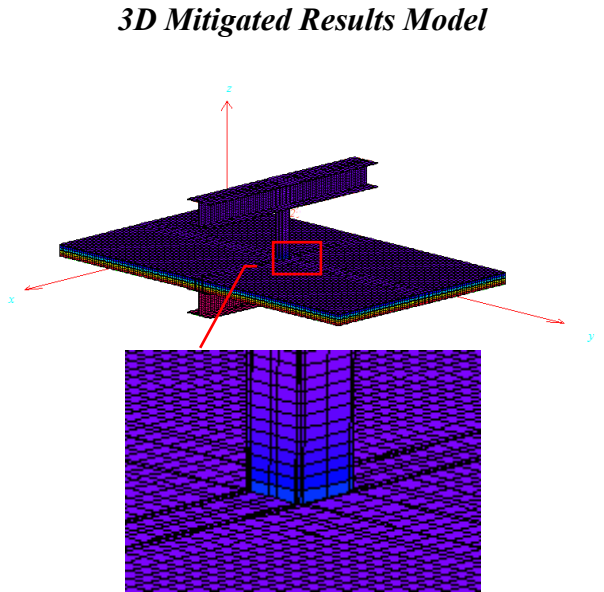
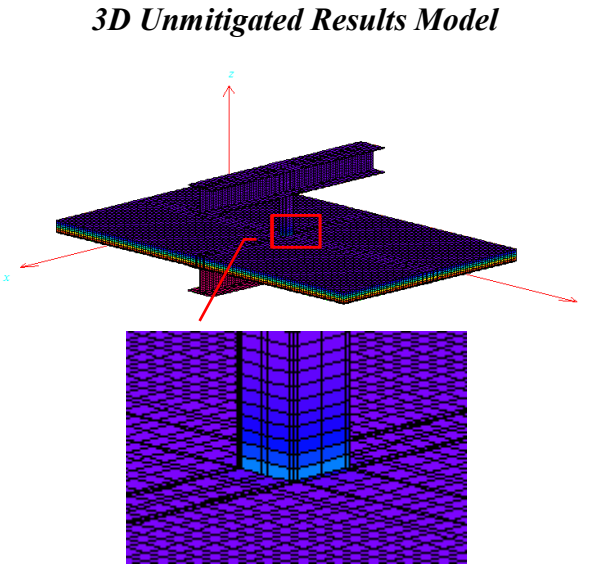
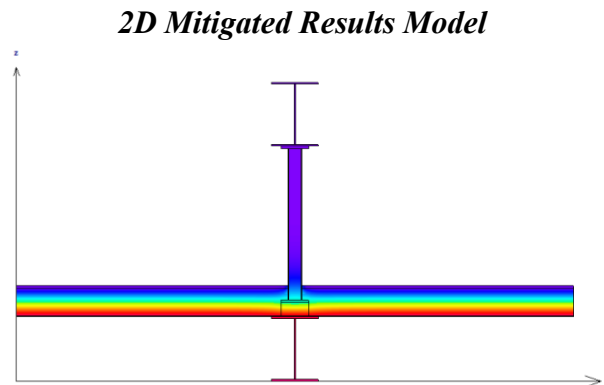
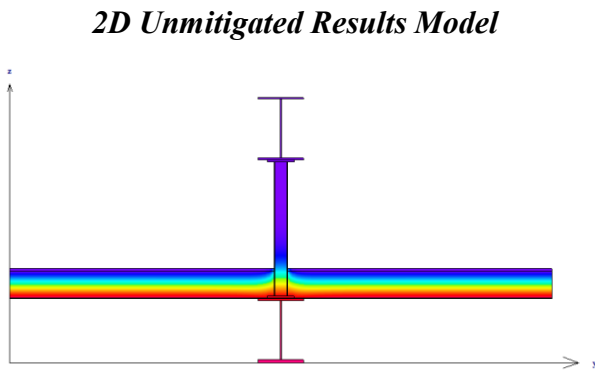
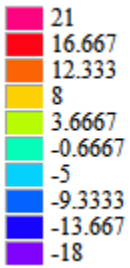
Detail:	Roof post	Climate Zone:	Zone 7
Mitigation Strategy:	9x9x3/8 FRP Shim	Interior Condition:	69.8°F
Area Dimensions:	72x120 inches	Exterior Condition:	-0.4°F
Shim Material:	Vinylester	Unmitigated Model:	RPU7-1-A
Shim Thickness:	6 inches	Mitigated Model:	RPM7-2-A
Insulation Thickness:	6 inches		
Rod Diameter:	0.75 inches		
Rod Spacing:	6 inches o.c.		



U-Value Unmitigated (BTU/h ft ² °F)	U-Value Mitigated (BTU/h ft ² °F)	χ (BTU/hr °F)	% Reduction in χ
0.035	0.032	0.29	40%

ROOF POST: CLIMATE ZONE 7, 3" VINYLESTER FRP SHIM

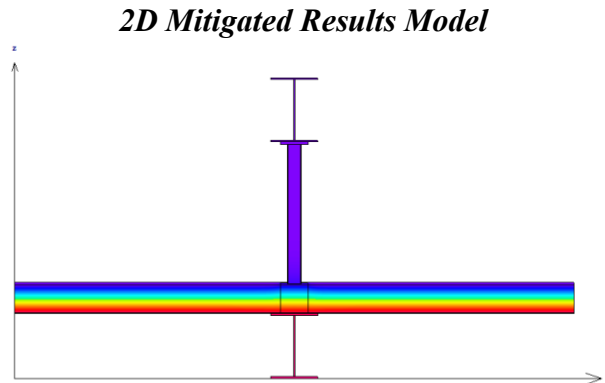
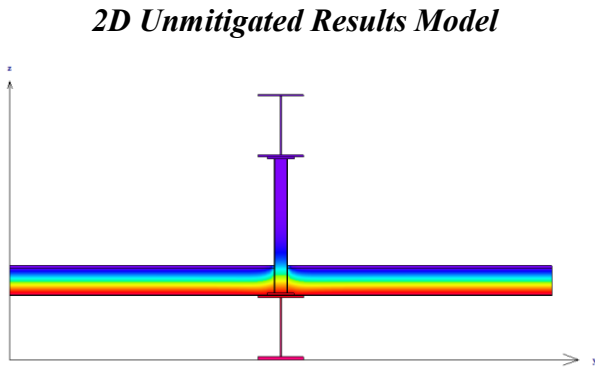
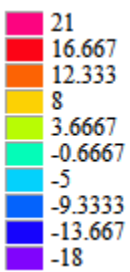
Detail:	Roof post	Climate Zone:	Zone 7
Mitigation Strategy:	9x9x3/8 FRP Shim	Interior Condition:	69.8°F
Area Dimensions:	72x120 inches	Exterior Condition:	-0.4°F
Shim Material:	Vinylester	Unmitigated Model:	RPU7-1-A
Shim Thickness:	3 inches	Mitigated Model:	RPM7-2-C
Insulation Thickness:	6 inches		
Rod Diameter:	0.75 inches		
Rod Spacing:	6 inches o.c.		



U-Value Unmitigated (BTU/h ft ² °F)	U-Value Mitigated (BTU/h ft ² °F)	χ (BTU/hr °F)	% Reduction in χ
0.035	0.032	0.34	31%

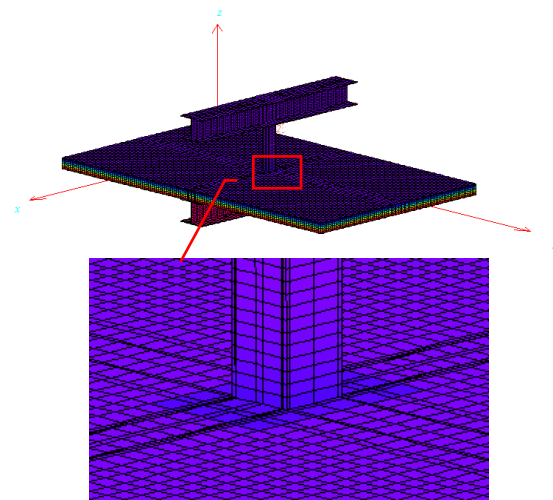
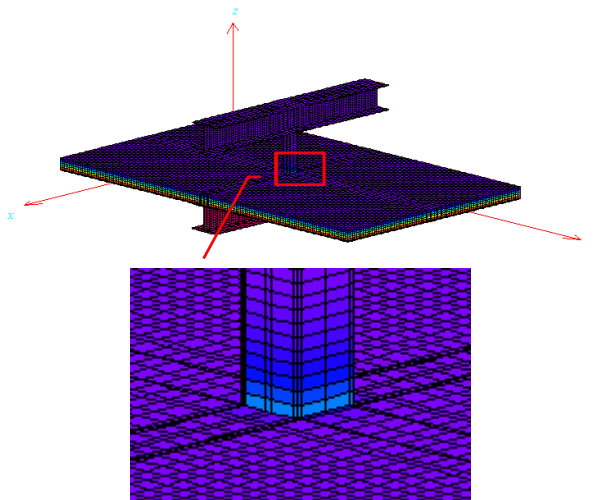
ROOF POST: CLIMATE ZONE 7, 6" PROPRIETARY 1 FRP SHIM

Detail:	Roof post	Climate Zone:	Zone 7
Mitigation Strategy:	9x9x3/8 FRP Shim	Interior Condition:	69.8°F
Area Dimensions:	72x120 inches	Exterior Condition:	-0.4°F
Shim Material:	Proprietary 1	Unmitigated Model:	RPU7-1-A
Shim Thickness:	6 inches	Mitigated Model:	RPM7-11-A
Insulation Thickness:	6 inches		
Rod Diameter:	0.75 inches		
Rod Spacing:	6 inches o.c.		



3D Unmitigated Results Model

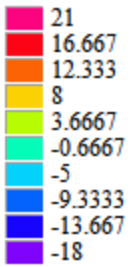
3D Mitigated Results Model



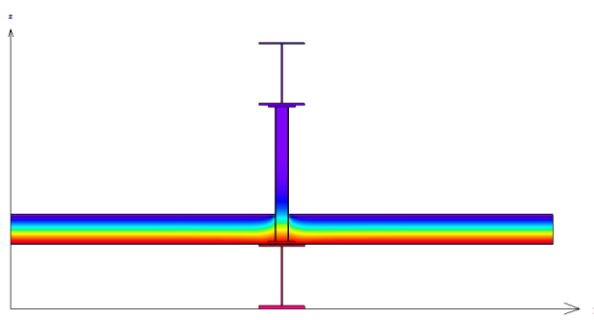
U-Value Unmitigated (BTU/h ft ² °F)	U-Value Mitigated (BTU/h ft ² °F)	χ (BTU/hr °F)	% Reduction in χ
0.035	0.030	0.17	65%

ROOF POST: CLIMATE ZONE 7, 3" PROPRIETARY 1 FRP SHIM

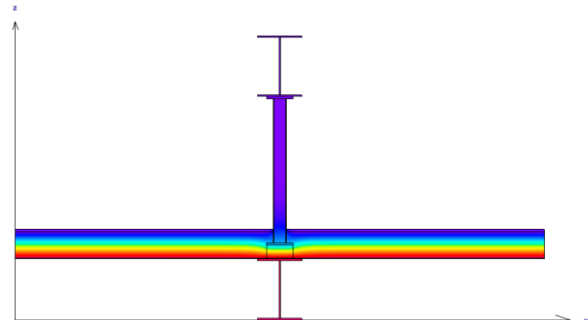
Detail:	Roof post	Climate Zone:	Zone 7
Mitigation Strategy:	9x9x3/8 FRP Shim	Interior Condition:	69.8°F
Area Dimensions:	72x120 inches	Exterior Condition:	-0.4°F
Shim Material:	Proprietary 1	Unmitigated Model:	RPU7-1-A
Shim Thickness:	3 inches	Mitigated Model:	RPM7-11-B
Insulation Thickness:	6 inches		
Rod Diameter:	0.75 inches		
Rod Spacing:	6 inches o.c.		



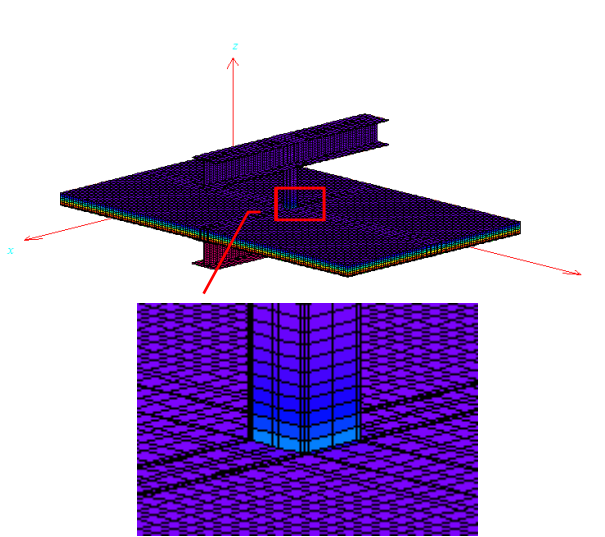
2D Unmitigated Results Model



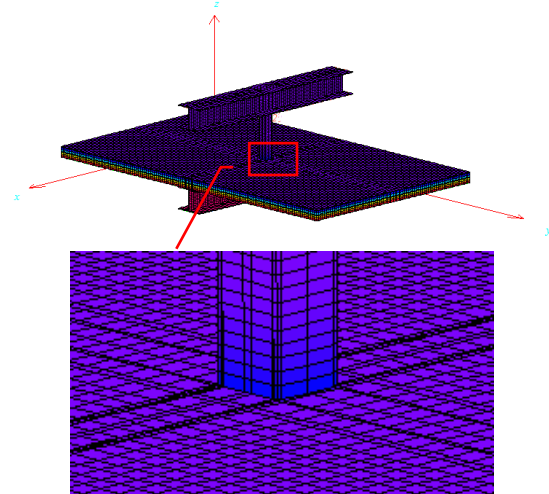
2D Mitigated Results Model



3D Unmitigated Results Model



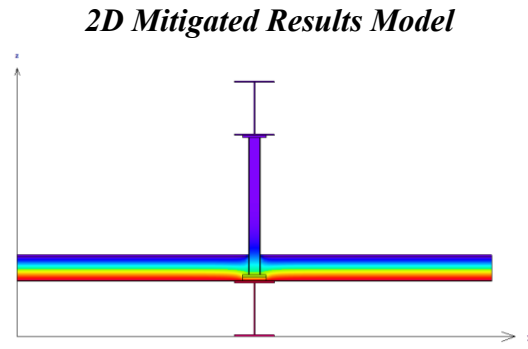
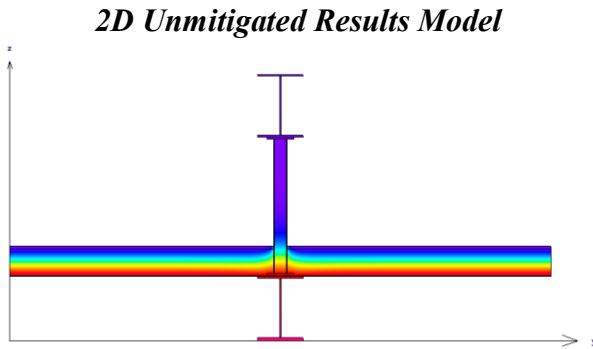
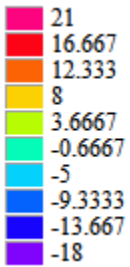
3D Mitigated Results Model



U-Value Unmitigated (BTU/h ft ² °F)	U-Value Mitigated (BTU/h ft ² °F)	χ (BTU/hr °F)	% Reduction in χ
0.035	0.031	0.24	52%

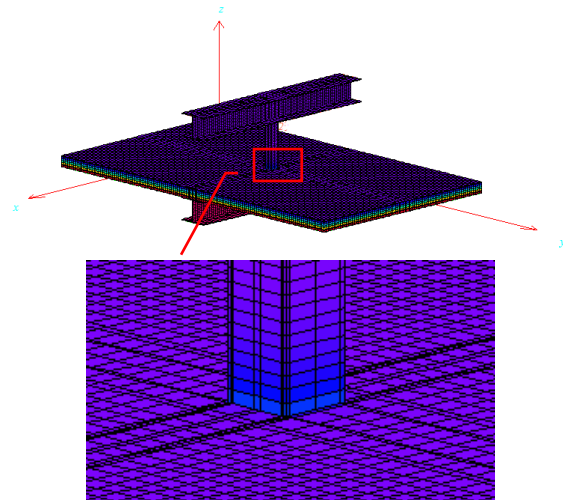
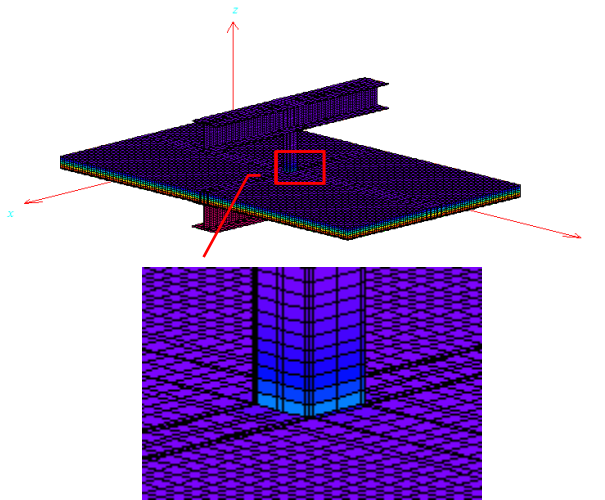
ROOF POST: CLIMATE ZONE 7, 1" PROPRIETARY 1 FRP SHIM

Detail:	Roof post	Climate Zone:	Zone 7
Mitigation Strategy:	9x9x3/8 FRP Shim	Interior Condition:	69.8°F
Area Dimensions:	72x120 inches	Exterior Condition:	-0.4°F
Shim Material:	Proprietary 1	Unmitigated Model:	RPU7-1-A
Shim Thickness:	1 inch	Mitigated Model:	RPM7-11-C
Insulation Thickness:	6 inches		
Rod Diameter:	0.75 inches		
Rod Spacing:	6 inches o.c.		



3D Unmitigated Results Model

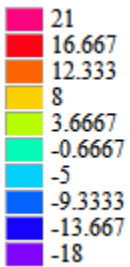
3D Mitigated Results Model



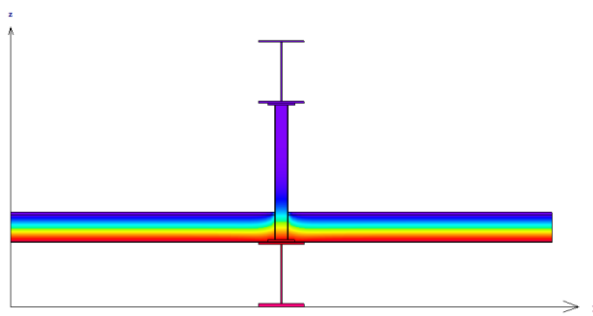
U-Value Unmitigated (BTU/h ft ² °F)	U-Value Mitigated (BTU/h ft ² °F)	χ (BTU/hr °F)	% Reduction in χ
0.035	0.032	0.34	31%

ROOF POST: CLIMATE ZONE 7, 6" PROPRIETARY 2 FRP SHIM

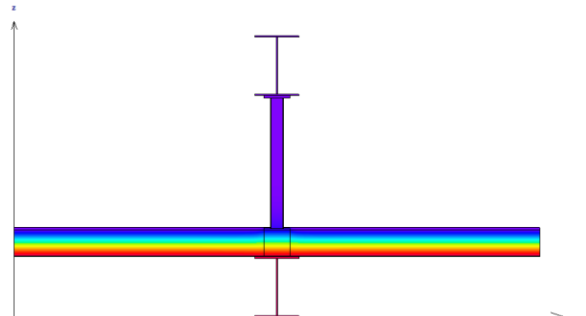
Detail:	Roof post	Climate Zone:	Zone 7
Mitigation Strategy:	9x9x3/8 FRP Shim	Interior Condition:	69.8°F
Area Dimensions:	72x120 inches	Exterior Condition:	-0.4°F
Shim Material:	Proprietary 2	Unmitigated Model:	RPU7-1-A
Shim Thickness:	6 inches	Mitigated Model:	RPM7-12-A
Insulation Thickness:	6 inches		
Rod Diameter:	0.75 inches		
Rod Spacing:	6 inches o.c.		



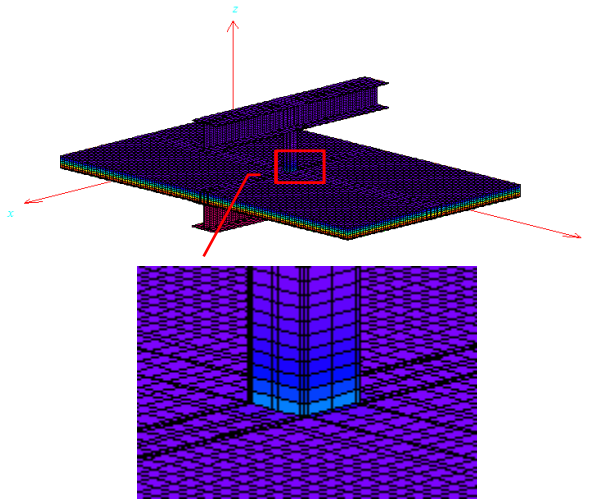
2D Unmitigated Results Model



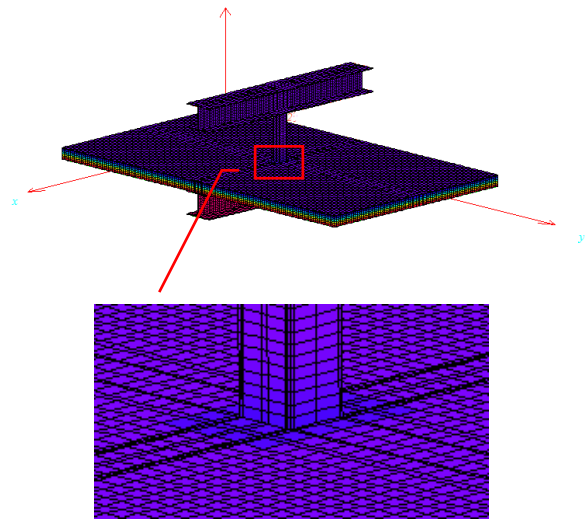
2D Mitigated Results Model



3D Unmitigated Results Model



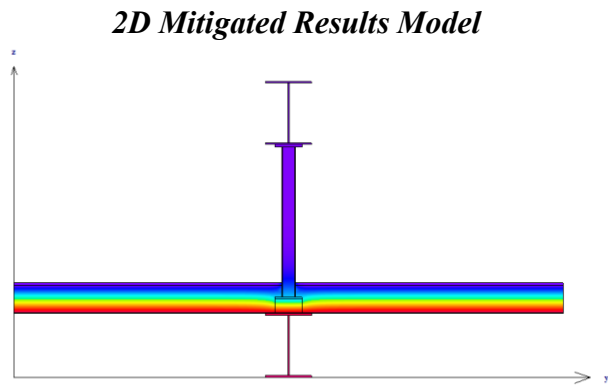
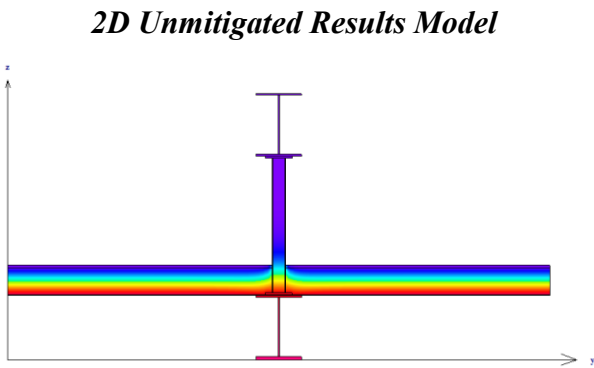
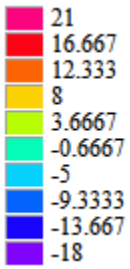
3D Mitigated Results Model



U-Value Unmitigated (BTU/h ft ² °F)	U-Value Mitigated (BTU/h ft ² °F)	χ (BTU/hr °F)	% Reduction in χ
0.035	0.030	0.20	60%

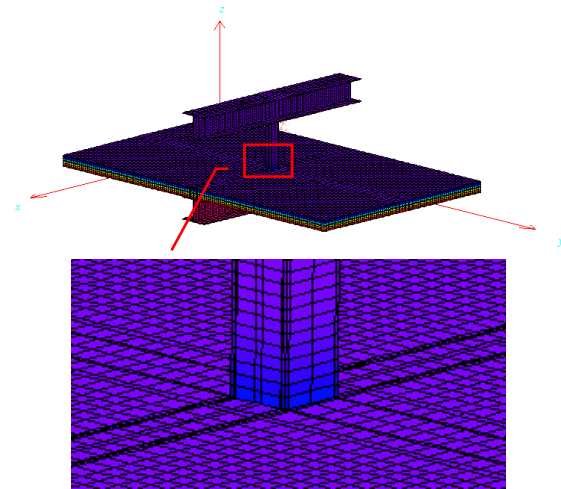
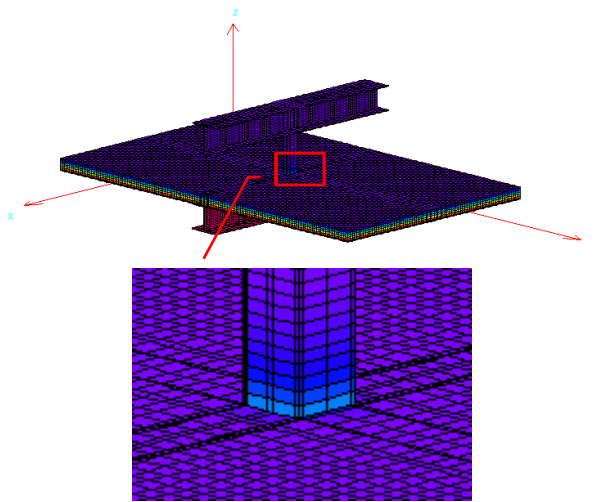
ROOF POST: CLIMATE ZONE 7, 3" PROPRIETARY 2 FRP SHIM

Detail:	Roof post	Climate Zone:	Zone 7
Mitigation Strategy:	9x9x3/8 FRP Shim	Interior Condition:	69.8°F
Area Dimensions:	72x120 inches	Exterior Condition:	-0.4°F
Shim Material:	Proprietary 2	Unmitigated Model:	RPU7-1-A
Shim Thickness:	3 inches	Mitigated Model:	RPM7-12-B
Insulation Thickness:	6 inches		
Rod Diameter:	0.75 inches		
Rod Spacing:	6 inches o.c.		



3D Unmitigated Results Model

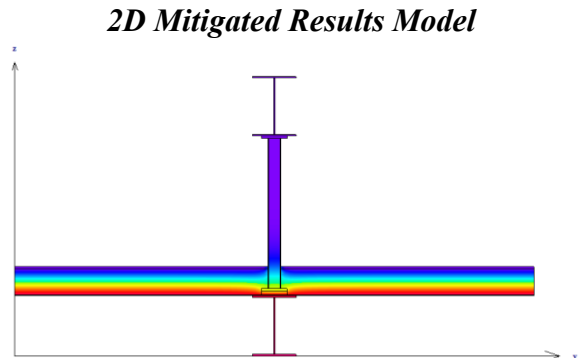
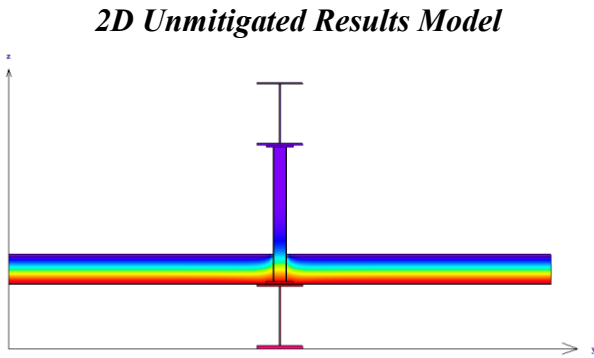
3D Mitigated Results Model



U-Value Unmitigated (BTU/h ft ² °F)	U-Value Mitigated (BTU/h ft ² °F)	χ (BTU/hr °F)	% Reduction in χ
0.035	0.031	0.26	47%

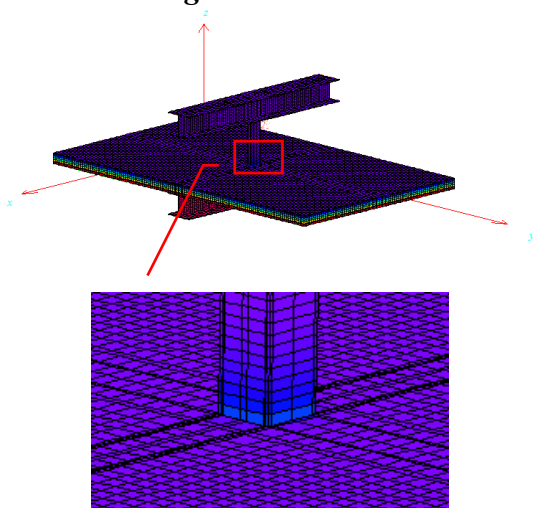
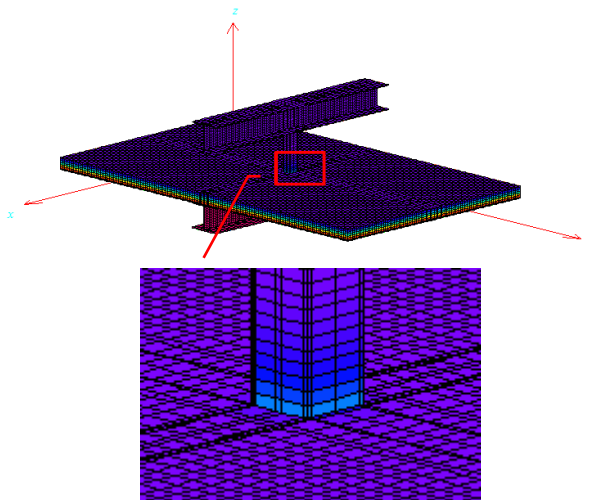
ROOF POST: CLIMATE ZONE 7, 1" PROPRIETARY 2 FRP SHIM

Detail:	Roof post	Climate Zone:	Zone 7
Mitigation Strategy:	9x9x3/8 FRP Shim	Interior Condition:	69.8°F
Area Dimensions:	72x120 inches	Exterior Condition:	-0.4°F
Shim Material:	Proprietary 2	Unmitigated Model:	RPU7-1-A
Shim Thickness:	1 inch	Mitigated Model:	RPM7-12-C
Insulation Thickness:	6 inches		
Rod Diameter:	0.75 inches		
Rod Spacing:	6 inches o.c.		



3D Unmitigated Results Model

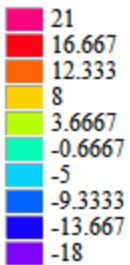
3D Mitigated Results Model



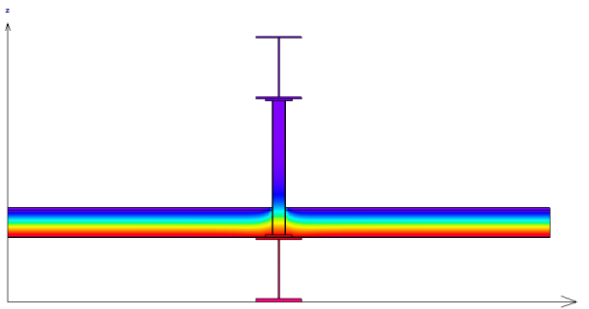
U-Value Unmitigated (BTU/h ft ² °F)	U-Value Mitigated (BTU/h ft ² °F)	χ (BTU/hr °F)	% Reduction in χ
0.035	0.033	0.36	27%

ROOF POST: CLIMATE ZONE 7, FRP HSS3x3x3/8 POST

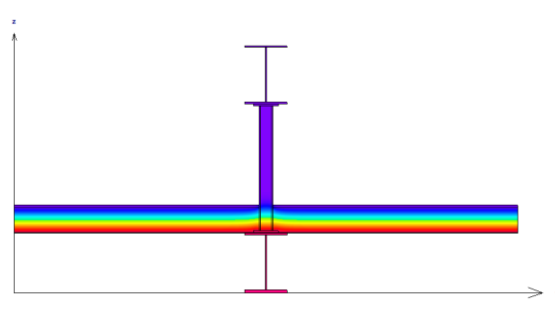
Detail:	Roof post	Climate Zone:	Zone 7
Mitigation Strategy:	9x9x3/8 FRP Shim	Interior Condition:	69.8°F
Area Dimensions:	72x120 inches	Exterior Condition:	-0.4°F
Shim Material:	N/A	Unmitigated Model:	RPU7-1-A
Shim Thickness:	N/A	Mitigated Model:	RPM7-1-C
Insulation Thickness:	6 inches		
Rod Diameter:	0.75 inches		
Rod Spacing:	6 inches o.c.		



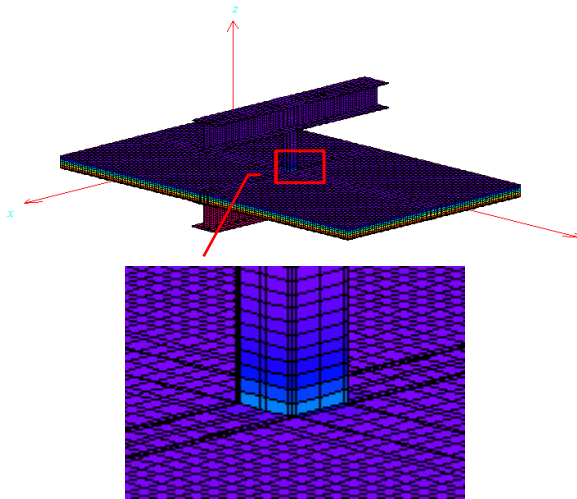
2D Unmitigated Results Model



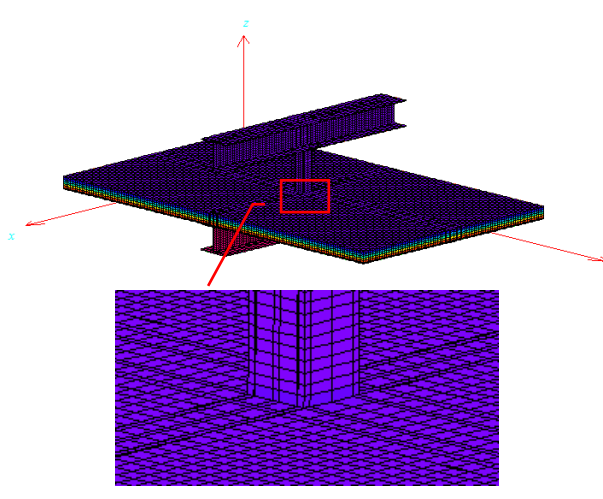
2D Mitigated Results Model



3D Unmitigated Results Model



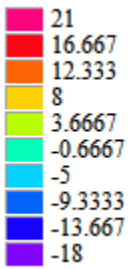
3D Mitigated Results Model



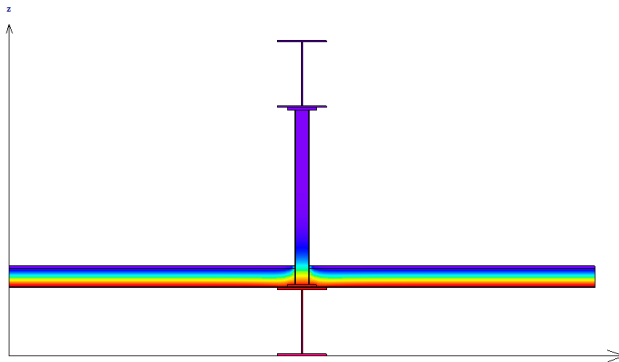
U-Value Unmitigated (BTU/h ft ² °F)	U-Value Mitigated (BTU/h ft ² °F)	χ (BTU/hr °F)	% Reduction in χ
0.035	0.027	0.03	95%

ROOF POST: CLIMATE ZONE 1, 3" VINYLESTER FRP SHIM

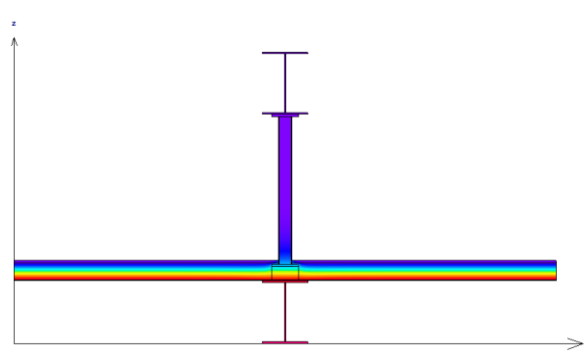
Detail:	Roof post	Climate Zone:	Zone 1
Mitigation Strategy:	9x9x3/8 FRP Shim	Interior Condition:	69.8°F
Area Dimensions:	72x120 inches	Exterior Condition:	-0.4°F
Shim Material:	Vinylester	Unmitigated Model:	RPU1-1-B
Shim Thickness:	3 inches	Mitigated Model:	RPM1-2-B
Insulation Thickness:	3.8 inches		
Rod Diameter:	0.75 inches		
Rod Spacing:	6 inches o.c.		



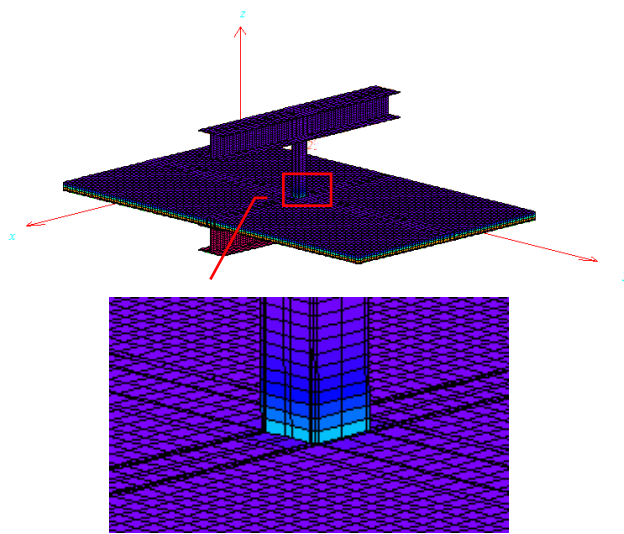
2D Unmitigated Results Model



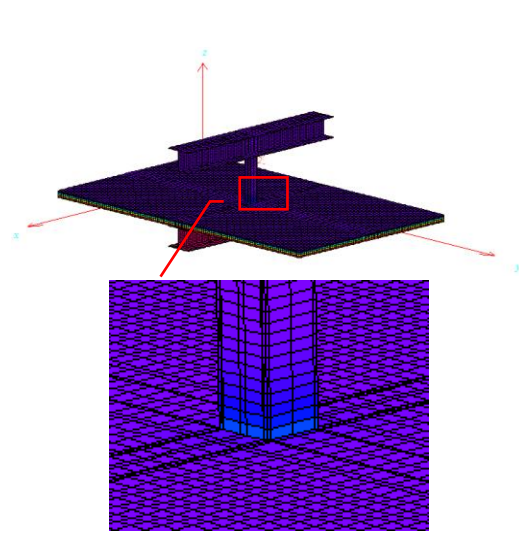
2D Mitigated Results Model



3D Unmitigated Results Model



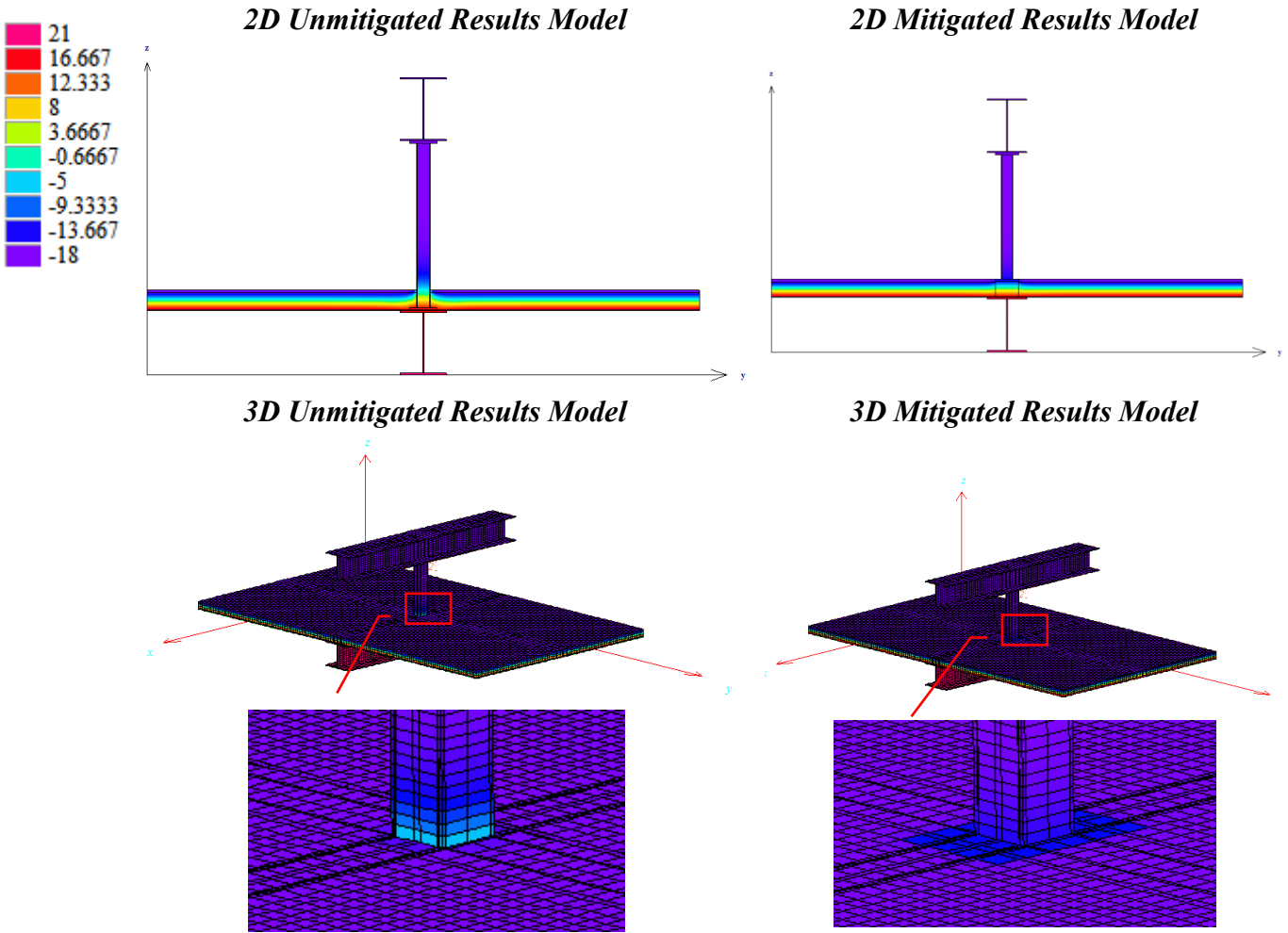
3D Mitigated Results Model



U-Value Unmitigated (BTU/h ft ² °F)	U-Value Mitigated (BTU/h ft ² °F)	χ (BTU/hr °F)	% Reduction in χ
0.052	0.048	0.40	34%

ROOF POST: CLIMATE ZONE 1, 4" VINYLESTER FRP SHIM

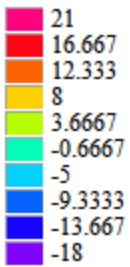
Detail:	Roof post	Climate Zone:	Zone 1
Mitigation Strategy:	9x9x3/8 FRP Shim	Interior Condition:	69.8°F
Area Dimensions:	72x120 inches	Exterior Condition:	-0.4°F
Shim Material:	Vinylester	Unmitigated Model:	RPU1-1-B
Shim Thickness:	4 inches	Mitigated Model:	RPM1-2-D
Insulation Thickness:	3.8 inches		
Rod Diameter:	0.75 inches		
Rod Spacing:	6 inches o.c.		



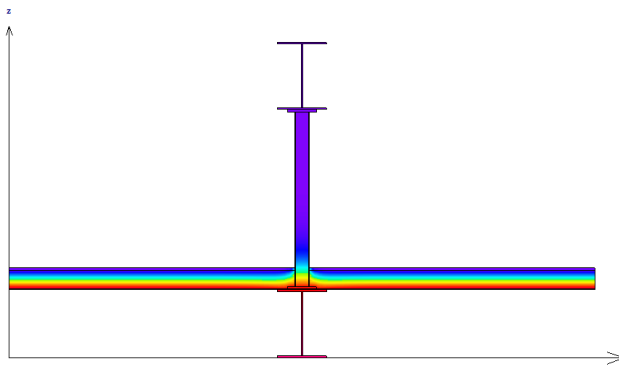
U-Value Unmitigated (BTU/h ft ² °F)	U-Value Mitigated (BTU/h ft ² °F)	χ (BTU/hr °F)	% Reduction in χ
0.052	0.048	0.41	33%

ROOF POST: CLIMATE ZONE 1, 1" VINYLESTER FRP SHIM

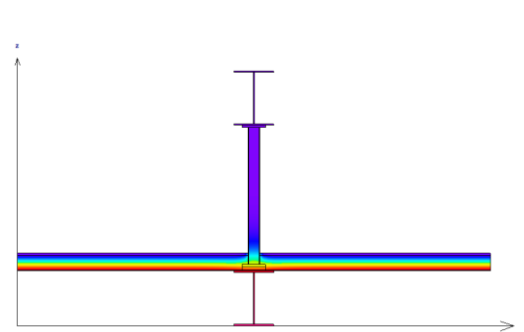
Detail:	Roof post	Climate Zone:	Zone 1
Mitigation Strategy:	9x9x3/8 FRP Shim	Interior Condition:	69.8°F
Area Dimensions:	72x120 inches	Exterior Condition:	-0.4°F
Shim Material:	Vinylester	Unmitigated Model:	RPU1-1-B
Shim Thickness:	1 inch	Mitigated Model:	RPM1-2-E
Insulation Thickness:	3.8 inches		
Rod Diameter:	0.75 inches		
Rod Spacing:	6 inches o.c.		



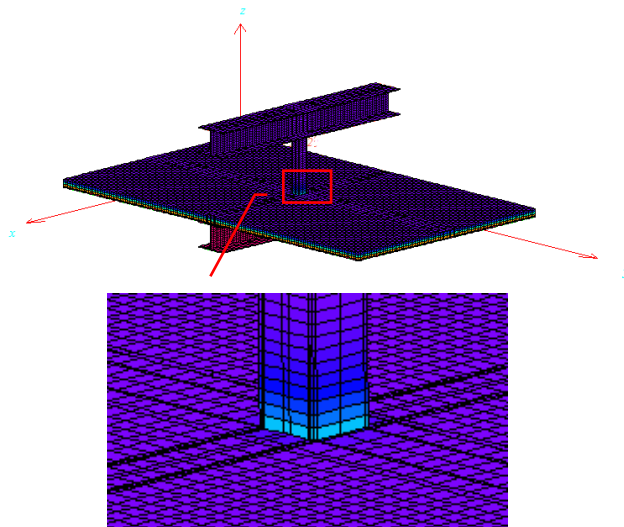
2D Unmitigated Results Model



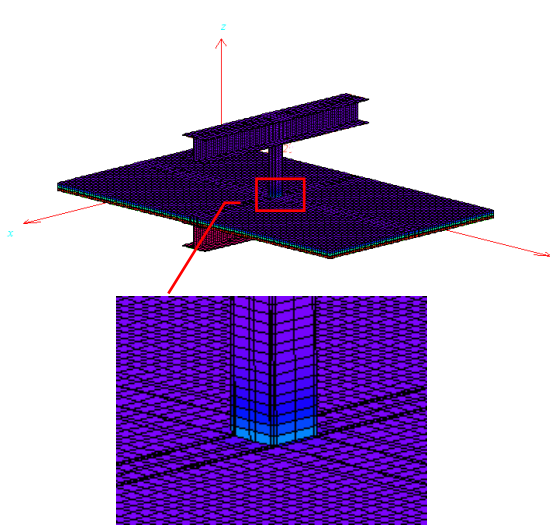
2D Mitigated Results Model



3D Unmitigated Results Model



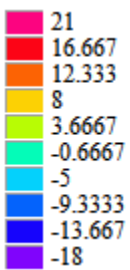
3D Mitigated Results Model



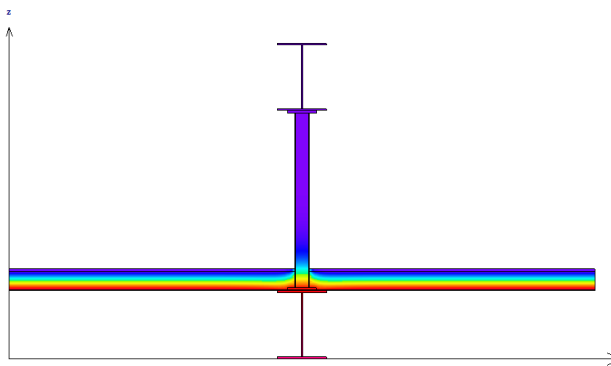
U-Value Unmitigated (BTU/h ft ² °F)	U-Value Mitigated (BTU/h ft ² °F)	χ (BTU/hr °F)	% Reduction in χ
0.052	0.050	0.50	18%

ROOF POST: CLIMATE ZONE 1, TWO 1" VINYLESTER FRP SHIMS

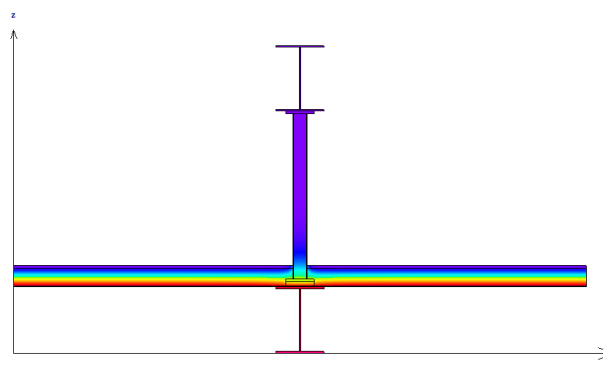
Detail:	Roof post	Climate Zone:	Zone 1
Mitigation Strategy:	9x9x3/8 FRP	Interior Condition:	69.8°F
Area Dimensions:	Shim	Exterior Condition:	-0.4°F
Shim Material:	72x120 inches	Unmitigated Model:	RPU1-1-B
Shim Thickness:	2 vinylester shims	Mitigated Model:	RPM1-2-F
Shim Thickness:	1 inch		
Insulation Thickness:	3.8 inches		
Rod Diameter:	0.75 inches		
Rod Spacing:	6 inches o.c.		



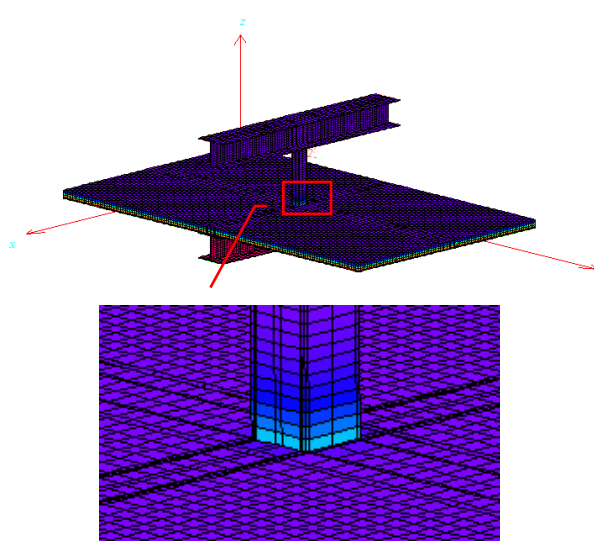
2D Unmitigated Results Model



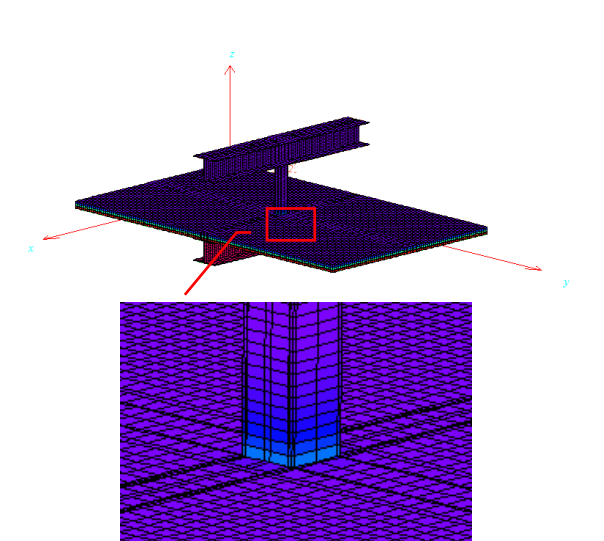
2D Mitigated Results Model



3D Unmitigated Results Model



3D Mitigated Results Model



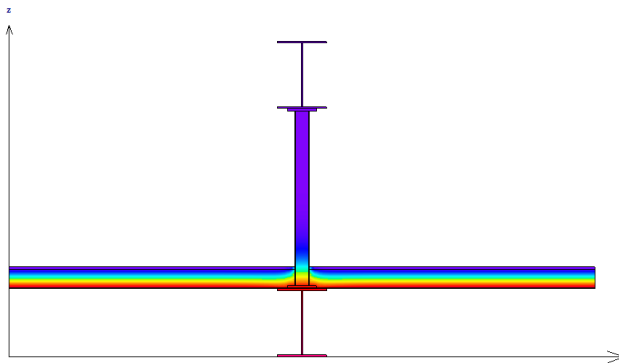
U-Value Unmitigated (BTU/h ft ² °F)	U-Value Mitigated (BTU/h ft ² °F)	χ (BTU/hr °F)	% Reduction in χ
0.052	0.049	0.46	25%

ROOF POST: CLIMATE ZONE 1, 1" VINYLESTER FRP SHIM WITH ROD BUSHINGS

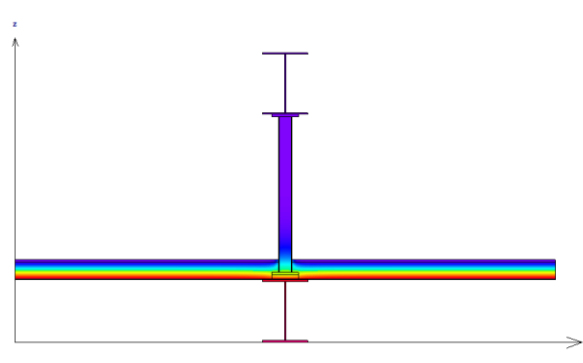
Detail:	Roof post	Climate Zone:	Zone 1
Mitigation Strategy:	9x9x3/8 FRP Shim	Interior Condition:	69.8°F
Area Dimensions:	72x120 inches	Exterior Condition:	-0.4°F
Shim Material:	Vinylester	Unmitigated Model:	RPU1-1-B
Shim Thickness:	1 inch	Mitigated Model:	RPM1-2-G
Insulation Thickness:	3.8 inches		
Rod Diameter:	0.75 inches with bushings		
Rod Spacing:	6 inches o.c.		



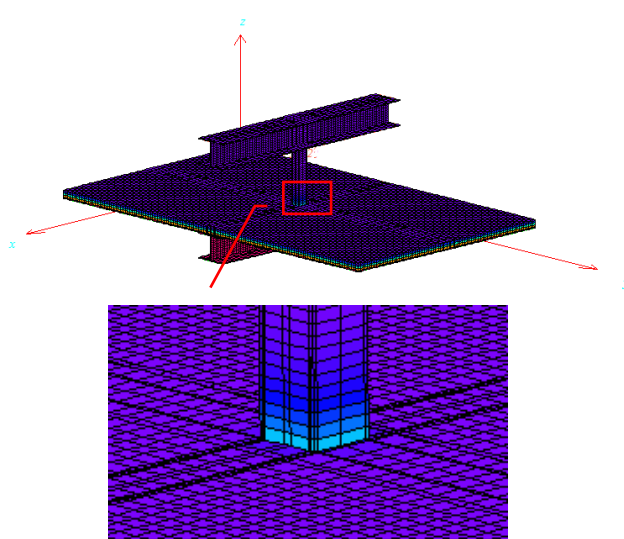
2D Unmitigated Results Model



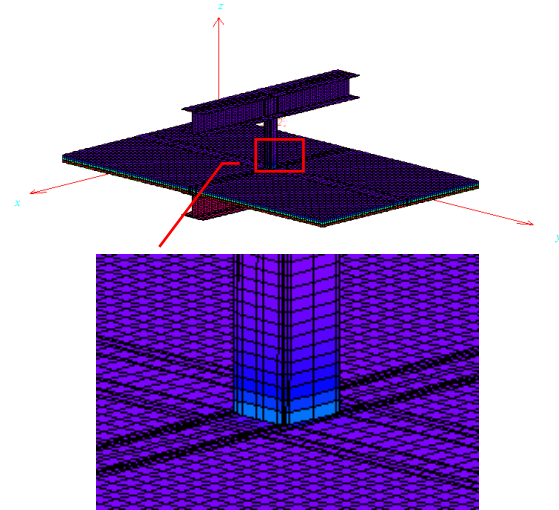
2D Mitigated Results Model



3D Unmitigated Results Model



3D Mitigated Results Model



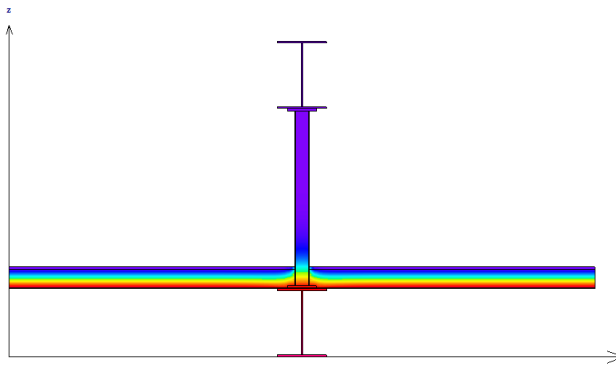
U-Value Unmitigated (BTU/h ft ² °F)	U-Value Mitigated (BTU/h ft ² °F)	χ (BTU/hr °F)	% Reduction in χ
0.052	0.049	0.45	25%

ROOF POST: CLIMATE ZONE 1, BUSHINGS AT STEEL RODS

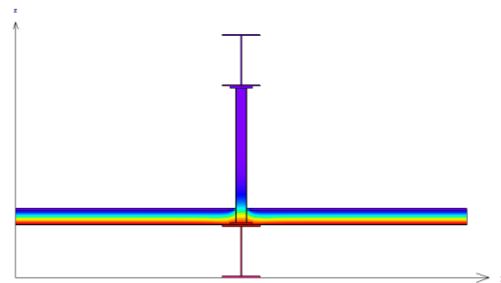
Detail:	Roof post	Climate Zone:	Zone 1
Mitigation Strategy:	9x9x3/8 FRP Shim	Interior Condition:	69.8°F
Area Dimensions:	72x120 inches	Exterior Condition:	-0.4°F
Shim Material:	N/A	Unmitigated Model:	RPU1-1-B
Shim Thickness:	N/A	Mitigated Model:	RPM1-2-H
Insulation Thickness:	3.8 inches		
Rod Diameter:	0.75 inches with bushings		
Rod Spacing:	6 inches o.c.		



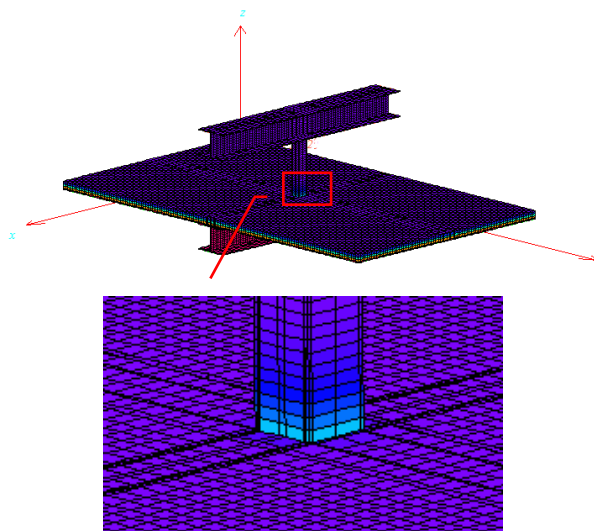
2D Unmitigated Results Model



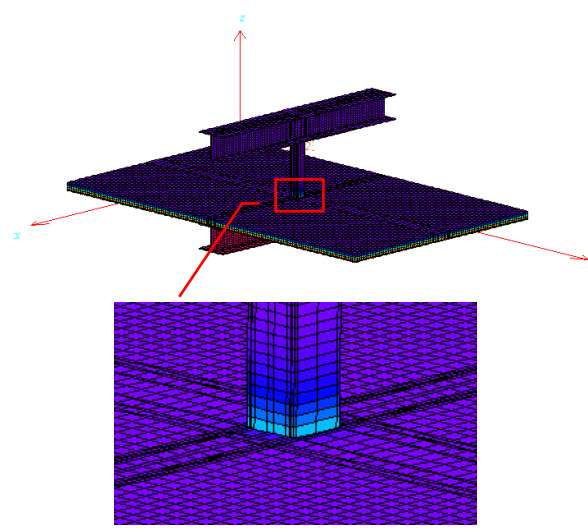
2D Mitigated Results Model



3D Unmitigated Results Model



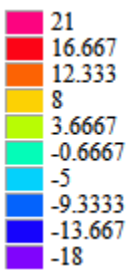
3D Mitigated Results Model



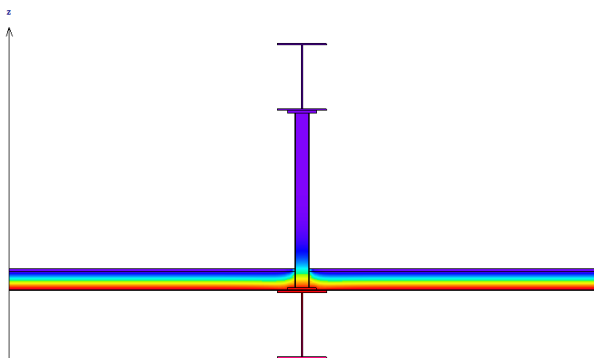
U-Value Unmitigated (BTU/h ft ² °F)	U-Value Mitigated (BTU/h ft ² °F)	χ (BTU/hr °F)	% Reduction in χ
0.052	0.052	0.61	0%

ROOF POST: CLIMATE ZONE 1, FRP HSS3x3x3/8 POST

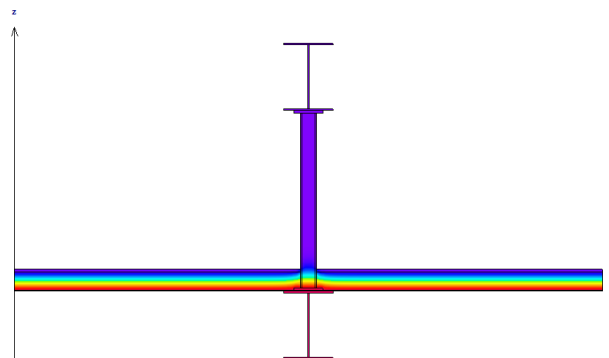
Detail:	Roof post	Climate Zone:	Zone 1
Mitigation Strategy:	9x9x3/8 FRP	Interior Condition:	69.8°F
	Shim	Exterior Condition:	-0.4°F
Area Dimensions:	72x120 inches	Unmitigated Model:	RPU1-1-B
Shim Material:	N/A	Mitigated Model:	RPM1-1-D
Shim Thickness:	N/A		
Insulation Thickness:	3.8 inches		
Rod Diameter:	0.75 inches		
Rod Spacing:	6 inches o.c.		



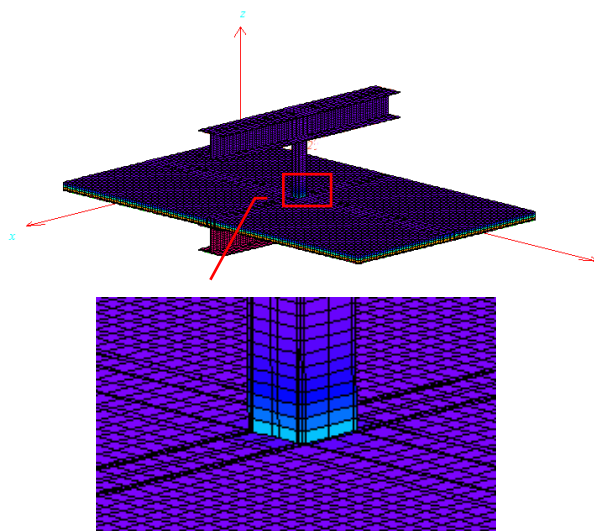
2D Unmitigated Results Model



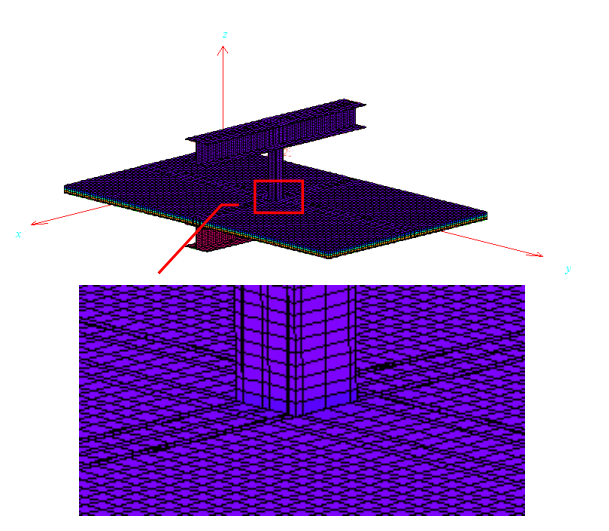
2D Mitigated Results Model



3D Unmitigated Results Model



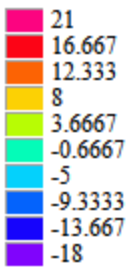
3D Mitigated Results Model



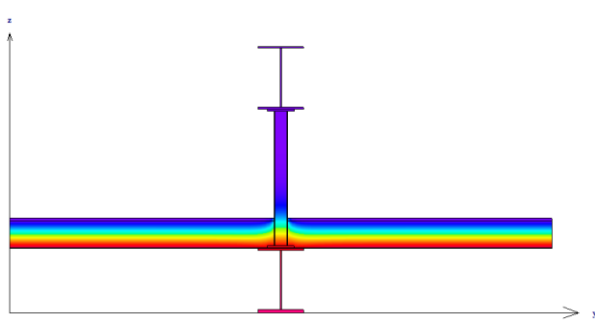
U-Value Unmitigated (BTU/h ft ² °F)	U-Value Mitigated (BTU/h ft ² °F)	χ (BTU/hr °F)	% Reduction in χ
0.052	0.042	0.04	94%

ROOF POST: CLIMATE ZONE 7, 6" VINYLESTER FRP SHIM, A307 RODS

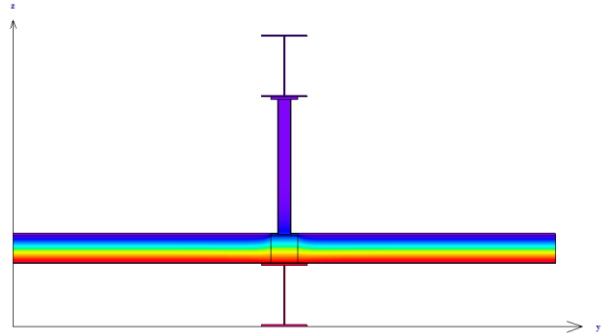
Detail:	Roof post	Climate Zone:	Zone 7
Mitigation Strategy:	9x9x3/8 FRP	Interior Condition:	69.8°F
	Shim	Exterior Condition:	-0.4°F
Area Dimensions:	72x120 inches	Unmitigated Model:	RPU7-7-A
Shim Material:	Vinylester	Mitigated Model:	RPM7-8-A
Shim Thickness:	6 inches		
Insulation Thickness:	6 inches		
Rod Diameter:	0.75 inches		
Rod Spacing:	6 inches o.c.		
Rod Spec:	A307		



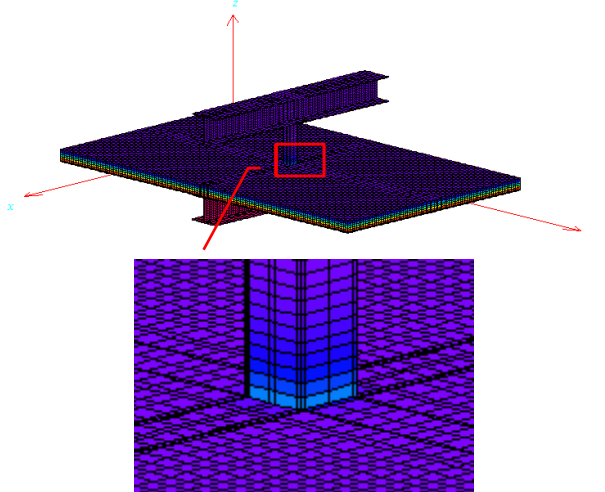
2D Unmitigated Results Model



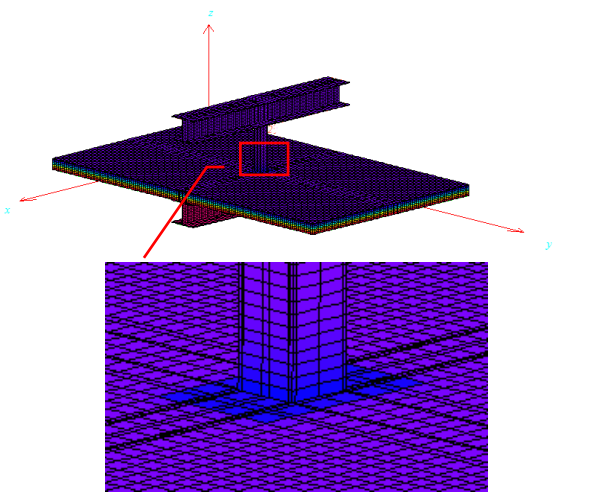
2D Mitigated Results Model



3D Unmitigated Results Model



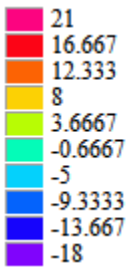
3D Mitigated Results Model



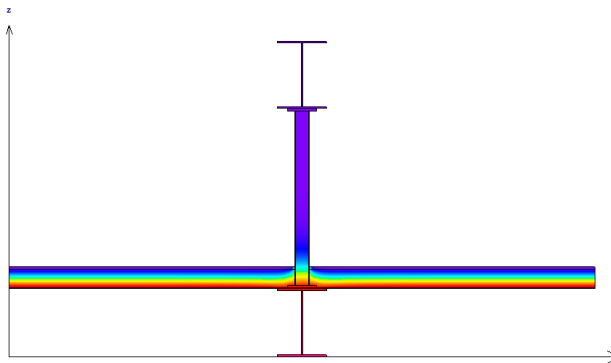
U-Value Unmitigated (BTU/h ft ² °F)	U-Value Mitigated (BTU/h ft ² °F)	χ (BTU/hr °F)	% Reduction in χ
0.035	0.034	0.44	10%

ROOF POST: CLIMATE ZONE 1, 3" VINYLESTER FRP SHIM, A307 RODS

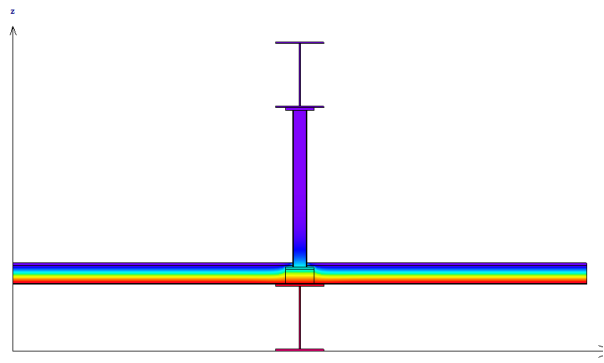
Detail:	Roof post	Climate Zone:	Zone 1
Mitigation Strategy:	9x9x3/8 FRP	Interior Condition:	69.8°F
Area Dimensions:	72x120 inches	Exterior Condition:	-0.4°F
Shim Material:	Vinylester	Unmitigated Model:	RPU1-7-B
Shim Thickness:	3 inches	Mitigated Model:	RPM1-8-B
Insulation Thickness:	3.8 inches		
Rod Diameter:	0.75 inches		
Rod Spacing:	6 inches o.c.		
Rod Spec:	A307		



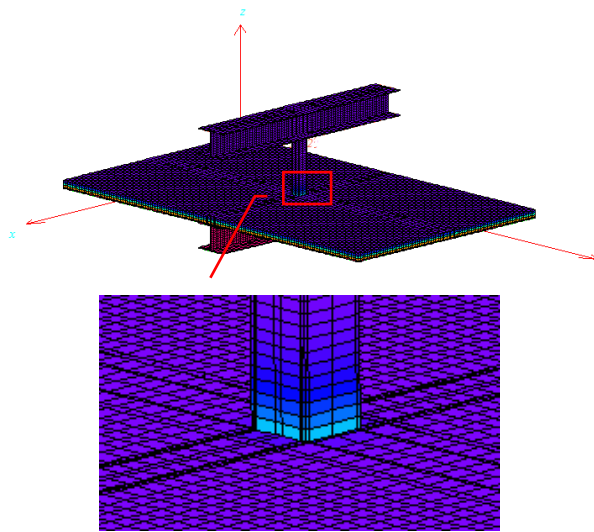
2D Unmitigated Results Model



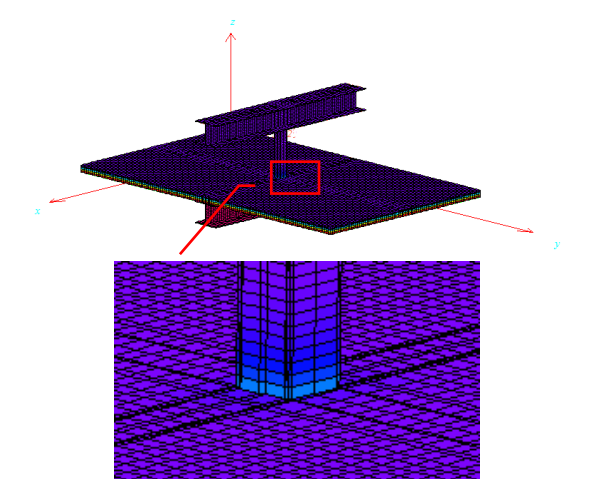
2D Mitigated Results Model



3D Unmitigated Results Model



3D Mitigated Results Model



U-Value Unmitigated (BTU/h ft ² °F)	U-Value Mitigated (BTU/h ft ² °F)	χ (BTU/hr °F)	% Reduction in χ
0.052	0.050	0.51	16%

Appendix E.3 – Results Sheets for Canopy Beams

CANOPY BEAM: CLIMATE ZONE 7, 3" VINYLESTER SHIM

Detail: Canopy Beam

Model length: 80"

Fastener: 3/4" dia. B8 Class 2 SS

Mitigation Strategy: 3" Vinylester shim

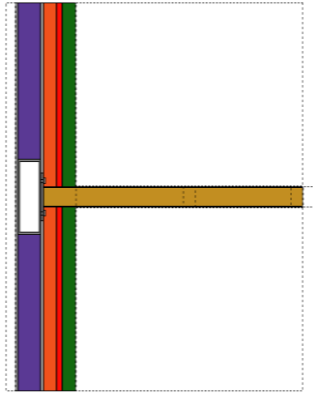
Climate Zone: 7

Exterior Temperature: -0.4 F

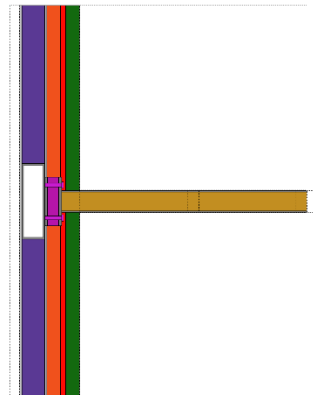
Interior Temperature: 69.8 F

Unmitigated filename: CBU7-7-A

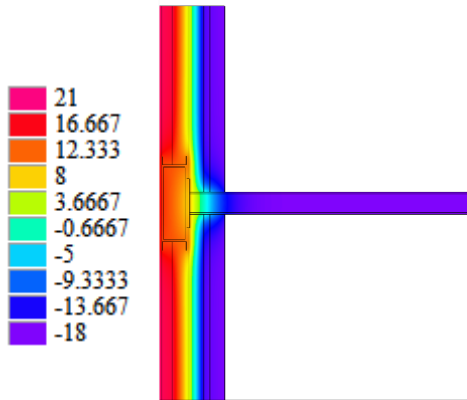
Mitigated filename: CBM7-2-A



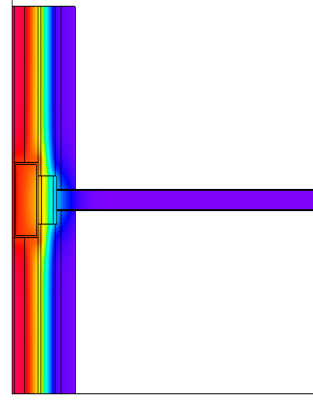
Unmitigated 2D Assembly Section



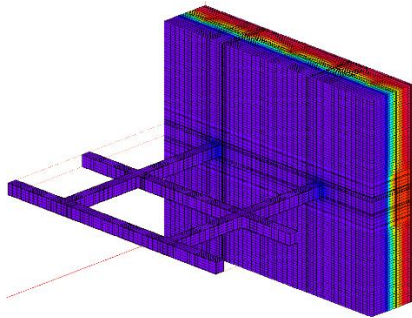
Mitigated 2D Assembly Section



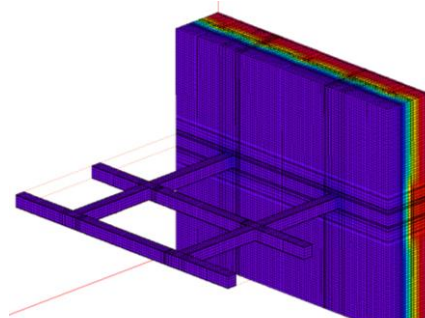
Unmitigated 2D Results Model



Mitigated 2D Results Model



Unmitigated 3D Results Model



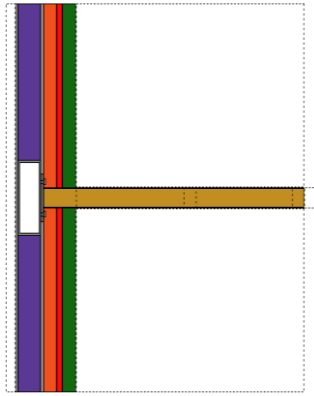
Mitigated 3D Results Model

U-Value Unmitigated (BTU/h ft ² °F)	U-Value Mitigated (BTU/h ft ² °F)	χ per beam (BTU/hr °F)	% Reduction in χ
0.067	0.065	0.46	8%

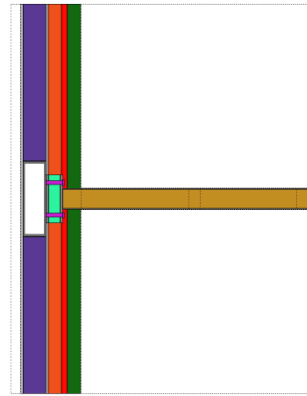
CANOPY BEAM: CLIMATE ZONE 7, 3" PROPRIETARY 1 SHIM

Detail: Canopy Beam
Model length: 80"
Fastener: 3/4" dia. B8 Class 2 SS
Mitigation Strategy: 3" Armadillo Armatherm shim

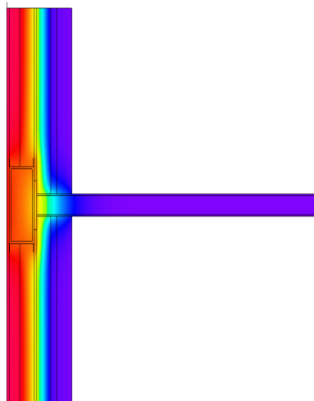
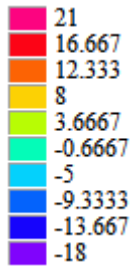
Climate Zone: 7
Exterior Temperature: -0.4 F
Interior Temperature: 69.8 F
Unmitigated filename: CBU7-7-A
Mitigated filename: CBM7-11-A



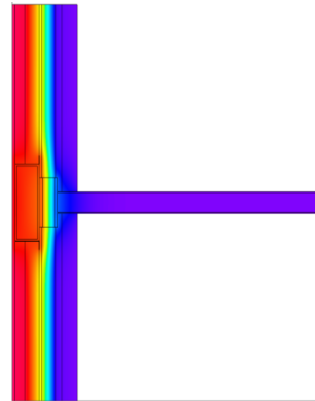
Unmitigated 2D Assembly Section



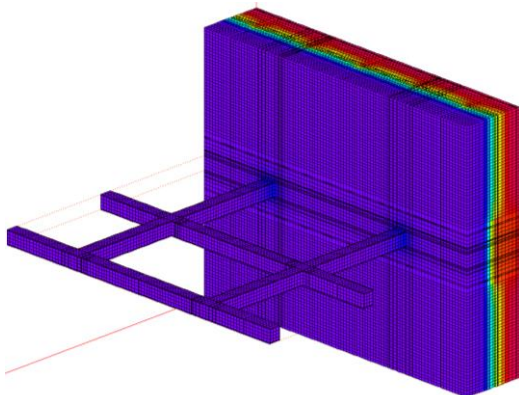
Mitigated 2D Assembly Section



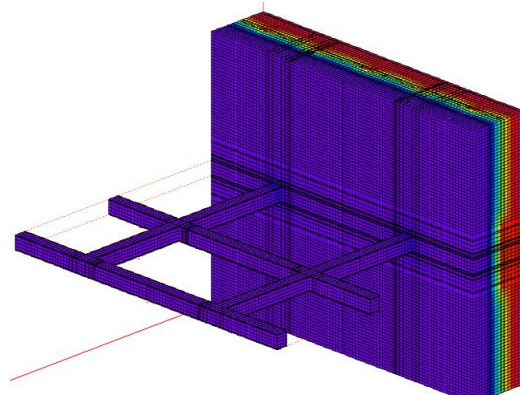
Unmitigated 2D Results Model



Mitigated 2D Results Model



Unmitigated 3D Results Model



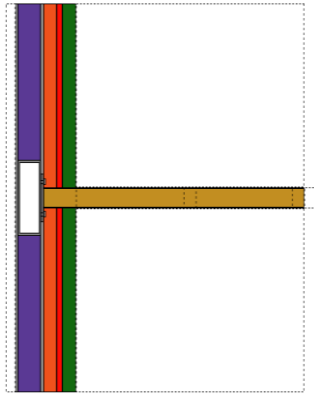
Mitigated 3D Results Model

U-Value Unmitigated (BTU/h ft ² °F)	U-Value Mitigated (BTU/h ft ² °F)	χ per beam (BTU/hr °F)	% Reduction in χ
0.067	0.059	0.35	30%

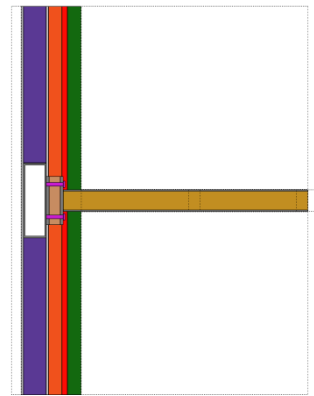
CANOPY BEAM: CLIMATE ZONE 7, 3" PROPRIETARY 2 SHIM

Detail: Canopy Beam
Model length: 80"
Fastener: 3/4" dia. B8 Class 2 SS
Mitigation Strategy: 3" Fabreeka TIM shim

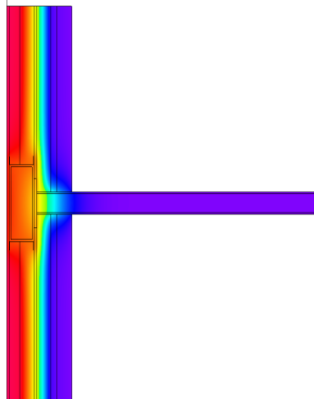
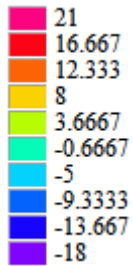
Climate Zone: 7
Exterior Temperature: -0.4 F
Interior Temperature: 69.8 F
Unmitigated filename: CBU7-7-A
Mitigated filename: CBM7-12-A



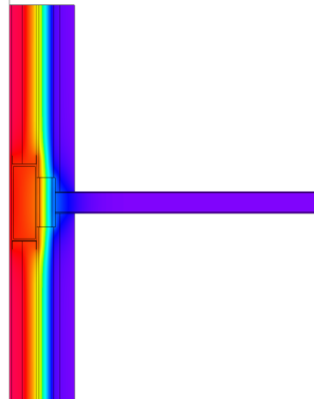
Unmitigated 2D Assembly Section



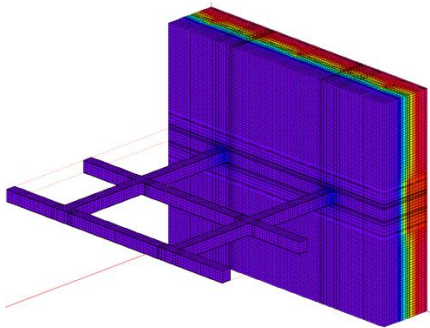
Mitigated 2D Assembly Section



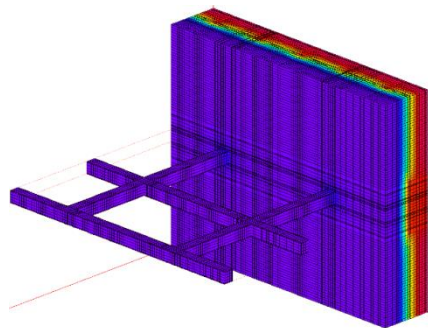
Unmitigated 2D Results Model



Mitigated 2D Results Model



Unmitigated 3D Results Model



Mitigated 3D Results Model

U-Value Unmitigated (BTU/h ft ² °F)	U-Value Mitigated (BTU/h ft ² °F)	χ per beam (BTU/hr °F)	% Reduction in χ
0.067	0.060	0.37	25%

CANOPY BEAM: CLIMATE ZONE 7, 1" VINYLESTER SHIM

Detail: Canopy Beam

Model length: 80"

Fastener: 3/4" dia. B8 Class 2 SS

Mitigation Strategy: 1" Vinylester shim

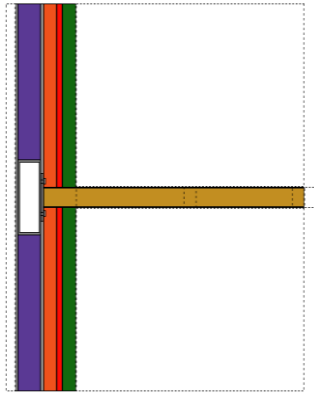
Climate Zone: 7

Exterior Temperature: -0.4 F

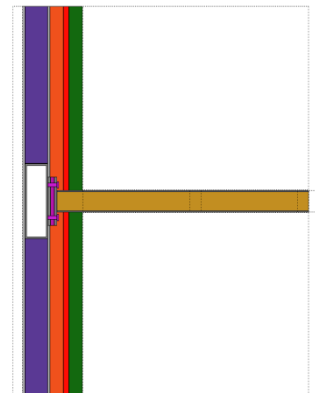
Interior Temperature: 69.8 F

Unmitigated filename: CBU7-7-A

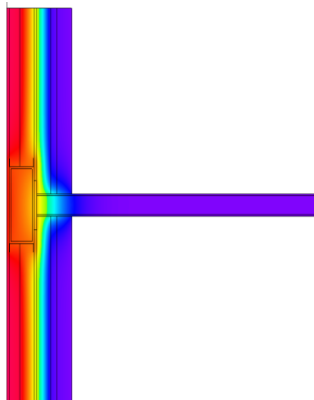
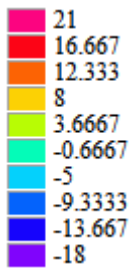
Mitigated filename: CBM-7-2-C



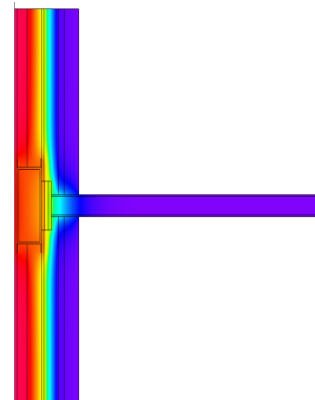
Unmitigated 2D Assembly Section



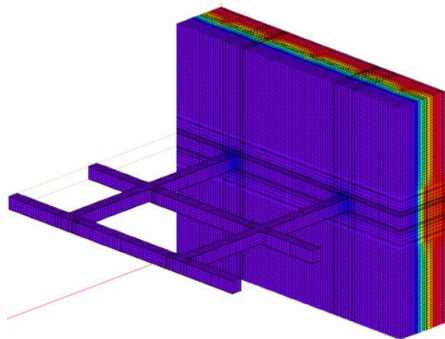
Mitigated 2D Assembly Section



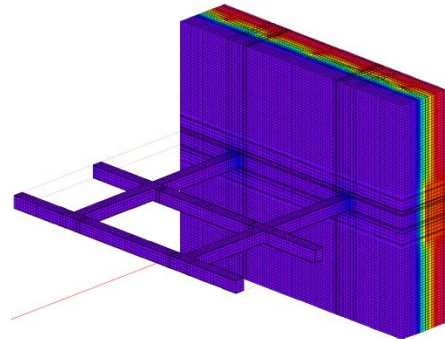
Unmitigated 2D Results Model



Mitigated 2D Results Model



Unmitigated 3D Results Model



Mitigated 3D Results Model

U-Value Unmitigated (BTU/h ft ² °F)	U-Value Mitigated (BTU/h ft ² °F)	χ per beam (BTU/hr °F)	% Reduction in χ
0.067	0.065	0.47	7%

Appendix E.4 – Structural Testing Matrix for Roof Posts

Test Name	Specimen Type	MITIGATION STRATEGY				SPECIMEN INFORMATION											
		Type	Material	Thick (in)	Length (in)*	Post	HSS Length (in)	Weld	Base Plate	Rod Dia. (in)	Rod Spacing (in)	Rod Spec	Top Plate	Bolt Dia. (in)	Bolt Spacing (in)	Bolt Spec	Loading
R1	designed	-	-	-	30	HSS 3x3x3/16	20.125	CJP	9x9x3/8"	0.5	6" oc	B8 Class 2	10x10x1"	1	6" oc	A325	Monotonic
R2	designed	shim	vinylester	3	30	HSS 3x3x3/16	14.125	CJP	9x9x3/8"	0.5	6" oc	B8 Class 2	10x10x1"	1	6" oc	A325	Monotonic
R3	designed	sleeve	FRP 4x4x1/2	-	30	HSS 3x3x3/16	20.125	CJP	9x9x3/8"	0.5	6" oc	B8 Class 2	10x10x1"	1	6" oc	A325	Monotonic
R4	designed	-	-	-	30	HSS 3x3x3/16	20.125	CJP	9x9x3/8"	0.5	6" oc	B8 Class 2	10x10x1"	1	6" oc	A325	Cyclic
R5	designed	shim	vinylester	3	30	HSS 3x3x3/16	14.125	CJP	9x9x3/8"	0.5	6" oc	B8 Class 2	10x10x1"	1	6" oc	A325	Cyclic
R6	designed	sleeve	FRP 4x4x1/2	-	30	HSS 3x3x3/16	20.125	CJP	9x9x3/8"	0.5	6" oc	B8 Class 2	10x10x1"	1	6" oc	A325	Cyclic
R7	over-designed	-	-	-	30	HSS 3x3x3/16	20	CJP	9x9x1/2"	0.75	6" oc	A307	10x10x1"	1	6" oc	A325	Cyclic
R8	over-designed	shim	vinylester	3	30	HSS 3x3x3/16	14	CJP	9x9x1/2"	0.75	6" oc	A307	10x10x1"	1	6" oc	A325	Cyclic
R9	over-designed	shim	phenolic	3	30	HSS 3x3x3/16	14	CJP	9x9x1/2"	0.75	6" oc	A307	10x10x1"	1	6" oc	A325	Cyclic
R10	over-designed	shim	polyurethane	3	30	HSS 3x3x3/16	14	CJP	9x9x1/2"	0.75	6" oc	A307	10x10x1"	1	6" oc	A325	Cyclic
R11	over-designed	shim	proprietary 1	3	30	HSS 3x3x3/16	14	CJP	9x9x1/2"	0.75	6" oc	A307	10x10x1"	1	6" oc	A325	Cyclic
R12	over-designed	shim	proprietary 2	3	30	HSS 3x3x3/16	14	CJP	9x9x1/2"	0.75	6" oc	A307	10x10x1"	1	6" oc	A325	Cyclic
R13	over-designed	shim	vinylester	1	30	HSS 3x3x3/16	14	CJP	9x9x1/2"	0.75	6" oc	A307	10x10x1"	1	6" oc	A325	Cyclic
R14	over-designed	sleeve	FRP 4x4x1/2	-	30	HSS 3x3x3/16	14	CJP	9x9x1/2"	0.75	6" oc	A307	10x10x1"	1	6" oc	A325	Cyclic
R15	over-designed	-	-	-	66	HSS 3x3x3/16	56	CJP	9x9x1/2"	0.75	6" oc	A307	10x10x1"	1	6" oc	A325	Cyclic

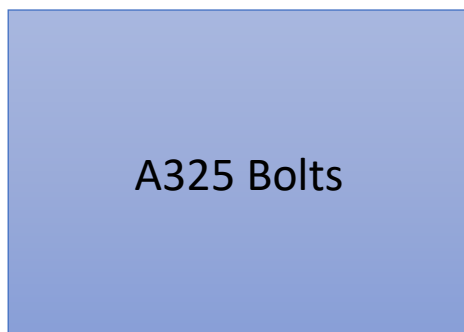
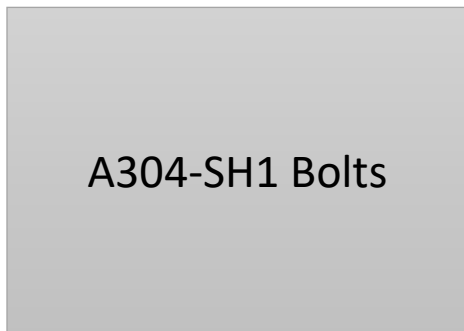
Appendix E.5 – Thermal Modeling Matrix for Roof Posts

TEST NAME		MITIGATION STRATEGY			SPECIMEN INFORMATION					THERMAL MODELING	
Structural Test	Thermal Modeling	Type	Material	Thickness	Insulation Thickness	Post	Base Plate	Rod Dia.	Rod Spec	Climate Zone	U-Value
-	-	-	-	(in)	(in)	-	(in)	(in)	-	-	(BTU/h*ft2**F)
R1	N/A	-	-	-	6	HSS 3x3x3/16	9x9x3/8	0.5	B8 Class 2	N/A	N/A
	RPU7-1-A	-	-	-	6	HSS3x3x3/16	6x9x1/2	0.75	B8 Class 2 SS	7	0.0351
	RPU1-1-B	-	-	-	3.8	HSS3x3x3/16	6x9x1/3	0.75	B8 Class 2 SS	1	0.0517
	RPU7-1-C	-	-	-	6	FRP HSS3x3x3/8	FRP 6x9x1/2	0.75	B8 Class 2 SS	7	0.0274
	RPU1-1-D	-	-	-	3.8	FRP HSS3x3x3/8	FRP 6x9x1/2	0.75	B8 Class 2 SS	1	0.0422
R2	N/A	shim	vinylester	3	6	HSS 3x3x3/16	9x9x3/8	0.5	B8 Class 2	N/A	N/A
	RPM7-2-A	shim	vinylester	6	6	HSS3x3x3/16	6x9x1/2	0.75	B8 Class 2 SS	7	0.0318
	RPM1-2-B	shim	vinylester	3	3.8	HSS3x3x3/16	6x9x1/2	0.75	B8 Class 2 SS	1	0.0482
	RPM7-2-C	shim	vinylester	3	6	HSS3x3x3/16	6x9x1/2	0.75	B8 Class 2 SS	7	0.0325
	RPM1-2-D	shim	vinylester	4	3.8	HSS3x3x3/16	6x9x1/2	0.75	B8 Class 2 SS	1	0.0484
	RPM1-2-E	shim	vinylester	1	3.8	HSS3x3x3/16	6x9x1/2	0.75	B8 Class 2 SS	1	0.0499
	RPM1-2-F	2 shims shim with bushings at steel rods	vinylester	1	3.8	HSS3x3x3/16	6x9x1/2	0.75	B8 Class 2 SS	1	0.0492
	RPM1-2-G	bushings at steel rods	vinylester	1	3.8	HSS3x3x3/16	6x9x1/2	0.75 with bushings	B8 Class 2 SS	1	0.0492
	RPM1-2-H	bushings at steel rods	vinylester	-	3.8	HSS3x3x3/16	6x9x1/2	0.75 with bushings	B8 Class 2 SS	1	0.0517
R3	N/A	sleeve	FRP 4x4x1/2	-	6	HSS 3x3x3/16	9x9x3/8	0.5	B8 Class 2	N/A	N/A
R4	N/A	-	-	-	6	HSS 3x3x3/16	9x9x3/8	0.5	B8 Class 2	N/A	N/A
R5	N/A	shim	vinylester	3	6	HSS 3x3x3/16	9x9x3/8	0.5	B8 Class 2	N/A	N/A
R6	N/A	sleeve	FRP 4x4x1/2	-	6	HSS 3x3x3/16	9x9x3/8	0.5	B8 Class 2	N/A	N/A
R7	N/A	-	-	-	6	HSS 3x3x3/16	9x9x1/2	0.75	A307	N/A	N/A
	RPU7-7-A	-	-	-	6	HSS3x3x3/16	6x9x1/2	0.75	A307	7	0.0351
	RPU1-7-B	-	-	-	3.8	HSS3x3x3/16	6x9x1/2	0.75	A307	1	0.0517
R8	N/A	shim	vinylester	3	6	HSS 3x3x3/16	9x9x1/2	0.75	A307	N/A	N/A
	RPM7-8-A	shim	vinylester	6	6	HSS3x3x3/16	6x9x1/2	0.75	A307	7	0.0342
	RPM7-8-B	shim	vinylester	3	3.8	HSS3x3x3/16	6x9x1/2	0.75	A307	7	0.0501
R9	N/A	shim	phenolic	3	6	HSS 3x3x3/16	9x9x1/3	0.75	A307	N/A	N/A
R10	N/A	shim	polyurethane	3	6	HSS 3x3x3/16	9x9x1/4	0.75	A307	N/A	N/A
R11	N/A	shim	proprietary 1	3	6	HSS 3x3x3/16	9x9x1/5	0.75	A307	N/A	N/A
	RPM7-11-A	shim	proprietary 1	6	6	HSS3x3x3/16	6x9x1/2	0.75	B8 Class 2 SS	7	0.0297
	RPM7-11-B	shim	proprietary 1	3	6	HSS3x3x3/16	6x9x1/2	0.75	B8 Class 2 SS	7	0.0308
	RPM7-11-C	shim	proprietary 1	1	6	HSS3x3x3/16	6x9x1/2	0.75	B8 Class 2 SS	7	0.0325
R12	N/A	shim	proprietary 2	3	6	HSS 3x3x3/16	9x9x1/6	0.75	A307	N/A	N/A
	RPM7-12-A	shim	proprietary 2	6	6	HSS3x3x3/16	6x9x1/2	0.75	B8 Class 2 SS	7	0.0301
	RPM7-12-B	shim	proprietary 2	3	6	HSS3x3x3/16	6x9x1/2	0.75	B8 Class 2 SS	7	0.0312
	RPM7-12-C	shim	proprietary 2	1	6	HSS3x3x3/16	6x9x1/2	0.75	B8 Class 2 SS	7	0.0328
R13	N/A	shim	vinylester	1	6	HSS 3x3x3/16	9x9x1/7	0.75	A307	N/A	N/A
R14	N/A	sleeve	FRP 4x4x1/2	-	6	HSS 3x3x3/16	9x9x1/8	0.75	A307	N/A	N/A
R15	N/A	-	-	-	6	HSS 3x3x3/16	9x9x1/2	0.75	A307	N/A	N/A

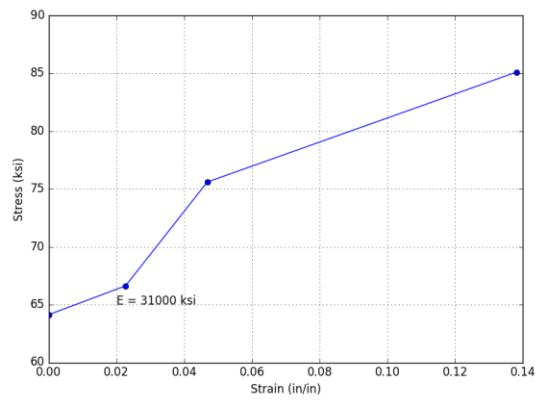
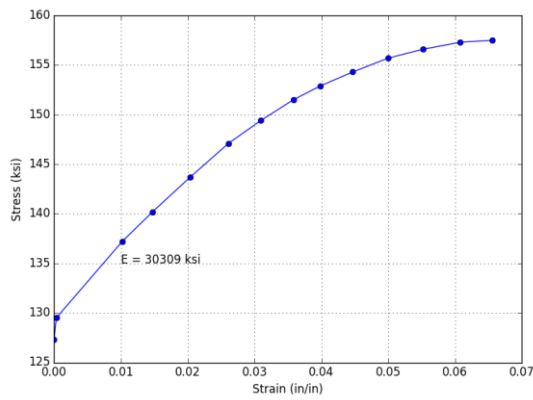
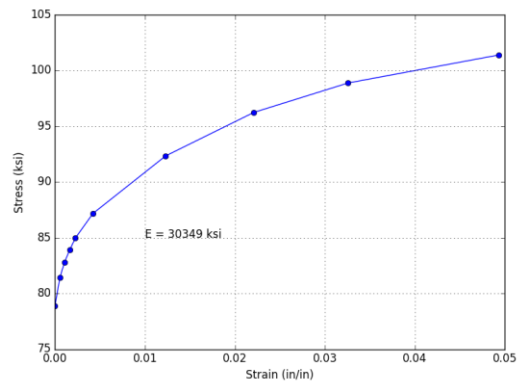
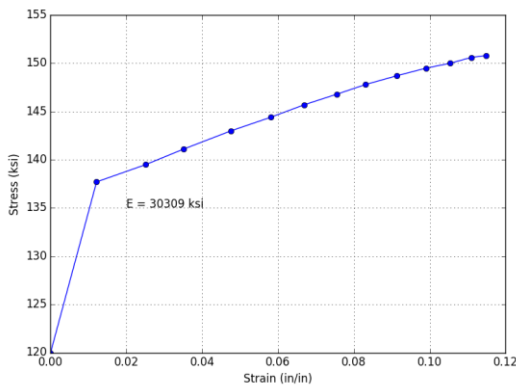
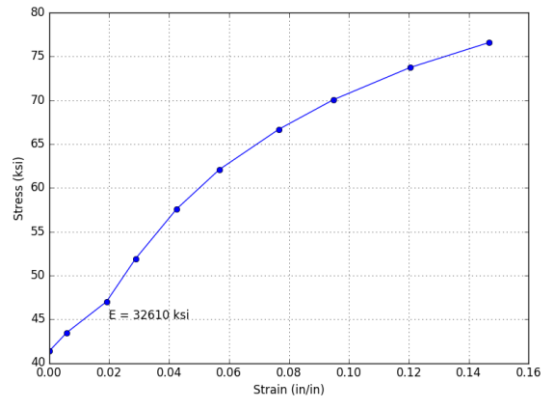
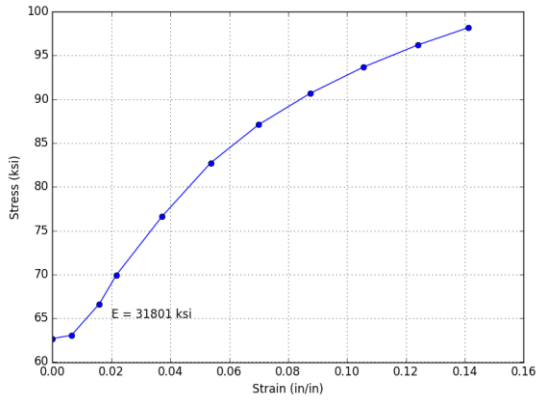
Appendix F: ABAQUS Supplementary Information and Results

Appendix F.1: ABAQUS Material Data

This appendix contains the material data used in ABAQUS. The E values on the plots are the initial modulus of elasticity from 0 to the first data point. A template for the layout of the plots for each material is shown below:



True Stress – True Strain



Appendix F.2: Data Plots

This appendix contains the data analysis of the ABAQUS results used to correct the experimental data. A template for the layout of the data plots for each tests is shown below:

Base Rotation
vs.
Displacement

Base Rotation
vs.
Base Moment

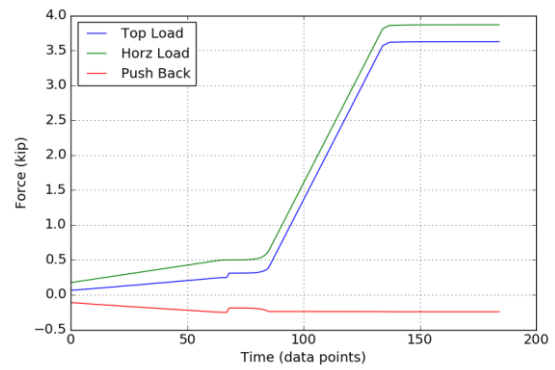
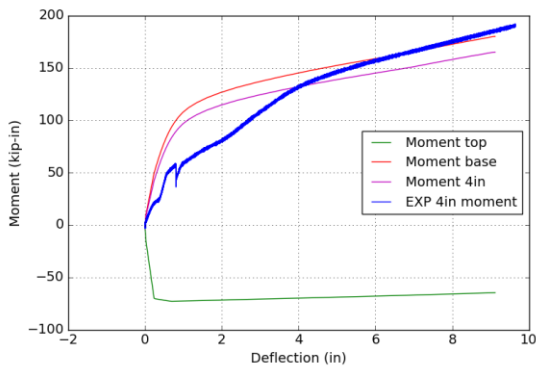
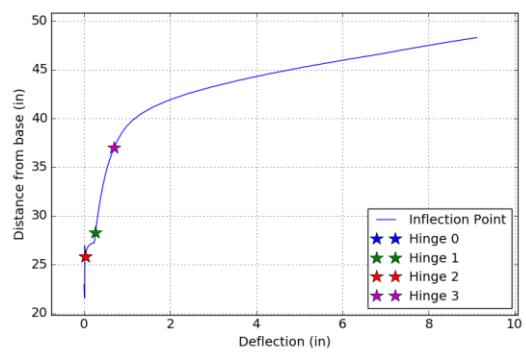
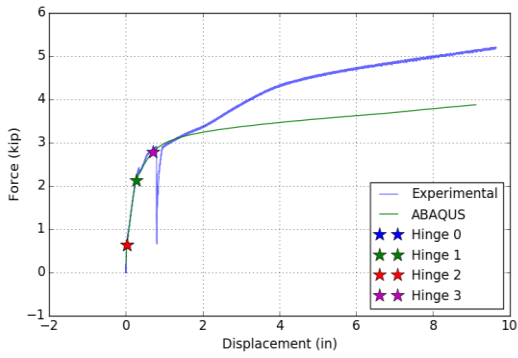
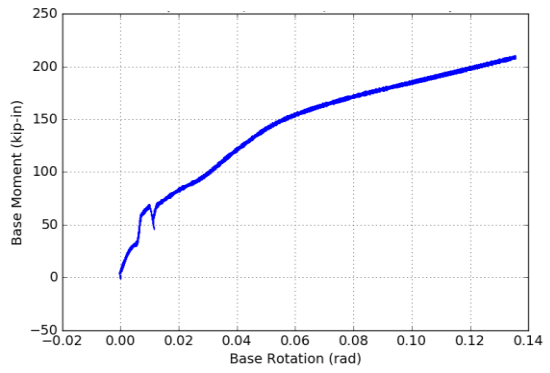
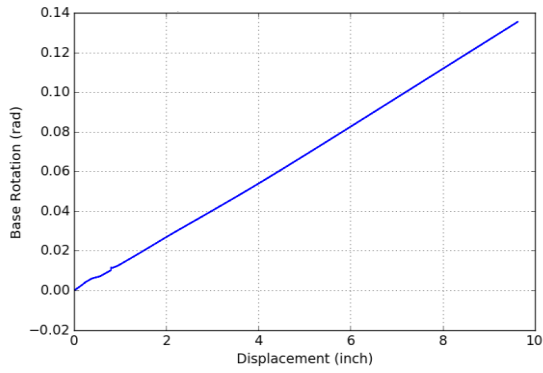
Force
vs.
Displacement

(Inflection Point)
Distance from Base
vs.
Displacement

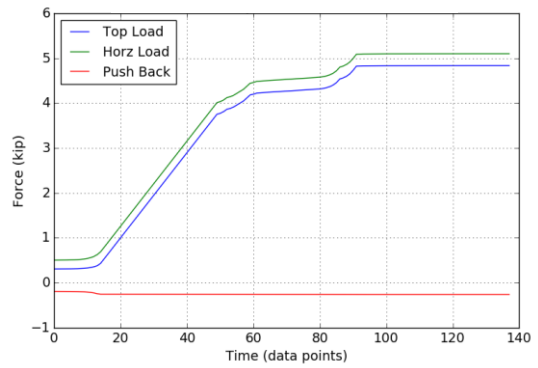
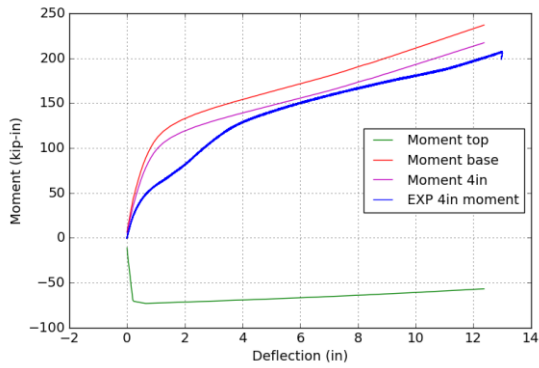
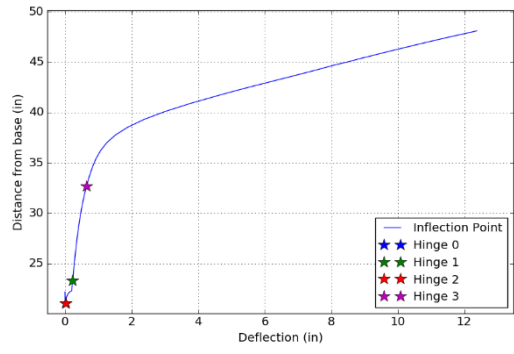
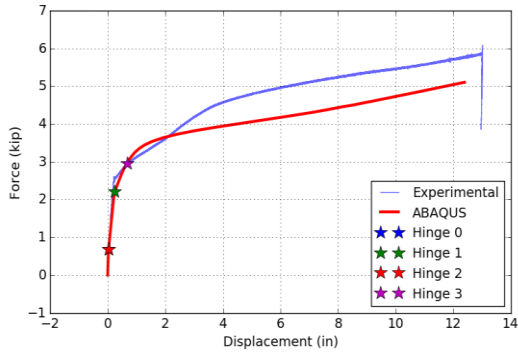
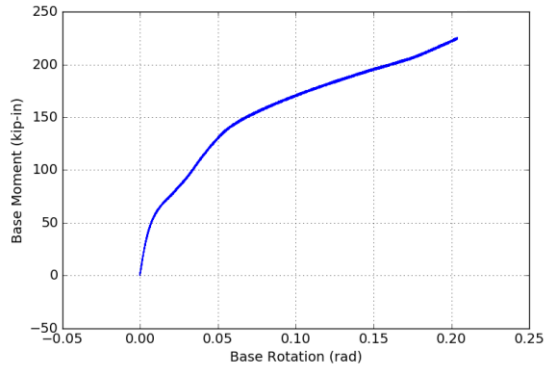
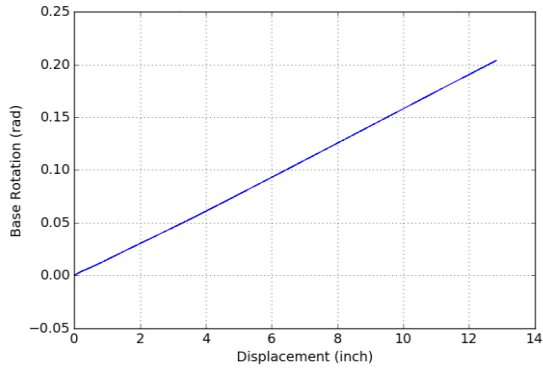
Moment
vs.
Deflection

(Top Push Back)
Force
vs.
Time

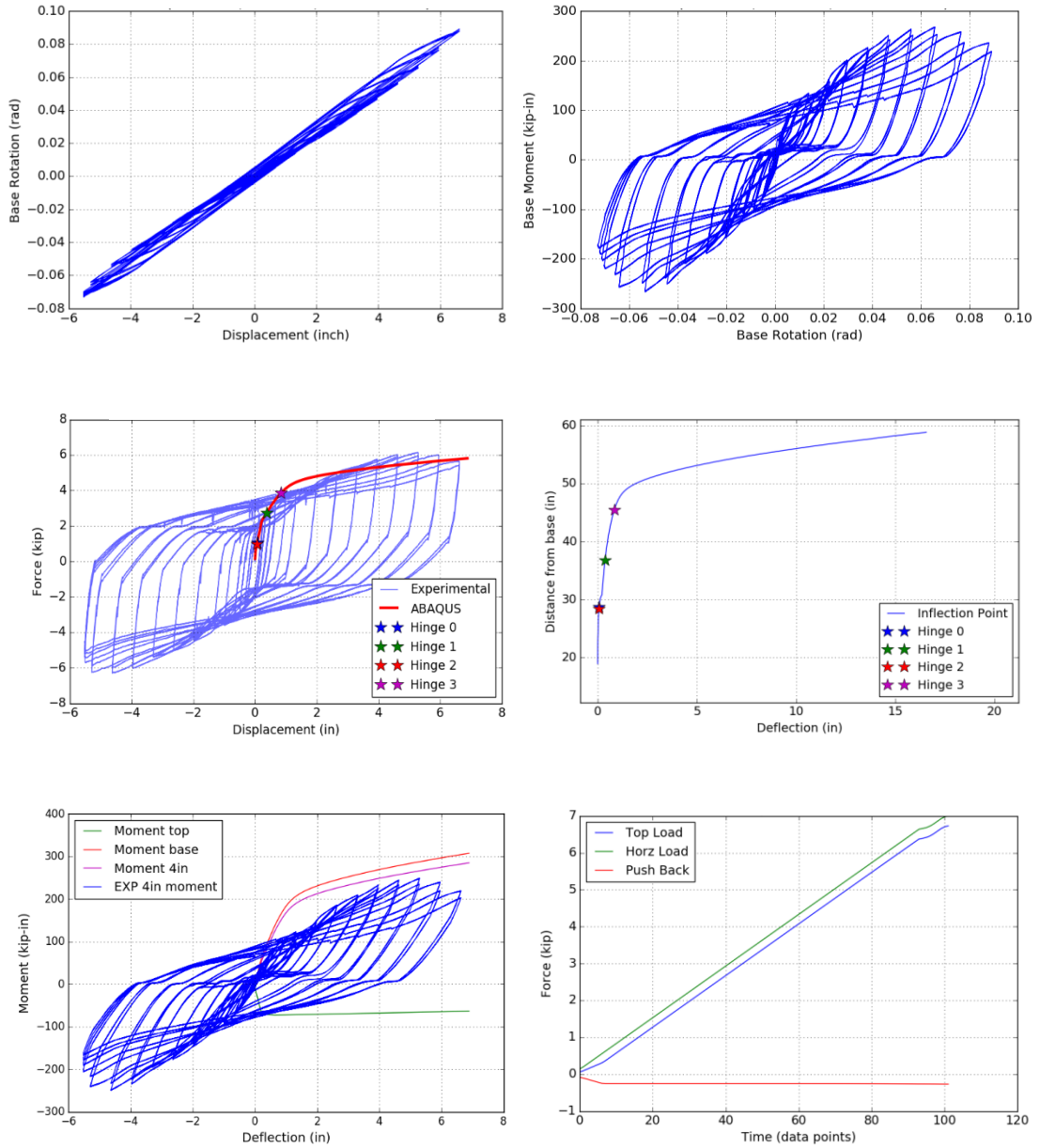
Canopy Beam: C1



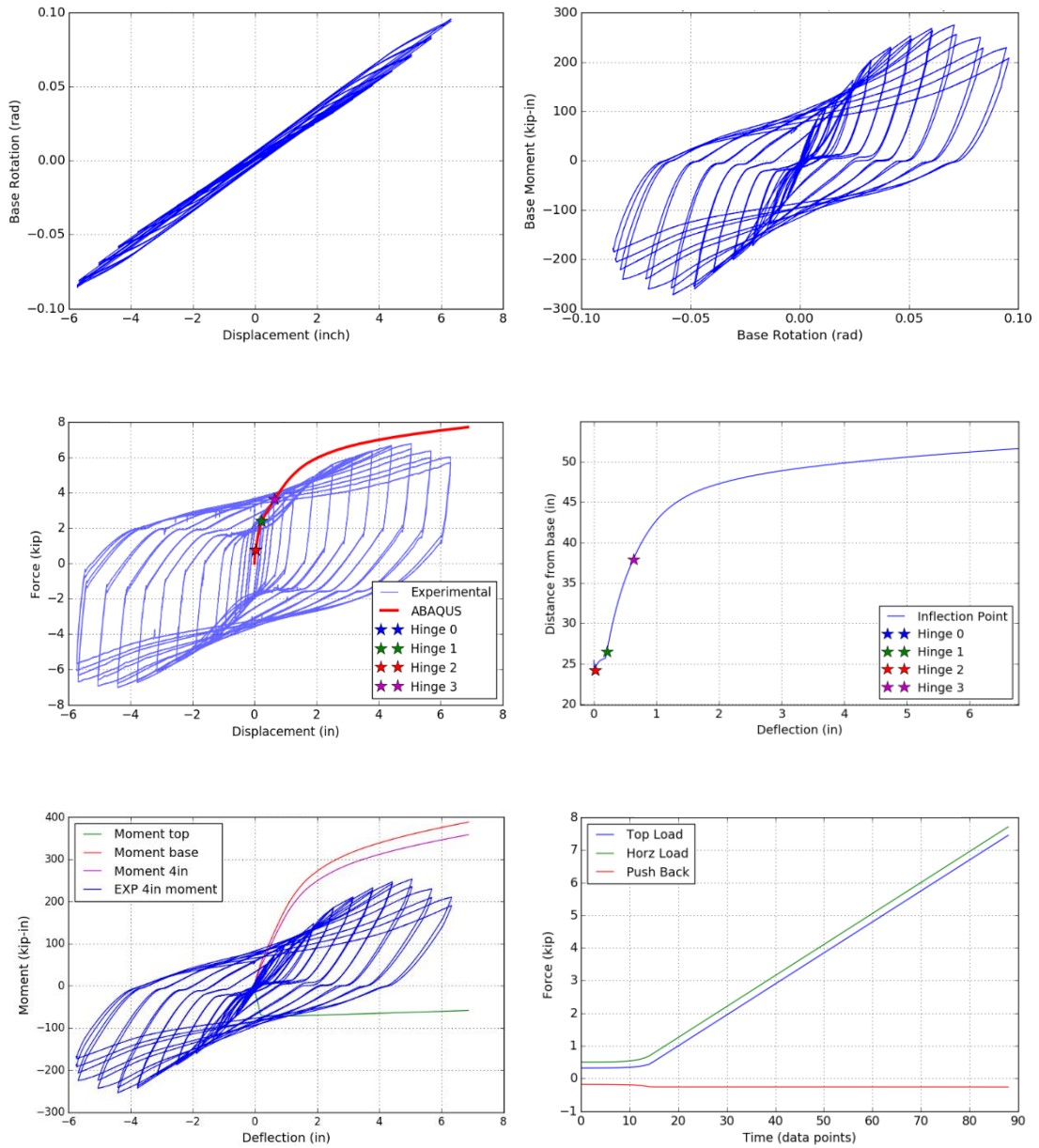
Canopy Beam: C2



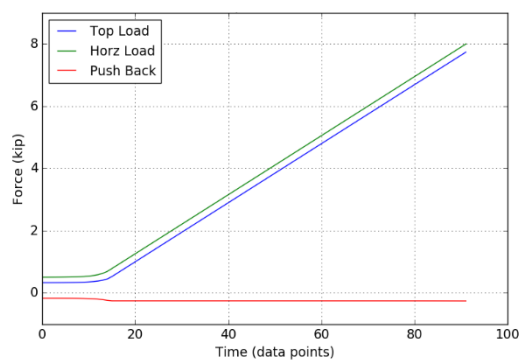
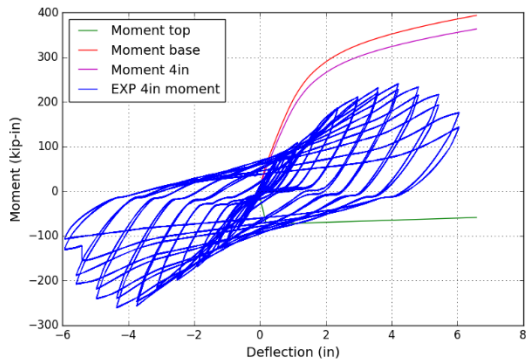
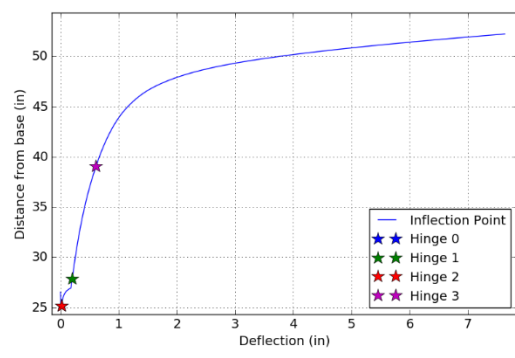
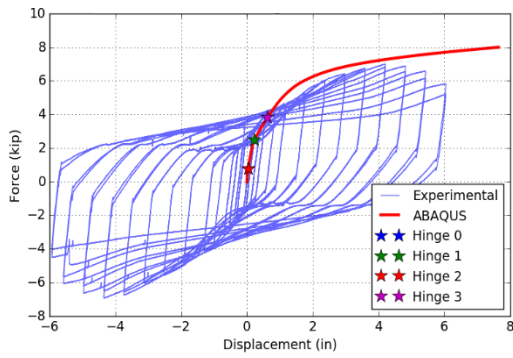
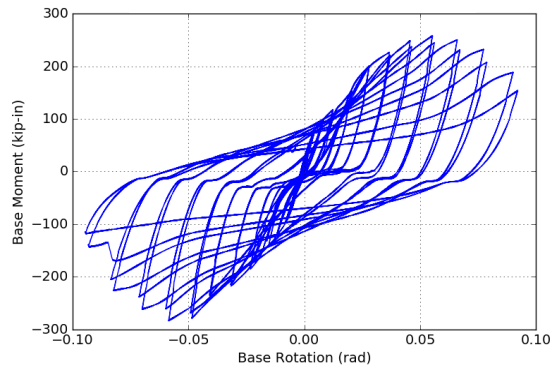
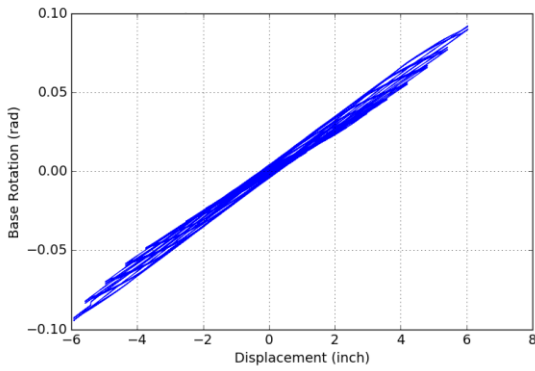
Canopy Beam: C7



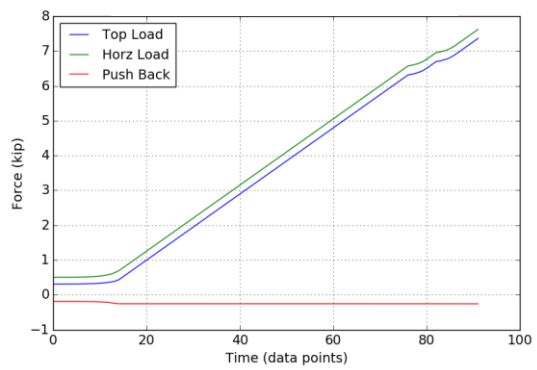
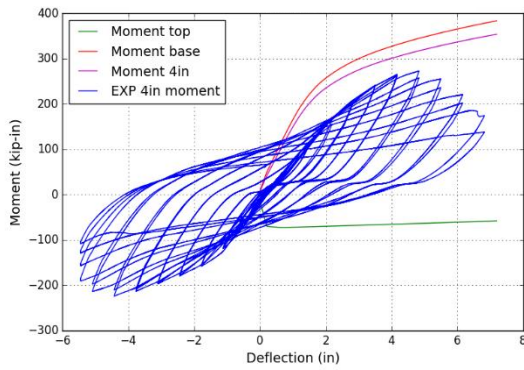
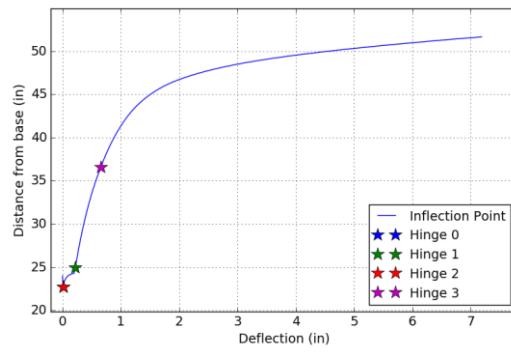
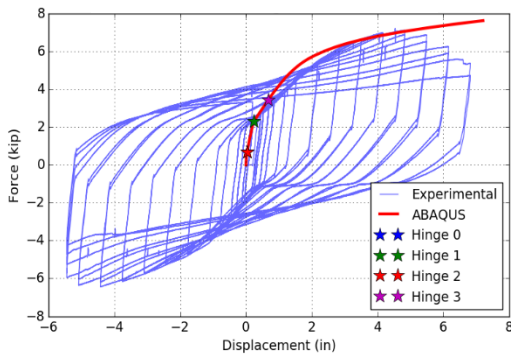
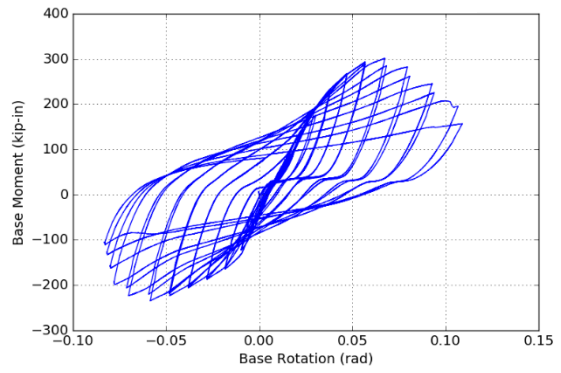
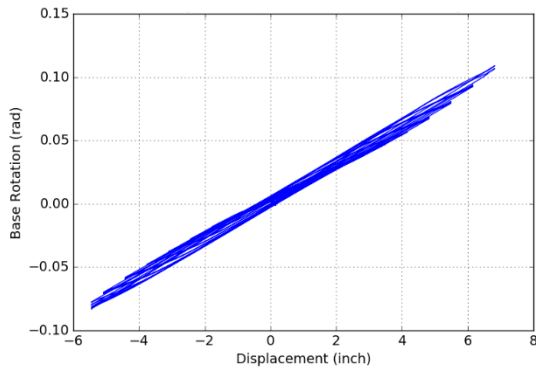
Canopy Beam: C8



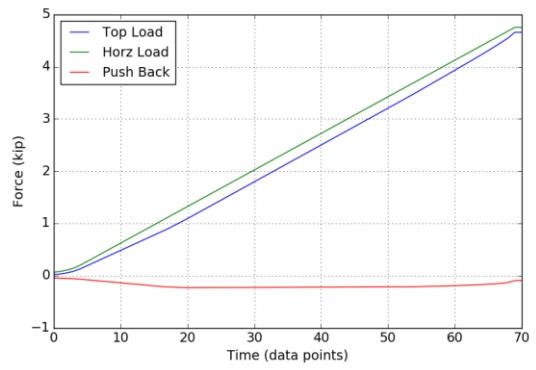
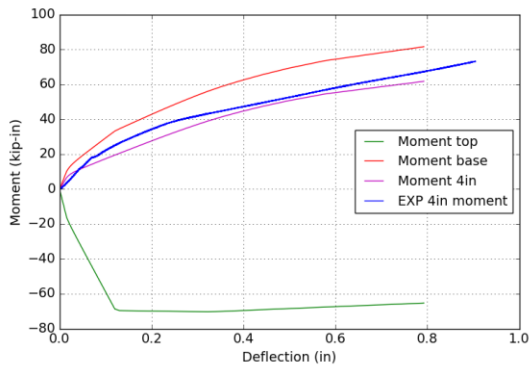
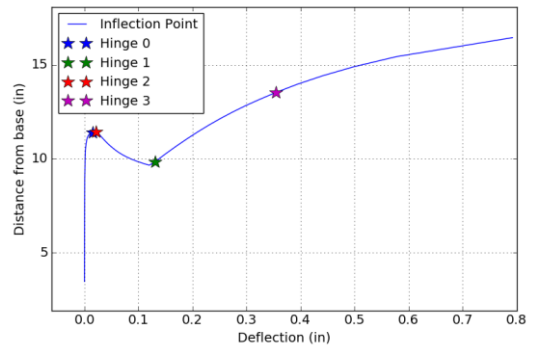
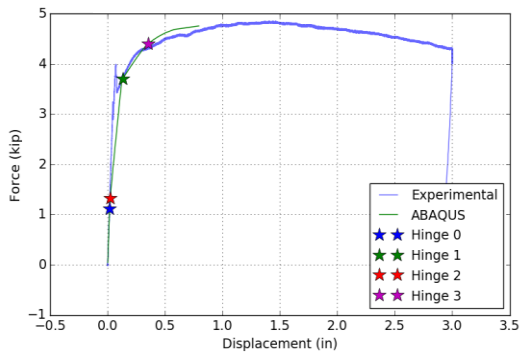
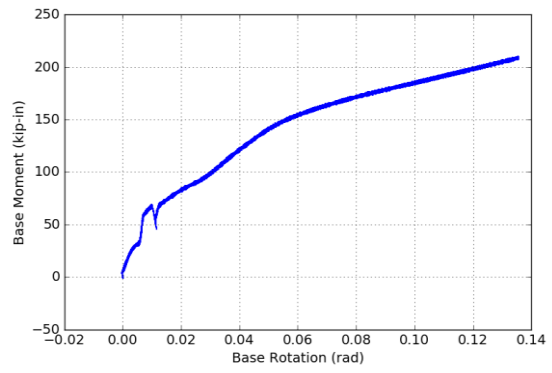
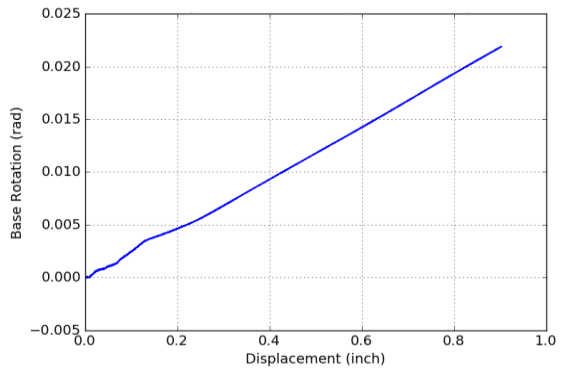
Canopy Beam: C13



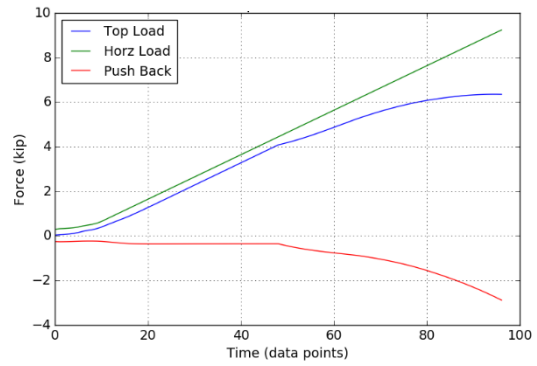
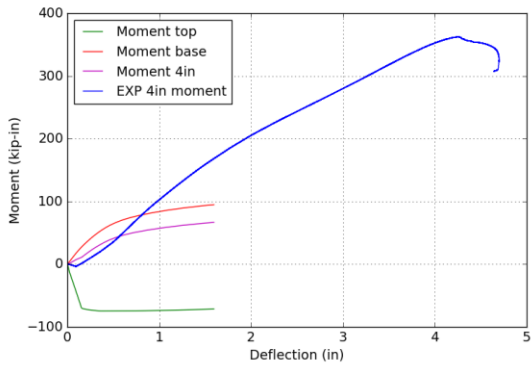
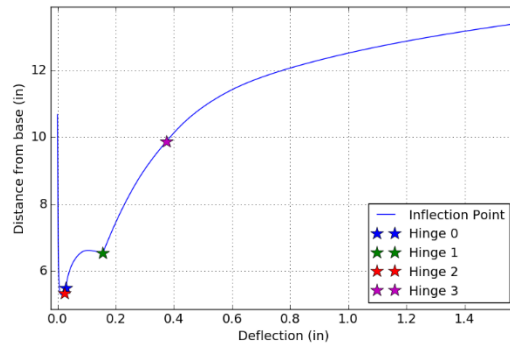
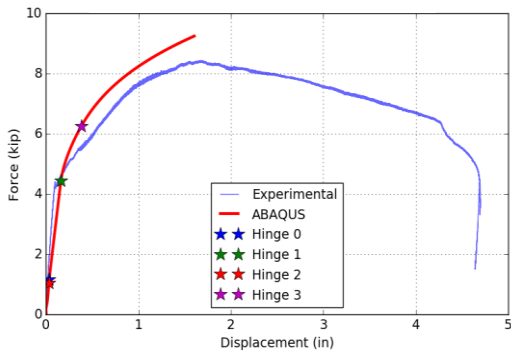
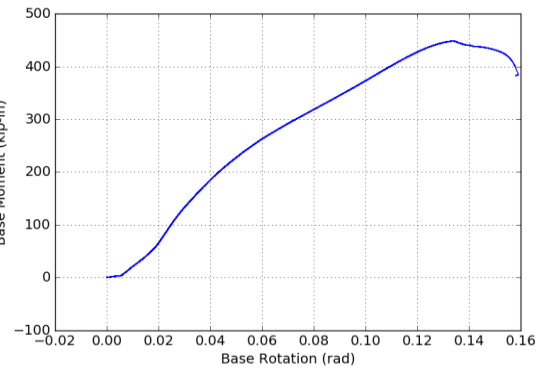
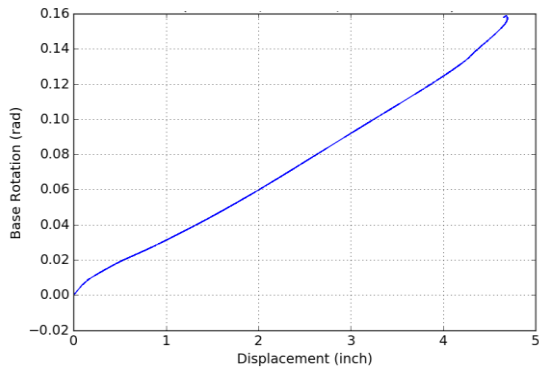
Canopy Beam: C15



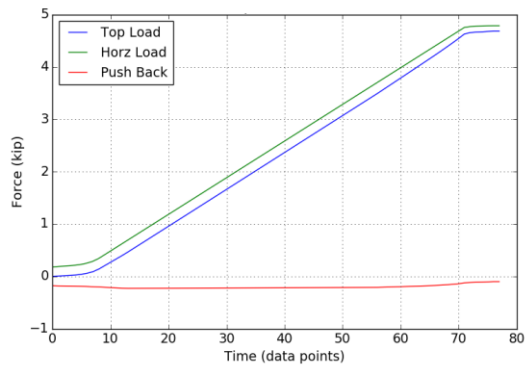
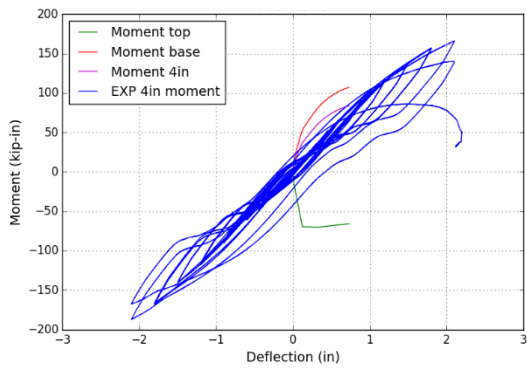
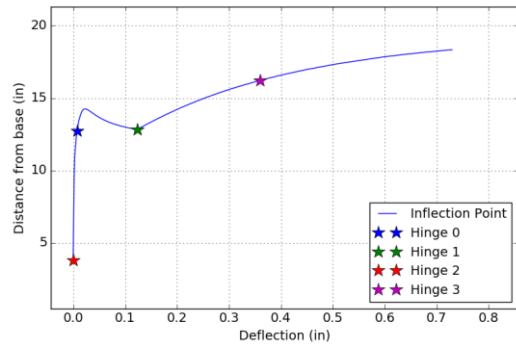
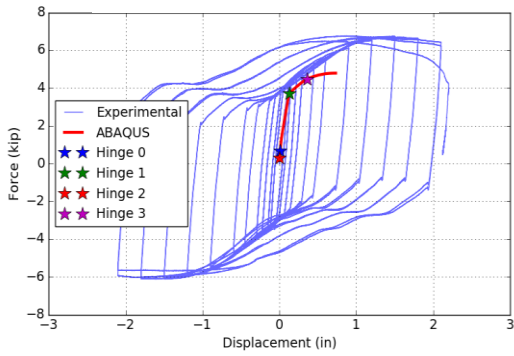
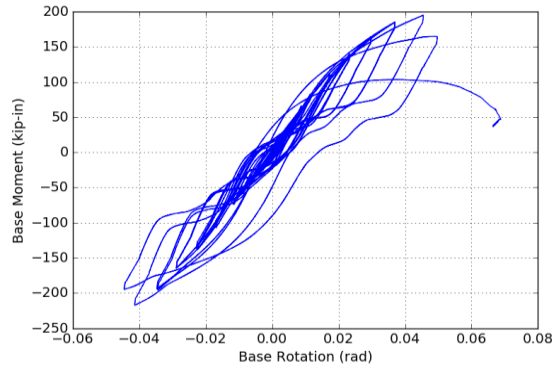
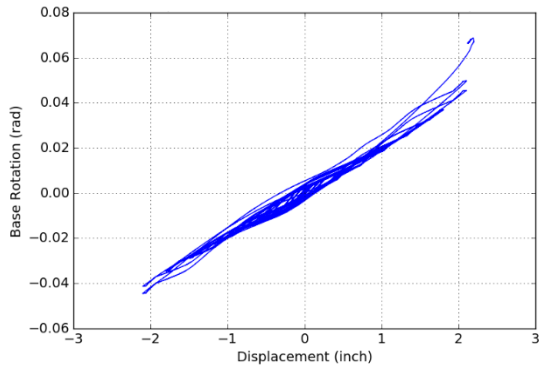
Roof Post: R1



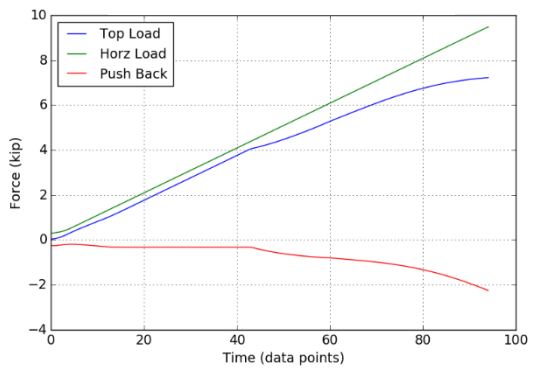
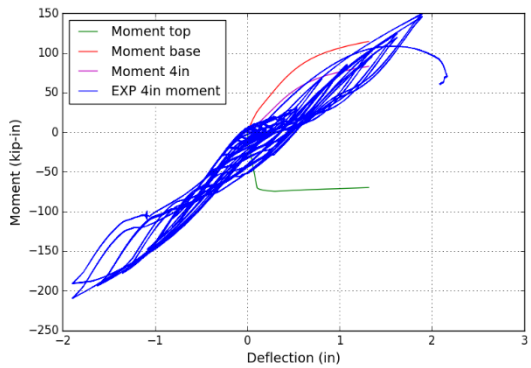
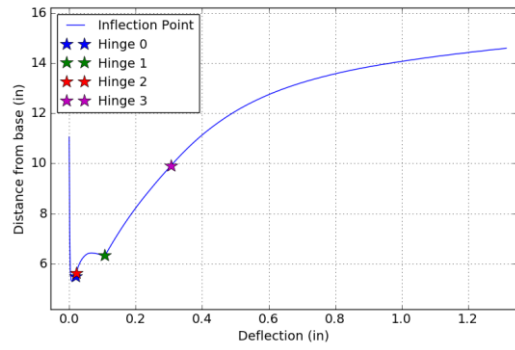
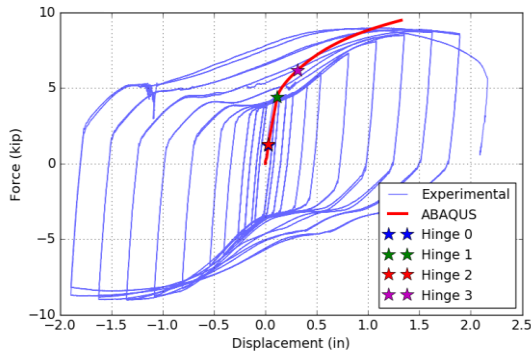
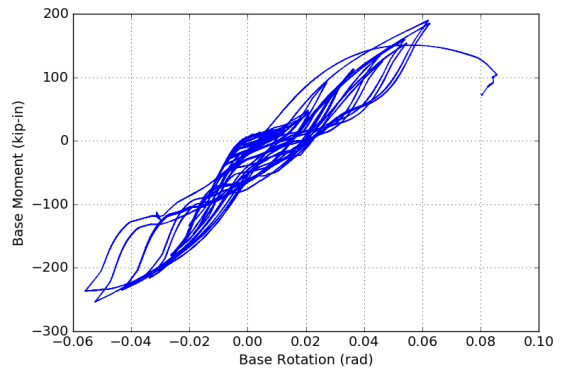
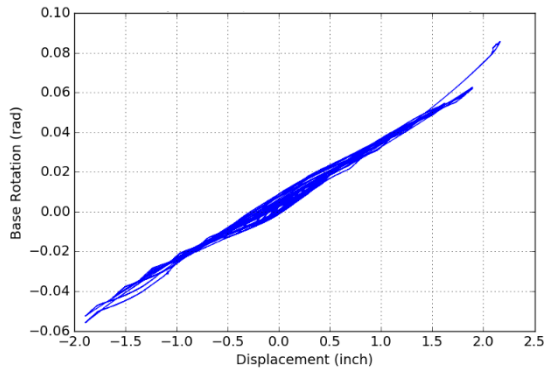
Roof Post: R2



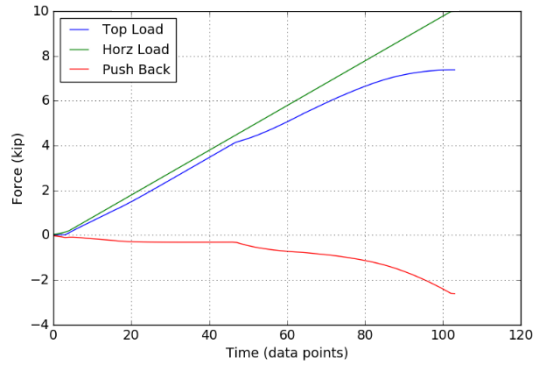
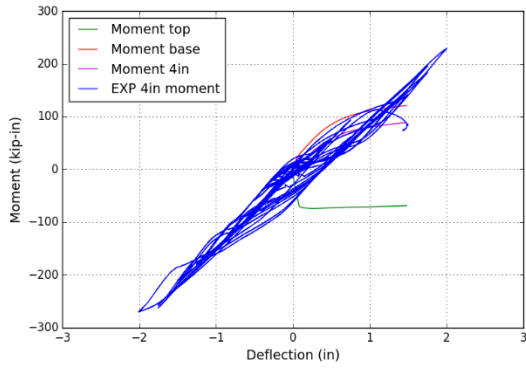
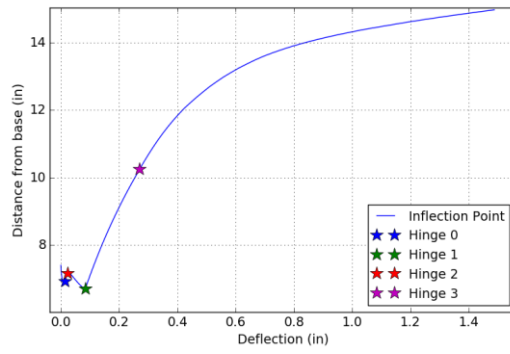
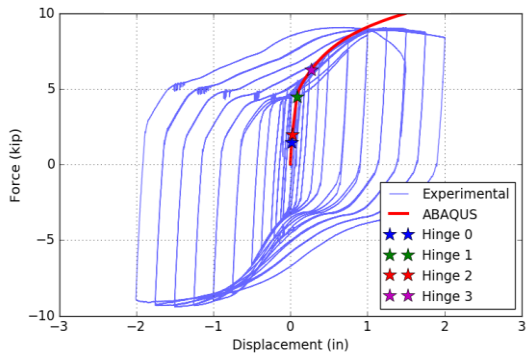
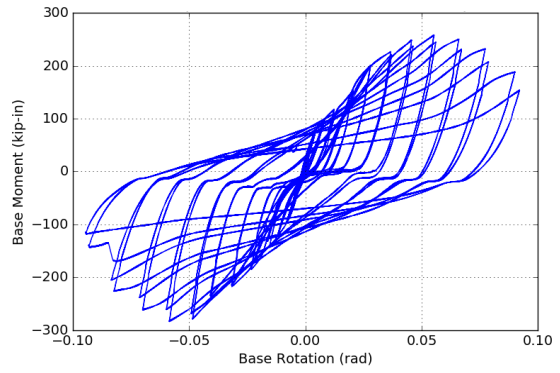
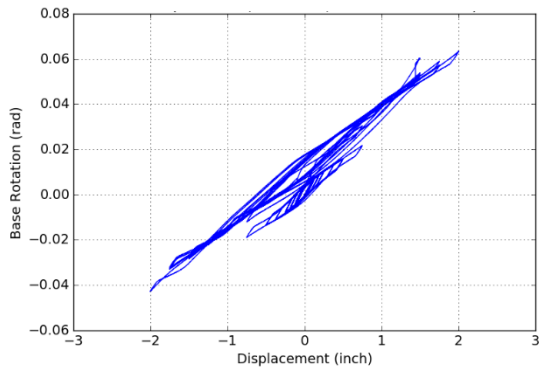
Roof Post: R7



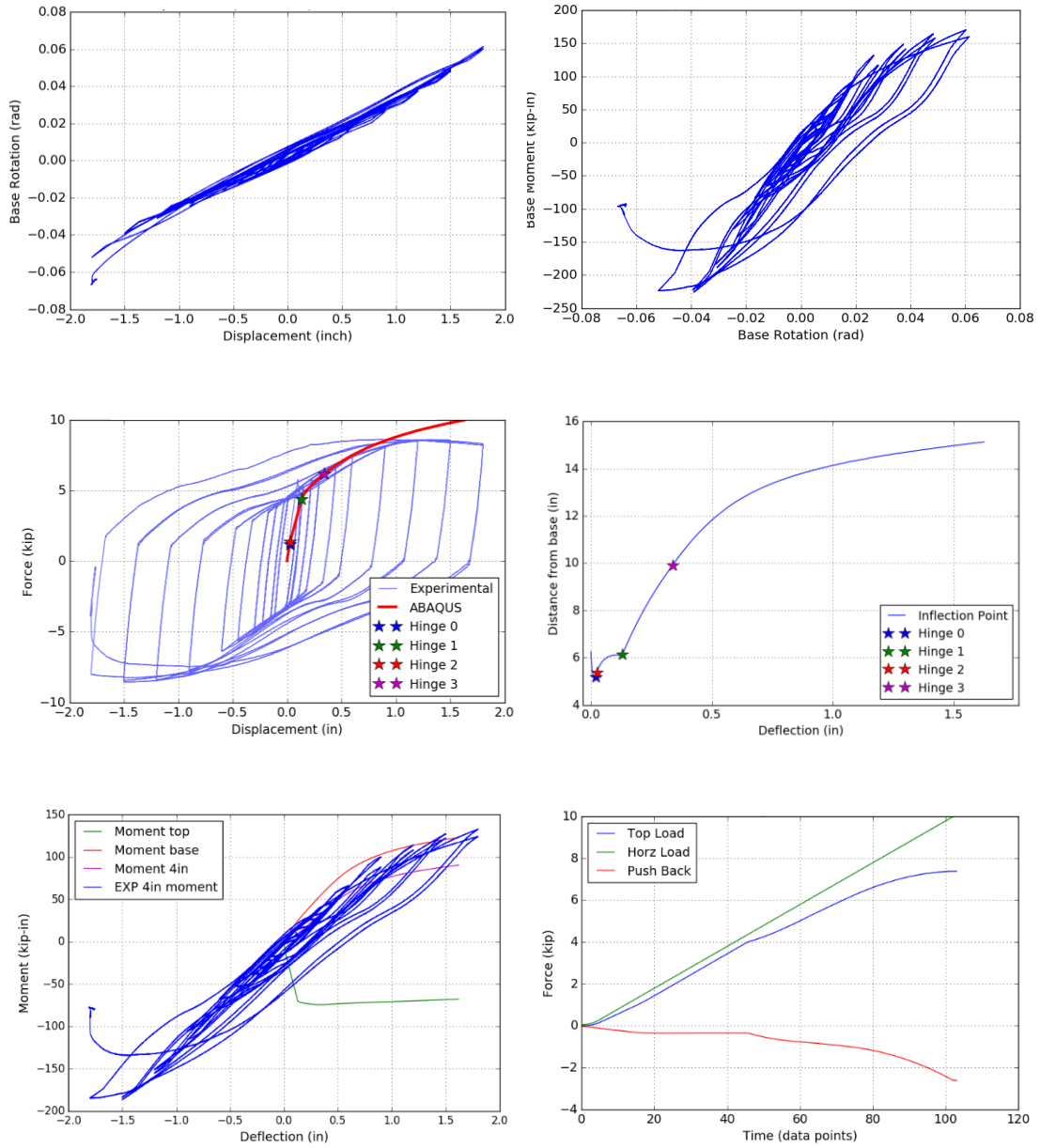
Roof Post: R8



Roof Post: R13

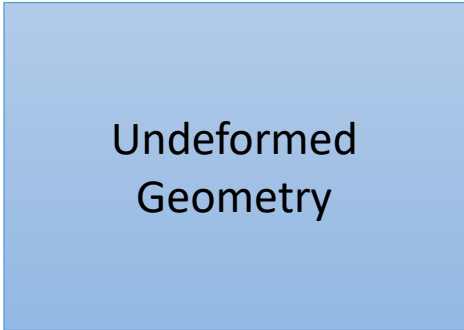


Roof Post: R15

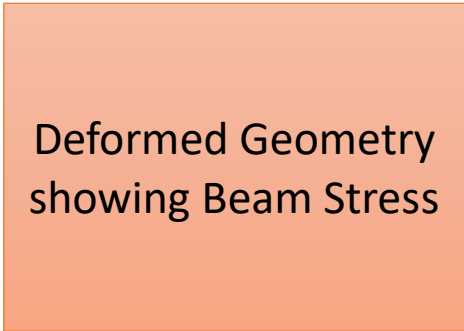


Appendix F.3: Deflected Shapes

This appendix contains the deflected shapes of the ABAQUS models. A template for the layout of the deflected shapes for each tests is shown below:



Undeformed
Geometry



Deformed Geometry
showing Beam Stress




FEM Side Deflection
von Mises Stress



FEM Front Deflection
von Mises Stress

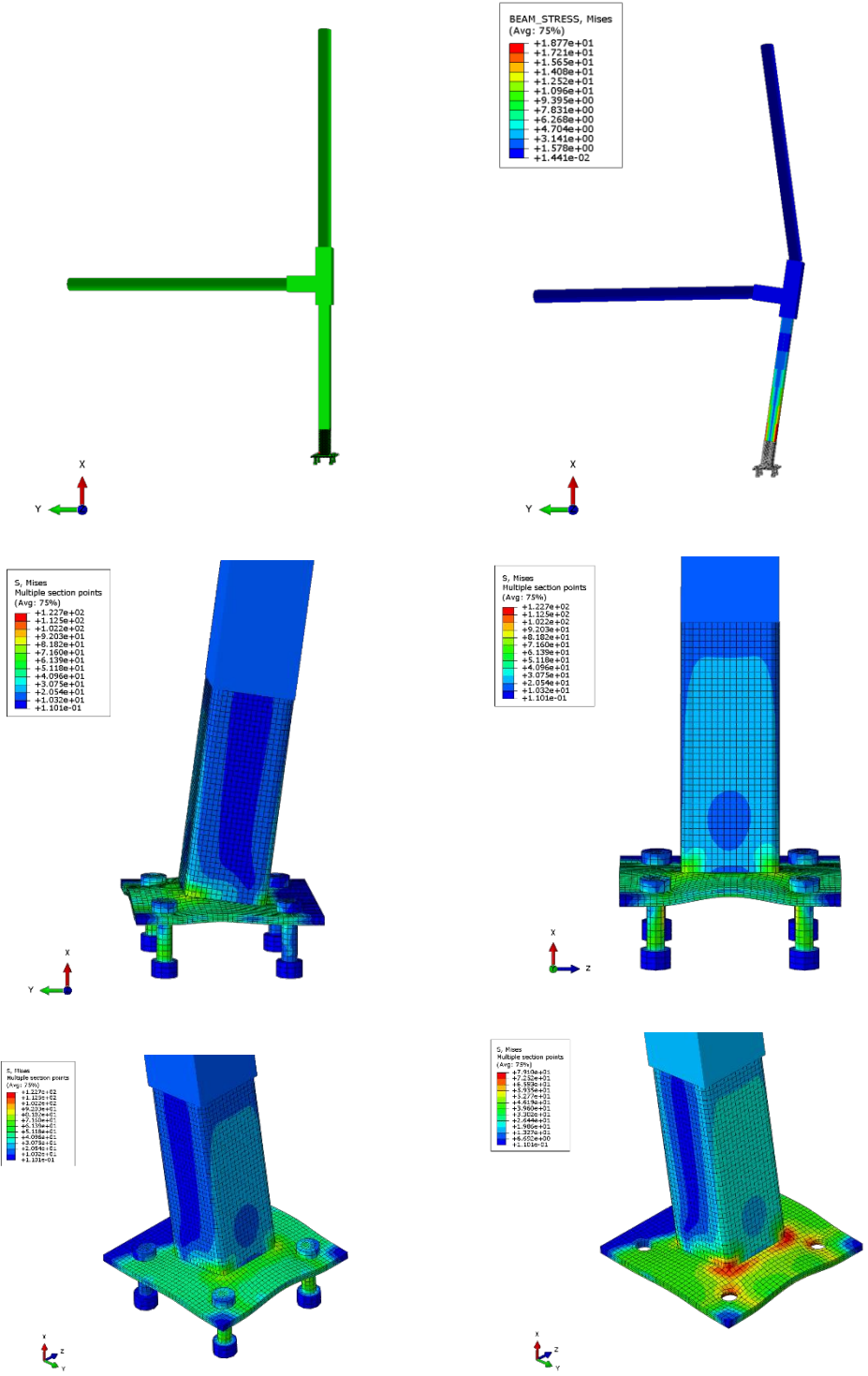


FEM Iso Deflection
von Mises Stress

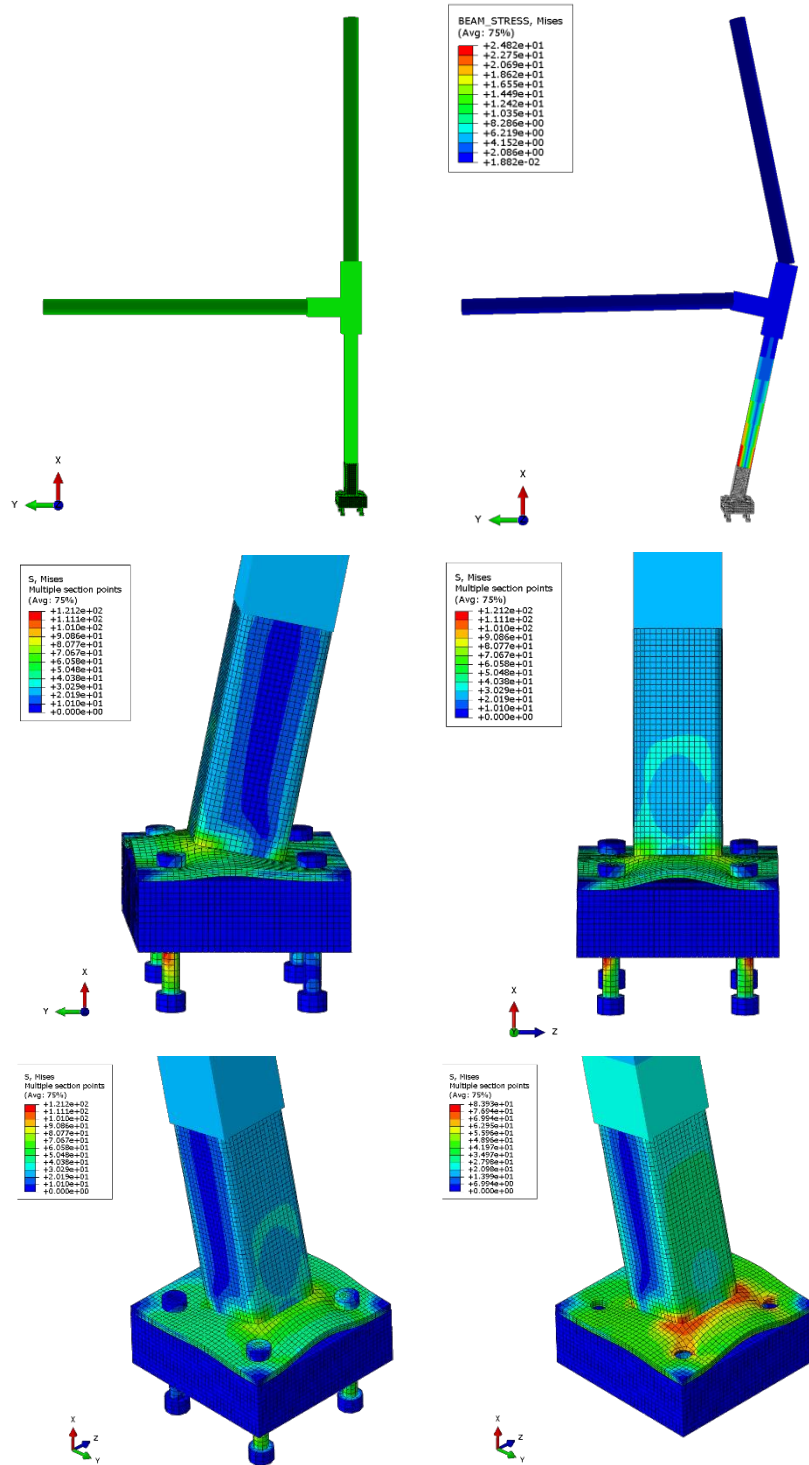


FEM Iso Deflection
von Mises Stress
No Bolts

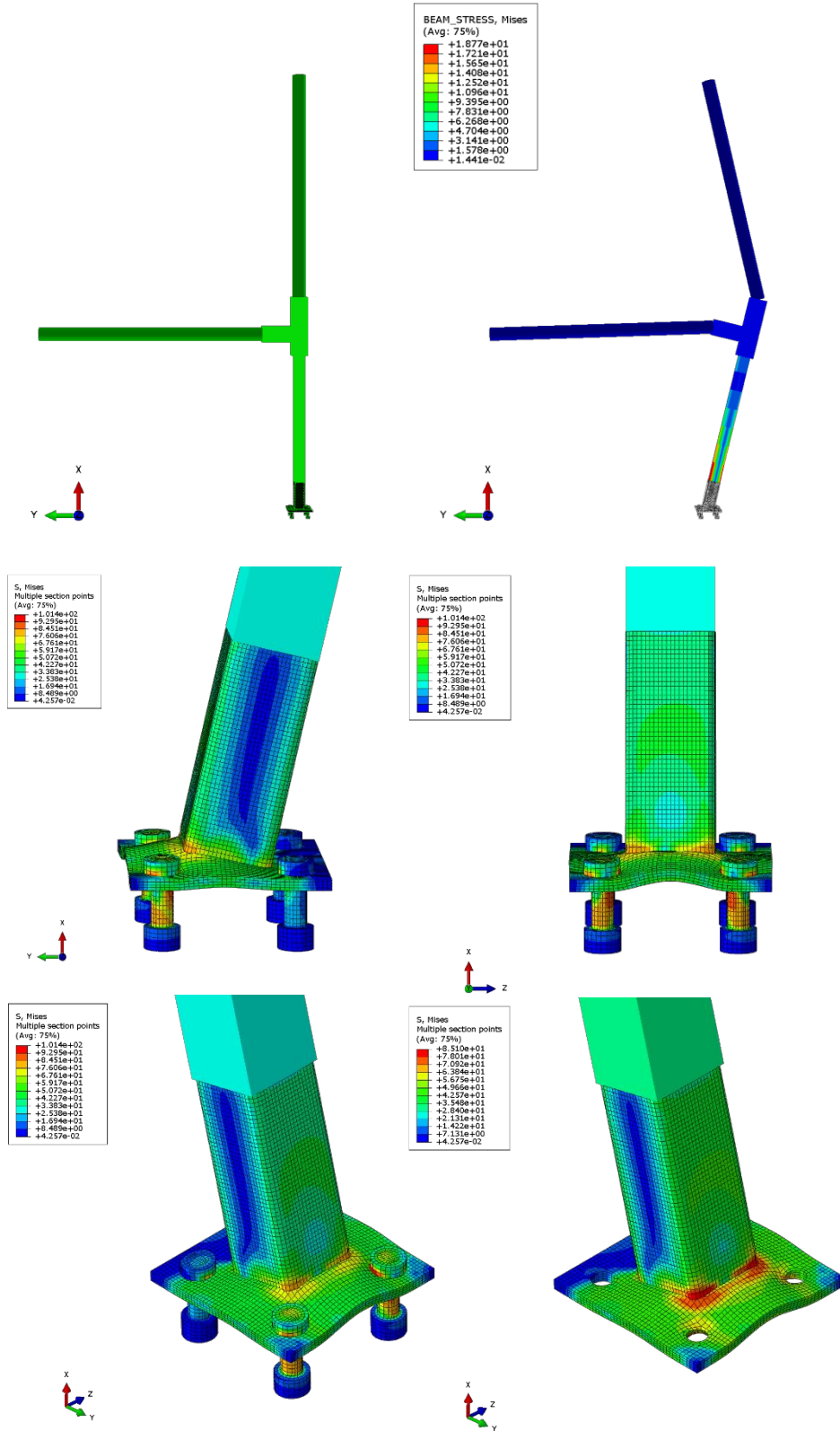
Canopy Beam: C1



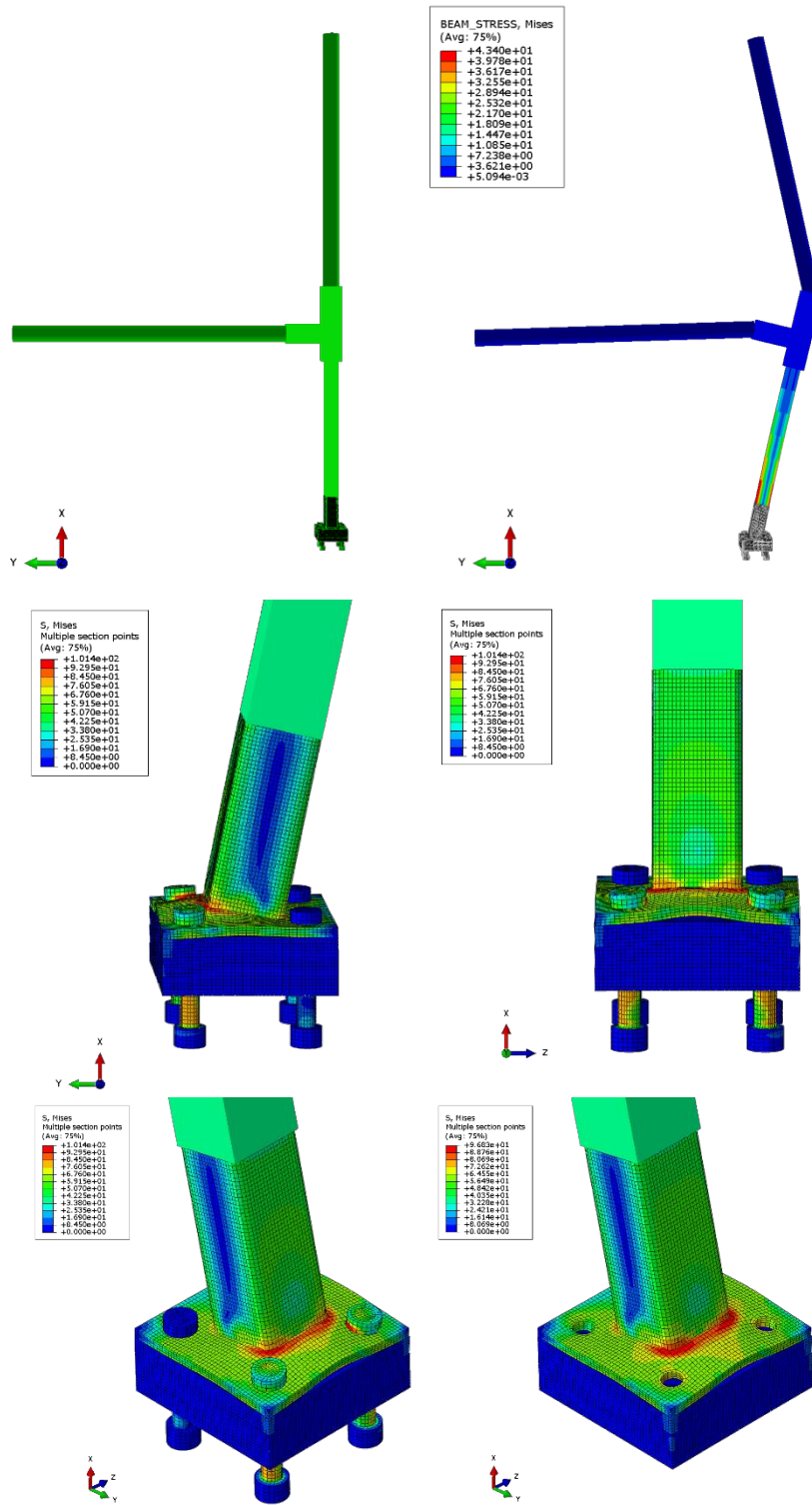
Canopy Beam: C2



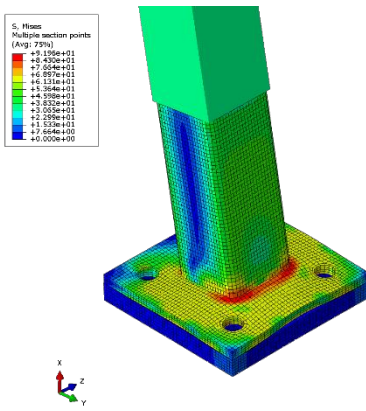
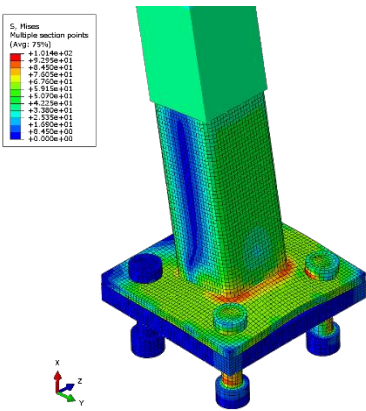
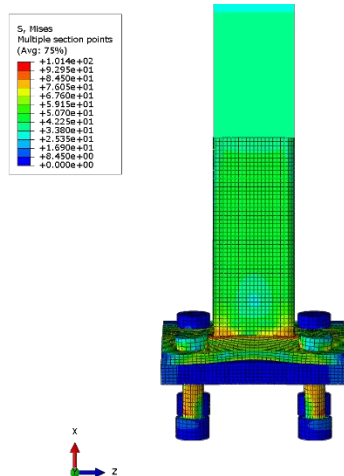
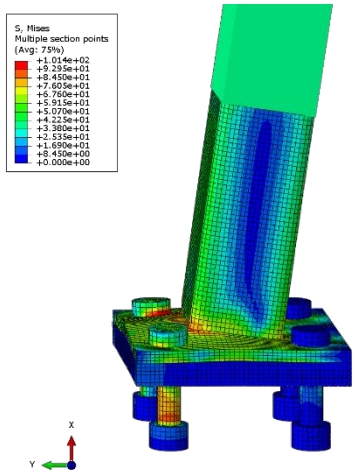
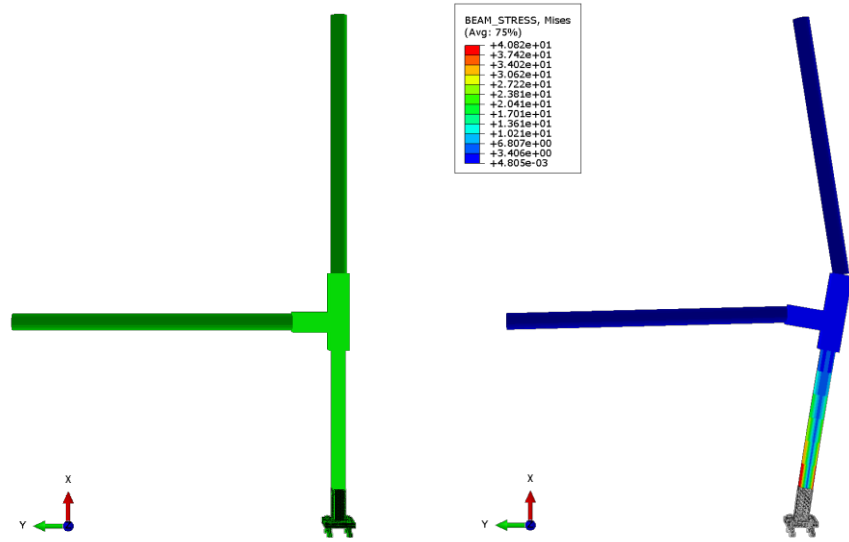
Canopy Beam: C7



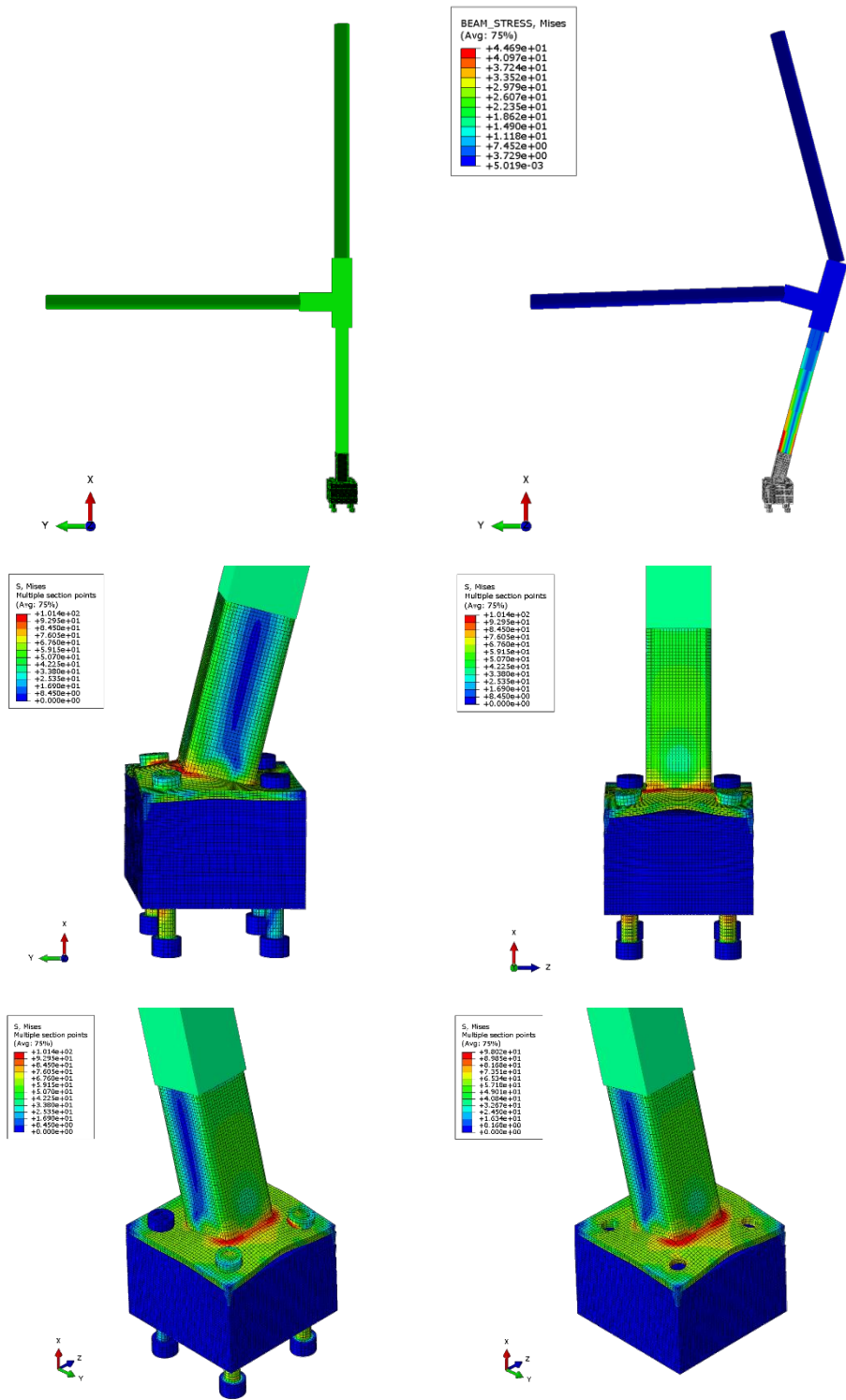
Canopy Beam: C8



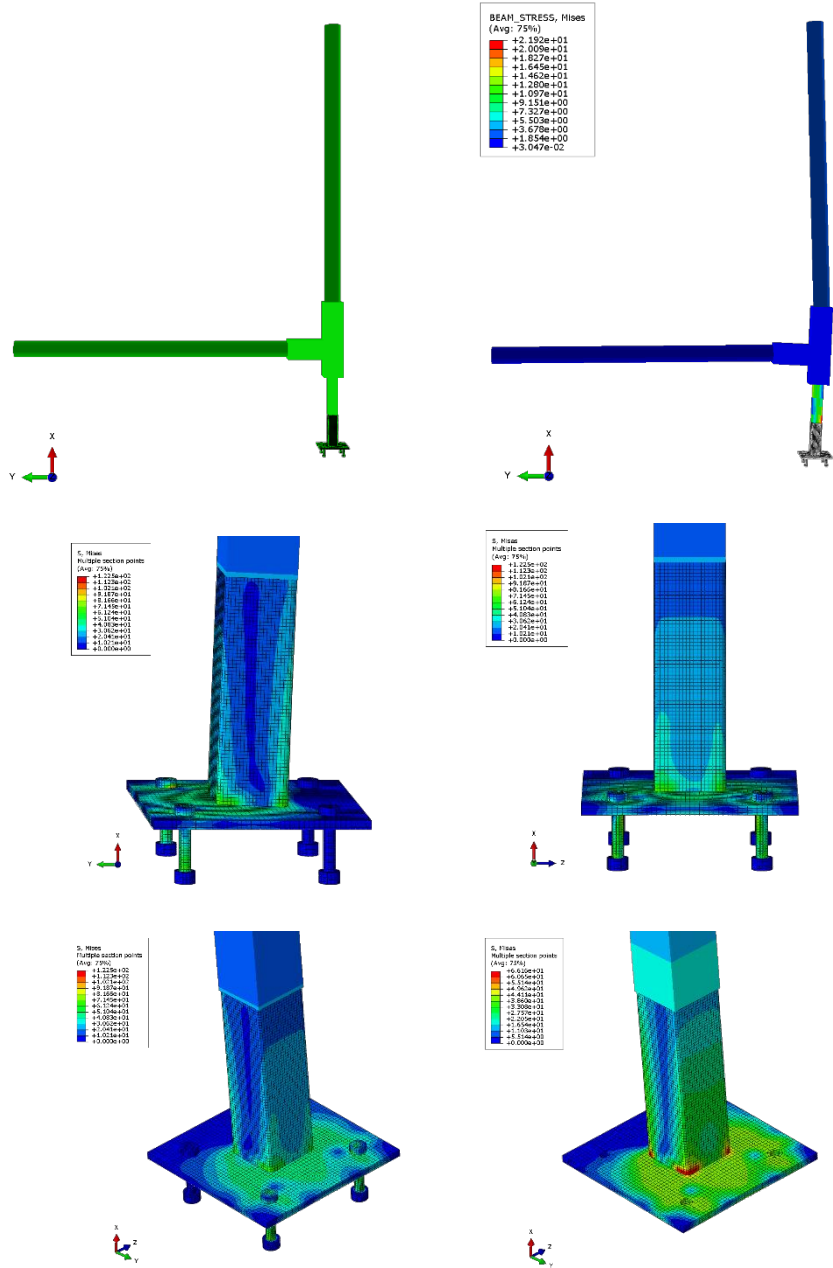
Canopy Beam: C13



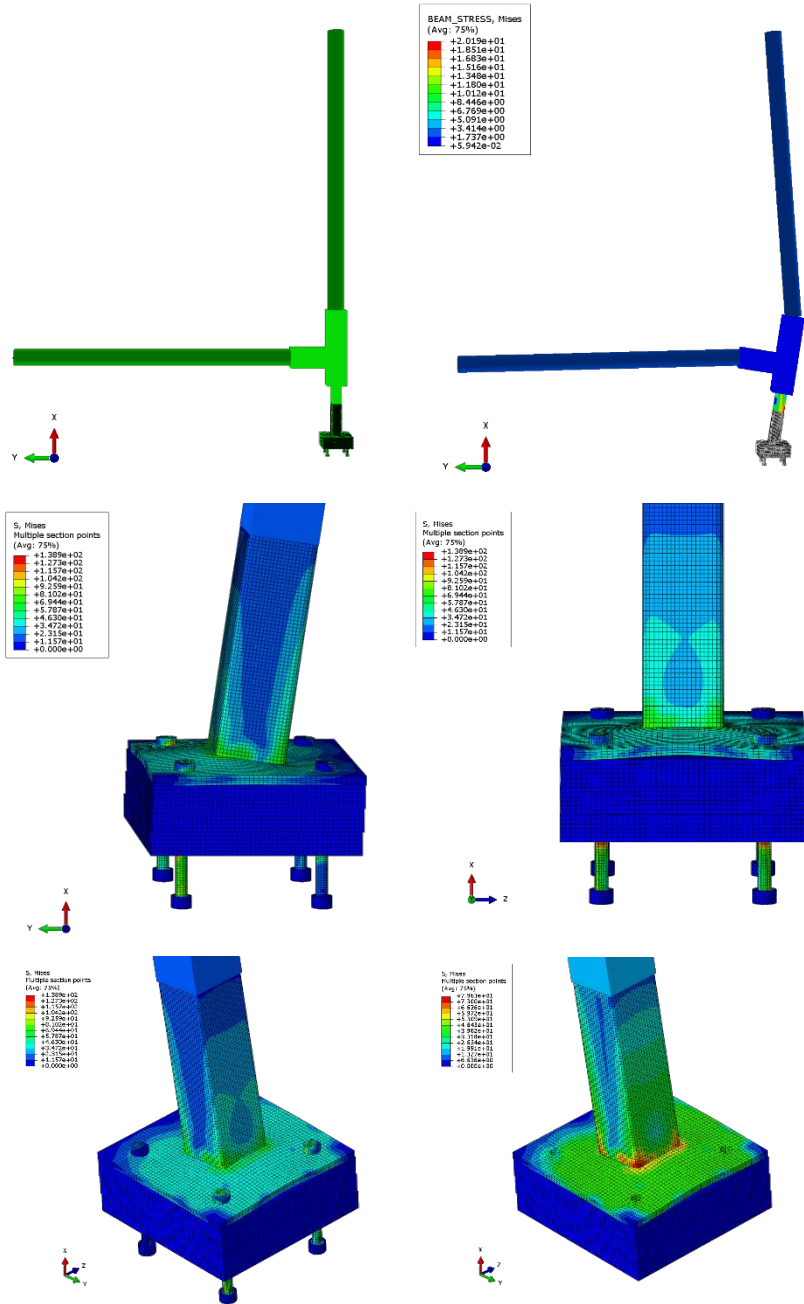
Canopy Beam: C15



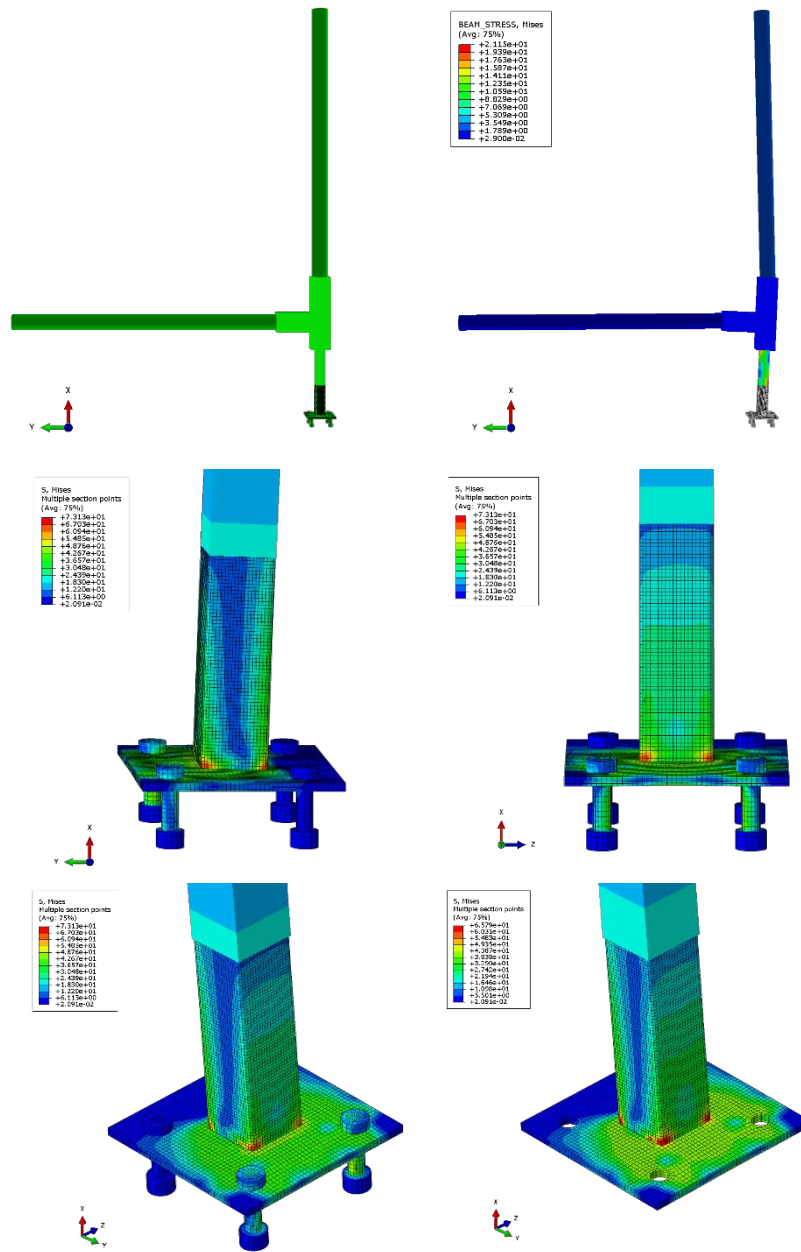
Roof Post: R1



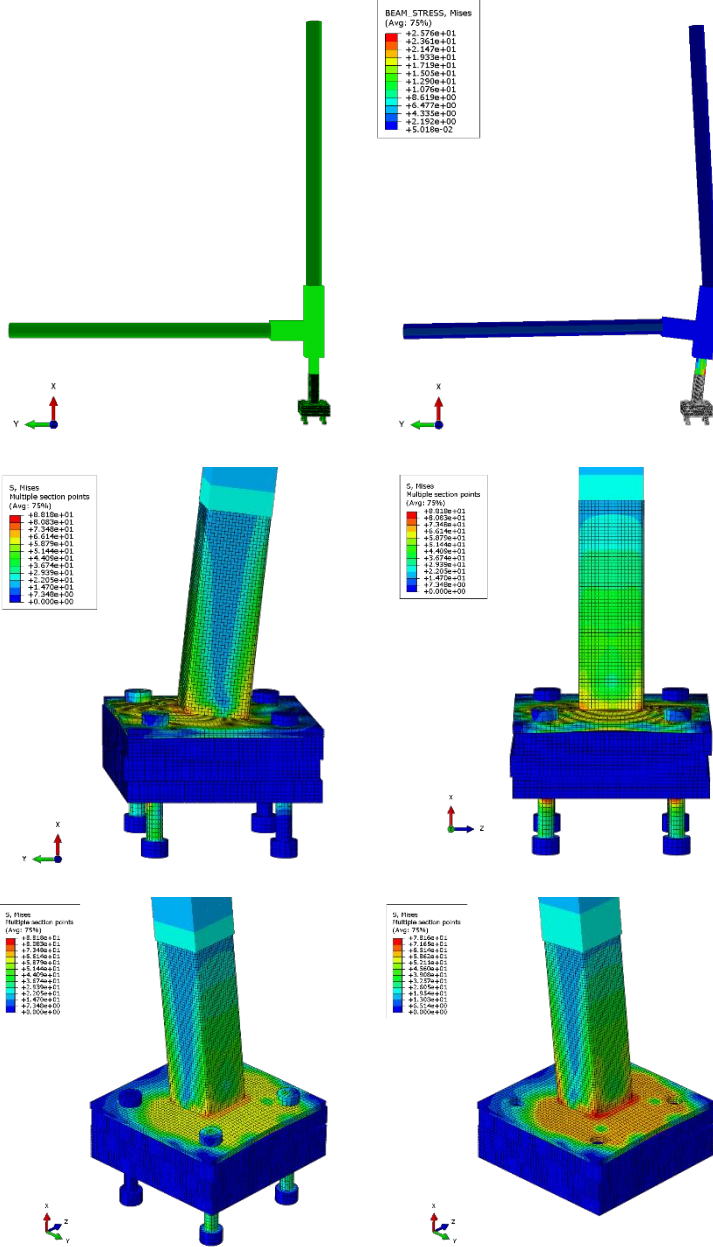
Roof Post: R2



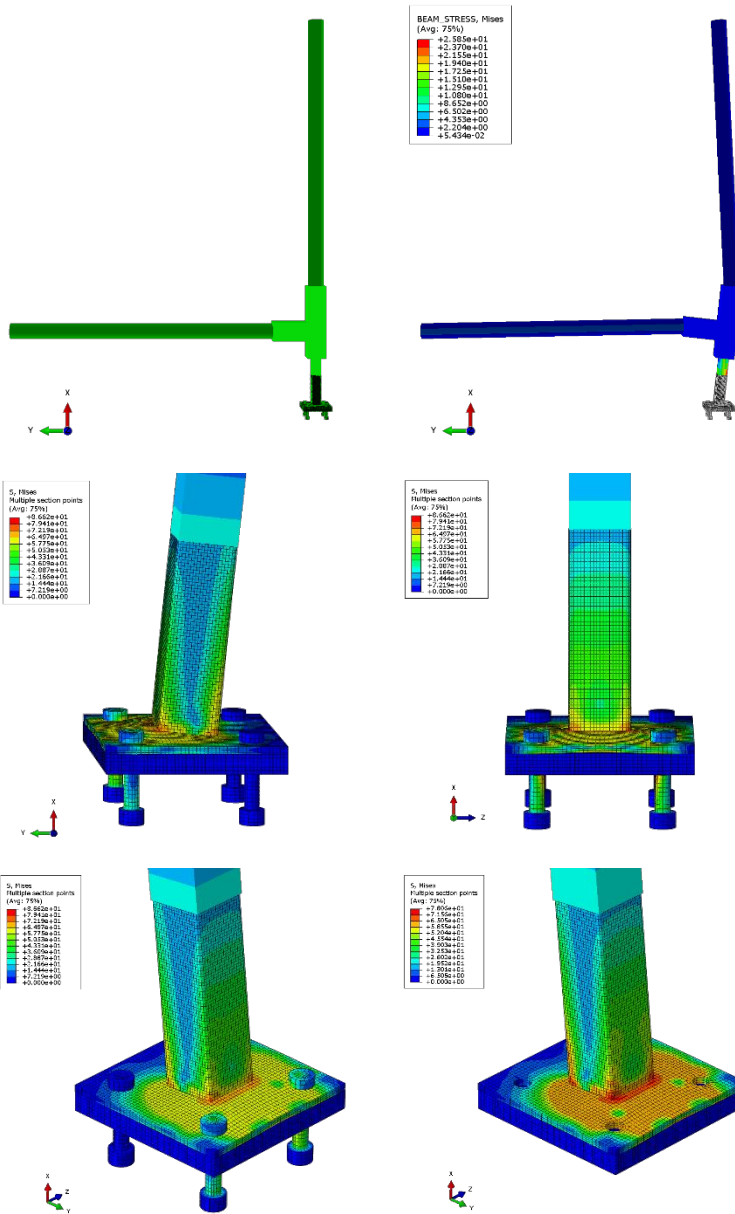
Roof Post: R7



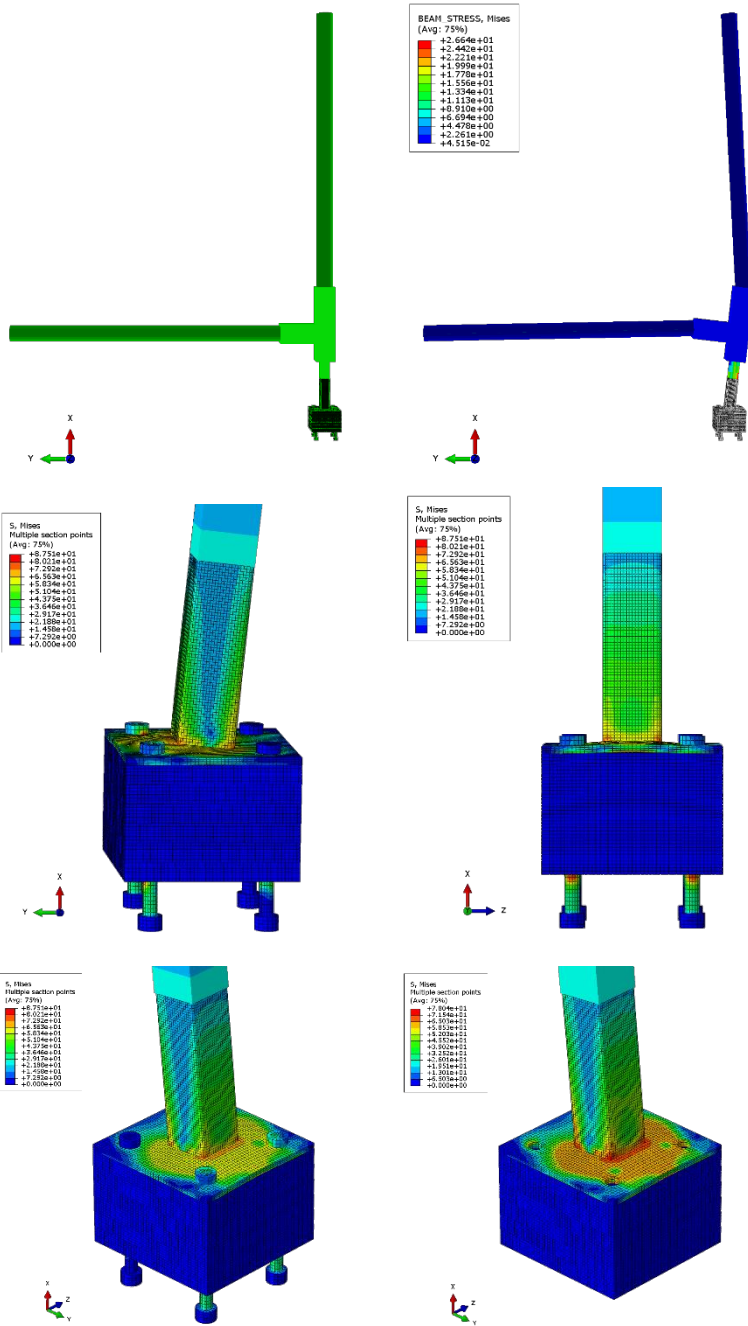
Roof Post: R8



Roof Post: R13



Roof Post: R15



Appendix G: Mill Certificates

The following mill certificates were provided by Capone Iron Corporation of Rowley, MA.



**WELDED TUBE
OF CANADA CORP.**
111 Rayette Rd
Concord, Ontario, L4K 2E9
Tel: (905) 669-1111
Fax: (905) 738-4070
Toll Free 1-800-565-TUBE (8223)

TEST REPORT
REPORT # ES5A1

NUMBER/NUMBER . 896392
DATE/M/M D/C Y/A : 2/01/16
PAGE: 1

10552 BUSINESSICK METALS
ATTN: CAROL L. STANTFORD
560 NORTH WASHINGTON AVE.
BRIDGEPORT
CT 06604 USA

Customer P.O. WTC BOLD Ship Date WTC Item#
01-21574-CS 510643 2/01/16 S10462
Description
ASTM A500 GR B & C, RM. 4, 000 4, 000 .50C 48C 003

CHEMICAL COMPOSITION

HEAT	TYPE	C	Mn	P	S	SI	CU	NI	Cr	Mo	Sn	V	Co	Ti	N	B	Al	Ca	CE
778126	HEAT	.170	.820	.012	.037	.015	.053	.013	.034	.003	.007		.002	.007	.003	.000	.047		.118
823989	HEAT	.170	.793	.010	.037	.018	.033	.022	.039	.004	.008		.002	.002	.005	.000	.035		.314

CE = C + Mn/6 + Ni + Cu/15 + Cr + Mo + V/5

TENSILE PROPERTIES

HEAT	TEST LOT	TYPE/SIZE	ORIENT	LOC	COND	10.2X OFFSET	YIELD	TENSILE	ELONG
						MIN	50.0	MIN	62.0
						MAX	KSI	KSI	(2")
778126	S-1.50"	L	R	AM		68.5	74.0	41	
823989	S-1.50"	L	B	AM		68.2	77.0	12	

LEGEND S: STR: P: L: LONGITUDINAL T: TRANSVERSE H: HOLE W: WELD M: AS WELDED N: NORMALIZED Q: QUENCHED AND TEMPERED SR: STRESS RELIEVED

Country of Origin: CANADA
Does not contain mercury, cadmium or lead.
Direct all inquiries to: sales@canadaweldtube.com

QANDJHEH02



**WELDED TUBE
OF CANADA CORP.**

111 Rayette Rd.
Concord, Ontario, L4K 2E9
Tel: (905) 669-1111
Fax: (905) 738-4070
Toll Free: 1-800-565-TUBE (8823)

TEST REPORT
RAPPORT D'ESSAI

NUMBER/NUMERO : 996992

DATE (M/M D/J) Y/N : 2/01/16

PAGE: 2

We hereby certify that the product was manufactured, sampled, tested and inspected in accordance with the latest edition of the specification at time of manufacture and any other requirements designated on the purchase order or contract. The tests were found to meet all such requirements.
This inspection certificate is in accordance with EN 10204 3.1.

Nous certifions par la présente que le produit a été fabriqué, échantillonné, testé et inspecté conformément à la dernière édition de la spécification au moment de la fabrication et de toutes les autres exigences désignées sur le bon de commande ou contrat. Les essais rencontrés, et respectent toutes ces exigences.
Ce certificat d'inspection a été établi en conformité avec la norme EN 10204 3.1.

Authorized By/Autorize Par : MR. METALLURGICAL SERVICES

0A033180A7

INSPECTION CERTIFICATE



Head Office
53, Jungbong-daero, Dong Gu,
Incheon 401-712, S. Korea

EN 10204(2004) TYPE 3.1

Certificate No. H20150202560 - 16

Class Cert. No.

Date of Issue 2015-02-16

Contract No.	
Customer	HYUNDAI CORPORATION
L/C No.	
P/O No.	46201501AW03
Commodity	H-BEAM ASTM A572 G50/A992/ CSA 350W
Specification	

Dimensions & Length	Heat No.	Pieces Weights (kg)	Chemical Composition (%)											Tensile Test			Impact Test (V-notch)			Remarks (Impact Specimen Size)	
			C	Mn	P	S	Cu	Mo	Al	Nb	Sn	CE(1)	Tensile Strength N/mm ²	Yield point N/mm ²	Elongation(2) %	Yield Ratio	AVG	1	2		3
14X14-1/2X132	N 027251	2	15	17	116	26	8	26	3	5	3	14	4	566	398	24.0	0.70				
60.00 FT		7,184												594	379	24.5	0.68				
14X14-1/2X132	N 027252	2	17	17	114	27	10	27	2	5	13	42	568	397	23.5	0.70					
60.00 FT		7,184												557	383	23.0	0.63				
14X14-1/2X73	N 026792	2	14	20	53	26	12	31	2	6	5	16	29	501	402	25.5	0.80				
40.00 FT		2,648												495	395	25.0	0.81				
14X14-1/2X73	N 026222	1	19	15	65	19	12	25	2	6	4	9	34	547	423	24.0	0.77				
50.00 FT		1,655												515	421	23.9	0.77				
14X14-1/2X89	N 026204	1	20	13	69	27	10	21	3	5	9	38	553	417	24.0	0.76					
40.00 FT		1,614												529	372	26.0	0.70				
14X14-1/2X89	N 027215	3	18	21	66	20	6	24	3	3	10	34	569	369	23.5	0.76					
40.00 FT		8,070												522	422	24.0	0.76				
14X14-1/2X89	N 026132	1	20	15	66	26	11	23	2	4	10	37	522	420	24.0	0.76					
50.00 FT		2,018												530	372	26.0	0.70				
14X14-1/2X89	N 027215	5	18	21	66	20	6	24	2	4	16	33	526	369	25.0	0.70					
50.00 FT		10,090												530	372	26.0	0.70				
14X14-1/2X89	N 027215	5	16	21	66	20	6	24	2	4	10	34	526	369	25.0	0.70					
60.00 FT		12,105												526	369	25.0	0.70				
SUBS TOTAL		24												52,568							

(Note) (1) Ceq [CE=C+Mn/6+Cr/5+V/5+Mo/5+Ni/15+Cu/15]

(2) Gauge length : 200 mm

(3) Yield Ratio = YP/TS

J. C. Ahn

General Manager of O.A Team

HMS1102(A)-3a

QR코드 "Qcert" App로 모바일 화면 확인에 사용되는 QR코드 (QRcode scanner App (Qcert))

2010632 A4(210x297)

WE HEREBY CERTIFY THAT THE MATERIAL HAS BEEN MADE AND TESTED IN ACCORDANCE WITH THE ABOVE SPECIFICATION AND ALSO WITH THE REQUIREMENTS CALLED FOR THE ABOVE ORDER

OLYMPIC STEEL
5080 RICHMOND ROAD
BEDFORD HEIGHTS, OH 44146 USA
PHONE: 216-292-3800

METALLURGICAL TEST REPORT

>>>>> CERTIFICATE OF ANALYSIS AND TESTS <<<<<<

Sold To: BUSHWICK-KOONS STEEL
P.O. BOX 476
PARKER FORD, PA 19457

Ship To: BUSHWICK
560 N WASHINGTON AVE
BRIDGEPORT, CT 06604

Sales Order: 364258 - 02 B/L No: 591790 Release: 2 Date: 03-Aug-2015
Reference: HALPIN, JOHN (31009) 2nd B/L: Cus Ord #: 01-00100
Cus Name: BUSHWICK-KOONS STEEL

Description of Material and Specification

Hot Rolled Plate A572/HSLAS50
875" x 96" x 240"

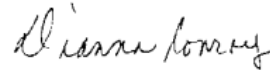
TAG#: 23902739
HEAT#: A5D910/SSAB - IOWA
MC # 23759247

Chem Elem Symbol / Elem Content Value:

<C : .17> <MN : 1.1> <P : .01> <S : .004> <SI : .13> <AL : .026> <V : .029> <CB : .002> <CU : .3> <NI : .12>
<CR : .15> <MO : .04> <TI : .007>

YIELD STRENGTH	MIN:	56000 PSI	MAX	56000 PSI
TENSILE STRENGTH	MIN:	75000 PSI	MAX	75000 PSI
ELONGATION 8"	MIN:	23 %	MAX	23 %

We hereby certify the above is correct as contained in the records of the corporation



Branch Certification Manager

USER: REPORTS@SEMSPRD
REPORT: ST MSR OSI

03-Aug-2015 2:00 PM
Page 4 of 5

USIMINAS
 USIMINAS SIDERURGICAS DE MINAS GERAIS S.A.
 Rua José Bonifácio, 100 - Vila Santa Helena - Belo Horizonte - Minas Gerais - Brasil
 CEP: 31280-000 - Fone: (051) 251-1111 - Telex: 5100000
 INCORPORADO EM 1974

INSPECTION CERTIFICATE/PACKING LIST
CERTIFICADO DE INSPEÇÃO
STEEL PLATE
 MARCA: MINOVA-FORTECO
 0150082786 non

Fabricated: 10/10/74
 Thickness: 10 mm
 Width: 2400 mm
 Length: 12000 mm
 Gross Weight: 47.000 kg
 Net Weight: 45.000 kg
 Date of Issue: 05/08/2014
 Certificate N°: 274839

Inspected by: [Signature]
 Date of Issue: 05/08/2014
 Certificate N°: 274839

Remarks: Observações
 COTA: CT 14 INSPERFI AC 101 14/07/2014 TRC/DOR WARKS BLANCO/RENEWELL 3M
 MSUD: Material Safety Data Sheet for the available at: www.usiminas.com.br
 P. 20 - 14/07/2014

Inspected by: [Signature]
 Date of Issue: 05/08/2014
 Certificate N°: 274839

Inspected by: [Signature]
 Date of Issue: 05/08/2014
 Certificate N°: 274839

Inspected by: [Signature]
 Date of Issue: 05/08/2014
 Certificate N°: 274839

Inspected by: [Signature]
 Date of Issue: 05/08/2014
 Certificate N°: 274839

Inspected by: [Signature]
 Date of Issue: 05/08/2014
 Certificate N°: 274839

Inspected by: [Signature]
 Date of Issue: 05/08/2014
 Certificate N°: 274839

Inspected by: [Signature]
 Date of Issue: 05/08/2014
 Certificate N°: 274839

Certificate of Mill Test Results

PHL-000003-000

Fig 1/1

PO/Rel

PART NO.

Attn:

NUCOR
PLATE MILL

P.O. Box 279
Winton, NC 27386
(552) 356-3700

Mill Test Report
Page 1

NUCOR
For Your

Issuing Date : 08/04/2015
Vehicle No : Reinsfelder 537674
Specification : 1.0000" x 96.000" x 240.000"
ASTM A572 50-55/ASTM A709 50-13a Type 2/CSA G40.21-50W/350W-
04/43 AASHTO M270-50

Load No. : 427898
Sold To : CHAPEL STEEL CORP
590 N BETHLEHEM PIKE
PO BOX 1000
SPRINGHOUSE, PA 19477

Our Order No. : 12941616

Cust. Order No. : PHL-11451
Ship To : CHAPEL STEEL CO (TRK CUST PAU)
POTTSTOWN INDUSTRIAL COMPLEX
BUILDING 2E
191 S KEIM ST
POTTSTOWN, PA 19464

Marking :

Heat No	C	Mn	P	S	Si	Cu	Ni	Cr	Mo	Al(tot)	V	Nb	Ti	N	Ca	B	Sn	Cuq	Pcm
5504700	0.19	1.28	0.011	0.000	0.17	0.23	0.11	0.10	0.02	0.032	0.042	0.003	0.002	0.0019	0.0002	0.012	0.46	0.28	

Plate Serial No	Tensile Test		Dir	Yield Tensile (psi)	Tensile (psi)	Elongation % in 2"	Elongation % in 8"	Dir.	Charpy Impacts					
	Pieces	Tons							(%) shear	(%) shear	(%) shear	Ave	Min	Max
5504700-04	6	19.80	1	59,200	82,900	21.0	19.4		1	2	3			

Manufactured to fully killed fine grain practice by Electric Arc Furnace. Welding or weld repair was not performed on this material. Mercury has not been used in the direct manufacturing of this material. Produced as continuous cast discrete plate as rolled, unless otherwise noted in Specification. For Mexico shipments: mhc-Sales@nuco.com Yield by 0.50UL method unless otherwise specified. Ceq = C+(Mn/6)+(Cr+Mo+V/5)+(Cu+Ni/15) Pcm = C+(Si/20)+(Mn/20)+(Cu/20)+(Ni/60)+(Cr/20)+(V/5)+(W/10)+S Melting and Manufactured in the USA. ISO 9001:2008 certified (#010940) by SRI Quality System Registrar (#0595-09). PED 9723EC 7/2 Annex 1. Para. 4.3 Compliant. DIN 58049 3 T 8/EN 10264 3.18(2004). DIN EN 10204 3.1(2005) compliant. For A55 grades only. Quality Assurance certificate 14-IMPQA-723

8/4/2015 8:58:54 AM

T. A. Deprets, Weiburgist

NUCOR
PLATE MILL

P.O.Box 279
 Winton, NC 27986
 (252) 356-3700

Mill Test Report

Page 2



Issuing Date : 12/01/2014 BIL No. : 403173 Our Order No. : 12339916 Cust. Order No. : DBP-1721

Vehicle No: TTPX 804324

Specification : 2.0000" x 96.000" x 240.000"

ASTM A572 Grade 50-13w/ASTM A709 Grade 50-13w/AAASHTO M270-50

Type 2

Load No. : 408274

Sold To : BUSHWICK METALS INC

185 GREAT NECK RD

STE 202

GREAT NECK, NY 11021

Ship To : ANASTASIO & SONS TRUCKING CO

158 MIDDLETOWN AVE

MIDDLETOWN, CT 06457

Marking :

Heat No	C	Mn	P	S	Si	Cu	Ni	Cr	Mo	Al(tot)	V	Nb	Ti	N	Ca	B	Sn	CEQ	PCM
4508338	0.17	1.17	0.010	0.002	0.18	0.26	0.11	0.09	0.01	0.024	0.043	0.002	0.002	0.002	0.0013	0.0000	0.0009	0.41	0.25

Plate Serial No	Tensile Test		Elongation		Charpy Impacts			Min Temp	Ave.
	Pieces	Tons	Dir.	Yield	(psi) Tensile	(%) Elongation % in 2"	(%) Elongation % in 8"		
4508338-03	6	39.20	T	50,500	76,500	19.3	19.3		
			T	60,100	82,800	19.9	19.9		

Manufactured to fully killed fine grain practice by Electric Arc Furnace. Welding or weld repair was not performed on this material. Mercury has not been used in the direct manufacturing of this material. Produced as continuous cast discrete plate as-rolled, unless otherwise noted in Specification. For Mexico shipments: rnc-SalesMX@Nucor.com
 Yield by 0.5EUT method unless otherwise specified. Ceq = C+(Mn/6)+(Cr+Mo+V/5)+(Cu+Ni/15)
 Form = C+(S/30)+(Mn/20)+(Cu/20)+(Ni/60)+(Cr/20)+(Mo/15)+(V/10)+5B
 Melted and manufactured in the USA. ISO 9001:2008 certified (#010940) by SRI Quality System Registrar (#0985-09) PED 87/23/EC 712 Annex 1, Para. 4.3 Compliant.
 DIN 50049 3.1/EN 10204 3.1B(2004), DIN EN 10204 3.1(2005) compliant. For ABS grades only, Quality Assurance certificate 14-MMPOA-723

T. A. Depreis
 T. A. Depreis, Metallurgist

12/01/2014 11:24:00 AM



US-ML-PETERSBURG
25801 HOFHEIMER WAY
PETERSBURG, VA 23803-8905
USA

CERTIFIED MATERIAL TEST REPORT

CUSTOMER SHIP TO
AZCO STEEL COMPANY
1641 NEW MARKET AVE
SOUTH PLAINFIELD, NJ 07080-1634
USA

CUSTOMER BILL TO
BUSHWICK METALS LLC
185 GREAT NECK ROAD
GREAT NECK, NY 11021-3352
USA

SALES ORDER
3222844/000030

GRADE
A992/A572-50

LENGTH
50'00"

SHAPE / SIZE
Wide Flange Beam / 12 X 58# / 310 X 86

WEIGHT
5,800 LB

HEAT / BATCH
60115479/03

Page 1/1

CUSTOMER PURCHASE ORDER NUMBER
02-27186

CUSTOMER MATERIAL N°

BILL OF LADING
1330-000064137

DATE
01/27/2016

SPECIFICATION / DATE OF REVISION
ASTM A6-14
ASTM A709-13A
ASTM A992-11, A572-15
CSA G40.21-13 345SWM

CHEMICAL COMPOSITION

C	%	0.10
Mn	%	1.04
P	%	0.018
S	%	0.021
Si	%	0.24
Cr	%	0.37
Ni	%	0.16
Mo	%	0.033
Sn	%	0.013
V	%	0.002
Nb	%	0.018
Al	%	0.003

CHEMICAL COMPOSITION

CEqvA6	%	0.34
--------	---	------

MECHANICAL PROPERTIES

YS	MPa	379
TS	MPa	404
UTS	MPa	538
YS	MPa	379
TS	MPa	404
UTS	MPa	538

MECHANICAL PROPERTIES

G/L	mm	200.0
Elong.	%	25.00
	%	25.50
Y/T ratio	%	0.751
	%	0.767
G/L	Inch	8.000
	Inch	8.000

COMMENTS / NOTES

The above figures are certified chemical and physical test records as contained in the permanent records of company. We certify that these data are correct and in compliance with specified requirements. This material, including the billets, was melted and manufactured in the USA. CMTR complies with EN 10204 3.1.

Shasthary

BHASKAR VALAMANCHILI
QUALITY DIRECTOR

Alice K. Pitchford

ALICE PITCHFORD
QUALITY ASSURANCE MGR.

18Dec15 18:34

T E S T C E R T I F I C A T E

No: MAR 381767

INDEPENDENCE TUBE CORPORATION
6226 W. 74TH STREET
CHICAGO, IL 60638
Tel: 708-496-0380 Fax: 708-563-1950

P/O No 02-24305-KB
Rel
S/O No MAR 298700-003
B/L No MAR 173893-005 Shp 22Dec15
Inv No Inv

Sold To: (615)
BUSHWICK METALS - SOUTH PLAINFIELD
25 ROCKWOOD PLACE
SUITE 320
ENGLEWOOD, NJ 07631

Ship To: (1)
BUSHWICK METALS - SOUTH PLAINFIELD
1641 NEW MARKET AVENUE
BLDG.6
908-754-8700
SOUTH PLAINFIELD, NJ 07080

Tel: 201-567-2400 Fax: 201 816-5865

CERTIFICATE of ANALYSIS and TESTS

Cert. No: MAR 381767
18Dec15

Part No
TUBING A500 GRADE B(C)
3" SQ X 3/16" X 40'

Pcs Wgt
24 6,595

Heat Number Tag No
541630 993409

Pcs Wgt
24 6,595

YLD=65450/TEN=74820/ELG=30.3

Heat Number
541630

*** Chemical Analysis ***
C=0.1900 Mn=0.8100 P=0.0120 S=0.0030 Si=0.0100 Al=0.0400
Cu=0.0100 Cr=0.0300 Mo=0.0100 V=0.0010 Ni=0.0100 Cb=0.0010
MELTED AND MANUFACTURED IN THE USA

WE PROUDLY MANUFACTURE ALL OF OUR HSS IN THE USA.
INDEPENDENCE TUBE PRODUCT IS MANUFACTURED, TESTED,
AND INSPECTED IN ACCORDANCE WITH ASTM STANDARDS.

CURRENT STANDARDS:

.....A500/A500M-13
.....A513-12
.....A252-10
.....A847/A847M-12

MATERIAL IDENTIFIED AS A500 GRADE B(C) MEETS BOTH
ASTM A500 GRADE B AND A500 GRADE C SPECIFICATIONS.



Steel Dynamics, Inc.

Structural and Rail Division • Columbia City, Indiana

(260) 625-8100 (260) 625-6950 FAX
Quality Steel 100% EAF Melted
and Manufactured in the USA

Recycled content: PC = 96.0%, PI = 3.8%
ISO 9001:2008 and ABS Certified

CERTIFIED MILL TEST REPORT

Customer # 000482

Printed: 08 / 05 / 2015

Produced: 07 / 14 / 2015

Ship to:
Bushwick Metals, Inc.
560 N. Washington Ave.
UNLOAD BY APPOINTMENT ONLY
Bridgeport CT, 06604 US
Attn: Receiving - ext. 3323 or 3324

Bill to:
BUSHWICK METALS
185 Great Neck Road Suite 320
Great Neck NY, 11021 US
Attn: Jim Zawisa

GENERAL INFORMATION		SPECIFICATIONS		SHIPMENT DETAILS	
Product	American Standard C	Standards		Bundle / ASN #	
Size	C 10X25	ASTM A616M - 14		Length	pcs
Heat Number	A112619	* ASTM A992/A992M - 11	A992 / A992M	8	01-06156
Condition(s)	As-Rolled Fine Grained Fully Killed No Weld Repair	ASTM A709/A709M - 13a	A709 gr50/gr345	8	01-06156
		ASTM A572/A572M - 13a	A572 gr50/gr345		
		AASHTO M270M/M270 - 12	M270 gr345/gr50		
		CSA G40.21-13	50W/550W		
		ASTM A36/A36M - 14	A36 / A36M		
				BOL #	0000378392 - 16000.00 lbs
				Cust PO	
				Recy PO	
				Job	

CHEMICAL ANALYSIS (weight percent)																				
C	Mn	P	S	Si	Cu	Ni	Cr	Mo	Sn	V	Nb/Cb	AI	N	B	*C1	*C2	*C3	*PC	*I	Analysis Type
.10	1.24	.014	.014	.22	.32	.10	.10	.034	.010	.036	.001	.001	.0144	.0004	.37	.40	.35	.20	5.71	Heat

MECHANICAL TESTING					
Test	Yield (fy)	Tensile (fu)	Elong. ratio (8" gage)	Temp F / C	Absorbed Energy ft-lbf / J
	Strength ksi / MPa	Strength ksi / MPa			
1	56 / 387	74 / 510	.76		
2	59 / 406	75 / 515	.79		
3					
4					

CHARPY IMPACT TESTS (available only when specified at time of order)					
Temp	F / C	Specimen 1	Specimen 2	Specimen 3	Minimum
Test					
1					
2					
3					
4					
5					
6					
7					

Notes: *Calculated Chemistry Values: Carbon Equivalents (Ct, C2, C3, PC), Corrosion Index (I) (ASTM G101)- 25.01(Cu)+3.88(Ni)+1.20(Cr)+1.49(Si)+17.25(P)+2.9(Cu)(Mn)+9.10(Ni)(P)+33.38(Cr)
 CEI (Mn+Cr+Mo+V)/5-(Ni+Cu)/15 CEZ (Mn+Si)/C-(Mn+Si)/5-(Ni+Cu)/15 CE3 (CE1) + C (Mn+Si) + (Si/24) + (Cr/3) + (P/40) + (Mn/4) + (Ni/4) Perm(AVZ) - C-5100-Min20-Cu20-MN60-Cr20-mr(15-V)(10-58)

I hereby certify that the material described herein has been made to the applicable specification by the electric arc furnace/continuous cast process and tested in accordance with the requirements of American Bureau of Shipping Rules with satisfactory results.

Signed: **Jeremy Cronkhite**
 Manager of Product Quality and Process Improvement

I hereby certify that the content of this report are accurate and correct. All tests and operations performed by this material manufacturer are in compliance with the requirements of the material specifications and applicable purchaser designated requirements.

Signed: _____ My commission expires: _____
 Notary Public

State of Indiana, County of Whitley Sworn to and subscribed before me this _____ day of _____

ASTM A6 - 14 G: A signature is not required on the test report; however, the document shall clearly identify the organization submitting the report. Notwithstanding the absence of a signature, the organization submitting the report is responsible for the content of the report.

Page 2 of 3



Steel Dynamics - Roanoke Bar Division
 P.O. Box 13948 Roanoke, VA 24038
 Office: 540-342-1831 Fax: 540-342-9437

Test and Inspection Report

NO. 03509-4
 ROANOKE

BUSHWICK METALS LLC
 185 GR NECK RD - 320
 GREAT NECK NY 11021-0000

Date 12/23/15

HEAT NUMBER	SIZE	1-YIELD Pt. KSI	ULTIMATE KSI	ELONG 8 IN. TEST	BEND TEST	GRADE					
JK7223	ANGLES 4 X 4 X 1/4	55.5	76.9	29.4		A36/A529					
PURCHASE ORDER NUMBER	NUMBER PIECES	2-YIELD Pt. KSI	ULTIMATE KSI	ELONG 8 IN. TEST	BEND TEST	GRADE					
01-03259	39 PIECES 20'	55.9	77.1	30.3		A36/A529					
HEAT NUMBER	SIZE	1-YIELD Pt. MPA	ULTIMATE MPA	ELONG 203mm TEST	BEND TEST	GRADE					
JK7223	ANGLES 101.6 X 101.6 X 6.4	382.7	530.2	29.4		A36/A529					
PURCHASE ORDER NUMBER	NUMBER PIECES	2-YIELD Pt. MPA	ULTIMATE MPA	ELONG 203mm TEST	BEND TEST	GRADE					
01-03259	39 PIECES 20'	385.4	531.6	30.3		A36/A529					
C	MN	S	P	SI	CR	NI	MO	CU	V	NB	CE
.14	1.05	.027	.011	.24	.11	.10	.02	.28	.021	.002	.41

MERCURY, RADIUM OR OTHER ALPHA SOURCE MATERIALS IN ANY FORM HAVE NOT BEEN USED IN THE PRODUCTION OF THIS MATERIAL. NO WELD REPAIR HAS BEEN PERFORMED.

Approved ABS QA Mill. Certificate No. 12-MMPQA-676

This material was melted and manufactured in the USA by basic Electric Furnace processes to meet specification: ASTM A36-14, A529-14 GR50, ASTM A572-15 GR50, A709-13A GR36 & GR50, ASME SA36-13 (01JUL13)

The tensile values stated in either inch-pound units or SI units are to be regarded as separate as defined in the ASTM scope for this material. Unless a metric specification is ordered, this material has been tested and meets the requirements of the inch-pound ranges.

This is to certify the above to be a true and accurate report as contained in the records of this company.

Engineer of Tests: Lewis E. Leftwich Jr.

A

ArcelorMittal

ArcelorMittal LaPlace
138 HWY 3217
LaPlace LOUISIANA 70068
Telephone (985) 652-4900
Export Country = USA

MATERIAL CERTIFICATION REPORT

BUSHWICK METALS LLC
SOUTH PLAINFIELD, NJ
1641 New Market Avenue
SOUTH PLAINFIELD NJ 07080
USA

Tested in Accordance
With: ASTM A6

Sales Order 140965-1 Date 10/21/2015 PO: 02-06075
Product Unequal Angles Cust 40005904 Ref. 80850412
Heat NO. L100623 Grade A3652950 Pieces 24
Cust.Mat. Length 40' 00" Weight 9889
Size 6"X4"X5/16"X10.300

CHEMICAL ANALYSIS	TEST 1		TEST 2		TEST 3	
	IMPERIAL	METRIC	IMPERIAL	METRIC	IMPERIAL	METRIC
C 0.12	56900 PSI	392 MPa	56400 PSI	389 MPa		
Mn 0.88	75800 PSI	523 MPa	76900 PSI	530 MPa		
P 0.012	34 %	34 %	29 %	29 %		
S 0.027	8 IN	203 mm	8 IN	203 mm		
Si 0.18						
Cu 0.32						
Ni 0.20						
Cr 0.20						
Mo 0.061						
Cb 0.010						
V 0						
B						
Al						
Sn 0.011						
N						
Ti						
Ci 5.9						
CE 0.36						

MECHANICAL PROPERTIES	TEST 1		TEST 2		TEST 3	
	IMPERIAL	METRIC	IMPERIAL	METRIC	IMPERIAL	METRIC
YIELD STRENGTH	56900 PSI	392 MPa	56400 PSI	389 MPa		
TENSILE STRENGTH	75800 PSI	523 MPa	76900 PSI	530 MPa		
ELONGATION	34 %	34 %	29 %	29 %		
GAUGE LENGTH	8 IN	203 mm	8 IN	203 mm		
BEND TEST DIAMETER						
BEND TEST RESULTS						
SPECIMEN AREA						
REDUCTION OF AREA						
IMPACT STRENGTH						

IMPACT STRENGTH AVERAGE TEST TEMP ORIENTATION	INTERNAL CLEANLINESS		GRAIN SIZE HARDNESS
	SEVERITY FREQUENCY RATING	GRAIN PRACTICE REDUCTION RATIO	

This heat makes the following grades: A36-0E, A57950-05, G40.21-CSA50W, CSA44W, A70936-09a, ASME SA36-2010, A57250-07, A70950-10, and the following AASHTO M270 Grades: 36, 50, and 345. Heat is free of Mercury contamination in the process.

I hereby certify that the material test results presented here are from the reported heat and are correct. All tests were performed in accordance to the specification reported above. All steel is electric arc furnace melted (billets), manufactured, processed, tested in the U.S.A with satisfactory results. No weld repair was performed on this heat.

Notarized upon request: _____ Signed: Mark Edwards
Sworn to and subscribed before me on this 21st day of October, 2015 MARK EDWARDS, QUALITY ASSURANCE SUPERVISOR

Notary Public _____ Parish/County _____
Direct any questions or necessary clarifications concerning this report to the Sales Department 1-800-535-7692 (USA)



ArcelorMittal LaPlace
 138 HWY 3217
 LaPlace LOUISIANA 70068
 Telephone (985) 652-4900
 Export Country = USA

MATERIAL CERTIFICATION REPORT
 BUSHWICK METALS LLC
 105 Great Neck Road, Suite 320
 GREAT NECK NY 11021
 USA

BUSHWICK METALS LLC
 SOUTH PLAINFIELD, NJ
 1641 New Market Avenue
 SOUTH PLAINFIELD NJ 07080
 USA

Tested in Accordance With: ASTM A6
 Sales Order 138386-1 Date 09/16/2015 PO: 02-06040
 Product Unequal Angles Cust 40005904 Ref. 80836698
 Heat No. L98235 Grade A3652950 Pieces 20
 Cust.Mat. Length 40' 00" Weight 10880
 Size 7"X4"X3/8"X13.600

CHEMICAL ANALYSIS	TEST 1		TEST 2		TEST 3	
	IMPERIAL	METRIC	IMPERIAL	METRIC	IMPERIAL	METRIC
C	0.14					
Mn	0.85					
P	0.007					
S	0.022					
Si	0.18					
Cu	0.27					
Ni	0.12					
Cr	0.14					
Mo	0.051					
Cb	0.010					
V	0					
B						
Al						
Sn	0.009					
N						
Ti						
Ci	5.4					
CF	0.34					

MECHANICAL PROPERTIES	TEST 1		TEST 2		TEST 3	
	IMPERIAL	METRIC	IMPERIAL	METRIC	IMPERIAL	METRIC
YIELD STRENGTH	56900 PSI	392 MPa	55700 PSI	384 MPa		
TENSILE STRENGTH	77400 PSI	534 MPa	76800 PSI	530 MPa		
ELONGATION	33 %	33 %	32 %	32 %		
GAUGE LENGTH	8 IN	203 mm	8 IN	203 mm		
BEND TEST DIAMETER						
BEND TEST RESULTS						
SPECIMEN AREA						
REDUCTION OF AREA						
IMPACT STRENGTH						

IMPACT STRENGTH AVERAGE TEST TEMP ORIENTATION	INTERNAL CLEANLINESS		GRAIN SIZE	
	IMPERIAL	METRIC	SEVERITY FREQUENCY RATING	HARDNESS GRAIN PRACTICE REDUCTION RATIO

This heat makes the following grades: A36-08, A52950-05, G40.21-CSA509, CSA44W, A70936-09a, ASME SA36-2010, A57250-07, A70950-10, and the following RASHTO M270 Grades: 36, 50, and 345. Heat is free of Mercury contamination in the process.

I hereby certify that the material test results presented here are from the reported heat and are correct. All tests were performed in accordance to the specification reported above. All steel is electric arc furnace melted (billets), manufactured, processed, tested in the U.S.A with satisfactory results. No weld repair was performed on this heat.

Notarized upon request: _____
 Sworn to and subscribed before me on this 16th day of September, 2015

Signed: Mark Edwards
 MARK EDWARDS, QUALITY ASSURANCE SUPERVISOR

Direct any questions or necessary clarifications concerning this report to the Sales Department 1-800-535-7692 (USA)

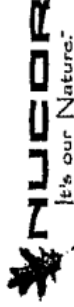
Parish/Country _____

Notary Public

NUCOR
P.O. Box 279
Winton, NC 27986
(252) 356-3700

Mill Test Report

Page 3



Issuing Date : 12/01/2014 B/L No. : 403173 Load No. : 408274 Our Order No. : 123399/11 Cust. Order No. : DBP-1721
 Vehicle No: TTPX 804324 Sold To : BUSHWICK METALS INC Ship To : ANASTASIO & SONS TRUCKING CO
 Specification : 0.6250" x 96.000" x 240.000" 185 GREAT NECK RD 158 MIDDLETOWN AVE
 ASTM A36-12/ASTM A709 Grade 36-13a/AASHTO M270 Grade 36/ASME STE 202 MIDDLETOWN, CT 06457
 SA36 2011 Addenda, 2013 AASHTO M270 36 GREAT NECK, NY 11021

Marking :

Heat No	C	Mn	P	S	Si	Cu	Ni	Cr	Mo	Al(tot)	V	Nb	Ti	N	Ca	B	Sn	CEQ	PCM
4508466	0.17	0.90	0.012	0.005	0.05	0.26	0.08	0.08	0.01	0.023	0.004	0.002	0.002	0.002	0.0018	0.0000	0.010	0.37	0.24

Plate Serial No	Tensile Test		Elongation		Charpy Impacts			Min Ave.
	Pieces	Yield (psi)	Tensile (psi)	% in 2"	Dir.	1 shear (%)	2 shear (%)	
4508466-01	5	39,100	68,800	21.6		1 shear	2 shear	Temp
		46,600	68,900	23.6		3 shear	3 shear	Ave.

Manufactured to fully killed fine grain practice by Electric Arc Furnace. Welding or weld repair was not performed on this material. We hereby certify that the contents of this report are accurate and correct. All test results and operations performed by the material manufacturer are in compliance with the applicable specifications, including customer specifications.

Mercury has not been used in the direct manufacturing of this material. Produced as continuous cast discrete plate as-rolled, unless otherwise noted in Specification. For Mexico shipments: nhc-sales@nuco.com

Yield by 0.5EUL method unless otherwise specified. Ceq = C+(Mn/6)+(Cr+Mo+V)/5+(Cu+N)/15

Form = C+(S/20)+(Mn/20)+(Cu/20)+(Ni/60)+(C/20)+(Mn/15)+(V/10)+SB

Melted and manufactured in the USA. ISO 9001:2008 certified (#010940) by SRI Quality System Registrar (#0985-09). PED 9 723/EC 7/2 Annex 1, Para. 4.3 Compliant.

DIN 50049 3.1.BVEN 10204 3.1E(2004), DIN EN 10204 3.1(2005) compliant. For ABS grades only. Quality Assurance certificate 14-MMPOA-723

T. A. Depraits
T. A. Depraits, Metallurgist

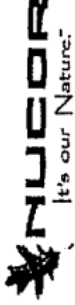
12/01/2014 11:24:00 AM

14468

NUCOR
PLATE MILL

P.O. Box 279
 Winton, NC 27986
 (252) 356-3700

Mill Test Report
 Page 1



Issuing Date : 12/01/2014
 Vehicle No: TTPX 804324
 Specification : 0.3750" x 96.000" x 240.000"
 ASTM A572 Grade 50-13si/ASTM A709 Grade 50-13si/AAASHTO M270-50
 Type 2

Load No.: 408274

Sold To: BUSHWICK METALS INC
 185 GREAT NECK RD
 STE 202
 GREAT NECK, NY 11021

Our Order No.: 123399/1

Cust. Order No.: DBP 1721

Ship To: ANASTASIO & SONS TRUCKING CO
 158 MIDDLE TOWN AVE
 MIDDLETOWN, CT 06457

Marking :

Heat No	C	Mn	P	S	Si	Cu	Ni	Cr	Mo	A1(tot)	V	Nb	Ti	N	Ca	B	Sn	CEQ	PCM
4508383	0.18	0.94	0.011	0.002	0.22	0.24	0.07	0.07	0.01	0.031	0.027	0.002					0.010	0.38	0.26

Plate Serial No	Tensile Test			Charpy Impacts			Min Temp Ave.													
	Pieces	Tons	Dir.	(psi) Tensile	Elongation % in 2"	Elongation % in 8"		Dir.	1 shear (%)	2 shear (%)	3 shear (%)									
4508383-08	6	7.35	T	52,400	77,700	19.8														
			T	54,000	77,000	19.9														
4508383-09	11	13.47	T	52,400	77,700	19.8														
			T	54,000	77,000	19.9														

Manufactured to fully killed fine grain practice by Electric Arc Furnace. Welding or weld repair was not performed on this material. We hereby certify that the contents of this report are accurate and correct. All test results Mercury has not been used in the direct manufacturing of this material. Produced as continuous cast discrete plate as-rolled, unless otherwise noted in Specification. For Mexico shipments, nbc-SalesMX@Nucor.com and operations performed by the material manufacturer are in compliance with the applicable specifications, including customer specifications.

Pcm = C-(S500-(Mn20)-(Cu20)-(Nb5)-(Cr20)-(Mo15)-(V10)-Sb

Melted and manufactured in the USA. ISO 9001:2008 certified (#010940) by SRI Quality System Registrar (#0985-09). PED 97/23/EC 7/2 Annex 1, Para. 4.3 Compliant.

DIN 50049 3.1B/EN 10204 3.1B(2004). DIN EN 10204 3.1(2005) compliant. For ABS grades only, Quality Assurance certificate 14-MMPQA-723

T. A. Depreits, Metallurgist

12/01/2014 11:24:00 AM

19468

14468

ARCELORMITTAL PLATE LLC TEST CERTIFICATE

SHIP TO:
ARCELORMITTAL USA LLC
110" LOADING BANK - .5" GA.
CONSHOHOCKEN PA 19428

PAGE NO: 01 OF 01
FILE NO: 0110-01-0
MILL ORDER NO: 75034-812
MELT NO: U6678
DATE: 01/25/16

SOLD TO:
ARCELORMITTAL USA LLC
SPP PROGRAM DISCRETE
CONSHOHOCKEN PA 19428

SEND TO:
TEST REPORT WITH SHIPMENT
FOR BOL # 90547

STEEL PLATE DIMENSIONS / DESCRIPTION						
TOTAL QTY	GAUGE	WIDTH	LENGTH	DESCRIPTION	PIECE WEIGHT	
	.5"	96"	240"	RECTANGLE	3267#	

CUSTOMER INFORMATION
CUSTOMER PO: SPP - 1/2"

SPECIFICATION(S)

THIS MATERIAL HAS BEEN MANUFACTURED AND TESTED IN ACCORDANCE WITH PURCHASE ORDER REQUIREMENTS AND SPECIFICATION(S).

ASTM A36 YR 14
THE MANAGEMENT SYSTEMS FOR MANUFACTURE OF THIS PRODUCT ARE CERTIFIED TO ISO 9001:2008 (CERTIFICATE NO. 30130) AND ISO 14001:2004 (CERTIFICATE NO. 49009).

CHEMICAL COMPOSITION (WT%) FOR ALL ELEMENTS EXCEPT H (PPM)

	C	MN	P	S	CU	SI	NI	CR	MO
MELT:U6678	.09	.70	.013	.018	.27	.23	.20	.12	.06
MELT:U6078		V	AL	CB					
		.001	.002	.001					

TENSILE PROPERTIES

LOC	DIR	YIELD STRENGTH PSI X 1000	TENSILE STRENGTH PSI X 1000	ELONGATION AFTER FRACTURE	
				GAGE LGTH	%
BOT.	TRANS.	52	65	8.00"	26.0
BOT.	TRANS.	52	67	8.00"	27.0

GENERAL INFORMATION

ALL STEEL HAS BEEN MELTED AND MANUFACTURED IN THE U.S.A.
ACID SOLUBLE ALUMINUM
FOR MORE INFORMATION AND PROCESSING GUIDELINES, REFER TO
WWW.USA.ARCELORMITTAL.COM/PLATE

WE HEREBY CERTIFY THAT THE ABOVE INFORMATION IS CORRECT:

ARCELORMITTAL PLATE LLC
QUALITY ASSURANCE LABORATORY
139 MODENA ROAD
COATESVILLE, PA 19320

SUPERVISOR - TEST REPORTING
ELINCIRE ZAPI ITNY